2 Recent advances in understanding of global mercury cycling

Authors: Peter Outridge, Robert Mason, Feiye Wang, Lars-Eric Heimburger, Xinbin Feng, [Milena Horvat]

Key messages

- *Considerable work has been published in the world literature concerning global Hg cycling and budgets, since the last Global Mercury Assessment in 2013. A major point of recent debate has been the impact of historical atmospheric emissions, mainly from silver and gold mining and amalgamation in the 16th to late 19th centuries, on current Hg levels in the environment, especially the oceans.*
- *Based on an evaluation of historic information, and of atmospheric Hg fluxes recorded in lake sediment, peat bog and glacier ice archives, the weight of evidence at present strongly supports a 'low mining emission' scenario.*
- *Building on a global model using the low emission scenario, this assessment estimates human activities to have increased total atmospheric Hg concentrations by about 450% above natural levels (i.e., those before 1450 AD). The anthropogenic effect represents an increase in mass of 3600 t above the natural value of 800 t for a current total of 4400 t. This increase includes the impact of revolatilization from soils and oceans of the 'legacy' Hg emitted from natural and human sources in the past but which is still circulating in the biosphere.*
- *Current anthropogenic emissions to air are estimated at 2500±500 t/y, which is the sum of the documented emission inventory presented later in this Assessment (2150 t/y) and undocumented releases from likely important sources such as agricultural waste burning, and municipal and industrial waste.*
- *Bearing in mind the uncertainties in natural and anthropogenic emission estimates, and the many deficiencies in our understanding of the processes and flux rates governing Hg transport and fate between the air, soil and ocean compartments, the best information currently available suggests that the increase in atmospheric Hg concentrations has driven a ~310% increase in average deposition rates to the Earth's surface in recent decades. This is the largest source (~90%) of Hg in the surface ocean; rivers are minor contributors.*
- *Surface marine waters have shown a 230% increase in Hg concentrations above natural levels. The increase in surface soils (~15%) has been an order of magnitude lower due to the large mass of natural Hg present in soils from rock weathering. Evasion of dissolved gaseous Hg from the ocean's surface back to the atmosphere has increased 250%. Deeper marine waters show increases of only 12–25% above natural levels owing to the slow rate of penetration of anthropogenic Hg and the large volume of mid- and deep-ocean waters.*
- *Even using the low mining emission scenario, the cumulative effect on today's oceanic Hg cycle of several centuries of emissions has been dramatic, with about two-thirds of the overall increase in marine Hg concentrations occurring before 1920 (mainly due to precious metal mining and associated cinnabar refining). About 20% of the overall increase is due to coal combustion since 1920, and another ~10% is due to other industrial activities.*
- *Marine Hg concentrations are expected to show a slow recovery following regulatory reductions in global Hg emissions (on the order of decades to centuries depending on the ocean basin and the trajectory of reductions). Mercury has a relatively long half-life in surface soils and marine waters, because of its recycling between the surface environment and atmosphere and between surface and intermediate ocean waters. Permanent removal of anthropogenic Hg from the biologically-active part of the environment will only occur once it is buried in deep ocean sediments and in mineral soils.*
- *Recommendations to improve the scientific knowledge base underpinning global models and budgets of Hg fall into two general areas: better understanding of natural inputs and processes, and more accurate and complete anthropogenic emissions inventories.*

2.1 General overview

An improved understanding of the global mercury (Hg) cycle is important for our capacity to predict how regulatory efforts to reduce current emissions to air, water and land will affect Hg concentrations in environmental compartments, biota and humans. The aim of this chapter is to provide a broad perspective for all subsequent chapters by describing the sources, transport and fate of Hg, especially anthropogenic Hg, in the global environment. Owing to its scale and chemical complexity, and the lack of detailed information for many aspects of it, the planetary Hg cycle is best described and communicated in a quantitative manner by using the budgets derived from global-scale models. This chapter presents a synthesis of recent advances in knowledge of the global Hg cycle, including the influence of historic emissions on current anthropogenic Hg levels in the environment, and provides updated global and oceanic total Hg budgets.

Mercury is released into the environment through human activities, as well as from natural sources and processes such as volcanoes and rock weathering. Following its release, Hg is transported and recycled between the major environmental compartments – air, soils and waters – until it is eventually removed from the system through burial in coastal and deep ocean sediments, lake sediments, and subsurface soils (Amos et al., 2014; Fitzgerald and Lamborg, 2014). Only a very small fraction of the Hg present in the environment is monomethylmercury – the only Hg form that biomagnifies in food chains. Hereafter, for the sake of simplicity, monomethylmercury is referred to by its generic name, methylmercury (MeHg). Methylmercury is produced from inorganic Hg mainly in aquatic ecosystems through biochemical processes mediated by naturally-occurring microorganisms. Recent findings on the methylation/demethylation part of the aquatic Hg cycle are presented in Chapter 7.2; many of these processes are only partly understood, which contributes to the

Table 2.1 Recent estimates of total, anthropogenic and natural[a] Hg masses in global air, soils and oceans (data in kilotonnes).

	Mason et al. (2012); AMAP/UNEP (2013)	Amos et al. (2013)	Zhang et al. (2014b)	Lamborg et al. (2014)	Present report[b]
Atmospheric Hg					
Total	5.1	5.3	4.4	n/a	4.4
Anthropogenic	3.4–4.1	4.6	3.6	n/a	3.6
Natural	1.0–1.7	0.7	0.8	n/a	0.8
Soil Hg (organic layers)					
Total	201	271	n/a	n/a	150
Anthropogenic	40	89	92	n/a	20
Natural	161	182	n/a	n/a	130
Oceanic Hg					
Total	358	343	257	316	313
Anthropogenic	53	222	66 (38–106)[c]	58±16[d]	55
Natural	305	122	191	258[e]	258

[a]The time point for designation of the 'natural' Hg state, and thus the quantification of 'natural' and 'anthropogenic' Hg masses, differed between studies: 2000 BC in the 'pre-anthropogenic period' by Amos et al. (2013), prior to 1450 AD by Zhang et al. (2014b) which preceded New World gold, silver and cinnabar mining, and about 1840 AD by Lamborg et al. (2014) which was prior to the North American Gold Rush and the expansion of coal-fired combustion sources. The anthropogenic Hg values from Mason et al. (2012) and Lamborg et al. (2014) are based on increases over the past ~100 to 150 years, and thus their 'natural' Hg masses may be over-estimated and the anthropogenic masses under-estimated compared with the other studies; [b]estimates modified from Zhang et al.'s (2014b) model (see Section 2.3), and thus the anthropogenic values represent the impact of human activities since before 1450 AD; [c]uncertainty range shown in brackets; [d]based on an oceanic anthropogenic Hg:anthropogenic CO_2 ratio for 1994; a more recent (higher) oceanic CO_2 estimate gave an Hg_{ant} estimate of 76 kt Hg (Lamborg et al., 2014); [e]calculated by subtraction.

difficulties in predicting the direct positive effects of regulatory action on biological Hg concentrations and human exposure.

In the 2013 technical background report to the Global Mercury Assessment (AMAP/UNEP, 2013), based on a global model and budget developed by Mason et al. (2012), it was estimated that human activities cumulatively had increased atmospheric Hg concentrations by 300–500% over the past century, whereas Hg in surface ocean waters less than 200 m deep had increased on average by ~200%. Deeper waters exhibited smaller increases (11–25%) because of limited exposure to atmospheric and riverine anthropogenic Hg inputs, and the century- to millennium-scale residence times of these slowly overturning, isolated water masses. Owing to the naturally large Hg mass present in soils, the average Hg increase was only ~20% in surface organic soils and was negligible in mineral soils. The revolatilization of 'legacy Hg' (i.e., the Hg that was emitted and deposited historically) from soils and oceans, and its long residence time in those compartments, act to maintain atmospheric Hg concentrations and deposition rates at higher levels than are supported by current primary emissions (Fitzgerald and Lamborg, 2014).

It is increasingly recognized, as a result of recent studies of Hg consumption and production in New World precious metal and cinnabar mining from the 16th century onwards (Guerrero, 2016, 2017), and re-examination of the atmospheric Hg flux rates recorded in long lake sediment and peat bog cores (Amos et al., 2015), that significant amounts of Hg were emitted by human activities during the 'pre-industrial period' (variably defined but generally accepted as ending about 1850) and that some fraction of this Hg is still circulating in the environment (Streets et al., 2011, 2017; Amos et al., 2013, 2015). Overall, studies since about 2012 indicate that the last few centuries of the 'pre-industrial period' are not a suitable reference point from which to gauge the full impact of human activities on the current global Hg cycle. However, there are different definitions of a time period that truly represents natural or 'pre-anthropogenic' conditions: for example, 2000 BC (Amos et al., 2013); 3000 BC to 1550 AD (Amos et al., 2015); or prior to 1450 AD (Zhang et al., 2014a).

Nonetheless, two new estimates generally agree that human activities have increased atmospheric Hg concentrations by 450% (Zhang et al., 2014b) to 660% (Amos et al., 2013), such that total atmospheric Hg concentrations today are 5.5-fold to 7.6-fold higher, respectively, than pre-anthropogenic 'natural' values (Table 2.1). These estimates include revolatilized legacy Hg. Zhang et al. (2014b) further calculated that the increased atmospheric concentrations had resulted in a 4.8-fold increase in average Hg deposition to oceans and a 7.8-fold increase in deposition to land above natural levels. However, Amos et al. (2015), based on a re-evaluation of long peat and lake sediment cores, proposed that substantially higher increases had occurred in deposition rates. Median increases in Hg accumulation rates between the pre-anthropogenic period – defined by Amos et al. (2015) as up to 1550 AD – and the 20th century peak were a factor of ~26 in peat bogs and ~14 in lake sediments, with both archive types showing increases of about 5-fold between the pre-anthropogenic and pre-industrial (1760–1880) periods. These total increases are several times higher than previous reviews of the sediment-based Hg literature indicated, of a ~3-fold increase since the pre-anthropogenic or 'pre-human' period (Fitzgerald et al., 1998; Engstrom et al., 2014; Fitzgerald and Lamborg, 2014). Amos et al. (2015) attributed the latter, lower value to an erroneous selection of 'natural' deposition values that were too high, based on 18th and early 19th century sediment samples that were already contaminated with mining-emitted Hg. Thus, recent studies since 2012 indicate that the true impact of anthropogenic emissions on atmospheric Hg, based on a comparison to pre-anthropogenic values, is greater than previous comparisons to the 19th century had suggested. But there is considerable variation in the estimates of the degree of that impact.

As with almost all modelled global budgets of elements and other chemical substances, large uncertainties exist regarding the amounts of Hg 'stored' in different environmental compartments, the fluxes of Hg between them, and the rates of removal of Hg from the biosphere (AMAP/UNEP, 2013). These uncertainties limit confidence in our understanding of the Hg cycle and in our ability to predict the responses of ecosystem Hg concentrations to changes in emissions due to international regulatory actions. Therefore, major ongoing efforts have been mounted to reduce these uncertainties and derive a more robust, accurate global budget. Since 2012, additional measurements of Hg concentrations and fluxes in oceans, the atmosphere and soils have led to suggested refinements of global budgets and models by several research groups. Nevertheless major uncertainties persist, especially in oceanic budgets.

The new estimates of the amounts of natural and anthropogenic Hg in the atmosphere by Amos et al. (2013) and Zhang et al. (2014b) agree to within about 30% of the estimates in the AMAP/UNEP (2013) budget (see Table 2.1). In the terrestrial system, both Amos et al. (2013) and Zhang et al. (2014b) suggested that soils globally contain more anthropogenic Hg than was stated in AMAP/UNEP (2013). This revision is supported by new modelling of the transport and fate of atmospheric Hg (Song et al., 2015). However, the balance of anthropogenic Hg distribution between global soils and oceans differs between models, with oceans holding either about as much anthropogenic Hg mass as soils (AMAP/UNEP, 2013; Zhang et al., 2014b) or substantially less (Amos et al., 2013). Again, the difference between model outcomes may be partly due to our lack of understanding of some of the basic processes governing Hg transport and fate. For example, recent studies on atmospheric Hg dynamics under a range of different plant communities – from tundra plants to forests – have indicated that the direct uptake of gaseous elemental Hg (Hg^0; GEM) through the stomata of plant leaves is more significant than previously thought (Enrico et al., 2016; Fu et al., 2016; Wang et al., 2016; Obrist et al., 2017, 2018; Risch et al., 2017). Risch et al. (2017) reported that at 27 forest sites across the eastern United States, litterfall Hg deposition equaled or exceeded the precipitation Hg flux in 70% of cases, and was on average 20% higher than in precipitation across all sites. Also, MeHg constituted ~0.5% of total Hg in litterfall, significantly higher than in precipitation (Risch et al., 2017). Thus, the litterfall total Hg flux was previously under-estimated, and litterfall MeHg could be a contributor to the terrestrially-sourced MeHg that is assimilated by some freshwater biota, especially in headwater streams (Tsui et al., 2014). Globally, GEM-containing litterfall and throughfall, and not wet and dry deposition of oxidized Hg species, may thus represent the largest net flux of atmospheric Hg to terrestrial ecosystems, at 1930 t/y (Fu et al., 2016). This flux via the GEM foliar uptake pathway has not been incorporated into global Hg models.

With respect to the world's oceans, there are significant differences between the new models concerning the quantity of anthropogenic Hg presently circulating in seawater (cf. Amos et al., 2013, 2015; Lamborg et al., 2014; Zhang et al., 2014b; see Table 2.1). Because much of the current risk from Hg to humans and wildlife originates in marine food webs, how much anthropogenic Hg is present in the oceans, its distribution, and its likely rate of clearance from seawater following emission reductions, are of fundamental importance.

Until 2012, published estimates of oceanic anthropogenic Hg exhibited more than an order of magnitude range, from 7.2 to 263 kt (Mason et al., 1994; Lamborg et al., 2002a; Sunderland and Mason, 2007; Selin et al., 2008; Soerensen et al., 2010; Strode et al., 2010; Streets et al., 2011; Mason et al., 2012). Since then, another estimate (222 kt) near the upper end of this range was derived by Amos et al. (2013) based on the putative inventory of all-time anthropogenic emissions by Streets et al. (2011), which indicated large releases from historic silver (Ag) mining activities (see also Streets et al., 2017). Zhang et al. (2014b) subsequently revised the historic mining emissions downward by 3-fold to make the trends in global Hg emissions more compatible with the Hg deposition histories recorded in 120 lake sediments world-wide (Figure 2.1), but retained all other elements of the Streets et al. (2011) inventory. Lake sediments and other natural archives of atmospheric deposition such as peat bogs and glacial ice are widely employed to reconstruct historic patterns of deposition flux, and the reconstructed fluxes are assumed to apply equally to deposition over both oceans and land.

The differences between the two most recent global budgets (i.e., Amos et al., 2013 and Zhang et al., 2014b) are primarily due to varying estimates of the amount and environmental fate of atmospheric emissions from historic Ag and gold (Au) mining in the Americas between the 16th and late-19th centuries, and to differences in the estimated amount of natural Hg originally present in the oceans. Overall, the different chemical rate constants used for modelling circulation processes within and between oceanic, atmospheric and terrestrial compartments are a secondary factor in uncertainty. Significant Hg releases to land, freshwaters and air occurred from the mining and amalgamation of Ag (and Au) in South/Central America during the Spanish colonial period (about 1520–1850 AD), and later from North American artisanal and small-scale mining during the 'Gold Rush' era (about 1850–1920) (Nriagu, 1993, 1994; Strode et al., 2009). Based on the relative importance of Spanish colonial Ag production for the three centuries after 1520 (~69% of total world Ag; TePaske and Brown, 2010), and the predominant use of Hg amalgamation to process the Spanish New World Ag (and Au) ores, Hg losses to the local environment from these operations must have been substantial (Guerrero, 2016, 2017). Smelting of Ag ores with lead was another, minor, production method (Guerrero, 2016). In terms of the global environment, it is generally agreed that some fraction of the Hg from both historic periods is still circulating within the biosphere, and that this has had an effect on present-day environmental Hg levels. But quantification of that effect is uncertain. Thus, before considering the question of how much anthropogenic Hg is in the biosphere, evidence for the impact of historic mining on the global environment and its relative importance in different models must be evaluated.

2.2 Influence of historic silver mining on anthropogenic mercury emission inventories

The total amount of Hg currently in the environment reflects a mixture of sources: historic anthropogenic releases to air, land and oceans; historic natural inputs; and present-day anthropogenic and natural releases. Global models need to estimate these quantities and how the historic emissions have been remobilized, transported and transformed over long (decadal to century) timescales. The influence of historic Ag mining on the oceanic Hg budget is particularly important (Zhang et al., 2014b).

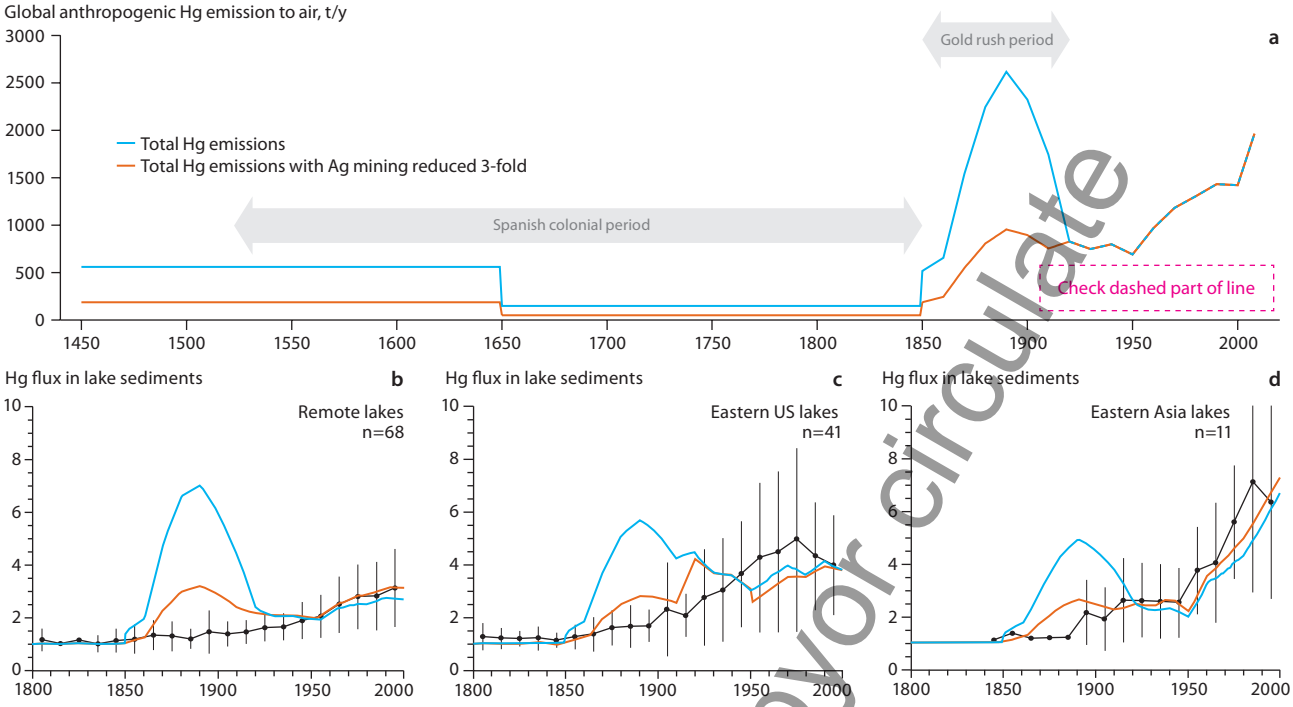

Figure 2.1. Two contrasting views of global anthropogenic Hg emissions to air through history, compared to Hg fluxes to lake sediments. The upper plot compares combined anthropogenic Hg emissions after 1450 from Streets et al. (2011; blue line) and the same emission inventory but with Ag mining emissions reduced three-fold (Zhang et al., 2014b). The lower plots show Hg fluxes in lake sediments after 1800 from remote lakes, lakes in the eastern USA and lakes in eastern Asia.

A historic analysis of liquid elemental Hg importation and consumption during Spanish colonial Ag mining operations in the 16th to 19th centuries, in what is today Mexico, Peru and Bolivia (Guerrero, 2012) indicated that large quantities of Hg were used during this period. Mercury was also refined from cinnabar at two sites in the Spanish New World (Guerrero, 2016). During the 250 years after ~1560, historic reports documented that over 120 kt of liquid Hg (average 0.48 kt/y) were imported from Europe or produced in the region (TePaske and Brown, 2010). Given the likely large scale of undocumented contraband Hg involved in mining, this amount may be considerably underestimated (S. Guerrero, pers. comm.).

Streets et al. (2011, 2017) assumed emission factors of 52% and 40%, respectively, to calculate airborne Hg emissions from historic Ag mining. By contrast, Guerrero (2012) calculated that only 7–34% of the Hg 'consumed' during New World Ag production was physically lost through volatilization, ground spills and in wastewater, with 66–93% of the consumed Hg chemically transformed into solid calomel (mercurous chloride, Hg_2Cl_2) that was accidentally lost or discarded into soils and streams. Volatilization was thus a relatively small fraction (<34%) of total Hg losses. The calomel transformation has been confirmed by controlled laboratory experiments (Johnson and Whittle, 1999). Subsequently, Guerrero (2016, 2017) cited observers in the 19th century who documented losses to air of less than 1% of the liquid Hg consumed, owing to improvements in the equipment used to recapture Hg after amalgamation and to efficiently condense gaseous Hg during the heating stage of amalgamation, as well as economic incentives for miners to limit Hg losses. The AMAP/UNEP (2013) report used an emission factor of 45% for Hg emissions from artisanal and small-scale gold mining (ASGM) in the present-day. That estimate is not affected by the new evidence concerning lower Hg losses from Ag mining. The Au amalgamation process with Hg does not involve calomel formation, and thus historic Hg losses from Ag mining are not representative of those from ASGM (Guerrero, 2017), which are likely to be higher.

These historical studies of the fate of Hg used in Ag mining represent an important advance in understanding the global Hg cycle because they concern a potentially major anthropogenic source. Streets et al. (2017) calculated that Ag production was the largest single atmospheric source of anthropogenic Hg throughout history, contributing several-times more Hg to air (146 kt, 31% of total atmospheric emissions) than combined large-scale Au production and ASGM (55.4 kt), and coal combustion (26.4 kt). Mercury production, much of which was destined for use in Ag and Au amalgamation, contributed the second highest amount, 91.7 kt.

Zhang et al. (2014b) adopted a median volatilization rate of 17% of Hg during historic Ag mining (based on Guerrero, 2012) and assumed that the same rate applied to 19th century Gold Rush Au and Ag mining. The resulting tally of cumulative atmospheric anthropogenic emissions was just over half that of Streets et al. (2011) (totals of 190 kt versus 351 kt, respectively), with markedly lower emissions during the Spanish colonial and Gold Rush mining periods (see Figure 2.1). Using their revised inventory, Zhang et al. (2014b) found a 3-fold lower current oceanic anthropogenic Hg mass compared to that derived by Amos et al. (2013), who incorporated Streets et al.'s (2011) larger mining estimate in their model (see Table 2.1).

Corroborative data supporting the lower New World mining emissions used by Zhang et al. (2014b) came from an independent analysis by Engstrom et al. (2014) of another large global set of lake sediment Hg profiles. Atmospheric Hg deposition was substantially increased during the Spanish colonial period in one South American lake (Laguna Negrilla) near the major cinnabar mining and Hg production site of Huancavelica, Peru, with less impact in another lake (El Junco, Galápagos Islands) further away from Ag and Hg mining and amalgamation operations. But little evidence of increased deposition at this time was found in sediment cores from

many remote North American, Arctic or African lakes, suggesting that most of the contamination from Spanish colonial mining operations was limited to surrounding terrestrial, freshwater and coastal marine ecosystems in western South/Central America (Engstrom et al., 2014). Thus, the world-wide lake sediment record appears to suggest a negligible global impact from Ag and Au production during the 16th to 19th centuries.

Similarly, there is little evidence in natural archives to support a dominant impact on the global atmosphere from late 19th-century North American Au and Ag mining, as suggested by Streets et al. (2011, 2017). Streets et al. (2017) proposed a bimodal pattern of anthropogenic Hg emissions from 1850 onwards, with values in the late 1890s that were as high or higher than in the mid- to late-20th century, due to a 450% increase in primary emissions between 1850 and 1890 (from 0.58 to 3.2 kt/y) mostly from the North American Gold Rush. Although increases in Hg accumulation occurred in remote lake sediments at this time, they were small relative to those observed later in the 20th century in the same core profiles (Strode et al., 2009; Engstrom et al., 2014; Zhang et al., 2014b). Coincident increases in emissions from other sources such as coal combustion and industrial Hg production and use (Streets et al., 2017, 2018) may have contributed to the elevated Hg deposition that was observed world-wide during the late 19th century. Commercial Hg-containing products have also been suggested to be significant contributors to global Hg releases to air, soil and water from the late 1800s onwards (Horowitz et al., 2014).

Amos et al. (2015) discounted this evidence by arguing that lake sediments in general respond relatively slowly and insensitively to changes in atmospheric Hg deposition compared with peat bogs. Amos et al. (2015) also proposed that the Guerrero (2012) volatilization estimate was unrealistically low because it omitted Hg losses during reprocessing of Hg-containing Ag and Au products, and revolatilization from solid mining wastes. There is some evidence that calomel may dissociate to GEM and gaseous mercuric chloride ($HgCl_2$) under ambient environmental temperatures and sunlight (Copan et al., 2015), but this has not been demonstrated under realistic controlled conditions. Evaluation of alternative global model scenarios by Amos et al. (2015) suggested that the 'mining reduced 3x' history of Zhang et al. (2014b) was inconsistent with Hg measurements in present-day environmental matrices, as well as with the magnitude of Hg enrichment in peat and some lake sediment archives. However, close examination of the published outputs shows that the 'mining reduced 3x' scenario gave better agreement with observed upper ocean total Hg concentrations and net oceanic evasion rates than the larger mining emission inventory of Streets et al. (2011), with similar estimates for present-day soil Hg concentrations and net terrestrial flux (see Amos et al., 2015: their figs. 3d, 3g, 3f and 3h, respectively). Furthermore, the sediment-based interpretations of Strode et al. (2009), Engstrom et al. (2014) and Zhang et al. (2014b) agreed with earlier peat bog Hg studies from the Faroe Islands (Shotyk et al., 2005), Maine, USA (Roos-Barraclough et al., 2006), and Swiss Jura Mountains (Roos-Barraclough and Shotyk, 2003) that also showed relatively muted Hg increases prior to 1900, and with 20th-century accumulation rates substantially higher than in the late 19th century.

Independent evidence supporting the lower Zhang et al. (2014b) emission history, and the lake sediment and peat bog patterns, was provided by three recent studies of glacier ice cores (Figure 2.2). In contrast to the 450% increase in global primary Hg emissions between 1850 and 1890 estimated by Streets et al.

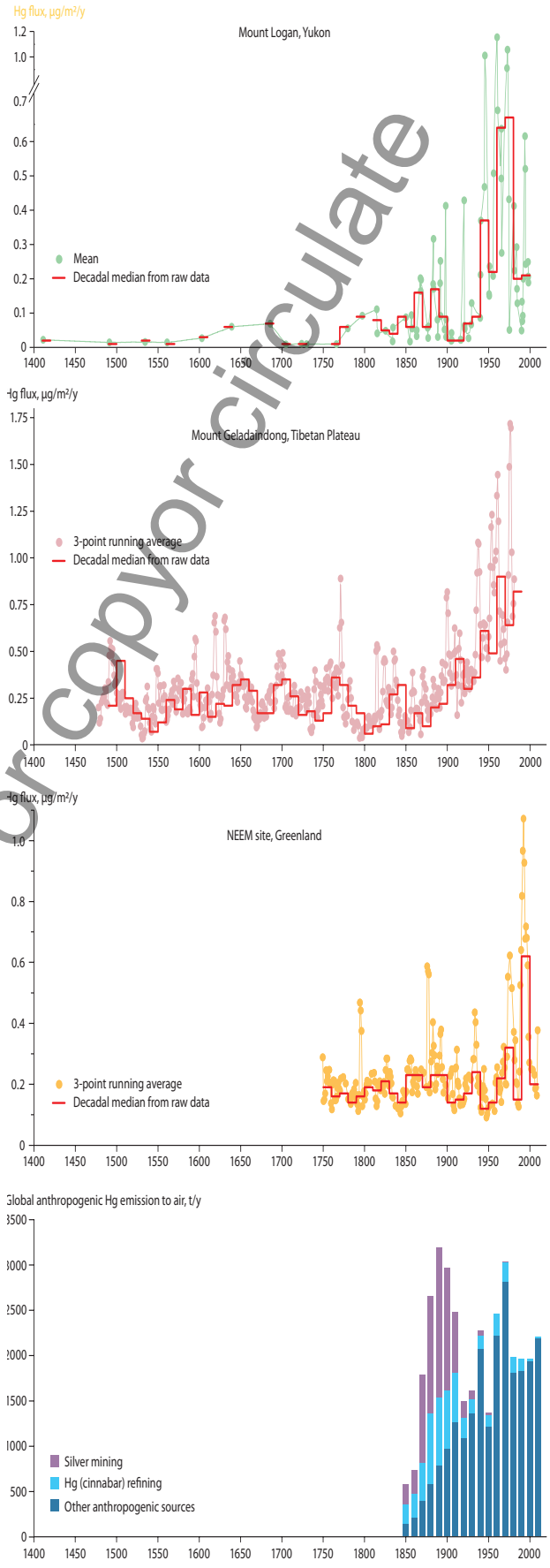

[GMA02-0020] Figure 2.2. Glacial ice core records of atmospheric Hg deposition from Mount Logan, Yukon (Beal et al., 2015), Mount Geladaindong, Tibetan Plateau, China (Kang et al., 2016), and the NEEM site, Greenland (Zheng, 2015), compared with the global atmospheric emission history since 1850 AD (Streets et al., 2017).

(2017), two Arctic or subarctic glacier records – Mount Logan, Yukon (Beal et al., 2015) and the North Greenland Eemian Ice Drilling (NEEM) site (Zheng, 2015) – showed increases in average Hg accumulation of only 150% and 40%, respectively, between 1840–1860 and 1880–1900, while an ice core from the Tibetan Plateau in central Asia (Mount Geladaindong, Kang et al., 2016) displayed a 140% increase. All three studies showed that Hg accumulation rates were substantially greater after 1950 than in the late 1800s, in contrast to Streets et al.'s (2011, 2017) inventory (see Figure 2.2). Furthermore, during the 16th to mid-19th centuries neither the Mount Logan core (which extended back to ~1400 AD) or the Mount Geladaindong core (which extended back to 1477 AD) revealed consistent or large increases in Hg fluxes that could represent a major atmospheric impact from the Spanish New World mining operations (compare Figure 2.1: upper plot, blue line, with Figure 2.2: upper three plots). Small increases in Hg accumulation were noted during the period 1600–1700 and again in the late 18th century at Mount Logan which could be a Spanish New World signal, but overall the peak periods of Spanish colonial mining (1600–1850) and the North American Gold Rush (1850–1900) represented only 8% and 14%, respectively, of total anthropogenic Hg deposition in the Mount Logan ice core, with 78% occurring during the 20th century (Beal et al., 2015).

Thus, the weight of evidence at present supports the Zhang et al. (2014b) emission history, and suggests that the atmospheric Hg emissions produced by historic precious metal and cinnabar mining and refining techniques were not globally or hemispherically distributed to a significant degree. That these historic emissions had effects on Hg levels in some areas around mining operations is not in dispute. Other studies have shown marked contamination of lake sediments and glacial ice by nearby historic Ag/Au mining (e.g., Cooke et al., 2013; Correla et al., 2017), although these regional effects are not seen everywhere. For example, reassessment of a glacier ice core Hg record from the western United States revealed no evidence of elevated Hg deposition from late 19th century Gold Rush mining operations (Chellman et al., 2017). To summarize, current evidence supports the interpretation that historic mining had much less impact on globally-distributed atmospheric emissions and deposition than coal combustion and other industrial sources had in the 20th century. A possible explanation for this finding is that modern high-temperature Hg sources, such as coal-fired power generators or cement kilns, which emit Hg tens to hundreds of meters above the ground, may have different Hg speciation and distribution profiles to historic mining sources, which were typically relatively low temperature emissions at ground level (Guerrero, 2016, 2017). High temperature sources emitting a larger fraction of GEM above the ground boundary layer would likely distribute more of that Hg further than historic mining sources.

2.3 Revised global and oceanic total Hg budgets

Even with the lower mining emissions inventory, Zhang et al.'s (2014b) modelling indicated that the cumulative impact of those emissions over four centuries on the current levels of oceanic anthropogenic Hg has been substantial, with 67% of the increase in oceanic Hg mass above natural levels occurring prior to 1920 mainly due to precious metal mining. A further 21% of the increase was from coal combustion and 11% from other industrial activities after 1920. The total anthropogenic

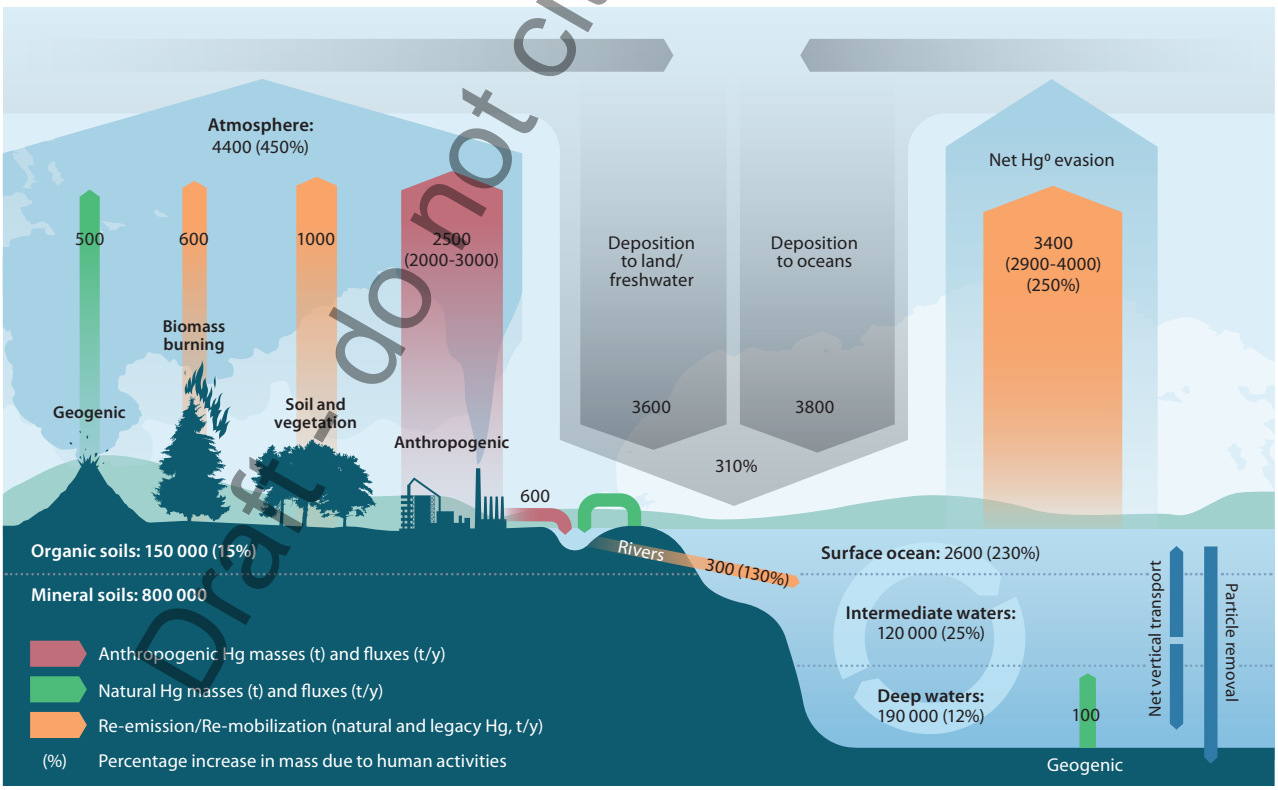

[GMA02-0030] Figure 2.3 Updated global Hg budget showing the anthropogenic impact on the Hg cycle since the pre-anthropogenic period (prior to 1450 AD) (see text for explanation of its derivation). Ranges are given in brackets after the best estimate values; percentages in brackets represent the estimated increase in mass or flux due to human activities since the pre-anthropogenic period (i.e., pre-1450 AD).

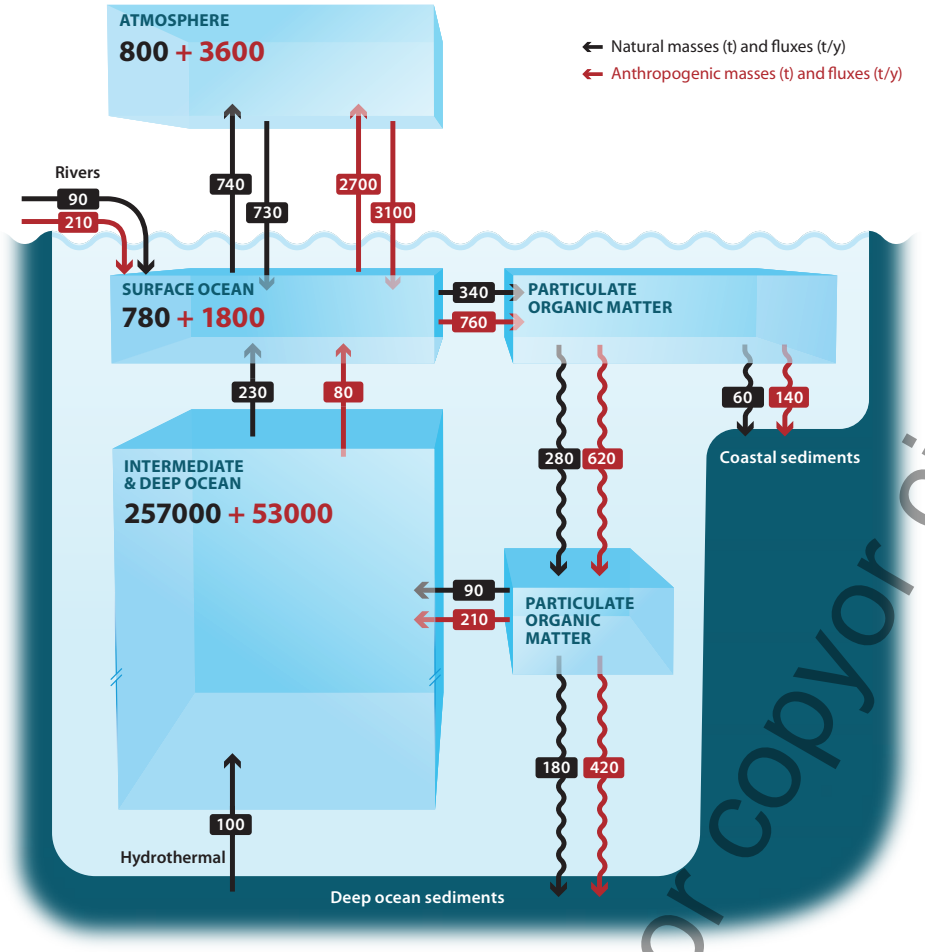

[GMA02-0040] Figure 2.4. Natural and anthropogenic Hg fluxes and masses in the world's oceans. Data adapted and revised from Zhang et al. (2014b), based on the revised global budget shown in Figure 2.3.

mass in today's oceans (66 kt) estimated by Zhang et al. (2014b) is in good agreement with another recent estimate of oceanic anthropogenic Hg (58±16 kt; Lamborg et al., 2014) derived using a different methodology based on seawater Hg concentration profiles combined with anthropogenic carbon dioxide (CO_2) and remineralized phosphate as proxies for oceanic Hg distribution. That the two studies, using different approaches, arrived at similar estimates increases confidence in the robustness of their conclusions. Both of these recent estimates fall within the lower half of the previous range of values and are close to the Mason et al. (2012) estimate of 53 kt used in AMAP/UNEP (2013) (see Table 2.1).

From these observations, a revised global total Hg budget (Figure 2.3) was constructed updating the previous version in AMAP/UNEP (2013; Mason et al. 2012). Changes in reservoirs and fluxes are based primarily on the discussion in Section 2.2 concerning more recent modeling efforts and budgets. Information and estimates from Lamborg et al. (2014) and Zhang et al. (2014b) were considered, and the revised ocean inventories are an average of the values in these two papers and the previous assessment. The new terrestrial reservoir and flux estimates are based largely on Driscoll et al. (2013) and Amos et al. (2015). Fluxes were also modified based on Pacyna et al. (2016) and Cohen et al. (2016), who advocated for specific values for the terrestrial fluxes from biomass burning, soil and vegetation emissions, and geogenic sources. These were adopted in the revised budget. The revised soil plus vegetation emissions are lower than the previous average, but for most of the remaining fluxes, the changes are relatively small (<30%) compared to the previous estimates.

Fluxes between terrestrial and oceanic reservoirs and the atmosphere were changed in accordance with the current best estimate for global atmospheric anthropogenic emissions (2500 t/y, which is 25% higher than in the previous assessment (AMAP/UNEP, 2013). This revised value reflects the fact that the current documented global inventory presented in this report (2150 t/y, range yyyy–zzzz for 2015; see Chapter 3) does not include emissions for several sectors that cannot yet be reliably quantified. Provisionally, these sectors, which include agricultural waste burning and municipal and industrial waste disposal (see Chapter 3) can be expected to contribute tens to hundreds of additional tonnes of atmospheric Hg. The 2500 t/y value adopted here is therefore considered to be a reasonable estimate for use in a contemporary global budget calculation. This estimate contains several acknowledged uncertainties (especially for emissions from ASGM, and waste combustion) and so a relatively wide range of ±500 t/y is included. Similarly, there is a large range in estimates for ocean evasion. A new estimate for total anthropogenic release to freshwaters, of 0.4 kt/y, is taken from Chapter 6; an estimate from that chapter for oil and gas releases to marine systems (0.015 kt/y) is insignificant compared with the other fluxes and so is not included in Figure 2.3. Fluxes in the budget should each be regarded as spanning a range of at least ±20%, and subject to future revision. The mass budget is balanced to within 5%.

Based on this revised global budget, the Hg budget in the world's oceans, as presented in the Zhang et al. (2014b) paper, was updated in light of the mass balance fluxes and reservoirs in Figure 2.3, and is presented in Figure 2.4. The ratios of natural to anthropogenic Hg as reported by Zhang et al. (2014b) were

retained for most of the reservoirs and fluxes, although the relative increase in oceanic Hg mass due to anthropogenic inputs reported by Zhang et al. (2014b) is higher than in other publications. This difference was taken into account in updating and revising their budget for this report. The graphic breaks down each reservoir and flux in terms of how much Hg is natural, and how much is anthropogenic. The graphic also shows the cycling of Hg in the ocean through uptake onto particulate organic matter, which is a major mechanism for transport of Hg between surface waters and deep ocean. In this graphic, the intermediate and deep waters are combined, whereas they are treated separately in the global budget (see Figure 2.3).

Inconsistencies remain in the evidence pertaining to the actual rates of atmospheric historic mining emissions that impacted the global environment, and thus, the evidence supporting these revised estimates of oceanic and global Hg cycling. Although the 3-fold reduction in mining emissions by Zhang et al. (2014b) brought their modelled emission history during the late 19th and early 20th centuries closer to the global lake sediment pattern, compared with the Streets et al. (2011) inventory, the modelled emissions remained relatively elevated compared to lake sediment Hg accumulation during the same period (see Figure 2.1). It may be that a further reduction in the assumed proportion of volatilized Hg from historic mining/amalgamation, which would not be inconsistent with the evidence discussed above, would bring the Zhang et al. (2014b) emission history, and the remote lake sediment, peat and ice core records, into even closer agreement. If implemented in future models, the additional reduction would reduce the relative amount of anthropogenic Hg in modern oceans and soils.

2.4 Distribution of anthropogenic Hg in the environment, especially the oceans

The Zhang et al. (2014b) global model projected that in the current global environment, 2% (3.6 kt) of the all-time cumulative anthropogenic emissions remains in the atmosphere, 48% (92 kt) is held in soils, and 50% (94 kt) in the oceans – 35% (66 kt) in seawater, and 15% (28 kt) buried in ocean sediments. For the oceans, atmospheric deposition from current primary emissions as well as revolatilization of legacy emissions contributes over 90% of the total (atmosphere + rivers) Hg inputs (4.0 out of 4.3 kt/y; Figure 2.3), with riverine inputs that reach the open ocean comprising a minor fraction (6%, 0.3 kt/y). Amos et al. (2014) estimated a substantially higher riverine contribution (1.5±0.8 kt/y; 30% of total 5.2 kt/y inputs) to the open ocean based on an observational database of riverwater Hg concentrations and consideration of river-offshore transport efficiencies for different estuary types. Most (72%) of the riverine Hg entering estuaries was scavenged and deposited in coastal marine sediments (Amos et al., 2014). By comparison, Mason et al. (2012) arrived at an estimate of 0.38 kt/y from rivers, which comprised ~10% of total ocean inputs. Recent data from Chinese rivers (Liu et al., 2016) support the lower estimates of Mason et al. (2012) and Zhang et al. (2014b), and so the revised oceanic budget proposes a total riverine input of 0.3 kt/y into oceans (see Figure 2.4).

Significant differences exist between recent models in their portrayal of the vertical distribution of oceanic anthropogenic Hg owing to the above-mentioned variance in historic emission estimates and different assumptions about the penetration rate of anthropogenic Hg into deep ocean waters. Zhang et al. (2014b) and Lamborg et al. (2014) largely agreed in their relative distribution, except that the deep ocean (below 1000 m depth) contained proportionally more anthropogenic Hg in Zhang et al.'s (2014b) simulation, 45% of total oceanic anthropogenic Hg vs 35% in the simulation by Lamborg et al. (2014). Compared to Zhang et al. (2014b), Streets et al. (2011) and Amos et al. (2013) calculated similar increases in the anthropogenic Hg content of the surface ocean (4.4 times natural concentrations vs. 3.6–5.9 times, respectively), but larger increases in the thermocline/intermediate depths (1.2 times vs 2.7–5.3 times) and deep ocean (1.2 times vs. 1.5–2.1 times). In addition to their use of larger historic mining emission estimates, Streets et al. (2011) and Amos et al. (2013) assumed faster vertical mixing rates compared with the other two studies.

Large inter-basin differences in the distribution of anthropogenic Hg were also apparent in intermediate and deep ocean waters, but were relatively uniform in surface waters, in the modelling of Zhang et al. (2014b). Vertical and horizontal advection of Hg inputs to the ocean which reflect ocean currents and areas of deep water formation, and high biological productivity and rapid particle scavenging of dissolved Hg in some tropical seas, account for the inter-basin patterns.

2.5 Rate of clearance of anthropogenic Hg from the world's oceans

The differences between models and their underpinning historic mining emission estimates are associated with significant differences in the implied response times of the oceans to emission reduction scenarios. All global ocean-atmosphere models predict that Hg clearance rates from most ocean basins will be slow relative to the rate of anthropogenic emission reductions in future, such that removal of anthropogenic Hg from the world's oceans will take many decades to centuries depending on the specific ocean basin and depth interval of the water mass in question, as well as the trajectory of emission controls (Mason et al., 2012; Lamborg et al., 2014; Zhang et al., 2014b; Amos et al., 2015). But according to Selin (2014) and Engstrom et al. (2014), the 'high emission' scenario of Streets et al. (2011; also 2017) and modelling by Amos et al. (2013, 2015) suggests much slower and delayed reductions in environmental Hg levels following emission curbs than the low emissions scenario by Zhang et al. (2014b), especially for the oceans. Even at current global emission levels, there is a general scientific consensus that seawater and marine foodchain Hg levels are likely to substantially increase over time, because of the slow clearance rate of legacy Hg from the world's oceans coupled with additional legacy anthropogenic Hg released from soil profiles into rivers and revolatilized into the air (Sunderland and Selin, 2013).

Until significant deficiencies in our current understanding of marine Hg cycling, and the rates of transformation between species that influence the major sinks for ocean Hg (evasion to the atmosphere and burial in sediments) are resolved, and

greater consistency is achieved in the interpretation of natural archives of Hg deposition from the atmosphere, the prediction of the timeline and effects of global emission reductions will remain uncertain. It is clear, however, that irrespective of these scientific uncertainties, emissions reductions are required to reverse the trend in oceanic anthropogenic Hg back towards natural levels, owing to the long response time of the ocean to changes in inputs (Sunderland and Selin, 2013; Engstrom et al., 2014; Selin, 2014).

2.6 Main uncertainties in global Hg models and budgets

This section summarizes the knowledge gaps and recommendations for further research stated in or developed from recent papers (Amos et al., 2013; Engstrom et al., 2014; Lamborg et al., 2014, 2016; Zhang et al., 2014b, 2016; Song et al., 2015; Kwon and Selin, 2016). Recommendations were selected on the basis of their relevance to global or oceanic models and budgets. Scientific uncertainties can be grouped under two headings: natural inputs and processes, and anthropogenic emissions.

2.6.1 Uncertainties in natural inputs and processes

Net removal rates of anthropogenic Hg from the surface ocean are the result of competition between three simultaneously occurring natural processes: the particulate flux from the surface to the deep ocean (the 'biological pump', involving particle scavenging, remineralization and settling); the mixing of surface and deep-ocean waters; and the reduction of inorganic Hg^{II} and subsequent evasion of Hg^0 back into the atmosphere. Some of the evaded Hg^0 is rapidly photo-oxidized in the lower troposphere and re-deposited to the ocean surface. Additional coupled ocean-atmosphere measurement studies are needed to comprehensively measure the concentrations of various Hg species spatially and temporally, and to better understand the transport and transformation rates of these co-occurring processes. The need is particularly acute in the Southern Hemisphere open oceans, as well as in regions where elevated anthropogenic Hg concentrations can be expected, such as the eastern equatorial Atlantic Ocean, eastern equatorial and high latitude Pacific Ocean, and northern Indian Ocean.

Uncertainties in the robustness of measurements of atmospheric and seawater Hg concentrations are exacerbated by relatively large inter-laboratory comparison errors, and so there is a particular need to improve the overall reliability of atmospheric and seawater Hg concentration and speciation measurements. Few inter-comparison efforts have been mounted (but see Gustin et al., 2015 for a review of atmospheric Hg determinations). Past intercalibration exercises for seawater have only addressed total Hg, and the results have indicated significant discrepancies among the participating laboratories (Lamborg et al., 2012). Future intercalibration exercises should continue the effort of attaining reliable data, and should be extended to include all Hg species, even unstable species such as dimethyl Hg and dissolved Hg^0. The development of suitable seawater reference materials is encouraged.

The role of natural inputs in the global Hg budget is poorly constrained but potentially of major importance. If the actual rate of emissions from natural sources such as volcanoes and marine hydrothermal vents is markedly higher or lower than currently thought, this would affect assumptions about the absolute amounts of, and relative balance between, natural and anthropogenic sources which are fundamental to modelling efforts and to our understanding of the global Hg cycle. Present estimates of global volcanic Hg emissions to air range over three orders of magnitude (0.1–1000 t/y) (Nriagu, 1989; Ferrara et al., 2000; Pyle and Mather, 2003; Nriagu and Becker, 2003; Bagnato et al., 2014). For oceans, the AMAP/UNEP (2013) report assigned a value of <600 t/y total Hg input from hydrothermal vents, which was based on few data and no systematic studies. Two recent GEOTRACES cruises sampled waters around hydrothermal vents in the North Atlantic and equatorial Pacific Oceans (Bowman et al., 2015, 2016). In the North Atlantic, elevated Hg concentrations were detected near the Mid-Atlantic Ridge (Bowman et al., 2015). In contrast, there was little evidence for hydrothermal Hg inputs over the East Pacific Rise in the equatorial Pacific (Bowman et al., 2016). These results suggest substantial variation in the extent of Hg inputs from different hydrothermal sources, as was found for other metals. Overall, there is insufficient new information to update the estimate of hydrothermal inputs made in 2013. In order to make direct estimations for global hydrothermal Hg fluxes, more observations of focused and diffuse-flow vent fluids and hydrothermal plumes are needed to better constrain the Hg flux, and its contribution to the global Hg cycle (German et al., 2016). In addition, analysis of sediments in regions close to hydrothermal sources relative to remote locations would help establish whether there is a strong hydrothermal signal. Submarine groundwater discharges are also likely to bring important amounts of Hg into the ocean, for which global models do not yet account. Several papers indicate that Hg inputs via submarine groundwater may be locally as important as atmospheric inputs, at least in coastal environments (Bone et al., 2007; Laurier et al., 2007; Black et al., 2009; Lee et al., 2011; Ganguli et al., 2012).

Given the importance of terrestrial soils as possibly the largest reservoir of natural and legacy anthropogenic Hg, global budget calculations will benefit from a better understanding of terrestrial Hg cycling. The lack of knowledge on the actual reservoir size that may be interacting with other parts of the biosphere has been highlighted by Schuster et al. (2018), who suggest that Arctic permafrost soils up to 300 cm deep are an unrecognized, globally significant repository of Hg. Currently, most models include only the shallow surface layer (10 cm active layer) of global soils in model parameterization and budgets. Although this permafrost Hg is mainly natural in origin, having been accumulated mostly during the early to mid-Holocene, it could represent an important potential source of Hg to the biosphere in future. There is little understanding of precisely how large and how rapidly releases from this source may develop with future climate warming, but they are expected to grow as permafrost thaws and releases its stored Hg and organic matter, both of which could lead to greater MeHg production in northern aquatic ecosystems (Stern et al., 2012). Other research priorities in this area include more measurements of the evasion rates of Hg from soils and the release rates of Hg to water following degradation of soil organic matter, as well as incorporation of the foliar uptake Hg^0 pathway into global models.

2.6.2 Uncertainties in anthropogenic emissions

The absolute amounts in historic emission inventories, and especially the role of precious metal mining, have been questioned in recent work comparing model outputs with past Hg deposition rates as reconstructed from natural archives of atmospheric deposition (see Section 2.2). Some of the uncertainty lies with the natural archives. For example, a recent paper has shown that the Hg accumulation rates in a Tibetan Plateau glacier ice core were one to two orders of magnitude lower than in a nearby lake sediment, yet both archives yielded remarkably similar trends (Kang et al., 2016). Similarly, the sediment, peat and ice core literature reviewed in Section 2.2 displays similar Hg deposition trends over time, but different absolute values, with ice cores exhibiting the lowest values of all. While the agreement in trends between archives is encouraging, the difference in absolute values begs the question of what is the most reliable quantitative estimate of past atmospheric deposition. Given the apparent importance of historic deposition to current world Hg budgets and to future emission reduction scenarios, a concerted effort to understand the reasons for the different findings from peat, lake sediment and glacial ice archives is called for that would build upon earlier work (e.g., Lamborg et al., 2002b; Biester et al., 2007; Outridge et al., 2011; Amos et al., 2015). Arriving at an agreed historic emission amount from precious metal mining would eliminate much of the uncertainty surrounding current anthropogenic Hg inventories in soils and the oceans.

The accuracy of the recent atmospheric emission inventories, including that of AMAP/UNEP (2013), has also been questioned, in part due to the inconsistency between the recent trends in primary industrial emissions, which are flat or rising, and the large (~30–40%) decreases in atmospheric GEM concentrations and wet deposition at background Northern Hemisphere monitoring stations since 1990 (see Engstrom et al., 2014; Zhang et al., 2016). Zhang et al. (2016) found that primary industrial emissions and GEM trends could be brought into closer agreement by accounting for the decline in Hg release from commercial products over this period, by reducing the atmospheric revolatilization rate of Hg from present-day ASGM, and by accounting for the shift in Hg^0/Hg^{II} speciation of emissions from coal-fired utilities after implementation of gaseous pollutant control measures. Because the emission inventories are the basis of global modelling efforts, resolving this discrepancy should improve the accuracy of global budgets and future trend scenarios. ASGM emissions were the largest single anthropogenic source of atmospheric Hg in the AMAP/UNEP (2013) report, but this finding has been disputed (Engstrom et al., 2014; Zhang et al., 2016). Verifiable and higher quality emission data from ASGM operations are therefore a priority need. Studies of the speciation and distribution of the Hg released into air, land and waters from present-day ASGM operations are also called for, given the evidence reviewed in Section 2.2 suggesting that historic emissions from Ag and Au mining were geographically restricted.

The identified uncertainties and knowledge gaps described above should not be construed as undermining the rationale for the Minamata Convention on Mercury. All models are based on field measurements and are in agreement that current levels of anthropogenic Hg emissions are likely to lead to increased environmental exposure of wildlife and humans (albeit of varying magnitude), and that reducing these emissions is essential for reducing their negative environmental and health impacts. The uncertainties and knowledge gaps mainly affect our capability to predict where and when, rather than if, the environment will respond to reduced emissions.

Note to reader

Tables S2 and C1 are still being developed/revised.

Chapter 2. Global Emissions of Mercury to the Atmosphere from anthropogenic sources

Key Findings/Messages:

Anthropogenic emissions of mercury to the atmosphere currently amount to approximately 2500 tonnes per year, accounting for about 30% of mercury emitted annually to the atmosphere, the remainder coming from environmental processes (60%) that result in re-emission of mercury previously deposited to soils and water (much of which is itself derived from earlier anthropogenic emissions and releases), and natural sources (ca. 10%).

A new global inventory of mercury emissions to air from anthropogenic sources in 2015 estimates emissions from 17 key sectors at ca. 2220 (2000 – 2820) tonnes. Additional emissions of the order of tens to hundreds of tonnes per year may arise from (generally smaller) anthropogenic sources not currently detailed in the global inventory work. Regional and sectoral attribution of the 2015 global emissions inventory indicates that emissions patterns in 2015 are very similar to those in 2010. The majority of the 2015 emissions occur in Asia (49%; primarily East and South-east Asia) followed by South America (18%) and Sub-Saharan Africa (16%). In the latter two regions, ASGM-associated emissions account for about 70-85% of the emissions. ASGM-related emissions constitute almost 38% of the global total and also account for a significant part of emissions in Central America and the Caribbean (31%) and East and South-east Asia (25%). In other regions (e.g., Europe and North America), emissions associated with energy production and industrial emissions predominate.

Stationary combustion of fossil fuels and biomass is responsible for about 24% of the estimated global emissions, with coal burning accounting for 21%. Emissions from combustion of biomass for energy production are quantified for the first time in the 2015 inventory work and comprise about 2.3% of the global inventory.

Main industrial sectors remain non-ferrous metal production (15% of the global inventory), cement production (10%) and ferrous metal production (2%). With a consumption of mercury estimated at more than 1500 tonnes in 2015, the chemicals industry is also identified as a significant emitter of mercury. The VCM and chlor-alkali chemical industries alone are estimated to be responsible for 3.3% of global emissions to air in 2015. Emissions from wastes from mercury-added products comprise ca. 7.3% of the global inventory estimate in 2015.

Inventory methodologies are constantly improved as new information and data become available.

Changes in emissions estimates for different periods therefore reflect both real-world trends and artefacts of improvements in inventory methods and data availability. Simple comparisons between the new inventory and previous inventories can result in misinterpretation and should therefore be avoided. Based on comparisons between the 2015 inventory and an updated inventory for 2010, estimated global emissions of mercury to the atmosphere in 2015 are approximately 20% higher than they were in 2010. However, different sectors contribute in different ways to this apparent overall increase.

Estimated emissions from ASGM are almost 160 tonnes higher in 2015 than in 2010 (accounting for about 45% of the overall increase); however, this increase is mainly a result of improved information rather than a real trend of increased ASGM-associated emissions over the 5 years between 2010 and 2015. Significant increases in emissions estimates for South America in particular are attributable mainly to the ASGM estimates.

If increases due to ASGM (and the VCM sector, not quantified in 2010) are discounted, the percentage increase is reduced to ca. 17% (equivalent to ca. 195 tonnes of emissions). Approximately 75% of this increase is associated with emissions from industrial sectors, 15% to stationary combustion, and 13% to (non-ASGM) intentional use sectors. Industrial emissions increased in Asia in particular, indicating that increased economic activity has more than offset any efforts to reduce emissions. In other regions, economic recovery following the financial crisis in 2008 (that may have influenced global emissions in 2010) may also have influenced observed trends in estimated emissions. Changes in fuel use and continuing action to reduce emissions resulted in modest decreases in emissions in North America and EU (ca. 11 tonnes in each region), and essentially unchanged emissions in the Australia, New Zealand and Oceania and South America regions. In all other regions, however, emissions increased by 10-20%, and 26% and 30% in South Asia and East and Southeast Asia, respectively.

Comparison between the 2015 global inventory estimates and other national and regional inventories is complicated by use of different sectoral breakdown and methods of quantification (including sources of information used, application of emission reporting thresholds, etc.). In general, however, GMA inventory estimates were in reasonable agreement with nationally compiled inventory estimates for most sectors, taking uncertainties into account. Additional comparisons with inventories compiled as part of Minamata Initial Assessments (MIAs) and National Action Plans (NAPs – specific to the ASGM sector) could, in most cases, only be made on the basis of preliminary MIAs and NAPs. The preliminary comparisons yielded a number of issues warranting follow-up when final

MIAs and NAPs are available.

Comparing emissions estimates produced using different methodologies and procedures (including both mass-balance and measurement-based estimates) provides important insights into limitations of reporting procedures, availability of key information and uncertainties associated with emissions quantification. Multiple approaches are essential for verifying emissions and release estimates and validating national reporting. Although challenging, harmonization of sector definitions between different reporting and inventory systems applied in different regions/countries, is an important consideration in relation to eventual Minamata emissions and release reporting requirements.

2.1 Sources of anthropogenic mercury emissions to the atmosphere

Previous assessments (UNEP, 2013; AMAP/UNEP, 2013) have described how industrial activities to produce energy, metals, cement and other commodities, together with a range of intentional uses of mercury in processes and products, result in anthropogenic emissions of mercury to the atmosphere. Present day anthropogenic emissions are estimated at more than 2200 tonnes per year (in 2015), accounting for about 30% of mercury emitted annually to the atmosphere; the remainder coming from environmental processes (60%) that result in re-emission of mercury previously deposited to soils and water (much of which is itself derived from earlier anthropogenic emissions and releases), and natural sources such as volcanoes (ca. 10%).

Mercury emissions to air are associated with a number of anthropogenic activities that can be broadly characterized into 'by-product' and 'intentional-use' sectors (AMAP/UNEP, 2013). Stationary combustion of fossil fuels (coal in particular), and high temperature processes involved in industrial activities such as primary metal smelting and cement production give rise to 'unintentional' mercury emissions (i.e., the mercury emissions are a 'by-product' of their presence in trace quantities in fuels and raw materials). Intentional-use sectors include use of mercury-containing products (e.g. lamps, batteries, instrumentation) and mercury use in dentistry (dental amalgam), where much of the mercury emissions to air (and releases to water) are associated with waste disposal. A further intentional use of mercury is in artisanal and small-scale gold mining (ASGM) where mercury is used to extract gold from gold-bearing sediments and rocks. Of these sources, stationary combustion of coal (for power, industry and domestic/residential heating) and artisanal gold mining were estimated to be responsible for over 60% of emissions to air in 2010 (UNEP, 2013).

Mercury emissions to air have changed over time. Historically gold and silver mining has been a major source of mercury emissions and releases. These emissions/releases have had local and regional impacts that can be traced today in sedimentary records (see Chapter 1). With the advent of the industrial revolution (ca. 1850s) and the subsequent rise of fossil fuel economies, mercury emissions increased, and are believed to have peakedaround the turn of the 20th century. Emissions have declined since then but remain high, estimated at around 2000-2500 tonnes per year during the first decades of the 21st century. These emissions give rise to global pollution; including long-range transport to remote regions (see Chapter 4), with associated concerns for impact on health of wildlife and human populations (see Chapters 7 and 8).

The GMA2013 (UNEP, 2013, AMAP/UNEP, 2013) included a first global inventory of anthropogenic mercury emissions to air for 2010 prepared according to an updated core methodology, an extension of methods employed to produce earlier global inventories for the years 1995-2005 (Pacyna et al. ref).

As part of the work to update the GMA2013, a new global inventory of anthropogenic mercury emissions to air has been produced, for the target year 2015. The 2015 inventory, presented in this report, addresses emissions from the following key emission sectors:

- Artisanal and small-scale gold mining
- Biomass burning (domestic, industrial and power plant energy production)
- Cement production (raw materials and fuel, excluding coal)
- Cremation emissions
- Chlor-alkali production (mercury process)
- Non-ferrous metal production (primary Al, Cu, Pb, Zn)
- Large-scale gold production
- Mercury production
- Oil refining
- Pig iron and steel production (primary)
- Stationary combustion of coal, gas and oil (domestic/residential, transportation)
- Stationary combustion of coal, gas and oil (industrial)
- Stationary combustion of coal, gas and oil (power plants)
- Secondary steel production
- Vinyl-chloride monomer (mercury catalyst)
- Waste (other waste)
- Waste incineration (controlled burning, including waste to energy)

These source sectors and related activities (identified in Table X1) include 3 new sectors not previously quantified, namely biomass combustion (for energy production), secondary steel production and mercury emitted during production of vinyl chloride monomer (VCM), a raw material for plastics including polymer polyvinyl chloride (PVC).

For the above-listed sectors it is possible to derive reasonably robust estimates of emissions at the regional and global scale that can also be assigned at a national level with some level of confidence.

It is important, however, to recognize that the inventory estimates reported here are not fully complete. Although the inventory includes the principle anthropogenic emission sectors, there remain sectors for which it is not yet possible to reliably quantify emissions, even at the global scale. These include sectors where information is currently inadequate to reliably quantify the scale of the activity or to define appropriate emission factors, such as agricultural burning and incineration of certain types of wastes including industrial and sewage sludge. Table S2 identifies additional sectors not yet fully quantified in global emission inventory work. Where possible, available information (e.g. national estimates for some countries) is used to provide some insight into the level of emissions that may be expected from sectors not included in the robust global inventory, but these values should be considered speculative at best.

2.2 Estimating 2015 global anthropogenic mercury emissions to air: General methodology and important considerations

2.2.1 General methodology

The methodology employed to produce the 2015 global inventory of anthropogenic emissions to air is essentially the same as that applied in developing the 2010 inventory reported in the GMA 2013 (AMAP/UNEP, 2013). The methodology applies a mass-balance approach (see Figure M1 and Annex 1) to derive emissions estimates that considers:

- the amounts of fuels and raw materials used, or commodities produced (activity data);
- the associated mercury content of fuels and raw materials and the types of process involved (reflected in 'unabated' emissions factors); and
- technology applied to reduce (abate) emissions to air (through technology profiles that reflect the degree of application and the degree of effectiveness of air pollution controls)

The ASGM and mercury-added product sectors employ a similar approach with some variations, combining activity data with emission factors and other factors that reflect distribution pathways to different environmental media and/or waste end-points (see Annexes 2-4).

Figure M1. General methodology

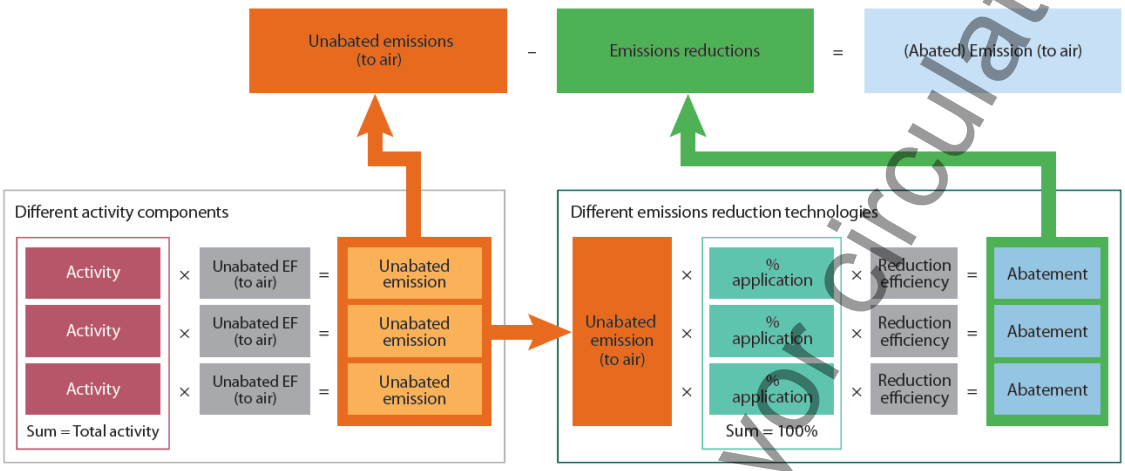

The general methodological approach and its development from earlier methods that were used to produce the original (1995, 2000 and 2005) global inventories of emissions to air is described in the GMA2013 report (AMAP/UNEP, 2013 - Section 2.2) and not repeated here. However, in order that the GMA inventory process remains transparent, the documentation in this report includes a discussion of some of the more significant changes that have been applied in the methods and/or to key parameters that influence calculated emissions estimates for particular sectors (Annex 5). Generally this reflects improvements in available information. The current report therefore also includes a comprehensive set of annexes that present the (updated) factors and assumptions applied in calculating the 2015 emissions estimates(Annex 6) and uncertainties (Annex 7), together with the activity data used (Annex 8) and the resulting emission estimates on a country/sector basis (Annex 10).

The methods employed to geospatially distribute national emissions estimates are described in REFs. In addition to improving the methods used to estimate global emissions by incorporating new information, the methodology used to geospatially distribute the global inventory has also been upgraded as part of the GMA2018 work (see Section 2.2.4).

2.2.1.1 Activity data

Information on amounts of fuel or raw materials used in different applications or amounts of products or commodities produced is one of the primary inputs for estimating emissions of mercury to air. Activity data are available from various sources, such as national statistics agencies, international organisations and industry associations. Activity data compiled in a consistent manner

for all countries that have a significant activity in a given sector are essential for the development of global inventories (and their temporal comparability). For this reason, the GMA inventory depends heavily on data compiled by the International Energy Agency (IEA) and sources such as the USGS (Minerals Yearbook). National data made available by some countries were also incorporated.

Sectors and sources of activity data used in preparing the 2015 global estimates are presented in Table X1. Sectors are grouped according to 4 main categories: Combustion of fuels; Industrial sectors; Artisanal and small-scale gold mining; and (non-ASGM) intentional use sectors. These main groups are also reflected in subsequent presentations of results. Activity data used to develop the 2015 GMA national emission estimates are presented in Annex 8.

Whenever available, statistics for the target year 2015 have been used for this emission inventory. In some cases, information for 2015 were not available at the time of preparing the inventory; therefore, data from 2014 (and in a few cases earlier) were used.

Table X1 –SECTORS / CODES FOR WHICH EMISSIONS HAVE BEEN ESTIMATED AND SOURCES OF ACTIVITY DATA USED

Sector Code	Sector description	Activity Code	Activity description	Sources of activity data.	Year of activity data
Artisanal and small-scale gold mining					
ASGM	Artisanal and small-scale gold mining	ASGM	Artisanal and small-scale gold mining	AGC, 2017; UN Environment 2017	2012+ for >80% of estimated emissions
Combustion of fuels for energy and in industry and domestic/residential uses					
BIO	Biomass burning (domestic, industrial and power plant)	PSB - DR	domestic residential burning	IEA 2017	2015
		PSB - IND	industry	IEA 2017	2015
		PSB - PP	power plants	IEA 2017	2015
SC-DR-coal	Stationary combustion of coal (domestic/residential, transportation)	BC-DR	brown coal	IEA 2017	2015
		HC-DR	hard coal	IEA 2017	2015
SC-DR-gas	Stationary combustion of gas (domestic/residential, transportation)	NG-DR	natural gas	IEA 2017	2015
SC-DR-oil	Stationary combustion of oil (domestic/residential, transportation)	CO-HF-IND	heavy fuel oil	IEA 2017	2015
		CO-IND	crude oil	IEA 2017	2015
		CO-LF-IND	light fuel oil	IEA 2017	2015

SC-IND-coal	Stationary combustion of coal (industrial)	BC-IND-CEM	brown coal (cement industry)	IEA 2017	2015
		BC-IND-NFM	brown coal (NFM industry)		2015
		BC-IND-OTH	brown coal (other industry)		2015
		BC-IND-PIP	brown coal (ferrous metal industry)		2015
		HC-IND-CEM	hard coal (cement industry)	IEA 2017	2015
		HC-IND-NFM	hard coal (NFM industry)		2015
		HC-IND-OTH	hard coal (other industry)		2015
		HC-IND-PIP	hard coal (ferrous metal industry)**		2015
SC-IND-gas	Stationary combustion of gas (industrial)	NG-IND	natural gas	IEA 2017	2015
SC-IND-oil	Stationary combustion of oil (industrial)	CO-HF-IND	heavy fuel oil	IEA 2017	2015
		CO-IND	crude oil	IEA 2017	2015
		CO-LF-IND	light fuel oil	IEA 2017	2015
SC-PP-coal	Stationary combustion of coal (power plants)	BC-L-PP	brown coal (lignite)	IEA 2017	2015
		BC-S-PP	brown coal (sub-bituminous)	IEA 2017	2015
		HC-A-PP	hard coal (anthracite)	IEA 2017	2015
		HC-B-PP	hard coal (bituminous)	IEA 2017	2015
SC-PP-gas	Stationary combustion of gas (power plants)	NG-PP	natural gas	IEA 2017	2015
SC-PP-oil	Stationary combustion of oil (power plants)	CO-HF-PP	heavy fuel oil	IEA 2017	2015
Industry sectors					
CEM	Cement production (raw materials and fuel, excluding coal)	CEM	cement (fuels excl.)	USGS 2016	2014
		PC- CEM	pet coke	IEA 2017	2015
		See also BC–IND-CEM and HC-IND-CEM			
NFMP	Non-ferrous metal production (primary Al, Cu, Pb, Zn)	AL-P	aluminium (primary production)	USGS 2017	2015
		CU-P	copper (primary production)	USGS 2017	2015
		CU-T	copper (total production)*	USGS 2017	2015
		PB-P	lead (primary production)	USGS 2017	2015
		PB-T	lead (total production)*	USGS 2017	2015

		ZN-P	zinc (primary production)	USGS 2017	2015
		ZN-T	zinc (total production)*	USGS 2017	2015
		See also BC–IND-NFM and HC-IND-NFM			
NFMP-AU	Large-scale gold production	GP-L	gold production	USGS 2017	2015
NFMP-HG	Mercury production	HG-P	mercury production	USGS 2016 UNEP 2017	2013/2014 2015
OR	Oil refining	CO-OR	oil refining	xxx	xxx
PISP	Pig iron and steel production (primary)	PIP	iron and steel (primary production)	USGS 2016	2014
SSC	Secondary steel production	SP-S	secondary steel production	Steel statistical yearbook 2015, World Steel Association 2015	2014
Intentional uses (other than ASGM)					
CREM	Cremation emissions	CREM	Cremation emissions	National reports and International Cremation Statistics	2014
CSP	Chlor-alkali production (mercury process)	CSP-C	capacity based	xxx	xxx
		CSP-P	production based	xxx	xxx
		See also BC–IND-PIP and HC-IND-PIP			
		CO-LF-PP	light fuel oil	IEA 2017	2015
		CO-PP	crude oil	IEA 2017	2015
VCM	Vinyl-chloride monomer (mercury catalyst)	VCM	Vinyl-chloride monomer	National and literature information on VCM production, mercury consumption and emissions	2015
WASOTH	Waste (other waste)	WASOTH	other waste	Estimated consumption of Hg in mercury added products in 2015 by world region (UNEP, 2017)	2015

WI	Waste incineration (controlled burning)	WI	waste incineration	Estimated consumption of Hg in mercury added products in 2015 by world region (UNEP, 2017)	2015

* PB-T, CU-T, ZN-T: total (primary+secondary) production used as activity for countries where activity data for primary production alone were not available.

** HC-IND-PIP: does not include 'non-energy coke' (see Annex METHODOLOGY UPDATE)

Lack of globally consistent activity data is one of the major obstacles to the inclusion (at the present time) of some additional sectors that are implicated in mercury emissions to the atmosphere in the global inventory. Some of these sectors are identified in Table S2.

2.2.1.2 Emission Factors and Technology Profiles

Information on (unabated and abated) emissions factors and technological profiles (reflecting degree of application and effectiveness of air pollution control (APC) technologies to reduce emissions of mercury; see AMAP/UNEP, 2013) are detailed in Annex 6. These factors are defined for individual countries where data are available. Where national data are lacking, default factors are applied to groups of countries based on assumptions regarding their level of technological development. For ASGM-associated emissions similar but more specific approach is employed (see Annex 2). The assignment of (emission and APC technology) factors for particular countries/sectors builds on work described in the GMA 2013, and utilises a considerable amount of new information that has become available since that time from published literature, in particular concerning China, as well as information acquired from national experts from more than 25 countries from all world regions during inventory workshops and meetings organized as part of the 2015 inventory compilation activity.

Revision to applied emission factors and assumptions regarding application and effectiveness of APC technologies can significantly affect derived (national-sector) emission estimates; some revisions reflect developments (e.g., in applied APC measures, or changes in sources of fuels or raw materials used nationally) since 2010; others reflect improved information on, e.g. mercury content of fuels and raw materials that would also apply in relation to revised 2010 emissions estimates. Revisions to factors applied in the 2015 inventory work are – for the most part – not yet reflected in the UNEP

Toolkits that are being used as the basis for most national Minamata Initial Assessments (MIAs), etc.; see section 2.3.3. The following section and Annex 5 discusses some of the more significant changes introduced for individual sectors.

2.2.2 Sector specific methodologies - significant changes and improvements

For the sectors: Stationary Combustion – oil burning; Stationary Combustion – gas burning; Primary production of non-ferrous metals – mercury from cinnabar ore, and; Chlor-alkali production, methods employed are essentially identical to those applied in the GMA2013 (AMAP/UNEP, 2013). Updated information on the basis for calculations applied in the 2015 inventory can be found in Annex 6.

For several other sectors, methods have been updated. Annex 5 details substantive methodological changes that have been introduced in relation to specific sectors. These changes can have implications for calculated estimates that need to be appreciated when comparing 2015 inventory estimates with previous estimates (including 2010 inventory estimates presented in GMA 2013). For a more detailed discussion of the results regarding emission estimates for selected emission source sectors see section 2.4.3.

2.2.3 Uncertainties

Estimating the uncertainties associated with mercury emissions is not a simple task: the nature of the data means that there will never be a single 'good' answer, only answers that are based on sensible approaches and can be considered 'reasonable' in relation to the context in which they are presented.

In the GMA2013 (AMAP/UNEP, 2013), a simplistic approach was applied to calculate uncertainties associated with the 2010 inventory estimates. Essentially, this involved calculating high- and low-range estimates for individual country-sector emissions based on assumptions regarding reliability of activity data and (unabated) emission factors and aggregating these to produce 'extreme' range values. Uncertainties associated with assumptions about applied technologies were ignored. It was noted that, since over- and under-estimation will to some extent cancel out in aggregated estimates, this approach would result in 'overstating' uncertainties associated with aggregated emissions estimates such as regional, sectoral or global totals. However, the method did promote awareness that inventory estimates – whatever their source or basis – have large associated uncertainties and need to be regarded in this light.

In the 2015 inventory work, a more detailed evaluation of uncertainties has been applied considering three different approaches: (i) calculating uncertainties using the approach applied in the GMA, 2013; (ii) applying a modification of this whereby uncertainties associated with technology assumptions were also introduced for most sectors, and (iii) employing the propagation of errors method (Frey, et al., 2006) to evaluate uncertainties associated with aggregated estimates. The latter method was adapted to apply a cut-off in extreme situations, e.g., so that abatement efficiency could not exceed 100%. Further assumptions were applied in relation to other factors; for example, unabated emissions factors used in range estimates were based on assumptions regarding skewed (log-normal) distribution of mercury-content of fuels and raw materials.

In the case of ASGM, the situation is somewhat different in that the main source of uncertainty in relation to emissions is considered to be associated with level of activity rather than the (unabated) emission factor. The emission factor from amalgam is effectively 100% of the mercury contained in the amalgam, and the quantity of amalgam is directly proportional to the amount of gold produced. This does not account for the use of retorts (mercury recycling); however, their use is small to negligible globally. Therefore, with respect to emissions of mercury to the atmosphere, the uncertainty in the estimate is largely equivalent to the uncertainty in the amount of gold produced. As a further consequence, if emissions to air are over-estimated, releases to land/water will be under-estimated, and vice versa.

Further details of the three approaches considered in evaluating uncertainty are described in Appendix 7. Results of the modified approach (approach (ii)) are reflected in the values for individual country-sector estimates tabulated in Annex 10 and Table C1.

The propagation of errors approach was considered to best represent the scale of the uncertainties for aggregated inventory estimates than those achieved by simply summing uncertainties for individual (country-sector) emission estimates. This is therefore the basis for uncertainty estimates associated with aggregated emission estimates presented in section 2.3, below.

At the global level, uncertainties calculated using approach (i) are -55% / +157%, using method (ii) -64% / +212%, and using method (iii) -10% / +27%.

2.2.4 Spatial distribution

The process of (geo-)spatially distributing national/sectoral emission estimates to reflect patterns of emission intensity across the globe is an essential pre-requisite to many approaches to model atmospheric transport and deposition (see Chapter AIR PATHWAYS). Methods previously applied (REF) have been updated and improved (Steenhuisen and Wilson (in prep)).

Principle new developments in the spatial distribution methodology include:

- Compilation of new information on point sources from available public domain resources (including geographical location, reported emissions where available from national inventories and PTRs (for Europe, USA, Canada, Australia)).
- Updated modelling of emissions from point sources lacking emissions estimates, using national emissions totals for the sector concerned and information on e.g. plant capacity; setting maximum values to avoid extreme values.
- Introduction of new procedures to allow national estimates to be mapped (gridded) at a finer resolution, for use in e.g. modelling work with flexibility to define different output resolutions.
- Introduction of new procedures to make it easier to incorporate and select proxy 'distribution masks' for application to different emission sectors and update proxy data for individual countries as opposed to global level only.
- Development of new distribution masks for population and urban population; a new distribution mask for ASGM using new information to better define relevant areas of countries concerned, etc. – including information for African countries from experts engaged in preparation of regional NAPs.
- Introduction of new options to allow more flexible introduction of alternative speciation schemes and emission height classification schemes for emissions from different sectors according to country groupings.
- Options to allow future applications to take advantage of improved information on individual plants (e.g. plant specific speciation schemes, emission stack heights, etc.)

Results of the spatial distribution of the GMA global inventory estimates of anthropogenic emissions to air in 2015 are presented in Section 2.5 (Figure X1); related datasets are available (xxxx) and were employed in modelling work reported in Chapter [AIR PATHWAYS]. The work undertaken to improve the spatial distribution procedures illustrates the importance of compiling better information on emissions at individual point source facilities, including the location of the facilities, associated (quantified) mercury emissions, and characteristics of the plants in relation to applied technology, fuels, and installed emission controls, etc. These data also need to be compiled in a manner that can track temporal changes in point-source emissions, to complement the development of temporally-consistent emission inventories. Facility level reporting systems are only available for a limited number of countries, and some employ thresholds for mandatory reporting that may result in under-estimation of total national emissions. Better information is also needed to improve 'proxy' data that are applied for distribution of non-point source emissions; for sectors, such as ASGM in particular,

where information on the (spatial) extent of the activity is difficult to determine from easily-accessible sources.

New information is also becoming available on speciation of emissions from point sources, in particular from China (e.g. Liu et al., 2018; Chen et al, 2013; Zhang et al., 2008; 2016) that needs to be evaluated as a basis for improving speciation schemes that are applied in connection with the spatial distribution work. Changes in APCD implemented in different countries over time influences the associated sectoral emission speciation of mercury. This is illustrated in recent work considering the impact on speciation of changes in (APC) technology at the national level (e.g. Wu et al., 2016). Speciation changes have not yet been adequately addressed in global inventories and failure to track the changes of Hg speciation can compromise assessment of air transport and deposition as well as environmental impact assessment of Hg emissions; see also discussions in Chapter AIR PATHWAYS (Section 5.2.1). Notwithstanding these observations, the results of the spatial distribution work, and basic speciation scheme applied in this work provide an important additional perspective on global emissions from anthropogenic sources, and are critical to the validity of work to investigate air transport and deposition and source-receptor relationships (see Chapter AIR PATHWAYS}.

2.3 Estimating 2015 global anthropogenic mercury emissions to air: Results

Results for the 2015 global inventory estimates are reviewed below from the perspective of regional- and sectoral-based summaries, followed by commentaries on comparisons with national inventories and air emissions on a sector by sector basis, and an evaluation of apparent trends in emissions between 2010 and 2015.

The global inventory of mercury emissions to the atmosphere in 2015 from the 17 major anthropogenic sources sectors quantitatively evaluated in this work is estimated at 2220 tonnes (range ca. 2000 – 2820 tonnes).

This global inventory total for 2015 does not include sectors that are not yet addressed discretely in the inventory work; that is, sectors that lack information required for detailed estimation at the regional level, such as 'contaminated sites' (e.g. old mines/mine tailings and decommissioned industrial facilities). Emissions to air from 'contaminated sites' in 2010 were estimated at ca. 80 tonnes in the GMA2013 work, and can be assumed to be similar in 2015. Sources not fully addressed in the quantitative inventory are discussed in Section 2.3.2 and Table S2).

Some key observations are as follows:

- The 2015 global inventory estimate of mercury emissions to air form anthropogenic sources of 2220 tonnes aligns with the GMA2013 statement that global emissions to air in the first part of the 21 century from principle anthropogenic sectors are of the order of 2000 tonnes per year.
- Uncertainties associated with the current air inventory estimate of 2220 tonnes are of the order of -10% and +30% (i.e., an approximate range of 2000-2820 tonnes).
- Estimated global mercury emissions to air from anthropogenic sources in 2015 are approximately 17% higher than the inventory for 2010, when 2010 estimates are retrospectively updated for comparable methodology and sectors not addressed in the original 2010 inventory excluded. Different sectors contribute to the increase to a different extent. High apparent increases in emissions from ASGM (almost 160 tonnes) are most likely associated primarily with improvements in the information upon which these estimates are based. The second major contributor to the increase is industrial sectors (142 tonnes) where increased economic activity in certain regions is reflected in activity data for production and use of raw materials. Changes in estimated emissions between 2010 and 2015 are discussed in more detail in sections 2.3.3 and 2.4.
- Sectors not yet addressed in the national-sector estimated inventory may contribute additional emissions to air of the order of some tens-to-hundreds of tonnes per year. These include, for example, ca. 70-95 tonnes of emissions from contaminated sites and XXX from other sectors noted in this report (see section 2.3.2 - *Anthropogenic sources not fully quantified in the inventory*).

2.3.1 Summary of results by region

The regional (sub-continental) contributions to the global inventory in 2015 are illustrated in Figure R1. The pattern of emissions is very similar to that in 2010, with the majority of the emissions occurring in Asia (49%, of which 39% in East and South-east Asia, compared with ca. 48% in 2010) followed by South America (18%) and Sub-Saharan Africa (16%) (see also Table R1). The consistency in the regional distribution of emissions between the 2010 (GMA 2013), 2010 updated and 2015 datasets discussed in this report (illustrated in Figure T2, section 2.4.2) indicates that these patterns are robust and not influenced to any undue extent by artefacts resulting from changes in methodology and additional sectors introduced since the GMA2013 work.

The relative pattern of contributions of the regions to the inventory total is heavily influenced by emissions from ASGM. ASGM-associated emissions account for about 70-75% of the emissions that occur in South America and Sub-Saharan Africa (see Figure R2, upper).

If ASGM-associated emissions are omitted (see Figure R2, lower), the East and South-east Asian region remains the region responsible for the majority of emissions (47% on the non-ASGM total), with South Asia responsible for a further 16%. The non-ferrous metals industry is the main source of emissions in Sub-Saharan Africa and the 'CIS and other European countries' region; thus these two regions, between them, contribute a further 16% of the total non-ASGM emissions. In the remaining

regions, coal combustion still accounts for the major part of the emissions in North America (almost 60%), the EU (ca. 54%) and Australia, New Zealand and Oceania (37%). In the Middle Eastern States and North Africa, the cement industry is the principle source of emissions (43% and 52% of the regional totals, respectively). Sources associated with wastes from mercury-containing products account for approximately 10-20% of emissions in most regions, somewhat higher in North Africa (27%) and lower in the EU and East and South-east Asian regions.

All percentage contributions need to be considered in relation to the total (absolute) amounts of mercury emitted in each sub-region. The sector-based emission discussion (section 2.3.3) provides additional insights into the relative amounts of emissions from different source sectors.

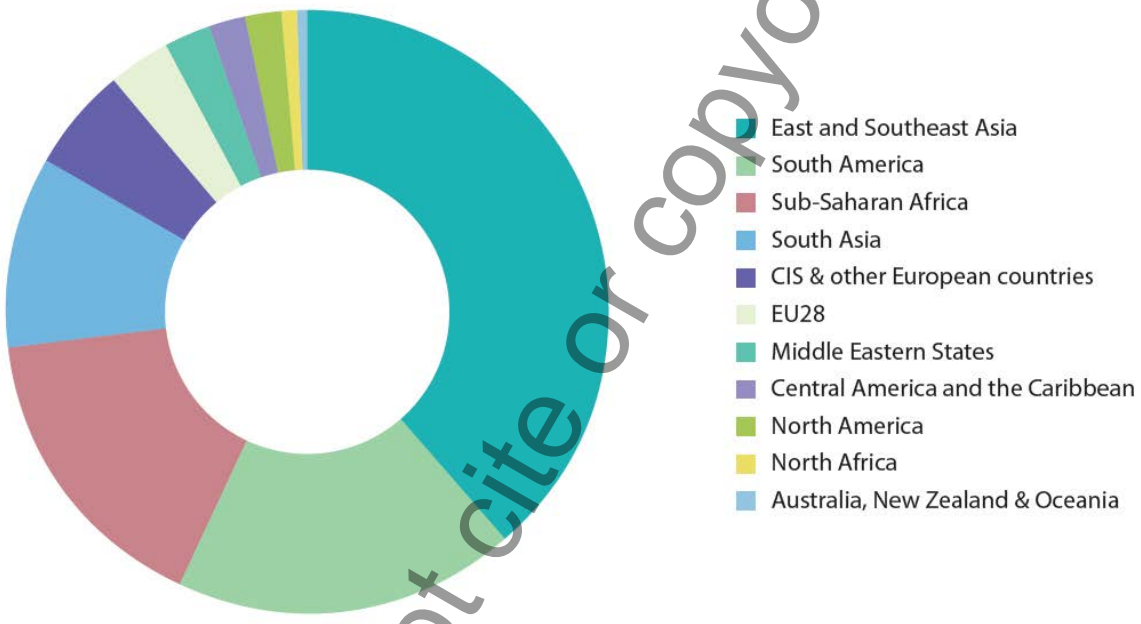

Figure R1: Regional breakdown of global emissions of mercury to air from anthropogenic sources in 2015.

Table R1: Regional breakdown of global emissions of mercury to air from anthropogenic sources in 2015, tonnes (to 3 significant figures)

	Sector group*				Regional total (and range), tonnes**	% of global total
	Fuel combustion	Industry sectors	Intentional-use (including product waste)	ASGM		
Australia, New Zealand & Oceania	3.57	4.07	1.15	0.0	8.79	0.4

					(6.93-13.7)	
Central America and the Caribbean	5.69	19.1	6.71	14.3	45.8 (37.2-61.4)	2.1
CIS & other European countries	26.4	64.7	20.7	12.7	124 (105-170)	5.6
East and Southeast Asia	229	307	109	214	859 (685-1430)	38.6
EU28	46.5	22.0	8.64	0.0	77.2 (67.2-107)	3.5
Middle Eastern States	11.4	29.0	12.1	0.225	52.8 (40.7-93.8)	2.4
North Africa	1.36	12.6	6.89	0.0	20.9 (13.5-45.8)	0.9
North America	27.0	7.63	5.77	0.0	40.4 (33.8-59.6)	1.8
South America	8.25	47.3	13.5	340	409 (308-522)	18.4
South Asia	125	59.1	37.2	4.50	225 (190-296)	10.1
Sub-Saharan Africa	48.9	41.9	17.1	252	360 (276-445)	16.2
Global inventory	533	614	239	838	2220 (2000-2820)	100.0

* See Table X1 for a definition of the sectors comprising each group

** Uncertainty ranges calculated using error propagation method (see Section 2.2.3)

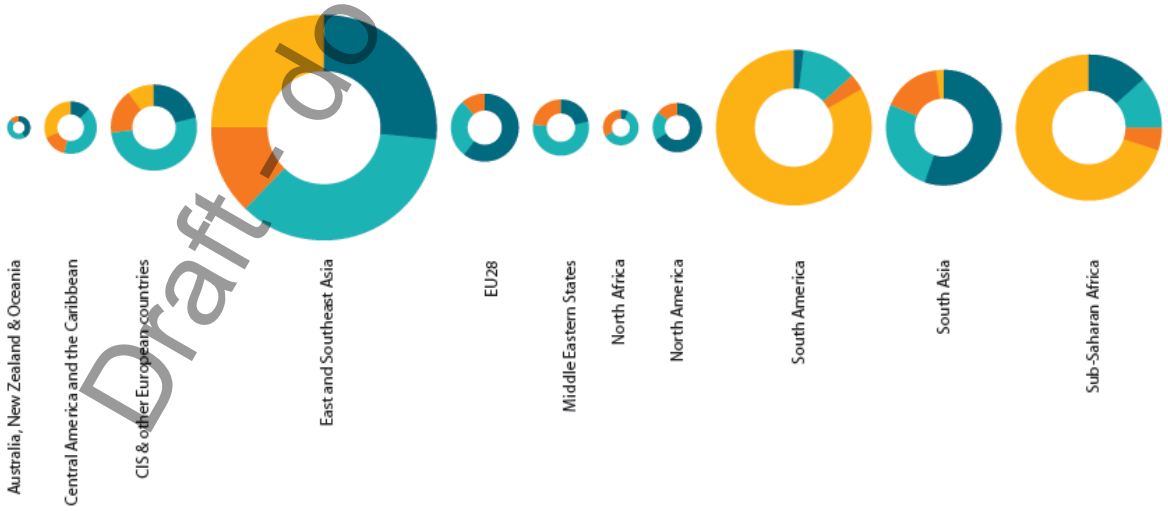

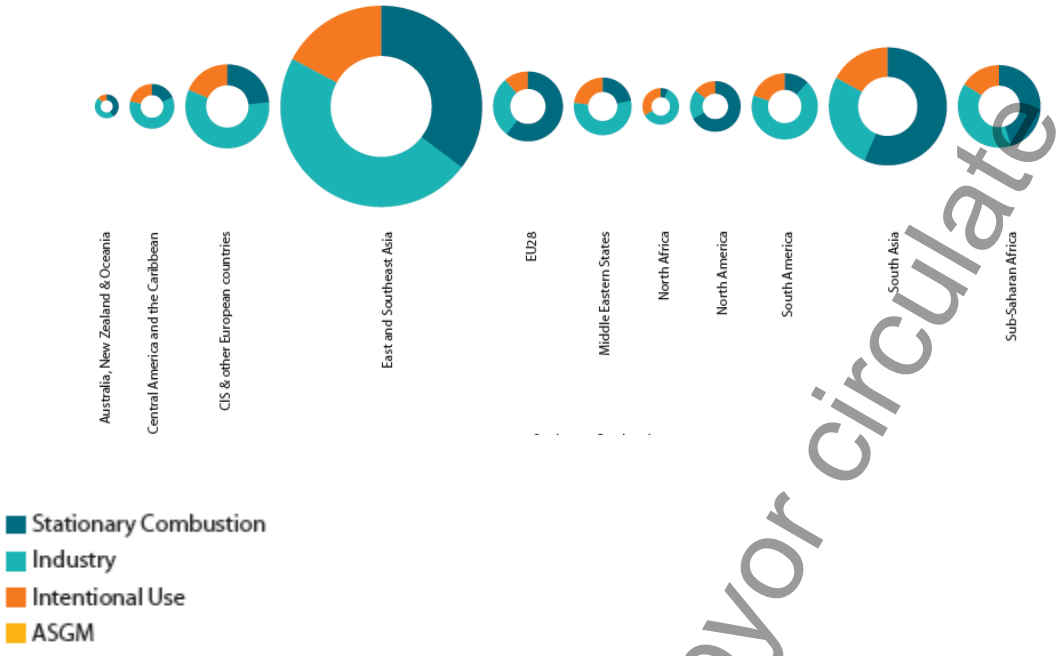

Figure R2: Contributions of main groups of sectors to total emissions in different sub-regions in 2015 (upper) including ASGM; (lower) with ASGM emissions excluded.

2.3.2 Summary of results by sector

As with the regional breakdown, the relative breakdown of anthropogenic mercury emissions in 2015 between sectors is, in most respects, very similar to that in 2010. The predominant source sector is ASGM (ca. 33.8%) followed by stationary combustion of coal (ca. 22.4%; of which 13.9%, 6% and 2.6% in, respectively, power plants, industrial uses and domestic/residential burning). These are followed by emissions from non-ferrous metal production (ca. 15.1%, of which 3.8% in large-scale gold production and 1% from production of mercury), and cement production (ca. 10.8%). Emissions associated with disposal of mercury-containing product waste (7.6%), ferrous-metal production (3.4%, of which 0.5% from secondary steel production), stationary combustion of other fuels (3%, from combustion of oil, gas and biomass – the latter a newly included component contributing 2.6%) and other (2.9%, with another newly included sector – VCM – responsible for 2.3% of this) make up the rest. See Figure S1 and Table S1.

More detailed discussions for individual sectors, also considering changes from 2010-2015 are presented in section 2.4.

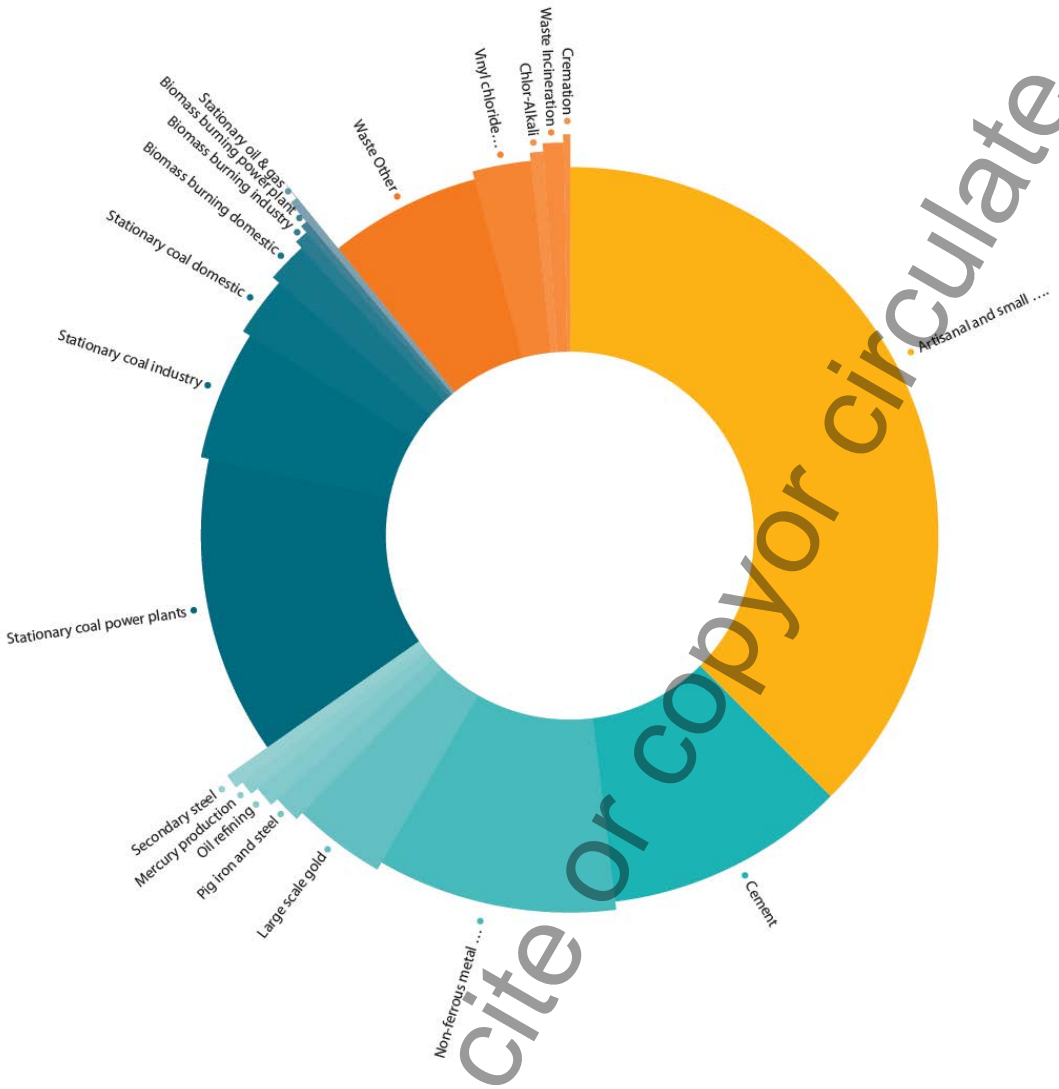

Figure S1: Proportions of global emissions of mercury to air from different anthropogenic source sectors in 2015.

Table S1: Global emissions of mercury to air from different anthropogenic source sectors in 2015, tonnes (values 3 significant figures); (colour code to reflect 4 main sector groupings, see Table X1)

Sector Code	Description	Activity Code	Description	Emission 2015*, tonnes	Sector emission (range), tonnes **	Sector % of total
ASGM	Artisanal and small-scale gold mining	ASGM	Artisanal and small-scale gold mining	838	838 (675-1000)	37.7

BIO	Biomass burning (domestic, industrial and power plant)	PSB - DR	domestic residential burning	38.3	51.9 (44.3-62.1)	2.33
		PSB - IND	industry	7.92		
		PSB - PP	power plants	5.68		
CEM	Cement production (raw materials and fuel, excluding coal)	CEM	cement (fuels excl.)	232	233 (117-782)	10.5
		PC- CEM	pet coke	1.14		
		See also BC–IND-CEM and HC-IND-CEM				
CREM	Cremation emissions	CREM	Cremation emissions	3.77	3.77 (3.51-4.02)	0.17
CSP	Chlor-alkali production (mercury process)	CSP-C	capacity based	13.5	15.1 (12.2-18.3)	0.68
		CSP-P	production based	1.61		
NFMP	Non-ferrous metal production (primary Al, Cu, Pb, Zn)	AL-P	aluminium (primary production)	6.61	228 (154-338)	10.3
		CU-P	copper (primary production)	48.4		
		CU-T	copper (total production)	0.424		
		PB-P	lead (primary production)	28.6		
		PB-T	lead (total production)	2.92		
		ZN-P	zinc (primary production)	17.5		
		ZN-T	zinc (total production)	124		
		See also BC–IND-NFM and HC-IND-NFM				
NFMP-AU	Large-scale gold production)	GP-L	gold production	84.5	84.5 (72.3-97.4)	3.8
NFMP-HG	Mercury production)	HG-P	mercury production	13.8	13.8 (7.9-19.7)	0.62
OR	Oil refining	CO-OR	oil refining	14.4	14.4 (11.5-17.2)	0.65
PISP	Pig iron and steel production (primary)	PIP	iron and steel (primary production)	29.8	29.8 (19.1-76.0)	1.34
		See also BC–IND-PIP and HC-IND-PIP				
SC-DR-coal	Stationary combustion of coal (domestic/residential, transportation)	BC-DR	brown coal	1.77	55.8 (36.7-69.4)	2.51
		HC-DR	hard coal	54.0		
SC-DR-gas	Stationary combustion of gas (domestic/residential, transportation)	NG-DR	natural gas	0.165	0.165 (0.13-0.22)	0.01

SC-DR-oil	Stationary combustion of oil (domestic/residential, transportation)	CO-DR	crude oil	0.001	2.70 (2.33-3.21)	0.12
		CO-HF-DR	heavy fuel oil	0.524		
		CO-LF-DR	light fuel oil	2.18		
SC-IND-coal	Stationary combustion of coal (industrial)	BC-IND-CEM	brown coal (cement industry)	2.15	126 (106-146)	5.67
		BC-IND-NFM	brown coal (NFM industry)	0.413		
		BC-IND-OTH	brown coal (other industry)	4.81		
		BC-IND-PIP	brown coal (ferrous metal industry)	0.151		
		HC-IND-CEM	hard coal (cement industry)	41.6		
		HC-IND-NFM	hard coal (NFM industry)	3.32		
		HC-IND-OTH	hard coal (other industry)	43.7		
		HC-IND-PIP	hard coal (ferrous metal industry)	30.1		
SC-IND-gas	Stationary combustion of gas (industrial)	NG-IND	natural gas	0.123	0.123 (0.10-0.15)	0.01
SC-IND-oil	Stationary combustion of oil (industrial)	CO-HF-IND	heavy fuel oil	1.11	1.40 (1.18-1.69)	0.06
		CO-IND	crude oil	0.085		
		CO-LF-IND	light fuel oil	0.206		
SC-PP-coal	Stationary combustion of coal (power plants)	BC-L-PP	brown coal (lignite)	59.3	292 (255-346)	13.1
		BC-S-PP	brown coal (sub-bituminous)	37.2		
		HC-A-PP	hard coal (anthracite)	3.14		
		HC-B-PP	hard coal (bituminous)	192		
SC-PP-gas	Stationary combustion of gas (power plants)	NG-PP	natural gas	0.349	0.349 (0.285-0.435)	0.02
SC-PP-oil	Stationary combustion of oil (power plants)	CO-HF-PP	heavy fuel oil	1.96	2.45 (2.17-2.84)	0.11
		CO-LF-PP	light fuel oil	0.164		
		CO-PP	crude oil	0.322		
SSC	Secondary steel production	SP-S	secondary steel production	10.1	10.1 (7.65-18.1)	0.46
VCM	Vinyl-chloride monomer (mercury catalyst)	VCM-P	Vinyl-chloride monomer production	12.3	58.2 (28.0-88.8)	2.6
		VCM-R	Vinyl-chloride monomer recycling	45.9		

WASOTH	Waste (other waste)	WASOTH	other waste	147	147 (120-223)	6.6
WI	Waste incineration (controlled burning)	WI	waste incineration	15.0	15.0 (8.9-32.3)	0.67
Total				2220	2220 (2000-2820)	100

* The indicated uncertainties are based on the propagation of errors approach; for by-product sectors, individual country-sector estimates were assigned uncertainties based on the modified GMA2013 approach (including uncertainties associated with APC technology); for ASGM and sectors concerning waste from mercury-containing products, the basic GMA2013 approach was used for country-estimates.

** Uncertainty ranges calculated using error propagation method (see Section 2.2.3)

Anthropogenic sources not fully quantified in the inventory

The robust global inventory presented above includes the source sectors that are responsible for the majority of anthropogenic emissions of mercury to air. There are, however, additional sources that cannot yet be reliably quantified at the regional and global scale. Table S2 lists a number of these sectors and summarises the state of available information and in some cases presents an indicative (often incomplete) estimates of possible emissions. These are only intended to provide an indication of the scale (order of magnitude) of emissions that may not yet be included in the quantified global inventory. Although it is not anticipated that sectors not currently included would significantly alter the total estimate of global anthropogenic emissions, they may be regionally and local important.

Table S2: Anthropogenic source sectors for which emissions cannot yet be reliably estimated.

Other potential emissions (sectors quantified only as global totals)	**Issues**	**Available information**	**Best estimate (contemporary emissions), tonnes**
Contaminated sites		Kocman et al. (ref) (quoted in 2010 GMA)	82 (70 – 95)
Agricultural burning	Agricultural burning (as well as biomass burning) are important sources, in particular in Sub-Saharan Africa and parts of Southeast Asia, and are also linked to climate change natural disasters. Lacking information on amounts incinerated and mercury content of materials burned	Emissions from China: Ca. 1 t (average for 2000-2010) from waste burning of crop residue (with an additional 2.3 t from burning of crop residue as fuel); 70% emitted as Hg^0. For comparison 2.15 t from fuelwood burning and 0.79 t from grassland and forest fires (Chen et al, 2013). Crop residue and wood burning for	1 (China)

		fuel should be covered under biomass burning for energy.	
Incineration of industrial and sewage sludge and some hazardous wastes	Lacking information on amounts incinerated and mercury content of wastes/sludge	Make an estimate and assume a Hg content? IEA data include waste separately as industrial waste, renewable MSW and non-renewable MSW IEA data (2014) includes global estimate for energy from industrial waste (801025 TJ-net); municipal waste (renewable) (658612 TJ-net); municipal waste (non-renewable) (645158 TJ-net)	To be inserted
Oil extraction (upstream of refineries)	General lack of information		No estimate available
Gas extraction (upstream of refineries)	General lack of information	NOAA/ World Bank Gas Flaring Project 2015 + UNEP Toolkit; no corresponding estimate for emissions from venting	0.15 (from flaring)
Geothermal power plant emissions		Study (Bravi and Bossi, 2014) indicating emissions of from plants in Italy in 2015; estimate based on 0.2g/MWh (a conservative estimate; Bravi, M. and R. Bossi study indicates 0.72 g/MWh); global geothermal energy production ca. 3 million TJ in 2015 (IEA)converted as ca. 833 million MWh)	1.2 (Italy) (166 tonnes global???)
Dental uses (production of amalgam, …)	Emissions associated with dental applications are not fully included in the inventory; emissions of Hg present in amalgam are included only as associated with human cremation. Emissions during the preparation of the amalgams and their subsequent removal and disposal in wastes are not included.		To be inserted
Other (including pulp and paper, secondary non-ferrous metals, food industry, chemical industry, production of bricks, ceramics, lime, coke, charcoal,		Residual totals from national PRT inventories covering primarily North America, Europe and Australia	To be inserted

fertilizers, combustion of peat, etc.)			
Informal/unorganised activities associated with a diverse range of industrial processes in developing countries (e.g. waste recycling); from small-scale to significantly large operations in some countries.			?
Speculative additional total global emissions			***10s to 100s tonnes per year***

2.3.3 Comparing GMA global inventory estimates with national inventories

The target for the 2018 GMA air emissions inventory activity remains the production of a robust global inventory for the target year of 2015, for a defined set of sectors for which reliable global estimates can be produced. Although it presents emission estimates broken down by sector for each of some 200 countries, the applied methodology is directed at global/regional rather than national level application.

All methods and approaches associated with generation of emissions estimates (whether produced by measurements or theoretical calculations) have - often large – associated uncertainties. It should therefore not be expected that estimates produced using different approaches (global vs national, etc.) will necessarily be identical. Estimates may differ for several reasons including:

- use of activity data corresponding to different years or different sources;
- differences in reporting/sector attribution;
- differences in applied EFs (amount and quality of measurement data used to derive emissions factors; high variability of mercury content in some raw materials and fuels);
- assumptions applied in deriving annual emissions estimates from measurements;
- assumptions regarding efficiency and degree of application of air pollution control equipment (and variability and uncertainty associated with APC efficiency)..

Comparison of (national-sectoral) estimates for 2015 that comprise the global inventory presented in this report (Annex 10) and national emission estimates from other sources is an important part of verification of estimates. Differences can often be explained, and even where this is not the case they can reveal methodological or data issues that need further investigation and guide future work.

A major development since the GMA2013 is that a large number of countries are engaged in preparing new national inventories or national emission/release estimates. Many of these are associated with the Minamata Initial Assessments (MIAs) or Minamata National Action Plans (NAPs).

This allows increased possibilities for comparing the global and nationally derived emissions estimates.

In relation to estimates compiled as part of the MIA process, most of the MIAs use an approach based on the UNEP Toolkit. The Toolkit was updated in 2013 to reflect new information compiled when developing the 2010 global inventory, and other updates of the Toolkit have been made in 2015 and 2017. In general, however, new refinements introduced in the work to produce the 2015 global inventory will not yet be reflected in the UNEP Toolkit.

Comparisons between GMA 2018 inventory estimates for the nominal year 2015 and national estimates are collated in Annex 9 [not yet available].

Information compiled as part of the GMA 2018 work, including information exchanged at international meetings organized as part of the inventory work identified the over 70 national inventories that may be suitable for comparison with the 2015 inventory estimates. These include:

i. Inventories prepared under the auspices of the UN ECE Convention on Long-range Transboundary Air Pollution (CLRTAP) reporting for 2015: covering 39 countries primarily in the EU and CIS and Other European countries regions, but also including Canada.

   An initial evaluation, based on total national mercury emission estimates for these countries indicated that GMA inventory estimates are generally somewhat higher than LRTAP reported emissions. For some countries (Azerbaijan, Bulgaria, Kazakhstan, Kyrgyzstan, Macedonia and Serbia) differences between GMA estimates and CLRTAP reported emissions are substantial and need further investigation. Comparing estimates for the remaining 33 countries, total estimated emissions to air were 67.5 tonnes in CLRTAP reporting vs. 86.7 tonnes in the GMA inventory. For 22 countries, national CLRTAP inventories were lower than the GMA estimates, and for 11 countries higher; GMA inventory estimates were on average ca. 36% greater than emissions reported to CLRTAP. It is possible that there are gaps in CLRTAP national mercury inventories; in recent years efforts to improve CLRTAP reporting have largely been directed at greenhouse gas emissions, while mercury and some other air pollutants have received low priority.

   Figure C1 presents comparisons between emission estimates reported to CLRTAP and GMA inventory estimates for 2015. Difficulties in precisely matching sectors defined under the CLRTAP reporting system and those applied in the GMA work are apparent. Harmonization of sector definitions between different reporting and inventory systems applied in different

regions/countries will be a challenge and an important consideration in relation to eventual Minamata emissions and release reporting requirements.

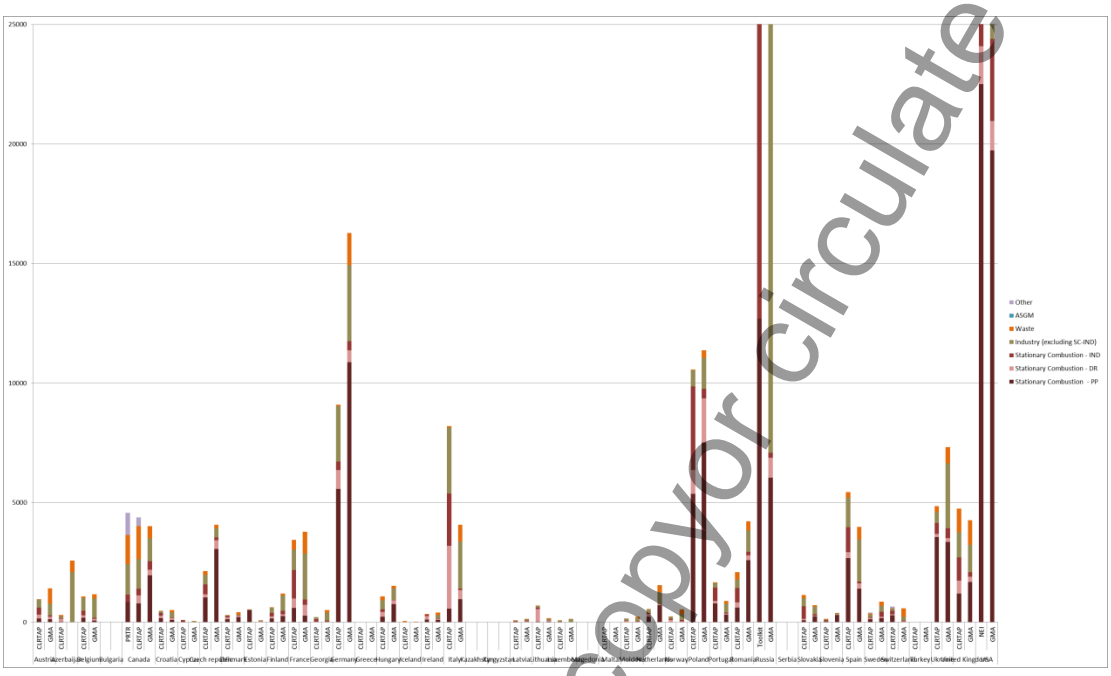

Figure C1. Comparisons of emission estimates reported to CLRTAP and GMA inventory estimates for 2015; also including national PTR estimates for Canada [delete bars for Russia and USA]

ii. Inventories currently being compiled as part of MIAs for about 30 countries from the Sub-Saharan Africa, East and South-east Asia, South Asia, South America and Central America and the Caribbean regions. At the time of preparation of the 2018 GMA, the majority of MIA inventories were preliminary, and not all were available for (provisional) comparison with GMA inventory estimates. Therefore only some provisional conclusions can be drawn based on comparisons of results from some countries, and discussions with MIA national and regional coordinators.

Comparisons between GMA inventory results and results presented in (preliminary) MIA inventories gave rise to the following general observations:

- With few exceptions, MIAs are being prepared using the UNEP Toolkit which is available in two versions: Level 1 and Level 2. The Toolkit Level 1 approach is designed to be employed for producing first rough estimates of mercury emissions and releases. The Toolkit's Level 2 is designed to represent national circumstances at a more detailed level, supported by available national data. There can be very substantial differences between emissions/release estimates for individual countries produced using the UNEP Toolkit Level 1 (REF) and Toolkit Level 2 (UNEP, 2017). For this reason, comparisons made between GMA inventory and MIA results focus on MIAs produced using Toolkit Level 2.

- In general, estimates of national emission totals agree fairly well, but there can be significant differences on the sector level. These differences may be due to methodological differences in the MIA and GMA approaches, or use of different years of (activity) data, but can also be due to errors in national data collection for the MIAs, or regarding the GMA estimates - application of default emission factors and technology profiles not sufficiently representative for the country concerned.
- The GMA inventory is based on activity data for a single year – nominally 2015. Most MIAs use this approach with a predefined base year (not always 2015), but when data from that year are not available, they use most recent available data, and sometimes the exact year of activity data concerned is not defined. Activity data is a major factor determining estimated emissions using the GMA and Toolkit approaches, and consequently lack of consistency in this respect is a possible explanation for substantial differences that can exist between GMA and MIA inventory estimates.
- Other reasons identified on the basis of preliminary comparisons that may explain differences between the GMA estimates and the MIAs are:

    - MIA estimates associated with oil and gas extraction – a component currently not included in the GMA inventory.
    - MIA estimates associated with waste categories such as industrial waste and waste waters, currently not included in the GMA inventory
    - Estimates of emissions from large scale gold mining, where the default factor in the Toolkit is 3 times higher than that applied in the GMA inventory methodology; data necessary to improve quantification of emissions from this sector are largely lacking.
    - For Cu production, the GMA approach may over-estimate the degree of application and effectiveness of abatement, at least for some African countries.
    - For cement production there are differences in assumptions applied in calculating emission estimates.
    - Some differences in ASGM/large-scale gold sector emissions estimates exist. The Toolkit default factors and methodology were revised in 2017; however many MIAs are still using earlier Toolkit versions.
    - Caution should be applied to avoid double counting in totals for inputs to waste and releases to some pathways from products in MIA results, as prescribed in the Toolkit
    - A major source of differences between GMA inventory estimates and preliminary MIA estimates can be traced to differences in estimates associated with use and disposal of waste (in particular waste burning) from mercury-added products. The methodology applied in the GMA work and the Toolkit approaches are very different. GMA emissions from waste are based on estimates of the amount of mercury in mercury-added products that are consumed in the country, while MIAs (using the UNEP Toolkit approach) calculate emissions using generic numbers for mercury-content of burned waste.
    - Discrepancies exist between estimates of amounts of mercury reported in MIAs for mercury-containing products and regional consumption estimates presented in the UNEP Trade and Supply report (UN Environment, 2017) that was used as the basis for GMA estimates. In some MIAs, problems have been identified with data collection, especially for mercury-added products, including differentiation of, for example, consumption of mercury-containing batteries and thermometers and mercury-free

batteries and thermometers. Similar difficulties exist for other products, such as paints and skin-lightening creams, where mercury-free product variants are predominant on the national market but it is difficult for countries to establish nationally if mercury is present in the products imported and/or consumed. Countries have used different assumptions in this regard, resulting in quite different results. Generally, countries have substantial data gaps for products. These problems may be exacerbated by insufficiently detailed customs statistics and lack of resources to contact producers and importers for supplementary information. Consequently, there are indications that the default factors for Hg content in general waste burnt (applied in many of the MIAs) may be too high.

iii. National inventories provided by Australia, Canada, Japan, Republic of Korea, Russia and United States. [Malaysia, Vietnam] National estimates for China from published sources.

Detailed comparisons between GMA estimates and national inventories provided by these countries are presented in Annex 9 [not yet complete]. Tables AC1-5; Table C1 below presents some example (preliminary) comparisons with GMA estimates for main sectors.

From this table it is apparent that estimates match to differing degrees for different sectors, and that this also varies between countries. However, in these example comparisons, the degree of consistency between national inventory estimates and the GMA estimates for this group of countries is generally good, and (with some exceptions) well within the bounds of associated uncertainties. As with the CLRTAP data comparisons (above), part of the differences can be explained by difference in the way emissions are assigned between sectors. This is particularly the case for some of the stationary combustion sectors and differentiation of power, industrial and domestic/residential burning sources, and whether or not fuels are included under stationary combustion or individual industrial sectors. One identified potential inconsistency is that activity data from IEA (used in GMA 2018) do not always match with nationally reported activity data; for example, for fuel consumption reported by Canada, where differences have been attributed to data set timing (monthly and annual, provisional and revised) and possible use of different factors for conversions from physical fuel units to energy units.

Some national inventories include additional emissions that are not yet quantified in the GMA inventory. Such 'other' sources include emissions from activities such as other chemical manufacturing processes; other mineral products (e.g., lime manufacturing), secondary non-ferrous metal production, oil and gas extraction, pulp and paper industry, and food industry, etc.). These emission sources are currently difficult to quantify at the global scale – largely due to lack of comprehensive activity data as well as lack of emission factors for highly variable process technologies. However, for the few (generally developed) countries

reporting emissions from ‘other’ sources the contribution is approximately 5-20% of the national inventory totals, which extrapolated globally (on non-ASGM emissions totals) could represent additional emissions of the order of 100-200 tonnes.

2000
2001

Table C1. Comparison between national inventory results and GMA 2015 (provisional) estimates (units: emissions to air in 2015, kg) [currently gma means are rounded to no decimals]

Sector	Australia***		Canada*		Japan		Republic of Korea		Russia		USA*		China(& Hong Kong)	
	national (2015)	GMA 2015	NPRI (2015) accessed 21/05/18	GMA 2015	national (2015)	GMA 2015	national (2015)	GMA 2015	national (2015)	GMA 2015	national (2014)	GMA 2015	national (2014 or 2015) **2014 emissions Wu et al, 2016b)**	GMA 2015
Stationary combustion in power plants														
- coal	2657	2878 (1210-4340)	790	1836 (897-3140)	1300	1297 (703-2100)	1167	1710 (820-3740)	10130	5782 (2500-10900)	20795	19145 (10100-37400)	73000 (Liu et al 2018)	81805 (41400-140200)
- oil	1	8 (1.36-17.3)		11 (2.03-24.4)	13	134 (25.4-295)	5**	33 (6.3-73.2)	277	171 (23.2-330)	39	37 (6.93-84.1)		89
- gas	7	4 (0.633-8.16)		11 (1.52-19.6)	2	18 (2.52-32.5)	0	4 (0.638-8.22)	1290	51 (6.83-97.4)	822	70 (9.93-128)		13
Stationary combustion in industry														
- coal	?	141 (68.9-244)	238	119 (51.9-333)	240	304 (152-519)	1433**	203 (103-343)	15700	186 (68.2-309)	1078	2257 (949-6490)		63363
- oil	?	10 (1.42-20)	48.6	17 (2.39-32.9)	2	51 (7.05-99.1)	51**	26 (3.62-51)	2	15 (2.03-29)	668	46 (6.27-88.1)		126
- gas	?	2 (0.256-3.3)	0	3 (0.471-6.08)	1	3 (0.369-4.76)	4	2 (0.246-3.17)		8 (1.12-15.9)	1150	27 (3.9-50.4)		9
Stationary combustion (domestic/ residential/other)														
- coal	?	1 (0.278-1.08)	264	3 (0.934-6.48)	0	0 (0.029-0.124)	0	0		661 (250-945)	0.8	168 (54-415)		37803
- oil	?	32 (4.55-58.6)		67 (9.50-123)	0	103 (14.6-189)	72*	49 (7.02-90.6)	229	60 (8.12-116)	1529	367 (52.3-675)		427

- gas	?	1 (0.166-2.14)		7 (1-12.9)	0	4 (0.598-7.71)	1*	3 (0.434-5.6)	25	17 (2.29-32.6)	58	47 (6.63-85.5)		13
Biomass burning	?	178 (27. 2-391)	0	485 (79.7-1050)	0	373 (66.3-843)	0**	86 (13.3-177)	81.7	145 (19.6-280)	853	2231 (368-4870)	4450 (Chen et al – see Table S2)	5119 (684-10000)
Ferrous metal production														
- primary pig iron and steel	165	5 (0.065-52.4)	630	200 (56.5-1360)	2000	2219 (1200-5320)	1337	687 (378-1090)	1910	4843 (1070-10000)	1551	513 (145-3410)	32 732 (Wu et al 2017)	8566 (2190-493000)
- secondary steel	21	24 (6.56-146)	0	117 (31.7-708)	540	599 (163-3630)	407	340 (93.5-647)	0	638 (135-3290)	4597	1288 (350-7810)		1023 (268-2490)
Non-ferrous metal production														
- primary copper/lead/zinc	611	803 (46.7-15500)	173	44 (12.4-9100)	260	1562 (67.2-47500)	16	296 (62.5-31900)	11460	12890 (2700-77000)	162	110 (19.6-15430)		126220 (25800-422000)
- primary aluminium	1635	41 (20.7-70.6)	19.8	36 (9.76-81.6)	0	0 (0.10-0.85)	0	0	133	1094 (230-2130)	362	123 (34.4-288)		3121 (869-10000)
- large-scale gold	3871	1833 (525-4230)	0	353 (2.94-1510)	0	18 (0.148-76)	0	1 (0.006-2.96)	32500	12474 (2430-27000)	521	494 (4.12-2110)		202 (4.1-1530)
- mercury production	0	0	0	0	0	0	0	0	0	0	0	0		8100 (1580-17600)
Other industry														
Cement	96	796 (211-5220)	262	128 (37.6-3070)	5500	3474 (861-8860)	2795	1258 (357-2590)	4120	2339 (877-4280)	2874	3120 (786-29500)		106283 (29300-1240000)
Oil refining	23	27 (7.75-42.9)		71 (20.3-112)	120	1138 (324-1790)	6	968 (203-1890)	226	201 (54.4-332)	338	1034 (295-1630)		2695 (728-4450)
Intentional use														
Chlor-alkali industry	0	0	8.88	0	0	0	0	0	360	3790 (796-7390)	82	183 (51.1-427)		405 (113-948)
VCM	0	0		0	0	0	0	0	124	310 (65.1-604)	0	0		57808 (12100-113000)
Waste														

- controlled incineration	0	235 (70.5-705)	673	117 (35.2-352)	1500	1210 (363-3630)	1366	570 (171-1710)	287	31 (9.29-92.9)	1640	1253 (376-3760)		8649 (2590-25900)
- other (landfill, etc.)	1	581 (174-1740)	141	307 (92.1-921)	3850	2399 (720-7200)	0	671 (201-2010)	759	9896 (2970-29700)	3249	3298 (989-9890)		19101 (5730-57300)
Cremation	29	70 (63-84)		89 (74.4-102)	69	101 (91.9-112)	5	41 (36.9-45)	335	122 (89.4-163)	1388	523 (438-600)		553 (503-614)
ASGM	0	0		0	0	0	0	0	0	5225 (1310-9140)	0	0		33750 (8440-59000)
Other	1074		1128		1351		519		8211		3245			
Total	10191	***7672 (2440-32900)***	***4377***	***4021 (1420-22070)***	***16747***	***15007 (4760-82200)***	***9186***	***6948 (2460-46400)***	***88164***	***60949 (15600-184000)***	***47004***	***36332 (15000-125000)***	***530000 Wu et al, 2016)***	***565244 (174000-2770000)***

Uncertainties for individual country-sector estimates reflect a maximum uncertainty range (see Annex xx; method 2)

*Canada also reports emissions (totalling 4387 kg) under the CLRTAP reporting system. Canada other includes: pulp and paper = 39.6; Municipal waste incineration = 673; solid waste disposal on land = 141. The United States reported their NEI 2014 v1 inventory to LRTAP; the data entered here are from the US NEI 2014 v2 inventory (updated January 2018).

**Estimated using UNEP emission factor.

Russia other: pulp and paper = 671; other NFM = 202; extraction/refining of gas = 443; combustion of peat/oil shale = 178; municipal waste incineration = 287; sewage sludge incineration = 670; medical waste incineration = 1090; mercury added consumer products = 4774

*** Australia – EPA 2015, sector attribution based on GMA author interpretation of EPA records.

**** US other: brick (34), chemical manufacturing (838), gypsum (141), lime manufacture (160), manufacture of mercury relays (38), mineral products (152), other (381), pulp and paper (164), recycling of EAF dust from steel manufacture (421), secondary metals and metal waste/non-ferrous (342), utility MACT pet coke (31), dental amalgam (419). Total 3245

Rep. Korea Other: Haz. waste (283.4) Sew sludge (32.99) Pulp-paper (177.82) On road (25.12)

Australia Other includes mining and processing of coal, iron and nfm (873), timber/pulp and paper (20), oil and gas production (28), lime production (42), chemical industry (26), brick manufacture (21), food industry (15)

2015

2016 Table C1. continued) [currently rounded to no decimals …. add uncertainty ranges to GMA]

Sector	**Malaysia (MIA version 12/5/17)**		**Vietnam (MIA version)**											
	national	GMA 2015	national	GMA 2015	national	GMA 2015	national	GMA 2015	national	GMA 2015	national	GMA 2015	national	GMA 2015
Stationary combustion in power plants														
- coal	2667	2389	4898	2652										
- oil	0	4		4										
- gas	0	6		3										
Stationary combustion in industry														
- coal	387	238		2447										
- oil	6	12		8										
- gas	3	1		0										
Stationary combustion (domestic/ residential/other)														
- coal	0	0		401										
- oil	0	20		13										
- gas	0	0		0										
Biomass burning	0	41	1168	736										
Ferrous metal production														
- primary pig iron and steel	0	0												
- secondary steel	21	101		128										
Non-ferrous metal production			561											
- primary copper/lead/zinc	0	0		249										
- primary aluminium	0	68		150										
- large-scale gold	0	128		0										
- mercury production	0	0		0										
Cement	3502	1655	5840	5770										
Oil refining	22	224		121										
Chlor-alkali industry	0													
VCM	0													
Waste														

- controlled incineration	0	49		5										
- other (landfill, etc.)	0	1694	1958	1741										
Cremation	0	5	92	61										
ASGM	0	1663	96.8	3562										
Other	1643		13230											
Total	8251	***8296***		***18053***										

***** Malaysia Other includes 1410 kg from extraction, refining and use of natural gas and mineral oils and 51 kg from incineration of hazardous waste

Vietnam other includes: natural gas extraction, refining and use = 159 kg; incineration of municipal/hazardous and medical waste = 11880; consumer products = 1236; dental amalgam product use = 12.4

2.4 Comparing 2010 and 2015 global inventory estimates

2.4.1 Cautionary Notes

Inventory methodologies are constantly improved as new information and data becomes available. With each new round of inventory development, methods are improved, both with respect to understanding of important factors/parameters and availability, and quality of essential data. This has implications for consistency over time. Changes in emissions estimates for different periods reflect both real-world trends and artefacts of improvements in inventory methods and data availability. Over-simplistic comparisons between the new inventory and previous inventories can result in misinterpretation and should therefore be avoided.

The increased focus on mercury emissions resulting from the adoption of the Minamata Convention, has also led to new research activities, national efforts and industrial focus related to mercury emissions. These efforts all contribute to providing more accurate and complete information on mercury emissions but unavoidably also introduce changes to both current and previous emission inventories.

It is inevitable that comparisons will be made between results presented in the GMA2013 (AMAP/UNEP, 2013) and the results in this update GMA – including comparing individual country-sector based estimates in the 2010 and 2015 inventories. If the implications of methodological refinements, addition of new sectors, improved quality of base information, etc. are not properly appreciated, such comparisons can result in inappropriate and misleading conclusions. It is strongly recommended that any such comparisons therefore refer to the information presented in this report only.

2.4.2 Observations on Changes from 2010 to 2015

As a first step in trying to address some of these issues and gain a reliable insight into whether apparent changes in emissions patterns between 2010 and 2015 represent real changes in emissions or are just artefacts of improved information and methodologies, an updated 2010 inventory was prepared in addition to the 2015 inventory. This updated 2010 inventory incorporated various 'improvements' including new (relevant) information on emission factors and application of APC technology, as well as updated activity data[1]. It also included a retrospective calculation of 2010 emissions for some sectors newly introduced in the 2015 inventory.

[1] In the 2010 inventory presented in the GMA 2013 much of the activity data used were preliminary, corresponding to the period for which latest-data were available (typically 2008 or 2009). The updated 2010 inventory values

Table T1 shows the estimated emissions for the main sector groups in the (updated) 2010 and 2015 inventories.

Table T1: Global emissions of mercury to air from different anthropogenic source sectors in 2015 and 2010 (updated)(to 3 significant figures)

Sector Code	Description	2010 (updated)	2015
ASGM	Artisanal and small-scale gold mining	679	838
BIO	Biomass burning (domestic, industrial and power plant)	49.5	51.9
CEM	Cement production (raw materials and fuel, excluding coal)*	187	233
CREM	Cremation emissions	4.91	3.77
CSP	Chlor-alkali production (mercury process)	21.0	15.2
NFMP	Non-ferrous metal production (primary Al, Cu, Pb, Zn)*	151	228
NFMP-AU	Large-scale gold production)	73.1	84.5
NFMP-HG	Mercury production)	12.2	13.8
OR	Oil refining	13.1	14.4
PISP	Pig iron and steel production (primary)*	26.7	29.8
SC-DR-coal	Stationary combustion of coal (domestic/residential, transportation)	54.4	55.8
SC-DR-gas	Stationary combustion of gas (domestic/residential, transportation)	0.162	0.165
SC-DR-oil	Stationary combustion of oil (domestic/residential, transportation)	2.63	2.70
SC-IND-coal	Stationary combustion of coal (industrial)	123	126
SC-IND-gas	Stationary combustion of gas (industrial)	0.115	0.123
SC-IND-oil	Stationary combustion of oil (industrial)	3.05	1.40
SC-PP-coal	Stationary combustion of coal (power plants)	268	292
SC-PP-gas	Stationary combustion of gas (power plants)	0.319	0.349
SC-PP-oil	Stationary combustion of oil (power plants)	2.58	2.44
SSC	Secondary steel production	9.69	10.1
VCM	Vinyl-chloride monomer (mercury catalyst)	**	58.3
WASOTH	Waste (other waste)***	115	147
WI	Waste incineration (controlled burning)***	15.4	15.0
Total		1810	2220

* Emissions from associated combustion of coal are accounted under SC-IND-coal

presented in this report include a number that have been revised for 'final' 2010 activity data. The 2015 inventory presented in this report is based on latest available activity data (see table X1).

** not estimated in original 2010 inventory (AMAP/UNEP, 2011) and lacking information for retrospective emissions estimates for 2010

*** In the original 2010 ca. 30% of mercury consumed in products was allocated as 'remaining in society'; in the 2015 (and revised 2010) values this amount is incorporated in the waste-stream estimates.

Figures T1 and T2 compare (in absolute and relative terms, respectively) the pattern of regional emissions in 2010 (GMA2013) with the updated-2010 inventory and the 2015 inventory. The updated estimate of total emissions to air for 2010 is very similar (at the global level) to the original global estimate for 2010 published in the GMA 2013 (AMAP/UNEP, 2013). This consistency is also apparent when considering aggregated emissions for (most) regions and sector groupings. The fact that changes in methods introduced for estimating emissions from specific sectors or country groups, the use of more representative 2010 activity data, and other 'artefacts' (including the introduction of at least one sector in 2015 not represented in the updated 2010 inventory) do not appear to have unduly influenced global or regional inventory results is considered a validation of the general approach employed for deriving global inventory estimates. At the same time, however, it should be noted that values for individual country-sector estimates have in some cases changed significantly.

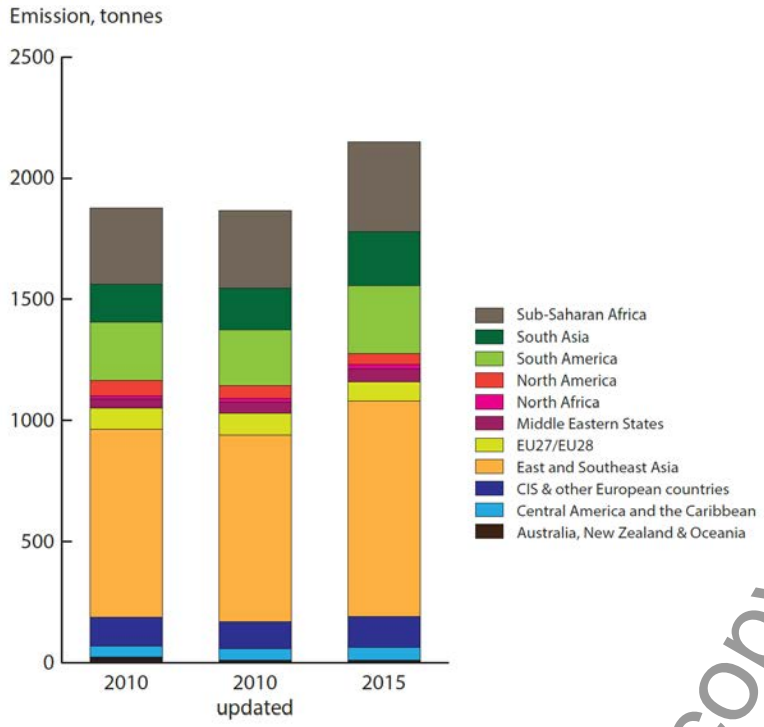

Figure T1: Regional breakdown of global emissions of mercury to air from anthropogenic sources in 2015 in relation to 2010.

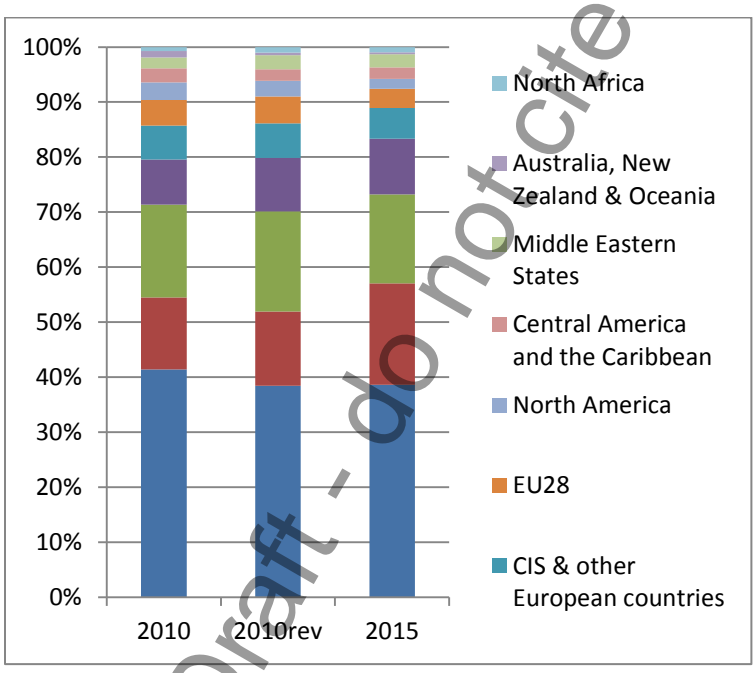

Figure T2: Proportion of global emissions of mercury to air from anthropogenic sources in different regions (results for 2015 compared with original and updated inventory for 2010).

Where possible, the discussions in section 2.4.3 (below) attempt to address the issue of whether apparent trends (between 2010 and 2015 estimates) reflect genuine changes in emissions over time or are artefacts related to improved information, etc. On the basis of this evaluation of apparent changes, the following observations are made:

GMA inventory estimates of global emissions of mercury to the atmosphere in 2015 are approximately 20% higher than they were in 2010; however, different sectors contribute to this overall increase in different ways (see Table T2).

The increase in estimated emissions from ASGM (160 tonnes more in 2015 than 2010) account for about 45% of the overall increase in inventory estimates from 2010 to 2015, with significant increases in estimated ASGM emissions for, in particular, South America. As noted above, changes in estimated emissions may be associated with both real world changes and changes in the underlying information or methods that are the basis for the estimates. In the case of ASGM, in particular, it is not a simple matter to distinguish between these two components. The judgment of those working in the area of ASGM is that the apparent increases in estimates from 2010 to 2015 are largely associated with improved information rather than a significant increase in real world emissions from ASGM in this 5-year period.

For other groups of sectors, estimates are based on more (temporally and methodologically) consistent sources of, e.g. activity data. This and knowledge of applied changes in calculation methods and assumptions makes it somewhat easier to draw general conclusions about factors that may be responsible for trends in emissions.

If increases due to ASGM (and emissions from the VCM sector, which are not quantified for 2010) are discounted, the percentage increase in the estimated global inventory from 2010 to 2015 is ca. 17% (equivalent to ca. 195 tonnes of emissions). This increase is mainly (ca. 75%) associated with emissions from industrial sectors, 15% with stationary combustion, and 13% with (non-ASGM) intentional use sectors.

Estimated mercury emissions to air decreased between 2010 and 2015 in two of the eleven world regions, namely North America and the EU region, by approximately 11 tonnes in each of these regions. Emissions over the period were relatively unchanged in Australia, New Zealand & Oceania, and (if ASGM

is discounted) in South America. In the case of North America in particular, shifts in fuel use (from coal to oil/gas) in the energy sector, combined with introduction of highly efficient APCD at major point sources appears to be a major factor in the changes observed. In both Canada and Australia closure or major changes in applied technology (including APC technology) at a few significant point sources associated with non-ferrous metal and large-scale gold production may have resulted in decreasing national emissions.

In all other regions, however, the estimated emissions to air increased, by approximately 10-20%, and 26% and 30% in South Asia and East and Southeast Asia, respectively (see Table T2).

Emissions associated with industrial sectors increased, in Asia in particular, indicating that economic growth and increased industrial activity has more than offset any efforts to reduce emissions. Cement production, ferrous (primary iron- and steel) and non-ferrous (primary Al, Cu, Pb, Zn) metal production, and large-scale gold and mercury production all had associated increases in emissions in 2015 compared with updated estimates for 2010. Estimated emissions from waste (from mercury-added products) also increased, although slightly lower from controlled waste burning. Estimated emissions from chlor-alkali production, however, decreased between 2010 and 2015. Other source sectors responsible for, at the global scale, relatively minor contributions to overall emissions were relatively similar in 2010 and 2015 (see Table T2). Estimated emissions from coal combustion in power plants in 2015 are approximately 9% higher in 2015 than 2010.

In some regions, economic recovery following the financial crisis in 2008 (that may have influenced global emissions in 2010) may also have influenced observed trends in estimated emissions.

Table T2, below, presents an overview of the scale of changes in estimated emissions in different regions for the main sectors addressed in the 2015 global emissions inventory.

Table T2: Percentage changes in emissions of mercury to air in different regions from different anthropogenic source sectors from 2010 (updated) to 2015. Colouring indicates increases (orange) and decreases (green) where changes in absolute estimates are greater than 500 kg.

Row Labe	ASGM	BIO	CEM	CREM	CSP	NFMP	NFMP-AU	NFMP-HG	OR	PISP	SC-DR-coa	SC-DR-gas	SC-DR-oil	C-IND-coa	SC-IND-gas	SC-IND-oil	SC-PP-coal	SC-PP-gas	SC-PP-oil	SSC	VCM	WASOTH	WI	Grand Tota
Australia,	New Zeal	1.6	7.4	-16.5		-1.9	1.3		-13.8	-10.4	-25.2	13.1	16.3	4.2	7.3	-38.8	-10.9	11.0	13.8	-11.2	#DIV/0!	46.2	46.2	0.2
Central A	18.4	11.0	9.3	-70.2	0.0	-22.1	100.1	1900.0	1.0	8.7		6.3	-1.0	438.6	8.5	-47.0	-19.1	6.2	-4.6	12.9	#DIV/0!	20.0	20.0	18.6
CIS & oth	5.6	14.1	27.8	40.9	-3.9	6.1	33.7	-57.3	5.8	2.4	-22.8	-7.6	-6.7	-28.7	-1.4	-26.1	-3.0	-4.8	-15.2	18.8	#DIV/0!	42.6	42.6	10.2
East and S	-12.4	-5.5	32.2	-33.2	0.0	158.0	-28.5	3.1	9.7	17.4	9.2	44.3	5.2	-5.5	33.6	-80.0	22.1	23.6	-18.5	-10.3	#DIV/0!	11.2	11.2	23.4
EU28		6.2	-14.0	-37.6	-66.2	-15.6	76.8		-3.3	2.7	-20.5	-17.9	-6.7	-8.6	-4.6	-36.8	-2.9	-31.0	-46.2	-7.2	#DIV/0!	-33.0	-33.0	-12.5
Middle Eastern Stat	-33.3	13.9	-20.5	0.0	2.9	47.8			14.2	19.3	-27.9	26.6	40.6	-19.5	16.4	1.3	4.9	26.8	1.6	36.9	#DIV/0!	51.4	51.4	14.5
North Africa	-2.7	4.8	-19.0	0.0	-53.4	316.2	-50.0	-14.2	-29.4		56.9	-0.6	-15.2	-13.9	-31.5	59.8	19.2	22.5	-4.1	#DIV/0!	66.7	66.7	15.8
North America	-1.4	23.0	-5.2	-83.3	-8.6	9.9		6.2	2.5	-51.5	1.6	-4.8	-19.0	7.8	-57.5	-23.0	27.0	-15.0	9.7	#DIV/0!	-44.7	-44.7	-21.8
South Am	91.6	6.1	19.8	-69.5	5.1	-5.0	7.9	0.0	-2.0	-8.4	69.1	10.7	5.0	11.8	-11.2	-40.8	66.5	27.5	21.4	0.8	#DIV/0!	1.5	1.5	67.6
South Asi	300.0	9.5	24.3	46.1	-74.0	12.7	-30.9		18.3	38.5	-8.8	15.9	5.0	25.4	-30.6	-13.9	38.0	-23.3	3.9	27.0	#DIV/0!	47.6	47.6	28.0
Sub-Sahar	8.6	10.1	62.0	-9.3	0.0	-32.4	11.0		-11.6	-13.6	58.5	400.0	26.5	6.9	129.0	0.0	-13.9	40.2	12.3	-12.3	#DIV/0!	164.3	164.3	9.1
Grand Tot	23.4	4.8	24.9	-23.3	-28.0	51.7	15.6	13.0	9.4	11.5	2.5	1.8	2.9	2.6	6.9	-54.1	9.0	9.4	-5.3	4.7	#DIV/0!	27.8	-2.9	22.8

2.4.3 Sector-based observations

Observations made below include comparisons between 2015 inventory estimates and updated 2010 inventory estimates.

1. Stationary Combustion – coal, oil and gas burning

Stationary combustion of fossil fuels (including biomass fuels for energy) is estimated to account for ca. 535 tonnes of mercury emitted to air in 2015, with coal-burning responsible for by far the largest amount (ca. 475 tonnes) followed by oil (7 tonnes) and gas (1 tonne). Of these emissions, about 295 tonnes are associated with burning of fossil fuels in power plants, 128 tonnes in industrial uses and the remaining 60 in other, primarily domestic and residential uses. Coal burning is therefore the second largest contributor to global mercury emissions after ASGM.

The 2015 inventory estimate (based on IEA activity data) includes 292 (255-346) tonnes from coal burning in power plants (an increase of 9% on a revised estimate for 2010) and 126 (106-146) tonnes in industry (close to the updated estimate for 2010). Mercury emissions from coal burning in other (mainly domestic and residential uses) are also relatively stable between 2010 and 2015 at around 56 (37-69) tonnes.

Considering the increase in emissions from coal burning in power plants in more detail, these are almost entirely due to increased emissions in the East and South-east Asian and South Asia regions. Increased mercury emissions of ca. 19 and 17 tonnes, respectively in these two regions, constitute a rise of ca. 21% in East and South-east Asia and 38% in South Asia. Decreasing mercury emissions from coal burning in power plants in Australia, New Zealand & Oceania (-11%), Central America and the Caribbean (-19%), CIS & other European countries (-3%), the EU region (-3%), North America (-23%) and Sub-Saharan Africa (-14%) amount to a cumulative reduction of ca. 14 tonnes of mercury emitted in these regions.

A new feature of the 2015 inventory is the differentiation of emissions from coal burning in industry between some major component activities. Of the total emissions from coal burning in industry of 126 tonnes, ca. 44 tonnes of this was associated with the cement industry; 30 tonnes with ferrous metal production (not including 'non-energy coke'); 3.7 tonnes with non-ferrous metal production; and 48 tonnes with other industrial uses. These emissions are accounted in the 2015 inventory under coal combustion but may also be taken into account as additional emissions when considering the cement, ferrous and non-ferrous metal sectors (see below).

2. Stationary Combustion – biomass burning

Biomass burning constitutes a new sector introduced in the 2015 inventory. Estimated emissions are based on IEA activity data and concern only biomass burning of primary solid biofuels for energy production (in power, industrial, and domestic/residential situation). Thus, they do not include biomass burning from, for example, agricultural burning or land clearance practises that take place in many countries.

The estimated mercury emissions from primary solid biofuel burning in 2015 are 52 tonnes (44-62 tonnes; ca. 2.3% of the global inventory). A comparable value of ca. 49 tonnes was calculated retrospectively for 2010.

The main emissions from biomass burning are associated with Sub-Saharan Africa, South Asia and East and Southeast Asia (ca. 28%, 25% and 21% of the biomass emissions total, respectively).

3. Cement production

Estimated total global mercury emissions to air from the cement sector are 233 (117-782) tonnes in 2015. However, the updated methodology allows an improved differentiation of the contribution to mercury emissions associated with fuels burned in cement-clinker production and the non-fuel raw materials. In the 2015 inventory, therefore, a part of the emissions accounted under 'industrial coal combustion' are identified with use of coal as fuel in the cement industry. If this additional 44 tonnes of emissions is accounted under cement production, the contribution of the cement sector in the global inventory rises from ca. 10.5% to ca. 12.5% making the cement sector the third largest contributor after ASGM and coal burning.

The total mercury emissions in 2015 directly associated with the cement sector (233 tonnes) is considerably higher than the ca. 187 tonnes associated with this sector in 2010 (updated), an

increase of 25%. Only in the EU region do the estimated emissions from the cement sector decrease between 2010 and 2015 (by ca. 14%); in all other regions increases are observed, of between ca. 7% in the Australia, New Zealand, Oceania region, up to 62% in Sub-Saharan Africa. These emission trends closely mirror the trends in cement production in the different regions, i.e. the primary activity data used in calculating emissions for the cement sector (see Figure S3).

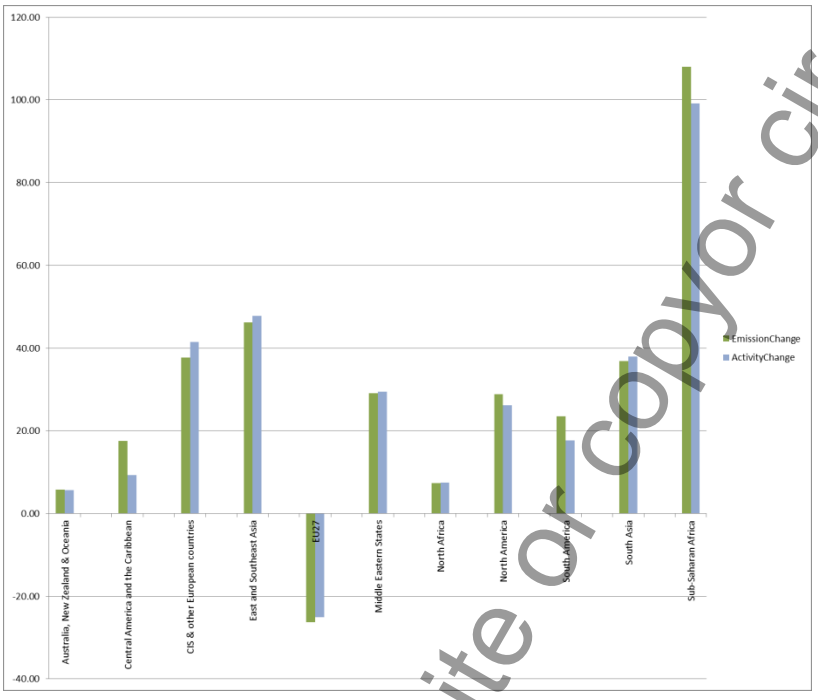

Figure S3: Relative (%) changes from 2010 to 2015 in activity data (cement production) and mercury emissions associated with cement production in different regions. [to be updated/revised]

4. Ferrous metal production (pig iron and steel and secondary steel)

Mercury emissions from primary ferrous metal (pig iron and steel) production are estimated at about 30 tonnes in 2015, with a relatively large uncertainty range (19-76 tonnes) which is somewhat higher than the updated 2010 estimate of 27 tonnes).

Of the increase in mercury emissions between 2010 (updated) and 2015, 1.8 tonnes of this amount is from increased emissions in East and Southeast Asia and 1.1 tonnes in South Asia. These two regions are responsible for, respectively 40% and 13.5% of emissions in 2015 from primary non-ferrous metal production. The other main region contributing to emissions from this sector is the CIS & other European countries region (responsible for about 22% of the sector emissions).

In the previous work (GMA2013) secondary steel production was not included but this sector has been added in the present work.

The resulting estimated emissions from secondary steel production in 2015 are 10 (7.6-18) tonnes of mercury (ca. 0.5% of the global inventory), with a (retrospectively calculated estimate of 9.7 tonnes in 2010). These totals are higher than might be expected for a process based on electric arc furnaces if relatively uncontaminated scrap metal is used and imply that significant amounts of mercury are present in the recycled scrap used in secondary steel production; assumptions applied in the calculation of the estimated emissions are presented in Annexes 5 and 6.

5. (Primary) non-ferrous metal production (Al, Cu, Pb, Zn)

Primary production of copper, lead and zinc, and aluminium, were together estimated to be responsible for some 228 tonnes of mercury emissions in 2015, significantly more than the ca. 150 tonnes in a revised estimate for 2010. It should be noted that the estimates for emissions from this sector have relatively large associated uncertainties (range 154-338 tonnes in 2015).

Aluminium production makes a modest contribution (6.6 tonnes) to the total estimated emissions for the primary NFM sector, with decreased emissions in several regions totalling ca. 0.5 tonnes offset by increases of 2.3 tonnes (approximately 85% of which occur in East and Southeast Asia).

Primary production of copper, lead and zinc make a significantly greater contribution to global mercury emissions, 222 tonnes in 2015 (from 146 tonnes in 2010). Again, increased estimated emissions in Asia (almost 85 tonnes, or 98% of the total increases), together with increased emissions in the CIS & other European countries region (1.7 tonnes) offset decreases in emissions (totalling ca. 9 tonnes) in other regions.

Secondary production of non-ferrous metals is not yet addressed as a separate activity in the global emissions inventory activity (see section 2.3.2).

ADD PLOT FOR NFM PRODUCTION REGIONAL ACTIVITY DATA TRENDS

6. (Primary) non-ferrous metal production (Hg)

Estimated mercury emissions to air associated with production of mercury increased between 2010 (12.2 tonnes) and 2015 (13.8 tonnes). With modest decreases in estimated emissions from mercury

production in the CIS and other European countries region and North Africa, the increase is almost entirely associated with emissions in Indonesia (estimated emissions of 3 tonnes in 2015 with no emissions documented for 2010) and Central America and the Caribbean region (where estimated emissions from mercury production in Mexico increased from 0.1 tonnes in 2010 to 2 tonnes in 2015). In absolute terms, China (8.1 tonnes in 2015) remains the main contributor to emissions from mercury production worldwide.

7. (Primary) non-ferrous metal production (large scale-gold production)

Mercury emissions from large-scale gold production in 2015 are estimated at ca. 84 (72-97) tonnes, 11 tonnes more than the revised 2010 estimate. In the Asian region, estimated emissions decreased by ca. 2.8 tonnes, partly explained by revisions in both activity data and emission factors to better reflect the current situation in e.g. East and South-east Asia. In other regions, in particular the CIS & other European countries region, Central America and the Caribbean, Sub-Saharan Africa and South America emissions increased, by an estimated total of 13 tonnes in these four regions in the period between 2010 and 2015.

Again, the large uncertainties associated with these emission estimates need to be borne-in-mind.

8. Oil and gas production and refining

Mercury is a trace contaminant present in varying concentrations in produced oil and gas. Mercury emissions associated with oil and gas production arise during different phases of operations. Emissions associated with the production (well-head) activities (including emissions from flaring) are currently not quantified in the global emission inventory due to lack of relevant information. Globally the quantity of mercury in produced gas is greater globally than in produced oil; however, mercury content varies greatly between regions and between gas fields depending on local geology.

A study by the US NOAA in 2015 estimated the total flared gas volume at 143 billion cubic metres (BCM) (about 3.5% of global gas production), with about 90% of the flaring occurring in upstream production areas, and 8% at refineries. Using the Toolkit estimate for mercury content of raw gas of 100 µg per m^3 this would yield a potential emission to air of ca. 0.15 tonnes of mercury per year from flaring.

Mercury is removed from oil and gas prior to its transport, in particular by pipelines, to avoid corrosion and damage to distribution systems. A significant part of the removal is done in

connection with oil refining operations. By-product mercury recovery or 'production' from non-ferrous mining operations and oil and gas processing are one of the five main sources of mercury supply with an estimated 30-100 tonnes of mercury captured from gas processing globally in 2015 (UN Environment, 2017).

GMA inventory estimates for emissions to air from oil refineries in 2010 (updated) and 2015 are 13.1 and 14.4 tonnes, respectively. In a commentary on the GMA (2010), the International Petroleum Industry Environmental Conservation Association (IPIECA) presented their view that the GMA estimates for emissions to air were significantly over-estimated; they estimate emissions to air (in 2012) at ca. 1.35 tonnes (IPIECA, 2013). Total inputs (i.e. amounts of oil refined multiplied by mercury content of the oil) associated with the refinery sector do not differ greatly between the approaches employed in the GMA and the IPIECA calculations. The main differences between the GMA and IPIECA estimates for emissions to air (and releases to water) appear to be associated with the assumptions regarding the fate of mercury at refineries. In the IPIECA approach, ca. 5% emissions to air are assumed, based on studies at US refineries (WSPA, 2009 REF in IPIECA, 2013) (with the major part of the mercury – 87% - associated with solid waste). The GMA (and UNEP Toolkit) methodology assumes higher emissions to air (ca. 25%) based on other industry reported studies (e.g., IKIMP, 2012 and references cited therein), with less of the mercury input being distributed to other media. No new information was identified that allowed this discrepancy regarding fate of mercury from oil refineries to be resolved, thus the GMA estimates of refinery emissions to air continue to differ from industry estimates by a factor of 10. Notwithstanding this degree of uncertainty, mercury emissions associated with oil and gas refining currently appear to constitute less than 1% of the total global anthropogenic emission to air.

9. Chlor-alkali production

Emissions from intentional use of mercury in the chlor-alkali industry have been decreasing for some time in most parts of the world. In part this is due to increased attention to best practices to reduce emissions, but primarily it is due to the shift from production based on the mercury-process to membrane production technology. The mercury cell process currently accounts for about 8% of the global chlorine production capacity of some 60 million tonnes, at about 75 plants worldwide (UN Environment, 2017).

GMA estimated emissions for this sector decreased from ca. 21 tonnes in 2010 to around 15 tonnes in 2015. It should also be noted that, depending on available information, emissions from some countries are based on caustic soda production statistics, and in other countries on plant production capacity.

For many parts of the world, updated activity data relevant to the 2015 inventory period are lacking; consequently, emission trends can only be described in relation to the EU, North America and South Asia regions, where emissions reportedly decreased by ca. 3 tonnes (66%), 0.9 tonnes (83%) and 1.9 tonnes (74%) between 2010 and 2015, respectively. In the case of South Asia, the reductions are largely associated with the phase-out of mercury-process chlor-alkali production in India where the last mercury-cell facility closed at the end of 2015. Within the EU, mercury-cell production is due to be phased out by the end of 2017, and as of 2015 only two mercury-cell facilities exist in the United States with scheduled to convert to membrane cell technology (UN Environment 2017).

The overall decrease in mercury emissions from the chlor-alkali industry would appear to be consistent with a reported 20% decrease in consumption of mercury in the chlor-alkali sector between 2010 and 2015; however, this is not entirely the case as the majority of the capacity that closed during that period involved the (relatively cleaner) plants in the EU and therefore it would not be expected that global emissions would have declined at the same rate as mercury consumption in this sector.

Although a relatively small component in the total global inventory, the continuing decrease in global mercury emissions from the chlor-alkali sector between 2010 and 2015 is a positive development, unrelated to changes in inventory methodology. However, with a total inventory of about 10 000 tonnes of mercury in use in the industry globally (UN Environment 2017), the fate of mercury recovered from phased-out mercury-cell production plants is a continuing concern.

10. Waste and waste incineration

Mercury emissions to air from disposal of waste from mercury-containing products are estimated at 162 tonnes in 2015; 147 (120-223 tonnes) from uncontrolled burning and landfill, and 15 (8.9-32.3) tonnes from controlled incineration.

The 2015 estimated emissions from these sectors are considerably higher than the estimate of 96 tonnes presented in the original 2010 inventory (AMAP/UNEP, 2011). This is to a large extent due to

a change in methodology where previously ca. 30% of mercury in mercury-containing products was assumed to be 'retained in society'. In the 2015 updated methodology, this amount is now accounted as part of the waste-stream and the updated 2010 emissions estimate of 130 tonnes reflects this methodological change.

Based on updated 2010 estimates, emissions from waste sectors declined in the EU and North America regions (by 33% and 45%, respectively; equivalent to 3-4 tonnes of mercury emitted in these regions). In all other regions, waste-associated mercury emissions increased, by more than 10 tonnes in South Asia and Sub-Saharan Africa, and around 3-5 tonnes in the Middle East, CIS and other European countries and East and South-east Asia. Emissions in Australia, New Zealand and Oceania and South America regions were relatively unchanged from 2010 to 2015.

Emissions from the waste sector have large associated uncertainties; quoted ranges are conservative and primarily reflect uncertainties attributed to activity data (i.e., estimates of regional consumption of mercury in mercury-added products).

In general, the estimates addressed in the global inventory do not include industrial wastes and only partially include waste that may be classified as hazardous or medical waste, some of which may also be incorporated in fuels used in, e.g. the cement industry.

Emissions associated with waste from mercury-added products is also an area where large discrepancies were identified between estimates made in the GMA inventory and those included in some national inventories produced as part of (preliminary) Minamata Initial Assessments (see section 2.3.4).

11. Crematoria emissions

Human cremation represents a relatively small but important source of emissions associated with intentional use of mercury – specifically mercury use in dental amalgam fillings. Estimated global mercury emissions to air from cremations are highly uncertain, but evaluated to be less than 5 tonnes per year (in 2015 and 2010) (ca. 0.25% of the global inventory). The proportion of regional emissions associated with cremation is slightly greater (around 1%) in the Australia, New Zealand and Oceania region and the EU and North America, likely reflecting comprehensive access to dental care that – in past decades at least – included widespread use of mercury amalgam fillings. Cultural

and religious practises associated with burial and cremation also play a role in determining whether cremation emissions are a significant part of the national air emission profile.

Cremation emissions are only part of the emissions associated with use of mercury in dental applications. The 2015 global inventory does not yet quantify emissions that can occur during preparation and routine disposal of mercury fillings. Other work has estimated emissions to air from these activities at XXX [REF]; they are also reported to contribute significantly to mercury releases to waste waters in many countries.

12. Artisanal and small-scale gold production

Intentional use of mercury in ASGM is the predominant source of mercury emissions to air at the global level in the 2015 inventory, as was also the case in 2010. There remain, however, large uncertainties associated with emission from ASGM.

ASGM activities take place in 7 of the 11 sub-regions considered in the current work. Of the estimated total global emissions from ASGM, of ca. 835 tonnes in 2015, ca. 41% is from South America, 30% from Sub-Saharan Africa and 26% from East and South-east Asia. Mercury emissions from ASGM activities in Central America and the Caribbean, the CIS region and South Asia are considerably lower (4.5 – 15 tonnes in 2015) with a very minor contribution also from Middle Eastern States.

ASGM-associated emissions are thus the predominant source of mercury emissions in some regions, accounting for more than 80% of the estimated emissions in South America, 70% of emissions in Sub-Saharan Africa, 30% of emissions in Central America and the Caribbean and about 25% of the emissions occurring in East and South-east Asia.

The estimated emissions from ASGM in 2015 (835 tonnes) are significantly higher than the value reported for 2010 in the GMA2013. A recalculation of the 2010 emissions using the improved information base on ASGM-related activities, and revised emission factor assumptions results in an estimated mercury emission from ASGM of ca. 680 tonnes in 2010. This would imply that ASGM emissions increased by ca. 23% between 2010 and 2015. There are, however, large differences in apparent trends in emissions between 2010 and 2015 in different regions. The most significant increases are for South America (mercury emissions increasing from ca. 177 in 2010 to 340 tonnes in 2015) and Sub-Saharan Africa (from ca. 230 to 250 tonnes); conversely, ASGM emissions from East

and South-east Asia declined from an estimated 245 tonnes in 2010 to 214 tonnes in 2015. In the latter region, estimates of ASGM emissions in China sharply declined (attributable to banning of mercury use in ASGM, but also uncertainty regarding the validity of high estimates for earlier years) but this was largely offset by increasing emissions in other countries in the region, Indonesia in particular. In South America and Sub-Saharan Africa the apparent trends may be influenced to a substantial extent by new information that has become available for these regions as a result of Minamata Initial Assessments and related work on NAPs for ASGM. This may also be the case for South-east Asia where, for example Myanmar has recently been identified as having significant ASGM emissions according to preliminary information from its MIA and NAP work. Consequently, the apparent increase in emissions from ASGM between 2010 and 2015 is considered to be more a reflection of improved information used in developing 2015 estimates than a 25% change in actual ASGM and stationary combustion of fossil fuels (primarily coal) are responsible for over 60% of the total estimated global emissions in 2015 (38% and 24%, respectively).

2.5 Conclusions (emissions to air)

Quantified descriptions of regional emission patterns and sector contributions to global emissions, as well as trends in emissions from 2010 to 2015 are presented in 'Key findings' at the start of this chapter and detailed in previous sections. To avoid repetition, findings and numerical results are only summarised briefly in the conclusions, or referred to within the context of a more general discussion of the air emissions inventory results.

The GMA2018 inventory of global emissions of mercury to air from anthropogenic sources in 2015 is the second inventory produced using the consistent and transparent 'GMA methodology' originally documented in the GMA 2013 (AMAP/UNEP, 2013).

The inventory produces an estimate of total emissions to air in 2015 of 2220 (2000-2820) tonnes and is presented in terms of regional and sectoral summaries (Section 2.3), as well as national-sector based estimates for some 17 key emission sectors (Annex 10). Regional emissions patterns and sector contributions were generally similar to those in 2010 reported in the 2013 GMA (AMAP/UNEP, 2013). Approximately 50% of estimated emissions to air occur in Asia, in particular the East and Southeast Asia region, followed by South America and Sub-Saharan Africa, with ASGM emissions dominating in the

latter two regions. ASGM activities and stationary combustion of fossil fuels (primarily coal burning) account for more than 60% of the estimated global emissions from anthropogenic sources in 2015, (38% and 24%, respectively) with the major industrial sectors (non-ferrous metals, cement and ferrous metals) responsible for a further 27%. Emissions from mercury-added product waste and intentional-use in the chemical industry contribute a further 7.3 and 3.3 %, respectively. Additional sectors for which it is not yet possible to prepare reliable global emission estimates are identified; the current evaluation, however, is that potential emissions from these sources are not expected to substantially increase the global emissions total or alter conclusions regarding, for example, regional emission patterns; they may however be of local or national significance in certain countries.

Geospatial distribution of the resulting inventory yields the pattern of mercury emissions shown in Figure CONC1. The distribution illustrates the concentration of emissions sources in Asia (in particular East and South-east Asia) associated with energy production and industry, and in some countries ASGM. It also shows the significant contribution to emissions in South America, Sub-Saharan Africa and Central America and the Caribbean associated with ASGM activities. In the industrialized population centres of Europe and North America, emissions associated with energy production and industrial sources predominate. Increased use of information on point-sources in the geospatial distribution procedure has resulted in more precise location of emissions – reflected by individual grid cells with high emission rates coincident with power plants and industrial facilities such as cement plants and non-ferrous metal smelters. The lower emission rates observed over wider areas are associated in some countries with activities such as ASGM (that are generally difficult to locate to specific areas at present), and in particular mercury emissions arising from disposal of waste from societal use of mercury-added products. Emissions from waste are assumed to be greatest in areas of high population and/or countries where consumption of mercury-added products is greatest.

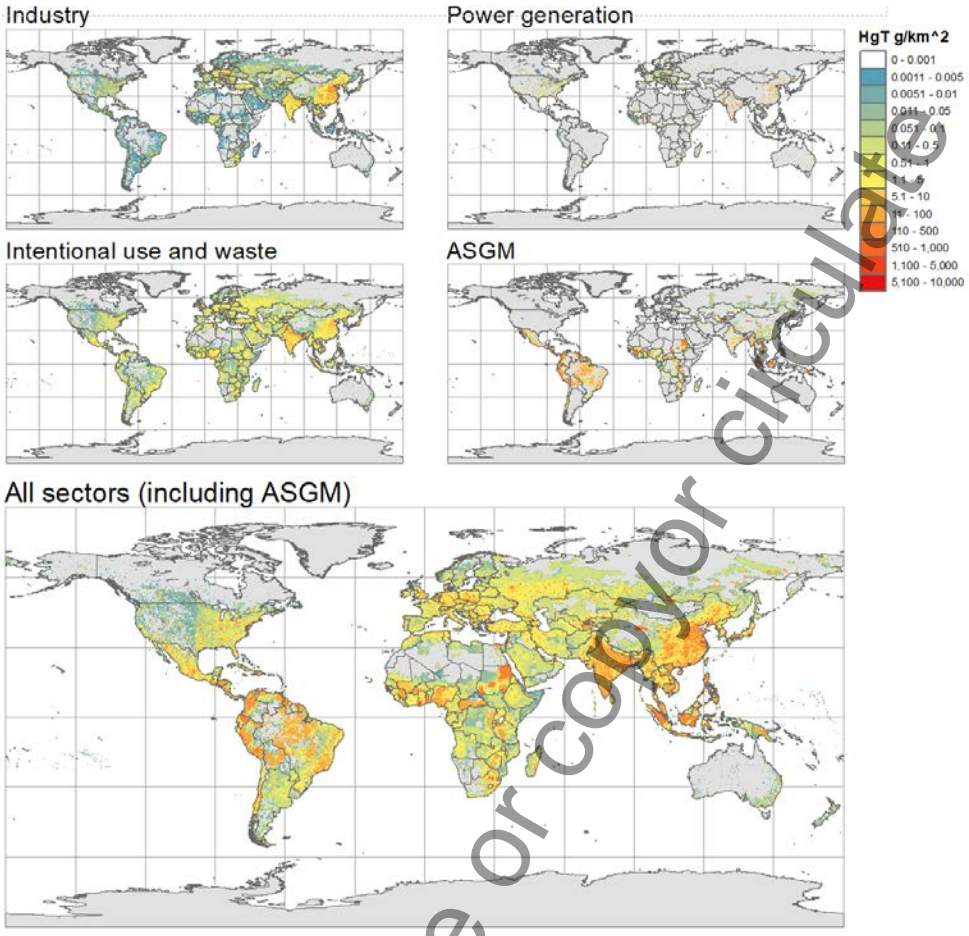

Figure CONC1 – Geospatially distributed (total) mercury emissions to air from anthropogenic sources in 2015.

The *Global mercury supply, trade and demand* report (UN-Environment, 2017) summarises the regional consumption of mercury in a range of applications (Table CONC1) including consumption in mercury-added products that are the source of much of the mercury emitted to air following waste disposal, as well as ASGM and chemical industry uses.

Table CONC1. Mercury consumption by region and application in 2015 (UN-Environment, 2017)

	ASGM	*VCM production*	*Chlor-alkali production*	*Batteries*	*Dental applicaitons*	*Measuring and control devices*	*Lamps*	*Electrical and electronic devices*	*Hg compounds and other applications*	*Regional totals*
East and Southeast Asia	645	1215	8	95	52	208	69	52	62	2407
South Asia	4	5	27	33	72	39	12	12	59	263
European Union (28 countries)	0	0	85	8	56	3	13	1	84	249
CIS and other European countries	24	6	45	13	19	12	7	7	37	171
Middle Eastern States	0	0	38	13	13	18	7	9	9	107
North Africa	0	0	11	8	4	6	4	2	5	41
Sub-Saharan Africa	366	0	1	24	7	11	5	19	15	447
North America	0	0	8	9	32	2	8	19	61	137
Central America and the Caribbean	16	0	19	9	6	9	4	6	8	78
South America	680	0	35	18	12	20	9	8	13	794
Australia, New Zealand and Oceania	0	0	0	1	3	1	3	13	1	22
Total per	1735	1226	277	231	274	330	142	147	354	4715

applicati on										

** 'consumption' is defined in terms of the end-use of mercury-added products (i.e. place of consumption), as opposed to regional 'demand' for mercury; tabulated values are means of wider ranges of estimates representing various levels of uncertainty (see source report); 'mercury compounds and other applications' include uses of mercury in cosmetics, pesticides, fungicides, catalysts, chemical intermediates, porosimeters, pycnometers, pharmaceuticals, traditional medicine, cultural and ritual uses, etc.*

Improvement in available information is identified as a reason for the increase in estimates of emissions from ASGM in 2015 relative to those in 2010. This is consistent with data indicating that consumption of mercury in ASGM was relatively stable between 2010 (range 912-2305 tonnes) and 2015 (range 872-2598 tonnes); this followed a large increase between 2005 (range 650-1000) and 2010 (UN Environment, 2017).

Estimated emissions to air from sources other than ASGM increased by ca. 17% (ca. 195 tonnes) from 2010 to 2015, the majority of this increase being associated with industrial sources. In the chemicals industry, a decrease in consumption of mercury in the chlor-alkali industry (by ca. 75 tonnes between 2010 and 2015; UN Environment, 2017) is reflected in decreasing emissions, from an estimated 21 tonnes in 2010 to 15 tonnes in 2015. However, over the same period, consumption in VCM production increased by around 280 tonnes, with emissions from this sector in 2015 estimated at ca. 60 tonnes. The majority of the VCM production is in China.

In industrial sectors where mercury emissions are a 'by-product' of presence of mercury in fuels and raw materials, the regional trends in emissions observed between 2010 and 2015 are determined largely by trends in 'activity' data. In the case of the cement industry for example, estimated emissions increased in all regions except for the EU28, the only region where cement production also declined between 2010 and 2015 (Figure CONC2). Steel production on the other hand declined between 2010 and 2015 in 6 of the 9 regions considered, but increased significantly in East and Southeast Asia, South Asia and the Middle East (by ca. 20%, 30% and 47%, respectively). Production volumes in the Middle East are far lower than in the Asian regions. Estimated emissions from pig iron and steel manufacture

correspondingly increased (by 17%, 38% and 19%) in these three regions, and 11% globally, and decreased (or were relatively unchanged) in 6 regions. At present, therefore, indications are that mitigation of emissions by implementing control technology is unable to offset increases due to increased activity in several industrial sectors in several regions; decreasing emissions are therefore primarily associated with decreasing activity or changes in fuel mix (reduced use of coal) in the energy sector.

Trends in activity data for coal consumption (source: … see note)

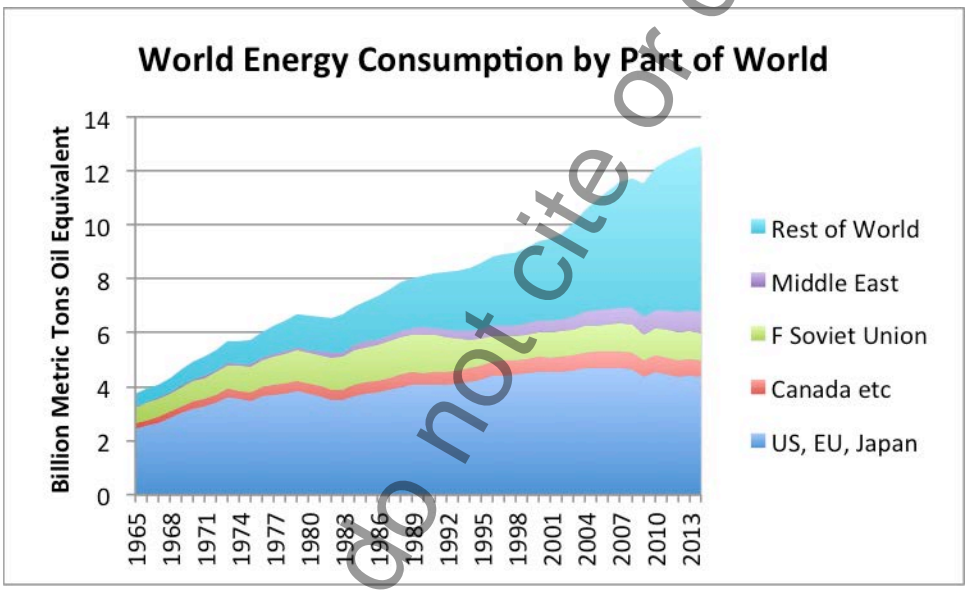

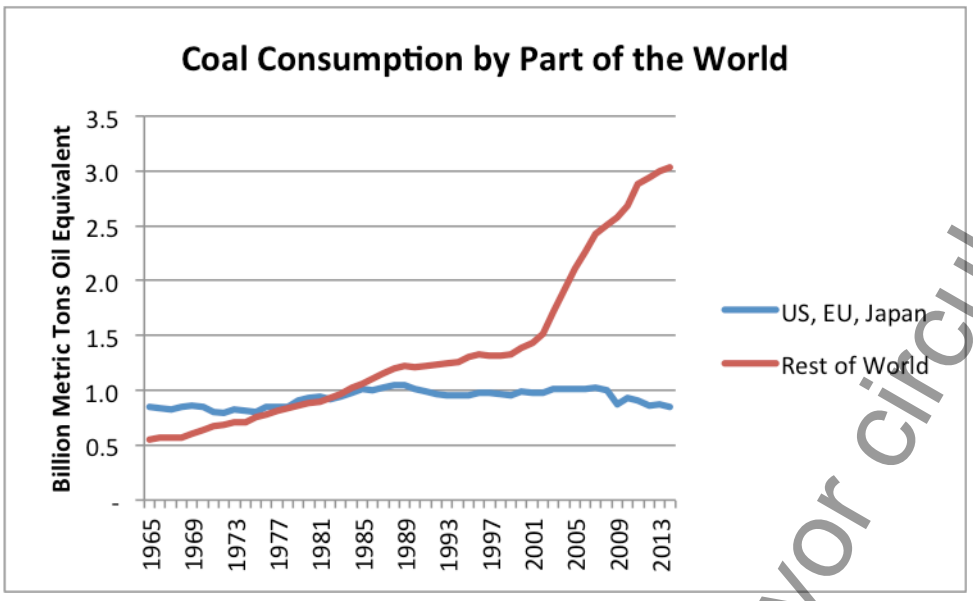

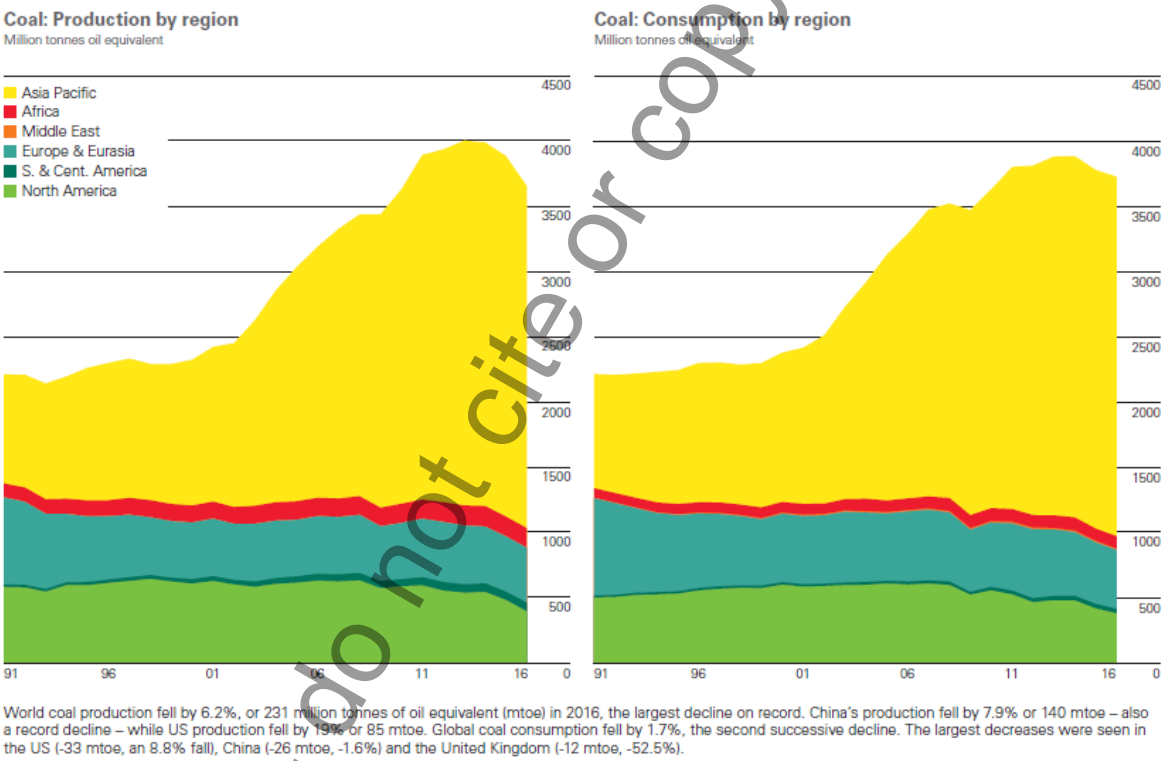

World coal production fell by 6.2%, or 231 million tonnes of oil equivalent (mtoe) in 2016, the largest decline on record. China's production fell by 7.9% or 140 mtoe – also a record decline – while US production fell by 19% or 85 mtoe. Global coal consumption fell by 1.7%, the second successive decline. The largest decreases were seen in the US (-33 mtoe, an 8.8% fall), China (-26 mtoe, -1.6%) and the United Kingdom (-12 mtoe, -52.5%).

Trends in activity data for steel production (source: World Steel Association, Steel statistical yearbook 2016)

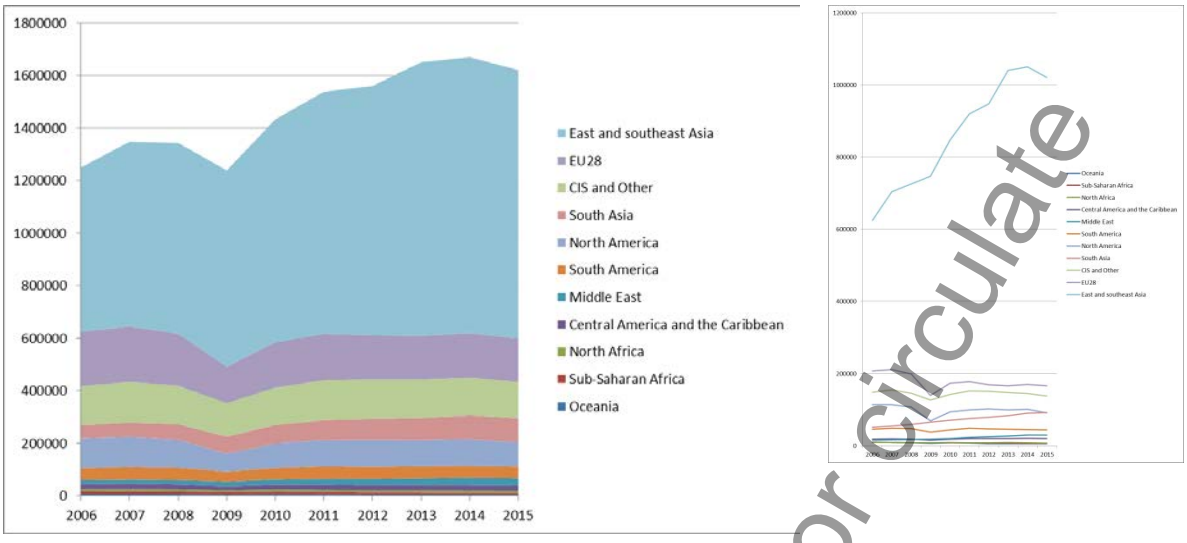

Trends in activity data for cement production (source: USGS, 2016)

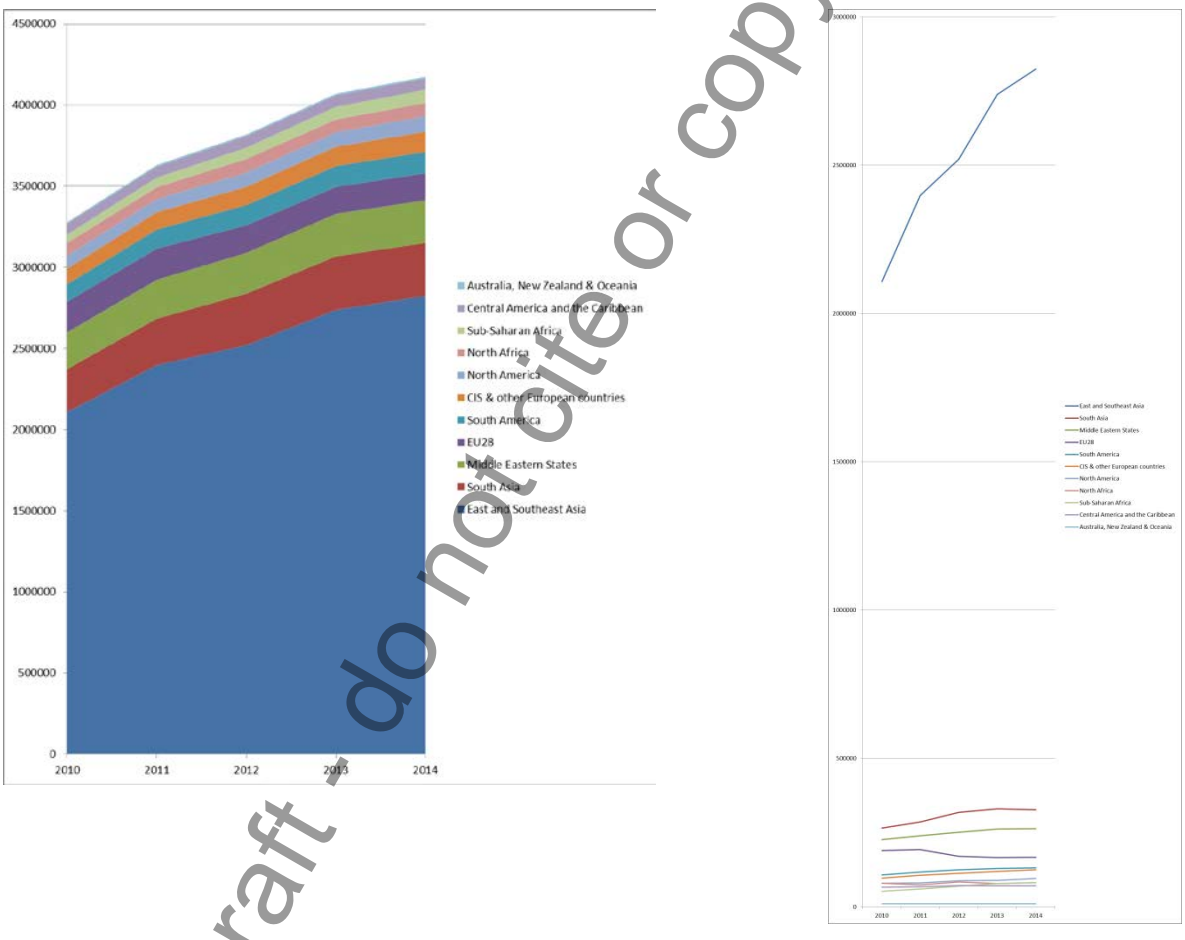

Figure CONC2, Trends in activity data for steel and cement production in different regions.

Estimated emissions from disposal of (mercury-added product) waste increased substantially (in percentage terms) in all regions – up to 165% in Sub-Saharan Africa and 28% globally - apart from the EU28 and North America, where emissions declined by 33% and 45%, respectively. Global consumption of mercury in mercury-added products (batteries in particular) declined or was relatively stable between 2010 and 2015 (Table CONC2); however, regional patterns appear to be changing as a result of increased use and disposal of these products in some regions, and decreased use combined with more efficient recycling in other regions.

Table CONC2. Mercury consumption in mercury-added products 2005-2015 (based on UN-Environment, 2017)

Sector mercury consumption (tonnes)	*2005*	*2010*	*2015*
Batteries	300 - 600	230 - 350	159 - 304
Dental applications	240 - 300	270 - 341	226 - 322
Measuring and control devices	150 - 350	219 - 280	267 - 392
Lamps	100 - 150	105 - 135	112 - 173
Electrical and electronic devices	150 - 350	140 - 170	109 - 185
Other (paints, laboratory, pharmaceutical, cultural/traditional uses, etc.)	30 - 60	222 - 389	215 - 492

** see source report for definitions of 'consumption'*

Possibilities to compare emissions (in 2015) estimated as part of the GMA2018 work are limited. No other global inventory produced using a consistent methodology is available; therefore, comparisons can only be made with estimates compiled at the regional or national level.

Comparisons between GMA inventory estimates and those prepared under other initiatives (including pollutant release and transfer inventories compiled by some countries) are not simple. In part this is due to differences in the categories covered, but the major obstacle remains differences in how emissions are characterised and reported under different activity or sector categories. Additional factors that need to be taken into account include reporting thresholds (i.e., the emissions level or alternative criteria

above which (facility level) reporting becomes mandatory). Also, whether measurements-based estimates derived to document that, e.g., air concentrations are below some regulatory limit, are appropriate for the purpose of establishing (annual) emissions estimates. Notwithstanding these issues, in many cases GMA and nationally-reported emissions estimates agree reasonably well (if uncertatinties are taken into consideration), especially in terms of national totals. Where differences exist, these can often be explained and attributed to factors mentioned above, and in particular differences in source categorisation.

Reporting systems currently in use are often adapted from systems not originally developed for reporting mercury emissions, and therefore may not be ideally suited for this purpose; the LRTAP reporting mechanism is an example. Emissions estimates compiled using the UN-Toolkit (employed in compiling the majority of MIAs), should be generally compatible with the GMA approach. Preliminary comparisons with MIAs, however, indicate that there are areas of inconsistency, especially where the Toolkit Level 1 has been employed or where countries have (uncritically) adopted default factors or employed inappropriate activity data (typically to fill gaps where appropriate data are simply not available). In all such comparisons, it is important to remember that there is no 'correct estimate' (all are based on some underlying and often very uncertain assumptions). For regulatory reasons, 'official' emissions estimates often lack any quantification of uncertainty, but this does not mean that the values are assured. The value of comparing emissions estimates from different sources, especially if derived using different methods, lies primarily in the possibilities that this gives for implying confidence in estimates or identifying areas where knowledge gaps exist. Streamlining and improvement of emissions estimation and reporting systems, including attention to underlying data used to calculate estimates, remains an important objective for future work. Efforts to harmonization reporting and inventory estimate systems will improve the ability to confidently measure the success of the Minamata Convention.

2.6 References

AGC, 2017 - Artisanal Gold Council, Kevin Telmer & Jennifer O' Neill (Artisanal Gold Council) pers. comm. (http://www.artisanalgold.org/)

AMAP/UNEP, 2013. Technical Background Report for the Global Mercury Assessment 2013. Arctic Monitoring and Assessment Programme, Oslo, Norway/UNEP Chemicals Branch, Geneva, Switzerland. vi + 263 pp

Artisanal Gold Council (AGC), 2016. Reducing the Use and Release of Mercury by Artisanal and Small-Scale Gold Miners in Nicaragua: Review of the Nicaragua ASGM sector.

BAT/BEP, 2017 – Guidance on best available techniques and best environmental practices (BAT/BEP) developed under the Minamata Convention, draft; status of February 2017 [cement, NFM, iron and steel methodology]
Boliden 2015 – Environmental report 2015 of the Boliden facility in Skelleftehamn, Sweden [cement, NFM, iron and steel methodology]
Bravi, M. and R. Basosi, 2014. Environmental impact of electricity from selected geothermal power plants in Italy. Journal of Cleaner Production 66 (2014) 301-308.
BREF CEM 2013 – Remus, R., Aguado Monsonet, M., Roudier, S., Delgado Sancho, L., 2013, Best Available Techniques (BAT) Reference Document for Iron and Steel Production [cement, NFM, iron and steel methodology]
BREF IS 2013 – Schorcht, F., Kourti, I., Scalet, B.M., Roudier, S., Delgado Sancho, L., 2013, Best Available Techniques (BAT) Reference Document for the Production of Cement, Lime and Magnesium Oxide [cement, NFM, iron and steel methodology]
BREF NFM 2014 – Joint Research Centre, 2014, Best Available Techniques (BAT) Reference Document for the Non-Ferrous Metal Industries, Final Draft (October 2014) [cement, NFM, iron and steel methodology]
Cementa 2015 – Environmental reports 2015 of the Cementa facilities in Slite, Dagerhamn, and Skövde, Sweden [cement, NFM, iron and steel methodology]
Chakraborty, 2013 – Chakraborty, L., Qureshi, A., Vadenbo, C. Hellweg, S., 2013, Anthropogenic Mercury Flows in India and Impacts of Emission Controls, Environmental Science and Technology, 47 (2013), 8105-8113 dx.doi.org/10.1021/es401006k [cement, NFM, iron and steel methodology] [VCM methodology]
Chen, L., L. Ming Liu, F. Ruifang Fan, S. Ma, X. Zhencheng, R. Mingzhong and H. Qiusheng, 2013. Mercury speciation and emission from municipal solid waste incinerators in the Pearl River Delta, South China. Science of the Total Environment 447 (2013) 396–402
Cordy, P., M.M. Veiga, I. Salih, S. Al-Saadi, S. Console, O. Garcia, M. Roeser, 2011. Mercury contamination from artisanal gold mining in Antioquia, Colombia: The world's highest per capita mercury pollution. Science of the Total Environment, 410-411, 154–60.
CSGB, 2017. Cremation Society of Great Britain – Cremation Statistics (2014). http://www.srgw.info/CremSoc4/Stats/
EMEP/EEA 2016 – EMEP/EEA air pollutant emission inventory guidebook – 2016 [cement, NFM, iron and steel methodology]
Frey, C., Penman, J., Hanle, L., Monni, S., & Ogle, S. (2006). Chapter 3 Uncertainties: 2006 IPCC Guidelines for National Greenhouse Gas Inventories. Geneva: IPCC. [2.2.3]
Friedli, H.R., A.F. Arellano, S. Cinnirella and N. Pirrone (2009). Initial Estimates of Mercury Emissions to the Atmosphere from Global Biomass Burning. Environ. Sci. Technol., 2009, 43 (10), pp 3507–3513. DOI: 10.1021/es802703g [biomass methodology]
GNR, 2014. GNR database 2014 – WBCSD Sustainability Initiative, Getting the Numbers Right Project, Emissions Report 2014 http://www.wbcsdcement.org/index.php/key-issues/climate-protection/gnr-database [cement, NFM, iron and steel methodology]
Gunson, A.J. (2004). Mercury and artisanal and small-scale gold miners in China (Master's thesis). Retrieved from https://open.library.ubc.ca/cIRcle/collections/ubctheses/
Huang, X., Li, M., Friedli, H., Song, Y., Chang, D., & Zhu, L. (2011). Mercury Emissions from Biomass Burning in China. Environmental Science & Technology, 9442-9448. [biomass methodology]
Hui 2016 – Hui, M., Wu, Q., Wang, S., Liang, S., Zhang, L., Wang, F., Lenzen, M., Wang, Y., Xu, L., Lin, Z., Yang, H., Lin, Y., Larssen, T., Xu, M., Hao, J., 2016, Mercury flows in China and Global Drivers, Environmental Science and Technology, November 2016 [cement, NFM, iron and steel methodology]
Hylander, L., & Herbert, R. (2008). Global Emission and Production of Mercury during the Pyrometallurgical Extraction of Nonferrous Sulfide Ores. Environ. Sci. Technol. 42,, 5971–5977. [2.2.3]
IEA, 2005. International Energy Agency (2005). Energy Statistics Manual, OECD/IEA, 2005 [biomass methodology]
IEA, 2016. Database [biomass methodology]
IPIECA, 2012. Industry input to the UN global mercury treaty negotiations focus on oil and gas. By: Doll, B.E., B.M. Knickerbocker and E. Nucci. The global oil and gas industry association for environmental and social issues (IPIECA).
IPIECA, 2013. IPIECA INC5 Fact Sheet.

Kindbom, K., Munthe, J. (1998) Hur påverkas kvicksilver i miljön av olika energialternativ? - En förstudie fokuserad på biobränslen. IVL B 1299 [biomass methodology]

Kribek 2010 – Kribek, B., Majer, V., Veselovsky, F., Nyambe. I., 2010, Discrimination of lithogenic and anthropogenic sources of metals and sulphur in soils of the central-northern part of the Zambian Copperbelt Mining District: A topsoil vs. subsurface soil concept, Journal of Geochemical Exploration 104 (2010), 69-86 [cement, NFM, iron and steel methodology]

Kumari 2011 – Kumari, R., 2011, Preliminary mercury emission estimates from non-ferrous metal smelting in India, Atmospheric Pollution Research 2 (2011), 513-519 – OBS not the same Kumari 2011 as in GMA-2013 – another article!! [cement, NFM, iron and steel methodology]

Lacerda, L. D. De., 2003. Updating global Hg emissions from small-scale gold mining and assessing its environmental impacts. Environmental Geology, 43, 308–314.

Lacerda L.D. and W. Salomons. Mercury from gold and silver mining: a chemical time bomb? Berlin, Heidelberg, New York: Springer-Verlag, 1998:146p.

Lin, Y., Wang, S., Wu, Q. and T. Larssen (2016). Material Flow for the Intentional Use of Mercury in China. Environ. Sci. Technol., 2016, 50 (5), pp 2337–2344. DOI: 10.1021/acs.est.5b04998 [VCM methodology]

Liu, K., S. Wang, Q. Wu, L. Wang, Q. Ma, L. Zhang, G. Li, H. Tian, L. Duan and J. Hao, 2018. A Highly Resolved Mercury Emission Inventory of Chinese Coal-Fired Power Plants. nviron. Sci. Technol., 2018, 52 (4), pp 2400–2408. DOI: 10.1021/acs.est.7b06209. Publication Date (Web): January 11, 2018

LKAB 2015 – Environmental reports 2015 of the LKAB facilities in Malmberget and Kiruna, Sweden [cement, NFM, iron and steel methodology]

Maxson, P. (2016 / 2017) [VCM methodology] [Annex Tables from DRAFT - Summary of supply, trade and demand information on mercury, (UN-Environment – need final version as draft not for citation)]

Mlakar 2010 – Mlakar, T., Horvat, M., Vuk, T., Stergarsek, A., Kotnik, J., Tratnik, J., Fajon. V., 2010, Mercury species, mass flows and processes in a cement plant, Fuel 89 (2010), 1936-1945 [cement, NFM, iron and steel methodology]

Muntean 2014 – Muntean, M., Janssens-Maenhout, G., Song, S., Selin, N., Olivier, J., Guizzardi, D., Maas, R., Dentener, F., 2014, Trend analysis from 1970 to 2008 and model evaluation of EDGARv4 global gridded anthropogenic mercury emissions, Science of the Total Environment 494-495 (2014), 337-350 [cement, NFM, iron and steel methodology]

Obrist, D., D.W. Johnson, S. E. Lindberg, Y. Luo O. Hararuk, R. Bracho, J. J. Battles, D. B. Dail, R. L. Edmonds, R. K. Monson, S. V. Ollinger S. G. Pallardy, K. S. Pregitzer, and D. E. Todd. (2011). Mercury Distribution Across 14 U.S. Forests. Part I: Spatial Patterns of Concentrations in Biomass, Litter, and Soils. Environ. Sci. Technol. 2011, 45, 3974–3981. dx.doi.org/10.1021/es104384m [biomass methodology]

Pacyna, J.M., E.G. Pacyna, F. Steenhuisen, S.J. Wilson, 2003. Mapping 1995 global anthropogenic emissions of mercury. Atmos. Environ. 01/2003 http://dx.doi.org/10.1016/S1352-2310(03)00239-5.

Pereira Filho, S.R., R.L.C. dos Santos, S. Boese-O'Reilly, 2004. Environmental and health assessment in two small-scale gold mining areas – Indonesia Final Report: Sulawesi & Kalimantan. Report Requested by UNIDO, United Nations Industrial Development Organization, No. P. 2003/007 – EG/GLO/01/G34 – Removal of Barriers to the Introduction of Cleaner Artisanal Gold Mining and Extraction Technologies

Pirrone, N., S. Cinnirella, X. Feng, R. B. Finkelman, H. R. Friedli, J. Leaner, R. Mason, A. B. Mukherjee, G. B. Stracher, D. G. Streets, and K. Telmer. Global mercury emissions to the atmosphere from anthropogenic and natural sources. Atmos. Chem. Phys., 10, 5951–5964, 2010. doi:10.5194/acp-10-5951-2010 [biomass methodology]

SSAB, 2015 – Environmental reports 2015 of the SSAB facilities in Luleå and Oxelösund, Sweden [cement, NFM, iron and steel methodology]

Telmer, K. H., & M. M. Veiga, 2009. World Emissions of Mercury from Artisanal and Small Scale Gold Mining. In R. Mason & N. Pirrone (Eds.), Mercury Fate and Transport in the Global Atmosphere. Boston, MA: Springer US.

USGS, 2016, U.S Geological Survey Minerals Yearbook, Vol . I, Metals & Minerals (https://minerals.usgs.gov/minerals/pubs/commodity/myb/)

UN Environment, 2017. Global mercury supply, trade and demand. United Nations Environment Programme, Chemicals and Health Branch. Geneva, Switzerland. 81 pp. – REPLACES SEVERAL MAXSON PERS COMMS

UN Environment, 2017b.Estimating Mercury Use and Documenting Practices in Artisanal and Small-scale Gold Mining (ASGM). Methods and Tools version 1. Artisanal Gold Council (AGC) document produced in conjunction with the UN Environment Global Mercury Partnership. 175 pp.

UNEP, 2011 – Toolkit for Identification and Quantification of Mercury Releases, Reference, Revised Inventory Level 2 Report Including Description of Mercury Source Characteristics, Version 1.1, 2011 [cement, NFM, iron and steel methodology]

UNEP, 2013. Global Mercury Assessment 2013: Sources, Emissions, Releases and Environmental Transport. UNEP Chemicals Branch, Geneva, Switzerland. 44pp

UNEP, 2013 – Technical report from GMA-2013 [cement, NFM, iron and steel methodology] [NB this ref. in these sections needs to be changed to AMAP/UNEP, 2013]

UNEP, 2015 – Toolkit for Identification and Quantification of Mercury Releases, Reference Report and Guideline for Inventory Level 2, Version 1.3, 2015 [cement, NFM, iron and steel methodology]

UNEP, 2017 – Toolkit for Identification and Quantification of Mercury Releases, Reference Report and Guideline for Inventory Level 2, Version 1.4, 2017 http://web.unep.org/chemicalsandwaste/what-we-do/technology-and-metals/mercury/toolkit-identification-and-quantification-mercury-releases [cement, NFM, iron and steel methodology] [biomass methodology]

Van Straaten, P., 2000. Mercury contamination associated with small-scale gold mining in Tanzania and Zimbabwe. Science of the Total Environment, 259(1-3), 105–13.

VDZ, 2015 – The German Cement Works Association, 2015, Environmental Data of the German Cement Industry 2014 [cement, NFM, iron and steel methodology]

Wang, 2014 – Wang, S., Wang, F., Zhang, L., Yang, H., Wu., Q, Hao, J., 2014, Mercury Enrichment and its effects on atmospheric emissions in cement plants in China, Atmospheric Environment 92 (2014) 421-428 [cement, NFM, iron and steel methodology]

Wang, 2016 – Wang, S., Wang, F., Zhang, L., Yang, H., Wu, Q., Hao. J., 2016, Mercury mass flow in iron and steel production process and its implications for mercury emission control, Journal of Environmental Sciences, 43 (2016), 293-301 [cement, NFM, iron and steel methodology]

Won, 2012 – Won, J., Lee, T., 2012, Estimation of total annual mercury emissions from cement manufacturing facilities in Korea, Atmospheric Environment 62(2012), 265-271 [cement, NFM, iron and steel methodology]

Wu, Y., Streets, D.G., Wang, S.X., & Hao, J.M. (2010). Uncertainties in estimating mercury emissions from coal-fired power plants in China. Atmos. Chem. Phys., 10, 2937–2947. [2.2.3]

Wu, 2012 – Wu, Q., Wang, S., Zhang, L., Song, J., Yang, H., Meng, Y., 2012, Update of mercury emissions from China's primary zinc, lead and copper smelters, 2000-2010, Atmospheric Chemistry and Physics 12 (2012), 11153-11163 [cement, NFM, iron and steel methodology]

Wu, 2016 – Wu, Q., Wang, S., Zhang, L., Hui, M., Wang, F, Hao, J., 2016, Flow analysis of the Mercury Associated with Nonferrous Ore Concentrates: Implications on Mercury Emissions and Recovery in China, Environmental Science and Technology, January 2016 [cement, NFM, iron and steel methodology] [PUBLISHED? CONFIDENTIAL?]

Wu, Q. S. Wang, G. Li, S. Liang, C.-J. Lin, Y. Wang, S. Cai, K. Liu and J. Hao, 2016b. Temporal Trend and Spatial Distribution of Speciated Atmospheric Mercury Emissions in China During 1978–2014. Environ. Sci. Technol., 2016, 50 (24), pp 13428–13435. DOI: 10.1021/acs.est.6b04308. Publication Date (Web): November 15, 2016

Wu, Q., G. Wei, S. Wang and J. Hao, 2017. Updated atmospheric speciated mercury emissions from iron and steel production in China during 2000–2015. Atmos. Chem. Phys., 17, 10423–10433, 2017. https://doi.org/10.5194/acp-17-10423-2017

Yang, 2016 – Yang, M., Wang, S., Zhang, L., Wu, Q., Wang, F., Hui, M., Yang, H., Hao, J., 2016, Mercury emission and speciation from industrial gold production using roasting process, Journal of Geochemical Exploration, 170 (2016), 72-77 [cement, NFM, iron and steel methodology]

Zhang 2012 – Zhang, L., Wang, S., Wu, Q., Meng, Y., Yang, H., Wang, F., Hao, J., 2012, Were mercury emission factors for Chinese non-ferrous metal smelters overestimated? Evidence from onsite measurements in six smelters, Environmental Pollution, 171 (2012), 109-117 [cement, NFM, iron and steel methodology]

Zhang, W., Wei, W., Hu, D., Zhu, Y., & Wang, X. (2013). Emission of Speciated Mercury from Residential Biomass Fuel Combustion in China. Energy & Fuels 27, 6792-6800. [biomass methodology]

Zhang 2015 – Zhang, L., Wang, S., Wang, L., Wu, Y., Duan, L., Wu, Q., Wang, F., Yang, M., Yang, H., Hao, J., Liu, X., 2015, Updated emission inventories for speciated atmospheric mercury from anthropogenic sources in China, Environmental Science and Technology 49 (2015), 3185-3194 [cement, NFM, iron and steel methodology]
Zhang, L., S. Wang, Q. Wu, F. Wang, C.-J. Lin, L. Zhang, M. Hui, M. Yang, H. Su and J. Hao, 2016. Mercury transformation and speciation in flue gases from anthropogenic emission sources: a critical review. Atmos. Chem. Phys., 16, 2417–2433. [SPECIATION FOR SPATIAL]

Personal comments:

National communication, South Africa – Rico Euripidou, mail 2016-11-11 [cement, NFM, iron and steel methodology]
National communication, Australia – Peter Nelson, mail February-March 2017 [cement, NFM, iron and steel methodology]
National communication, China – Qingru Wu, mail 2017-03-14 (clarifications) [cement, NFM, iron and steel methodology]
National communication, Korea – Yong-Chil Seo, mail 2016-02-25 [cement, NFM, iron and steel methodology]
AUST Cu - http://www.ga.gov.au/scientific-topics/minerals/mineral-resources/copper#heading-5 (link from Peter Nelson) [cement, NFM, iron and steel methodology]
NAM Zn - http://www.exxaro.com/pdf/icpr/a/mining_assets/base_metals.htm [cement, NFM, iron and steel methodology]

(Other references are as in GMA 2013 Technical report)

Annex 1 Description of method used to estimate 2015 mercury emissions to air from main 'by-product' emission sectors and the chlor-alkali industry, including an example calculation

Annex 2 Description of method used to estimate 2015 mercury emissions to air from artisanal and small-scale gold mining, including an example calculation

Annex 3 Description of method used to estimate 2015 mercury emissions to air from wastes associated with mercury added products, including an example calculation

Annex 4 Description of method used to estimate 2015 mercury emissions to air from use in dental amalgam and human cremation

Annex 5 Methodological update - principle changes in methodologies applied to specific sectors

Annex 6 Emission factors and technology profiles used in the calculation of emission estimates

Annex 7 Details of methods for calculating uncertainty ranges

Annex 8 Activity data used in the calculation of emission estimates

Annex 9 Comparisons with National Inventories (to be completed)

Annex 10 Global Inventory Estimates 2015

GMA 2018 Chapter 3

Levels of mercury in air

Leading author: Nicola Pirrone

Co-Authors: Mariantonia Bencardino, Sergio Cinnirella, Aurélien Dommergue, JosephTimothy Dvonch, Ralf Ebinghaus, Xinbin Feng, Alessandra Fino, Xuewu Fu, Katarina Gårdfeldt, Antonella Macagnano, David Schmeltz, David Gay, Milena Horvat, Dan Jaffe, Joze Kotnic, Henrik Skov, Francesca Sprovieri, Hélène Angot, Alexandra Steffen, Amanda Cole, Elsie Sunderland, Kjetil Tørseth, Simon Wilson (Members of the UNEP Fate & Transport Partnership Group, - Air Subgroup Technical Expert Team).

Contents

Chapter 3 - Levels of mercury in air

3.1 Background

The aim of this chapter is to provide an up-to-date overview of mercury (Hg) levels in air (since the GMA 2013). In particular, this chapter focuses on atmospheric Hg measurements and regional/worldwide spatial and temporal trends. The information presented here includes an overview of measurements currently collected in regional monitoring networks around the world. This chapter also includes an overview of high altitude and vertical profile measurements and Hg exchange fluxes at the air/water/soil/vegetation/snow-ice interfaces. A summary of new non-standard/conventional methods available (under development) for monitoring Hg in air is also presented. The chapter concludes with an overall assessment of the state of atmospheric Hg measurements and our current understanding of the state of the science.

Specifically, this chapter highlights recent key findings on:

- Atmospheric Hg measurements and trends worldwide and at the regional/continental scale with a focus on the spatial and temporal variability of Hg and its compounds concentrations at ground-based sites, at different altitudes and latitudes in the Southern and Northern Hemispheres.
- Atmospheric Hg in the polar environment (Arctic and Antarctica) and the specific aspects related to these regions in terms of impact caused by Long Range Transport (LRT) and in-situ formation and transformation processes.
- Recent studies on vertical profile measurements over background regions and over impacted (industrial/urban) regions to support modelling uncertainty and advance our understanding of LRT and deposition/re-emission patterns.
- Temporal and spatial variability in Hg exchange fluxes between air and soil/vegetation/snow-ice interfaces, and also including contaminated sites (industrial, mining areas).
- Recent advances in monitoring applications using new/non-standard methods for measuring Hg species in the atmosphere.

3.2 Atmospheric mercury measurements and trends worldwide

3.2.1 Introduction

Atmospheric Hg is monitored in national programs driven by national legislation or international agreements and conventions. Extensive monitoring is also conducted as a part of long-term research

6066 programs. Table 1 provides a global review of mercury monitoring programmes at national, regional and
6067 local scales, based on the 'Global Review of Mercury Monitoring networks' (UNEP, 2016), produced
6068 within the framework of the Global Environmental Facility (GEF)-funded project "Development of a Plan
6069 for Global Monitoring of Human Exposure to and Environmental Concentrations of Mercury", with
6070 supplementary information collected through the negotiations of the Minamata Convention and reported
6071 by countries and experts. Many national networks operate in order to support environmental policy within
6072 international conventions or agreements and this cooperation also includes development of joint
6073 procedures both for measurements and reporting of data and for regular evaluation of trends and patterns.
6074 For example, in Europe, air monitoring data on Hg is reported to The European Monitoring and
6075 Evaluation Programme (EMEP) under the Convention on Long-range Transboundary Air Pollution
6076 (CLRTAP). Arctic countries report data to The Arctic Monitoring and Assessment Program under the
6077 Arctic Council (AMAP). Several countries in the Asian/Pacific region are participating to the Asia-Pacific
6078 Mercury Monitoring Network (APMMN network). National networks differ in terms of ambition level
6079 e.g. relating to sampling frequency and whether speciation of airborne Hg is included.

6080 National monitoring can provide the basis and infrastructure for research programs where routine
6081 monitoring can be expanded to include more advanced methodologies for e.g. speciation of airborne Hg,
6082 and also new sites in locations where measurement data were previously not available. Examples of
6083 programs contributing results to this chapter are the Global Mercury Observation System (GMOS)
6084 program and several other research projects focused on Polar regions. The GMOS network continues to
6085 operate many of the sites in coordination with national programs and regional agreements. Monitoring
6086 stations are located mostly at background sites in order to intercept major intercontinental and continental
6087 air mass transport patterns. GMOS monitoring sites have been classified as "Master" or "Secondary"
6088 sites. Master stations are those where Gaseous Elemental Mercury (GEM, i.e. the gas phase mercury in its
6089 ground electronic state), Gaseous Oxidized Mercury (GOM, i.e. the oxidized gas phase mercury
6090 compounds), Hg associated with suspended particulate matter (PBM2.5) and Hg in precipitation are
6091 continuously measured. Secondary stations are those where only Total Gaseous Mercury (TGM, i.e. the
6092 summary of gas phase species of mercury, including ground state and reactive forms) and Hg in
6093 precipitation are continuously measured. (see www.gmos.eu for further details).

6094 **Table 1:** Global Review of mercury monitoring sites in national or regional/global areas (UN
6095 Environment, 2016).

National / regional area	Program/ network/ inventory - dates of mercury measurements	Number of monitoring stations/ sites	Managing Institution	Main URLs

National networks				
Andorra	Andorran Air Quality network - from 2011 onwards	Not available	Department of Environment and Sustainability	
Australia	The Australian National Pollutant inventory (NPI) - from 1996 onwards	2		https://data.gov.au/dataset/npi
Austria	Network for Mercury impacts in forest foliage - - from 1983 (as bio-monitoring) onwards	Not available	Austrian Federal Research Centre for Forests controls	http://www.bioindikatornetz.at
Brazil	Mercury monitoring sites – Running dates na	Not available	CETESB, the environmental agency of the State of São Paulo	http://www.cetesb.sp.gov.br/2014/10/27/cetesb-realiza-treinamentos-internacionais-sobre-pops-e-mercurio/
Canada	The Canadian Air and Precipitation Monitoring Network (CAPMoN) & others (including AMAP) – from 1994 onwards (see section 3.2.5)	3 for air meas..	CAPMoN	https://www.ec.gc.ca/rs-mn/default.asp?lang=En&n=6C2AD92E-1 http://nadp.sws.uiuc.edu/
		+7 for air meas.	Environment and Climate Change Canada	
		+ 2 remote	Canadian Northern Contaminants Program (NCP) – Environment Canada	
China	Mercury monitoring sites (including GMOS sites) – Running dates na	9 for air meas.	Institute of Geochemistry, CAS	
China (Taiwan)	Wet deposition Network - from 2009 onwards	11	Environmental Protection Administration	
		+ 1 remote		
Hungary	Hungarian Air Quality Monitoring Network - from 2010 onwards	1	Hungarian Meteorological Service	
Republic of Korea	Mercury Monitoring Network in Korean Air Pollution Monitoring Network - from 2009 onwards	12 TGM / 1 Hg speciation / 4 Hg precipitation	National Institute of Environmental Research in the Ministry of Environment.	https://seoulsolution.kr/en/content/air-pollution-monitoring-network www.airkorea.or.kr (Korean only)

Japan	Mercury Monitoring Networks - from 1998 onwards	5	National Institute for Minamata Disease (NIMD) and the National Institute for Environmental Studies (NIES)/Ministry of Environment (MOE).	https://www.env.go.jp/en/chemi/mercury/bms.html http://www.env.go.jp/press/104568.html (Japanese only) http://www.env.go.jp/air/osen/monitoring/mon_h27/index.html (Japanese only)
Poland	Polish State Environmental Monitoring programme - from 2000 onwards	5	Inspection of Environmental Protection	http://www.gios.gov.pl/en/state-of-the-environment/state-environmental-monitoring
Indonesia	Mercury Monitoring Site	1		http://apmmn.org
Switzerland	Mercury Monitoring Site	1		https://www.hfsjg.ch
Romania	Mercury Monitoring Network - from 2000 onwards		Ministry of Environment, NEPA and the National Environmental Guard	
United Kingdom	National Metals Network and National Atmospheric Emission Inventory – Running dates na	2	UK DEFRA; CEH	http://www.auchencorth.ceh.ac.uk/node/211 https://uk-air.defra.gov.uk/networks/network-info?view=metals http://naei.defra.gov.uk/overview/pollutants?pollutant_id=15
Vietnam	- from 2014 onwards	1	Vietnamese Centre for Environmental Monitoring (CEM) of the Vietnam Environment Administration (VEA)	
Regional/Global networks				
Global network	Global Mercury Observation System (GMOS)	Many stations in both hemispheres (see sect. 3.2.2)	CNR-IIA Division of Rende, Italy	www.gmos.eu
Regional Network	European Union Network under EU Directive 2004/107/EC	Several stations in Europe	European Environment Agency (EEA)	http://cdr.eionet.europa.eu/ https://www.eea.europa.eu/publications/92-9167-058-8/page010.html

Regional network	European Monitoring and Evaluation Programme (EMEP)	Several stations in Europe	EMEP Organization	http://emep.int/index.html
Regional network	National Atmospheric Deposition Program (NADP)	Many stations in USA, Canada (see section 3.2.4)	NADP Program Office Illinois State Water Survey, 2204 Griffith Drive Champaign, IL 61820-7495	http://nadp.sws.uiuc.edu/mdn/
Regional network	Asia-Pacific Mercury Monitoring Network (APMMN)	Several stations in the Asia-Pacific Region	APMMN Organization	http://apmmn.org/
Regional network	Arctic Monitoring and Assessment Programme (AMAP)	Several stations across the circum-Arctic Region	AMAP Organization	https://www.amap.no/about/the-amap-programme

The 2016 UN Environment Global Review lists main information on existing national and regional/global monitoring networks but doesn't include data on Hg concentrations and depositions.

Figure 1 provides a global picture of major Hg monitoring networks that are part of global and regional networks mentioned in several sections of this chapter. It shows that though we have monitoring sites in both hemispheres, there are regions (even large regions) that are completely lacking of monitoring data/sites which makes it infeasible to evaluate the current geospatial distribution (gradients and variability) of Hg concentration in ambient air.

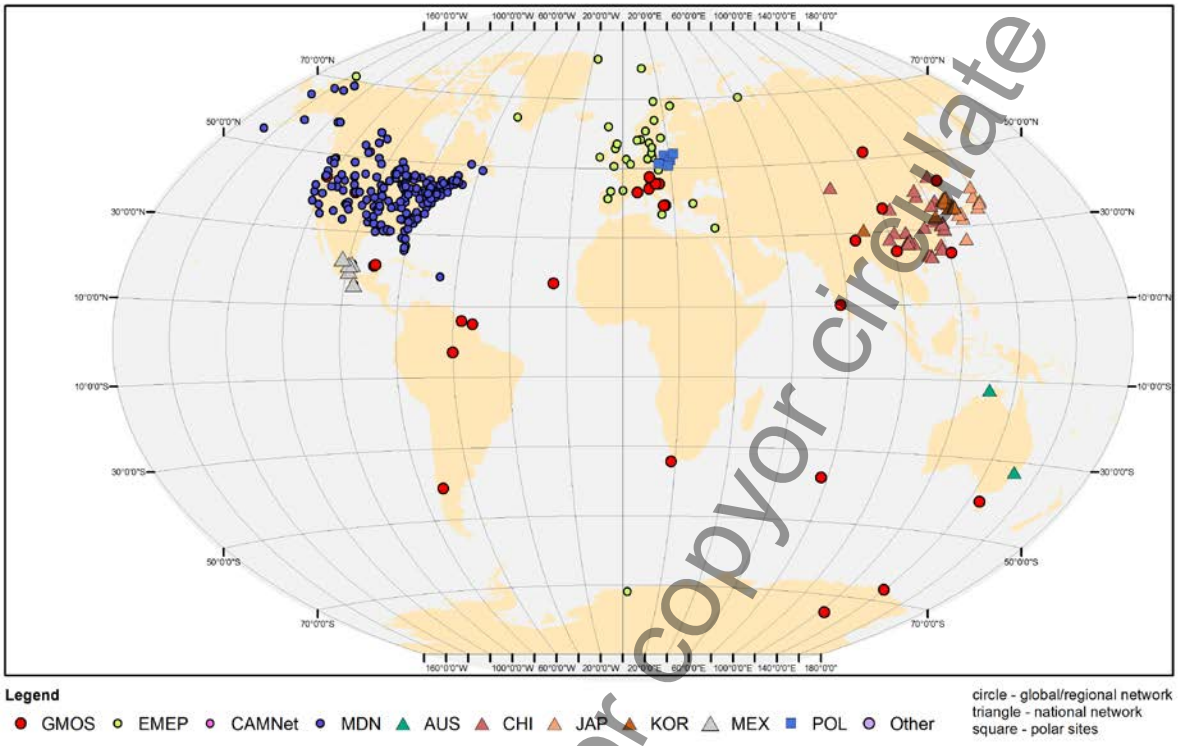

Figure 1: Global map of Hg monitoring networks

3.2.2 Spatial variability in the Southern and Northern Hemispheres

This section presents atmospheric Hg concentrations recorded worldwide in the framework of the GMOS program network, analysing Hg measurement results in terms of temporal and spatial variability within the network. Particularly, measurements and data analysis across several ground-based sites related to the 2012-2014 years have been discussed. Major findings highlighted in this section include a clear gradient of Hg concentrations between the Northern and Southern hemispheres, confirming that the gradient observed is mostly driven by local and regional sources, which can be anthropogenic, natural or a combination of both. Tables 2 and 3 show annual values for speciated Hg concentrations at all sites from 2012 to 2014. In both Tables 2 and 3, the stations are ordered by latitude, thus describing the spatial atmospheric Hg variations moving from Northern to Southern Hemisphere. Mean GEM values of most of the sites located in the Northern Hemisphere were between 1.3 and 1.6 ngm^{-3}, which is comparable to the concentrations measured at the long-term monitoring stations at Mace Head, Ireland (Ebinghaus et al., 2011; Slemr et al.,2011; Weigelt et al., 2015; Cole et al. 2014), and Zingst, Germany (Kock et al.,2005). In contrast, GEM concentrations from the EVK site, located at 5050 m above sea level in the Eastern Himalaya of Nepal, reported mean values below 1.3 ngm^{-3}. This value is comparable to free tropospheric

concentrations measured in August 2013 over Europe (Weigelt et al., 2016). GEM concentration means observed at the stations in the Northern Hemisphere are also in good agreement with the overall mean concentrations observed at multiple sites in Canada (ranging from 1.23±0.37 to 3.75 ± 2.22 ng m^{-3} overall, measurements collected from 1994-2011) (Cole et al., 2014) and those reported from two Arctic stations (VRS, PAL) (Sprovieri et al., 2016). Seasonal variations of GEM concentrations have also been observed at all European sites in the Northern Hemisphere, with most of them showing higher concentrations during the winter and spring and lower concentrations in summer and fall seasons. For the sites located in the Southern Hemisphere as part of GMOS network (see Table 2), mean GEM concentrations (~ 1.0 ngm^{-3}) are lower than those reported in the Northern Hemisphere (~ 1.5 ngm^{-3}) but are in good agreement with the previously reported southern hemispherical background levels (Sprovieri et al., 2010; Angot et al., 2014; Slemr et al., 2015) and the expected range for remote sites in this region. A small (within ~ 0.1 ngm^{-3}) seasonal variability in GEM concentrations was observed at Cape Point and Amsterdam Island with highest values during the winter and lowest values in summer (Slemr et al., 2015) but the variability in concentrations is much lower than in the Northern Hemisphere. GEM concentrations are comparable at all Southern Hemisphere monitoring sites, whereas the lower concentrations of GEM observed (<1ngm^{-3}), were associated with air masses coming from the southern Indian Ocean and the Antarctic continent (Angot et al., 2014).

6140 **Table 2:** Annually averaged GEM mean concentrations from 2012 to 2014 at the GMOS stations (Sprovieri et al., 2016).

	Code	Site	Type of Site	Elev (m asl)	Lat	Lon	Country	2012 GEM Mean ± St.Dev. (ng m^{-3})	2013 GEM Mean ± St.Dev. (ng m^{-3})	2014 GEM Mean ± St.Dev. (ng m^{-3})
Northern Hemisphere	VRS	Villum Research Station	Remote	30	81.58033	-16.60961	Greenland	1.44 ± 0.27	1.61 ± 0.41	1.41 ± 0.35
	PAL	Pallas	Remote	340	68.00000	24.23972	Finland	- ± -	1.45 ± 0.11	1.47 ± 0.17
	RAO*	Råö	Remote	5	57.39384	11.91407	Sweden	1.33 ± 0.20	1.43 ± 0.16	1.48 ± 0.23
	MHE	Mace Head	Remote	5	53.32511	-9.90500	Ireland	** ± **	1.46 ± 0.17	1.41 ± 0.14
	LIS	Listvyanka	Rural	670	51.84670	104.89300	Russia	- ± -	1.34 ± 0.38	1.39 ± 0.40
	CMA	Col Margherita	Rural	2545	46.36711	11.79341	Italy	- ± -	- ± -	1.69 ± 0.29
	LON*	Longobucco	Rural	1379	39.39408	16.61348	Italy	- ± -	1.43 ± 0.33	- ± -
	MIN	**Minamata**	**Rural**	**20**	**32.23056**	**130.40389**	**Japan**	1.95 ± 0.48	1.86 ± 0.40	1.91 ± 0.40
	EVK	Ev-K2	Remote	5050	27.95861	86.81333	Nepal	1.14 ± 0.17	1.11 ± 0.42	1.33 ± 0.22
Tropics	SIS	Sisal	Rural	7	21.16356	-90.04679	Mexico	- ± -	1.20 ± 0.24	1.11 ± 0.37
	CAL	Calhau	Remote	10	16.86402	-24.86730	Cape Verde	- ± -	1.22 ± 0.14	1.20 ± 0.09
	KOD	Kodaicanal	Rural	2333	10.23170	77.46524	India	- ± -	1.54 ± 0.20	1.54 ± 0.26
	NIK	Nieuw Nickerie	Rural	1	5.95679	-57.03923	Suriname	- ± -	1.13 ± 0.42	1.28 ± 0.46
	MAN*	Manaus	Remote	110	-2.89056	-59.96975	Brazil	- ± -	1.08 ± 0.23	0.99 ± 0.23
Southern Hemisphere	AMS*	Amsterdam Island	Remote	70	-37.79604	77.55095	Terres Australes et Antarctiques Françaises	1.03 ± 0.07	1.03 ± 0.09	1.05 ± 0.05
	CPT	Cape Point	Remote	230	-34.35348	18.48983	South Africa	1.07 ± 0.10	1.03 ± 0.11	1.09 ± 0.12
	BAR	Bariloche	Rural	801	-41.12873	-71.42010	Argentina	1.01 ± 0.11	0.89 ± 0.15	0.87 ± 0.15
	DDU	Dumont d'Urville	Remote	40	-66.66281	140.00292	Antarctica	0.91 ± 0.2	0.85 ± 0.19	0.86 ± 0.38
	DMC	Concordia Station	Remote	3220	-75.10170	123.34895	Antarctica	0.76 ± 0.24	0.84 ± 0.27	- ± -

6141 **** to be included; *GMOS Master stations with speciation Hg data; in bold External GMOS Partners**

Table 3: Annually-averaged Particle Bound Mercury (PBM) and Gaseous Oxidised Mercury (GOM) mean concentrations from 2012 to 2014 at the GMOS stations (Sprovieri et al., 2016).

							2012		2013		2014	
	Code	**Site**	**Elev (m asl)**	**Lat**	**Lon**	**Country**	**PBM** Mean ± St.Dev. (pg m^{-3})	**GOM** Mean ± St.Dev. (pg m^{-3})	**PBM** Mean ± St.Dev. (pg m^{-3})	**GOM** Mean ± St.Dev. (pg m^{-3})	**PBM** Mean ± St.Dev. (pg m^{-3})	**GOM** Mean ± St.Dev. (pg m^{-3})
NH	RAO	Råö	5	57.39384	11.91407	Sweden	2.89 ± 3.27	0.63 ± 1.73	3.96 ± 3.77	0.54 ± 0.85	4.41 ± 5.87	1.25 ± 1.87
	LON	Longobucco	1379	39.39408	16.61348	Italy	-	-	3.28 ± 3.82	11.33 ± 29.90	-	-
	CHE	**Cape Hedo**	**60**	**26.86430**	**128.25141**	**Japan**	1.77 ± 2.46	1.10 ± 1.80	3.70 ± 3.60	1.46 ± 2.19	4.03 ± 5.25	2.26 ± 3.71
T	MAN	Manaus	110	-2.89056	-59.96975	Brazil	-	-	5.04 ± 4.13	1.72 ± 0.72	1.45 ± 1.81	1.61 ± 1.75
SH	AMS	Amsterdam Island	70	-37.79604	77.55095	Terres Australes et Antarctiques Françaises	1.76 ± 1.20	1.65 ± 0.82	2.05 ± 1.37	1.53 ± 0.45	2.22 ± 1.83	2.03 ± 1.44

6148
6149 Table 4 reports the summary of the annual wet deposition fluxes and the weighted total mercury (THg)
6150 concentrations observed at the 17 GMOS sites from the Northern, Tropical, and Southern Hemispheres
6151 between 2011 and 2015 (Sprovieri et al., 2017). Seasonal trend analysis of THg in precipitation showed
6152 increasing Hg concentrations and Hg deposition during the spring and summer months. However, the
6153 patterns of THg concentrations and precipitation amounts reveal that, at most of the sites, the seasonal
6154 THg wet deposition maximum corresponds to the maximum in precipitation amounts collected (Sprovieri
6155 et al., 2017). The dominant factor in determining the Hg wet deposition loading recorded at all the
6156 European sites was then generally related to the amounts of the collected precipitation (Sprovieri et al.,
6157 2017).

6158

Table 4: Annual wet deposition fluxes [$\mu g m^{-2} yr^{-1}$] and weighted THg concentrations [$ng L^{-1}$] observed at GMOS stations from 2011 to 2015 (Sprovieri et al., 2017).

	Code	**Station**	**Elev (m asl)**	**Lat**	**Lon**	**Country**	**2011**		**2012**		**2013**		**2014**		**2015**	
							Annual Wet Dep. Flux [$\mu g m^{-2} yr^{-1}$]	Weighted HgT [$ng L^{-1}$]	Annual Wet Dep. Flux [$\mu g m^{-2} yr^{-1}$]	Weighted HgT [$ng L^{-1}$]	Annual Wet Dep. Flux [$\mu g m^{-2} yr^{-1}$]	Weighted HgT [$ng L^{-1}$]	Annual Wet Dep. Flux [$\mu g m^{-2} yr^{-1}$]	Weighted HgT [$ng L^{-1}$]	Annual Wet Dep. Flux [$\mu g m^{-2} yr^{-1}$]	Weighted HgT [$ng L^{-1}$]
Northern Hemisphere	NYA	Zeppelin	474	78.90806	11.88139	Norway	-	-	0.9	**3.8**	0.9	**4.1**	1.7	**5.7**	0.8	**4.4**
	PAL	Pallas	340	68	24.23972	Finland	2.9	**7.1**	1.9	**6.8**	1.3	**4.5**	2.3	**6.1**	-	-
	RAO	Råö	5	57.393835	11.914066	Sweden	5.8	**8.9**	6.5	**10.4**	4.2	**8.2**	6.3	**9.9**	-	-
	MHE	Mace Head	5	53.325106	-9.905	Ireland	-	-	0.9	**2.2**	4.8	**4.6**	4.1	**6.6**	-	-
	LIS	Listvyanka	670	51.8467	104.893	Russia	-	-	0.2	**9.7**	0.1	**2.6**	-	-	-	-
	CMA	Col Margherita	2545	46.36711	11.79341	Italy	-	-	-	-	-	-	4.4	**7.8**	-	-
	ISK	Iskrba	520	45.561217	14.858047	Slovenia	5.1	**7.5**	8.4	**6.2**	7.2	**5.3**	10.0	**6.1**	3.0	**3.0**
	MCH	Mt. Changbai	741	42.40028	128.11250	China	2.8	**10.6**	4.8	**8.4**	1.2	**3.9**	1.0	**5.4**	-	-
	LON	Longobucco	1379	39.39408	16.61348	Italy	-	-	0.3	**3.9**	3.1	**6.6**	-	-	-	-
	MWA	Mt. Walinguan	3816	36.28667	100.89797	China	-	-	0.3	**4.3**	0.4	**6.4**	2.2	**15.0**	-	-

	MAL	Mt. Ailao	2503	24.53791	101.03024	China	4.3	**2.8**	3.2	**3.3**	5.5	**5.3**	0.2	**6.7**	-	-
Tropics	SIS	Sisal	7	21.16356	-90.04679	Mexico	-	-	-	-	7.4	**11.0**	6.5	**9.1**	-	-
	CST	Celestun	3	20.85838	-90.38309	Mexico	-	-	2.4	**8.1**	0.1	**13.5**	-	-	-	-
Southern Hemisphere	AMS	Amsterdam Island	70	-37.79604	77.55095	Terres Australes et Antarctiques Françaises	-	-	-	-	1.95	**2.34**	1.55	**1.80**	-	-
	CPT	Cape Point	230	-34.35348	18.48983	South Africa	0.3	**2.1**	3.8	**14.6**	5.2	**19.6**	0.57	**1.84**	0.6	**3.0**
	CGR	Cape Grim	94	-40.683333	144.689444	Australia	-	-	-	-	3.1	**4.0**	3.8	**6.7**	3.1	**6.5**
	BAR	Bariloche	801	-41.12873	-71.42010	Argentina	-	-	-	-	-	-	0.1	**0.4**	0.5	**0.6**

Mercury deposition measurements are scarce in tropical latitudes; hence there have been few scientific publications within the past decade from this region (Shanley et al., 2015 and references therein). The tropics are a particularly important region with regard to global atmospheric chemistry and 49% of total GOM deposition globally occurs in the tropical oceans (Horowitz et al., 2017). Due to intense ultraviolet radiation and high water-vapour concentrations, high OH concentrations oxidize inorganic and organic gases, and induce an efficient removal from the atmosphere of the oxidized products. To address the regional gap of information, the GMOS program initiated Hg deposition measurements in Mexico at Sisal station (see Table 3). High wet Hg deposition flux at this site suggested that other tropical areas maybe hotspots for Hg deposition as well. A number of studies have suggested that this could be due to higher precipitation and the scavenging ratios from the global pool in the subtropical free troposphere where high concentrations of oxidized Hg species exist (Selin and Jacob, 2008). These findings were also highlighted in previous studies in the south of Florida and the Gulf of Mexico coastal areas, confirming that local and regional Hg emissions play only a minor role in wet Hg deposition (Sillman et al., 2013) and suggesting that the primary source of scavenged oxidized Hg could be the global pool. In remote areas particularly in the Southern Hemisphere, far from any local sources, atmospheric deposition has been recognized as the main source of Hg to the ocean (Lindberg et al., 2007; Pirrone et al., 2008; Sunderland and Mason, 2007). THg exhibited annual and seasonal patterns in Hg wet deposition samples. Inter-annual differences in total wet deposition are mostly linked with precipitation volume, with the greatest deposition flux occurring in the wettest years (see Table 4) (Sprovieri et al., 2017).

3.2.3 Northern–Southern Hemispheric gradients

A summary of descriptive statistics of GEM, GOM and PBM from all GMOS sites distributed from the Northern to the Southern Hemisphere is reported in Tables 2 and 3, whereas Figure 2 shows a focus on GEM yearly distribution for 2013 (blue) and 2014 (green). The sites have been organized in the graphic as well as in the tables according to their latitude from those located in the Northern Hemisphere to those located in the tropics and in the Southern Hemisphere. The box-and-whisker plot of GEM shows a downward trend from the 13 northern sites which had significantly higher median concentrations than those recorded at the southern sites, confirming the assessment previously performed at long-term monitoring sites such as Mace Head (MHD), Ireland (Ebinghaus et al., 2011; Weigelt et al., 2015), and at Cape Point (CPT), South Africa (Slemr et al., 2015). At MHD the annual baseline GEM means observed by Ebinghaus et al. (2011) decreased from 1.82 ngm^{-3} earlier in 1996 to 1.4 ngm^{-3} in 2011, showing a downwards trend of 1.4–1.8% per year. Recently across the GMOS network, a decrease of 1.6% at MHD

from 2013 and 2014 was observed and a slight increase (see Slemr et al., 2015) in Hg concentrations at CPT from 2007 to 2013 that continued through 2014 (Slemr et al., 2015). The clear north–south gradient, in line also with previous studies (Soerensen et al., 2010a, b, 2012; Sommar et al., 2010; Lindberg et al., 2007; Sprovieri et al., 2010), has been confirmed also by the probability density functions (PDFs) calculated on the data (Sprovieri et al., 2016).

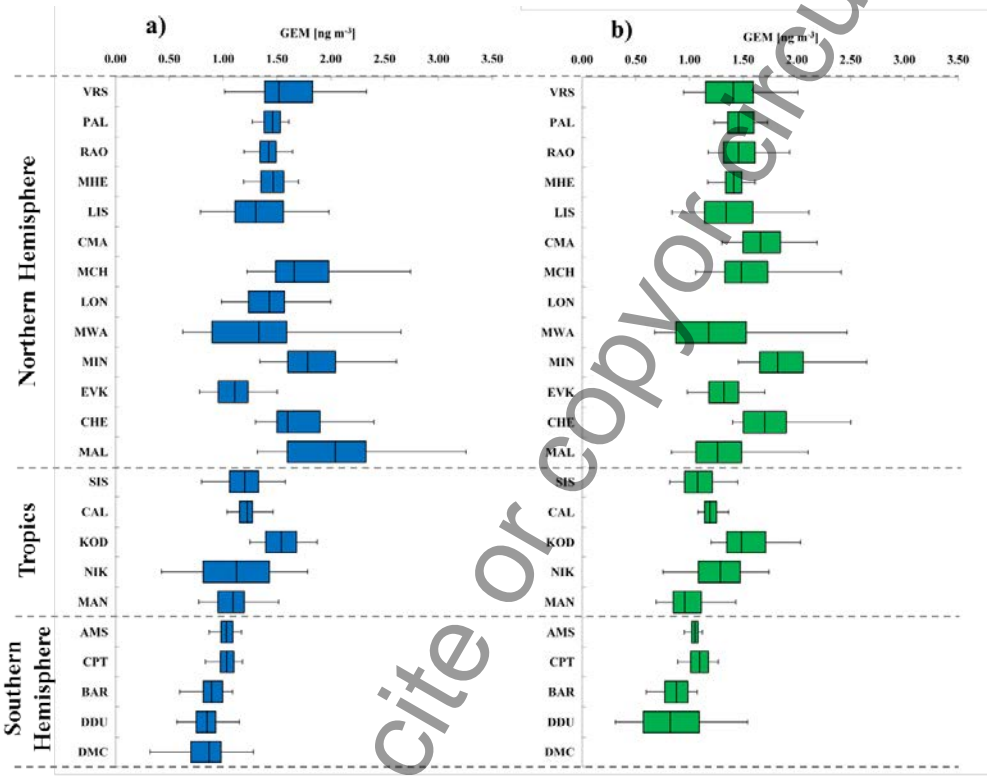

Figure 2: Box-and-whisker plots of GEM yearly distribution at the GMOS stations for (a) 2013 and (b) 2014. The sites are organized according to their latitude from the northern to the southern locations. Each box includes median (midline), 25th and 75th percentiles (box edges), 5th and 95th percentiles (whiskers) (Sprovieri et al., 2016).

3.2.4 Spatial and temporal variability in North America

3.2.4.1 NADP's Mercury Deposition Network

The National Atmospheric Deposition Program's (NADP) Mercury Deposition Network (MDN) makes long-term measurements of Hg in precipitation (wet deposition) across North America. The MDN began monitoring in 1996. The MDN sites follow standard procedures, and uniform precipitation collectors and rain gages to make weekly-integrated measurements of THg in precipitation (wet-only deposition) from

Tuesday to Tuesday. Some daily samples are available. Sample bottles are pre-charged with acid to preserve the Hg sample. Currently, the MDN has 106 active sites. All MDN samples are analysed for THg concentration using Cold Vapour Atomic Florescence Spectroscopy (CVAFS). Invalid samples are identified using standard protocols. Subsamples for some sites are analysed for methyl mercury (MeHg). Valid and invalid results are provided for use by the scientific community (http://nadp.isws.illinois.edu/mdn/).

All observations are used to determine THg concentration and deposition over North America in annual maps of precipitation weighted-mean concentration (ng/L) and flux (ug/m^2 year, see Figure 3). Precipitation-weighted average concentrations from earlier years are shown for comparison (Table 5). Over the MDN measurement area, significant wet deposition is found along the U.S. Gulf Coast, and somewhat inland. Wet Hg deposition in these areas strongly correlates with higher precipitation (40-60 inches per year or >1000 cm/year). This pattern is repeated annually. Highest concentrations are found in the western areas where precipitation is lowest, and dominated by winter snow.

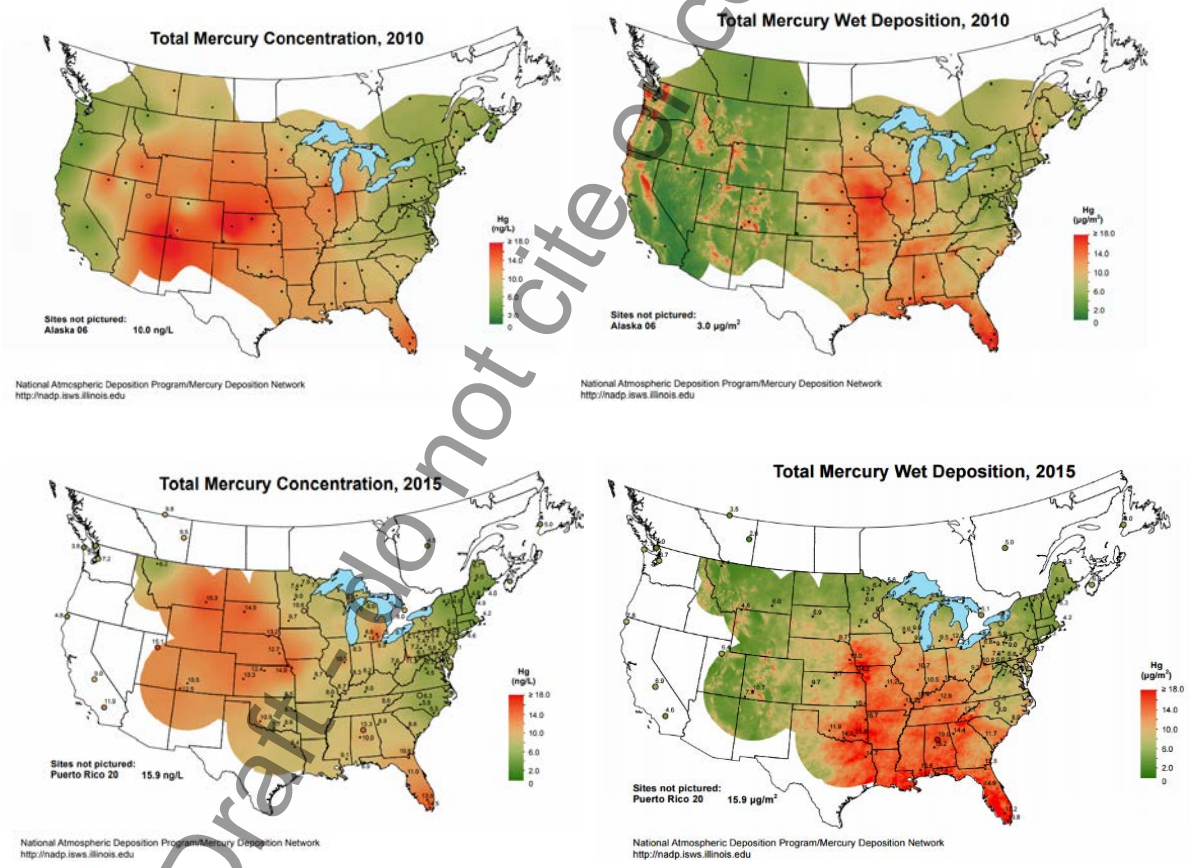

Figure 3: Total mercury wet concentration and deposition as measured across North America for 2010 (above) and for 2015 (below). All years available at http://nadp.isws.illinois.edu.

Table 5: Annual Hg concentration means and medians for all sites in North America

Year	Valid Observations	PW Mean	Median	Units
2010	4,495	8.51	6.33	ng/L
2011	4,286	9.01	6.99	ng/L
2012	4,357	9.15	7.03	ng/L
2013	4,391	9.02	7.17	ng/L
2014	4,848	8.83	6.98	ng/L
2015	4,798	8.04	6.40	ng/L

Trends over time in MDN data have been investigated by several research groups (Butler et al., 2008; Prestbo and Gay, 2009; Risch et al., 2012; Weiss-Penzias et al., 2016). Evaluating data through the mid 2000s, Butler et al. showed general decreases in eastern U.S. concentrations, with significant decreases at about half of these sites. Fewer significant trends were seen in the Southeast, but the general tendency was for decreasing concentrations. Prestbo and Gay found significant decreasing concentration trends at about half of the sites (mostly in the East), particularly across Pennsylvania and extending up through the Northeast, and fully consistent with Butler et al. Two sites in the West (Colorado, Washington) showed the same decreases. No significant concentration increases were noted, with little change in the Upper Midwest concentration or deposition. Risch et al., focusing on the Great Lakes region, found only "small localized decreases" in Hg concentration. Deposition trends were present, but not at these same sites; Overall, Hg deposition in the Great Lakes area remained unchanged between 2002 and 2008. Weiss-Penzias et al reported wet concentrations almost exclusively decreasing between 1997 and 2013, with over 50% of the MDNsites showing significant decreases (of 19 sites). However, for the time period 2007–2013 (with 71 sites), increasing concentrations were just as numerous as decreasing concentrations, and this tendency increased with a shorter time period (2008-13), and positive tendencies were wide spread. Regional trend analyses revealed significant positive trends in Hg concentration in the Rocky Mountains, Plains, and Upper Midwest regions for the more recent time periods.

3.2.4.2 NADP's Atmospheric Mercury Network

The NADP's Atmospheric Mercury Network (AMNet) measures atmospheric Hg that contributes to Hg deposition using automated, continuous measurement systems, and standardized methods. Currently, the network consists of 22 active AMNet sites (Figure 3); data from the AMNet are available on the NADP website (http://nadp.isws.illinois.edu/ amn). AMNet observations have been made continuously since 2009 (five-minute and two-hour averages). Data are qualified and averaged to one-hour (GEM in ng m^{-3}) and two-hour values (GOM, and $PBM_{2.5}$, in pg m^{-3}).

Valid data are released for use by the scientific community, and also released in annual figures of Hg variability for sites meeting certain criteria. Annual average statistics for the network are shown in the Table 6, with annual GEM values by site and year in Table 7. The median GEM concentration found in the network is 1.38 ng/m3, and varies somewhat across the network. However, larger differences were present between sites for GOM and PBM concentrations in AMNet. GOM concentrations are generally higher in the urban environment, with lowest concentrations along the Pacific Ocean and other coastal sites. $PBM_{2.5}$ concentrations measured were generally the same as with GOM. The occurrence of very high outlier concentrations were noted at almost all of the sites (Table 7 and Figure 5).

Investigations of AMNet trends over time are currently ongoing. Data are also being used to estimate speciated and total mercury dry deposition at select locations in North America (Zhang et al., 2016 & 2012).

Table 6: Annual GEM, GOM, and PBM concentrations [ng m^{-3}, pg m^{-3}] for all AMNet stations from 2010 to 2015. Number of observations are included.

	Atmospheric Mercury Concentrations	Valid Observations	Mean	Median	Units
2010	GEM	51,289	1.57	1.43	ng/m3
	GOM	38,744	6.5	1.39	pg/m3
	PBM	38,099	6.67	3.78	pg/m3
2011	GEM	54,541	1.59	1.44	ng/m3
	GOM	44,864	15.92	1.35	pg/m3
	PBM	44,817	8.23	4.09	pg/m3
2012	GEM	42,924	1.47	1.42	ng/m3
	GOM	36,226	19.74	1.22	pg/m3
	PBM	37,386	13.13	4.18	pg/m3
2013	GEM	39,078	1.49	1.44	ng/m3
	GOM	30,806	14.35	1.29	pg/m3
	PBM	30,919	10.33	4.45	pg/m3
2014	GEM	49,348	1.47	1.4	ng/m3
	GOM	35,390	12.64	1.52	pg/m3
	PBM	35,238	10.99	4.96	pg/m3
2015	GEM	52,938	1.58	1.38	ng/m3
	GOM	44,179	12.47	1.59	pg/m3
	PBM	43,022	8.62	4.11	pg/m3

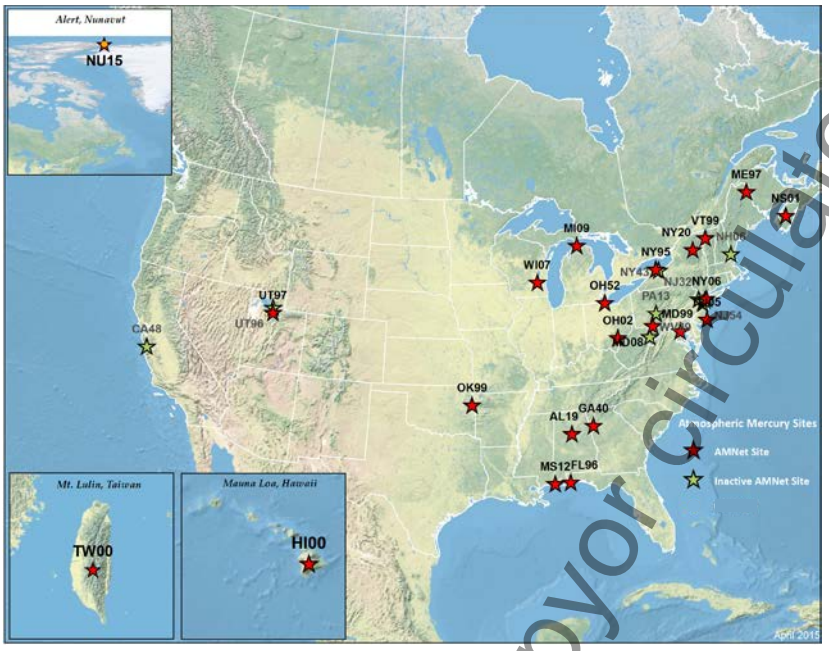

Figure 4: AMNet sites as of 12/31/2015.

Table 7: Annual GEM concentrations [ng m^{-3}] observed at AMNet stations from 2009 to 2015. Only average values with greater than 2000 valid two-hourly averages are included.

Site	Site Name	State	Latitude	Longitude	Elev.	Start Date	Stop Date	2009 GEM (ng/m3)	2010 GEM (ng/m3)	2011 GEM (ng/m3)	2012 GEM (ng/m3)	2013 GEM (ng/m3)	2014 GEM (ng/m3)	2015 GEM (ng/m3)
AK03	Denali NP-Mt. McKinley	AK	63.7232	-148.9676	661	03/10/14							1.34 ± 0.16	1.35 ± 0.14
AL19	Birmingham	AL	33.5530	-86.8148	200	01/01/09	06/30/16	2.06 ± 4.70	2.16 ± 1.28	2.23 ± 1.28	1.95 ± 1.39	1.85 ± 2.08	1.80 ± 0.70	1.67 ± 1.11
CA48	Elkhorn Slough	CA	36.8100	-121.7800	15	01/01/10	01/01/11		1.48 ± 0.17	1.48 ± 0.15				
FL96	Pensacola	FL	30.5499	-87.3750	45	01/01/09	10/01/16	1.36 ± 0.15	1.42 ± 0.14	1.38 ± 0.16	1.41 ± 0.14	1.37 ± 0.20	1.35 ± 0.20	1.28 ± 0.13
GA40	Yorkville	GA	33.9282	-85.0451	395	01/01/09	10/01/16	1.28 ± 0.16	1.31 ± 0.21	1.41 ± 0.30	1.45 ± 0.20	1.42 ± 0.32	1.44 ± 0.24	1.37 ± 0.28
HI00	Mauna Loa	HI	19.5392	-155.5792	3399	12/30/10				1.45 ± 0.51	1.33 ± 0.52	1.42 ± 0.42	1.34 ± 0.33	1.37 ± 0.32
MD08	Piney Reservoir	MD	39.7053	-79.0122	769	01/01/08		1.29 ± 0.21	1.39 ± 0.17	1.43 ± 0.17		1.34 ± 0.19	1.34 ± 0.20	
MD98	Beltsville #2	MD	39.0280	-76.8171	46	01/26/07		1.30 ± 0.23	1.45 ± 0.43	1.51 ± 0.23	1.42 ± 0.19	1.40 ± 0.21	1.32 ± 0.20	1.31 ± 0.19
MD99	Beltsville	MD	39.0280	-76.8171	46	11/07/06		1.33 ± 0.20	1.45 ± 0.43	1.46 ± 0.20	1.43 ± 0.20	1.37 ± 0.20	1.41 ± 0.18	
ME97	Presque Isle	ME	46.6964	-68.0332	165	12/06/13							1.58 0.28	
MS12	Grand Bay NERR	MS	30.4294	-88.4277	2	09/29/06		1.36 ± 0.18	1.40 ± 0.13	1.44 ± 0.14	1.36 ± 0.17	1.41 ± 0.14	1.41 ± 0.25	1.35 ± 0.24
MS99	Grand Bay NERR #2	MS	30.4294	-88.4277	2	10/18/07	11/12/12	1.40 ± 0.23	1.39 ± 0.13	1.45 ± 0.16				
NH06	Thompson Farm	NH	43.1100	-70.9500		01/01/09	11/29/11	1.33 ± 0.25	1.32 ± 0.15	1.36 ± 0.21				
NJ05	Brigantine	NJ	39.4649	-74.4488	1	06/01/09	10/01/15							
NJ30	New Brunswick	NJ	40.4728	-74.4226	21	10/01/15								
NJ54	Elizabeth Lab	NJ	40.6414	-74.2084	11	10/01/15								
NS01	Kejimkujik NP, Canada	NS	44.4328	-65.2056	155	01/26/09		1.37 ± 0.31	1.35 ± 0.20	1.41 ± 0.19	1.28 ± 0.19	1.32 ± 0.20	1.27 ± 0.21	1.24 ± 0.23
NY06	Bronx	NY	40.8680	-73.8782	68	08/27/08		1.50 ± 0.34		1.51 ± 0.34	1.60 ± 0.39		2.05 ± 0.74	1.80 ± 0.42
NY20	Huntington Wildlife	NY	43.9731	-74.2231	500	11/21/07		1.25 ± 0.28	1.39 ± 0.55	1.23 ± 0.27	1.32 ± 0.27			1.24 ± 0.25
NY43	Rochester	NY	43.1463	-77.5482	136	09/26/08		1.41 ± 0.19	1.43 ± 0.19	1.33 ± 0.16	1.41 ± 0.42		1.73 ± 1.14	1.50 ± 0.75
NY95	Rochester_B	NY	43.1463	-77.5481	136	11/21/07	11/13/09	1.58 ± 0.29						
OH02	Athens Super Site	OH	39.3078	-82.1182	275	01/01/07		1.33 ± 0.16	1.43 ± 0.19	1.40 ± 0.24			1.54 ± 0.22	1.49 ± 0.23
OH52	South Bass Island	OH	41.6582	-82.8270	177	12/31/11				. .		1.72 ± 0.71		
OK99	Stilwell	OK	35.7508	-94.6700	299	10/20/08		1.32 ± 0.19	1.40 ± 0.18	1.36 ± 0.18				
TW01	Mt. Lulin	TW	23.5100	120.9200	2862	01/01/10								
UT96	Antelope Island	UT	41.0467	-112.0248	1287	06/18/09	06/30/11		1.68 ± 0.93					
UT97	Salt Lake City	UT	40.7118	-111.9609	1297	11/23/08		2.19 ± 0.98		1.80 ± 0.80	1.81 ± 1.14	1.85 ± 0.94	1.74 ± 0.48	
VT99	Underhill	VT	44.5283	-72.8684	399	01/01/08	01/04/16	1.41 ± 0.23	1.51 ± 0.15	1.46 ± 0.19	1.33 ± 0.17	1.08 ± 0.14	1.33 ± 0.19	1.30 ± 0.17
WI07	Horicon Marsh	WI	43.4660	-88.6210	287	01/02/11				1.34 ± 0.17	1.49 ± 0.15	1.53 ± 0.20	1.47 ± 0.22	1.52 ± 0.41

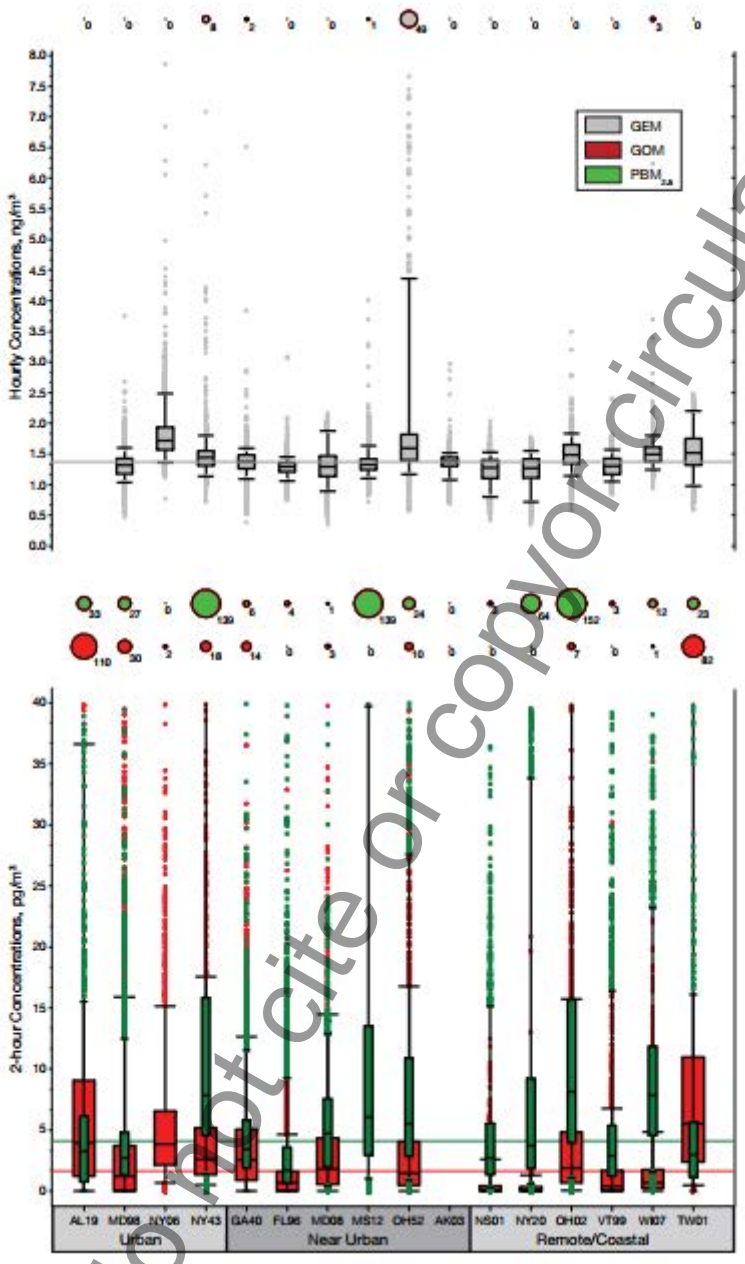

Figure 5: Hourly GEM concentrations in ng/m3 for each AMNet site (top) and 2-hour GOM and PBM2.5 concentrations in pg/m3 for each AMNet site (bottom), 2015. The bubble charts indicate the number of valid observations for GEM values above 8 ng/m3, and GOM and PBM2.5 above 40 pg/m3, the upper limit shown with the box plots. Horizontal lines in each graph represent the respective 2015 median values. From NADP, 2016.

Reference: National Atmospheric Deposition Program, 2016. National Atmospheric Deposition Program 2015 Annual Summary. NADP Data Report 2016-02. Illinois State Water Survey, University of Illinois at Urbana-Champaign, IL.

3.2.5 Environment and Climate Change Canada – Atmospheric Mercury Monitoring

Since 1994, considerable atmospheric Hg monitoring has taken place across Canada as well as many focused Hg research projects. The parameters measured have evolved over time and the breadth and volume of data collected are significant. Atmospheric monitoring in Canada is undertaken to serve 3 main goals: 1) To measure atmospheric input/deposition into vulnerable Canadian ecosystems; 2) To measure ambient levels of mercury resulting from domestic and regional emission sources and 3) To assess transboundary transport of mercury into and around Canada[1]. Ongoing continuous monitoring of Hg in Canada has been rationalized, in part, because Canada has been shown to be a net recipient of mercury, by means of atmospheric transport and deposition (ECCC 2016).

Most monitoring in Canada began as independent research programs to measure TGM in the early 1990s. Since that time, the number and location of measurement sites has changed and, as of 2017, the current sites for atmospheric mercury monitoring have been consolidated and fall under *Environment and Climate Change Canada – Atmospheric Mercury Monitoring or ECCC-AMM network*. Table 8 shows all the atmospheric Hg measurements that have been taken across Canada (current sites are highlighted in grey) and Figure 6 shows the time periods over which measurements were made at each location. In 1996, Canada joined the United States-led Mercury Deposition Network (MDN) and began collecting wet deposition samples for THg and, at some sites, methyl mercury (MeHg). The sites where these precipitation measurements have been made over time are listed in Table 8. Finally, during the early 2000s, to meet increasing research needs, considerable advancements were made in instrument capabilities to collect and analyse Hg species in the air. From 2002 onward, some sites began continuous measurements that could distinguish among GEM, GOM and PBM (collectively termed speciated atmospheric mercury). The sites which have made these measurements over time are also listed in Table 8. As of December 2017, the ECCC-AMM monitors TGM at 11 sites, atmospheric speciated mercury at 4 sites and wet deposition at 6 sites; Figure 7 shows a map of the active ECCC-AMM sites.

[1] A description of which sites address these goals is in the Canadian Mercury Science Assessment – Summary of Key Results (ECCC, 2016).

6320 **Table 8:** Mean concentrations of mercury data collected in Canada, the location of each site and the time
6321 period over when measurements were collected.

Station	Long (°W) Lat (°W)	Measurement period TGM	Mean TGM (ng m^{-3})	Measurement period Speciated Hg	Mean GEM (ng m^{-3})	Mean GOM (pg m^{-3})	Mean PBM (pg m^{-3})	Measurement period wet deposition	Mean Total Hg (ng L^{-1})
Little Fox Lake YK [a,g]	135.63 61.35	Jun 2007 – Dec 2016	1.39 ± 0.15	-	-	-	-	-	-
Ucluelet BC [b]	125.54 48.92	Aug 2013 – Dec 2016	1.34 ± 0.13	-	-	-	-	-	-
Reifel Island BC [c, d]	123.17 49.10	Mar 1999 – Feb 2004	1.67 ± 0.19	-	-	-	-	Apr 2000 – Feb 2004	5.6
Saturna BC [c, d, e]	123.13 48.78	Feb 2010 – Aug 2016	1.31 ± 0.16	-	-	-	-	Sep 2009 – Dec 2015	5.2
Whistler BC [b]	122.93 50.07	Aug 2008 – Dec 2015	1.26 ± 0.20	-	-	-	-	-	-
Fort Vermilion AB [f]	116.02 58.38	-	-	-	-	-	-	Dec 2006 – Jan 2008	4.3
Meadows AB	114.64 53.53	May 2005 – Dec 2008	1.51 ± 0.21	-	-	-	-	-	-
Genesee AB [b,d]	114.20 53.30	Mar 2004 – Dec 2010	1.53 ± 0.25	Jan 2009 - Dec 2010	1.38 ± 0.17	5.0 ± 4.6	5.0 ± 4.3	Jul 2006 – Dec 2015	11.6
Crossfield AB [f]	114.00 51.29	-	-	-	-	-	-	May 2006 – Dec 2007	9.3
Fort Chipewyan AB [c]	111.12 58.78	Jun 2000 – July 2001	1.36 ± 0.15	-	-	-	-	-	-
Henry Kroeger AB [d]	110.83 51.42	-	-	-	-	-	-	Oct 2004 – Dec 2015	12.3
Esther AB [d, e]	110.20 51.67	Jun 1998 – Apr 2001	1.65 ± 0.15					Apr 2000 – May 2001	14.9
Fort McKay South AB [h]	111.64 57.15	Jan 2016 – Dec 2016	1.24 ± 0.38	Aug 2013 – Dec 2016	1.18 ± 0.19	0.7 ± 1.5	4.4 ± 8.7	-	-
Patricia McInnis AB [h]	111.48 56.75	Oct 2010 – Dec 2016	1.32 ± 0.22	-	-	-	-	-	-
Pinehouse Lake SK [e]	106.725 55.5121							May 2015 – Dec 2015	8.4
Bratt's Lake SK [d,e]	104.71 50.20	May 2001 – Apr 2013	1.44 ± 0.24	-	-	-	-	Jun 2001 – Apr 2013	11.3
Flin Flon MB [b]	101.88 54.77	Jul 2008 – Dec 2016	3.23 ± 1.87	Jul 2010 – Mar 2011	2.04 ± 0.58	3.9 ± 8.4	11 ± 16	Sep 2009 – Dec 2010	59.9
ELA ON [d,e,]	93.72 49.66	-	-					Nov 2009 – Jan 2011	13.4
Burnt Island ON [c]	82.95 45.81	May 1998 – Dec 2007	1.55 ± 0.22					Dec 2001 – Mar 2003	10.1
Egbert ON [c,d,e]	79.78 44.23	Dec 1996 – Dec 2016	1.51 ± 0.31	-	-	-	-	Mar 2000 – Dec 2015	8.1
Kuujjuarapik QC [c]	77.73 55.30	Aug 1999 – Sep 2009	1.68 ± 0.46	-	-	-	-	-	-
Point Petre ON [c]	77.15 43.84	Nov 1996 – Dec 2007	1.75 ± 0.33	-	-	-	-	Nov 2001 – Mar 2003	8.4
Chapais QC [d,e]	74.98 49.82	-	-	-	-	-	-	Dec 2009 – Dec 2015	5.2
St. Anicet QC [b,c,d]	74.03 45.20	Aug 1994 – Dec 2016	1.53 ± 0.35	Jan 2003 – Dec 2015	1.43 ± 0.30	2.7 ± 4.1	17.2 ± 25.8	Apr 1998 – Aug 2007	8.0
St. Andrews NB [c,d]	67.08 45.08	Jan 1996 – Jul 2007	1.38 ± 0.24	-	-	-	-	Jul 1996 – Dec 2003	6.5
Kejimkujik NS [c,d,e]	65.21 44.43	Jan 1996 – Dec 2016	1.36 ± 0.28	Jan 2009 – Dec 2016	1.31 ± 0.20	0.6 ± 1.3	5.4 ± 8.8	Jul 1996 – Dec 2015	5.1
Mingan QC [b,c]	64.17 50.27	Jan 1997 – Dec 2015	1.42 ± 0.23	-	-	-	-	Apr 1998 – Aug 2007	5.1
Halifax NS [b]	63.67 44.67			Oct 2009 – Dec 2011	1.53 ± 0.42	2.0 ± 2.1	2.1 ± 1.8		
Southampton PE [c]	62.58 46.39	Jan 2005 – Dec 2006	1.23 ± 0.19	-	-	-	-	-	-

Alert NU [a]	62.33 82.50	Jan 1995 – Dec 2016	1.47 ± 0.38	Jan 2002 – Dec 2016	1.25 ± 0.40	25 ± 54	42 ± 77	-	-
Stephenville NL [d,e]	58.57 48.56	-	-	-	-	-	-	Feb 2010 – Dec 2015	5.2
Cormak NL [d,e]	57.38 49.32	-	-	-	-	-	-	May 2000 – Jul 2010	4.3

Legend: a-h are the previous network names under which the data were collected: a) Northern Contaminants Program (NCP); b) Clean Air Regulatory Agenda Mercury Science Program (CARA) currently Climate Change and Air Pollution program (CCAP); c) Canadian Atmospheric Mercury Measurement Network (CAMNet); d) The Mercury Deposition Network (MDN); e) The Canadian Air and Precipitation Monitoring Network (CAPMoN); f) Geological Survey of Canada (GSC); g) Intercontinental Atmospheric Transport of Anthropogenic Pollutants to the Arctic (INCATPA); h) Joint Oil Sands Monitoring Program (JOSM). Long = Longitude; Lat = Latitude. Note: Fort McKay south is collecting THg as of October 2017, no results were available at the time of writing.

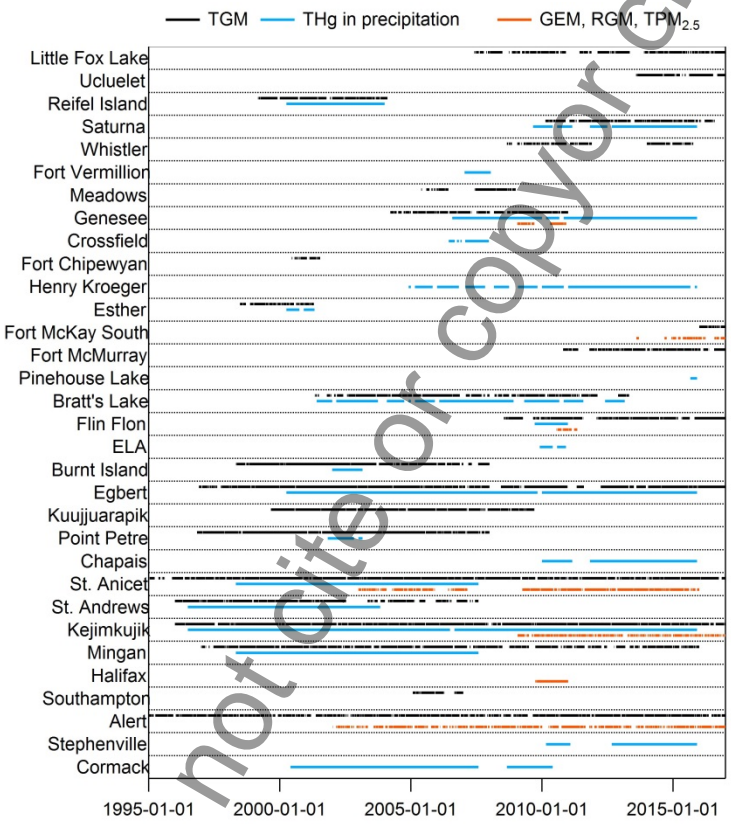

Figure 6: Time period of mercury measurements at Canadian monitoring sites

From the measurements collected over the past 20+ years, concentration levels of TGM in Canada are generally within the ranges reported by other northern hemispherical countries, with some exceptions. One exception is the annual concentrations reported from Alert (located in the high Arctic) which are, in general, lower than the national average, with low GEM levels and high speciated mercury concentration levels (Steffen et al., 2008 and 2014). This difference is seen at many coastal Arctic locations and is primarily explained by the springtime chemistry known as Atmospheric Mercury Depletion Events (AMDEs). The other Canadian location that deviates from the norm is Flin Flon, Manitoba, which shows

higher concentrations than the national average. Flin Flon was the location of Canada's largest copper and zinc smelter from 1927 to its closure in 2010. While mercury levels have decreased over time since the closure; atmospheric mercury concentration levels around this site remain the highest in Canada. These levels are attributed to the re-emission of previously deposited mercury in the vicinity of the smelter (ECCC, 2017). The remainder of the sites in Canada have distinct seasonal and diurnal patterns reflective of the surrounding environment (be it rural or urban) (Cole et al., 2014).

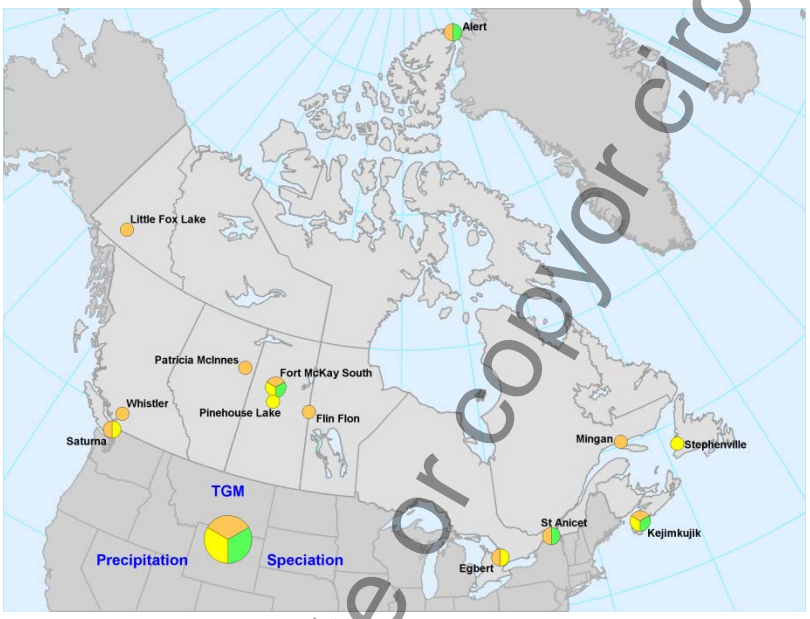

Figure 7: Environment and Climate Change Canada – Atmospheric Mercury Monitoring sites currently operating in Canada as of December 2017.
Measurements include: TGM (total gaseous mercury) - orange; speciated mercury - green (gaseous elemental mercury, reactive gaseous mercury and total particulate mercury) and precipitation – yellow (total mercury (THg (wet))

Trends of mercury over time, including TGM, speciated mercury and THg (wet) mercury in precipitation (Cole et al., 2014), have been investigated for several Canadian measurement sites. Updated trends of monthly median TGM and monthly volume-weighted mean concentrations of mercury in precipitation (total mercury or THg) are listed in Table 9. The most recent available data were used in the analysis, where monthly values were deemed valid with at least 75% data coverage, and a minimum of 5 years of data were required to perform the trend analysis. Trends were calculated using the seasonal Kendall test for trend and the related Sen's slope calculation (Gilbert, 1987; van Belle and Hughes, 1984). This method is an extension of the non-parametric Mann-Kendall test for trend, which is recommended when there are missing values and when the data are not normally distributed; both of these conditions apply to these datasets.[2] The areas shaded in blue in Table 8 are currently operated sites in Canada as of December

[2] In the seasonal Kendall method, data from the 12 months are treated as 12 separate datasets. For each month, the presence of a trend is confirmed or rejected by the Mann-Kendall test, and a slope is estimated using Sen's nonparametric estimator of slope. An overall annual trend is

2017. Monthly long-term trends for speciated mercury have been made for some sites in Canada (Cole et al., 2014); however, they do vary greatly by season and are not easily summarized by an overall annual trend. Therefore, they are not included in Table 9.

Table 9: Annual trends over time of mercury data collected in Canada

Station	Measurement period TGM	Trend TGM (% yr^{-1})	Measurement period wet deposition	Trend Total Hg (THg) in precip
Little Fox Lake YK	Jun 2007 – Dec 2016	+1.3 (+0.7 to +1.9)	-	-
Reifel Island BC	Mar 1999 – Feb 2004	-3.3 (-4.2 to -2.4)	-	-
Saturna BC	Feb 2010 – Aug 2016	-4.1 (-5.1 to -2.2)	Sep 2009 – Dec 2015	ns (-2.5 to +6.7)
Genesee AB	Mar 2004 – Dec 2010	-0.4 (ns) (-1.4 to +0.1)	Jul 2006 – Dec 2015	ns (-6.6 to +0.3)
Patricia McInnis AB	Oct 2010 – Dec 2016	-3.6 (-5.4 to -2.1)	-	-
Henry Kroeger AB	-	-	Oct 2004 – Dec 2015	ns (-4.2 to +3.8)
Bratt's Lake SK	Nov 2001 – Apr 2013	-1.5 (-2.3 to -0.9)	Jun 2001 – Apr 2013	ns (-2.7 to +4.1)
Flin Flon MB	Jul 2008 – Dec 2016	-4.2 (-6.5 to -2.4)	-	-
Burnt Island ON	May 1998 – Nov 2007	-2.5 (-3.4 to -1.6)	-	-
Egbert ON	Dec 1996 – Dec 2016	-1.7 (-1.9 to -1.5)	Apr 2000 – Dec 2015	ns (-1.2 to +0.6)
Point Petre ON	Nov 1996 – Nov 2007	-1.7 (-2.2 to -1.2)	-	-
Chapais QC	-	-	Dec 2009 – Dec 2015	-6.4 (-10.8 to -1.8)
Mingan QC	Jan 1997 – Dec 2015	-1.1 (-1.4 to -0.9)	Apr 1998 – Aug 2007	ns (-5.1 to +0.5)
St. Anicet QC	Jan 1995 – Dec 2016	-1.5 (-1.6 to -1.3)	May 1998 – Aug 2007	-3.0 (-5.3 to -1.0)
St. Andrews NB	Jan 1996 – Jun 2007	-1.0 (-1.4 to -0.5)	Jul 1996 – Dec 2003	ns (-7.0 to +0.5)
Kejimkujik NS	Jan 1996 – Dec 2016	-0.9 (-1.1 to -0.7)	Jul 1996 – Dec 2015	-1.5 (-2.3 to -0.8)
Alert NU	Apr 1995 – Dec 2016	-0.9 (-1.1 to -0.7)		
Cormak NF			May 2000 – Jul 2010	ns (-3.5 to +0.5)

The trends in the TGM data show that for most sites in Canada there are decreasing levels of mercury. Figure 8 shows the trends for both TGM and THg based on the more recent data. Stations in Figure 8 are oriented from western to eastern Canada. The blue bars represent TGM, the green bars represent THg and the starred bars indicate that no significant trend was determined. If the bar is above zero, the trend is increasing, and if it is below zero the trend is decreasing. The only location reporting an increasing trend in the TGM concentration is Little Fox Lake, Yukon. Conversely, all other locations indicate decreasing

estimated from the monthly trend statistics; however, this estimate may be questionable if the monthly trends are not homogeneous. Thus, to ensure reliability of the data, a test for seasonal homogeneity was performed as well. If seasonal trends were homogeneous, the results were used to determine an overall trend for the entire period. The disadvantage of this technique is that it produces a linear trend over the entire period and can miss complex patterns such as a decrease followed by an increase.

trends. The THg wet deposition data shows decreasing trends at 3 eastern locations (St Anicet, Chapais and Kejimikujik). No statistically significant increases or decreases were observed at other sites. This is consistent with other reports of THg in wet deposition in North America (Weiss-Penzias et al., 2016). The majority of the TGM decreasing trends in Canada shown in Figure 7 reflect typical northern hemispherical declines (Cole et al., 2014; Zhang et al., 2016 and Zhou et al., 2017) or declines reflective of changes in local emissions (e.g. Flin Flon). These decreases are primarily resulting from decreases in regional emission changes. The decrease at Alert is less than that at other sites, likely a reflection of northern hemispheric background levels decreasing in addition to the Arctic atmospheric chemistry processes that occur at this site (Cole et al., 2013). Interestingly in the recent trend analysis, Kejimikujik shows the same low % decrease as Alert than other locations in Canada. This shift to a lower decreasing trend could result from both decreases in emissions in the area (Zhou et al, 2017) and potential increases in the release of mercury from the nearby ocean (Amos, 2013). The increasing trend reported in the Yukon site is still being investigated; however, analysis of long-range transport events of mercury to Little Fox Lake indicates that Asia significantly contributes to the ambient mercury levels (Dastoor et al., 2015).

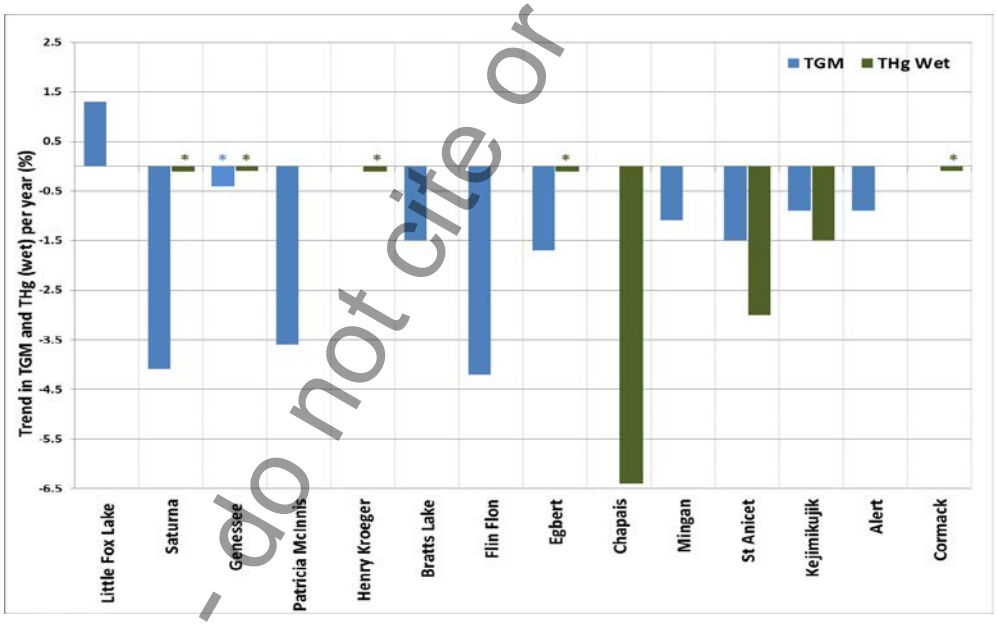

Figure 8: Trend as expressed as a percent per year for total gaseous mercury (TGM) and total mercury (THg) from wet deposition in Canada from most current data including the data ending in 2010 for some sites. Blue bars indicate trends for TGM, green bars indicate trends for THg (wet deposition) and bars with an asterisk indicate trends that are not statistically significant.

3.2.6 Atmospheric mercury in Asia

Before the establishment of the GMOS global network, independent programs and networks for monitoring atmospheric Hg species and deposition have been developed in Asia, including those in Korea, Japan and China supported by the National Science Foundation in each of the Asian countries and region. Since 2010, some of these Asian sites have been incorporated within the global network (Sprovieri et al., 2016), including Mt. Waliguan, Mt. Ailao, Shangri-La and Mt. Changbai in mainland China, Lulin in Taiwan, Cape Hedo, Okinawa and Minamata, Kyushu islands in Japan, Kanghwa Island in Korea, and Kodaikanal in India. A statistical summary of speciated atmospheric Hg concentrations and associated site information (urban and remote areas) in Asia is shown in Table 10 whereas Table 11 reports Hg concentrations and deposition fluxes in precipitation, throughfall, and litterfall. GEM and PBM concentrations recorded at remote Chinese sites are elevated compared to that observed at background/remote areas in Europe and North America, and at other sites in the Northern Hemisphere (Sprovieri et al., 2016; Fu et al., 2015). In Chinese urban areas, the highly elevated GEM, GOM and PBM were mainly derived from local anthropogenic Hg emissions, whereas regional anthropogenic emissions and long-range transport from domestic source regions are the primary causes of the elevated GEM and PBM concentrations at remote sites (Fu et al., 2015). Mean GOM concentrations at remote sites in China ranged from 2.2 to 10.1 pgm^{-3}, significantly lower than those observed in the Chinese urban areas but comparable to the values in Europe and North America (Fu et al., 2015; Table 4).

Wet-only deposition fluxes of THg and MeHg ranged between 1.8–7.0 $\mu gm^{-2}\ yr^{-1}$ and 0.01–0.06 $\mu gm^{-2}yr^{-1}$, respectively, at remote sites, and 13.4-56.5 $\mu gm^{-2}yr^{-1}$ and 0.05–0.28 $\mu gm^{-2}yr^{-1}$ at urban sites, respectively. Wet deposition fluxes of THg and MeHg at urban sites in China were higher compared to those in North America and Europe, but wet deposition fluxes of THg at remote sites were in the lower range of those observed in North America and Europe. Regarding the Chinese GMOS sites, details on THg recorded from 2011 to 2015 are reported in Table 11.

Table 10: Atmospheric Hg concentrations at ground-based stations in Asia (Fu et al., 2015).

Site	Country	Elev (m asl)	Lat	Lon	Type	Study period	TGM or GEM Mean ± St.Dev. (ng m^{-3})	PBM/TPM Mean ± St.Dev. (pg m^{-3})	GOM Mean ± St.Dev. (pg m^{-3})	Reference
An-myun	Korea	45.7	36.533°N	126.317°E	Background	12/2004-04/2006	4.61±2.21	-	-	Nguyen et al. (2007)
Beijing	China	48	38.898° N	116.392° E	Urban	02&09/1998	10.4±3.25	-	-	Liu et al. (2002)
						01-12/2006	-	272	-	Schleicher et

							-	573±551*	-	al. (2015)
Cape Hedo	Japan	60	26.864° N	128.251° E	Background	04/2009 – 03/2017	1.86±0.22	2.6±0.9	1.6±0.5	www.env.go.jp/press/104568.html
Changchun	China	270	43.824° N	125.319° E	Urban	-/2001	18.4	276*	-	Fang et al. (2004)
Chemgshantou	China	30	37.38° N	122.68° E	Remote coast	07&10/2007, 01&04/2009	2.31±0.74	-	-	Ci et al. (2011)
Chongming Island	China	11	31.522° N	121.908° E	Remote coast	2009-09-12	2.5±1.50	-	-	Dou et al. (2013)
Chongqing	China	350	29.6° N	106.5° E	Urban	08/2006-09/2007	6.74±0.37	-	-	Yang et al. (2009)
Chuncheon	Rep.Korea	120	37.999ºN	127.810E	Residential town	03-12/2006	1.580.62	-	-	Han et al., 2014
						01-12/2007	2.41±1.56	4.7±4.3	2.7±3.2	
						01/2008-02/2009	2.52±1.8	2.5±3.2	2.8±2.4	
Guangzhou	China	60	23.124° N	113.355° E	Urban	11/2010-10/2011	4.6±1.60	-	-	Chen et al. (2013)
Guiyang	China	1040	26.57°N	106.72° E	Urban	11/2011-11/2012	8.4±4.87	-	-	Feng et al. (2004)
						12/2009-11/2010	10.2±7.06	-	-	Fu and Feng (2015)
						08-12/2009	9.72±10.2	368±276	35.7±43.9	Fu et al. (2011)
Jeju Island (Go-san)	Rep.Korea	67	33.294 ºN	126.163 ºE	Remote coast/ Background	2014-2016	0.55±0.88	-	-	www.airkorea.or.kr
Jiaxing	China	10	30.833° N	120.7° E	Urban	09/2005	5.4±4.10	-	-	Wang et al. (2007)
Lanzhou	China	1540	36.067° N	103.79° E	Urban	-/2004	28.6	-	-	Su et al. (2007)
						04&07&10&12/1994	-	955*	-	Duan and Yang (1995)
Lulin	Chinese Taipei	2862	23.51°N	120.92° E	Background	04/2006-12/2007	1.73±0.61	2.3±3.9	12.1±20.0	Sheu et al. (2010)
Minamata[T]	Japan	20	32.231°N	130.403° E	Rural	04/2011-12/2014	1.89±0.43	-	-	Sprovieri et al. (2016a)
Miyun	China	220	40.481°N	116.775° E	Remote forest	12/2008-11/2009	3.22±1.94	98.2±113	10.1±18.8	Zhang er al. (2013)
Mt. Ailao	China	2450	24.533°N	101.017° E	Remote forest	05/2011-05/2012	2.09±0.63	31.3±28.0	2.2±2.3	Zhang et al. (2015b)
Mt. Changbai	China	740	42.402°N	128.112° E	Remote forest	10/2008-10/2010	1.6±0.51	-	-	Fu et al. (2012b)
						07/2013-07/2014	1.73±0.48	18.9±15.6	5.7±6.8	Fu et al. (2014)
Mt. Damei	China	550	29.632°N	121.565° E	Remote forest	04/2011-04/2013	3.31±1.44	154±104	6.3±3.9	Yu et al. (2015)
Mt. Dinghu	China	700	23.164°N	112.549° E	Remote forest	09/2009-04/2010	5.07±2.89	-	-	Chen et al. (2013)
Mt. Gongga	China	1640	29.649° N	102.117° E	Remote forest	05/2005-07/2007	3.98±1.62	30.7±32.0*	6.2±3.9	Fu et al. (2008)
Mt. Jiuxian	China	1700	25.71° N	118.11° E	Remote forest	11/2010. 01&04&08/2010	-	24.0±14.6	-	Xu et al. (2013)
Mt. Leigong	China	2178	26.39° N	108.2° E	Remote forest	05/2008-05/2009	2.8±1.51	-	-	Fu et al. (2010)
Mt. Walinguan	China	3816	36.287°N	100.898°E	Remote grassland	09/2007-09/2008	1.98±0.98	19.4±18.0	7.4±4.8	Fu et al. (2012a)
Nanjing	China	100	32.05° N	118.78° E	Urban	01-12/2011	7.9±7.00	-	-	Zhu et al. (2012)
						06/2011-02/2012	-	1100±570*	-	Zhu et al. (2014)
Ningbo	China	10	29.867° N	121.544° E	Urban	10/2007-01/2008	3.79±1.29	-	-	Nguyen et al. (2011)

Pohang	Rep.Korea	10	35.992ºN	129.404ºE	Urban/Industry	08&10/2012, 01&03&04/2013	5.00±4.70	-	-	Seo et al. (2016)
Qingdao	China	40	36.16° N	120.5° E	Urban	01/2013	2.8±0.90	245±174*	-	Zhang er al. (2014)
Seoul	Rep.Korea	77	37.610 ºN	126.934 ºE	Urban	2014-2016	2.15±1.21	-	-	www.airkorea.or.kr
Seoul	Rep.Korea	17	37.514ºN	127.001ºE	Urban	02/2005~12/2006	3.44±2.13	-	-	Choi et al. (2009)
Seoul	Rep.Korea	17	37.514ºN	127.001ºE	Urban	01/2006~12/2009	-	16.7±23.7	11.7±15.1	Seo et al. (2015)
Shangai	China	19	31.23° N	121.54° E	Urban	08-09/2009	2.7±1.70	-	-	Friedli et al. (2011)
						07/2004-04/2006	-	560±220*	-	Xiu et al. (2009)
Shangri-La	China	3580	28.017° N	99.733° E	Remote forest	11/2009-10/2010	2.55±2.73	37.8±31.0	7.9±7.9	Zhang er al. (2015)
Southeastern coastal cities	China	-	-	-	Urban	11/2010, 01&04&08/2011	-	141±128	-	Xu et al. (2013)
Tae-An	Rep.Korea	23	36.738 ºN	126.133 ºE	Rural	2014-2016	2.15±1.29	-	-	www.airkorea.or.kr
Tokai-mura	Japan	15	36.27°N	140.36°E	Urban	10/2005-08/2006	3.78±1.62	-	-	Osawa et al. (2007)
Wanqingsha	China	3	22.7° N	113.55° E	Remote coast	2009-11-12	2.94	-	-	Li et al. (2011)
Wuhan	China	20	30.6° N	114.3° E	Urban	-/2002	14.8	-	-	Xiang and Liu (2008)
Xiamen	China	7	24.60° N	118.05° E	Urban	03/2012-02/2013	3.5	174±280	61.0±69.0	Xu et al. (2015)
Yongheung island	Rep.Korea	32	37.279 ºN	126.457 ºE	Rural / but, coal-fired power plant is located.	01/2013-08/2014	2.8±1.10	10.9±11.2	8.3±9.7	Xu et al. (2015)

(PBM/TPM: * Indicates TPM, otherwise indicates PBM.)

6426 **Table 11:** Hg concentrations and deposition fluxes in precipitation, throughfall, and litterfall in China (from Fu et al., 2015).

Site	Elev (m asl)	Lat	Lat	Type	Study period	Samples	Hg concentration (ng L^{-1} or ng g^{-1})		Deposition flux (μg m^{-2} yr^{-1})		Reference
							THg	MeHg	THg	MeHg	
Chuncheon, Korea	120	37.999	127.810	Residential town	08/2006-07/2008	Precipitation	8.8	-	9.4	-	Ahn et al., 2011
Jeju Island (Go-san), Korea	67	33.294	126.163	Remote coast/Back ground	04/2015-11/2016	Precipitation	5.3	-	8.4	-	Kim et al., 2016
Seoul, Korea	77	37.610	126.934	Urban	04/2015-11/2016	Precipitation	12	-	19	-	Kim et al., 2016
Tae-An. Korea	23	36.738	12.133	Rural	04/2015-11/2016	Precipitation	21	-	11	-	Kim et al., 2017
Mt. Ailao, Yunnan	2500	24.53	24.53	Remote	06/2011-05/2012	Precipitation	3.0	-	5.4	-	Zhou et al. (2013)
						Litterfall	54.0	-	71.2	-	
Mt. Leigong, Guizhou	2178	26.39	26.39	Remote	05/2008-05/2009	Precipitation	4.0	0.04	6.1	0.06	Fu et al. (2010b)
						Throughfall	8.9	0.1	10.5	0.12	
						Litterfall	91.0	0.48	39.5	0.28	
Mt. Damei, Zhejiang	550	29.63	29.63	Remote	08/2012-07/2013	Precipitation	4.1	-	7.0	-	Lang (2014)
						Litterfall	46.6	-	26.0	-	
Nam Co, Tibet	4730	30.77	30.77	Remote	07/2009-07/2011	Precipitation	4.8	0.03	1.8	0.01	Huang et al. (2012)
Mt. Gongga[1], Suchuan	1640	29.65	29.65	Remote	2006-01-12	Precipitation*	9.9	-	9.1	-	Fu et al. (2008)
Mt. Gongga[2], Suchuan	3000	29.58	29.58	Remote	05/2005-04/2007	Precipitation*	14.2	0.16	26.1	0.3	Fu et al. (2010a)
						Throughfall	40.2	0.3	57.1	0.43	
						Litterfall	35.7	-	35.5	-	
Mt. Changbai, Jilin	750	42.40	42.40	Remote	08/2005-07/2006	Precipitation*	13.4	-	8.4	-	Wan et al. (2000a)
Puding, Guizhou	1145	26.37	26.37	Remote	08/2005-07/2006	Precipitation*	20.6	0.18	24.8	0.22	Guo et al. (2008)
Hongjiadu, Guizhou	1130	26.88	26.88	Remote	08/2005-07/2006	Precipitation*	39.4	0.18	34.7	0.16	Guo et al. (2008)
Yinzidu, Guizhou	1088	26.57	26.57	Remote	08/2005-07/2006	Precipitation*	35.7	0.18	38.1	0.19	Guo et al. (2008)
Dongfeng, Guizhou	970	26.85	26.85	Remote	08/2005-07/2006	Precipitation*	37.4	0.2	36.3	0.19	Guo et al. (2008)

Wujiangdu, Guizhou		27.32	27.32	Remote	08/2005-07/2006	Precipitation*	57.1	0.25	39.6	0.17	Guo et al. (2008)
Guiyang	1040	26.57	26.57	Urban	2008-07-09	Precipitation	13.3	0.05	13.4	0.05	Liu et al. (2011)
Xiamen	50	24.60	24.60	Urban	07/2013-02/2014	Precipitation	26.6	-	30.4	-	Wu (2014)
Chongqing				Urban	06/2010-06/2011	Precipitation	30.7	0.31	28.7	0.28	Wang et al. (2012); Y.M. Wang et al. (2014)
Tieshanping, Chongqing	500	29.63	29.63	Urban	03/2005-03/2006	Precipitation	32.3	-	29.0	-	Wang er al. (2009)
						Throughfall	69.7	-	71.3	-	
						Litterfall	105	-	220	-	
Nanjing	100	32.05	32.05	Urban	06/2011-02/2012	Precipitation	52.9	-	56.5	-	Zhu et al. (2014)

(Precipitation: * indicates bulk precipitation, otherwise indicates wet-only precipitation. Mt. Gongga: 1 elevation of the sampling site was 1600m above sea level. 2 Elevation of the sampling site was 3000m above sea level).

3.2.7 Mercury concentrations and pattern analysis in polar areas (Arctic and Antarctica)

The Arctic Monitoring and Assessment Programme (AMAP) established in 1991, is a coordinated air monitoring programme covering the circum Arctic are as of North America and Eurasia. The AMAP programme has an active ambient air Hg monitoring component with sites in Canada, USA, Russia, Norway and Greenland (Denmark). The Global Atmospheric Watch (GAW) site at Alert operated by Environment and Climate Change Canada – and funded through the Northern Contaminants Program (NCP) of Indigenous and Northern Affairs Canada (INAC) – has the longest continuous record of GEM (22 years) and Hg speciation (15 years) in the Arctic (Cole et al., 2013; Steffen et al., 2014). Continuous monitoring for long periods has also occurred at: (1) Amderma (Russia) (Steffen et al., 2005), (2) GAW Ny-Ålesund 'Zeppelin' site (Svalbard,Norway) (Berg et al., 2013), (3) AMAP Villum Research Station at Station Nord (hereafter named Station Nord, Greenland-Denmark) (Skov et al., 2004) and (4) Andøya (northern Norway) (Berg et al., 2001). Four multi-year records over the 2011-2015 period from high arctic (Alert, Station Nord and Zeppelin) and European sub-arctic (Andøya) sites were recently analysed (Angot et al., 2016a). Additionally, summer time measurements were performed in 2004 over the North Atlantic Ocean (Aspmo et al., 2004), and in 2005, 2010 and 2012 in the marine boundary layer over the Arctic Ocean (Sommar et al., 2010, Yu et al., 2014).

Table 12: Annually based statistics (number of hourly-averaged data (n.), mean, median, standard deviation (SD), of GEM concentrations (in ng m^{-3}) at ground-based polar sites over the 2011-2015 period.

		ALT	SND	NYA	AND	TR	DC	DDU
2011	*n*	8040	4712	8173	7444	5978	NA	NA
	mean	1.39	1.26	1.51	1.61	0.95	NA	NA
	median	1.35	1.34	1.59	1.61	0.99	NA	NA
	SD	0.45	0.32	1.61	0.15	0.20	NA	NA
2012	*n*	8447	7932	8181	8428	7808	3761	5949
	mean	1.21	1.44	1.51	1.61	0.98	0.76	0.91
	median	1.21	1.44	1.54	1.61	0.97	0.70	0.92
	SD	0.35	0.26	0.21	0.13	0.15	0.24	0.20
2013	*n*	8048	6605	6980	7862	8197	2900	5121
	mean	1.31	1.57	1.47	1.53	0.90	0.84	0.85
	median	1.39	1.49	1.52	1.56	0.93	0.87	0.85
	SD	0.46	0.44	0.30	0.15	0.15	0.27	0.19
2014	*n*	8358	4991	6730	8146	7421	NA	1958
	mean	1.45	1.36	1.48	1.50	0.95	NA	0.85
	median	1.45	1.36	1.57	1.51	1.00	NA	0.82
	SD	0.33	0.35	0.33	0.16	0.21	NA	0.38
2015	*n*	NA	1059	8342	7146	3670	8383	3114
	mean	NA	1.11	1.49	1.50	0.94	1.06	0.86
	median	NA	1.11	1.49	1.50	0.93	1.12	0.87
	SD	NA	0.32	0.21	0.10	0.31	0.41	0.19

While the Arctic has been extensively monitored, measurements are more sporadic in Antarctica. Several short-term ambient air measurements campaigns were carried out in summer in the 2000s at Terra Nova

Bay, McMurdo, South Pole and Concordia stations (Sprovieri et al., 2002; Brooks et al., 2008a, b; Dommergue et al., 2012). A year-round record (January 2000-February 2001) was reported at Neumayer (Ebinghaus et al., 2002; Temme et al., 2003) while multi-year records of GEM were initiated at the Norwegian Antarctic Research Station, Troll (TR) in 2007 (Pfaffhuber et al., 2012). In 2012, GMOS (2011-2015) supported the implementation of two other monitoring stations: Dumont d'Urville on the East Antarctic coast and Concordia station on the East Antarctic ice sheet (Angot et al., 2016b, c). Monitoring at Concordia station is now supported by the French Polar Institute IPEV. Additionally, short-term field campaigns dedicated to atmospheric Hg (Nerentorp Mastromonaco et al., 2016; Wang et al., 2016) and Hg deposition (Han et al., 2011; 2014; 2017) were performed in recent years over the Austral Ocean and the East Antarctic ice sheet, producing supplementary data. In Nerentorp Mastromonaco et al., 2016, the authors suggested a seasonal increase of total mercury in the sea-water due to a contribution of Hg(II) deposition combined with contributions from melting sea ice and snow.

First discovered in 1995 (Schroeder et al., 1998), atmospheric mercury depletion events (AMDEs) are observed in springtime throughout the Arctic (Lindberg et al., 2001; Berg et al., 2003a; Poissant and Pilote, 2003; Skov et al., 2004; Steffen et al., 2005) as a result of the oxidation of GEM by reactive bromine species (Lu et al., 2001; Brooks et al., 2006; Sommar et al., 2007). AMDEs can lead to the deposition of ~100 t of mercury per year to the Arctic (Ariya et al., 2004; Skov et al., 2004; Dastoor et al., 2015). The fraction of mercury retained in snowpack during AMDEs is still a matter of debate in the scientific mercury community because a number of studies have observed rapid re-volatilization (Steffen et al., 2008; Soerensen et al., 2016).

Several studies have reported significant re-emission, (e.g., Ferrari et al., 2005; Brooks et al., 2006; Kirk et al., 2006; Sommar et al., 2007; Dommergue et al., 2010a) reducing the amount of mercury that accumulates within the snowpack (Hirdman et al., 2009; Larose et al., 2010). Until today no one has determined a net accumulation based on flux measurements of wet deposition, dry deposition and reemission. During AMDEs, dramatically higher levels of both GOM and / or $PBM_{2.5}$ are observed (Luetal.,2001; Lindberg et al., 2002; Luand Schroeder, 2004; Sprovieri et al.,2005; Steffenetal., 2008). Lindberg et al.(2002) for instance reported GOM concentrations up to 900pg m^{-3} during an AMDE at Barrow (Alaska) and showed a strong positive correlation between GOM production and both UV-B radiation and surface snow Hg concentrations. Preliminary multi-year trends of GOM and $PBM_{2.5}$ concentrations at Alert were analysed (Coleetal.,2013), indicating increases from 2002 to 2009 in both GOM and $PBM_{2.5}$ during spring when concentrations are highest. Steffen et al. (2014) investigated the behaviour of the GOM and $PBM_{2.5}$ over 10 years at Alert and showed that there is a transition to a regime

of high $PBM_{2.5}$ levels in March and April to a regime of high GOM levels in May. This transition was found to be driven by air temperature and presence of springtime particles (sea salts and arctic haze). They further reported that the highest deposition of mercury to the snow occurs when the GOM levels peak and not when $PBM_{2.5}$ levels are highest. They concluded that, using this information, one can predict when the most mercury will be deposited to the snow and ice surfaces in the high Arctic.

Despite the significant challenges in the measurements, the behaviour of mercury over the Arctic sea ice has been investigated (Nghiem et al., 2012; Steffen et al., 2013; Moore et al, 2014). Nghiem et al (2012) showed that the ever decreasing amount of perennial sea ice in the Arctic Ocean will impact the amount of active bromine in this area. Since the depletion of GEM is driven by the bromine photochemistry, the decrease in perennial sea ice will certainly impact the amount of mercury depleted in the atmosphere over the Arctic sea ice. Further, Moore et al. (2014) showed that with the changes of sea ice from perennial to annual, the dynamics of the sea ice also change. Annual sea ice creates more dynamic sea ice, enabling it to provide more turbulence within the ice and produce more open leads. These open leads cause convective forcing of the overlying atmosphere to pull down air masses that contain more mercury than those which are depleted at the surface and replenish the pool of mercury available for conversion and eventual deposition. Finally, it has also been shown that some of the mercury deposited to the surfaces is reemitted to the atmosphere (references above); however, several studies have shown that photo-reduction of the mercury in the snow is dependent on the amount of chlorine in the surface snow (Poulain et al., 2004 and Lehnherr and St Louis, 2009). Thus, the more chlorine in the snow, the less mercury will re-emit. Steffen et al. (2013) demonstrated that there is significantly more GEM re-emitted to the atmosphere from inland snow than from snow over the sea ice. All of these studies combined demonstrate that the mercury chemistry in the Arctic is very dependent on the sea ice and its overlying atmosphere. With significant changes occurring in the Arctic and the dynamics of the sea ice, the springtime mercury cycle will be impacted including the amount of mercury deposited and retained in the Arctic ecosystem.

As presented in Fig. 9, a different seasonal pattern is observed in the high Arctic (ALT, SND, NYA – latitude ranging from 78 to 82°N) as compared to lower latitudes (AND, northern Norway - 69°N). As noted by Angot et al. (2016a), a variability is observed at high Arctic sites in spring due to the occurrence of AMDEs (see above). Summertime (June-August) measurements also differ from what is seen at lower latitudes likely due to re-emission of GEM by the Arctic Ocean and/or by snow surfaces (Angot et al. 2016a and references therein). Yu et al. (2014) reported highly variable GEM concentrations (0.15-4.58 ng m^{-3}) over the central Arctic Ocean in summer, highlighting the need for additional oceanographic campaigns to better understand and constrain oceanic fluxes of GEM.

6519 The analysis of ten-year trends of TGM (GEM+GOM) concentrations (Coleetal.,2013) revealed
6520 discrepancies among Arctic sites. While no trend was observed at Zeppelin station, a slight decreasing
6521 trend (-0.9% per year) was reported at Alert. This difference in trends may be due to several factors
6522 including different air masses origin and local scale processes (e.g., oceanic evasion).

6523

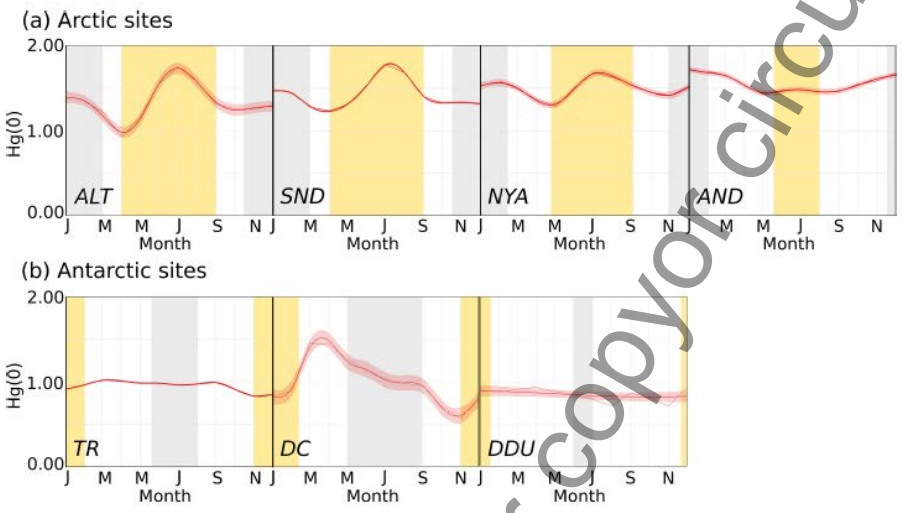

6524
6525 **Figure 9:** Seasonal variation (monthly mean along with the 95% confidence interval for the mean) of
6526 GEM (Hg(0)) concentrations (in ngm^{-3}) at (a) four Arctic and (b) three Antarctic sites for the period
6527 2011-2015 (Angot et al., 2016a). ALT: Alert, SND: Villum Research Station at Station Nord, NYA:
6528 Zeppelin station at Ny-Ålesund, AND: Andøya, TR: Troll, DC: Concordia Station at Dome C, DDU:
6529 Dumont d'Urville. Periods highlighted in yellow (grey) refer to 24h sunlight (darkness).
6530
6531 Similar to the Arctic, AMDEs can be observed at coastal Antarctic sites after polar sunrise (e.g.,
6532 Ebinghaus et al., 2002). However, major differences between the Artic and the Antarctic Hg atmospheric
6533 cycles have been identified in recent studies, primarily because of their different geography; While the
6534 Arctic is a semi-enclosed ocean almost completely surrounded by land, Antarctica is a land mass –
6535 covered with an immense ice shelf – surrounded by ocean. In summer (November to mid-February,
6536 permanent sunlight), GEM concentrations exhibit a distinct diurnal cycle on the East Antarctic ice sheet,
6537 with a maximum at noon, attributed to a dynamic daily cycle of GEM oxidation, deposition to the
6538 snowpack, and re-emission from the snowpack (Dommergue et al., 2012, Angot et al., 2016c, Wang et al.,
6539 2016). Additionally, GEM depletion events can be observed on the ice sheet in summer, with GEM
6540 concentrations remaining low (~ 0.40 ng m^{-3}) for several weeks (Angot et al., 2016c). These depletion
6541 events do not resemble the ones observed in springtime in the Arctic since they are not associated with
6542 depletion of ozone. They are observed when air masses stagnate over the East Antarctic ice sheet, likely
6543 favouring an accumulation of oxidants within the shallow (few hundreds of meters) atmospheric

boundary layer. These observations, along with GOM/ $PBM_{2.5}$concentrations up to 1000 pg m^{-3} recorded at South Pole (Brooks et al., 2008), suggest that the inland atmospheric reservoir is depleted in GEM and enriched in GOM in summer. Observations at coastal Antarctic stations suggest that divalent Hg species produced inland can be transported – due to the large-scale airflow pattern flowing from the East Antarctic ice sheet towards the coast (katabatic winds) – leading to Hg deposition and accumulation in coastal ecosystems (Angot et al., 2016b, Bargagli, 2016). Atmospheric models are currently unable to reproduce this complex reactivity (Angot et al., 2016a). Field studies also show that the sea ice environment is a significant interphase between the polar ocean and the atmosphere and should be accounted for when studying how climate change may affect the mercury cycle in polar regions (Nerentorp Mastromonaco et al., 2016b).

3.2.8 Atmospheric mercury measurements and trends in Europe

Heavy metals were considered by the Convention on Long-Range Transboundary Air Pollution (CLRTAP) beginning in the 1980s. At that time, mercury was only of secondary priority, as it was considered that measurements of the relevant chemical forms, and the understanding of chemistry involved, was not mature enough for any regional scale harmonized monitoring to be initiated (EMEP-CCC, 1985). The European Monitoring and Evaluation Programmes (EMEP) first data report on heavy metals (EMEP, 1986) thus does not include any Hg data, even though the first measurements were already available at that time. By 1990, the number of sites measuring mercury in air had increased to seven, with sites located in Norway, Sweden, Denmark, Germany and the UK. Mercury was included in the first priority list of measurements for the late 1990s, and since then the number of sites have increased gradually. The CLRTAP Aarhus Protocol on Heavy metals was adopted in 1998, and countries agreed to reduce their emission rates compared to year 1990 levels. Currently monitoring efforts include about 37 sites across 17 countries (Fig. 10). Considering all years, the total number of sites is 64 sites and 23 countries.

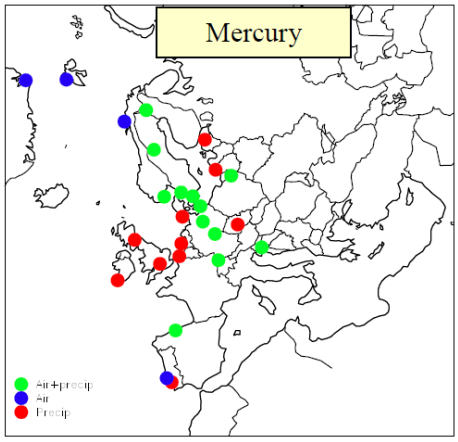

Figure 10: EMEP Mercury observation network.

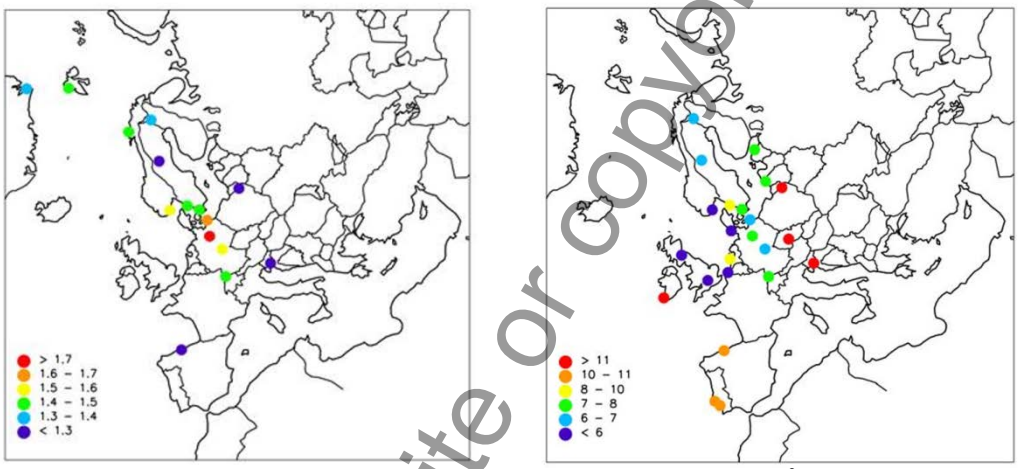

Figure 11: Concentration levels of Mercury in air (left, unit: ng/m^3) and precipitation (right, unit ng/L) at EMEP sites, year 2014.

Compared to other heavy metals, relatively few stations are measuring mercury in precipitation in Europe, and many of them are related to the OSPARCOM programme. There are several sites (in PT, LV, IE) with high detection limits and these are only giving an indication of upper concentration limit. There is no clear regional distribution of mercury in precipitation; the highest concentration is seen at NL0091 with 10 µg/L (when excluding uncertain data from Portugal and Ireland), followed by sites in Czech Republic and Sweden with concentrations of 8 µg/L, while the lowest levels (less than 5 µg/L) are seen in Great Britain.

Annual averages of Hg concentrations in precipitation and in air in 2014 are presented in Figure 11. There is an indication of elevated levels in central Europe as expected due to influence from anthropogenic sources like coal combustion. An interesting observation is that the coastal Arctic sites in Norway has

slightly higher levels than what is observed at Greenland and more inland in Finland and Sweden, which might be due to the summertime evasion from the ocean or due to the fact that Svalbard receives several direct transport episodes from the continent, especially in winter and spring. PL05 and SI08 show unexpected low concentrations, 1.2 ng m^{-3} and 0.8 ng m^{-3} respectively. The latter concentration level is even lower than observed in Antarctica (Pfaffhuber et al, 2012). Given the locations of these stations and the proximity to emission sources, it seems likely there may be a bias in the concentration level for these two sites. This bias is larger at ES08, which has an annual mean of 0.3 ng m^{-3}, which seems improbable.

In precipitation, the highest levels are seen in Eastern Europe (SI, PL and CZ), which seem reasonable since the anthropogenic emission sources are highest in this region. Taking into account that precipitation measurements of mercury are more complex than air measurements, and that the expected measurement uncertainty is 42% (Umweltbundesamt, 2006), the observed concentrations and spatial pattern seems reasonable, for Poland most of the data is below detection limit so it is difficult to fully assess the spatial concentration pattern. Also, Ireland and Portugal report most of the data below detection limit.

Two recent publications and reports present the spatial and temporal trends of mercury in EMEP, namely Tørseth et al. (2012) and Colette et al. (2016). The first paper provides a very broad introductory overview of the full dataset available for the study, but does not go into any details on site level and individual time series. The latter report focuses primarily on the period 1990-2012, and relies heavily on model results from the EMEP-MSC-E model, using official emissions data. An overall assessment based on these two publications is given below.

Figure 12 presents annual time series of mercury measured at sites with long-term data series across Europe. As can be seen, most of these sites are located in Northern Europe, and there are obvious gaps in the time series in the early 1990s. Inter-annual variability is large, but a significant reduction has occurred since. Trends based on this analysis suggest reductions in the order of 5-10% since the late 1990s. More recent work by Zhang et al. (2016) suggests declines of greater than 2% per year since the mid-1990s in Western Europe and a total reduction of greater than 30% due to declines in primary anthropogenic source releases.

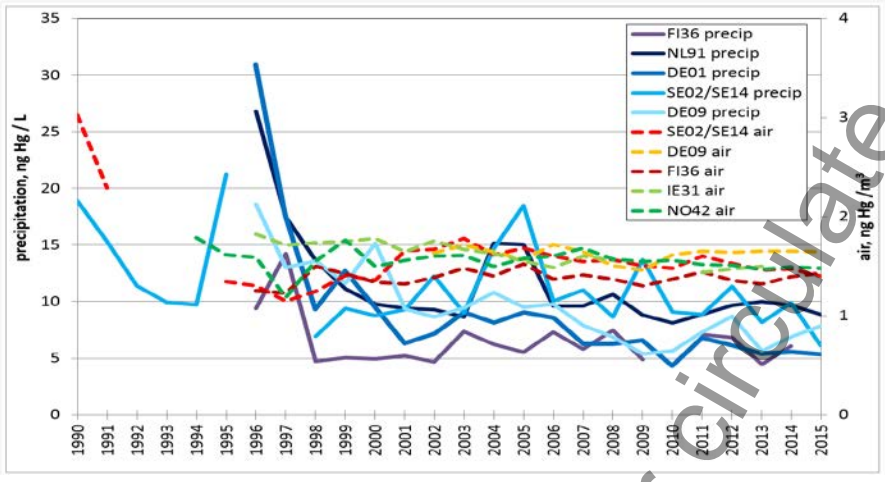

Figure 12: Time series of mercury in air and precipitation at selected EMEP stations, 1990-2015.

Tørseth el al., 2012 also include reference to various studies on trends in emissions and observations, to assess the levels before the late 1980s. They conclude that a major decline of the European Hg emissions occurred at the end of the 1980s. The measurements of TGM for the period from 1980 to about 1993 indicate a dramatic decrease of about 60% in ambient concentrations. Concentration changes reflect the emission change in Europe. Reduced emissions in Europe and the long lifetime of Hg have resulted in an increased focus on non-European sources (HTAP, 2010). Measurements of TGM indicate a dramatic decrease in concentrations during 1980 to about 1993.

For mercury, the European emission sources have been reduced significantly resulting in a relatively large contribution from non-European sources to ambient levels. The monitoring efforts within Europe have gradually improved in Northern Europe, while other regions have little data available.

3.3 Vertical profile and UTLS measurements

3.3.1 Vertical profiles

Vertical profiling of GEM from inside the boundary layer to the free troposphere was carried out during European Tropospheric Mercury Experiment (ETMEP) flights in 2013 (Weigelt et al. 2015). Several flights were performed with a CASA-212 research aircraft equipped with scientific instruments to measure GEM, GOM, and TGM as well as the trace gases CO, O_3, SO_2, NO, NO_2, and meteorological parameters temperature, pressure, and relative humidity. A specially designed gas inlet system was

installed at the aircraft fuselage. In total five vertical profiles were flown over flat and mountainous rural- and industrialized sites in Slovenia and Germany. On the contrary to previously measured vertical profiles, a significant difference between boundary layer- and free tropospheric air was detected. While the free tropospheric overall GEM background concentration over central Europe is ~ 1.3 ng m^{-3}, inside the boundary layer the GEM background concentration was found to be 10 to 30% higher (~ 1.6 ng m^{-3}). At all measurement locations, a clear vertical gradient was not apparent in either the boundary layer or in the free troposphere. This finding indicates that inside the particular layers of the atmosphere, GEM is homogeneously distributed. The combination of ETMEP measurements over Leipzig with CARIBIC measurement over Western Europe (Fig. 13) revealed for the first time a complete vertical profile from 0.5 km (lower boundary layer) to 10.5 km (upper free troposphere). From above the boundary layer to the top of the free troposphere, the GEM background concentration was on average 1.3 ng m^{-3}. All concentrations are given at STP (0°C, 1013.25 hPa).

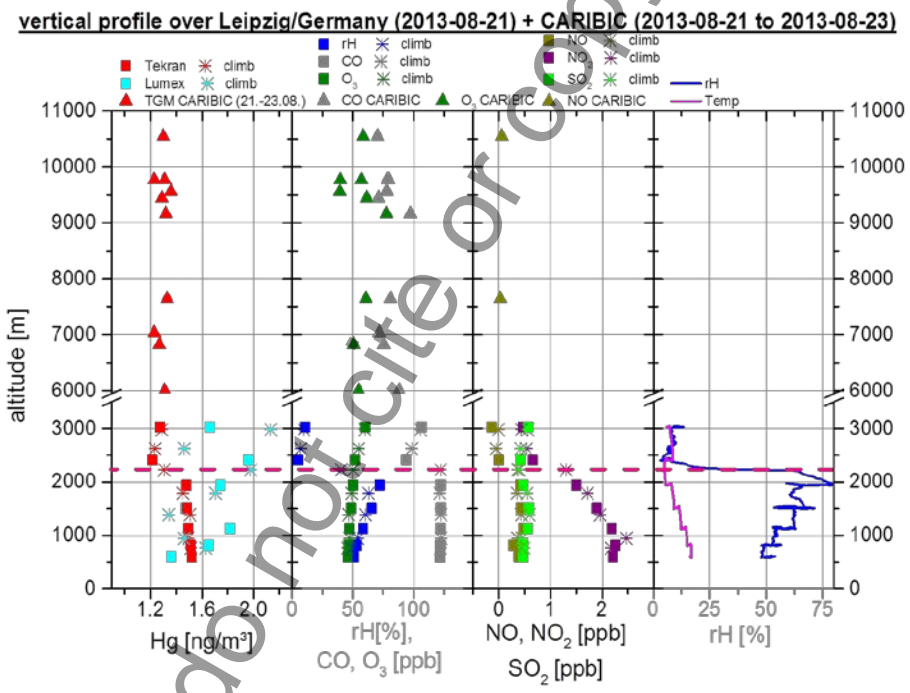

Figure 13: Vertical profile of GEM, CO, O3, SO2, NO, NO2, T, RH over Leipzig, Germany during ETMEP and CARIBIC flights.

3.3.2 Aircraft-based emission estimates for point and area sources

On several Nitrogen, Oxidants, Mercury and Aerosol Distributions, Sources and Sinks (NOMADSS) project flights, large Hg point sources were sampled, mainly coal-fired power plants (CFPP) in the

Southeast U.S. Ambrose et al. (2015) developed a unique method to use the NOMADSS data to evaluate Hg point source emissions. This method relies on the simultaneous C-130 observations of NO_x, SO_2, CO and CO_2 observations. A key conclusion is that for some CFPPs, including some of the largest Hg emitters in the U.S., the observations suggest substantially higher Hg emissions compared to the emission inventories.

During ETMEP flights over central Europe significant mercury emissions were measured from a modern coal-fired power plant south of Leipzig/Germany. Inside the plume GEM peaked to 10 ng/m³. The denuder sample inside the plume indicated modern coal-fired power plants may be an overestimated source of GOM. The measured fraction of GOM inside the plume was between 0.5% and 2%. This is in contrast to the 40%, given by the "AMAP/UNEP geospatially distributed mercury emissions dataset 2010v1" (AMAP/UNEP, 2013). The yearly emission of gaseous mercury from that power plant was estimated to be 268-283kg/a for GEM and 2-12 kg/a for GOM (Weigelt et al. 2015).

The Chicago-Gary area is highly industrialized with significant emissions of Hg and other pollutants. Using data from NOMADSS flight RF-15, Gratz et al. (2016) developed a novel method to evaluate the Hg emission inventory from this region. The observations showed a region of enhanced Hg, CO, SO2 and NOx. Combining the observations with the Flexpart model allowed for the characterization of the "footprint" of the observations and therefore a good comparison between the observations and expectations based on the emission inventory. Gratz' analysis indicated "that there are many small emission sources that are not fully accounted for within the inventory, and/or that the re-emission of legacy Hg is a significant source of THg to the atmosphere in this region (Gratz et al., 2016).

3.3.3 Large-scale Tropospheric distribution and plumes

During the Civil Aircraft for the Regular Investigation of the atmosphere Based on an Instrument Container (CARIBIC) project more than 100 large-scale pollution plumes have been detected in the global upper troposphere. The largest plume with an extension of 1000 km was detected on a flight from Frankfurt to Osaka between the Korean peninsula and the Yellow Sea. This mixed plume could be attributed to large forest fires in Southern Siberia as well as industrial sources in Chinese provinces of Shandong, Henan, Shanxi and Hebei.

Most of the plumes were found over East Asia during the flights from Frankfurt to Guangzhou, Osaka, Seoul and Manila, in the African equatorial region during the flights to South Africa, over South America

during the flights to Sao Paulo and Santiago de Chile, and over Pakistan and India during the flights to Chennai. The plumes encountered over the African equatorial region and over South America originate from biomass burning as evidenced by low Hg/CO emission ratios and elevated mixing ratios of acetonitrile, CH_3Cl and CH_3Br. Backward trajectories point to the region around Rift Valley and Amazon basin with its outskirts as the source areas. The plumes encountered over the East Asia and over Pakistan and India are predominantly of urban/industrial origin, sometimes mixed with products of biomass/biofuel burning. Numerous plumes with elevated mercury concentrations were encountered during the tropospheric sections of the CARIBIC flights since May 2005. Mercury correlated significantly with CO in more than 50% of the observed plumes and with CO_2 in about 30% of the plumes for which CO_2 data were available. Extensive ancillary data on chemical fingerprint of the air within these plumes and backward trajectories provide additional means to identify the origin and the type of the source (Slemr et al., 2014).

Large plumes over equatorial Africa were observed during all flights between Frankfurt and South Africa. These plumes which extend over thousands of km are embedded in north-south gradient of mercury, CO, and CO_2, and consist of a number of overlapping smaller plumes. Due to the changing background, the inhomogeneity of the plumes and low precision of the mercury measurements, only a few of the plume encounters provided significant Hg vs. CO correlations. Most plumes were observed over Far East Asia and relative to the number of flights to Far East destinations the yield of plumes with significant Hg vs CO correlations was the second highest after the African flights. Lower yields of plume occurrence were found for flights to South America and to South Asia. Only one plume was encountered over North America and one over Europe. (Slemr et al., 2009, Slemr et al., 2013, Slemr et al., 2014)

The Hg/CO emission ratios derived from these correlations are consistent with the previous data and tend to smaller values of ~1 pg m^{-3} ppb^{-1} for plumes from biomass burning and larger values of ~6 pg m^{-3} ppb^{-1} for urban/industrial emissions. Most of the plumes observed over South America and Africa originate from biomass burning and one plume observed over mid-Atlantic could be attributed to forest fires in the southeastern U.S. The plumes observed over the Far East Asia are mostly of urban/industrial or mixed origin. Only a few Hg/CO_2 emission ratios have been reported so far. The range of the Hg/CO_2 emission ratios from CARIBIC flights is comparable to the range observed at Cape Point (Brunke et al., 2012). The Hg/CO_2 emission ratios of 107 – 964 pg m^{-3} ppm^{-1} observed in the plumes over Far East, however, are substantially higher than 2 – 30 pg m^{-3} ppm^{-1} calculated by Brunke et al. (2012) for coal burning. If confirmed by further measurements, the higher observed than calculated Hg/CO_2 emission ratios would imply substantial other mercury emissions than from coal burning. Generally, it can be concluded from

CARIBIC data that the major industrial sources for atmospheric mercury are located in East-Asia, Pakistan and India whereas major contribution to mercury emissions from biomass burning are originating from Equatorial Africa (Rift-Valley) and the Amazon region.

In the tropospheric CARIBIC data an El Niño Southern Oscillation (ENSO) signal could be detected. (Slemr et al., 2016a). The highest mercury concentrations are always found at the most negative SOI (Southern Oscillation Index) values i.e. are related to the El Niño events. A cross-correlation reveals that peak mercury concentrations are delayed by 6 – 12 months against SOI. This delay is similar to the delay of CO which has been shown to originate from biomass burning in aftermath of El Niño events. Slemr et al. (2016) suggested that the ENSO signal in the worldwide mercury concentrations is also due to mercury emissions from biomass burning (Slemr et al., 2009, Slemr et al., 2013, Slemr et al., 2014).

3.3.4 Airborne observations of speciated Hg

Mercury observations on the NCAR C-130 were made by the University of Washington in summer 2013 with specially developed Detector for Oxidized Hg Species (DOHGS) (Ambrose et al., 2015), which measures both gaseous elemental mercury (Hg0), gaseous oxidized mercury (GOM), plus a fraction of particle-bound oxidized Hg. GOM is believed to consist of Hg(II) compounds, such as $HgCl_2$, $HgBr_2$, etc. The measurements were routinely calibrated in-flight with a high precision source of Hg0, and in the laboratory with sources of gaseous $HgBr_2$ and $HgCl_2$. The dual channel difference method avoids problems with earlier measurements based on KCl denuders, which are known to have significant interferences. We believe these are the most carefully calibrated and accurate measurements of speciated Hg made to date on an aircraft platform. Details on the methodology and further information on calibrations, accuracy, and precision are given in Ambrose et al. (2015). On several flights, substantial concentrations of Hg(II) were identified. Although the location and timing of these events were correct in the GEOS-Chem Hg model, the concentrations were much higher (2–4x). Figure 14 shows an example from research flight 6 (RF-06), along with the base simulations from GEOS-Chem (Gratz et al., 2015). This flight was also one of the few with detectable concentrations of BrO. We concluded that the likely source of Hg(II) on this flight was oxidation of gaseous elemental mercury (GEM) by Br radicals. This was supported by a detailed chemical mechanism and box-model calculation. This is a major finding and has implications for both Hg and halogens. Note that the halogen chemistry and mercury oxidation mechanism in the GEOS-Chem model were recently updated, as reported in Horowitz et al. (2017).

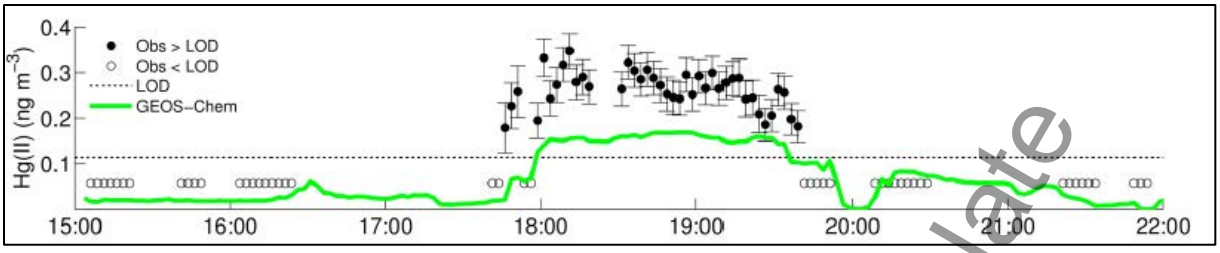

Figure 14: Oxidized Hg (Hg(II); ng m^{-3}) concentrations measured during RF-06 on June 19, 2013, (black points) and modelled Hg(II) from the base model simulations (green line).

Shah et al. (2016) further analysed the origins of oxidized mercury using a variety of sensitivity studies with the GEOS-Chem model. For observations above the detection limit it was found that modelled Hg(II) concentrations are a factor of 3 too low (observations: 212 ± 112 ng m^{-3}, model: 67 ± 44 ng m^{-3}). The highest Hg(II) concentrations, 300–680 pg m^{-3}, were observed in dry (RH < 35 %) and clean air masses during two flights over Texas at 5–7 km altitude and off the North Carolina coast at 1–3 km. The GEOS-Chem model, back trajectories and observed chemical tracers for these air masses indicate subsidence and transport from the upper and middle troposphere of the subtropical anticyclones, where fast oxidation of elemental mercury (Hg0) to Hg(II) and lack of Hg(II) removal lead to efficient accumulation of Hg(II). Shah et al. (2016) suggested that the most likely explanation for the model bias is a systematic underestimate of the Hg0 +Br reaction rate, which has now been updated in Horowitz et al. (2017). It was shown that sensitivity simulations with tripled bromine radical concentrations or a faster oxidation rate constant for Hg0 +Br, result in 1.5–2 times higher modelled Hg(II) concentrations and improved agreement with the observations. The modelled tropospheric lifetime of Hg0 against oxidation to Hg(II) decreases from 5 months in the base simulation to 2.8–1.2 months in our sensitivity simulations. In order to maintain the modelled global burden of THg, the in-cloud reduction of Hg(II) was increased, thus leading to faster chemical cycling between Hg0 and Hg(II). Observations and model results for the NOMADSS campaign suggest that the subtropical anticyclones are significant global sources of Hg(II).

In the lower stratosphere, TGM concentrations always decrease with increasing PV and O_3. This behaviour is similar to all trace species with ground sources and stratospheric sinks such as CO and CH_4. Opposite to such species, mercury as an element can only be transformed to other mercury species such as GOM or PBM. The transformation rate of TGM to PBM can be calculated using SF_6 as a timer. SF_6 is a very long-lived tracer whose concentration increases by about 0.230 ppt yr-1. Correlations of TGM with SF_6 suggest a seasonally dependent TGM conversion rate of about 0.43 ng m-3 yr-1 resulting in a stratospheric TGM lifetime of about 2 yr. This lifetime is longer than several weeks claimed recently by

Lyman and Jaffe (2012) but is closer to the 1 yr estimated by Holmes et al. (2010) using the GEOS-Chem model with included bromine oxidation chemistry.

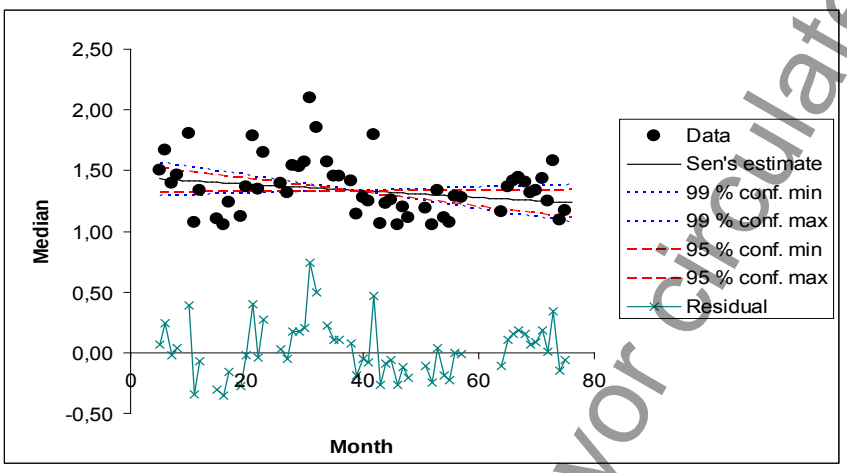

Figure 15: Monthly averages of TGM concentrations in the troposphere (PV < 1.5 PVU) north of 15°N from May 2005 to April 2011 with Sen´s slope estimate.

3.4 Temporal and spatial variability of Hg exchange fluxes between air and soil/vegetation/snow-ice

Air–soil (or vegetation covered) exchange fluxes are an important part of global and regional Hg biogeochemical cycle (Lindberg et al. 2007, Gustin et al. 2008, Gustin et al. 2010, Pierce et al. 2015). Much of Hg(II) deposited in precipitation or taken up by plants is subject to reduction to Hg(0) and may be evaded back to the atmosphere. Smith-Downey et al. (2010) estimated based on a global terrestrial mercury model that evasion of mercury linked to decomposition of soil organic carbon pools and subsequent liberation of Hg(II) sorbed to soil organic matter is greater than 700 Mg per year, reflecting the large pool of Hg stored in terrestrial ecosystems globally (>240 Gg). In total, this study estimated 56% of Hg deposited to terrestrial ecosystems is reemitted. Similarly, Graydon et al. (2012) found that 45-70% of isotopically labelled Hg(II) wet deposited to a forested watershed had been reemitted to the atmosphere after one year. Recent observations suggest the evasion flux of mercury from global soils may be slightly lower and the reservoir even higher (e.g., Hararuk et al., 2013).

Hg exchange flux between soil (vegetation) depends on several environmental factors (soil moisture, soil porosity substrate temperature, etc.), chemical factors (Hg species and its content in soil, organic matter, atmospheric oxidants, etc.), meteorological factors (e.g. pressure, air temperature, wind speed and turbulence, solar radiation, snow cower) and surface characteristics (e.g. type of vegetation, substrate type, roughness of the surface) (Schroeder et al. 2005, Gustin et al. 2004). These factors are leading to

highly variable Hg fluxes in different landscapes and determine spatial and temporal variability in deposition or evasion of GEM (Schroeder et al. 2005). All forms of atmospheric Hg can be deposited from atmosphere to soils or differently vegetated surfaces by wet or by dry deposition processes (Gustin 2011) where it can either remain in terrestrial system and undergo further biogeochemical cycle or emitted back to atmosphere with relative importance of different controlling factors (Gustin 2011). Changes in direction of the flux were observed on several soil types covered by different types of vegetation (Gustin and Jaffe 2010, Poissant et al. 2005), and can happen quickly, within a few hours (Bash and Miller 2008, Converse et al. 2010).

Soil types, moisture, and Hg content and speciation in soil are important factors influencing GEM flux between soil and air (Kocman and Horvat 2010, Lin et al. 2010). Soil porosity and disturbance promote Hg(II) reduction and GEM transport from soil (Fu et al. 2012, Bash and Miller 2007). Soils with small grain size, silt and clay with higher surface area showed higher GEM fluxes to air (Gustin et al. 2002). Rainfall and soil moisture promote GEM emission by an order of magnitude (Lindberg et al. 1999). Irrigation of soil enhances Hg (II) reduction and added water replaces GEM binding sites and thus promotes GEM emission. Organic matter in soil was reported to be one of main factors affecting GEM emissions as organic matter forms stable complexes with Hg(II) and thus reduces GEM flux (Grigal 2003, Skyllberg et al. 2006, Yang et al. 2007). Microbial activity in soil and increasing soil pH may promote GEM flux by Hg(II) reduction (Fritshe et al. 2008, Choi and Holsen 2009, Yang et al. 2007). High ambient air GEM concentrations were reported to reduce GEM flux by reducing Hg(0) concentration gradients and thus deposition is dominated despite the influence of other factors (Xin and Gustin 2007, Bash and Miller 2007, Wang et al. 2007, Zhu et al. 2016). Flux measured from background soils was between -51.7 to 97.8 with a mean of 2.1 ng $m^{-2}h^{-1}$ (Zhu et al. 2016 and references therein).

Vegetation is changing environmental factors at ground surfaces by reducing solar radiation, temperature, wind velocity (Gustin et al. 2004), and serves as surfaces for Hg uptake (Zhu et al. 2016). Deforestation can increase GEM emissions due to higher solar irradiation and temperature (Zhu et al. 2016, Carpi et al. 2014, Mazur et al. 2014). Recent measurements showed that GEM exchange flux between plants and air is bidirectional and that growing plants acts as a net sink (Ericksen et al. 2003, Stamenković et al. 2008, Hartman et al. 2009, Zhu et al. 2016). Most fluxes measured in forest foliage and grasslands were between -9.6 and 37 (6.3), and -19 to 41 (5.5) ng $m^{-2}h^{-1}$, respectively (Zhu et al. 2016 and references therein).

Air-snow exchange fluxes were mostly investigated in polar regions. During AMDEs, air GEM is oxidized and deposited in snow as GOM and PBM which can be rapidly volatilized back to the atmosphere by photochemical reduction on snow or in melted snow (Dommergue et al. 2003, Fain et al. 2007, Kirk et al. 2006). Photo-reduction was found to be a predominant factor for re-emission from snow and was linearly correlated to UV intensity (Lalonde et al. 2002, Mann et al. 2015). An important factor controlling snow-air fluxes is temperature, also by changing the solid-liquid water ratio (Mann et al. 2015). Similar factors in polar regions control snow-air Hg exchange in temperate regions (Maxwell et al. 2013). Measured fluxes from snowpack are within same range reported for vegetation cover and were between -10.8 to 40 ng $m^{-2}h^{-1}$ with mean of 5.7 ng $m^{-2}h^{-1}$ (Zhu et al. 2016 and references therein).

Polar air-sea water exchange of elemental mercury was for the first time measured continuously in the remote seas of western Antarctica. The measurements were performed during winter and spring (2013) in the Weddell Sea and during summer (2010/2011) in the Bellingshausen, Amundsen and Ross Seas, and show spatial and seasonal variations. The average DGM concentration in surface water in open sea was highest during spring (12±7 pg L^{-1}) and lowest during summer (7±6.8 pg L^{-1}), resulting in a net evasion of mercury during spring (1.1±1.6 ng m-2 h^{-1}) and a net deposition during summer (-0.2±1.3 ng m-2 h^{-1}). In open sea, higher average concentrations of GEM (or TGM) and DGM were found close to the Drake Passage compared to in the Bellingshausen and Weddell Seas. Emission sources from the South American continent, identified with back trajectories, were suggested to explain the observed variations. The yearly mercury evasion from open sea surfaces in the Southern Ocean was estimated at 30 (-450-1700) tons, using the average (and min and max) flux rates obtained in this study. Higher DGM was measured under sea ice (19-62 pg L^{-1}) compared to in open sea due to a capsuling effect, resulting in a theoretical prevented evasion of 520 (0-3400) tons per year. Diminishing sea ice and higher water temperatures in polar regions could result in increased mercury evasion to the atmosphere. However, the contribution of the Southern Ocean to the global modelled annual emissions of mercury from sea surfaces would probably only be a few percentage (Nerentorp et al 2017).

Hg evasion from contaminated or naturally enrich soils was recognized as an important input to regional and global budgets (Ferrara et al. 1998, Kotnik et al. 2005). The average evasion flux over urbanized areas and agricultural fields is 5 to 10 times higher than over background soils (Zhu et al. 2016). Measured Hg exchange fluxes over natural enriched surfaces were reported to be 5.5 to 239 (5.6) µg m^{-2} h^{-1}, and from anthropogenically contaminated sites 0.001 to 14 (0.6) µg m^{-2} h^{-1} (Zhu et al. 2016 and references therein).

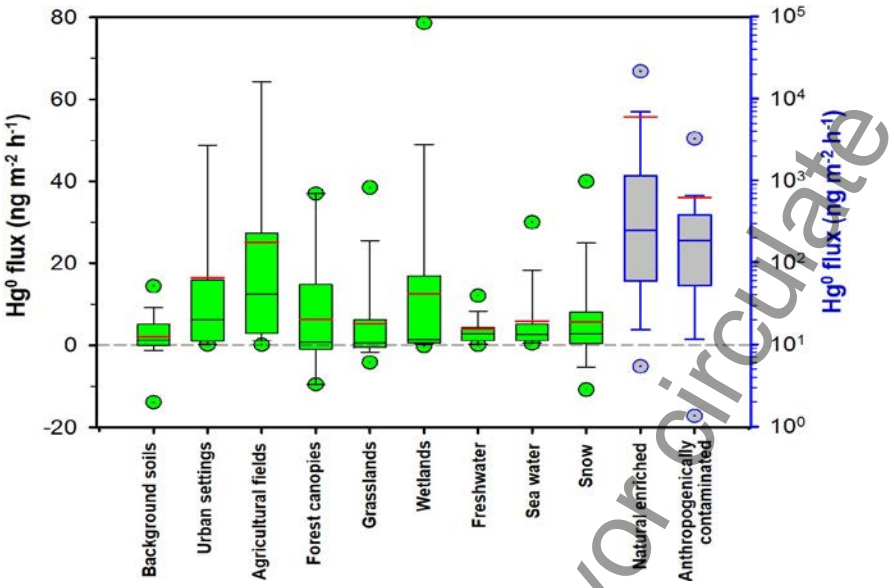

Figure 16: Box and whisker plots of global field-observed GEM fluxes obtained from various landscapes. The two-box horizontal border lines indicate 25th and 75th percentiles, whiskers represent 10th and 90th percentiles and outliers (green circles) indicate 5th and 95th percentiles from bottom to top. Red line and black line indicate mean and median flux. Figure from Zhu et al. 2016.

Fluxes from soils, mines and snow surfaces, where GEM can be formed due to photoreduction, are typically higher during daytime compared to night time (Zhu et al. 2016). Higher evasion flux was observed during warm seasons, compared to cold seasons, from different soils and enriched surfaces (Zhu et al. 2016). Hg flux measurements over soil, vegetation or snow-covered surfaces were consistently higher in East Asia than those measured in Europe, North and South America, Australia and South Africa. This is explained by higher anthropogenic emissions and re-emissions of deposited Hg (Zhu et al. 2016 and references therein).

3.5 Existing data by new monitoring technologies and new methods

Complex commercial instruments (Gustin et al., 2015) as well as sensors and sensing systems have been recently redesigned and improved by introducing innovative technologies. Thus, many sensors have been developed to detect the several forms of mercury making use of nanotechnology. Over the last 20 years, biomolecules, macromolecules, nanostructures (rods, tubes, fibres, particles, dots) and nanocomposite-based systems have been found to be the most intriguing and effective devices for mercury detection in several environmental compartments. Most of them have exploited the strong affinity between mercury and gold, others the affinity of mercury ions to specific biomolecules. The possibility to manipulate and

6882 investigate the features of the nano materials allowed the opportunity to fabricate selective and more
6883 sensitive tools. The Table 13 comprises some of the most recent technologies used to develop sensors and
6884 devices for mercury detection.

6885 **Table 13:** Recent technologies used to develop sensors and devices for mercury detection.

Sampling	Materials/device	Linearity range	LOD	Samples	Reference
Hg ions	CV-AAS +SDS-coated chromosorb P + 2-mercaptobenzo xazole	0.05-85.6 ug L^{-1} 90 ugL^{-1}- 9.6 mgL^{-1}	0.1ug L^{-1}	Real samples in liquids	Ghaedi, M. et al., 2006
TGM-Continuous Emission Monitor	Catalysts to oxidize + polymer composites to absorb + chemicals to remove (CVA-AFS)	60 pptv-228 ppbv	6 pptv	Real samples	Tekran331OXi (www.tekran.com)
Optical sensors: Hg^{2+}, FRET bio-sensor (gold nanoparticles-DNA)	Fluorescence quenching		8 ug L^{-1}	Water	Miyake, Y. et al., 2006
Optical sensors: Hg^{2+}, surface energy transfer probe-Rhodamine B-AuNPs	Fluorescence quenching		2 ug L^{-1}	Buffer solution, water, river water, contaminated soil	Darbha, G.K., et al., 2007
Optical sensor: surface-enhanced resonance Raman scattering (SERRS) sensor	structure-switching double stranded DNAs (dsDNAs)		0.02 ug L^{-1}	Aqueous solution	Kang T., et al. 2011
Electrochemical sensors: Hg^{2+}, array of 256 gold microelectrodes	anodic stripping voltammetry	10 ug L^{-1}-200 ug L^{-1}x10^{-8}-1x10^{-6} M	3.2 µg L^{-1} (16 nM)	Chloride media	Ordeig, O., et al., 2006
FET sensors: Hg^{2+}	Thioglycolic acid (TGA)-functionalized - AuNPs-reduced graphene oxide		5 ug L^{-1}	Aqueous solution	Chen, K., et al., 2012

	(rGO)				
Colorimetric sensors: Hg^{2+} (naked eye)	Au-nanorods/glass	2.0 µg L^{-1} to 0.58 mg L^{-1}	1 ug L^{-1}	Aqueous solution	Chemnasiri W., et al., 2012
LSPR (prediction model)	Au-nanorods (shift wavelength)		4.5 attograms (mass)	Hg^0 vapour	James J.Z., et al., 2013
Conductive sensors	CNT-AuNP		2 ppbv	Hg^0 vapour	McNicholas T.P., et al., 2011
Conductive sensors	TiO2NFs-AuNPs (tens of min)		2 pptv	Hg^0 vapour	Macagnano A., et al. 2017
Conductive sensors	TiO2NF-AuNPs	20-100 ppbv	1.5 ppbv	Hg^0 vapour	Macagnano et al. 2017
QCM sensor (AT cut quartz)	nanostructured gold electrode		2.5 ppbv	Hg^0 vapour	Kabir K.M., et al., 2015
Jerome® J405 Mercury Vapour Analyzer	gold thin film (750 ccmin-1)	60 pptv-120 ppbv	60 pptv	Hg^0 vapour	www.azi.com

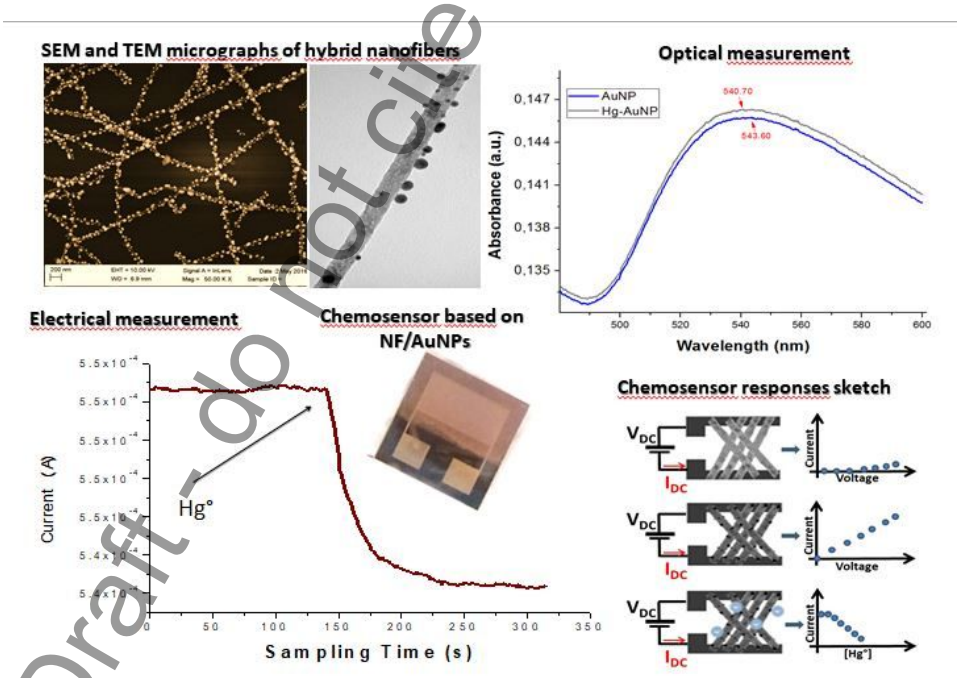

Figure 17: Recent results from sensors based on electrospinning technology: nanofibers of titaniadoped with AuNPs to detect traces of elemental mercury in air (*Macagnano et al., 2017, a,b).*

On the other hand, identifying as well monitoring both GOM and PGM in the atmosphere, that are commonly present at ultra-trace concentration (pg/m^{-3}), look even more difficult due to their complex fundamental physiochemical properties (Gustin et al. 2013). To date, strategies based on ultrasensitive GC/MS systems (Jones et al., 2016), soft ionization mass spectrometry coupled with nanostructured preconcentrators (Deeds et al. 2015), detectors for oxidized Hg species (DOHGS)(Ambrose et al., 2013) and proper calibrators and filters associated to a Tekran system (Lyman et al., 2016) appear as the most advanced technologies to quantify GOM and PGM in a quasi-real time from air.

However, given the uncertainty and restrictions associated with automated measurements, passive sampling systems currently are a useful alternative for making regional and global estimates of air Hg concentrations. Some passive samplers applied for Hg have been biological materials, i.e. leaves, lichens, tree cores, and mosses (Grangeon et al., 2012; Harmens et al., 2008). Further passive samplers have been designed using a variety of synthetic materials (like sulphur-impregnated carbon (SIC), chlorine-impregnated carbon (CIC), bromine-impregnated carbon (BIC) gold-coated (GCS) sorbents, etc.) (Lin, H. et al., 2017) and housings for Hg collection (McLagan et al., 2016). These latter samplers work on the basis of diffusion. Additionally, surrogate surfaces have been developed for passive measurement of Hg dry deposition. Most commercially available passive/diffusive samplers are planar or axial in shape and offer lower sampling rates and limited sampling capacity. As a result, sensitivity can suffer during short-term analysis (due to low sampling rates), or long-term sampling (analyte back-diffusion due to low capacity) (Huang et al. 2014). Alternatively, radial samplers, consisting of a columnar sorbent surrounded by a cylindrical diffusive barrier, have the purpose to increase the sampling rate by maximizing the surface area across which diffusion occurs (Radiello®, Krol et al., 2010). Passive Samplers (PASs) have been also designed with external shields to protect the sampler components from direct wind, sunlight, and precipitation and to reduce turbulent airflow. A collection of passive samplers more recently developed has been reported in Table 14.

Table 14– Passive samplers developed in recent years to measure TGM [ng m^3] and GOM [pg m^3].

Target	Location	TGM (ng m^{-3}) GOM (pg m^{-3})	Materials/ sampler	Sampling rate (ml min^{-1})	Blank	DL (pg m^3)	Influences	Reference
TGM	Rural	i) 1-4 ii) 0.8-1.5	i) Gold coated plate ii) silver wire /radial	i) 87 (lab); 51+/-19 (field); 260 theoretic	i) ii) 80 pg	i) 90 (3 days) ii) 430 (3 days)		Gustin et al., 2011

			sampler	al ii) 20 measured ; 33 theoretic al				
TGM	Industr.	25	Gold solution with LDPE/passive integrative mercury sampler (PIMS)	1.4	0.3 ng	2000 (4 weeks)		Brumbaugh et al., 2000
TGM	Chamber	10	Gold coated tube/laboratory scale	57 measured 114 theoretic al	0.02 ng	50 (2.8 days); 140 (1 day)	Wind speed	Skov et al., 2007.
TGM	Chamber indoor, outdoor	2-3.5	Gold-coated silica/axial sampler	0.22 measured 0.32 theoretic al		30% (uncertainty)		Brown et al., J., 2012
TGM	Industrial , suburban , rural	2-5.5	Sulphur-impregnated carbon/axial sampler	90		80 (30 days)	Wind speed	Zhang et al., 2012
TGM	Industrial	2	Gold-coated filter-cation exchange membrane/two-bowl sampler	460 measured 556 theoretic al	0.17 ng	10 (3 days)	Wind speed; humidity	Huang et al., 2012
TGM	Chamber , indoor, outdoor	1.35−2.16 ng m^{-3} (indoor); d 1.17− 3.29 ng m^{-3} (outdoor)	Sulphur impregnated carbon sampler/radial in a protective shield	0.158-0.121 $m^3 day^{-1}$ indoor-outdoor		11-12 months		Mc. Lagan D., et al., 2016
GOM	Rural, suburban	DL-65	Cation-exchange membrane/mu	0.7-3.2 measured	0.27 ng to 0.68	5 (2 weeks)	Wind speed	Lyman et al., 2010

			ltiple configurations	0.055 theoretic al	ng			
GOM	Remote	DL-67	Cation-exchange membrane/aerohead configuration		0.56 ng	2.3 (2 weeks)	Wind speed	Wright et al., 2013
GOM	Industrial, suburban, rural	DL-35	Cation-exchange membrane/ two-bowl sampler	1042 measured 486 theoretic al	0.02-0.04 ng	3 (3 days)	Wind speed; humidity	Huang et al., 2012

3.7 Conclusions

Data from existing air mercury monitoring networks show a clear gradient of mercury concentration between the northern and southern hemispheres. The map of existing networks and their spatial distribution, however, show geographical coverage gaps of large areas (i.e., Africa, Latin America and Caribbean, Russia) that are key for long-range transport analysis and identification of source-receptor regions relationship.

Sufficient data do not exist to assess the global temporal trend in atmospheric mercury concentration and deposition. Data from Europe, Canada, the United States show general decrease in the level of mercury in air.

Close cooperation among existing monitoring networks is needed to support global actions to reduce mercury emissions by:

- Ensuring sustainability of a long-term monitoring program covering both hemispheres
- Assuring comparability among different monitoring data sets by promoting the adoption of common methods and standards
- Promoting experiments for testing and validating new methods and technologies for mercury monitoring
- Supporting nations as they develop their own monitoring programs by promoting a continuous capacity building and transfer of knowledge program in cooperation with UN Environment.

3.8 References

Aas, W., Pfaffhuber, K.A., & Nizzetto, P.B. (2016). Heavy metals and POP measurements, 2014 (EMEP/CCC, 04/2016). Kjeller: NILU.

Ambrose, J.L., Gratz, L.E., Jaffe, D.A., Campos, T., Flocke, F., Knapp, D., Stechman, D., Stell, M., Weinheimer, A., Cantrell, C., and Mauldin, R. Mercury Emission Ratios from Coal-Fired Power Plants in the Southeastern United States during NOMADSS. Envir. Sci. Tech. 49 (17), 10389–10397, doi: 10.1021/acs.est.5b01755, 2015.

Ambrose J.L., Lyman S.N., Huang J., Gustin M.S., Jaffe D.A, Fast time resolution oxidized mercury measurements during the Reno Atmospheric Mercury Intercomparison Experiment (RAMIX), Environ Sci Technol. 2013 Jul 2;47(13):7285-94

Amos, H.M., D.J. Jacob, D.G. Streets, E.M. Sunderland. Legacy impacts of all-time anthropogenic emissions on the global mercury cycle. Global Biogeochemical Cycles. 27, 1-12, 410–421, doi:10.1002/gbc.20040, 2013.

Amos, H.M., D.J. Jacob, D. Kocman, H.M. Horowitz, Y. Zhang, S. Dutkiewicz, M. Horvat, E.S. Corbitt, D.P. Krabbenhoft, E.M. Sunderland. 2014. Global biogeochemical implications of mercury discharges from rivers and sediment burial. Environmental Science and Technology. 48, 9514-9522.

Angot, H., Barret, M., Magand, O., Ramonet, M., and Dommergue, A.: A 2-year record of atmospheric mercury species at a background Southern Hemisphere station on Amsterdam Island, Atmos. Chem. Phys., 14, 11461–11473, doi:10.5194/acp-14-11461-2014, 2014.

Angot, H., Dastoor, A., De Simone, F., Gårdfeldt, K., Gencarelli, C.N., Hedgecock, I.M., Langer, S., Magand, O., Mastromonaco, M.N., Nordstrøm, C., Pfaffhuber, K.A., Pirrone, N., Ryjkov, A., Selin, N.E., Skov, H., Song, S., Sprovieri, F., Steffen, A., Toyota, K., Travnikov, O., Yang, X., Dommergue, A., 2016a. Chemical cycling and deposition of atmospheric mercury in polar regions: review of recent measurements and comparison with models. Atmos Chem Phys 16, 10735–10763. doi:10.5194/acp-16-10735-2016

Angot, H., Dion, I., Vogel, N., Legrand, M., Magand, O., Dommergue, A., 2016b. Multi-year record of atmospheric mercury at Dumont d'Urville, East Antarctic coast: continental outflow and oceanic influences. Atmos Chem Phys 16, 8265–8279. doi:10.5194/acp-16-8265-2016.

Angot, H., Magand, O., Helmig, D., Ricaud, P., Quennehen, B., Gallée, H., Del Guasta, M., Sprovieri, F., Pirrone, N., Savarino, J., Dommergue, A., 2016c. New insights into the atmospheric mercury cycling in central Antarctica and implications on a continental scale. Atmos Chem Phys 16, 8249–8264. doi:10.5194/acp-16-8249-2016.

Ariya, P.A., Dastoor, A.P., Amyot, M., Schroeder, W.H., Barrie, L., Anlauf, K., Raofie, F., Ryzhkov, A., Davignon, D., Lalonde, J., Steffen, A., 2004. The arctic: a sink for mercury. Tellus 56B, 397cling.

Aspmo, K., Temme, C., Berg, T., Ferrari, C., Gauchard, P-A., Fain, X., Wibetoe, G., 2004. Mercury in the atmosphere, snow and melt water ponds in the North Atlantic Ocean during Arctic summer. Environ. Sci. Thecnol 40, 4083–4089.

Banic, C.M., Beauchamp, S.T., Tordon, R.J., Schroeder, W.H., Steffen, A., Anlauf, K.A., Wong, K.H.T. Vertical distribution of gaseous elemental mercury in Canada, J. Geophys. Res. 108, D9, 4264.

Bargagli, R., 2016. Atmospheric chemistry of mercury in Antarctica and the role of cryptogams to assess deposition patterns in coastal ice-free areas. Chemosphere 163, 202–208. doi:10.1016/j.chemosphere.2016.08.007

Bash, J. O. and Miller, D. R.: A note on elevated total gaseous mercury concentrations downwind from an agriculture field during tilling, Sci. Total Environ., 388, 379–388, 2007.

Bash, J. O. and Miller, D. R.: A relaxed eddy accumulation system for measuring surface fluxes of total gaseous mercury, J. Atmos. Ocean. Tech., 25, 244–257, 2008.

Berg, T., Bartnicki, J., Munthe, J., Lattila, H., Hrehoruk, J., Mazur, A., 2001. Atmospheric mercury species in the European Arctic: measurements and modelling. Atmos. Environ. 35, 2569016/j.

Berg, T., Pfaffhuber, K.A., Cole, A.S., Engelsen, O., Steffen, A., 2013. Ten-year trends in atmospheric mercury concentrations, meteorological effects and climate variables at Zeppelin, Ny-Alesund. Atmospheric Chem. Phys. 13, 6575–6586.

Berg, T., Sommar, J., W.A., Cg, Gardfeldt, K., Munthe, J., Schroeder, B., 2003. Arctic mercury depletion events at two elevations as observed at the Zeppelin Station and Dirigibile Italia, Ny-Ålesund, spring 2002. J Phys IV Fr. 107, 151–154.

Brenninkmeijer, C.A.M. P., Crutzen, T., Dauer, D.B., Ebinghaus, R., Filippi, D., Fischer, H., Franke, H., Freiß, U. J., Heintzenberg, H.M., Kock, H.H., Leuenberger, M., Martinsson, B.G., Miemczyk, S., Nguyen, H.N.,

Oram, D., O'Sullivan, S., Penkett, U., Platt, M., Pupek, M., Ramonet, B., Reichelt, R.M., Rhee, T.S., Rohwer, J., Rosenfeld, K., Scharffe, D., Schlager, H., Schumann, U., Slemr, F., Sprung, D., Stock, P., Thaler, R., van Velthoven, P., Waibel, A., Wandel, A., Waschitschek, K., Wiedensohler, A., Zahn, A., Zech, U., Ziereis H.(2007): Civil Aircraft for the Regular Investigation of the Atmosphere Based on an Instrumented Container; the new CARIBIC system, Atmospheric Chemistry and Physics, 7, 5277–5339, 2007.

Brooks, S., Saiz-Lopez, A., Skov, H., Lindberg, S.E., Plane, J.M.C., Goodsite, M.E., 2006. The mass balance of mercury in the springtime arctic environment. Geophys. Res. Lett. 33, L13812. doi:10.1029/2005GL025525.

Brooks, S.B., Arimoto, R., Lindberg, S.E., Southworth, G., 2008a. Antarctic polar plateau snow surface conversion of deposited oxidized mercury to gaseous elemental mercury with fractional long-term burial. Atmos. Environ. 42, 2877–2884.

Brooks, S.B., Lindberg, S.E., Southworth, G., Arimoto, R., 2008b. Springtime atmospheric mercury speciation in the McMurdo, Antarctica coastal region. Atmos. Environ. 42, 2885th fra.

Butler, T. J., Cohen, M. D., Vermeylen, F. M., Likens, G. E., Schmeltz, D., & Artz, R. S. (2008). Regional precipitation mercury trends in the eastern USA, 1998–2005: Declines in the Northeast and Midwest, no trend in the Southeast. Atmospheric Environment, 42(7), 1582-1592.

Carbone, F., M. S. Landis, C. N. Gencarelli, A. Naccarato, F. Sprovieri, F. De Simone, I. M. Hedgecock, **N. Pirrone** (2016) Sea surface temperature variation linked to elemental mercury concentrations measured on Mauna Loa. *Geophysical Research Letters*, *43*, doi:10.1002/2016GL069252.

Carpi, A., Fostier, A. H., Orta, O. R., dos Santos, J. C., and Gittings, M.: Gaseous mercury emissions from soil following forest loss and land use changes: Field experiments in the United States and Brazil, Atmos. Environ., 96, 423–429, 2014.

Choi, H. D. and Holsen, T. M.: Gaseous mercury emissions from unsterilized and sterilized soils: The effect of temperature and UV radiation, Environ. Poll., 157, 1673–1678, 2009.

Cinnirella S., D'Amore F., Bencardino M., Sprovieri F., Pirrone N. 2014. The GMOS cyber(e)-infrastructure: advanced services for supporting science and policy. Environmental Science and Pollution Research, 21(6): 4193-4208.

Cole, A.S., Steffen, A., Pfaffhuber, K.A., Berg, T., Pilote, M., Poissant, L., Tordon, R., Hung, H. Ten-year trends of atmospheric mercury in the high Arctic compared to Canadian sub-Arctic and mid-latitudes sites. Atmospheric Chem. Phys. 13, 1535–1545, 2013.

Cole, A. S., Steffen, A., Eckley, C. S., Narayan, J., Pilote, M., Tordon, R., Graydon, J. A., St Louis, V. L., Xu, X., & Branfireun, B. (2014). A Survey of Mercury in Air and Precipitation across Canada: Patterns and Trends. Atmosphere, 5, 635-668, 2014.

Cole, A. S., Steffen, A., Aspmo Pfaffhuber, K., Berg, T., Pilote, M., Poissant, L., Tordon, R., and Hung, H., 2013. Ten-year trends of atmospheric mercury in the high Arctic compared to Canadian sub-Arctic and mid-latitude sites. Atmospheric Chemistry and Physics 13: 1535-1545, doi:10.5194/acp-13-1535-2013.

Colette, A., Aas, W., Banin, L., Braban, C.F., Ferm, M., González Ortiz, A., Ilyin, I., Mar, K., Pandolfi, M., Putaud, J.-P., Shatalov, V., Solberg, S., Spindler, G., Tarasova, O., Vana, M., Adani, M., Almodovar, P., Berton, E., Bessagnet, B., Bohlin-Nizzetto, P., Boruvkova, J., Breivik, K., Briganti, G., Cappelletti, A., Cuvelier, K., Derwent, R., D'Isidoro, M., Fagerli, H., Funk, C., Garcia Vivanco, M., González Ortiz, A., Haeuber, R., Hueglin, C., Jenkins, S., Kerr, J., de Leeuw, F., Lynch, J., Manders, A., Mircea, M., Pay, M.T., Pritula, D., Putaud, J.-P., Querol, X., Raffort,V., Reiss, I., Roustan, Y., Sauvage, S., Scavo, K., Simpson, D., Smith, R.I., Tang, Y.S., Theobald, M., Tørseth, K., Tsyro, S., van Pul, A., Vidic, S., Wallasch, M., Wind, P. (2016). Air pollution trends in the EMEP region between 1990 and 2012. Joint Report of the EMEP Task Force on Measurements and Modelling (TFMM), Chemical Co-ordinating Centre (CCC), Meteorological Synthesizing Centre-East (MSC-E), Meteorological Synthesizing Centre-West (MSC-W) (EMEP: TFMM/CCC/MSC-E/MSC-W Trend Report) (EMEP/CCC, 01/2016). Kjeller: NILU, 2016.

Colleen P.J, Lyman S.N., Jaffe D.A:, Allen T., O'Neil T.L., Detection and quantification of gas-phase oxidized mercury compounds by GC/MS, Atmos. Meas. Tech., 9, 2195–2205, 2016

Converse, A. D., Riscassi, A. L., and Scanlon, T. M.: Seasonal variability in gaseous mercury fluxes measured in a high-elevation meadow, Atmos. Environ., 44, 2176–2185, 2010. doi:10.1029JD002116, 2003.

D'Amore F., M. Bencardino, S. Cinnirella, F. Sprovieri, **N. Pirrone** (2015)Data quality through a web-based QA/QC system: implementation for atmospheric mercury data from the Global Mercury Observation System. *Environmental Science: Processes Impacts*, 2015, DOI:10.1039/C5EM00205B.

Dastoor, A., Ryzhkov, A., Durnford, D., Lehnherr, I., Steffen, A., Morrison, H. Atmospheric mercury in the Canadian Arctic. Part II: Insight from modeling. Sci. Total Environ., Special Issue: Mercury in Canada's North 509–510, 16–27, 2015. doi:10.1016/j.scitotenv.2014.10.112

Deeds D.A., Ghoshdastidar, Raofie F., Guerette E.A., Tessier A., Ariya P.A., Development of a Particle-Trap Preconcentration-Soft Ionization Mass Spectrometric Technique for the Quantification of Mercury Halides in Air, Anal. Chem. 2015, 87, 5109−5116

Dommergue, A., Barret, M., Courteaud, J., Cristofanelli, P., Ferrari, C.P., Gall 2015. Atmospheric mercury in the Canadian Arctic. Part II: Insight frondary layer of the Antarctic Plateau. Atmos Chem Phys 12, 11027–11036. doi:10.5194/acp-12-11027-2012

Dommergue, A., Larose, C., Faurteaud, J., Cristofanelli, P., Ferrari, C.P., Gall 2015. Atmospheric mercury in the Canadian Arctic. Part II: Insight frondar-Ålesund Area (79°N) and Their Transfer during Snowmelt. Environ. Sci. Technol. 44, 901–907. doi:10.1021/es902579m.

Dommergue, A., Ferrari, C. P., Gauchard, P.-A., Boutron, C. F., Poissant, L., Pilote, M., Jitaru, P., and Adams, F. C.: The fate of mercury species in a sub-arctic snowpack during snowmelt, Geophys. Res. Lett., 30, 1621, doi:10.1029/2003GL017308, 2003.

Ebinghaus, R., Jennings, S., Kock, H., Derwent, R., Manning, A., and Spain, T.: Decreasing trends in total gaseous mercury observations in baseline air at Mace Head, Ireland from 1996 to 2009, Atmos. Environ., 45, 3475–3480, 2011.

Ebinghaus, R., Kock, H. H., Coggins, A. M., Spain, T. G., Jennings, S. G., and Temme, C.: Long-term measurements of atmospheric mercury at Mace Head, Irish west coast, between 1995 and 2001, Atmos. Environ., 36, 5267–5276, 2002.

Ebinghaus, R., Kock, H.H., Temme, C., Einax, J.W., Lowe, A.G., Richter, A., Burrows, J.P., Schroeder, W.H., 2002. Antarctic springtime depletion of atmospheric mercury. Environ. Sci. Technol. 36, 123876, 20.

Ebinghaus, R., Slemr, F. Aircraft measurements of atmospheric mercury over southern and eastern Germany, Atmos. Environ. 34, 895-903, 2000.

Ebinghaus, R., Slemr, F., Brenninkmeijer, C.A.M., van Velthoven, P., Zahn, A., Hermann, M., O´Sullivan, D.A.,Oram, D.E. Emissions of gaseous mercury from biomass burning in South America in 2005 observed during CARIBIC flights, Geophys. Res. Lett. 34, L08813, doi:10.1029/2006GL028866, 2007.

ECCC, Canadian Mercury Science Assessment, Executive Summary. Steffen, A., 2016. ISSN: 978-0-660-03315-0, En84-130/1-2016E-PDF, 1-6, 2016.

ECCC, Canadian Mercury Science Assessment, Report. Steffen, A. ISBN: 978-0-660-04499-6, En84-130/3-2016E-PDF, 1-793, 2017.

Ericksen, J. A., Gustin, M. S., Schorran, D. E., Johnson, D. W., Lindberg, S. E., and Coleman, J. S.: Accumulation of atmospheric mercury in forest foliage, Atmos. Environ., 37, 1613–1622, 2003.

Faïn, X., Grangeon, S., Bahlmann, E., Fritsche, J., Obrist, D., Dommergue, A., Ferrari, C. P., Cairns, W., Ebinghaus, R., and Barbante, C.: Diurnal production of gaseous mercury in the alpine snowpack before snowmelt, J. Geophys. Res.-Atmos., 112, D21311, doi:10.1029/2007JD008520, 2007.

Ferrara, R., Maserti, B. E., Andersson, M., Edner, H., Ragnarson, P., Svanberg, S., and Hernandez, A.: Atmospheric mercury concentrations and fluxes in the Almadén district (Spain), Atmos. Environ., 32, 3897–3904, 1998.

Ferrari, C.P., Gauchard, P.-A., Aspmo, K., Dommergue, A., Magand, O., Bahlmann, E., Nagorski, S., Temme, C., Ebinghaus, R., Steffen, A., Banic, C., Berg, T., Planchon, F., Barbante, C., Cescon, P., Boutron, C.F., 2005. Snow-to-air exchanges of mercury in an arctic seasonal snowpack in Ny-Alesund, Svalbard. Atmos. Environ. 39, 7633–7645.

Fisher, J.A., D.J. Jacob, A.L. Soerensen, H.M. Amos, A. Steffen, E.M. Sunderland. 2012. Riverine source of Arctic Ocean mercury inferred from atmospheric observations. Nature Geoscience. 5: 499-504.

Friedli, H.R., Radke, L.F., Lu, J.Y., Banic, C.M., Leaitch, W.R., MacPherson, J.I. Mercury emissions from burning of biomass from temperate North American forests: laboratory and airborne measurements, Atmos. Environ. 37, 253-267, 2003.

Fritsche, J., Obrist, D., Zeeman, M. J., Conen, F., Eugster, W., and Alewell, C.: Elemental mercury fluxes over a sub-alpine grassland determined with two micrometeorological methods, Atmos. Environ., 42, 2922–2933, 2008.

Fu, X., Feng, X., Zhang, H., Yu, B., and Chen, L.: Mercury emissions from natural surfaces highly impacted by human activities in Guangzhou province, South China, Atmos. Environ., 54, 185– 193, 2012a.
Fu, X.W., Zhang, H., Yu, B.,Wang, X., Lin, C.-J., and Feng, X. B.: Observations of atmospheric mercury in China: a critical review, Atmos. Chem. Phys., 15, 9455–9476, doi:10.5194/acp-15-9455- 2015, 2015.
Gilbert, R. O. Statistical Methods for Environmental Pollution Monitoring. New York, Van Nostrand Reinhold Company, 1987.
Grangeon S., Guedron S., Asta J., Sarret G., Charlet L.,Lichen and soil as indicators of an atmospheric mercury contamination in the vicinity of a chlor-alkali plant, *Ecol. Indic.*, 2012, **13**, 178–183
Gratz, L., et al. Airborne Observations of Mercury Emissions from the Chicago/Gary Urban/Industrial Area during the 2013 NOMADSS Campaign. Atmos. Env., 145, 415–423, doi: 10.1016/j.atmosenv.2016.09.051, 2016.
Gratz, L.E., et al. Oxidation of mercury by bromine in the subtropical Pacific free troposphere. Geophys. Research Letters, 42, 10492–10502, doi: 10.1002/2015GL066645, 2015.
Graydon, J.A., V. St. Louis, S. Lindberg, K.A. Sandilands, J.W.M. Rudd, C.A. Kelly, R. Harris, M. Tate, D.P. Krabbenhoft, C.A. Emmerton, H. Asmath, M. Richardson. The role of terrestrial vegetation in atmospheric Hg deposition: Pools and fluxes from the METAALICUS experiment. Global Biogeochemical Cycles, 2012, 2610.1029/2011GB004031.
Grigal, D. F.: Mercury sequestration in forests and peatlands: A review, J. Environ. Qual., 32, 393–405, 2003.
Gustin M.S., Amos H.M., Huang J., Miller M.B. and Heidcorn K. Measuring and modeling mercury in the atmosphere: a critical review, Atmos. Chem. Phys., 15, 5697–5713, 2015
Gustin, M. S., Huang, J., Miller, M. B., Peterson, C., Jaffe, D. A., Ambrose, J., Finley, B. D., Lyman, S. N., Call, K., Talbot, R., Feddersen, D., Mao, H., and Lindberg, S. E.: Do We Understand What the Mercury Speciation Instruments Are Actually Measuring? Results of RAMIX, Environ. Sci. Technol., 47, 7295–7306, 2013
Gustin, M. and Jaffe, D.: Reducing the Uncertainty in Measurement and Understanding of Mercury in the Atmosphere, Environ. Sci. Technol., 44, 2222–2227, 2010.
Gustin, M. S., Biester, H., and Kim, C. S.: Investigation of the light-enhanced emission of mercury from naturally enriched substrates, Atmos. Environ., 36, 3241–3254, 2002.
Gustin, M. S., Ericksen, J. A., Schorran, D. E., Johnson, D. W., Lindberg, S. E., and Coleman, J. S.: Application of controlled mesocosms for understanding mercury air-soil-plant exchange, Environ. Sci. Technol., 38, 6044–6050, 2004.
Gustin, M. S.: Exchange of mercury between the atmosphere and terrestrial ecosystems, in: Environmental Chemistry and Toxicology of Mercury, edited by: Liu, G. L., Cai, Y., and O'Driscoll, N., 423–451, 2011.
Gustin, M.; Jaffe, D. Reducing the uncertainty in measurement and understanding of mercury in the atmosphere. Environ. Sci. Technol. 2010, 44, 2222–2227.
Gustin, M.S.; Lindberg, S.E.; Weisberg, P.J. An update on the natural sources and sinks of atmospheric mercury. Appl. Geochem. 2008, 23, 482–493.
Han, Y., Huh, Y., Hong, S., Hur, S.D., Motoyama, H., 2014. Evidence of air-snow mercury exchange recorded in the snowpack at Dome Fuji, Antarctica. Geosci. J. 18, 105i, 3. doi:10.1007/s12303-013-0054-7.
Han, Y., Huh, Y., Hong, S., Hur, S.D., Motoyama, H., Fujita, S., Nakazawa, F., Fukui, K., 2011. Quantification of total mercury in Antarctic surface snow using ICP-SF-MS: spatial variation from the coast to Dome Fuji. Bull. Korean Chem. Soc. 32, 4258–4264.
Han, Y., Huh, Y., Hur, S.D., Hong, S., Chung, J.W., Motoyama, H., 2017. Net deposition of mercury to the Antarctic Plateau enhanced by sea salt. Sci. Total Environ. 583, 81patial variation from thtenv.2017.01.008.
Hararuk, O., D. Obrist, Y. Luo. 2013. Modeling the sensitivity of soil mercury to climate-induced changes in soil-carbon pools. Biogeosciences. 10, 2393-2407.
Harmens, H., Norris, D.A., Koerber, G.R., Buse, A.,Steinnes E. and Rühling, Å., Temporal trends (1990–2000) in the concentration of cadmium, lead and mercury in mosses across Europe, *Environ. Pollut.*, 2008, **151**, 368–376
Hartman, J. S., Weisberg, P. J., Pillai, R., Ericksen, J. A., Kuiken, T., Lindberg, S. E., Zhang, H., Rytuba, J. J., and Gustin, M. S.: Application of a rule-based model to estimate mercury exchange for three background biomes in the Continental United States, Environ. Sci. Technol., 43, 4989–4994, 2009.
Hirdman, D., Aspmo, K., Burkhart, J.F., Eckhardt, S., Sodemann, H., Stohl, A., 2009. Transport of mercury in the Arctic atmosphere: Evidence for a spring-time net sink and summer-time source. Geophys. Res. Lett. 36, L12814. doi:10.1029/2009GL038345.

Horowitz, HM, DJ Jacob, Y Zhang, TS Dibble, HM Amos, JA Schmidt, ES Corbitt, EA Marais, EM Sunderland. (2017). A new mechanism for atmospheric mercury redox chemistry: implications for the global mercury budget. Atmospheric Chemistry and Physics. 17, 6353-6371.

Kalinchuk, V.V., Mishukov, V.F., Astakhov, A.S., 2017. Arctic source for elevated atmospheric mercury (Hg0) in the western Bering Sea in the summer of 2013. J. Environ. Sci. doi:10.1016/j.jes.2016.12.022

Kim, S. H., Han, Y. J., Holsen, T. M., & Yi, S. M. (2009). Characteristics of atmospheric speciated mercury concentrations (TGM, Hg (II) and Hg (p)) in Seoul, Korea. Atmospheric Environment, 43(20), 3267-3274.

Kirk, J. L., St. Louis, V. L., and Sharp, M. J.: Rapid reduction and reemission of mercury deposited into snowpacks during atmospheric mercury depletion events at Churchill, Manitoba, Canada, Environ. Sci. Technol., 40, 7590–7596, 2006.

Kock, H., Bieber, E., Ebinghaus, R., Spain, T., and Thees, B.: Comparison of long-term trends and seasonal variations of atmospheric mercury concentrations at the two European coastal monitoring stations Mace Head, Ireland, and Zingst, Germany, Atmos. Environ., 39, 7549–7556, 2005.

Kocman, D. and Horvat, M.: A laboratory based experimental study of mercury emission from contaminated soils in the River Idrijca catchment, Atmos. Chem. Phys., 10, 1417–1426, doi:10.5194/acp-10-1417-2010, 2010.

Kotnik, J., Horvat, M., and Dizdarevic, T.: Current and past mercury distribution in air over the Idrija Hg mine region, Slovenia, Atmos. Environ., 39, 7570–7579, 2005.

Król, S., Zabiegała, B., and Namiesnik, J.: Monitoring VOCs in atmospheric air II. Sample collection and preparation, TRACTrend. Anal. Chem., 29, 1101–1112, 2010.

Kwon, S.Y., Selin, N.E., 2016. Uncertainties in Atmospheric Mercury Modeling for Policy Evaluation. Curr. Pollut. Rep. 2, 103–114. doi:10.1007/s40726-016-0030-8.

Lalonde, J. D., Poulain, A. J., and Amyot, M.: The role of mercury redox reactions in snow on snow-to-air mercury transfer, Environ. Sci. Technol., 36, 174–178, 2002.

Larose, C., Dommergue, A., De Angelis, M., Cossa, D., Averty, B., Marusczak, N., Soumis, N., Schneider, D., Ferrari, C., 2010. Springtime changes in snow chemistry lead to new insights into mercury methylation in the Arctic. Geochim. Cosmochim. Acta 74, 6263–6275.

Lehnherr, I., & St. Louis, V. (2009). Importance of ultraviolet radiation in the photodemethylation of methylmercury in freshwater ecosystems. Environmental Science and Technology, 43(15), 5692-5698.

Lin, C. J., Gustin, M. S., Singhasuk, P., Eckley, C., and Miller, M.: Empirical models for estimating mercury flux from soils, Environ. Sci. Technol., 44, 8522–8528, 2010.

Lin, H., Zhang, W., Deng, C. et al. Evaluation of passive sampling of gaseous mercury using different sorbing materials, Environ Sci Pollut Res (2017) 24: 14190. doi:10.1007/s11356-017-9018-1

Lindberg, S. E., Zhang, H., Gustin, M., Vette, A., Marsik, F., Owens, J., Casimir, A., Ebinghaus, R., Edwards, G., Fitzgerald, C., Kemp, J., Kock, H. H., London, J., Majewski, M., Poissant, L., Pilote, M., Rasmussen, P., Schaedlich, F., Schneeberger, D., Sommar, J., Turner, R.,Wallschlager, D., and Xiao, Z.: Increases in mercury emissions from desert soils in response to rainfall and irrigation, J. Geophys. Res.-Atmos., 104, 21879–21888, 1999.

Lindberg, S.; Bullock, R.; Ebinghaus, R.; Engstrom, D.; Feng, X.B.; Fitzgerald, W.; Pirrone, N.; Prestbo, E.;Seigneur, C. A synthesis of progress and uncertainties in attributing the sources of mercury in deposition. Ambio 2007, 36, 19–32.

Lindberg, S.E., Brooks, S., Lin, C.-J., Scott, K., Meyers, T., Chambers, L., Landis, M., Stevens, R., 2001. Formation of Reactive Gaseous Mercury in the Arctic: Evidence of Oxidation of Hg. Res.-Atd irrigation, J. Geophys. Resrctic Sunrise. Water Air Soil Pollut. Focus 1, 295–302. doi:10.1023/a:1013171509022

Lindberg, S.E., Brooks, S., Lin, C.-J., Scott, K.J., Landis, M.S., Stevens, R.K., Goodsite, M.E., Richter, A., 2002. Dynamic oxidation of gaseous mercury in the arctic troposphere at polar sunrise. Environ. Sci. Technol. 36, 1245ic Sun.

Lu, J.Y., Schroeder, W.H., 2004. Annual time-series of total filterable atmospheric mercury concentrations in the Arctic. Tellus 56B, 213–222.

Lu, J.Y., Schroeder, W.H., Barrie, L.A., Steffen, A., Welch, H.E., Martin, K., Lockhart, L., Hunt, R.V., Boila, G., Richter, A., 2001. Magnification of atmospheric mercury deposition to polar regions in springtime: the link to tropospheric ozone depletion chemistry. Geophys. Res. Lett. 28, 3219–3222.

Lyman S., Jones C., O'Neil T., Allen T., Miller M., Gustin M.S., Pierec A.M., Winston L., Ren X., Kelley P., Automated Calibration of Atmospheric Oxidized MercuryMeasurements, Environ. Sci. Technol. 2016, 50, 12921−12927

Lyman, S.N., Jaffe, D.A. Formation and fate of oxidized mercury in the upper troposphere and lower stratosphere, Nature Geoscience, doi:10.1038/NGEO1353, 2011.
Macagnano A., Perri V., Zampetti E., Bearzotti A., De Cesare F., Sprovieri F., Pirrone N. A smart nanofibrous material for adsorbing and detecting elemental mercury in air. Atmos. Chem. Phys., 17, 6883-6893, 2017. Https://doi.org/10.5194/acp-17-6883-2017 (b)
Macagnano A., Perri V., Zampetti E., Ferretti A.M., Sprovieri F., Pirrone N., Bearzotti A., Esposito G., De Cesare F. Elemental mercury vapor chemoresistors employing TIO_2 nanofibers photocatalytically decorated with Au-nanoparticles. Sensors and Actuators B 247 (2017) 957–967 (a)
Mann, E. A., Mallory, M. L., Ziegler, S. E., Avery, T. S., Tordon, R., and O'Driscoll, N. J.: Photoreducible mercury loss from Arctic snow is influenced by temperature and snow age, Environ. Sci. Technol., 49, 12120–12126, 2015.
Maxwell, J. A., Holsen, T. M., and Mondal, S.: Gaseous elemental mercury (GEM) emissions from snow surfaces in Northern New York, PloS One, 8, e69342, 2013.
Mazur, M., Mitchell, C. P. J., Eckley, C. S., Eggert, S. L., Kolka, R. K., Sebestyen, S. D., and Swain, E. B.: Gaseous mercury fluxes from forest soils in response to forest harvesting intensity: A field manipulation experiment, Sci. Total Environ., 496, 678–687, 2014.
McLagan D.S., Mazur M.E.E., Mitchell C.P.J., Wania F. Passive air sampling of gaseous elemental mercury: a critical review. Atmos. Chem. Phys., 16, 3061-3076, 2016. Http://www.atmos-chem-phys.net/16/3061/2016/; doi:10.5194/acp-16-3061-2016.
Moore, C. W., Obrist, D., Steffen, A., Staebler, R. M., Douglas, T. A., Richter, A., & Nghiem, S. V. (2014). Sea Ice Lead-induced Convective Forcing of Mercury and Ozone in the Arctic Boundary Layer. Nature
Nerentorp Mastromonaco, M., G, Eckley, C. S., Eggert, S. L., Kolka, R. K., Sebfors, A., Ahnoff, M., Dommergue, A., Meld manipulation experiment, Sci. Total Environ., 496, 678harvesting intensity: A field manipulation experimentn. 129, 125l Env.
Nerentorp Mastromonaco, M., Gårdfeldt, K., Langer, S., Dommergue A., Seasonal Study of Mercury Species in the Antarctic Sea Ice Environment. Environ. Sci. Technol. 50 (23), pp 12705–12712, 2016b.
Nerentorp Mastromonaco, M., Gårdfeldt, K., , Assmann, K M., Langerc, S., Delalid, T., Shlyapnikovd, M Y., Zivkovicd, I., Horvat, M. Speciation of mercury in the waters of the Weddell, Amundsen and Ross Seas (Southern Ocean) Marine ChemistryVolume 193, 20 July 2017, Pages 20–33, 2017.
Nerentorp Mastromonaco, M., Gårdfeldt, K., Jourdain, B., Abrahamsson, K., Granfors, A., Anhoff, M., Dommergue, A., Mejan, G., Jacobi, H-W. 2016 a Antarctic winter mercury and ozone depletion events over sea ice. Atmospheric Environment, 129:125-132, 2016a.
Nerentorp Mastromonaco, M., Gårdfeldt, K., Langer, S. Seasonal Flux of mercury over west Antarctic Seas. Marine Chemistry 193 20:44-54, 2017.
Nghiem, S., Rigor, I., Richter, A., Burrows, J. P., Shepson, P. B., Bottenheim, J., Barber, D. G., Steffen, A., Latonas, J., Wang, F., Stern, G., Clemente-Colón, P., Martin, S., Hall, D. K., Kaleschke, L., Tackett, P., Neumann, G., & Asplin, M. J. (2012). Field and satellite observations of the formation and distribution of Arctic atmospheric bromine above a rejuvenated sea ice cover. Journal of Geophysical Research D: Atmospheres, 117(5), D00S05.
Nguyen, H. T., Kim, K. H., Kim, M. Y., Hong, S., Youn, Y. H., Shon, Z. H., & Lee, J. S. (2007). Monitoring of atmospheric mercury at a global atmospheric watch (GAW) site on An-Myun Island, Korea. Water, air, and soil pollution, 185(1-4), 149-164.
Nguyen, H. T., Kim, M. Y., & Kim, K. H. (2010). The influence of long-range transport on atmospheric mercury on Jeju Island, Korea. Science of the Total Environment, 408(6), 1295-1307.
Osawa, T., Ueno, T., & Fu, F. (2007). Sequential variation of atmospheric mercury in Tokai-mura, seaside area of eastern central Japan. Journal of Geophysical Research: Atmospheres, 112(D19).
Pacyna, E. G., Pacyna, J. M., Fudala, J., Strzelecka-Jastrzab, E., Hlawiczka, S., and Panasiuk, D.: Mercury emissions to the atmosphere from anthropogenic sources in Europe in 2000 and their scenarios until 2020, Sci. Total Environ., 370, 147–156, 2006.
Pfaffhuber, K.A., Berg, T., Hirdman, D., Stohl, A., 2012. Atmospheric mercury observations from Antarctica: seasonal variation and source and sink region calculations. Atmos Chem Phys 12, 3241–3251. doi:10.5194/acp-12-3241-2012.
Pierce, A.H.; Moore, C.W.; Wohlfahrt, G.; HÖrtang, L.; Kljun, N.; Obrist, D. Eddy covariance flux measurements of gaseous elemental mercury using cavity ring-down spectroscopy. Environ. Sci. Technol. 2015, 49, 1559–1568.

Pirrone, N., Hedgecock, I., and Sprovieri, F.: Atmospheric mercury, easy to spot and hard to pin down: impasse?, Atmos. Environ., 42, 8549–8551, doi:10.1016/j.atmosenv.2008.09.004, 2008.

Poissant, L., Pilote, M., 2003. Time series analysis of atmospheric mercury in Kuujjuarapik/Whapmagoostui (Quebec). J Phys IV Fr. 107, 10798551,

Poissant, L.; Pilote, M.; Beauvais, C.; Constant, P.; Zhang, H.H. A year of continuous measurements of three atmospheric mercury species (GEM, RGM and Hgp) in southern Quebec, Canada. Atmos. Environ. 2005, 39, 1275–1287.

Poulain, A. J., Lalonde, J. D., Amyot, J. D., Shead, J. A., Raofie, F., & Ariya, P. A. (2004). Redox transformations of mercury in an Arctic snowpack at springtime. Atmospheric Environment, 38, 6763-6774.

Prestbo, E. M., & Gay, D. A. (2009). Wet deposition of mercury in the US and Canada, 1996–2005: Results and analysis of the NADP mercury deposition network (MDN). Atmospheric Environment, 43(27), 4223-4233.

ResSteffen, A., Douglas, T., Amyot, M., Ariya, P., Aspmo, K., Berg, T., Bottenheim, J., Brooks, S., Cobbett, F., Dastoor, A., Dommergue, A., Ebinghaus, R., Ferrari, C., Gardfeldt, K., Goodsite, M.E., Lean, D., Poulain, A.J., Scherz, C., Skov, H., Sommar, J., Temme, C., 2008. A synthesis of atmospheric mercury depletion event chemistry in the atmosphere and snow. Atmos Chem Phys 8, 1445–1482. doi:10.5194/acp-8-1445-2008.

Risch, M. R., Gay, D. A., Fowler, K. K., Keeler, G. J., Backus, S. M., Blanchard, P., ... & Dvonch, J. T. (2012). Spatial patterns and temporal trends in mercury concentrations, precipitation depths, and mercury wet deposition in the North American Great Lakes region, 2002–2008. Environmental pollution, 161, 261-271.

Schartup, AT, U. Ndu, P.H. Balcom, R.P. Mason, E.M. Sunderland. 2015. Contrasting effects of marine and terrestrially derived organic matter on mercury speciation and bioavailability in seawater. Environmental Science and Technology. 49: 5965-5972.

Schroeder, W. H., Beauchamp, S., Edwards, G., Poissant, L., Rasmussen, P., Tordon, R., Dias, G., Kemp, J., Van Heyst, B., and Banic, C. M.: Gaseous mercury emissions from natural sources in Canadian landscapes, J. Geophys. Res.-Atmos., 110, D18302, 2005.

Schroeder, W.H., Anlauf, K.G., Barrie, L.A., Lu, J.Y., Steffen, A., Schneeberger, D.R., Berg, T., 1998. Arctic spingtime depletion of mercury. Nature 394, 331 sout.

Selin, N. E., Jacob, D. J., Yantosca, R. M., Strode, S., Jaeglé, L., and Sunderland, E. M.: Global 3-D land-ocean-atmosphere model for mercury: Present-day versus preindustrial cycles and anthropogenic enrichment factors for deposition, Global Biogeochem. Cy., 22, GB2011, doi:10.1029/2007GB003040, 2008.

Shah, V., Jaeglé, L., Gratz, L.E., Ambrose, J.L., Jaffe, D.A., Selin, N.E., Song, S., Giang A., et al. Origin of oxidized mercury in the summertime free troposphere over the Southeast United States. Atmos. Chem. Phys., 16, 1511–1530, doi: 10.5194/acp-16-1511-2016, 2016.

Shanley, J. B., Engle, M. A., Scholl, M., Krabbenhoft, D. P., Brunette, R., Olson, M. L., & Conroy, M. E. (2015). High mercury wet deposition at a "clean air" site in Puerto Rico. Environmental Science & Technology, 49(20), 12474-12482.

Sheu, G. R., Lin, N. H., Wang, J. L., Lee, C. T., Yang, C. F. O., & Wang, S. H. (2010). Temporal distribution and potential sources of atmospheric mercury measured at a high-elevation background station in Taiwan. Atmos. Environ. 2010, *44*(20), 2393-2400.

Sillman, S., Marsik, F., Dvonch, J. T., & Keeler, G. J. (2013, January). Assessing atmospheric deposition of mercury in Florida, USA: Local versus global sources and models versus measurements. In E3S Web of Conferences (Vol. 1). EDP Sciences.

Skov, H. Brooks, S. Goodsite, M.E. Lindberg, S.E. Meyers, T.P. Landis, M.S. Larsen, M.R.B. Jensen, B. McConville, G. Christensen, J. (2006) Measuring reactive gaseous mercury flux by relaxed eddy accumulation. Atm. Env. vol 40, 5452-5463.

Skov, H. Christensen, J. Goodsite, M.E. Heidam, N.Z. Jensen, B. Wåhlin, P. and Geernaert, G. (2004) "The fate of elemental mercury in Arctic during atmospheric mercury depletion episodes and the load of atmospheric mercury to Arctic" ES & T. vol. 38, 2373-2382. . doi:10.1021/es030080h.

Skov, H. Sørensen, B.T. Landis, M.E. Johnson, M.S. Lohse, C. Goodsite, M.E. and Sacco, P. (2007) Performance of a new diffusive sampler for Hgo determination in the troposphere. Environmental Chemistry, vol. 4. 75-80.

Skov, H., Christensen, J.H., Goodsite, M.E., Heidam, N.Z., Jensen, B., With reduced sulfur groups, Environ. Sci. T. Sci. Tr groups, Environ. Sci. Tci. Ton with reduced sulfur groups, Environ. Sci. Tn. Sci. Tn.hnol., 40, 4174si180, 2006.iences.viron. Sci. Technol. 38, 2373–2382. doi:10.1021/es030080h

Skyllberg, U., Bloom, P. R., Qian, J., Lin, C. M., and Bleam, W. F.: Complexation of mercury(II) in soil organic matter: EXAFS evidence for linear two-coordination with reduced sulfur groups, Environ. Sci. Technol., 40, 4174–4180, 2006.

Slemr, F., Angot, H., Dommergue, A., Magand, O., Barret, M., Weigelt, A., Ebinghaus, R., Brunke, E.-G., Pfaffhuber, K. A., Edwards, G., Howard, D., Powell, J., Keywood, M., and Wang, F.: Comparison of mercury concentrations measured at several sites in the Southern Hemisphere, Atmos. Chem. Phys., 15, 3125–3133, doi:10.5194/acp-15-3125-2015, 2015.

Slemr, F., Brunke, E.-G., Ebinghaus, R., and Kuss, J.: Worldwide trend of atmospheric mercury since 1995, Atmos. Chem. Phys., 11, 4779–4787, doi:10.5194/acp-11-4779-2011, 2011.

Slemr, F., Ebinghaus, R., Brenninkmeijer, C.A.M., Hermann, M., Kock, H.H., Martinsson, B.G., Schuck, T.,Sprung, D., van Velthoven, P., Zahn, A., Ziereis, H. Gaseous mercury distribution in the upper troposphere and lower stratosphere observed onboard the CARIBIC passenger aircraft, Atmos. Chem. Phys. 9, 1957-1969, 2009.

Slemr, F., Ebinghaus, R., Brenninkmeijer, C.A.M., Hermann, M., Kock, H.H., Levine, I., Martinsson, B., Schuck, T., Sprung, D., van Velthoven, P., Zahn, A., Ziereis H.: Gaseous mercury distribution in the upper troposphere and lower stratosphere observed during the CARIBIC flights from Frankfurt to southern China and to South America, Atmospheric Chemistry and Physics, 9 (6): 1957-1969, 2009.

Slemr, F., Ebinghaus, R., Weigelt, A., Kock, H. H., Brenninkmeijer, C. A. M., Schuck, T., Hermann, M., et al.: CARIBIC observations of gaseous mercury in the upper troposphere and lower stratosphere. E3S Web of Conferences, 1(2013), 17001. (doi:10.1051/e3sconf/20130117001), 2013.

Slemr, F.; Brenninkmeijer, C.A.; Rauthe-Schöch, A.; Weigelt, A.; Ebinghaus, R.; Brunke, E.-G.; Martin, L.; Spain, T.G.; O´Doherty, S.: El Niño–Southern Oscillation influence on tropospheric mercury concentrations. Geophysical Research Letters 43, 1766–1771 (doi:10.1002/2016GL067949), 2016a.

Slemr, F.; Weigelt, A.; Ebinghaus, R.; Brenninkmeijer, C.; Baker, A.; Schuck, T.; Rauthe-Schöch, A.; Riede, H., Leedham, E.; Hermann, M.; van Velthoven, P.; Oram, D.; O'Sullivan, D.; Dyroff, C.; Zahn, A.; Ziereis, H.: Mercury Plumes in the Global Upper Troposphere Observed during Flights with the CARIBIC Observatory from May 2005 until June 2013, Atmosphere, 5, 342-369; doi:10.3390/atmos5020342, 2014.

Slemr, F.; Weigelt, A.; Ebinghaus, R.; Kock, H.H.; Bödewadt, J.; Brenninkmeijer, C.A.M.; Rauthe-Schöch, A.; Weber, S.; Hermann, M.; Becker, J.; Zahn, A.; Martinsson, B.: Atmospheric mercury measurements onboard the CARIBIC passenger aircraft. Atmospheric Measurement Techniques 9, 2291–2302 (doi: 10.5194/amt-9-2291-2016), 2016b.

Smith-Downey, N.V., E.M. Sunderland, D.J. Jacob. 2010. Anthropogenic impacts on global storage and emissions of mercury from terrestrial soils: Insights from a new global model. Journal of Geophysical Research, 115, G03008.

Soerensen, A., Skov, H., Soerensen, D. J. B., and Johnson, M.: Global concentrations of gaseous elemental mercury and reactive gaseous mercury in the marine boundary layer, Environ. Sci. Technol., 44, 7425–7430, doi:10.1021/es903839n, 2010a.

Soerensen, A., Sunderland, E., Holmes, C., Jacob, D., Yantosca, R., Skov, H., Christensen, J., Strode, S., and Mason, R.: An improved global model for air-sea exchange of mercury: high concentrations over the North Atlantic, Environ. Sci. Technol., 44, 8574–8580, doi:10.1021/es102032g, 2010b.

Soerensen, A.L., D.J. Jacob, A.T. Schartup, J.A. Fisher, I. Lehnherr, V.L. St. Louis, L-E. Heimberger, J.E. Sonke, D.P. Krabbenhoft, E.M. Sunderland. (2016). A mass budget for mercury and methylmercury in the Arctic Ocean. Global Biogeochemical Cycles, 30, 560–575, doi:10.1002/2015GB005280.

Soerensen, A.L., D.J. Jacob, D.G. Streets, M.L.I. Witt, R. Ebinghaus, R.P. Mason, M. Andersson, E.M. Sunderland. 2012. Multi-decadal decline of mercury in the North Atlantic atmosphere explained by changing subsurface seawater concentrations. Geophysical Research Letters, 39, L21810.

Soerensen, A.L., R.P. Mason, P.H. Balcom, D.J. Jacob, Y. Zhang, J. Kuss, E.M. Sunderland. 2014. Elemental mercury concentrations and fluxes in the tropical atmosphere and ocean. Environmental Science and Technology. 48, 11312-11319.

Soerensen, A.L., R.P. Mason, P.H. Balcom, E.M. Sunderland. 2013. Drivers of surface ocean mercury concentrations and air-sea exchange in the West Atlantic Ocean. Environmental Science and Technology. 47, 7757-7765.

Sommar, J., Andersson, M. E., and Jacobi, H.-W.: Circumpolar measurements of speciated mercury, ozone and carbon monoxide in the boundary layer of the Arctic Ocean, Atmos. Chem. Phys., 10, 5031–5045, doi:10.5194/acp-10-5031-2010, 2010.

Sommar, J., W, Sunderland, E., Holmes, C., Jacob, D., Yantosca, R., Skov, H., Christensen, J., Strode, S., and Mason, R.: ACircumpolar transport and air-surface exchange of atmospheric mercury at Ny- over the North ASvalbard, spring 2002. Atmos Chem Phys 7, 151–166. doi:10.5194/acp-7-151-2007.

Sprovieri F., N. Pirrone, M.S. Landis, R.K. Stevens (2005a) Oxidation of gaseous elemental mercury to gaseous divalent mercury during 2003 polar sunrise at Ny-Alesund. Environmental Science & Technology 39 (23), 9156-9165.

Sprovieri F., N. Pirrone, M.S. Landis, R.K. Stevens (2005b) Atmospheric mercury behavior at different altutudes at Ny Alesund during Spring 2003. Atmospheric Environment 39 (39), 7646-7656.

Sprovieri, F., Pirrone, N., Bencardino, M., D'Amore, F., Angot, H., Barbante, C., Brunke, E.-G., Arcega-Cabrera, F., Cairns, W., Comero, S., Diéguez, M. D. C., Dommergue, A., Ebinghaus, R., Feng, X. B., Fu, X., Garcia, P. E., Gawlik, B. M., Hageström, U., Hansson, K., Horvat, M., Kotnik, J., Labuschagne, C., Magand, O., Martin, L., Mashyanov, N., Mkololo, T., Munthe, J., Obolkin, V., Ramirez Islas, M., Sena, F., Somerset, V., Spandow, P., Vardè, M., Walters, C., Wängberg, I., Weigelt, A., Yang, X., and Zhang, H.: Five-year records of mercury wet deposition flux at GMOS sites in the Northern and Southern hemispheres, Atmos. Chem. Phys., 17, 2689-2708, doi:10.5194/acp-17-2689-2017, 2017.Temme, C., Blanchard, P., Steffen, A., Banic, C., Beauchamp, S., Poissant, L., Tordon, R., andWiens, B.: Trend, seasonal and multivariate analysis study of total gaseous mercury data from the Canadian atmospheric mercury measurement network (CAMNet), Atmos. Environ., 41, 5423–5441, 2007.

Sprovieri, F., Pirrone, N., Bencardino, M., D'Amore, F., Carbone, F., Cinnirella, S., Mannarino, V.,Landis, M., Ebinghaus, R., Weigelt, A., Brunke, E-G., Labuschagne, C., Martin, L., Munthe, J.,Wängberg, I., Artaxo, P., Morais, F., de Melo Jorge Barbosa, H., Brito, J., Cairns, W., Barbante,C., del Carmen Diéguez, M., Garcia, P.E., Dommergue, A., Angot, H., Magand, O., Skov, H.,Horvat, M., Kotnik, J., Read, K.A., Neves, L.M., Gawlik, B.M., Sena, F., Mashyanov, N.,Obolkin, W., Wip, D., Feng, X.B., Zhang, H., Fu, X., Ramachandran, R., Cossa, D., Knoery, J.,Marusczak, N., Nerentorp, M., Norstrom, C., 2016. Atmospheric mercury concentrationsobserved at ground-based monitoring sites globally distributed in the framework of theGMOS network. Atmos. Chem. Phys., 16, 11915-11935,

Sprovieri, F., Pirrone, N., Bencardino, M., D'Amore, F., Angot, H., Barbante, C., Brunke, E.-G., Arcega-Cabrera, F., Cairns, W., Comero, S., Diéguez, M. D. C., Dommergue, A., Ebinghaus, R., Feng, X. B., Fu, X., Garcia, P. E., Gawlik, B. M., Hageström, U., Hansson, K., Horvat, M., Kotnik, J., Labuschagne, C., Magand, O., Martin, L., Mashyanov, N., Mkololo, T., Munthe, J., Obolkin, V., Ramirez Islas, M., Sena, F., Somerset, V., Spandow, P., Vardè, M., Walters, C., Wängberg, I., Weigelt, A., Yang, X., and Zhang, H.: Five-year records of mercury wet deposition flux at GMOS sites in the Northern and Southern hemispheres, Atmos. Chem. Phys., 17, 2689-2708, doi:10.5194/acp-17-2689-2017, 2017.Stamenkovic, J., Gustin, M. S., Arnone, J. A., Johnson, D. W., Larsen, J. D., and Verburg, P. S. J.: Atmospheric mercury exchange with a tallgrass prairie ecosystem housed in mesocosms, Sci. Total Environ., 406, 227–238, 2008.

Sprovieri, F., Pirrone, N., Ebinghaus, R., Kock, H., and Dommergue, A.: A review of worldwide atmospheric mercury measurements, Atmos. Chem. Phys., 10, 8245–8265, doi:10.5194/acp-10-8245-8265, 2010, 2010.

Sprovieri, F., Pirrone, N., Hedgecock, I.M., Landis, M.S., Stevens, R.K., 2002. Intensive atmospheric mercury measurements at Terra Nova Bay in antarctica during November and December 2000. J. Geophys. Res. 107, 4722. doi:10.1029/2002JD002057.

Steffen, A., Schroeder, W., Macdonald, R., Poissant, L., Konoplev, A., 2005. Mercury in the Arctic atmosphere: An analysis of eight years of measurements of GEM at Alert (Canada) and a comparison with observations at Amderma (Russia) and Kuujjuarapik (Canada). Sci. Total Environ., Sources, Occurrence, Trends and Pathways of Contaminants in the ArcticBidleman S.I. 342, 185–198. doi:10.1016/j.scitotenv.2004.12.04, 2005.

Steffen, A., Douglas, T., Amyot, M., Ariya, P., Aspmo, K., Berg, T., Bottenheim, J., Brooks, S., Cobbett, F. D., Dastoor, A., Dommergue, A., Ebinghaus, R., Ferrari, C., Gardfeldt, K., Goodsite, M. E., Lean, D., Poulain, A. J., Scherz, C., Skov, H., Sommar, J. and Temme, C. (2008). "A synthesis of atmospheric mercury depletion event chemistry in the atmosphere and snow." Atmospheric Chemistry and Physics 8: 1445-1482, 2008.

Steffen, A., Bottenheim, J., Cole, A., Douglas, T. A., Ebinghaus, R., Friess, U., Netcheva, S., Nghiem, S., Sihler, H., & Staebler, R.. Atmospheric mercury over sea ice during the OASIS-2009 campaign. Atmospheric Chemistry and Physics, 13, 7007-7021, 2013.

Steffen, A., Bottenheim, J., Cole, A., Ebinghaus, R., Lawson, G. and Leaitch, W. R.. "Atmospheric mercury speciation and mercury in snow over time at Alert, Canada." Atmospheric Chemistry and Physics 14: 2219-

2231, 2014.
Sunderland, EM, RP Mason. (2007) Human impacts on open ocean mercury concentrations. Global Biogeochemical Cycles. GB4022, doi:10.1029/2006GB002876, 2007.
Swartzendruber, P. C., Jaffe, D.A., Finley, B., 2009. Development and First Results of an Aircraft-Based, High Time Resolution Technique for Gaseous Elemental and Reactive (Oxidized) Gaseous Mercury. Environ. Sci. Technol. 43, 7484–7489.
Temme, C., Einax, J.W., Ebinghaus, R., Schroeder, W.H., 2003. Measurements of atmospheric mercury species at a coastal site in the antarctic and over the atlantic ocean during polar summer. Environ. Sci. Technol. 37, 22ol.
Tørseth, K., Aas, W., Breivik, K., Fjæraa, A.M., Fiebig, M., Hjellbrekke, A.G., Lund Myhre, C., Solberg, S., Yttri, K.E. (2012). Introduction to the European Monitoring and Evaluation Programme (EMEP) and observed atmospheric composition change during 1972-2009. Atmospheric Chemistry and Physics, 12, 5447-5481. doi:10.5194/acp-12-5447-2012.
Travnikov O., H. Angot, P. Artaxo, M. Bencardino, J. Bieser, F. D'Amore, A. Dastoor, F. De Simone, M. del Carmen Diéguez, A. Dommergue, R. Ebinghaus, X. B. Feng, C. N Gencarelli, I. M Hedgecock, O. Magand, L. Martin, M. Volker, N. Mashyanov, N. Pirrone, R. Ramachandran, K. A. Read, A. Ryjkov, N. E Selin, F. Sena, S. Song, F. Sprovieri, D. Wip, I. Wängberg, X. Yang, 2017. Multi-model study of mercury dispersion in the atmosphere: atmospheric processes and model evaluation. Atmos. Chem. Phys., 17, 5271–5295.
United Nations Environment, 2015. Global mercury modelling: update of modelling results in the global mercury assessment 2013.
United Nations Environment, Global Review of Mercury Monitoring Networks, 1- 48, November 2016.
van Belle, G. and Hughes, J. P. "Nonparametric tests for trend in water quality." Water Resources Research 20(1): 127-136, 1984.
Wang, J., Zhang, L., Xie, Z., 2016. Total gaseous mercury along a transect from coastal to central Antarctic: Spatial and diurnal variations. J. Hazard. Mater. 317, 362 Guizhou,:10.1016/j.jhazmat.2016.05.068
Wang, S. F., Feng, X. B., Qiu, G. L., Fu, X. W., and Wei, Z. Q.: Characteristics of mercury exchange flux between soil and air in the heavily air-polluted area, eastern Guizhou, China, Atmos. Environ., 41, 5584–5594, 2007.
Weigelt, A., Ebinghaus, R., Manning, A., Derwent, R., Simmonds, P., Spain, T., Jennings, S., and Slemr, F.: Analysis and interpretation of 18 years of mercury observations since 1996 at Mace Head, Ireland, Atmos. Environ., 100, 85–93, doi:10.1016/j.atmosenv.2014.10.050, 2015.
Weigelt, A., Ebinghaus, R., Pirrone, N., Bieser, J., Bödewadt, J., Esposito, G., Slemr, F., van Velthoven, P. F. J., Zahn, A., and Ziereis, H.: Tropospheric mercury vertical profiles between 500 and 10 000m in central Europe, Atmos. Chem. Phys., 16, 4135–4146, doi:10.5194/acp-16-4135-2016, 2016.
Weigelt A., Franz Slemr, Ralf Ebinghaus, Nicola Pirrone, Johannes Bieser, Jan Bödewadt, Giulio Esposito, and Peter F. J. van Velthoven (2016) Mercury emissions of a coal-fired power plant in Germany**.** *Atmospheric Chemistry & Phys*ics, 16, 13653-13668, doi:10.5194/acp-16-13653-2016, 2016.
Weigelt, A.; Temme, C.; Bieber, E.; Schwerin, A.; Schuetze, M.; Ebinghaus, R.; Kock, H.H. : Measurements of atmospheric mercury species at a German rural background site from 2009 to 2011 – methods and results, Environmental Chemistry, 10(2), 102-110 (DOI: 10.1071/EN12107), 2013.
Weiss-Penzias, P. S., Gay, D. A., Brigham, M. E., Parsons, M. T., Gustin, M. S., & ter Schure, A. Trends in mercury wet deposition and mercury air concentrations across the US and Canada. Science of the Total Environment, 568, 546-556, 2016.
Xin, M. and Gustin, M. S.: Gaseous elemental mercury exchangewith low mercury containing soils: Investigation of controlling factors, Appl. Geochem., 22, 1451–1466, 2007.
Yang, Y. K., Zhang, C., Shi, X. J., Lin, T., andWang, D. Y.: Effect of organic matter and pH on mercury release from soils, J. Environ. Sci., 19, 1349–1354, 2007.
Yu, J., Xie, Z., Kang, H., Li, Z., Sun, C., Bian, L., Zhang, P., 2014. High variability of atmospheric mercury in the summertime boundary layer through the central Arctic Ocean. Sci. Rep. 4, 6091. doi:10.1038/srep06091.
Zhang, Y., D.J. Jacob, H.M. Horowitz, L. Chen, H.M. Amos, D.P. Krabbenhoft, F. Slemr, V.L. St. Louis, E.M. Sunderland. Observed dcrease in atmospheric mercury explained by global decline in anthropogenic emissions. Proceedings of the United States National Academy of Sciences. 113(3): 526-531, 2016.

7480 Zhang, Y., D.J. Jacob, S. Dutkiewicz, H.M. Amos, M.S. Long, E.M. Sunderland. (2015). Biogeochemical drivers of
7481 the fate of riverine mercury discharged to the global and Arctic oceans. Global Biogeochemical Cycles, 29,
7482 854-864.
7483 Zhou, H., Zhou, C., Lynman, M.M. Dvonch, J.T., Barres, J.A., Hopke, P.K., Cohen, M. and Holsen, T.M,
7484 Atmospheric Mercury Temporal Trends in the Northeastern United States from 1992 to 2014: Are
7485 measured concentrations responding to decreasing regional emissions? *Environmental Science and*
7486 *Technology* Letters, 4, 91-97, 2017.
7487 Zhu W., Lin CJ., Wang X., Sommar J., Fu X., and Feng X., Global observations and modeling of atmosphere–
7488 surface exchange of elemental mercury: a critical review. Atmos. Chem. Phys., 16, 4451–4480, 2016.

5. Atmospheric pathways, transport and fate

Authors: Oleg Travnikov, Hélène Angot, Johannes Bieser, Mark Cohen, Ashu Dastoor, Francesco De Simone, Ian Hedgecock, Sae Yun Kwon, Che-Jen Lin, Andrei Ryjkov, Noelle Selin, Colin P. Thackray, Xun Wang

Key messages

- *Significant progress has been made since GMA 2013 in all key areas of interest regarding the atmospheric mercury (Hg) cycle. Uncertainties remain in quantifying emissions, particularly from certain regions and sectors and in Hg speciation. Emission rates from natural surfaces need to be better constrained. New information has solidified our knowledge about Hg oxidation reactions, including the importance of bromine chemistry.*
- *Both model simulations and natural archives provide evidence for peak atmospheric Hg concentrations during the latter half of the 20th century and declines in more recent decades. Future changes under policy scenarios could reduce Hg deposition in the future, but the influence of climate change and legacy Hg complicates our ability to assess this.*
- *Atmospheric Hg concentrations are highest in the temperate latitudes of the Northern Hemisphere and lowest in the high latitudes of the Southern Hemisphere. Highest concentrations are found in East, South, and Southeast Asia due to high anthropogenic emissions as well as in equatorial Africa and South America because of active artisanal and small-scale gold mining (ASGM). Total Hg deposition is more equally distributed between the Northern and Southern Hemispheres, highest in large industrial regions and lowest in remote unpopulated regions. Regions with active ASGM are also subject to a relatively high total Hg deposition rate.*
- *Atmospheric deposition from direct anthropogenic emissions is the mixture of domestic emissions and atmospherically transported Hg from sources in other regions. The share of domestic sources varies from more than 65% in Asia to less than 5% in the Arctic and Antarctica. In East and South Asia, anthropogenic Hg deposition is dominated by the contribution from domestic sources (77% and 66%, respectively). Domestic and foreign anthropogenic sources contribute almost equally to the total anthropogenic Hg deposition in Europe.*
- *Mercury removal from the atmosphere occurs via wet and dry deposition. Dry deposition remains more poorly quantified than wet deposition, and there remains disagreement among models on its global magnitude.*
- *In North America, the contribution of domestic sources to regional deposition has declined from 23% to 17%, due to the reduction in North American anthropogenic emissions since 2010. Regions with active ASGM (Africa, South and Central America) also receive a relatively large fraction of anthropogenic deposition from domestic sources (30–38%). The largest foreign contributors to various receptor regions are East Asia, Africa, South America, and Southeast Asia.*
- *East Asia and Africa remain the largest contributors to the global ocean reservoirs, owing to their large anthropogenic emissions (20–50% and 10–27%, respectively). The only exception is the Mediterranean and Black Seas, where the contribution from European anthropogenic emissions (20%) dominates over East Asian and African sources.*
- *Mercury deposition from the power generation sectors is largely restricted to a few industrial regions, with the largest contribution in Europe and South Asia. Deposition from industrial sources covers wider areas in Asia, Europe, North and South America, and Africa. The impact of emissions from intentional use and product waste is insignificant in all regions. Mercury emissions from ASGM are transported globally, but the most significant deposition occurs closer to the sources and largely impacts South America, equatorial Africa, and East and Southeast Asia.*

5.1 Introduction

Mercury (Hg) has a long environmental lifetime and cycles between the atmosphere, ocean, and land. Mercury released to the atmosphere can travel globally: it undergoes atmospheric redox reactions, deposits to the Earth's surface, and can continue to cycle between surface and atmosphere for decades to centuries and longer. Using a combination of models and measurements, work since the 2013 Global Mercury Assessment (GMA 2013) (AMAP/UNEP 2013) has addressed various aspects of Hg transport and fate, including emissions, atmospheric chemistry, removal processes, modelling, and historical trends. A number of other studies have also provided insights into regional and local Hg cycling.

Emissions and their speciation: The emergence of new regional and global emissions inventories provides alternatives to the UNEP/AMAP inventories for the present day as well as new historical estimates. Uncertainties remain in quantifying emissions, particularly from certain regions and sectors and in Hg speciation.

Atmospheric chemistry: New information has solidified knowledge about Hg oxidation reactions, including the importance of bromine (Br) chemistry in Hg oxidation. Models including these reactions have shorter Hg lifetimes and can reproduce some free tropospheric observations. It should be noted that use of oxidation reactions with hydroxyl radical (OH) and ozone (O_3) in Hg modelling studies also allows reproducing of spatial and temporal patterns of Hg measurements. However, while oxidation in the presence of OH and O_3 has been observed in laboratory experiments, direct reactions of Hg with OH and O_3 are not supported by the theoretical chemical literature implying the possibility of heterogeneous pathways. Thus, significant uncertainties remain in the understanding of atmospheric Hg oxidation

and reduction. Recent model intercomparison studies have shown that there remain challenges in reproducing observed concentrations and patterns when varying atmospheric redox mechanisms are used in the models. In particular, uncertainty remains in atmospheric speciation (Jaffe et al., 2014), the potential importance of heterogeneous chemistry (Ariya et al, 2015), and the mechanism and rate of atmospheric reduction reactions (de Foy et al., 2016).

Removal processes: Measurement and model comparison studies of wet deposition, especially in convective storms, have provided insight into the vertical distribution of Hg in the troposphere as well as oxidation processes. Dry deposition remains more poorly quantified than wet deposition, and there remains disagreement among models on its global magnitude. New measurement analyses of dry deposition have shown the importance of gaseous elemental mercury (Hg^0) uptake into the terrestrial environment, in addition to deposition of oxidized Hg forms.

Mercury modelling: Recent model development has advanced the ability to simulate Hg transport in the atmosphere between different geographical regions and to account for multi-media cycling of Hg, including the importance of legacy Hg. New modelling results based on the updated global Hg emissions inventory for 2015 provided up-to-date estimates of Hg dispersion on a global scale, source apportionment of Hg deposition to various terrestrial and aquatic regions and the contribution of different emission sectors to Hg atmospheric loads (see Section 5.3).

Historical trends and future scenarios: Recent declines have been observed in both atmospheric Hg concentration and wet deposition, on the order of 1–2% per year, that differ by region. Some modelling studies have reproduced these trends, attributing some regional variations to declines in emissions. The observed trends, however, are small compared with uncertainties in surface-atmosphere fluxes, anthropogenic sources, and their attributable fraction. Future changes in Hg emissions under policy scenarios could reduce Hg deposition in the future; however, the influence of climate change and legacy Hg complicates the ability to identify sources and mechanisms that may lead to future changes in atmospheric Hg.

5.2 Atmospheric processes

In GMA 2013, the atmospheric chemistry section (section 3.2) focused on emission speciation, atmospheric Hg redox chemistry, processes governing the exchange of Hg at environmental interfaces and atmospheric Hg dynamics. Progress has since been made in all key areas of interest regarding atmospheric Hg chemistry as well as in some that were not included, especially progress in the last few years of using Hg isotope fractionation to probe Hg processes and origins. However, it may seem that more questions have been posed than answered. Atmospheric Hg processes have been studied or inferred using theoretical, experimental, monitoring and modelling techniques, and usually a combination of all four. The chemical nature of atmospheric Hg, whether elemental, oxidized or bound (tightly or loosely) to atmospheric particulate matter, and its interconversion between these forms, continues to pose a challenge for the emission inventory, modelling and measurement communities alike.

5.2.1 Emissions and their speciation

As discussed in Chapter 2, there are numerous uncertainties in estimating current and historical anthropogenic Hg emissions as well as natural and legacy emissions. In addition to the AMAP/UNEP emission inventories of 2008 and 2013 (AMAP/UNEP, 2008, 2013) new global Hg emission inventories have been developed. In particular, the EDGAR global inventory of Hg anthropogenic emissions for the period 1970–2008 (Muntean et al., 2014) uses different approaches to determine emissions from anthropogenic activity sectors and differs in both total Hg emissions and their speciation compared to the AMAP/UNEP inventory. The EDGAR inventory total Hg emissions are roughly two-thirds of the AMAP/UNEP totals for 2008 and 2013 (1287 and 1960 Mg, respectively), and the relative contributions of elemental, oxidized, and particulate Hg also differ, 81:14:5 for AMAP/UNEP and 72:22:6 for EDGAR. Geographical distribution is broadly similar in the two emission inventories (see De Simone et al., 2016). All-time emissions to the atmosphere have also been quantified by taking into account estimates of releases (Streets et al., 2011, 2017). Other developments include regional inventories (Rafaj et al., 2014; Wu et al., 2016), estimates of historical and legacy Hg emissions (Amos et al., 2013, 2015), and the contribution of the past and current use of Hg in commercial products (Horowitz et al., 2014). A model comparison study of the effect of using different global emission inventories (De Simone et al., 2016) showed a consistent geographical pattern across the models, in which anthropogenic emissions contribute less than 15% of total Hg deposition in the Southern Hemisphere, 15–20% in the Tropics and 20–30% in the Northern Hemisphere. Exceptions were observed in industrial 'hotspots', where domestic anthropogenic emissions accounted for the majority of Hg deposition.

The importance of accurate emission inventories and how their uncertainty relates to the effectiveness evaluation of the Minamata Convention was discussed by Kwon and Selin (2016). The observed decrease in atmospheric Hg species concentrations (e.g., Castro and Sherwell, 2015; Ren et al., 2016; Zhou et al., 2017) in the USA is consistent with significant regional decreases in emissions upwind of measurement sites as shown in global as well as U.S. and Canadian national inventories. In addition, the observed increase in Hg concentrations measured in the Southern Hemisphere at Cape Point (South Africa) over the past decade is consistent with the estimated increase in Hg emissions from artisanal and small-scale gold mining in the Southern Hemisphere over the same period (Martin et al., 2017). However, some authors call into question the accuracy of current global emission inventories, particularly in their estimation of European and North American sources (Zhang et al., 2016c), and suggest that there has been a 20% decrease in global anthropogenic Hg emissions between 1990 and 2010, with a 30% decrease in anthropogenic Hg^0. Some additional factors that could result in underestimated reduction of Hg levels in the atmosphere were discussed by Amos et al. (2015) and include the overestimation of geogenic emissions and oceanic evasion of Hg.

Since GMA 2013, some progress has been made in emission speciation. Regional and global modelling studies have also called into question the speciation in emission inventories for specific areas (Kos et al., 2013; Bieser et al., 2014; Zhang et al., 2015). The partitioning of oxidized Hg compounds (Hg^{II})

between the gas and particulate phases is still difficult to determine. This is partly due to the lack of information on the Hg^{II} species present in the atmosphere, but also to the vast range of particulate chemical composition. Ariya et al. (2015) discussed heterogeneous reactions of Hg in some detail as well as interactions between Hg and fly ash generated at coal-fired power plants, which is particularly important during the combustion processes leading to Hg emissions. Uncertainties in the atmospheric measurements of speciated Hg further complicate this issue. The tendency of models to produce oxidized Hg concentrations higher than measured may be at least partly due to the measurements being biased low in some situations, rather than solely because of emissions speciation errors.

While Hg emission and speciation from anthropogenic sources have been quantified and updated with a reasonable consistency, estimates of natural Hg emission from the Earth's surfaces, including re-emission of previously deposited Hg, are poorly constrained and have large uncertainties (±2000 Mg/y). This limits the understanding of global and regional Hg cycling budgets (Pirrone et al., 2010; Song et al., 2015; Zhu et al., 2016). The primary challenge in quantifying Hg^0 release from natural surfaces is the lack of understanding in fundamental processes driving the release from different types of surface. Measurements of Hg stable isotope ratios in soil, biomass and air samples suggests that Hg^0 re-emitted from soil and leaf litter is derived from Hg previously bound in the soils and leaf interior, which is subsequently sequestered and recycled, rather than originating from Hg deposited recently on soil and foliage surfaces (Demers et al., 2013; Yu et al., 2016; Yuan et al., 2018).

5.2.2 Atmospheric chemistry

Atmospheric redox reactions can occur homogeneously in the gas and aqueous phases, and heterogeneously on the surface of fog/cloud droplets and atmospheric particulate matter. It is clear that the heterogeneous reactions are more complex to study than the homogenous reactions due to the very wide range of composition of the surfaces at which reactions may take place. A recent review by Ariya et al. (2015) provides an in-depth overview of Hg reactions and transformations in environmental media.

Perhaps the major obstacle to understanding the processes by which Hg is oxidized, reduced, adsorbed and desorbed in the atmosphere and both in and on atmospheric particles is because the nature of the oxidized Hg compounds in the atmosphere remains uncertain. While it seems clear that O_3, OH, and Br are all implicated in the oxidation of atmospheric Hg, the precise nature of the reactions occurring and the identity (and phase) of the products remains the subject of speculation. Recent theoretical studies have given further insight into the Br-initiated oxidation of Hg; this reaction proceeds via an unstable $HgBr^*$ intermediate which may react further to form oxidized Hg species or decompose back to Hg and Br (Goodsite et al., 2004, 2012). Several theoretical studies have investigated the possibility that $HgBr^*$ may react with a series of small atmospheric compounds (Dibble et al, 2012, 2013, 2014; Jiao and Dibble, 2015, 2017) and volatile organic compounds (Dibble and Schwid, 2016). Based on these studies, it appears likely that the $HgBr^*$ intermediate may react further with the relatively abundant radicals HO_2 and NO_2. Meanwhile the likelihood that elemental Hg is oxidized by molecular halogens has been shown to be improbable and that oxidation to Hg halides requires either halogen atom initiation or the presence of a reactive surface (Auzmendi-Murua et al., 2014).

Discussion of atmospheric Hg oxidation by halogens and their compounds must come with the caveat that while the latitudinal, vertical and seasonal variations in O_3 and OH concentrations have been well studied and documented, those of the halogens have not. Thus the halogen concentration fields used in Hg modelling studies are themselves the subject of not insignificant uncertainty, meaning that it remains difficult to draw firm conclusions on the precise role of individual Hg oxidants in the atmosphere. Nonetheless ever more studies on halogen and halogen compounds are becoming available as their impact on numerous aspects of atmospheric chemistry, beyond their role in stratospheric O_3 depletion becomes clear (see, for example, Hossaini et al., 2015; Simpson et al., 2015; Wang et al., 2015; Jourdain et al., 2016; Sherwen et al., 2016).

Considering only oxidation reactions can lead to atmospheric lifetimes for Hg^0 which cannot be reconciled with its global distribution and relatively uniform background hemispheric concentrations. Experimental and observational evidence (in particular the rapid depletion of Hg^0 concentrations seen during atmospheric mercury depletion events; AMDEs) as well as the results from theoretical kinetics studies, point to an atmospheric lifetime against oxidation shorter than that previously estimated of around 12 months (Schroeder and Munthe, 1998). Two recent model studies (Shah et al., 2016; Horowitz et al., 2017) suggested that it may be less than three months; however, these studies both use hypothetical reduction mechanisms to constrain the Hg^0 concentration to observed values. There is, therefore, likely to be Hg reduction taking place in the atmosphere, and over the years several mechanisms have been suggested, most of which have involved the atmospheric aqueous phase, cloud and fog droplets and deliquesced aerosols, as the reaction medium. See Ariya et al. (2015) for a thorough discussion of possible reduction pathways. Most recently it has been suggested that atmospheric reduction occurs in cloud droplets via the photo-reduction of organic Hg compounds. This mechanism was tested in a model study using simulated organic aerosol concentrations as an indicator of organic Hg compound concentrations (Horowitz et al., 2017). However, it should be noted that the rate of reduction in global models is largely tuned to reproduce observed Hg species concentrations. As for the stratosphere, estimates based on long-term aircraft measurements show that the stratospheric lifetime of Hg (72± 37 years) is longer than was previously estimated (Slemr et al., 2018).

Further information concerning Hg oxidation at different levels in the atmosphere has been obtained as a result of the increasing availability of observational data available from high-altitude measurement sites and aircraft measurements. Observations combined with modelling can help determine which Hg atmospheric oxidation pathways are more or less likely. Weiss-Penzias et al. (2015) found that, during one high Hg^{II} free tropospheric event, there was almost quantitative oxidation of Hg^0 to Hg^{II}. Interestingly, a better model reproduction of the observations (using the GEOS-Chem model prior to the update

of the Hg chemistry scheme as described by Horowitz et al., 2017) was found when employing the O_3/OH rather than the $HgBr^*$ oxidation scheme. Recent model-measurement comparison studies have shown episodes of high oxidized Hg concentrations that can be explained by Br oxidation (Gratz et al., 2015; Coburn et al., 2016) and that this is consistent with constraints from global biogeochemical cycling (Shah et al., 2016). These studies collectively show that measurements in free tropospheric air can significantly aid understanding of the atmospheric chemistry and dynamics of Hg.

Kos et al. (2013) performed a detailed analysis of the uncertainties associated with Hg^{II} measurement and modelling. Several model sensitivity runs were carried out to evaluate different chemical mechanisms and speciation of anthropogenic Hg emissions. In particular, Kos et al. (2013) found evident inconsistencies between the emission speciation in existing emission inventories and the measured Hg^{II} concentration in surface air. Besides, the OH oxidation chemistry provided better agreement with observations at simulation of the seasonal cycle of wet deposition in North America.

A complex analysis of the major Hg oxidation mechanisms was carried out by Travnikov et al. (2017) involving both measured data from ground-based sites and simulation results from four global chemical transport models. It was shown that the Br oxidation mechanism can reproduce successfully the observed seasonal variation of the Hg^{II}:Hg^0 ratio in the near-surface air, but predicts a wet deposition maximum in spring instead of summer as observed at monitoring sites in North America and Europe. Model runs with OH chemistry correctly simulated both the periods of maximum and minimum values and the amplitude of observed seasonal variation but shift the maximum Hg^{II}:Hg^0 ratios from spring to summer. Ozone chemistry did not predict significant seasonal variation in Hg oxidation. Travnikov et al. (2017) suggested the possibility of more complex chemistry and/or multiple Hg oxidation pathways occurring concurrently in various parts of the atmosphere.

Bieser et al. (2017) used the same model ensemble and various aircraft observations to study vertical and hemispheric distributions of atmospheric Hg. They also found that different chemical mechanisms were better at reproducing observed Hg^{II} patterns depending on altitude. Increased Hg^{II} concentrations above the planetary boundary layer in spring and summer could only be reproduced by models using O_3 and OH chemistry. On the other hand, the use of the Br oxidation mechanism generated better agreement with observed intercontinental gradients of total Hg in the upper troposphere.

As shown above, measurements of oxidized Hg are an important tool for assessing Hg chemistry and fate. However, uncertainties in the measurement techniques challenge our ability to further advance model-measurement comparison of Hg species (Gustin et al., 2015). There is growing evidence that oxidized Hg measurements performed using a Tekran speciation technique suffer from significant biases and interferences (Lyman et al., 2010; Gustin et al., 2013; Jaffe et al., 2014; Marusczak et al., 2016). While modelled results discussed in this report as well as other studies are often evaluated against available measurements, further coordination between measurement and modelling communities to address measurement biases will enhance our understanding of atmospheric Hg processes.

5.2.3 Removal process

Mercury removal from the atmosphere occurs via wet and dry deposition (Risch et al., 2012; Weiss-Penzias et al., 2016). Studies of Hg deposition are providing insights into atmospheric oxidation through the study of Hg in precipitation according to precipitation type (Dvonch et al., 2005; Holmes et al., 2016; Kaulfus et al., 2017). These studies show that precipitation system morphology influences Hg deposition, with convective systems showing enhanced Hg deposition by a factor of 1.6. The magnitude of Hg deposition via precipitation also differs by season and region. The nature of the precipitation system is of particular interest because convective systems scavenge Hg from much higher altitudes than stratiform systems. Thus indirectly these studies provide information regarding the atmospheric oxidation of Hg because the scavenging height of different cloud types differs significantly and combined with information on the vertical distribution of potential Hg oxidants, modelling studies can help to evaluate possible, probable and unlikely oxidation mechanisms at varying levels in the troposphere. This does of course require the models to more or less accurately reproduce precipitation system morphologies. More sites measuring Hg in precipitation would clearly help estimate ecosystem deposition fluxes and so refine models.

Nair et al. (2013) carried out cloud-resolving simulations of Hg wet deposition processes in several case studies in the northeastern and southeastern USA. This study is of particular interest as many modelling simulations have tended to underestimate Hg wet deposition in the southeastern USA. It was found that wet deposition in typical northeastern thunderstorms would generally be less than in comparable storms in the southeast – assuming identical atmospheric concentrations of Hg – due to differences in typical cloud dynamics between the two regions. In addition, it was found that stratiform precipitation typically only scavenges Hg from the lowest ~4 km of the atmosphere, while southeastern thunderstorms can scavenge Hg up to ~10 km.

In another wet deposition process analysis, apparent scavenging ratios based on ground-level measurements of speciated air concentrations of Hg and total Hg in precipitation were studied at four sites in the northeastern USA (Huang et al., 2013). While the use of ground-based measurements introduced inherent uncertainties, the authors suggested that gaseous oxidized mercury (GOM) concentrations may be underestimated by current measurements, because scavenging ratios based on existing GOM measurements appeared anomalously high.

Several studies investigated Hg dry deposition processes. Zhang et al. (2012) compared CMAQ- and GRAHM-modelled dry deposition against field measurements in the Great Lakes region for 2002 and in some cases, 2005. Dry deposition from the different models varied by as much as a factor of 2 at regional scales, and larger variations were found at local scales. Zhang et al. (2012) suggested that the model-estimated dry deposition values were upper estimates given the tendency of the models to produce atmospheric concentrations of GOM and particulate-bound mercury (PBM) that are significantly higher than measured concentrations. Following a proposed methodology to estimate bi-directional Hg^0 surface exchange (Wright and Zhang, 2015), dry deposition of Hg was estimated

at 24 measurement sites in the USA and Canada (Zhang et al., 2016b). In this analysis, the dry deposition flux of Hg^0 was estimated to be significantly larger than that of GOM or PBM at most of the sites.

Foliar uptake of Hg (usually assumed to be Hg^0) and Hg dynamics in forests in general have been studied in a number of locations since GMA 2013. Risch et al. (2012) studied Hg deposition in the eastern USA, while Laacouri et al. (2013) examined Hg in the leaves of deciduous trees. Two recent studies in China have shown that more study is needed. Yu et al. (2017) found that forests can be a source of Hg. In contrast, Fu et al. (2016b) suggested that at a mountain forest site Hg^0 uptake via foliage predominates, which explains the observed Hg depletion events. Fu et al. (2016b) concluded that "such depletion events of GEM are likely to be a widespread phenomenon, suggesting that the forest ecosystem represents one of the largest sinks (~1930 Mg) of atmospheric Hg on a global scale", which is the equivalent of all annual anthropogenic emissions as estimated in GMA 2013. Moreover, it was found that stomatal uptake of Hg^0 is more effective than previously expected and thus is a significant sink for atmospheric mercury (Jiskra et al., 2018). In particular, based on global Hg^0 and carbon dioxide (CO_2) measurements it was estimated that the annual Hg^0 removal through stomatal uptake is on the order of 1000 Mg. While the precise level of Hg^0 uptake via foliage is uncertain, it does seem reasonably certain that deciduous trees are a Hg sink, especially during the growing season.

The importance of Hg^0 dry deposition was also supported by Obrist et al. (2017) who showed that most of the Hg (about 70%) in the interior Arctic tundra is derived from Hg^0 deposition, with only minor contributions from the deposition of Hg^{II} from precipitation or AMDEs. Additional work is required to reconcile these results with those of many fate-and-transport models (e.g., Selin et al., 2007; Holmes et al., 2010; Lei et al., 2013; Song et al., 2015; Cohen et al., 2016) and estimates based on field measurement surveys (e.g., Pirrone et al., 2010; Denkenberger et al., 2012; Eckley et al., 2016) that suggest that the overall net flux of Hg^0 from terrestrial surfaces is upward.

Another aspect of Hg removal from the atmosphere that has been studied by a number of groups is the deposition of Hg via litterfall. Forest canopies seem to be effective sinks for both particulate and oxidized Hg (Fu et al., 2016a; Wang et al., 2016a; Wright et al., 2016).

5.3 Global atmospheric transport and fate modelling

5.3.1 Recent modelling studies

Since GMA 2013 (AMAP/UNEP, 2013) and GMA Update 2015 (AMAP/UNEP, 2015), various modelling studies have addressed the issue of Hg dispersion and fate on a global scale. Global chemical transport models have been used for simulations of Hg atmospheric transport (Lei et al., 2013, 2014; De Simone et al., 2014, 2015, 2016), source apportionment of Hg deposition in various geographic regions (Lei et al., 2013; Chen et al., 2014, 2015a; Dastoor et al., 2015; Cohen et al., 2016), and study of processes governing Hg cycling in the atmosphere (Song et al., 2015; Angot et al., 2016; Shah et al., 2016; Bieser et al., 2017; Horowitz et al., 2017; Travnikov et al., 2017).

Some of the above-mentioned modelling studies were focused on assessing source-receptor relationships, that is, how emissions in one region or country contribute to deposition in others. These assessments are based on emission inventories describing current anthropogenic emissions. All models also include estimates of emissions from natural surfaces. These emissions are a mixture of natural emissions and re-emissions of Hg emitted from anthropogenic activities in previous years. A summary of source-receptor relationship estimates from several recent studies including the GMA Update 2015 and the current assessment is presented in Table 5.1. This contains model estimates of the relative contributions of direct anthropogenic emissions from selected source regions (East Asia, Europe, North America) to total Hg deposition in some receptor region (East Asia, Europe, North America, Arctic). The total deposition here implies contributions from both direct anthropogenic emissions and natural and secondary emissions. It should be noted that the model studies concern different years and, in particular, used essentially different inventories of both Hg anthropogenic emissions and estimates of Hg natural/secondary emissions.

As seen from Table 5.1, the contribution of domestic sources to total Hg deposition in East Asia varies from 37% to 62%. The upper estimates published by Chen et al. (2014, 2015a) are based on outdated inventories for 2000 (Pacyna et al., 2006) and 2005 (AMAP/UNEP, 2008), respectively, which were characterized by significantly higher emissions in this region compared to more recent inventories for 2010 (AMAP/UNEP, 2013) and 2015 (Chapter 2) used in other studies. Another reason is the higher proportion of

Table 5.1 Summary of source apportionment estimates for selected source and receptor regions. Data show the relative percentage contribution of direct anthropogenic emissions from a source region to total Hg deposition in a receptor region.

Receptor region	Source region		
	East Asia	Europe	North America
East Asia	62[a], 50[b], 37[c], 37[d]	1.0[c], 0.8[d]	0.6[c], 0.3[d]
Europe	3.0[a], 8.2[c], 6.1[d]	19[b], 20[c], 16[d]	0.6[c], 0.5[d]
North America	9[e], 4.8[a], 10[c], 7.4[d]	1.6[c], 1.2[d]	22[e], 9.3[b], 7.1[c], 3.7[d]
Arctic	12[f], 11[c], 9.3[d]	2.5[f], 2.5[c], 2.3[d]	2.2[f], 1.2[c], 0.7[d]

[a] Chen et al. (2015a); Hg emissions for 2000 (Pacyna et al., 2006); [b] Chen et al. (2014); Hg emissions for 2005 (AMAP/UNEP, 2008); [c] GMA Update 2015; Hg emissions for 2010 (AMAP/UNEP, 2013); [d] Current study; Hg emissions for 2015 (see Chapter 2); [e] Lei et al. (2013); Hg emissions for 2000 (Pacyna et al., 2006); [f] Dastoor et al. (2015); Hg emissions for 2005 (AMAP/UNEP, 2008).

oxidized Hg species in anthropogenic emissions from East Asia accepted in the older inventories that leads to shorter Hg dispersion from emission sources. This effect can also explain discrepancies in simulations of the East Asia contribution to total Hg deposition over Europe and North America, which vary within the ranges 3–8.2% and 4.8–10% respectively. The lower estimates are based on the emissions inventory for 2000 with a significant share of oxidized Hg (Chen et al., 2015a). The studies provide consistent estimates of the contribution of domestic sources to total Hg deposition in Europe (16–20%). In contrast, similar estimates for North America vary over a wide range (3.7–22%). It should be noted that all four available estimates were based on different inventories, with the lower values referring to more recent years. This agrees with the gradual reduction in total emissions of Hg in North America from 145 t/y in 2000 (Pacyna et al., 2006) to 44 t/y in 2015 (Chapter 2). Besides, the upper estimate (22%) obtained by Lei et al. (2013) relates to the USA and, probably, overestimates the contribution of domestic sources to the continent as a whole. Thus, model evaluation of source-receptor relationships is strongly dependent on the availability of reliable emissions inventories. More detailed discussion of multi-model simulations of Hg dispersion on a global scale using updated emissions data for 2015 is presented in Sections 5.3.2 to 5.3.4.

5.3.2 Deposition to terrestrial and aquatic regions

The current state of Hg dispersion in the atmosphere and deposition to various terrestrial and aquatic regions was studied by an ensemble of chemical transport models using the new inventory of Hg anthropogenic emissions discussed in Chapter 2. Four global-scale chemical transport models for Hg were applied in the study – ECHMERIT, GEM-MACH-Hg, GEOS-Chem (v11-02), and GLEMOS. A short summary of major model characteristics is given in Appendix 5.1. All models cover the global atmosphere (the entire troposphere and at least the lower stratosphere) with somewhat different spatial resolution ranging from 0.5 to 2.8 geographical degrees. Three of the four models (ECHMERIT, GEM-MACH-Hg, GLEMOS) are atmospheric transport models simulating the processes of Hg transport and fate in the atmosphere as well as air-surface exchange leading to Hg input to and removal from the atmosphere. The fourth model (GEOS-Chem) is a coupled multi-media transport model simulating Hg processes both in the atmosphere and in slab oceanic and terrestrial layers. The models differ in terms of major Hg oxidation mechanisms using chemical schemes based on Hg oxidation by atomic Br (GEOS-Chem), OH initiated reactions (GEM-MACH-Hg) or a combination of OH and O_3 initiated reactions (ECHMERIT and GLEMOS). See Travnikov et al. (2017) for a more detailed description of the models along with a discussion of their differences.

All models used the new global Hg anthropogenic emissions inventory for 2015 described in Chapter 2. The dataset consists of gridded emission data with a spatial resolution of 0.1° × 0.1° for three Hg species (Hg^0, GOM, PBM), which were redistributed into the native model grids using mass conservation methods. The total global emission of Hg from anthropogenic sources is estimated at 2224 t/y. The overall proportions of Hg^0, GOM, and PBM emissions are 82%, 14% and 4%, respectively. In contrast to the anthropogenic emissions, total values of natural and secondary emissions differed significantly among the models. Parameterization of these processes is an essential part of the model setup and describes Hg cycling between the Earth's surface and the atmosphere. Particular approaches used by the models vary between empirically prescribed and dynamically simulated air-surface exchange fluxes and are based on different theoretical assumptions. More details on applied parameterizations can be found in the sources provided in Appendix 5.1. It should be noted that there is a significant gap in understanding of major processes determining Hg cycling within environmental media (soil, vegetation, ocean) and air-surface exchange. Therefore, existing model estimates of natural and secondary emissions contain considerable uncertainties and disparity.

The analysis presented in this section and the next contains information on emissions and deposition fluxes averaged over a number of geographical regions. The definition of source and receptor regions is consistent with the GMA Update 2015 and is shown in Figure 5.1. The regions are divided into six continents (Europe, North, Central, and South America, Africa, and Australia and New Zealand), five large subcontinents (Middle East, countries of the Commonwealth of Independent States (CIS), and South, East, and Southeast Asia), and two polar regions (Arctic and Antarctica). Aquatic regions of the world ocean are defined in accordance with the Major Fishing Areas of the UN Food and Agriculture Organization (FAO, 2018).

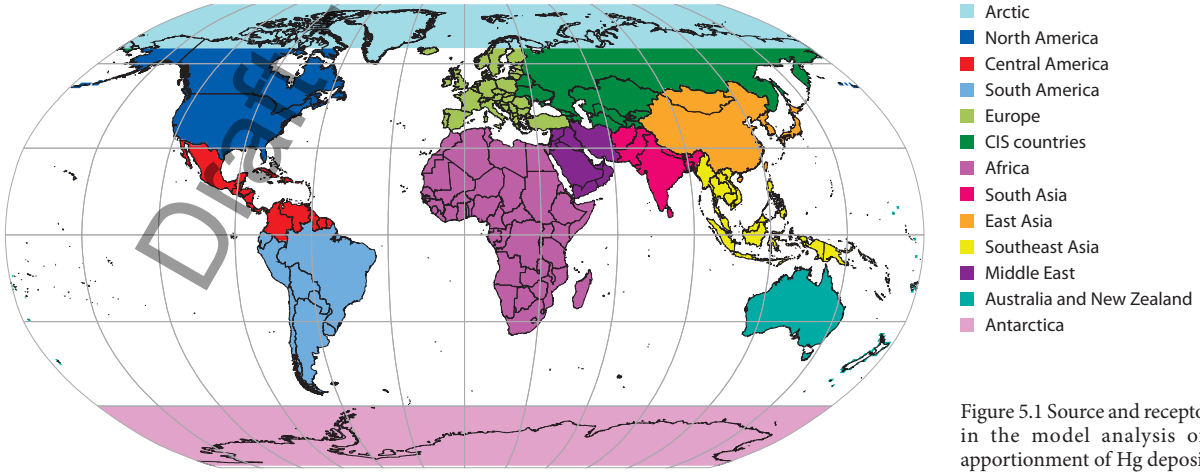

Figure 5.1 Source and receptor regions in the model analysis of source apportionment of Hg deposition.

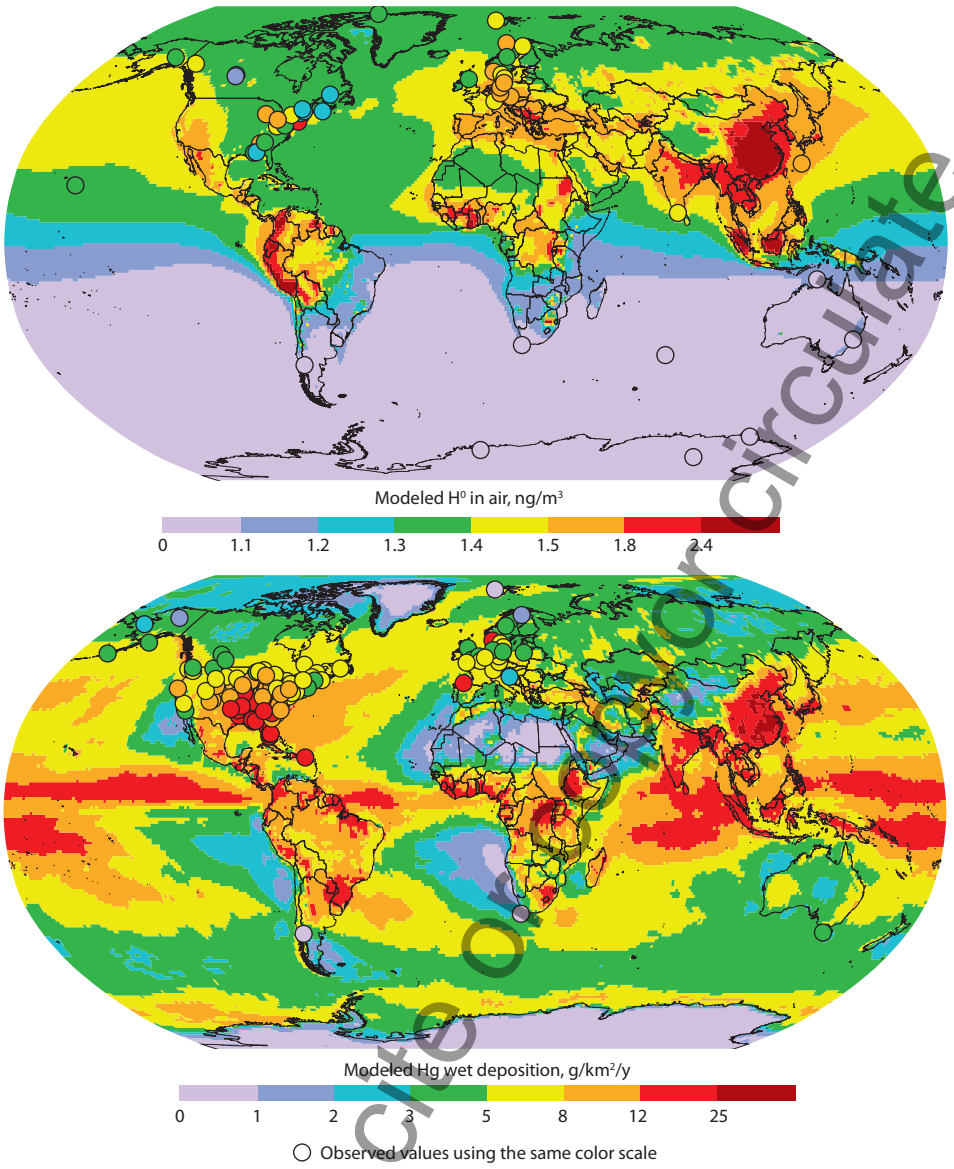

Figure 5.2 Model ensemble median global distributions of Hg^0 concentration in surface air and Hg wet deposition flux in 2015.

The global distribution of Hg^0 concentration in surface air in 2015 as simulated by the model ensemble is shown in Figure 5.2 in terms of the model ensemble median. The spatial pattern is characterized by the latitudinal gradient with elevated concentrations (above 1.4 ng/m^3) in the temperate latitudes of the Northern Hemisphere and the lowest concentrations (below 1 ng/m^3) in the southernmost parts of the Southern Hemisphere. The highest concentrations (above 2 ng/m^3) are located in East, South and Southeast Asia due to high levels of anthropogenic emissions as well as in equatorial Africa and South America owing to high emission amounts attributed to artisanal and small-scale gold mining (ASGM). The simulated Hg^0 concentration pattern is very similar to previous estimates presented in the GMA Update 2015. The modelling results were evaluated against observations from global and regional monitoring networks (GMOS, EMEP, AMNet and NAtChem). Available measurement data generally confirm large-scale spatial variation of simulated Hg^0 (Figure 5.2) with the interhemispheric gradient and elevated concentrations in the major industrial regions. There are still some discrepancies between the modelling results and observations in particular locations, which characterize more complicated small-scale spatial patterns in Hg^0 levels that are not captured by the models.

Both simulated and observed levels of Hg wet deposition are shown in Figure 5.2. The measurement data were obtained from the GMOS, NADP/MDN and EMEP networks. Wet deposition is relatively equally distributed between the Northern Hemisphere and Southern Hemisphere and reflects the influence of multiple factors including anthropogenic emissions, oxidation chemistry and precipitation pattern. Elevated fluxes of Hg wet deposition are found in areas inside and downwind of the industrial regions of Asia, North America and Europe as well as over the high precipitation zones in the Tropics. The lowest model-estimated wet deposition levels are in arid areas of Greenland, northern Africa and Antarctica. The simulations reproduce measured levels of wet deposition in North America, Europe and Australia relatively well.

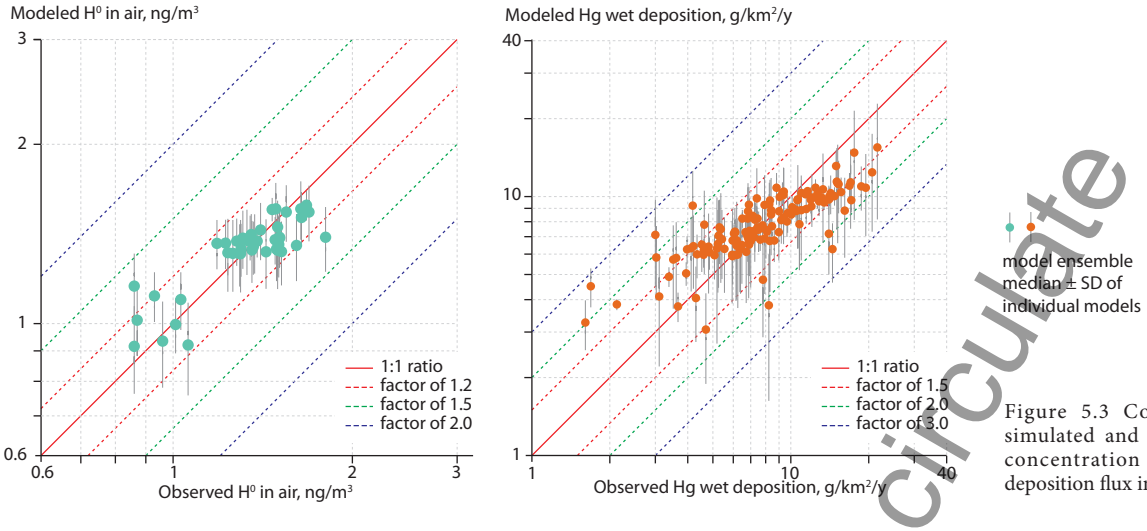

Figure 5.3 Comparison of simulated and observed Hg^0 concentration and Hg wet deposition flux in 2015.

A detailed comparison between model results and observations is illustrated in Figure 5.3. The model ensemble median of Hg^0 concentration agrees with observed values within ±20% at most of the measurement sites. The scatter of simulated values among the models presented by the standard deviation is relatively small and does not exceed 20%. The model-to-measurement difference is larger for wet deposition. The model ensemble demonstrates good correlation ($r^2 = 0.7$) with observations but tends to overestimate low and underestimate high deposition fluxes. The deviation between the modelling results and measurements does not exceed a factor of 2 at the majority of measurement sites. However, it should be noted that available measurement data cover limited regions of North America and Europe and cannot provide complete evaluation of the global spatial pattern. The inter-model variance is also larger for wet deposition, which can be explained by the differences in parameterizations of Hg oxidation chemistry, and the scavenging and precipitation amount between the models.

A comprehensive evaluation of the participating models against a variety of ground-based and aircraft measurements as well as their sensitivity to various parameters and processes can be found in a series of recent publications (Angot et al., 2016; Bieser et al., 2017; Travnikov et al., 2017).

It should be noted that measurements of Hg^0 air concentration and Hg wet deposition obtained from global and regional networks may not provide a complete evaluation of model performance. Mercury removal from the atmosphere is largely determined by the oxidation/reduction chemistry and air-surface exchange. Therefore, reliable measurements of oxidized Hg forms and air-surface exchange fluxes (including Hg^0 gaseous exchange, Hg^{II} dry deposition as well as Hg throughfall and litterfall deposition) are critical for understanding the distribution, cycling and fate of Hg in the atmosphere and, ultimately, for improving Hg chemical transport models. Available measurements of reactive Hg concentration in air and air-surface exchange are relatively scarce and uncertain (see discussion in Section 5.2).

Figure 5.4 shows Hg^0 air concentration and Hg wet and dry deposition (including dry deposition of Hg^0) averaged over various geographic regions. The regional pattern of deposition fluxes generally follows that of Hg^0 concentration with the exceptions of relatively low wet and dry deposition in the Middle East and CIS countries and elevated deposition fluxes in

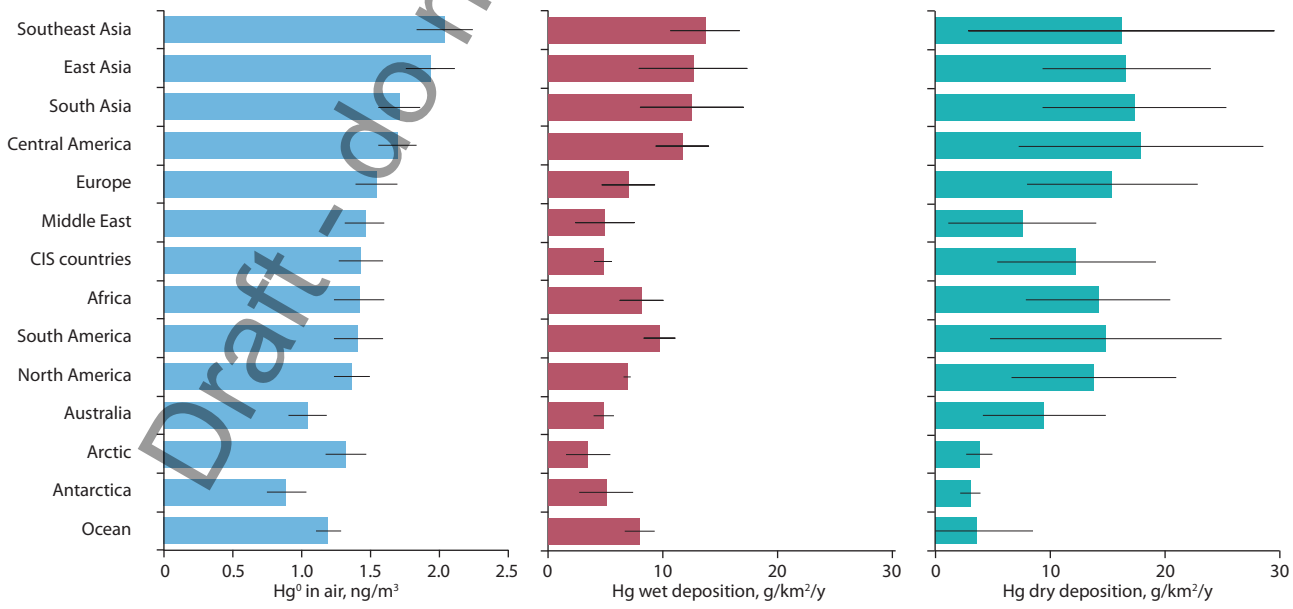

Figure 5.4 Model ensemble median Hg^0 concentration, Hg wet deposition and Hg dry deposition in 2015 averaged over the various geographic regions defined in Figure 5.1. Whiskers show the standard deviation of the models from the ensemble median.

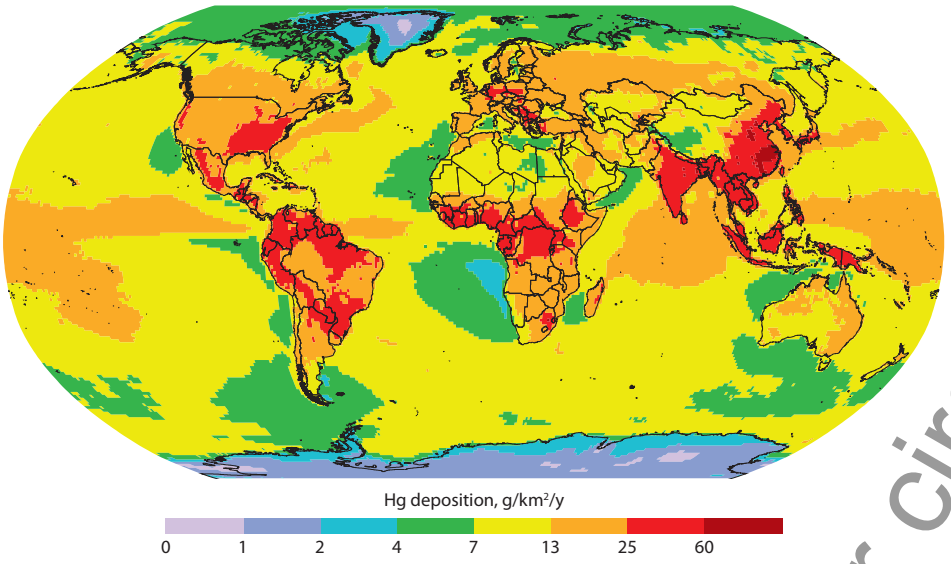

Figure 5.5 Global distribution of the model ensemble median total (wet and dry) Hg deposition in 2015.

Africa and South America relative to Hg^0 concentration. These exceptions can be explained by the regional precipitation and climatic characteristics. In most receptor regions, the average dry deposition is higher than wet deposition by 20–120%. In contrast to terrestrial regions, wet deposition to the ocean is higher than dry deposition. The inter-model variation also demonstrates significantly higher uncertainty for dry deposition (±28–85%) in comparison to wet deposition (±4–55%) and Hg^0 concentration (±7–16%). Thus, the uncertainty of total deposition (wet and dry) discussed in this and the two following sections, consists largely of the uncertainty of dry deposition.

The global distribution of Hg deposition in 2015 simulated by the model ensemble is shown in Figure 5.5. The spatial pattern partly follows the spatial distribution of wet deposition with elevated deposition fluxes over the major industrial regions and areas of intensive precipitation. In comparison to wet deposition, however, much higher deposition fluxes are observed over land than the ocean due to the large contribution of dry deposition. The deposition pattern does not reveal any considerable difference in Hg deposition to the ocean in the Northern Hemisphere and Southern Hemisphere. Levels of Hg deposition to land vary within the continents reflecting the spatial pattern of anthropogenic emissions as well as surface and climatic characteristics. There are increasing north-to-south gradients of Hg deposition in North America and Eurasia with the exception of the desert and mountain regions in Central and East Asia. Most territory in South America is subject to high Hg fluxes determined by both wet and dry deposition, except for the most southern part of the continent, due to the significant contribution of ASGM emissions and oxidized chemistry. In Africa, Hg deposition differs significantly from relatively low fluxes in the desert north to high deposition fluxes in the equatorial and southern parts of the continent.

Figure 5.6 summarizes the total Hg deposition fluxes to terrestrial and aquatic receptor regions as well as the relative contributions of direct anthropogenic and natural/secondary sources simulated by the model ensemble. Total Hg deposition fluxes are highest in large industrial regions such as South, East, and Southeast Asia (25–30 g/km²/y). Regions with active ASGM (Central and South America), which emit Hg in the form of Hg^0, are also subject to a high total Hg deposition flux of 25 g/km²/y due to intensive *in situ* Hg^0 oxidation in the atmosphere of

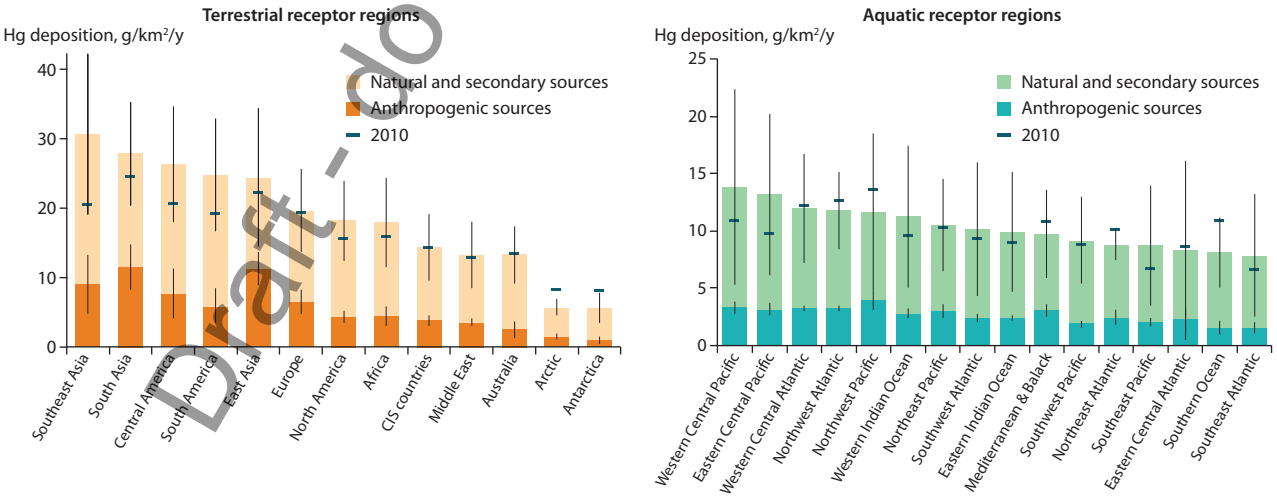

Figure 5.6 Total Hg deposition fluxes and the relative contributions of direct anthropogenic and natural and secondary sources to various terrestrial and aquatic receptor regions in 2015. Whiskers show the standard deviation of the models from the ensemble median for direct anthropogenic and natural/secondary sources, respectively. Results of the GMA Update 2015 (year 2010 anthropogenic Hg emission inventory) are shown for comparison.

the Tropics (Horowitz et al., 2017). The lowest deposition levels are in remote regions such as the Arctic and Antarctic (below 6 g/km^2/y). A comparison between the modelled results here and the GMA Update 2015 (year 2010 anthropogenic Hg emission inventory) shows an average 20% (2–40%) increase in total Hg deposition flux to most receptor regions, except in the polar regions, which show a 30% reduction. This is consistent with the global increase in anthropogenic emissions (~12%) since 2010 (Chapter 2). Southeast Asia, South America and Central America demonstrate the largest increase in total Hg deposition fluxes of 50%, 30% and 27%, respectively. This is explained by the large magnitude change in their domestic anthropogenic emissions in the new emissions inventory and indicates refinement of emissions data rather than a real temporal trend of anthropogenic emissions in these regions. The reduction of Hg deposition in the polar regions is mostly due to refinement of the model parameterizations for polar-specific processes and the interannual variation in meteorological conditions.

Total Hg deposition consists of contributions from direct anthropogenic emissions as well as natural and secondary sources, which account for 53–81% of the total Hg deposition. The contribution of natural and secondary sources evaluated here is very similar to that reported in the GMA Update 2015 (52–79%). As illustrated in Figure 5.6, the relative contributions of direct anthropogenic sources show a regional pattern – decreasing from regions of the highest (South, East and Southeast Asia; 30–47%) to the lowest total Hg deposition flux (the polar regions; 20–25%). The contribution of direct anthropogenic sources to other receptor regions is within 25–35%. The regional pattern can be explained by the level of domestic anthropogenic emissions, which generate a substantial fraction of oxidized Hg that deposits rapidly within the source region. It should be noted that there can be substantial variation in the relative contributions of anthropogenic and natural/secondary sources within a given region.

Mercury deposition to various regions of the world ocean is shown in Figure 5.6. Deposition flux averaged over the regions varies from 8 g/km^2/y over the Southeast Atlantic to 14 g/km^2/y over the Western Central Pacific. This agrees well with model deposition fluxes to the ocean reported in the GMA Update 2015 (6.5–13.6 g/km^2/y). The new estimates show higher deposition fluxes in the Tropics (Western Central Pacific, Eastern Central Pacific, Indian Ocean) due to refinement of Hg oxidation chemistry (Horowitz et al., 2017). Mercury deposition to the ocean is also influenced by direct anthropogenic emissions as well as by natural and secondary sources. The relative contribution of direct anthropogenic sources to ocean reservoirs evaluated here varies from 19% (Southern Ocean) to 35% (Northwest Pacific) and is slightly lower compared to the direct anthropogenic contribution of terrestrial reservoirs (20–50%).

The inter-model differences in the simulated total Hg deposition fluxes from anthropogenic and natural/secondary sources are shown in Figure 5.6 in terms of the standard deviation. The inter-model difference in deposition from direct anthropogenic sources (±9–52% for terrestrial and ±8–47% for aquatic regions) is mostly determined by the differences in the chemical mechanisms implemented in the models and the parameterizations of removal processes. The inter-model differences in simulated deposition from natural/secondary sources is much lower compared to those of anthropogenic sources (±28–76% for terrestrial and ±20–130% for aquatic regions), which is also affected by the model parameterizations of natural and secondary emissions. The source apportionment analysis of Hg deposition from direct anthropogenic emissions shown in the two following sections represents the sources that can be most easily regulated by environmental policy.

5.3.3 Source apportionment of anthropogenic Hg deposition

Source apportionment of Hg deposition, illustrating atmospheric transport of Hg between different continents and regions, was evaluated in the GMA 2013 and the GMA Update 2015. This section provides an updated source-receptor analysis of Hg deposition generated from the same four global chemical transport models. It should be noted that the results discussed in this section present shares of source regions to deposition from direct anthropogenic emissions instead of the share of total deposition, which also includes a contribution from natural and secondary sources. The source apportionment of total deposition is briefly discussed in Section 5.3.1 along with a comparison with results of other recent studies.

Figure 5.7 illustrates the source apportionment of Hg deposition from direct anthropogenic sources to various receptor regions. The direct anthropogenic emissions represent the mixture of domestic emissions and atmospherically transported Hg from sources located in other regions (foreign emissions). The share of foreign sources varies from 100% in Antarctica to 23% in East Asia. The largest foreign contributors to various receptor regions are East Asia, Africa, South America, and Southeast Asia, with their contributions ranging between 10–34%, 4–24%, 3–23%, 3–11%, respectively. The largest foreign contributors are characterized by large anthropogenic emissions as well as active ASGM, which contributes to the global Hg burden and thus to long-range transport via Hg^0 emissions. The smallest foreign contributors are the Middle East (<2%), Australia (<1%), and the polar regions (<1%), which are characterized by the lowest anthropogenic emissions. It should be noted that there are substantial variations in the overall averages within particular regions. In general, the results shown here are in accord with the GMA Update 2015.

As illustrated in Figure 5.7, the share of domestic sources to various receptor regions is ranked in the order of East Asia (77%), South Asia (66%), Europe (48%), Southeast Asia (39%), Africa (38%), South America (34%), Central America (30%), CIS countries (28%), Middle East (18%), North America (15%), Australia and New Zealand (6%), Arctic (3%), and Antarctica (0%). In East and South Asia, anthropogenic Hg deposition is dominated by the contribution from domestic sources. This is due to the significant domestic anthropogenic emissions mainly from the industrial and power sectors, which emit a substantial fraction of oxidized Hg. The domestic shares in East and South Asian anthropogenic deposition show some increase since 2010 (GMA Update 2015; 76% and 58% respectively), which is explained by the increase in Asian anthropogenic emissions since 2010 (Chapter 2). Consistent with the GMA Update 2015, both domestic and foreign anthropogenic sources contribute almost equally to the total anthropogenic Hg deposition in Europe. The largest foreign contributors are ranked in the order of East Asia (18%), Africa (8%), CIS countries (6%), and

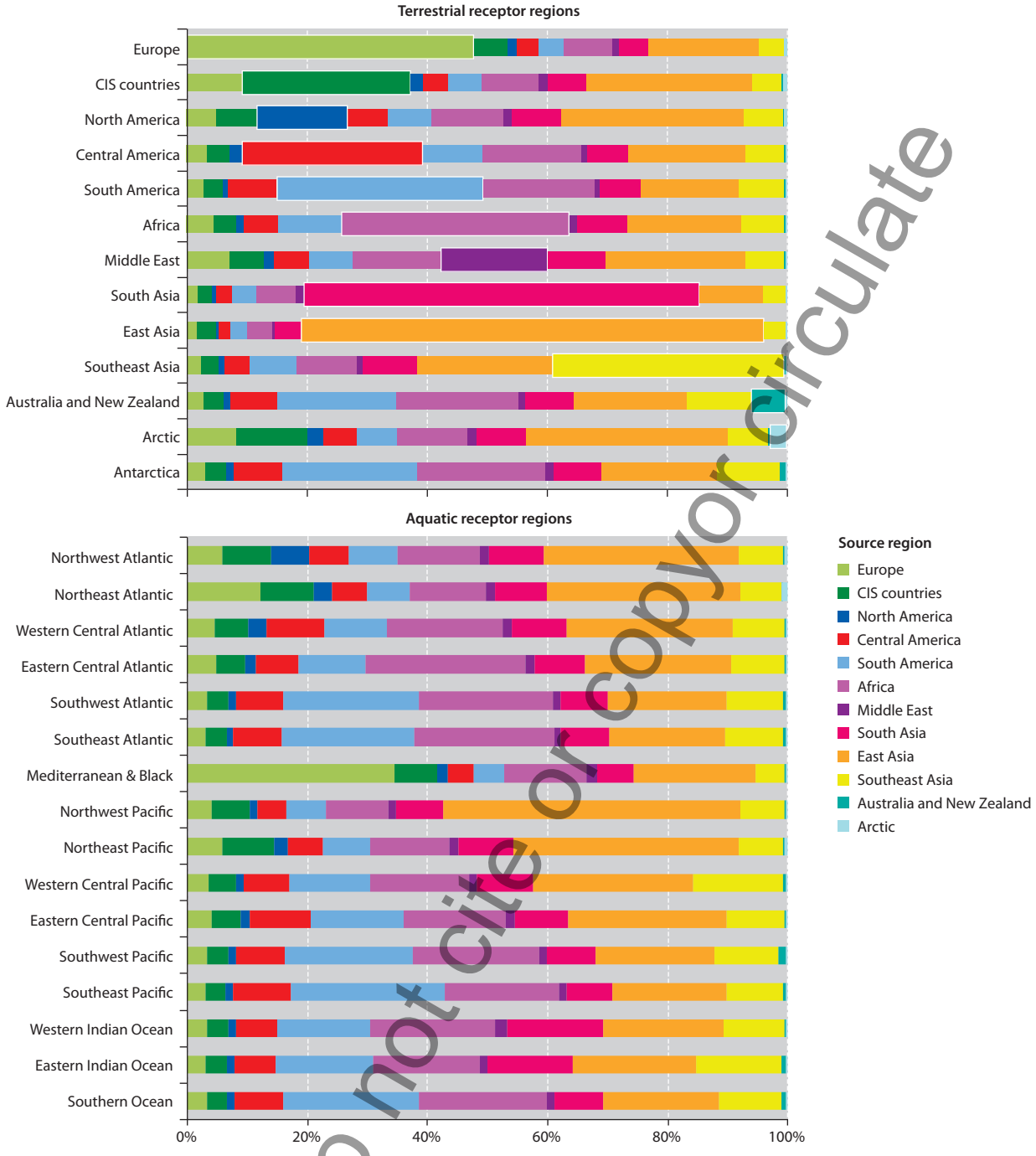

Figure 5.7 Model ensemble median source apportionment of Hg deposition from direct anthropogenic emissions to various terrestrial and aquatic regions in 2015. The colors depict source regions, which are consistent with Figure 5.1. The contribution of domestic sources is shown by wider bars. Source apportionment for individual models are given in Appendix 5.2.

South Asia (5%). Regions with active ASGM (Africa, South and Central America) also receive a relatively large fraction of anthropogenic deposition from domestic sources as well as from East Asia. In North America, the share of domestic sources shows a reduction from 23% to 15% (GMA Update 2015). This is consistent with the reduction in North American anthropogenic emissions since 2010 (Chapter 2). Significant foreign contributors to North American anthropogenic deposition are ranked in the order East Asia (31%), Africa (12%), South Asia (8%), and Southeast Asia (7%). Remote regions including the Arctic and Antarctic are predominantly influenced by the long-range transport of atmospheric Hg from East Asia and Africa.

Figure 5.7 also illustrates the source apportionment of Hg deposition from direct anthropogenic sources to various ocean regions. Overall, the results shown here are in accord with the GMA Update 2015. East Asia and Africa remain the largest contributors to the global ocean regions, owing to their large anthropogenic emissions. The contributions from East Asia and Africa to various ocean regions range between 20–50% and 11–27%, respectively. Northwest (50%) and Northeast Pacific (38%) receive the largest contribution from East Asian anthropogenic emissions. Eastern Central (27%), Southeast (23%), and Southwest Atlantic (22%) receive the largest contribution from African anthropogenic emissions. South America also significantly contributes to Hg deposition to the

ocean (5–26%), particularly, over the Southeast Pacific (26%), Southwest Atlantic (23%), and Southeast Atlantic (22%). The only exceptions are the Mediterranean Sea and Black Sea, where the contribution from European anthropogenic emissions (20%) dominates over East Asian, African, and South American anthropogenic emissions. A number of the ocean regions – particularly the Northwest Pacific – receive high anthropogenic Hg deposition and demonstrate a large total capture fisheries production as reported in the GMA Update 2015. The lowest contributors to the global ocean regions are the Arctic (<2%) and Australia (<1%), which are characterized by the lowest anthropogenic emissions.

5.3.4 Contribution of different emission sectors to Hg deposition

The four global chemical transport models were also applied for simulating Hg deposition from different anthropogenic emissions sectors. In this study, all the sectors of anthropogenic emissions discussed in Chapter 2 were aggregated into four general groups: power generation; industrial sources; intentional use and product waste; and ASGM. Total emissions from these four sector groups in 2015 amount to 347 t/y, 874 t/y, 166 t/y and 838 t/y, respectively. Chemical speciation of Hg emissions differs considerably between different sector groups (Figure 5.8). According to the applied inventory (Chapter 2), emissions from power generation roughly comprise equal contributions of elemental mercury (Hg^0) and oxidized forms (GOM, PBM). The proportion of oxidized Hg is much smaller in emissions from industrial sources (20%). A quarter of total Hg emissions from intentional use and product waste is emitted in the oxidized forms. It is expected that all Hg emitted from ASGM is in the elemental gaseous form. It should be noted that available estimates of Hg emissions speciation are associated with significant uncertainties (Section 5.2).

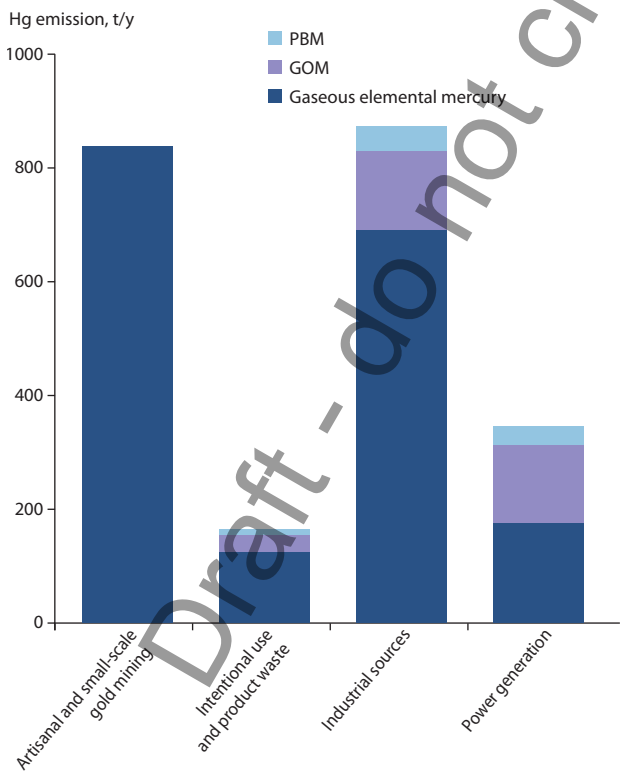

Figure 5.8 Chemical speciation of Hg emissions from the four groups of emission sectors in 2015.

The model simulated patterns of Hg deposition from the four emission sectors are shown in Figure 5.9. Mercury deposition from the power generation group is largely restricted to industrial regions in East and South Asia, Europe, North America, and South Africa, where the majority of large stationary combustion sources are located. It results from the large proportion of oxidized Hg in emissions from this sector. Mercury deposition flux from power generation in these regions exceeds 2.5 g/km²/y, whereas in other regions it falls below 1.4 g/km²/y. The relatively short distance of Hg dispersion from this sector group is caused by the substantial proportion of oxidized Hg in the emissions. Emissions from the industrial sectors group are more widely distributed over the world and contain a substantial fraction of Hg^0 (80%). Therefore, significant deposition (above 2.5 g/km²/y) from industrial sources covers wide areas in Asia, Europe, North and South America, and Africa. In South and East Asia, deposition from this sector group exceeds 5 and 10 g/km²/y, respectively. Deposition from the intentional use and product waste group is also mostly related to major industrial regions but its contribution is much lower and generally does not exceed 1.4 g/km²/y except for South and East Asia. The majority of ASGM emission sources are located in the low latitudes of both hemispheres. Being in the elemental form, Hg emissions from this sector are transported globally, however, most significant deposition fluxes (above 2.5 g/km²/y) occur close to emission sources and largely impact South America, equatorial Africa, East and Southeast Asia.

The relative contribution of the emission sectors to Hg deposition from direct anthropogenic emissions varies substantially between different geographic regions (Figure 5.10). Power generation contributes from 11% to 35% of total anthropogenic deposition with the largest contribution in Europe and South Asia, and the smallest contribution in Central and South America and Antarctica. The contribution of industrial sources ranges from 33% (South America) to 60% (East Asia). The share of the intentional use and product waste sector group in Hg anthropogenic deposition is less significant in all regions (6–12%). The relative contribution of ASGM is the largest over the continents of the Southern Hemisphere: South America (50%), Antarctica (49%), Australia and New Zealand (46%); and the smallest in industrial regions of the Northern Hemisphere: Europe (17%), South Asia (15%) and East Asia (12%).

Aquatic regions of the global ocean are also differently affected by the emission sectors (Figure 5.10). Most regions of the Northern Hemisphere are predominantly influenced by industrial sources (43–50%). The contribution of the power generation group commonly does not exceed 20% with the exception of the Mediterranean Sea and Black Sea (30%), which are located close to European emission sources. The relative contribution of ASGM to the aquatic regions of the Northern Hemisphere is below 30%. In contrast, this sector makes up the largest contribution (40–50%) to Hg deposition over the ocean in the Southern Hemisphere. The group of sectors associated with intentional use and product waste contributes less than 10% of Hg anthropogenic deposition to all regions of the global ocean.

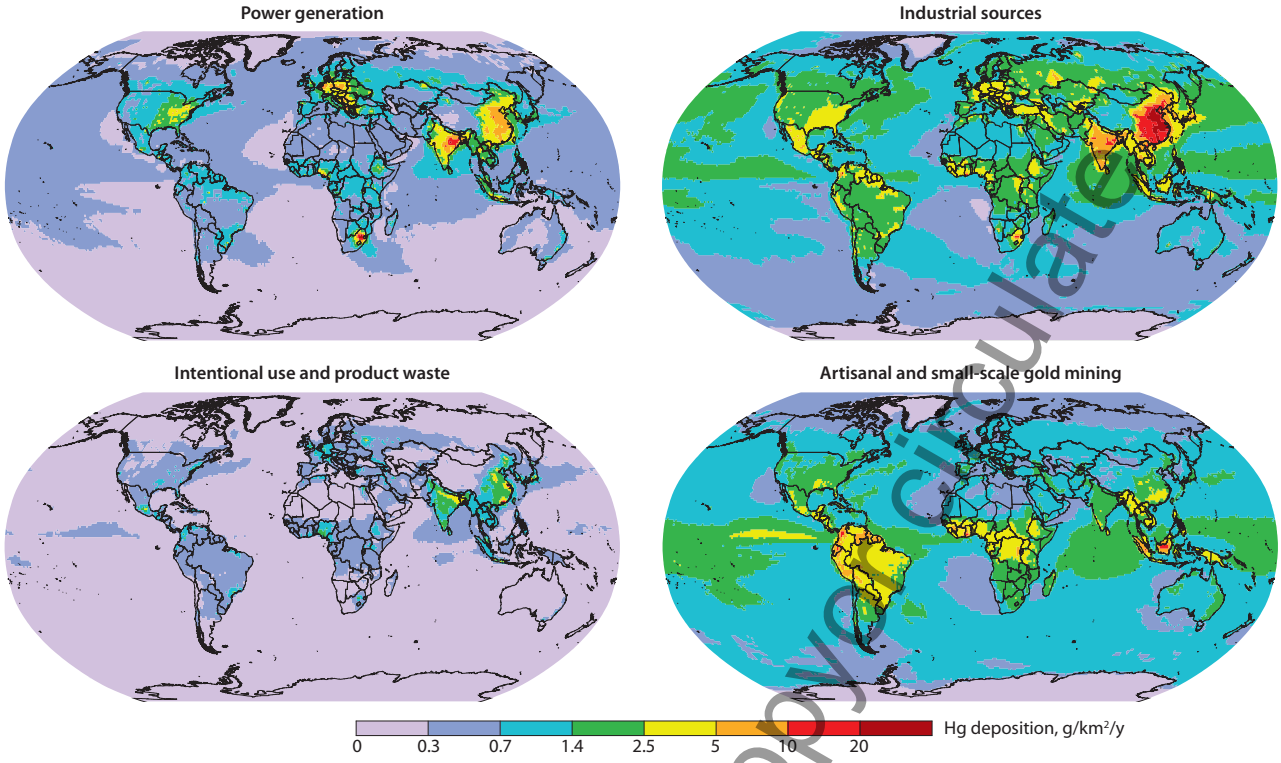

Figure 5.9 Global distribution of Hg deposition (model ensemble median) from the four groups of emission sectors in 2015: power generation, industrial sources, intentional use and product waste, and artisanal and small-scale gold mining.

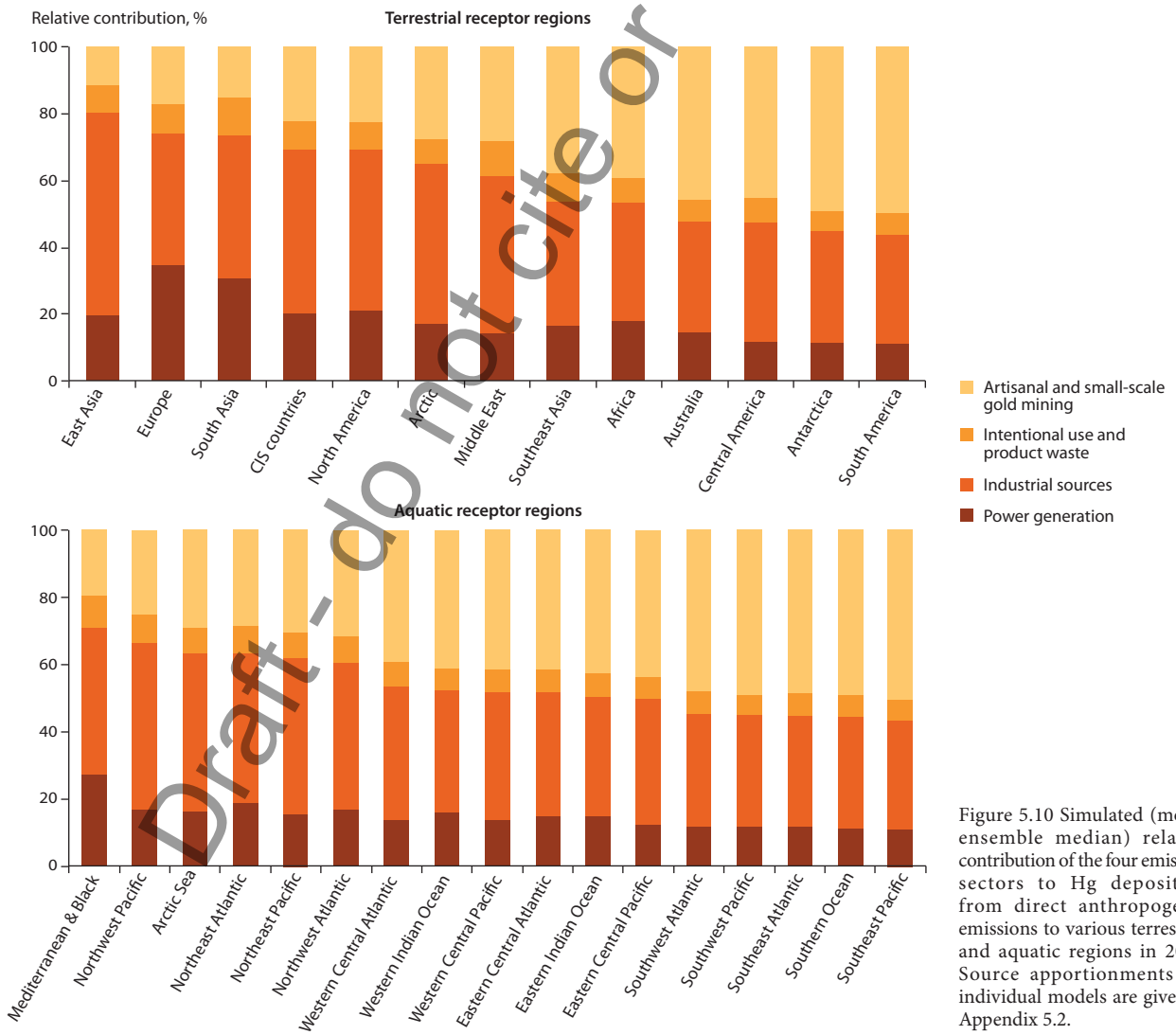

Figure 5.10 Simulated (model ensemble median) relative contribution of the four emission sectors to Hg deposition from direct anthropogenic emissions to various terrestrial and aquatic regions in 2015. Source apportionments for individual models are given in Appendix 5.2.

5.4 Historical trends and future scenarios

Evaluation of historical changes in Hg atmospheric concentration and deposition to other environmental media is important because it explains how legacy Hg (previously emitted and deposited anthropogenic Hg) affects present-day Hg levels and future environmental responses to expected emission control measures. Human disturbance of natural Hg cycling in the environment by mining and industrial activities has led to significant enrichment of atmospheric Hg since pre-industrial times (e.g., Fitzgerald et al., 1998; Biester et al., 2007; Lindberg et al., 2007). Amos et al. (2013, 2014, 2015) recently applied a multi-media box model coupling the atmosphere, ocean, and terrestrial reservoirs to reconstruct historical Hg cycling among geochemical reservoirs at the millennial scale. They found that present-day atmospheric deposition has increased by a factor of 2.6 relative to the preindustrial period (~1850), which is consistent with sediment archives. Moreover, all-time anthropogenic emissions (since ~2000 BC) have enriched present-day Hg levels in the atmosphere, surface ocean, and deep ocean by factors of 7.5, 5.9, and 2.1, respectively, relative to natural conditions (Amos et al., 2013). Amos et al. (2014) also showed that accounting for the additional loss of Hg to ocean margin sediments showed that the all-time relative enrichment in surface reservoirs was two-fold higher than was previously estimated [*please check*]. Application of a coupled 3D atmospheric and ocean transport model by Zhang et al. (2014) on 600 years cycling of Hg in the global environment provides lower enrichment factors for Hg levels in the atmosphere, surface ocean and deep ocean (5.5, 4.4 and 1.2, respectively). This difference is attributed to lower estimates of Hg emissions from historical mining and more complex vertical mixing in the ocean by Zhang et al. (2014). Model simulations and natural archives both provide evidence for peak atmospheric Hg concentrations during the latter half of the 20th century and declines in more recent decades (Amos et al., 2015).

Changes in atmospheric Hg deposition over the past two decades in different geographic regions were evaluated in several recent modelling studies. Long-term trends in Hg deposition in Europe were analyzed by the Task Force on Measurements and Modelling under the Co-operative Programme for Monitoring and Evaluation of the Long-range Transmission of Air Pollutants in Europe (Colette et al., 2016). According to the modelling results presented in the study, total Hg deposition in the EMEP region considered (Europe and Central Asia) decreased on average by 23% during the period 1990–2012 (about -1%/y). However, the deposition trend was essentially non-linear with the rates of deposition reduction being higher at the beginning and lower at the end of the period. The trend broadly agrees with available long-term measurements of Hg in precipitation in this region (Tørseth el al., 2012; Colette et al., 2016). The magnitude of deposition changes differs significantly between individual countries ranging from a 70% decrease to a 10% increase. The decrease in deposition was generally larger in the countries of the European Union (EU28) (35% for the period 1990–2012 or -1.5%/y) than in other parts of the region (Eastern Europe and Central Asia). Similar rates (-1.5±0.7%/y) of Hg wet deposition reduction at monitoring sites in Western Europe were simulated for the period 1996–2008 (Muntean et al., 2014) and were two-fold lower than the observed trend at these sites [*please check*]. Zhang et al. (2016c) estimated a steeper trend in Hg wet deposition in the same region (-2.0±0.14%/y). Muntean et al. (2014) estimated a Hg wet deposition decline in North America of -2.4±0.7%/y for the period 1996–2008. Zhang et al. (2016c) utilized an updated emissions inventory and obtained a smaller decline of -1.4±0.1%/y for a longer period (1996–2013) in the same region.

Using a global Hg model (GEOS-Chem) that coupled the atmosphere, soil, and surface ocean, Soerensen et al. (2012) found a long-term decline in Hg^0 concentration over the northern Atlantic. They concluded that existing inventories of Hg anthropogenic emissions cannot explain the substantial decrease in observed Hg^0 concentration (-2.5%/y) for the period 1990–2009 since significant emissions reductions in North America and Europe are balanced by the rise in Hg emissions in East Asia. Instead, it was hypothesized that the reduction in riverine and wastewater Hg inputs to ocean margins could lead to a reduction in subsurface seawater Hg concentration as well as lower Hg emissions from the ocean (Soerensen et al., 2012). Amos et al. (2014) later showed that riverine Hg inputs to the North Atlantic did not contribute substantially to these changes. Zhang et al. (2016c) demonstrated that revised anthropogenic emissions can explain the observed decline in atmospheric Hg. Thus, there are multiple plausible explanations for the decline in Hg concentration over the past two decades which cannot be resolved without a better understanding of past Hg emissions.

Despite increases in global anthropogenic emissions since the mid-20th century (Streets et al., 2011), atmospheric Hg levels in the Arctic have decreased or remained constant (Cole and Steffen, 2010; Berg et al., 2013; Cole et al., 2013). The effects of climate change-related factors such as increased air temperatures (particularly in spring) and reduced sea-ice extent and thickness on Hg levels in Arctic ecosystems are complex and multidirectional (Bekryaev et al., 2010; Cavalieri and Parkinson, 2012; Stern et al., 2012).

Fisher et al. (2013) investigated the factors controlling Hg^0 trends in the Arctic between 1979 and 2008 by using the global historical anthropogenic emissions inventory of Streets et al. (2011) in GEOS-Chem. The model simulated a small increasing trend in Hg^0 concentrations over the 30 year-period mainly reflecting the growth in emissions. The authors also suggested that climate warming may lead to decreased fluxes of Hg from the atmosphere to the cryosphere and increased Hg^0 concentrations in the Arctic. Chen et al. (2015b) extended the study of Fisher et al. (2013) to quantitatively determine the contributions of changes in environmental variables and anthropogenic emissions to Hg trends in the Arctic using the anthropogenic emission inventories of AMAP/UNEP for 2000, 2005, and 2010. In addition to confirming the results of Fisher et al. (2013) for spring and summer, the study found that a decrease in Atlantic Ocean evasion of Hg at lower latitudes contributed to the decrease in Hg^0 concentrations in the Arctic from November to March.

Dastoor et al. (2015) assessed the impact of changing anthropogenic emissions and meteorology on Hg^0 concentrations and deposition in the Canadian Arctic from 1990 to 2005 using GEM-MACH-Hg and AMAP anthropogenic emissions (AMAP, 2011). Changes in meteorology and decline in emissions in North America and Europe were found to contribute equally to the decrease in surface air Hg^0 concentrations in the Canadian

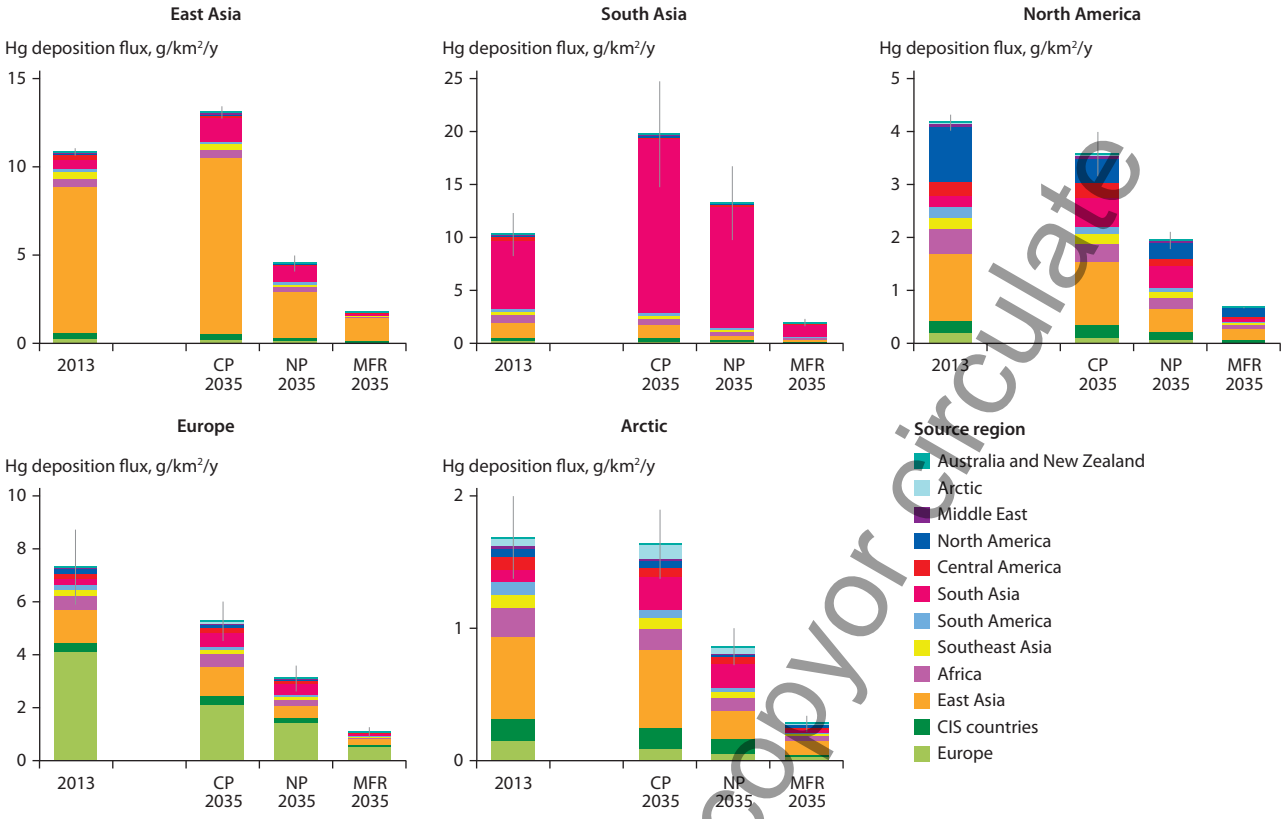

Figure 5.11 Source apportionment of Hg deposition from direct anthropogenic sources (average of two models) in 2013 and 2035 in various regions: East Asia, South Asia, North America, Europe, and the Arctic. Whiskers show deviation between the models. Contributions of natural and secondary emissions are not shown. Source: Pacyna et al. (2016).

Arctic with an overall decline of ~12% from 1990 to 2005, which is in accord with measurements at Alert (Cole and Steffen, 2010; Cole et al., 2013). In contrast, a slow increase (10%) in Hg net deposition is found in the Canadian Arctic in response to combined changes in meteorology and emissions. Changes in snowpack and sea-ice characteristics and an increase in precipitation in the Arctic related to climate change are found to be primary causes for the meteorology-related changes in Hg air concentration and deposition. Increasing precipitation results in some increase in wet deposition, whereas increasing areas of snowpack on first-year sea ice and decreasing snow cover extent both lead to a decline in Hg re-emission and air concentration. Although the link between Hg deposition and lake sediment fluxes is not fully understood, an increase in deposition of Hg in the Arctic appears to be consistent with observed increases in Hg fluxes in some Arctic lake sediments in recent decades (Goodsite et al., 2013).

Despite modelling differences, all studies suggested a dominant role of climate warming-related changes in environmental factors on Hg trends in the Arctic. Current Hg models lack a complete representation of the complexity of climate sensitive Hg processes. Fully interactive atmosphere-land-ocean biogeochemical Hg models including detailed representation of sea-ice dynamics are required to reduce the discrepancy between modelling results. Moreover, field measurements together with model parametrization of climate warming-related environmental factors (temperature, ultraviolet radiation, nutrients etc.) are needed to gain process-based understanding and project future changes in atmospheric Hg trends.

Recently, several modelling studies have investigated future changes in atmospheric Hg concentration and deposition as a result of changes in anthropogenic emissions, land use and land cover as well as climate change. Pacyna et al. (2016) used two chemical transport models (GLEMOS, ECHMERIT) to evaluate future changes in Hg deposition in various geographic regions using three anthropogenic emissions scenarios of 2035 (Figure 5.11). The 'current policy' scenario (CP 2035) predicted a considerable decrease (20–30%) in Hg deposition in Europe and North America and a strong (up to 50%) increase in South and East Asia. According to the 'new policy' scenario (NP 2035) a moderate decrease in Hg deposition (20–30%) was predicted in all regions except South Asia. Model predictions based on the 'maximum feasible reduction' scenario (MFR 2035) showed a consistent Hg deposition reduction on a global scale. It should be noted that the geogenic and legacy sources were assumed to be unchanged in this study.

The combined effect of emissions changes and warming associated with climate change was studied by Lei et al. (2014) with the CAM-Chem model using three emissions scenarios of 2050 (B1, A1B, A1FI) based on projections developed by the Intergovernmental Panel on Climate Change (IPCC). It was found that all three scenarios predict a general increase in total gaseous mercury (TGM) concentration around the globe due to increasing use of fossil fuel energy. The increase in temperature enhances emissions from land and ocean and accelerates oxidation of Hg^0 leading to increased deposition. The effect of climate change as well as change in land use on future Hg levels were studied more thoroughly by Zhang et al. (2016a) by combining a chemical transport model (GEOS-

Chem), a general circulation model (GISS GCM 3), and a dynamic vegetation model (LPJ). Using the IPCC A1B scenario for simulating 2000–2050 climate change they found a global increase in surface Hg^0 concentration with significant changes occurring over most continental and ocean regions due to changes in atmospheric Hg redox chemistry. The study also found that changes in natural vegetation and anthropogenic land use can lead to general increases in Hg^0 dry deposition. The gross Hg deposition flux is expected to increase over most continental regions driven by the combined changes in climate and land use. However, these results do not take into account the possible feedback of the deep ocean and terrestrial reservoirs to the future emissions and climate changes. Besides, current understanding of processes governing Hg cycling in the aquatic and terrestrial environments as well as the air-surface exchange is very limited. Interactions between the Hg cycle and important environmental constituents (e.g. organic carbon, nutrients and biota) and dependence on ambient parameters (e.g. temperature, moisture, radiation) requires further refinement in the model to improve future projections.

Amos et al. (2013) used a fully coupled biogeochemical model and showed that even if anthropogenic emissions remain constant, Hg deposition will continue to increase due to the legacy of anthropogenic production emissions accumulated in the ocean. Generally, the atmosphere responds quickly to a change in emissions but long-term changes are sensitive to various factors, including historical changes in anthropogenic emissions, air-sea exchange, and Hg burial in deep ocean and coastal sediments (Amos et al., 2014, 2015).

5.5 Region-specific modelling studies

5.5.1 Polar regions

Since GMA 2013, three global Hg models have been applied to study Hg cycling in polar regions - GLEMOS (Travnikov and Ilyin, 2009), GEOS-Chem (Holmes et al., 2010; Fisher et al., 2012), and GEM-MACH-Hg (formerly GRAHM; Dastoor et al., 2008; Durnford et al., 2012; Kos et al., 2013). The greatest differences among models in the polar regions concern the representation of Hg^0-Br oxidation rates, Br concentrations, parameterization of photo-reduction and re-emission of Hg^0 from the snowpack, and Hg evasion fluxes from the Arctic Ocean (Angot et al., 2016). Durnford et al. (2012) developed and implemented a dynamic multi-layer snowpack-meltwater parameterization in GEM-MACH-Hg. Fisher et al. (2012) and Durnford et al. (2012) introduced enhanced evasion of Hg from the Arctic Ocean during summer to explain the observed summer maximum in Hg^0 concentrations (Steffen et al., 2005; Berg et al., 2013). Dastoor and Durnford (2014) found that summer concentrations in the Arctic are characterized by two distinct maxima with the peaks varying in time with location and year. Using GEM-MACH-Hg, the authors demonstrated that an early summer peak in Hg^0 concentrations is supported primarily by re-emission of Hg from melting snowpack and meltwater and a late summer peak is supported by evasion of Hg^0 from the Arctic Ocean. Toyota et al. (2014) developed a detailed one-dimensional air-snowpack model for interactions of Br, O_3, and Hg in the springtime Arctic which provided a physical-chemical mechanism for AMDEs and concurrently occurring ozone depletion events (ODEs). The authors also developed a temperature dependent GOM-PBM partitioning mechanism explaining the observed seasonal transition between oxidized Hg species (Steffen et al., 2014) and demonstrated that PBM is mainly produced as $HgBr_4^{2-}$ through uptake of GOM into Br-enriched aerosols after O_3 is significantly depleted in the Arctic air masses.

Dastoor and Durnford (2014) conducted a comprehensive evaluation of GEM-MACH-Hg simulated concentrations of Hg^0 and Hg^{II} in air, total Hg concentrations in precipitation and seasonal snowpack, and snow/air Hg fluxes with measurements for 2005–2009 at four Arctic sites – Alert, Ny-Ålesund, Amderma, and Barrow (see Figure 5.12). The model median concentrations of Hg^0 and Hg^{II} were found within the range of observed medians at all locations. Mercury concentrations in snow collected during the springtime (AMDE season) are significantly higher at Barrow than Alert, which was simulated well by the model. Modelled Hg concentrations in seasonal snowpack were also within the measured range.

Angot et al. (2016) evaluated GEM-MACH-Hg, GEOS-Chem and GLEMOS using atmospheric monitoring data of Hg concentrations for 2013 at four Arctic sites (Alert, Station

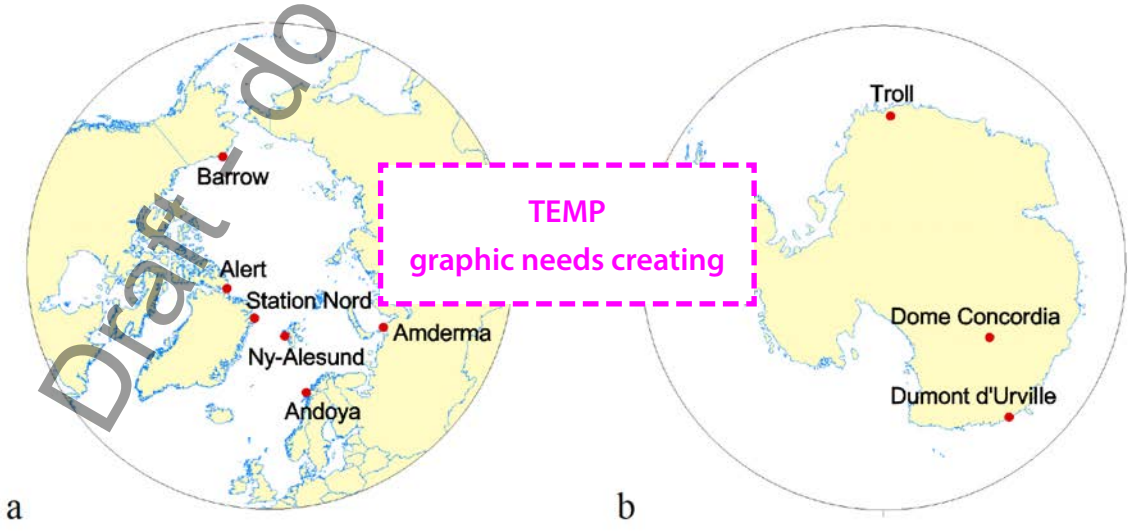

Figure 5.12 Location of Arctic and Antarctic ground-based sites used for model evaluation.

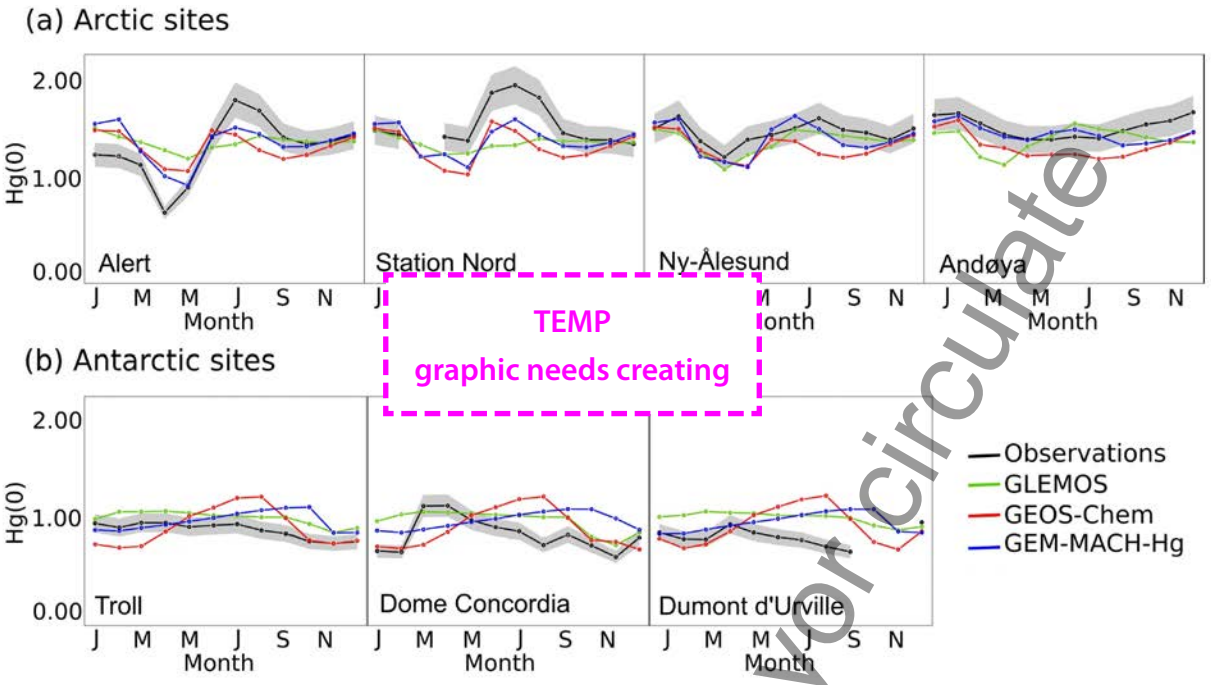

Figure 5.13 Year 2013 monthly-averaged Hg^0 concentrations at Arctic and Antarctic ground-based sites. Adapted from Angot et al. (2016). Only models that explicitly implement high-latitude specific processes are shown.

Nord, Ny-Ålesund, Andøya) and three Antarctic sites (Troll, Dome Concordia, Dumont d'Urville; see Figure 12). In addition, interannual variability in Hg^0 concentrations was evaluated using GEOS-Chem and GEM-MACH-Hg simulations for 2011–2014. The models captured the broad spatial and seasonal patterns in Hg^0 concentration observed in the Arctic. The decline in Hg^0 concentrations from Andøya (the site closest to European industrialized areas) to Alert (the most northerly site) was reproduced well by the models and suggests transport of anthropogenic Hg from lower latitudes to the Arctic. The more pronounced seasonal cycle observed at Alert and Station Nord than at Ny-Ålesund and Andøya was also captured by the models (Figure 5.13).

All models reproduced the characteristic low Hg^0 concentrations in spring and high Hg^0 concentrations in summer. Consistent with observations, the models simulated enhanced total oxidized Hg concentrations (i.e., oxidized gaseous and particulate Hg) at Alert and Ny-Ålesund during the AMDE season but underestimated the values compared to measurements. At Ny-Ålesund all the models overestimated Hg wet deposition along with overestimation of precipitation amount. The model-measurement discrepancy was attributed to lower collection efficiency for precipitation in polar regions due to frequent strong winds and blowing snow conditions (Lynch et al., 2003; Prestbo and Gay, 2009) and to the uncertainties in gas-particle partitioning of oxidized Hg in the models.

Simulated Hg^0 interannual variability in GEOS-Chem and GEM-MACH-Hg in winter was lower than measured which suggests an impact of interannual variability in anthropogenic emissions; the models used 2010 global anthropogenic Hg emissions (AMAP/UNEP, 2013) for simulations over the 2011–2014 period. Interannual variability in the frequency of AMDEs was fairly well reproduced by GEM-MACH-Hg but not by GEOS-Chem. Real-time modelling of the distribution of Br concentrations and sea-ice dynamics is needed to improve the models (Moore et al., 2014).

In contrast, at Antarctic sites, the models overestimated Hg^0 concentrations and failed to reproduce observed seasonal patterns in Hg^0 concentration (Figure 5.13). GEM-MACH-Hg and GEOS-Chem simulated increasing Hg^0 concentrations at all sites over the course of winter in contrast to the pattern shown by observations; whereas, GLEMOS simulated a lower than observed winter decline in Hg^0 concentrations at Dumont d'Urville and Dome Concordia (Angot et al., 2016). High summer variability and a strong diurnal cycle in Hg^0 concentrations observed at Dumont d'Urville and Dome Concordia were also not well reproduced by the models. GEM-MACH-Hg did not simulate the infrequent AMDEs observed at Troll and Dumont d'Urville in spring; whereas, GEOS-Chem simulated AMDEs at Dumont d'Urville with somewhat higher frequency than observed. Angot et al. (2016) attributed poor model simulation of Hg at the Antarctic sites to missing local Hg^0 oxidation pathways involving OH, O_3, NO_X, organic peroxy radicals and air circulation, and bias in Southern Hemisphere emissions including oceanic evasion in the models.

Modelling estimates of Hg mass fluxes in the Arctic including the Arctic Ocean were provided by Fisher et al. (2012), Durnford et al. (2012) and Dastoor and Durnford (2014). Using GEOS-Chem, Fisher et al. (2012) estimated Hg deposition of 55 Mg/y (25 Mg/y directly to open ocean, 20 Mg/y to ocean via snow melt on sea ice, 10 Mg/y to land via snow melt), evasion from ocean of 90 Mg/y and a net surface loss of 35 Mg/y in the Arctic north of 70°N. In contrast, using GEM-MACH-Hg, Durnford et al. (2012) estimated Hg deposition of 153 Mg/y (58 Mg/y directly to open ocean, 50 Mg/y to ocean via snow melt on sea ice, 29 Mg/y directly to land, 16 Mg/y to land via snow melt), emission of 36 Mg/y (33 Mg/y from ocean, 3 Mg/y

from land) and a net surface gain of 117 Mg/y in the Arctic north of 66.5°N. Thus, Fisher et al. (2012) concluded that the Arctic Ocean is a net source of Hg to the atmosphere, i.e., 45 Mg/y; whereas, Durnford et al. (2012) concluded that the Arctic Ocean is a net sink of atmospheric Hg, i.e., 75 Mg/y. In comparison, GLEMOS estimated the yearly net gain of Hg in the Arctic to be 131 Mg/y (Travnikov and Ilyin, 2009).

Model disagreements in the estimates of atmosphere-ocean-snowpack Hg fluxes indicate sources of uncertainty in the models. Constraining models in the polar regions is challenging due to insufficient measurements (Dastoor and Durnford, 2014; Angot et al., 2016). Fisher et al. (2012) inferred that a 95 Mg/y input of Hg from circumpolar rivers (and coastal erosion) resulting in a 90 Mg/y evasion of Hg from the Arctic Ocean was required to balance the observed summer peak in Hg^0 concentrations at the Arctic sites. In contrast, Durnford et al. (2012) found that 33 Mg/y Hg evasion from the Arctic Ocean was sufficient to reproduce the summer peak in Hg^0 concentrations in the Arctic. Dastoor and Durnford (2014) estimated riverine Hg export to the Arctic Ocean from North American, Russian and all Arctic watersheds to be in the range 2.8–5.6, 12.7–25.4 and 15.5–31.0 Mg/y, respectively, based on GEM-MACH-Hg simulated Hg in meltwater. Using the MITgcm ocean model and GEOS-Chem, Zhang et al. (2015) concluded that an input of 63 Mg/y of Hg discharge from rivers and coastal erosion to the Arctic Ocean was needed to reproduce the observed summer maximum in atmospheric Hg^0 concentrations. River discharge to the Arctic Ocean is poorly constrained by observations with estimates ranging from 12.5 to 44 Mg/y (Outridge et al., 2008; Amos et al., 2014). Zhang et al. (2015) noted that enhanced turbulence associated with sea-ice dynamics facilitates increased evasion of Hg discharged by Arctic rivers in estuaries resulting in a much larger proportion of riverine Hg in the Arctic Ocean subject to evasion than estimated by Fisher et al. (2012). In addition, Fisher et al. (2012) assumed that the Hg input from rivers is uniformly distributed across the entire Arctic Ocean; whereas, latitudinal variation in Hg evasion from the Arctic Ocean was assumed by Durnford et al. (2012) and Zhang et al. (2015), which is supported by observations (Andersson et al., 2008; Hirdman et al., 2009; Sommar et al, 2010). Other sources of differences between models were related to the parameterizations of Br concentrations and Hg snowpack/meltwater processes (Dastoor and Durnford, 2014).

5.5.2 Europe

In recent years, the development of regional atmospheric Hg models for Europe was supported by the FP7 project GMOS (Global Mercury Observations System). Mercury chemistry was incorporated into the on-line coupled meteorological CTM WRF-Chem model by Gencarelli et al. (2014) and the CCLM-CMAQ model was further developed (Bieser et al., 2014; Zhu et al., 2015). These models have been used to evaluate key processes and identify their impact on Hg dispersion and deposition in Europe (Gencarelli et al., 2016; Bieser et al., 2017).

Historically, Europe has been one of the major emitters of Hg (Streets et al., 2011). A major decline in European Hg emissions occurred at the end of the 1980s (Pacyna et al., 2009). Since 1990 atmospheric Hg emissions have been reduced by 60% (Maas and Grennfelt, 2016). A large proportion of this reduction is due to regulatory and economic changes in the late 20th century. However, based on the recent estimates of Muntean et al. (2014) Hg emissions in Europe continue to decrease, but at different rates for each Hg species. Coal-fired power plants are the main source of Hg in Europe. Due to technological development, emissions of GOM are declining faster than total Hg emissions, which affects the regional deposition and global transport patterns. This finding was further confirmed by model studies where the models' tendency to overestimate ground-based GOM concentrations could be attributed to the speciation of primary anthropogenic Hg emissions (Bieser et al., 2014, 2017). Moreover, airborne *in situ* measurements at a modern coal-fired power plant did not detect any GOM 1 km downwind from the stack (Weigelt et al., 2016).

The models have in common that the modelled annual wet deposition fluxes are in good agreement with observations. This was found for regional models (Bieser et al., 2014; Gencarelli et al., 2014) and global models (Muntean et al., 2014). At the same time, models tend to underestimate total gaseous mercury concentrations for Europe; something also seen in the results from global models (Muntean et al., 2014; Chen et al., 2015a). The reason for this is not yet understood. In a global long-term simulation with the GEOS-Chem model, Muntean et al. (2014) showed that modelled total gaseous mercury concentrations were closer to observations in the 1990s but that the model overestimates the decreasing trend of recent decades. This, in turn, can be explained by overestimation of the emissions trend. It is also in line with the fact that new regional emission models lead to higher estimates for European Hg emissions (Rafaj et al., 2014).

A recent study with a newly developed regional multi-media model indicates that an underestimation of air-sea exchange from regional oceans could be a source of model bias for Europe (Bieser and Schrum, 2016). Comparing the impact of air-sea exchange on Hg concentrations at two ground-based stations in Europe (Figure 5.14) shows that air-sea exchange has a larger impact on Hg^0 concentrations near the ocean (Zingst) than 200 km inland (Waldhof).

A first model analysis on the vertical distribution of Hg in Europe was recently published by Bieser et al. (2017). Based on the combination of ground-based observations and aircraft measurements in the troposphere and lower stratosphere a comprehensive Hg vertical profile in Europe was reconstructed up to 12 km in altitude. The measurements were compared with multi-model simulations of Hg vertical distribution in the atmosphere. This showed that models are generally able to reproduce the Hg^0 gradient from the surface to the tropopause (Figure 5.15). Moreover, models were also able to reproduce the GOM gradient inside the planetary boundary layer (not shown), in those cases where a small GOM fraction in the anthropogenic emissions was assumed (Bieser et al., 2017). This is in line with the findings on decreasing GOM fraction in European Hg emissions discussed earlier in this section.

The impact of long-range atmospheric transport on European Hg deposition was investigated in the GMA Update 2015. Since then, there has only been one new study on the global transport of Hg from Asia (Chen et al., 2015a). In this study, the estimated contribution of Chinese emissions to Hg deposition in Europe is 3%, which is less than estimates of 8% by other models (AMAP/UNEP, 2015). It should be noted that most global model results appear to be relatively consistent

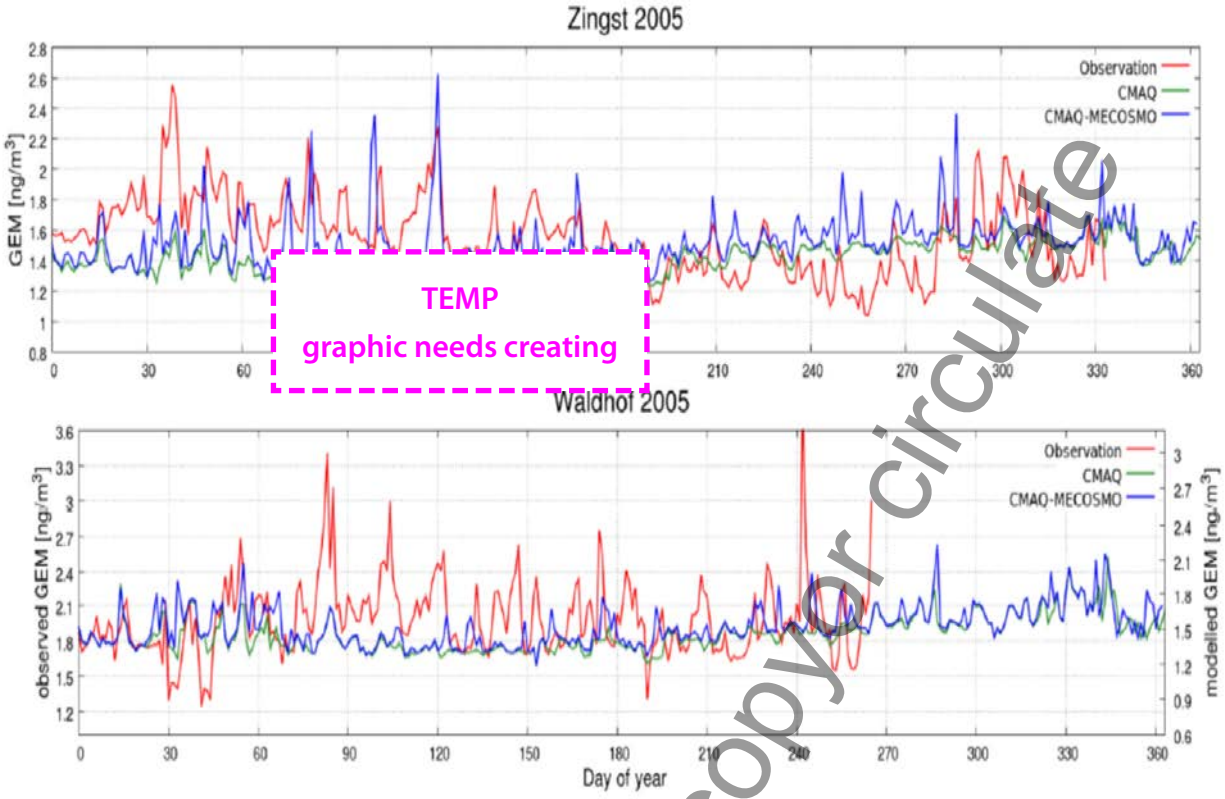

Figure 5.14 Impact of air-sea exchange on atmospheric Hg concentrations at two ground-based observations sites in Germany: Zingst (near the coast) and Waldhof (200 km inland). Source: Bieser and Schrum (2016).

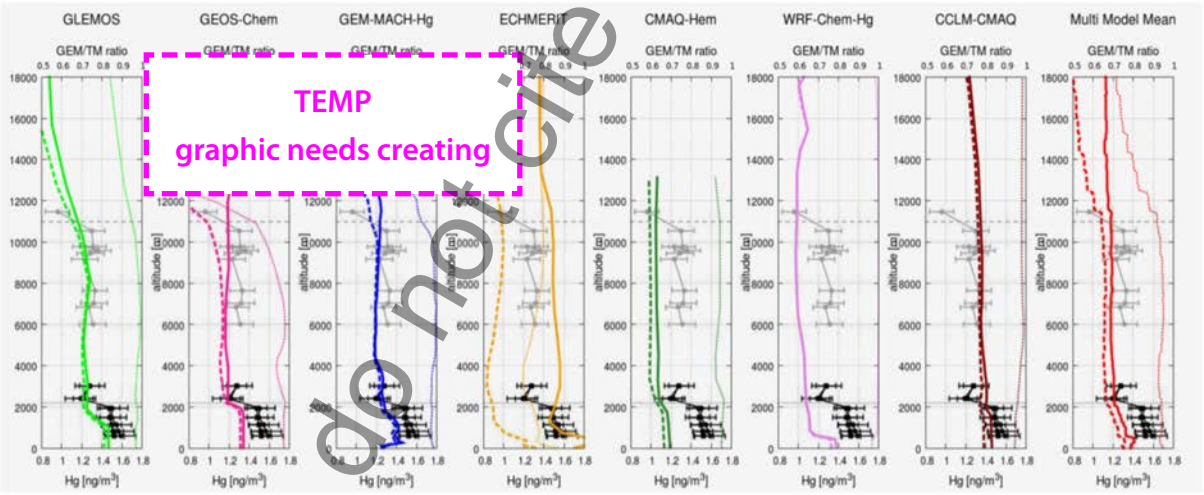

Figure 5.15 Vertical profiles at Leipzig, Germany 23 August 2013 from two aircraft campaigns and simulations with seven atmospheric chemistry transport models. Source: Bieser et al. (2017).

in terms of estimating the contribution of Asian emissions to European deposition values and so the study by Chen et al. (2015a) seems to be an outlier (see also Section 5.3.1). The impact of long-range transport on regional Hg deposition in Europe is strongly dependent on the lifetime of Hg in the atmospheric models. An important factor is the speciation of emissions in China, as Hg^0 and PBM have much longer atmospheric lifetimes than GOM. Thus, if novel technology leads to a similar shift in Hg emission speciation in Asia as recently observed in Europe, a longer lifetime of Hg emitted in Asia could be expected.

De Simone et al. (2015, 2017) investigated the impact of biomass burning on atmospheric Hg concentrations and deposition. Wildfires in the boreal forests can have an especially large impact on regional Hg concentration and deposition. For Europe, De Simone et al. (2015, 2017) estimated the fraction of Hg deposition due to biomass burning at between 5% and 10%.

5.5.3 North America

The model CMAQ, with global boundary conditions estimated with the MOZART model, was used to estimate atmospheric Hg deposition to the Great Lakes in 2005 (Grant et al., 2014). Emissions from U.S. power plants had the greatest impact on Lake Erie. The model tended to overestimate wet deposition in the Great Lakes region. In another CMAQ-based investigation, the model was used with boundary conditions from GEOS-Chem, and alternatively GRAHM, to estimate atmospheric Hg deposition in the United States (Myers et al., 2013) in a series of 2001–2005 case studies. Simulation results were significantly influenced by the choice of boundary conditions. CMAQ, with a new aqueous-phase oxidized Hg reduction chemical mechanism (involving dicarboxylic acids) and GEOS-Chem boundary conditions, was used to simulate Hg fate and transport in the USA during the period 2001–2002 (Bash et al., 2014). Results for wet deposition with the new chemical mechanism were found to be more consistent with observations than earlier mechanisms used in CMAQ. Using a weight-of-evidence approach, Sunderland et al. (2016) argued that historical EPA CMAQ-based modelling may have underestimated the impact of local and regional sources on near-field Hg deposition, and consequently underestimated the benefits of Hg emissions reductions.

The GEOS-Chem model was used to estimate the cumulative benefits of domestic and international Hg controls for atmospheric deposition – and subsequent public health impacts – in the USA through 2050 (Giang and Selin, 2016). For the same amount of avoided Hg emissions, domestic reductions were estimated to have nearly an order of magnitude higher public health benefit than international actions. The CAM-Chem-Hg model was used to estimate present day (~2000; Lei et al., 2013) and future (~2050; Lei et al., 2014) atmospheric Hg concentrations and deposition in the USA, as influenced by different scenarios of changes in domestic and global emissions, and different climate change scenarios. Concentrations and deposition in the USA increased significantly in scenarios with higher future emissions and higher air temperatures. Under the scenario of highest impact considered, climate change alone caused an approximate 50–100% increase in atmospheric Hg concentrations in the USA. When increased Hg emissions in this scenario were included, the average Hg^0, GOM, and PBM concentrations in the USA increased by factors of ~2.5, ~5, and ~3, respectively. The GRE-CAPS model – which included a version of the regional CAMx model – was used to investigate the influence of climate change on atmospheric Hg deposition in the eastern USA (Megaritis et al., 2014). Simulations for the present day (~2000s) were compared with climate change-influenced simulations for 2050, assuming constant 2001 Hg emissions. The study found that average deposition in the USA increased by about 5% due to climate-change impacts (e.g., enhanced atmospheric oxidation of Hg^0 at higher temperatures), but regional differences were found (e.g., related to changes in precipitation patterns).

The HYSPLIT-Hg, a special version of the NOAA HYSPLIT model developed to simulate the fate and transport of atmospheric Hg, including chemical transformations, was used to estimate 2005 atmospheric Hg deposition to the Great Lakes (Cohen et al., 2016). Results for a base case and ten alternative model configurations were developed, examining the sensitivity

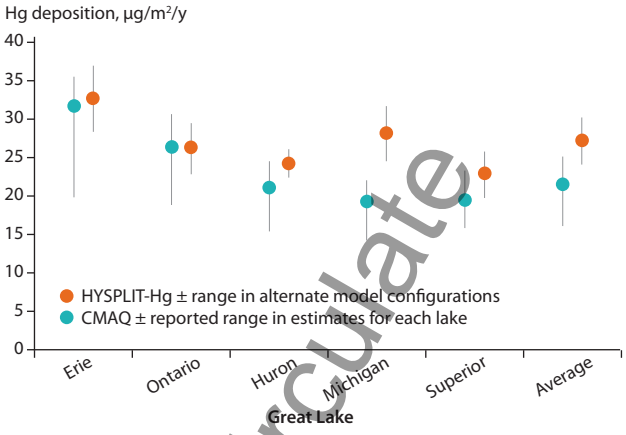

Figure 5.16 Atmospheric Hg deposition flux to the Great Lakes for 2005, estimated by CMAQ (Grant et al., 2014) and HYSPLIT-Hg (Cohen et al., 2016). CMAQ error bars shown are the reported range in estimates for each lake. HYSPLIT-Hg error bars shown are the range found in the ten alternate model configurations used in the analysis. The Great Lakes summary values shown are based on an area-weighted average of individual-lake results.

of the results to different assumptions regarding atmospheric reaction rates and chemical mechanisms. Model evaluation against measurements in the Great Lakes region showed good agreement between modelled and measured wet deposition and Hg^0 concentrations, but also that the model tended to overestimate reported GOM and PBM concentrations. The total deposition and source-attribution for that deposition was similar to that found by Grant et al. (2014) (see Figure 5.16). Lake Erie, downwind of significant local/regional emissions sources was estimated by the model to be the most impacted by direct anthropogenic emissions (58% of the base-case total deposition), while Lake Superior, with the fewest upwind local/regional sources was the least impacted (27%). On average, the USA was the largest national contributor (25%) for the Great Lakes, followed by China (6%). The contribution of U.S. direct anthropogenic emissions to total Hg deposition varied between 46% for the base case (with a range of 24–51% over all model configurations) for Lake Erie and 11% (range 6–13%) for Lake Superior. The relative contributions of different sources are illustrated in Figure 5.17 for the base-case simulation. These results were used in an International Joint Commission report (IJC, 2015) which called for increased monitoring and modelling of atmospheric Hg in the Great Lakes region.

A number of analyses were conducted in which measurements of atmospheric concentration were combined with back-trajectory and other receptor-based modelling approaches to assess the relative importance of different source regions and other factors to the atmospheric Hg arriving at the measurement site (see Table 5.2 for examples). In most cases, the HYSPLIT model (Stein et al., 2015) was used for simulating back-trajectories. Similar studies were carried out for flight-based measurements of atmospheric Hg concentration above the surface, utilizing back-trajectories and/or other model simulations, above Tullahoma, TN (Brooks et al., 2014), Texas and the southeastern USA (Ambrose et al., 2015; Gratz et al., 2015; Shah et al., 2016), and Lake Michigan (Gratz et al., 2016).

In a hybrid analysis combining fate-and-transport modelling with measurements, GEOS-Chem was used to examine trends in Hg wet deposition over the United States over the 2004–2010 period (Zhang and Jaeglé, 2013). The modelling results were subtracted from the observations to assess the

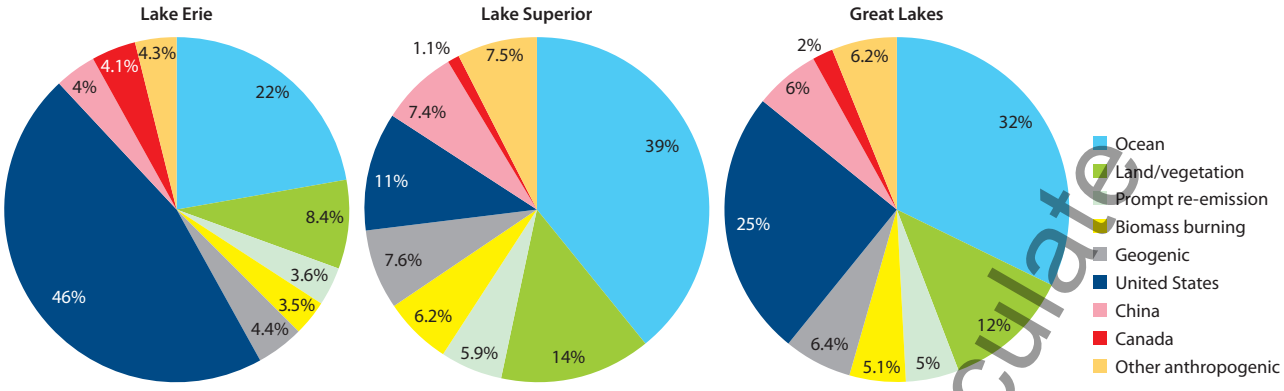

Figure 5.17 Relative contributions of different source categories to the 2005 atmospheric Hg deposition to Lake Erie, Lake Superior, and an area-weighted average for the Great Lakes as a whole, estimated by the HYSPLIT-Hg model (Cohen et al., 2016) (base-case simulation). The values shown for specific countries (United States, China, and Canada) and for all other countries ('Other anthropogenic') include only the contributions from direct, anthropogenic emissions and do not include contributions arising from re-emissions of previously deposited material from terrestrial or oceanic surfaces.

roles of changing meteorology and emissions on observed wet deposition at 47 U.S. sites. In the northeast and midwest USA, approximately half of the decreasing trend in Hg concentrations in precipitation could be explained by decreasing U.S. emissions over the study period. The use of receptor-based analyses to investigate source-receptor relationships for atmospheric Hg has been reviewed by Cheng et al. (2015).

Table 5.2 Measurement sites analyzed with receptor-based modelling.

Measurement site	Back-trajectory study
Canada	
Dartmouth, NS	Cheng et al., 2013a, 2016
Kejimkujik, NS	Cheng et al., 2013a, 2016
Windsor, ON	Xu et al., 2014
USA	
Beltsville, MD	Ren et al., 2016
Chicago, IL	Gratz et al., 2013a
Grand Bay, MS	Rolison et al., 2013; Ren et al., 2014
Holland MI	Gratz et al., 2013a
Huntington Forest, NY	Cheng et al., 2013b; Choi et al., 2013; Zhou et al., 2017;
Illinois (several sites)	Gratz et al., 2013b; Lynam et al., 2014
Oxford, MS	Jiang et al., 2013
Pensacola, FL	Demers et al., 2015; Huang et al., 2016
Piney Reservoir, MD	Castro and Sherwell, 2015
Reno, NV	Gustin et al., 2016
Rochester, NY	Choi et al., 2013
Steubenville, OH	White et al., 2013
Underhill, VT	Zhou et al., 2017
Western U.S. (several sites)	Wright et al., 2014; Huang and Gustin, 2015; Gustin et al., 2016
Mexico	
Celestun, Yucatan	Velasco et al., 2016

5.5.4 East Asia

East Asia (including Southeast Asia) is the largest source region for atmospheric Hg release worldwide, with China contributing the largest amount of anthropogenic Hg emissions. According to GMA 2013, Hg release in East and Southeast Asia accounted for 40% of global anthropogenic emission in 2010. Mercury outflow from East Asia has been regarded as a global Hg pollution issue (Jaffe et al., 2005; Lin et al., 2010; Chen et al., 2014).

Rapid economic growth and improving air emission control in East Asia are causing changes in anthropogenic Hg emission and speciation over a relatively short period. As better emission data become available, reassessment using updated emission data is necessary. For example, Wu et al. (2016) applied updated industrial activity statistics and emission factors to estimate anthropogenic Hg release in China between 1978 and 2014, and found the emission varied significantly due to increased industrial production, energy use and implementation of emission control measures. Atmospheric Hg emission in China peaked in 2011 at 565 Mg/y and then fell to 531 Mg/y in 2014 (Wu et al., 2017). More importantly, the emission speciation gradually shifted to a larger fraction of oxidized Hg (Wu et al., 2016). Such a shift implies increased local deposition and reduced emission outflow.

Wang et al. (2016b) re-evaluated the natural release of Hg^0 vapor from soil, vegetation and water surfaces using new soil Hg data in China and updated model schemes with recently reported physical-chemical parameters. They found a different spatial distribution of estimated Hg release compared to the data reported by Shetty et al. (2008), despite a similar net natural release at ~460 Mg/y in China.

Several regional and global modelling studies have simulated atmospheric Hg levels in China and the East Asian region (e.g., Lin et al., 2010; Pan et al., 2010; Chen et al., 2014, 2015a; Zhu et al., 2015; Wang et al., 2018). It should be noted that most model results are not directly comparable due to differences in the emission inventory (particularly, natural emissions since many earlier studies did not specify the quantity and spatial distribution), Hg chemistry and model configuration. In general, regional models reproduced Hg concentrations that were more representative of the observed elevated levels in urban and industrial areas. Previous global model results estimated that Asian emissions contributed 16–25% of Hg

TEMP
graphic needs creating

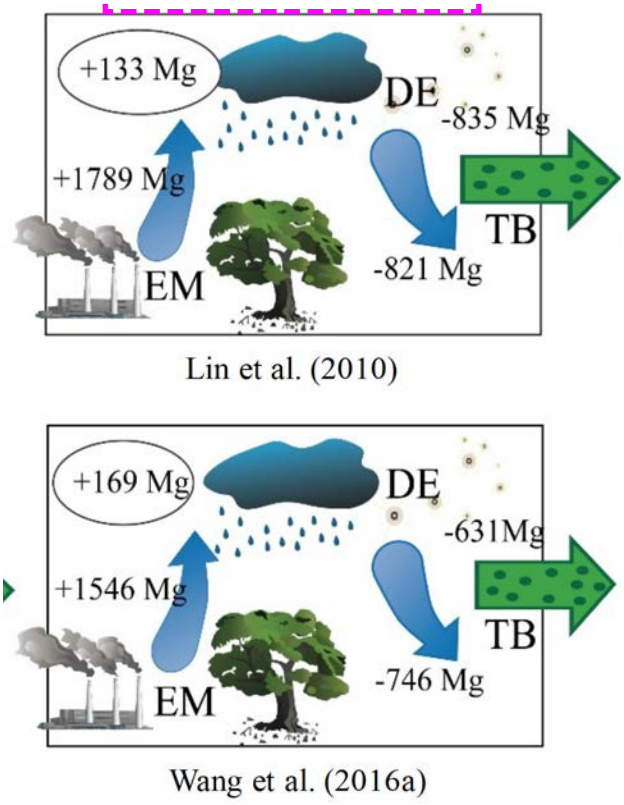

Figure 5.18 Comparison of annual Hg mass budget in East Asia by Lin et al. (2010) and Wang et al. (2018).

deposition in North America and 10–15% in the European region. More recent modelling studies provide lower values (8–10% for North America and 7–8% for Europe), except for one study (Chen et al., 2014) which reported a contribution of <5% for both regions (see also Section 5.3.1). Recently, It was estimated that the contribution of foreign countries to the Hg^0 concentration on the Korean Peninsula averaged ~15% (Seo et al., 2016; Sung et al., 2016).

The results of two regional modelling studies using CMAQ-Hg with identical model specifications are directly comparable (Lin et al., 2010; Wang et al., 2018). The two studies use the same model configuration of CMAQ-Hg with different emission inventories: from Streets et al. (2005) and Shetty et al. (2008) for the former and Wu et al. (2016) and Wang et al. (2016b) for the latter. The difference in the annual budgets is mainly caused by the reduced anthropogenic emission in the region, increased fraction of Hg^{II}, and a change in the spatial distribution of natural emissions. Given the changes in emissions, the transport budget from East Asia by Wang et al. (2018) is 25% lower than the earlier estimate by Lin et al. (2010), as shown in Figure 5.18. In addition, the greater Hg mass accumulated within the regional domain of Wang et al. (2018) also better explains the elevated atmospheric Hg concentrations in China. More modelling studies are still needed in this region. Recent observational data obtained from the ambient monitoring network in China (Fu et al., 2015) provide a unique opportunity to better understand the chemical transport of atmospheric Hg in a region undergoing dynamic emission changes.

5.6 Conclusions

A number of regional and global models have been used to simulate the atmospheric transport and fate of Hg, using meteorological data and emissions inventories as inputs and atmospheric measurements to evaluate the results. In particular, the new modelling results based on the updated global Hg emissions inventory for 2015 present up-to-date estimates of Hg transport and fate on a global scale, including source apportionment of Hg deposition in various terrestrial and aquatic regions as well as an evaluation of contributions from different emission sectors. A comparison between the current modelled results and GMA Update 2015 (year 2010 anthropogenic Hg emission inventory) shows an average 20% increase in total Hg deposition flux to most geographic regions, except in the polar regions, which show a 30% reduction. This is consistent with the global increase in anthropogenic Hg emissions (~12%) between 2010 and 2015. Overall, the new analysis of Hg intercontinental transport is consistent with previous results presented in GMA Update 2015. The changes include an increase in deposition from sources in East and South Asia and a reduction in deposition from domestic sources in North America since 2010 due to emission changes in these regions. The contribution of Hg emissions from artisanal and small-scale gold mining to Hg deposition worldwide was estimated for the first time, indicating global dispersion but with the largest effect closer to emission sources in South America, equatorial Africa, and East and Southeast Asia.

Significant uncertainties remain in model physics (e.g., gas-particle partitioning and deposition processes) and chemistry (e.g., elemental Hg oxidation mechanisms, reaction kinetics and oxidation products), as well as in model inputs (e.g., emission amounts and speciation) and measurements used for evaluation. Nevertheless, scientific understanding of atmospheric Hg as represented in the models has progressed to the point where useful policy-relevant information about source-receptor relationships can be derived. This also implies that models can be used to provide first estimates of the effects on Hg deposition of emission reductions, both regionally and globally.

Atmospheric measurements are essential to evaluate and improve models; given the uncertainties noted in Section 5.2, models must continually be tested by comparison against measurements. At the same time, measurements alone cannot provide the depth of source-receptor and trend explanation information that can be obtained by models. Likewise, uncertainties in emissions inventories (e.g., speciation of emissions from power plants and industrial sources, contribution of emissions from ASGM, natural and secondary emissions) have emerged as a critical limitation in atmospheric model analyses. In particular, the quantity of Hg^0 release from natural surfaces needs to be better constrained, and the parameterization of estimating the re-emission of previously deposited Hg in models must be further improved to more realistically determine the source-receptor relationship of global Hg emission and deposition. Improvement in these fundamental model inputs is essential to enhance model accuracy.

Appendix 5.1 Model ensemble

Characteristics of the participating global chemical transport models.

	ECHMERIT	GEM-MACH-Hg	GEOS-Chem (v11-02)	GLEMOS
Institution performing model simulation	CNR-Institute of Atmospheric Pollution Research, Italy	Environment and Climate Change Canada, Canada	Massachusetts Institute of Technology, USA	Meteorological Synthesizing Centre – East of EMEP
Model type	Atmospheric	Atmospheric	Multi-media [a]	Atmospheric
Spatial resolution				
Horizontal	T42 (~ 2.8° × 2.8°)	0.5° × 0.5°	2.5° × 2°	1° × 1°
Vertical (atmosphere)	19 levels, top 10 hPa	58 levels, top 7 hPa	47 levels, top 0.01 hPa	20 levels, top 10 hPa
Atmospheric chemistry				
Gas-phase oxidation (major oxidants)	O_3, OH	OH, Br [b]	Br, NO_2, HO_2 [c]	O_3, OH
Gas-phase reduction	no	no	no	no
Aqueous chemistry (in cloud water)	yes	no	yes [d]	yes
Emissions				
Anthropogenic, t/y	2224	2224	2224	2224
Average speciation GEM:GOM:PBM	82:14:4	87:10:3 [e]	82:18:0 [f]	82:14:4
Natural and secondary, t/y [g]	8600 [h]	5460 [i]	4900 [j]	3730 [k]
Reference	De Simone et al. 2014; Jung et al. 2009	Durnford et al. 2012; Kos et al. 2013; Dastoor et al. 2015	Holmes et al. 2010; Amos et al. 2012; Horowitz et al. 2017	Travnikov and Ilyin 2009; Travnikov et al. 2009

[a] Off-line land and ocean according to Horowitz et al., (2017); [b] OH is a main oxidizing agent globally, Br is a main oxidizing agent in the polar regions; [c] Two-step oxidation initiated by Br. The second-stage HgBr oxidation is mainly by the NO_2 and HO_2 radicals; [d] Oxidation of $Hg^0_{(aq)}$ takes place in clouds only. Photo-reduction of $Hg^{2+}_{(aq)}$ takes place in both aqueous aerosols and clouds (Horowitz et al., 2017); [e] The original speciation of Hg emissions from coal-fired power plants is corrected by converting 80% of GOM and PBM to GEM; [f] Dynamic gas-particle partitioning of reactive Hg in the atmosphere according to Amos et al. (2012); [g] Gross emissions from natural and secondary sources; [h] Prescribed emission from terrestrial surfaces as a function of temperature and solar radiation, dynamically calculated ocean emissions based on prescribed seawater concentrations; [i] Prescribed emission from terrestrial surfaces as a function of temperature and solar radiation, dynamic re-emission from snow and aquatic surfaces; [j] Prescribed emission from terrestrial surfaces as a function of temperature and solar radiation, dynamic fluxes from aquatic surfaces based on multi-media modelling; [k] Prescribed emission from terrestrial and aquatic surfaces as a function of temperature and solar radiation, dynamic re-emission from snow.

Appendix 5.2 Source apportionment results for individual transport models

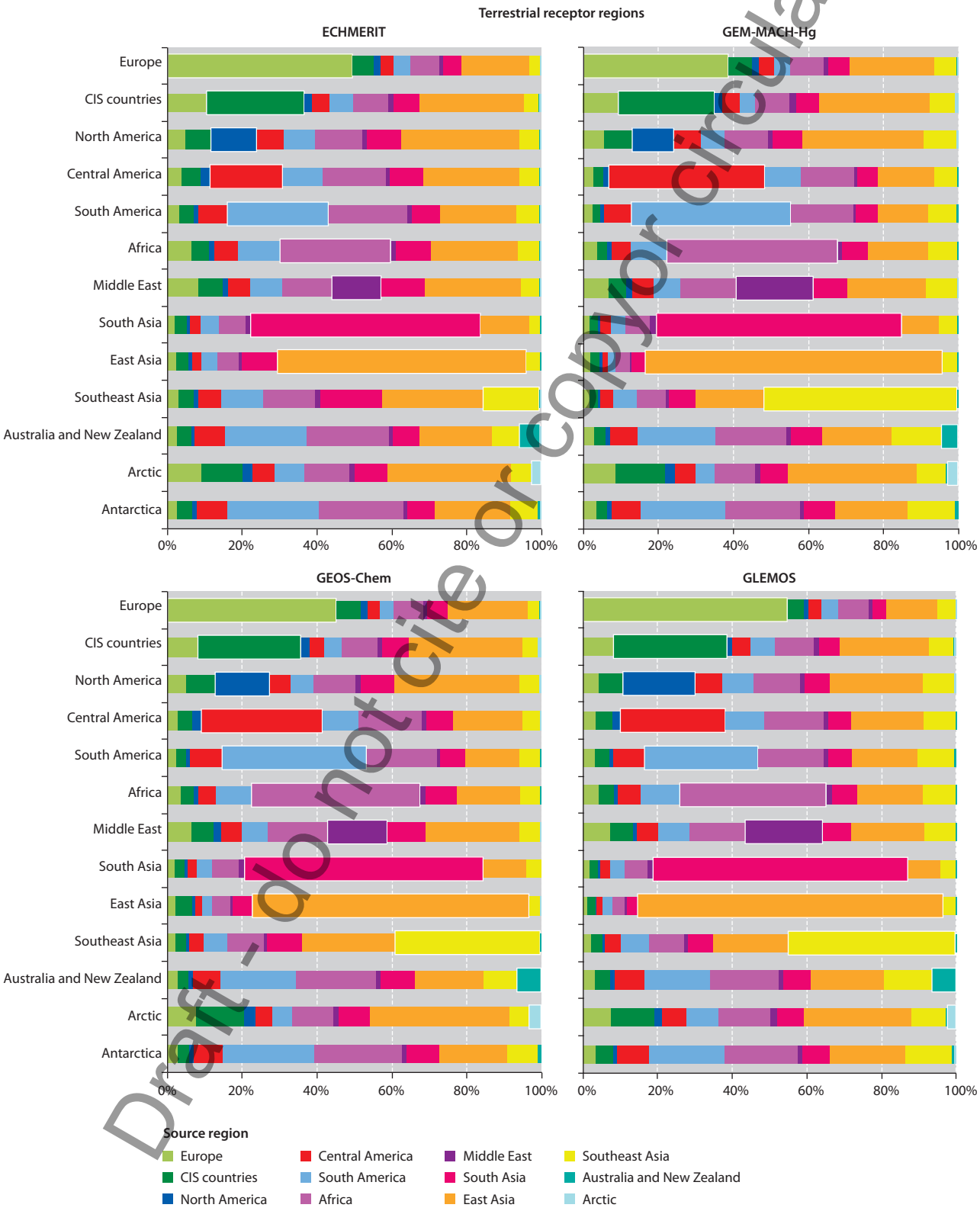

Figure A5.2.1 Source apportionment of Hg deposition from direct anthropogenic emissions to terrestrial receptor regions in 2015 simulated by four models: ECHMERIT, GEM-MACH-Hg, GEOS-Chem, and GLEMOS. Contribution of domestic sources is shown by wider bars.

Figure A5.2.2 Source apportionment of Hg deposition from direct anthropogenic emissions to aquatic receptor regions in 2015 simulated by four models: ECHMERIT, GEM-MACH-Hg, GEOS-Chem, and GLEMOS.

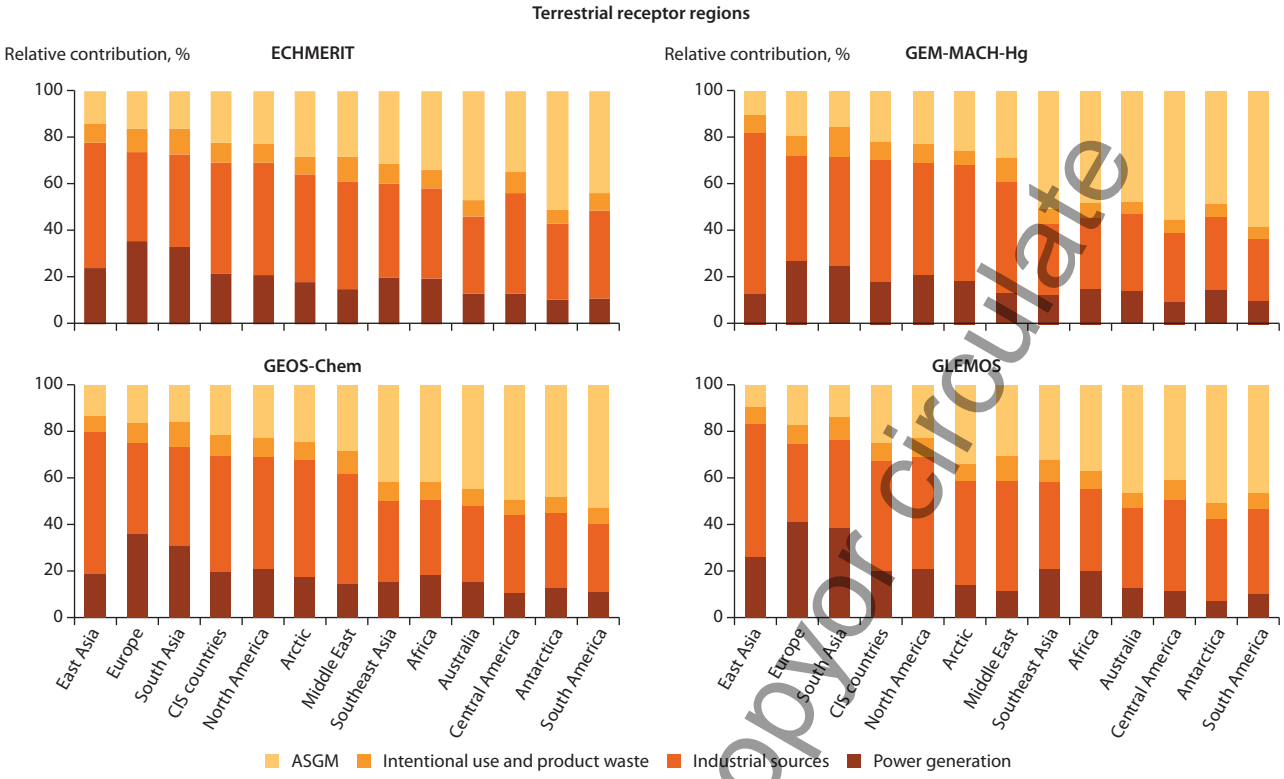

Figure A5.2.3 Simulated relative contribution of the four emission sectors to Hg deposition from direct anthropogenic emissions to terrestrial receptor regions in 2015 simulated by four models: ECHMERIT, GEM-MACH-Hg, GEOS-Chem, and GLEMOS.

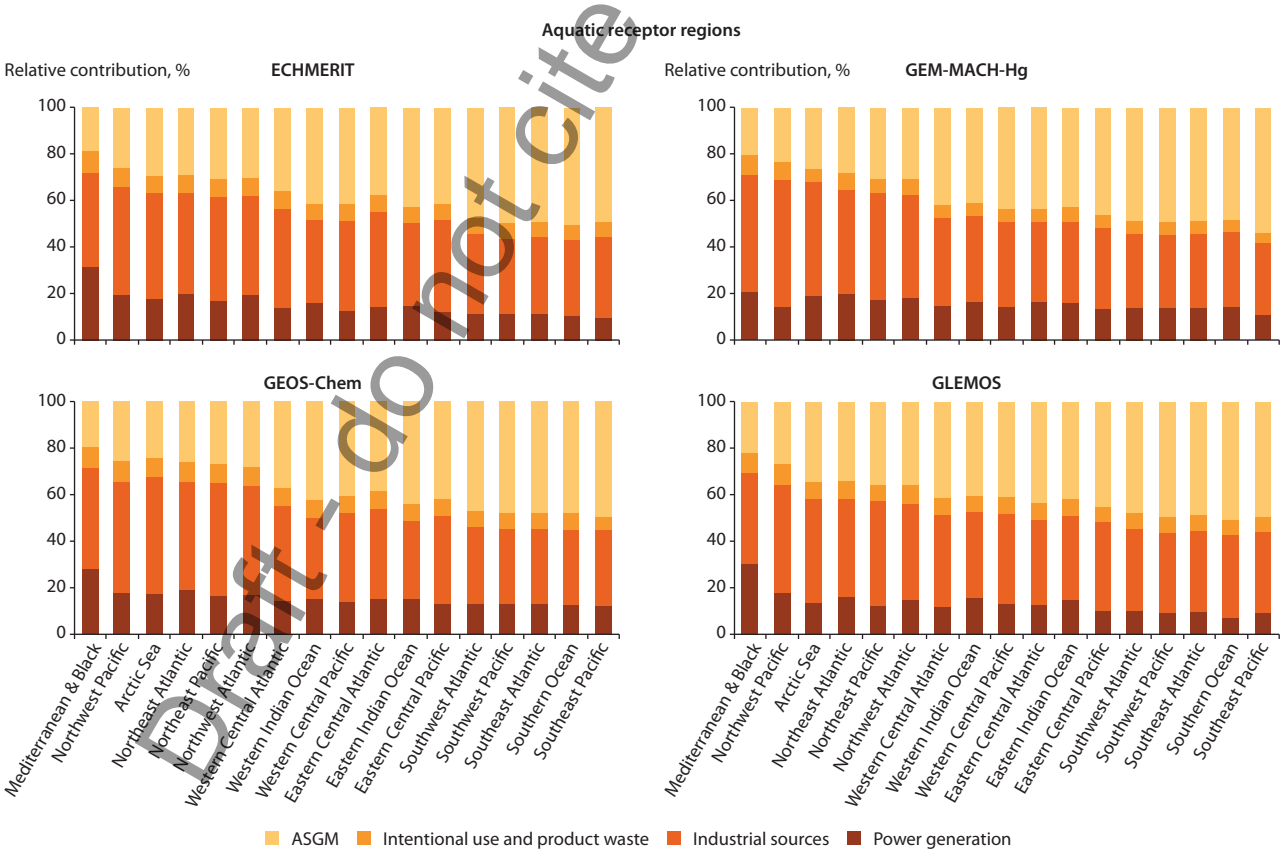

Figure A5.2.4 Simulated relative contribution of the four emission sectors to Hg deposition from direct anthropogenic emissions to aquatic receptor regions in 2015 simulated by four models: ECHMERIT, GEM-MACH-Hg, GEOS-Chem, and GLEMOS.

Contents

Key Findings/Messages:

The 2015 global inventory of mercury releases to aquatic environments from anthropogenic sources currently amounts to ca. 600 t/y (x-y). The new inventory is more complete and reinforces the importance of these sources in the global context.

The current inventory of global anthropogenic Hg releases to aquatic systems is a work in progress, and an important step towards filling a major gap in inventories of anthropogenic Hg releases to the environment.

Quantifiable releases to water from anthropogenic sources comprising 10 key sectors are included in the inventory, with some new important sectors added and newly evaluated in 2015 compared to 2010, such as releases associated with municipal wastewater, coal washing and that from coal fired power plants. In addition to methodological changes introduced to derive the estimates, these newly added sectors are driving the relatively large difference between the 2010 and 2015 anthropogenic Hg release inventory.

For the first time, the inventory was extended to include primary releases to land and solid waste streams from some of the sources considered. The magnitude of these terrestrial mercury pathways can be substantial. It was established that releases of the order of tens to hundreds of tonnes per year may arise following these pathways, and this mercury initially accumulated in terrestrial systems, if not treated properly, can act as potential secondary source of mercury for both water and atmosphere.

Regional and sectoral attribution of global release inventory indicates both similarities and differences with atmospheric emission patterns. Excluding ASGM sector for which combined releases to water and land are estimated, the majority of releases to water occur in Asia (56%; primarily East and South-east Asia) followed by Europe and CIS countries (14%, primary EU28), Latin America (11%) and Sub-Saharan Africa (8%).

Sector-wise the majority of the global anthropogenic releases of Hg to aquatic systems are relatively equally distributed between ore mining and processing (40%) and waste treatment sectors (43%),

followed by energy sectors (17%). Relative contribution of sectors within individual region varies a lot and depends on technological and socio-economic status of the region. For example, releases resulting from ASGM, sector that is considered as the major single current anthropogenic source of Hg for aquatic systems, occur primarily in South America (50%) and East and South East Asia (35%).

In future assessments of aquatic mercury releases, it is reasonable to anticipate additional releases may arise from sectors and activities not quantified in the 2015 inventory due to the lack of information that would enable any reliable global quantification, or from smaller anthropogenic sources not currently detailed in the global inventory work.

Uncertainties associated with release estimates for 2015 are still large (+-X) and are mainly the result of either unavailable or unreliable/inconsistent information on global-scale sector-specific production rates, waste-water generation, treatment practices etc.

5.1 Introduction

This chapter is an extension to work on the global inventory of air emissions discussed in Chapter 2. The results presented represent an attempt to compile a comprehensive global inventory of releases of mercury to water from anthropogenic sources for which sufficient information is available. The work builds on, updates and extends the aquatic Hg release inventory prepared as a part of the UNEP global mercury assessment 2013 (AMAP/UNEP, 2013).

This is the second time only that the content of the updated report has been expanded to include information on Hg releases to aquatic environments. General lack of data in the literature reporting Hg releases to aquatic systems and related information needed for estimation of the releases (e.g. waste-water amounts) is still an issue restricting accuracy and completeness of these estimates. Therefore, methods employed to derive the estimates are largely driven by the type and the amount of information available for various source category. Part of this work is directly linked to the air emissions inventory work and utilise factors employed in the UNEP Toolkit that are used to derive releases to water from sectors responsible for emissions to air. Some newly evaluated releases from other sectors not covered by the Toolkit and air emission sources covered in Chapter 2, but recognised as relevant with respect to

releases to water, are also addressed, using independent methods and assumptions to derive the estimates.

To the extent possible, our estimates are compared with available national and other estimates/inventories of releases to water. For some of the release sectors covered in the 2015 inventory - to evaluate if obtained results are realistic - alternative release estimates were made using independent assumptions and information. Information regarding global releases of Hg to aquatic systems is still incomplete, and therefore a substantial part of this chapter is devoted to discussion on data sources and their availability, data gaps and associated uncertainties, as well as different methods for estimating the releases (see Annex X for details).

The focus of this chapter is on Hg released from current primary anthropogenic sources to adjacent freshwater systems. If should be pointed out that this inventory does not represent the total global load of Hg to aquatic systems. Namely, in addition to primary anthropogenic sources for which lack of information prevented reliable quantification, releases associated with leaching and runoff of legacy Hg accumulated in terrestrial environments over time can also be important contributors. Moreover, significant quantities of Hg that is currently being released to land and waste pathways from primary sources have a potential to eventually end in the nearby aquatic systems. While magnitude and relative importance of primary Hg releases to land is discussed for some selected sources for which information exists, associated potential secondary aquatic releases are not quantified. In this chapter, relative contribution and significance of sources quantified is assessed by comparing inventory results with magnitudes of sources and pathways of other components of the global Hg cycle as established before (section 5.3.5).

In contrast to air emission estimates (Chapter 2), the numbers presented here do not necessarily correspond to the year 2015. For example, the underlying assumptions for estimating Hg releases with industrial wastewaters are based on information corresponding to latest available information, while releases from point sources were derived from atmospheric inventory data for 2015 presented in Chapter 2.

Inventory results for individual release sectors are summarised and discussed according to sub-continental regions. The purpose of this regionalisation is comparability with air emissions inventory.

It should be noted that the fate of terrestrial Hg once entering aquatic systems will largely depend on site-specific environmental conditions that govern its transport and transformation processes within catchments, and have the control over its ultimate delivery to downstream marine environments. Moreover, it is known that global climate change can alter processes controlling mobility of terrestrial Hg and can facilitate its delivery to aquatic systems. This is especially critical in sensitive ecosystems like the Arctic (AMAP, 2016). However, these aspects are not addressed in the inventory as the focus of this chapter is on quantification of releases only.

5.2 Estimating global anthropogenic mercury releases for 2010-2015: Methodology

A key component of this work to update the 2010 Global Atmospheric Mercury Assessment: Sources, Emissions and Transport report (AMAP/UNEP, 20013) is the production of a new global inventory of primary anthropogenic Hg releases to aquatic systems. This new inventory has the target year of 2015 – however recognising that information required to produce such inventories may not yet be available for all countries and release categories the basis for most of this new inventory is latest available data which mostly dates in the 2000–2015 period.

5.2.1 Methods for estimating releases

Various methods are employed to estimate releases of Hg at the plant/facility, national, regional and global level. The approaches used and underlying assumptions depend on the data availability. Assumptions have been validated to the extent possible permitting the availability of information For reasons of transparency, details on the approaches and assumptions made in the GMAAR to derive the estimates are given in Annex X., with a summary given in the following sections. In general, they fall under one of the three main groups schematically shown in Figure 1. In order to avoid confusion with the atmospheric and other independent inventories, we named our inventory of global primary anthropogenic aquatic Hg releases *Global Mercury Assessment Aquatic Release* (GMAAR) inventory.

Group 1: This group comprise sectors covered by the UNEP Toolkit (chlor-alkali industry, oil refining, large scale Au and non-ferrous metal production) and for which the Toolkit (UNEP, 2017) provides 'distribution factors' that proportionally 'distribute' total Hg releases between emissions to air and releases to water and land. We use these factors together with the most recent Global Mercury

Assessment (GMA) atmospheric Hg emission inventory (Chapter 2) to calculate the corresponding magnitudes of releases to water. Sectors included in this first group are those included also in 2010 inventory. However, in contrast to 2010 inventory where DF were directly adopted from the Toolkit, in 2015 inventory country/group-specific abatement profiles used to derive atmospheric emissions were taken into account and DFs adjusted accordingly (see Appendix X.1 for details).

Group 2: This group is comprised of sectors for which estimates were derived based on measured Hg concentrations reported in the literature for selected case studies and associated volumes of wastewater released and other relevant activity data, respectively. Following the approach recently used by Liu et al. (2016) to develop aquatic Hg release inventory for China, sectors considered important in terms of their relative contribution and included in this inventory, in addition to those from the first group, are: Hg releases associated with produced municipal wastewater, wastewater from coal-fired power plants and coal washing. All sectors from the second group are new addition to the global inventory and have not been addressed in the 2010 inventory.

Group 3: This group covers Hg releases from wastes associated with the use of Hg-added products: batteries, measuring devices, lamps, electrical and electronic devices, and other uses. Releases are produced using approach comparable to that applied to calculate emission to air (See section 2.2.2. of Chapter 2 and Annex 3 for details), adjusted to aquatic Hg fate. The model used considers regional patterns of consumption of Hg and Hg-containing products and initially distributes Hg in products to different pathways using distribution factors. Releases to water are then assumed for breakage during use, waste recycling and from waste landfills, using fate-specific release factor (see Annex X.5 for details). This is a new methodological approach, as releases from the use of Hg-added products in 2010 inventory were derived using the UNEP Toolkit distribution factors approach.

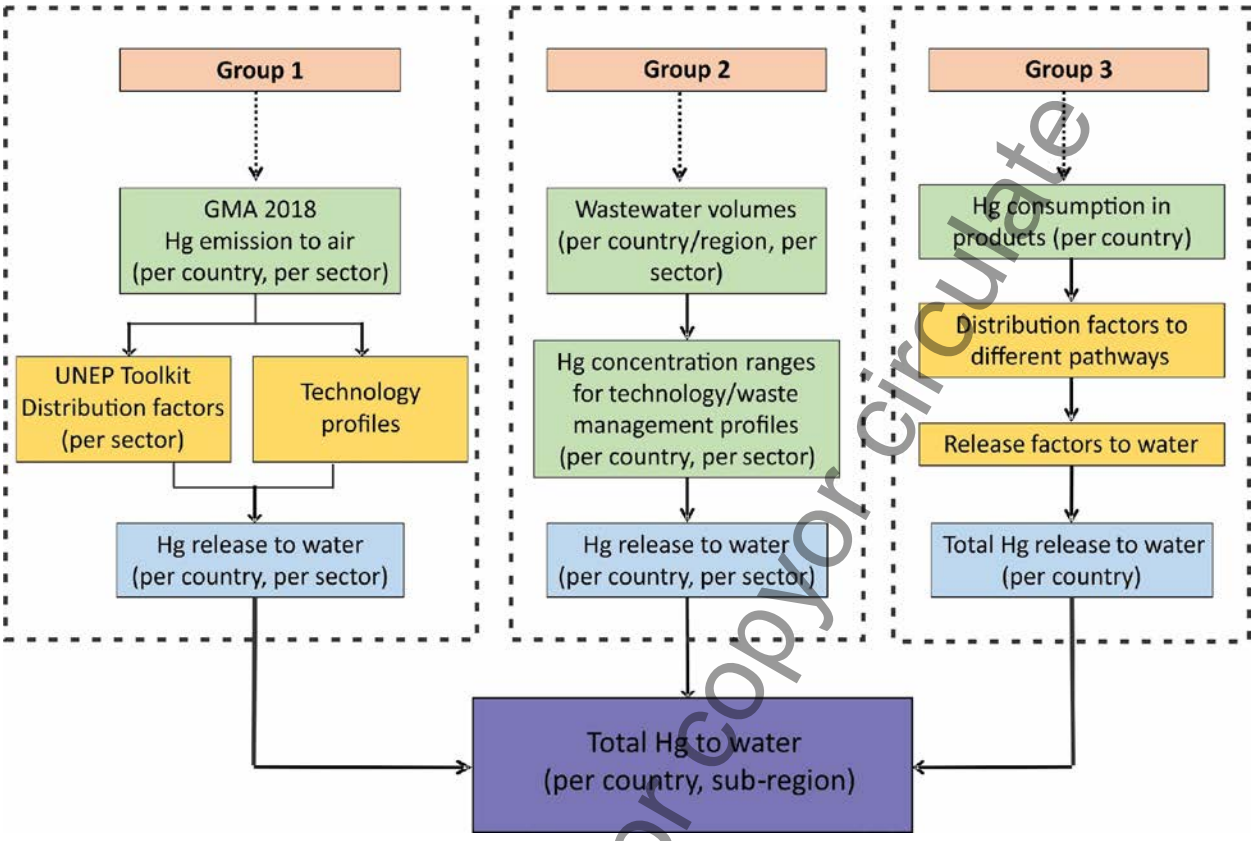

Figure 1. Methods for estimating releases

Initially, estimates of Hg releases for all sectors were made on the country level, as majority of input data used are country specific. Technology and waste-management profiles of individual country (cross ref.) were used for selection of Hg concentration ranges and other related activity data. Based on the country-level information, Hg release estimates were then summarised according to sub-continental regions, using the same regionalisation as that used for the air emission inventory.

5.2.2 Sectors and activities

5.2.2.1 Sectors and activities quantified in the inventory

Selection of the sectors and activities for the aquatic inventory is driven by previously established knowledge and assumptions about their relative importance, while their categorisation depends mainly on the data and type of information available for individual sector/activity. To the extent possible, categorisation was kept comparable with that used for the air emission sectors. The release estimates in the new 2015 GMAAR inventory comprise the following ten key release sectors:

1. Production of non-ferrous metals (primary production of aluminium, copper, lead and zinc) (O1)
2. Production of mercury metal (O2)
3. Production of gold from large-scale mining (O3)
4. Mercury releases from oil refining (E1)
5. Production of gold from artisanal and small-scale gold mining (O4)
6. Mercury releases from chlor-alkali industry (Hg cell technology) (W1)
7. Mercury releases from Hg-added products (batteries, measuring devices, lamps, electrical and electronic devices and other uses) use and waste disposal (W2)
8. Mercury releases with municipal waste-water (W3)
9. Mercury releases from coal-fired power plants (E2)
10. Mercury releases from coal washing (E3)

In broader terms these sectors can be divided into three general categories: ore mining and processing sector (O), energy sector (E) and waste treatment and disposal (W). The first seven items on the list are those included previously in the 2010 inventory. Among these the first four sectors are associated with by-product or unintentional Hg releases and latter three with intentional uses of Hg. The last three items from the list are new addition to the 2015 inventory and comprise categories for which relative contribution of Hg releases to aquatic systems is considered to be significant, following mostly the example of Liu et al. (2016) and their release estimates for China.

5.2.2.2 Sectors and activities not quantified in the inventory

We recognise that there are additional sectors and anthropogenic activities not taken into account in this inventory, but might be responsible for the delivery of additional Hg to local aquatic systems. For example, in the Hg release inventory from anthropogenic sources in China, releases from iron and steel industry, fabrication of textiles and apparel and printing industry were also considered, however estimated at less than 5% of total releases (Liu et al., 2016). Similar, according to recent global estimate of Streets et al. (2017), cumulative releases of Hg to land and water for sectors like iron and steel manufacturing, as well as dental industry, represent a relatively low share of total releases. Considering relative low importance of these sectors, especially in the light of the fact that there is no data available that would allow any reasonable global quantitative estimate, these sectors were not included in the 2015 inventory. Some other possible sources of Hg for aquatic systems also not assessed here include VCM production, aluminium fluoride production, cellulose-production and titanium dioxide production.

On the other hand, it should be pointed out that there are processes associated with some of the sectors covered in the inventory that might result in additional quantities of Hg released, however not accounted for in the current inventory due to lack of sufficient information to develop a global inventory. One such example are releases that might occur during the production stage of Hg-added products (e.g. thermometers, lamps and batteries), as only releases associated with the use, disposal and recycling of these products are considered in this inventory. Similar, in the case of Hg releases from coal industry, large quantities of water used during coal mining and transport, apart from those associated with coal washing, might release significant amounts of Hg.

5.2.2.3 Primary releases to land and waste

In addition to direct releases to air and water, releases of Hg from anthropogenic sources can follow other pathways, such as releases to various terrestrial systems and waste disposal sites that can in the long term act as secondary sources of Hg releases and final receiving media can be also nearby aquatic systems. While detailed quantification of these potential secondary sources was out of the scope of this work, the magnitude and relative importance of primary Hg releases to land and waste is discussed for selected sectors. In this section an overview of information sources and sectors for which such information is available is given, followed by discussion in Section 5.3.3.

For the Group 1 sectors for which water release estimates are based on distribution factors provided by the UNEP Toolkit, primary releases to land and waste are also derived using the same approach (see Annex X.1 for details). In addition to the three environmental media that receive Hg directly (air, water and land/soil), the Toolkit considers also three intermediate output pathways "products", "general waste" and "sectors specific waste treatment". By definition, “products” as output pathway are mercury containing by-products sent back into the market and cannot directly be allocated to environmental releases, “general waste” pathway considers bulk of general waste that undergoes a general treatment (e.g. incineration or deposition) under controlled circumstances, while “sector specific waste treatment” pathway covers waste from industry and consumers that is collected and treated in separate systems, and in some cases recycled (UNEP, 2017).

Some of the information on Hg releases to terrestrial ecosystems is available as part of independent both global as well as country-level estimates. These estimates use different approaches and assumptions to follow various environmental pathways of Hg, and are broken down to diverse

combination of sectors where mercury is/was intentionally or unintentionally used and/or present in products and processes, which makes the comparisons difficult. For example, Streets et al. (2017) estimated combined releases to water and land as part of the estimated all-time total Hg released to the environment by human activities globally up to 2010. For the commercially used Hg, Horowitz et al. (2014) quantified global time-dependent historical releases to different environmental reservoirs including air, water, soil and landfills. Similar method using a mass-balance material flow-model of Hg with air, water, soil, landfill and Hg reclaimed by recycling as final environmental fates was used by Lin et al. (2016) for intentional use of Hg in China. Recently, in addition to quantification of releases of Hg from municipal sewage to aquatic environments in China, Liu et al. (2018) evaluated associated Hg releases into other sinks including landfills, croplands, urban areas, natural land and the atmosphere.5.2.3 Sources of data and information used in the inventory

Primary sources of data and information used in the production of the release inventory are described in Table 1. The following section briefly summarises data and information used to produce the estimates.

Table 1. Primary sources of activity and other related data used do derive release estimates

Release category	**Activity data[a]**	**Distribution/release factors[b]**	**Hg content[c]**	**Other**
Non-ferrous metal (Cu, Pb, Zn, Al, Hg, large-scale Au) production	GMA 2015 air emissions	UNEP, 2017a,b	-	
Chlor-alkali industry	GMA 2015 air emissions	UNEP, 2017a,b	-	
Oil refining	GMA 2015 air emissions	UNEP, 2017a,b	-	
Artisanal and small-scale gold mining	Artisanal Gold Council	Artisanal Gold Council/ UNEP Partnership on Reducing Mercury in ASGM	Artisanal Gold Council/ UNEP Partnership on Reducing Mercury in ASGM	Annex 2
Municipal sewage	AQUASTAT, 2017	-		Malik et al., 2015; Sato et al., 2013 UNEP, 2017
Coal-fired power plants	Liu et al. (2016); GCPT, 2017;	-	Liu et al., 2016	Biesheuvel et al., 2016
Coal washing	Enerdata, 2016	UNEP, 2017b; Liu et al, 2016; ENM, 2016	Annex 6 and Hg in coal reported therein	Carbon Locker, 2017
Hg-added products use and waste disposal	UN Environment, 2017P	UNEP, 2017b; Lin et al., 2016	-	

Group 1 sources: For release categories using UNEP Toolkit distribution factors (chlor-alkali industry, oil refining, large scale Au and non-ferrous metal production), respective air emissions developed in

Chapter 2 of this report were used as input data to calculate corresponding releases to water. For the ASGM category, releases are discussed based on the amounts of Hg used in these activities and practices employed in individual country, as discussed in detail in Annex 2 of this report.

Group 2 sources*:* For estimation of Hg releases associated with municipal sewage, information on amounts of municipal wastewater generated and its treatment practices in individual countries were used. Amounts of municipal wastewater were obtained mostly from AQUASTAT, the FAO's global water information system, while national waste-water treatment practices were obtained from Malik et al. (2015) and, Sato et al. (2013). For countries with no data general regional averages were adopted based on data from Malik et al. (2015) and recent UNEP report (UNEP, 2017). Ranges of Hg concentrations for untreated wastewater and water treated in treatment plants were selected based on ranges usually reported in literature, taking the waste management profile of individual country into account (see Annex X.1 for details).

Releases associated with wastewater from coal-fired power plants were estimated based on amounts of waste-water generated per MWh of energy produced, as estimated from data presented by Liu et al. (2016). Hg concentration ranges applied were taken from the same source. Realized total energy output from CFPPs in individual country which was calculated from electricity generation capacities obtained from the Global Coal Plant Tracker database (GCPT, 2017) using country-specific capacity factors adopted from Biesheuvel et al. (2016).

Global releases due to coal washing are estimated using information on production rates, Hg coal content, the Hg removal efficiency of coal washing and the coal washing rates. Activity levels of raw coal production for individual country were obtained from the global energy statistical yearbook (Enerdata, 2016), information on type of coal produced from international energy statistics (EIA, 2017), Hg content of various coal types was selected based on ranges reported in scientific literature (see Annex 6), coal washing rates in major producing countries adopted from Energy News Monitor (ENM, 2016) and Hg removal efficiency from UNEP (2017) and Liu et al. (2016).

Group 3 sources: For estimation of Hg releases associated with the use and disposal of Hg added products information consist of estimated Hg consumption in one year covering the product groups: batteries, measuring devices, lamps, electrical and electronic devices, dental applications, and other

uses (UN Environment, 2017). The same distribution factors as in the case of air emissions were used to follow the fate of mercury through major pathways (see Annex 3 for details). Water specific release factors were selected and adjusted according to waste management profile of individual country based on factors from the Toolkit (UNEP, 2017) and Lin et al. (2016).

5.2.5 Uncertainties and limitations

It should be pointed out that, given the global scope of this assessment, there are several limitations of this work and the estimates presented here are just that – the estimates. Numbers discussed in the following sections are derived using a number of different approaches and various assumptions, and the use of alternative approaches and assumptions might result in significantly different values. It was out of the scope of this work, however, to address these aspects into detail.

In order to provide some quantification of the uncertainties associated with the 2015 inventory, upper and lower range releases were produced for all sectors. For the sectors using the Toolkit approach, upper and lower range release estimates were calculated using the methodology used for emission inventory and described in Chapter 2 of this report. For the Group 2 and Group 3 sectors, upper and lower range releases were produced using the respective upper and lower ranges of Hg levels and associated activity data, respectively. Uncertainties related to the input data selected are further discussed for selected sectors in Section 5.3.2.

In addition to the above mentioned uncertainties, an additional limitation of this work is the possible double counting on one hand and the potential for underestimation of releases on the other. All sectors included in the inventory have a distinctive Hg sources and their pathways are clearly identified. The exception are releases associated with municipal waste-water which might contain a fraction of releases accounted for in the Hg-added products sector, releases resulting from breakage during use pathway to be specific. This latter pathway is however a minor share representing only 5% of releases from Hg-added products sector. As to the possible underestimation, a number of sectors and activities are identified in Section 5.2.2.2 that are not included in the current inventory, but might be important contributors to Hg releases on global scales. For example, sectors like iron and steel industry and others considered relatively less important in China (Liu et al., 2016) might be more important elsewhere. The current inventory of global anthropogenic Hg releases to aquatic systems is a work in progress, and an

important step towards filling a major gap in inventories of anthropogenic Hg releases to the environment.

5.3 Estimating global anthropogenic mercury releases: Results

Given the specific nature of releases associated with artisanal and small scale gold mining (see section 5.3.2.6 for details), results for ASGM and non-ASGM sectors are discussed separately. In section 5.3.1 overall results are discussed considering releases summarised based on three general source categories (ore mining and processing, energy sector and waste treatment) and sub-regions, while details for selected sectors are given in section 5.3.2, including discussions on trends where possible and the associated uncertainties.

Using the methods described above, the total estimated inventory of anthropogenic Hg releases from sources for which there was enough information to provide quantitative estimates, is 593 (x-y) t/y (ASGM not included).

5.3.1 Inventory results by region and sectors

Table 2 summarises the distribution of the estimates of global anthropogenic Hg releases to aquatic systems according to sub-continental regions. Table 3 presents the results per region on a per capita basis, for ASGM and other sectors.

Table 2. Global anthropogenic mercury releases to aquatic systems from different regions

Sub-continent	Releases[a] (range), t	%
Australia, New Zealand & Oceania	7.22 (x – y)	1.2
Central America and the Caribbean	22.4 (x – y)	3.8
CIS & other European countries	49.5 (x – y)	8.4
East and Southeast Asia	272 (x – y)	46
European Union	34.1 (x – y)	5.7
Middle Eastern States	16.8 (x – y)	2.8
North Africa	10.6 (x – y)	1.8
North America	32.4 (x – y)	5.5
South America	43.6 (x – y)	7.2
South Asia	57.5 (x – y)	9.7
Sub-Saharan Africa	48.6 (x – y)	8.0
Total	593(x – y)	100

[a]Values rounded to three significant figures, ASGM not included

Table 3. Per capita anthropogenic mercury releases to aquatic systems in different regions

Sub-continent	Per capita releases from non-ASGM sectors, g	Per capita releases from ASGM [a], g	Per $INT of GDP at PPP
Australia, New Zealand & Oceania	-	-	-
Central America and the Caribbean	-	-	-
CIS & other European countries	-	-	-
East and Southeast Asia	-	-	-
European Union	-	-	-
Middle Eastern States	-	-	-
North Africa	-	-	-
North America	-	-	-
South America	-	-	-
South Asia	-	-	-
Sub-Saharan Africa	-	-	-
Global	-	-	-

[a]To both land and water

Figure 2 and Table 4 summarise the distribution of the estimates of global anthropogenic Hg releases to aquatic systems according to sector. Apart from combined releases to water and land resulting from ASGM activities, the majority of the global anthropogenic releases of Hg to aquatic systems are associated with the waste treatment sectors (43%), followed by ore mining and processing group of sectors (41%) and energy sectors (17%). Overall, the new inventory is dominated by releases from non-ferrous metal production (Cu, Pb, Zn, Al) and both waste-treatment related sectors, namely releases resulting from the use and disposal of Hg added products, and those associated with municipal wastewater. These three sectors alone contribute more than 70%) of the total releases from all the sectors included. Other major release sectors include waste-water from coal fired power plants (9%), coal washing (7%) and production of gold from large-scale mining (10%).

In addition to methodological changes introduced to derive the estimates on releases associated with the Group 1 sectors (see Annex X.1 for details), the three newly added sectors (municipal wastewater, CFPPs and coal washing) are driving the relatively large difference between the 2010 and 2015 anthropogenic Hg release inventory (185 t/y in 2010 compared to 600 t/y in 2015). Here it should be noted that compilation of the global aquatic Hg inventory including identification of new sources is an ongoing activity, and as recognised in the 2010 inventory already, global releases are assumed to be underestimated due to the lack of information for some sources. In any case, both inventories cannot be directly compared. Moreover, it must be pointed out that the three newly added sectors have the

largest associated uncertainty among all included sectors. Methodological changes and uncertainties are further discussed in Section 5.3.2.

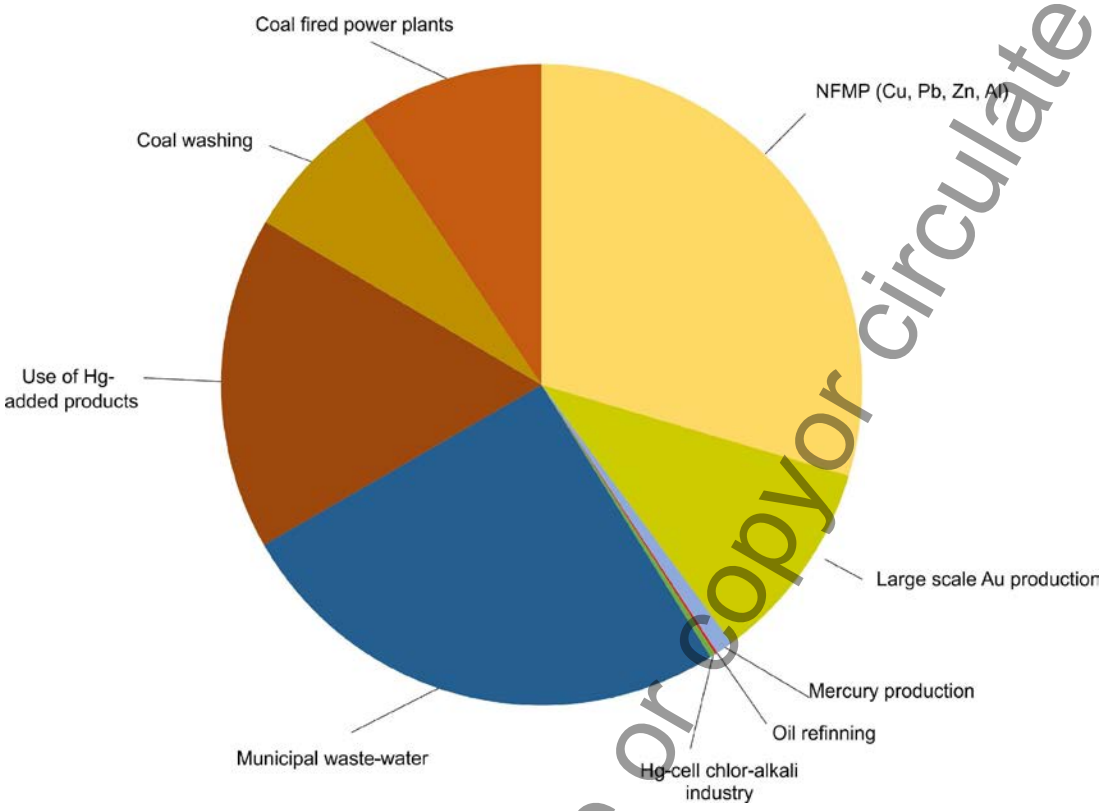

Figure 2. Proportions of global anthropogenic mercury releases to water in 2015 inventory from different sectors

Table 4. Global anthropogenic mercury releases to aquatic systems from different sectors

Sector	Releases (range), t[a]	%[b]
Production of non-ferrous metals (primary production of copper, lead, zinc and aluminium)	175 (x - y)	30
Production of mercury metal	5.18 (x - y)	0.9
Production of gold from large-scale mining	61.2 (x - y)	10
Mercury releases from oil refining	0.56 (x - y)	0.1
Mercury releases from chlor-alkali industry (Hg cell technology)	1.74 (x - y)	0.4
Mercury releases with municipal sewage	150 (50 - 250)	25
Mercury releases from coal-fired power plants	55.6 (12.3 - 123)	9.4
Mercury releases from coal washing	42 (23 - 65)	7.1
Mercury releases from Hg-added products use and waste disposal	99.4 (66.5 - 133)	17
Total [b]	600 (x – y)	
Production of gold from artisanal and small-scale gold mining[c]	1221 (585-1858)	-

[a]Values rounded to three significant figures; [b]ASGM not included; [c]Releases to both land and water

Figure 3 presents the 2015 inventory graphically by region and sector. It can be clearly seen from the illustration that relative contribution to the total global anthropogenic Hg releases to water is by far the greatest in East and Southeast Asia. This is driven by large population and associated large industrial and other activities. As this region is a dominant source of Hg releases from most sectors, distribution of releases between sectors reflects the global one.

On the other hand, relative contributions of individual sectors are distributed unevenly between the regions. In case of ore mining and ore processing sectors, majority of associated releases occur in East and Southeast Asia (59%), followed by EU-28 region (9%), South America (7%) and CIS and other European countries (7%). Similar, contribution from energy sectors is by far the largest in East and Southeast Asia (59%), then followed by North America (12%) and South Asia (10%). In contrast to these two general group of sectors, contribution of releases from waste treatment sectors is more equally distributed with East and South Asia contributing 25%, followed by South Asia (17%), Sub-Saharan Africa (12%), CIS and other European countries (11%) and South America (10%).

Consequently, relative contribution to total releases from various sectors within individual region varies a lot, clearly reflecting differences in types of industrial activities, and technological and socio-economic status of the region. For example, non-ferrous metal processing dominates releases in East and Southeast Asia, EU-28 countries and to a lesser degree in Australia, New Zealand and Oceania. In many regions, releases associated with waste streams, both form the municipal waste-water and that from the use and disposal of Hg-added products dominate, such as in North Africa, Central America and Caribbean, Middle Eastern States, South Asia and Sub-Saharan Africa. Large-scale Au production is important contributor to releases in Australia, New Zealand and Oceania, Central America and Caribbean, North America, South America and Sub-Saharan Africa. In North America and Australia, New Zealand and Oceania releases associated with coal washing and from coal-fired power plants, respectively, are also important contributor.

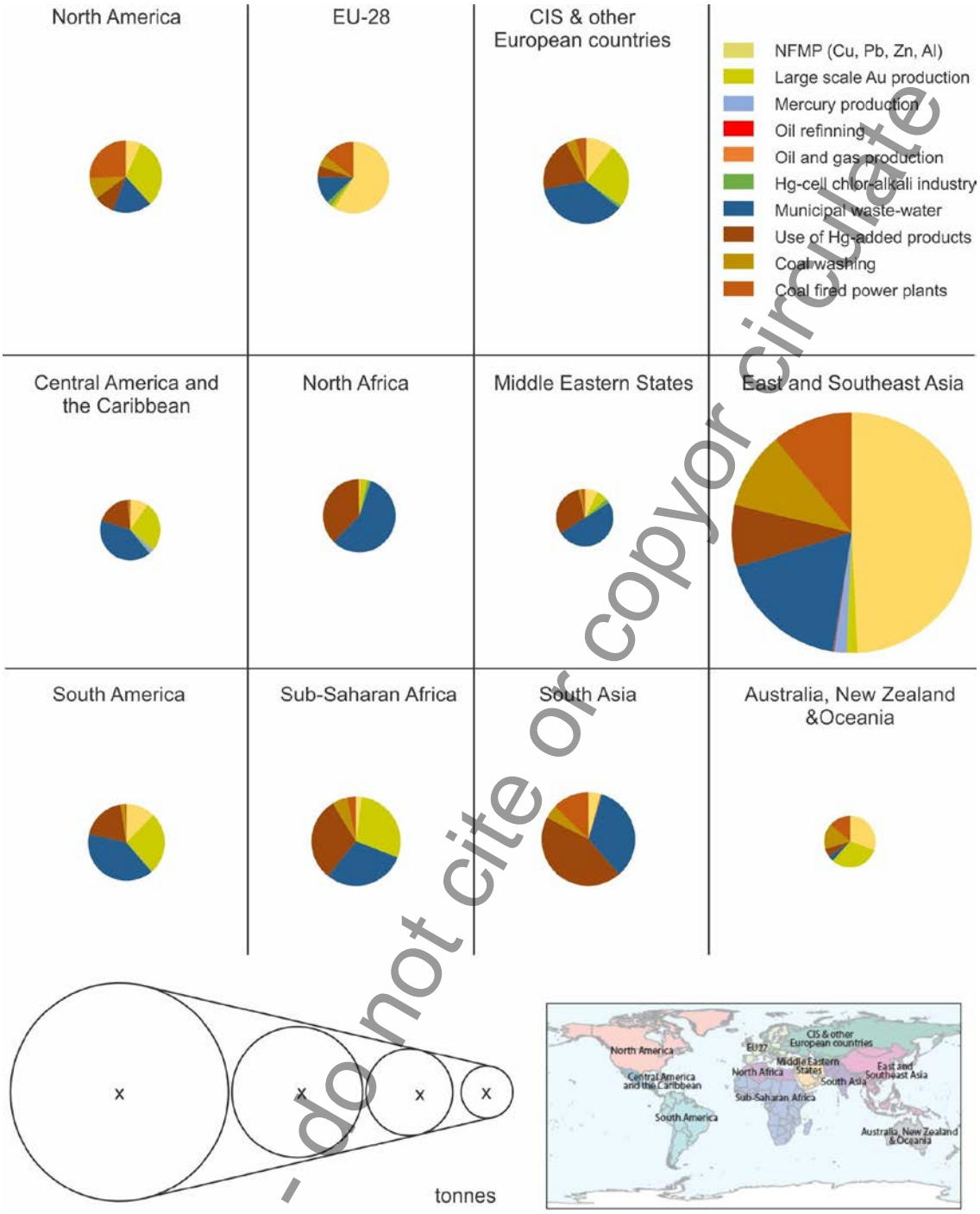

Figure3. Regional pattern of global anthropogenic mercury releases to water in 2015 inventory from different sectors (circle sizes provisional only)

5.3.2 Discussion of results for selected sectors

The following sections discuss details on Hg releases associated with major release sectors. For the sectors included in both 2010 and 2015 inventory, differences in release estimates are also addressed, as well as differences in methods used to derive the estimates.

5.3.2.1 NFMP including Cu, Pb, Zn, Al, Hg and large scale Au production

The estimates included in the current inventory for releases from copper (Cu), lead (Pb), zinc (Zn), aluminium (Al), mercury (Hg) and large scale gold (Au) production were all included previously in the 2010 inventory. Compared to 2010, sum of releases from these sectors for 2015 is almost three times higher (242 vs. 88.5 t/y). There are some differences in the input data between the two inventories, as discussed in Chapter 2, however this large difference is mostly a result of methodological changes incorporated in the 2015 inventory. Namely, in the new inventory country/group-specific abatement technologies are considered as part of the approach used to derive the release estimates, resulting in more releases to water in case when wet gas cleaning technologies dominate technology profiles (see Annex X.1 for details). Using the new approach, among the NFMP sectors, a vast majority of releases (58%) is associated with production of zinc mostly taken place in East and Southeast Asia, followed by large scale Au production (25%), Cu (8%) and Al (5%) production. It should be noted that some of the NFMP installations considered here might use water pollution abatement technologies which would decrease the actual Hg releases. This is not considered here and therefore some of the numbers discussed here might be overestimated. On the other hand, NFMP sectors have a large potential for secondary Hg releases to water to occur, as large quantities of Hg from these sector are distributed to land and waste, respectively. (see Section 5.3.3 for details).

5.3.2.2 Municipal sewage

Releases from municipal sewage have not been addressed in the 2010 inventory. Estimates suggest that this sector is an important sector contributing significant amounts (25%) to the total global inventory. Given the input data and approach used for estimating Hg releases (details in Annex X.2), Hg releases from this sector are linked closely to water-use patterns and wastewater treatment practices in individual countries. Substantial part of municipal waste-water results from domestic water uses, but also from commercial and industrial effluents and storm water. While developed nations have very large per-capita water use and efficient wastewater treatment, people in developing countries use much less

water, however with poorly developed wastewater collection and treatment systems (Sato et al., 2013). It is expected that with increases in population of developing nation's water demand and associated Hg releases will increase in these regions. On the other hand, it should be noted that global distribution and consumption of Hg containing products as one of the most important sources of Hg for this sector, is not uniform, and will largely depend on individual country's economy, with more products being consumed in developed parts of the world. Phase out of many products that contain Hg under the Minamata Convention is expected to result in decreases of Hg releases with municipal sewage, and so is the anticipated increased treatment of wastewater.

While Hg concentrations in both treated and untreated municipal waste-water are relatively well documented in the literature, Hg release estimates for this sector depend largely on data on global water use patterns, information that is considered as the least reliable and most inconsistent of all water resources information (Gleick et al., 2014). The major limitations are lack of reporting standards, differences in approaches used to derive the information on water usages, and large inconsistencies in reporting years (Gleick et al., 2014). Another source of uncertainties lies in the fact that country-scale wastewater treatment levels (i.e. primary, secondary, and tertiary), practices that have significantly influence on effluent Hg concentrations, are mostly unknown. In our estimates, different Hg removal efficiencies for treated water were assigned to individual countries based on their waste management profile.

5.3.2.3 Coal industry

Releases from coal industry have not been addressed in previous global inventories. In the 2015 inventory we consider two types of releases resulting from associated water use: Hg releases with wastewater from coal-fired power plants and those resulting from coal washing. Together both releases are estimated to contribute 16% to the global inventory. Both types of release estimates are considered preliminary and have large associated uncertainties. In the case of coal-fired power plants, this reflects the fact that information on actual profiles of installations - water use practices, treatment and wastewater generation - is missing for most of the world's CFPPs and so is information on Hg concentrations in respective effluents. In case of coal washing the major uncertainties are the result of assumptions that had to be made regarding coal washing rates, removal efficiencies and especially

selected share of Hg reaching aquatic systems in individual countries. Estimates are therefore made based on gross generic assumptions as described in Annexes X.3 and X.4.

Coal-fired power plants. CFPPs are recognised as one of the major anthropogenic Hg emission sources. However, due to the lack of quantitative information, Hg releases to water from this sector were neglected in previous inventories. Large releases are the result of the fact that coal industry is by far the greatest water demanding anthropogenic activity in the world, and it was estimated that in 2013 CFPPs alone consumed 19 billion m^3 of freshwater globally (Cheng and Lammi, 2016). While the vast majority of this water is used for cooling, and is usually not contaminated with Hg, additional water uses such as pollution control can also generate large amounts of Hg contaminated wastewater. Here, an attempt was made to quantify Hg releases with this latter non-cooling water-use types.

Despite many uncertainties, there is now much more evidence based on both measured and estimated data about the significance of aquatic Hg releases from CFPPs. It is known that plants using wet scrubbers can discharge up to tens of kg of Hg to local surface waters per year (EIP, 2016, E-PRTR, 2014). In addition to discharges to surface water, even larger amounts of Hg (up to hundreds kg per year) are dumped into ash ponds which are prone to leaks (EIP, 2016). In a recent aquatic release inventory for China, wastewater discharged from CFPPs, although in gradual decline in the last decade, is recognised as one of the most important anthropogenic sources of Hg (Liu et al., 2016). Similar, according to European Pollutant Release and Transfer Register (E-PRTR, 2017), Hg releases from thermal power stations and other combustion installations are the second largest source – second only to urban waste-water treatment plants. Global Hg releases from this sector using assumptions described in Annex X.3 are based on information available for China (Liu et al., 2016) and are estimated in the 12-123 t/y range. Alternative to this approach would be an estimate made based on simple global upscaling of ratio of anthropogenic Hg released to water and air for China for this sector which is approximately 1:4. This would result in a global release of 50-110 t/y, which is a range comparable to the first approach.

Coal washing. In addition to water used in CFPPs, large amounts of water are used during coal mining and washing. The latter is used to remove impurities and ash from the coal and results in the generation of a slurry of toxic material (Cheng and Lammi, 2016). Here, in the absence of detailed information, we use the approach similar to that of Liu et al. (2016) and make a preliminary estimate of likely magnitude of global Hg releases due to coal washing based on global coal production, coal Hg content, assumed Hg

removal efficiencies, washing rates and environmental fate in individual countries (see Appendix X.4 for details). Given the fact that coal washing results in higher caloric value of coal and consequently a higher economic value, coal beneficiation is increasing throughout the world. Available information suggests that a higher share of the coal produced is treated in more developed countries but is also in increase in developing economies (Budge et al., 2000). Estimates available for China, the major coal producer in the world, indicate rapid increase of Hg releases from coal mining and washing with an annual average growth rate of 25% in the 2001-2012 period, making this sector the second largest anthropogenic source of aquatic Hg in China (Liu et al., 2016). Overall releases from this sector are largely dominated by releases from China (>60%), followed by other important coal producing countries such as United States, India, Australia and Indonesia. In addition to high uncertainty of the approach and sensitivity of all input information used to derive these estimates, it should be pointed out that these numbers are obtained based on very gross assumptions regarding environmental fate of Hg once washed from coal. It should be pointed out that releases associated with this sector can occur as part of mining operations or later on before the actual use of coal, e.g. at sites where coal-fired power plants are located. Nevertheless, even larger quantities of Hg in the magnitude of tens of tonnes per year are assumed to accumulate in the slurry ponds at coal washing sites globally, representing a great environmental hazard for local aquatic systems, as these ponds are often very prone to brakeage and leaking (Cheng and Lammi, 2016). Moreover, coal-washing practices result in millions of tonnes of coal-washing products, and in China for example, a significant share of these by-products is being reported to be re-used for various industrial and domestic purposes, and from which secondary emissions and releases can occur (Zhao et al., 2017).

5.3.2.4 Oil industry

Hg releases from oil refining were included previously in the 2010 inventory. Given the fact that in 2015 oil refineries processed similar amounts of crude as in 2010, and that the same method was used to estimate releases, differences between the two inventories are negligible. In addition to oil refining, there are releases from this industrial activities associated with discharge of produced water during crude oil and gas extraction, as well as transportation of oil and gas. According to a preliminary assessment made by IPIECA, Hg releases with produced water during oil production are 13.5 t/y globally, with a vast majority (~90%) of releases occurring off-shore. It should be noted however, that this estimate is based on a very gross generic assumptions and additional work is needed to better quantify these releases.

5.3.2.5 Hg-added products – use and waste disposal

Hg-added products sector comprise of releases from the following product groups: batteries, measuring devices, lamps, electrical and electronic devices, , and other uses (see Annex 3 for details). In the 2010 inventory, releases for this sector were estimated based on Hg emission inventory by using the distribution factors from the UNEP Toolkit to calculate the corresponding magnitudes of releases to water. The 2015 inventory adopts the model used to estimate mercury emission from waste streams associated with intentional use sectors and considers releases for three main pathways of Hg-added products: breakage during use, waste recycling and waste landfilling (see details in Annex X.6). In addition to the new method used to derive the estimates, there is a change in the models input data. In the 2010 inventory part of the mercury from Hg-added products (approx. 30%) was considered as "retained in use" and is now included in the waste streams and consequently in emission and release pathways, respectively.

Our estimates suggest significant Hg releases due to usage and disposal of Hg added products (66-133 t/y), a vast majority (91%) being associated with uncontrolled landfilling of waste which is primarily occurring in developing countries, followed by releases during breakage (5%) and recycling (4%). Due to environmental regulations and new technologies available, the use of Hg in products is in decline and so are environmental releases of Hg, especially in developed countries. Substitution of Hg-added products with non-Hg containing alternatives, however, is also becoming evident in developing countries. An exception are products without the adequate Hg-free alternatives such as lightning devices which are also excluded from the Minamata Convention.

It should be noted that these estimates depend largely on estimates of regional consumption of Hg-added products. While this information is available for developed countries, very little information is available on the real consumption patterns for Hg-added products in developing countries.

5.3.2.6 Artisanal and small-scale gold mining (ASGM)

Given the fact that there is still not enough information and knowledge to separate terrestrial releases between water and land, releases associated with artisanal and small-scale gold mining (ASGM) remain a "special" sector in the inventory. The detailed reasoning for this is given in 2010 inventory (AMAP/UNEP, 2013). In summary, Hg releases for this sector are based on amounts of Hg used in ASGM activities and the characteristics of the mining practices applied in individual countries. The

methodological approach used differentiates between emissions to air and releases to both land and water (details including example calculation is given in Annex 2). At this point, it is not possible to directly determine what the proportion is of Hg associated with this later pathway that will enter hydrosphere. In addition to the direct losses occurring during ore amalgamation, large quantities of Hg are accumulating in soils and sediments surrounding ASGM sites over the time. This accumulated Hg has potential to be remobilised and enter aquatic systems, however with a time-lag usually unknown, depending largely on site-specific environmental conditions. It is estimated that ASGM releases to water and land in 2015 are 1221 t/y (range, 585-1858 t/y). The vast majority of these releases are occurring in South America (55%) and East and Southeast Asia (30%), followed by Sub-Saharan Africa (7%) and Central America and the Caribbean (5%), while other regions where ASGM activities are carries out - CIS and other Europeans countries, South Asia and Middle East – contribute a minor share to the total.

5.3.3 Comparison of estimates with independent inventories and approaches

Compared to air emission inventories, there are fewer national inventories of mercury releases to water available for comparison with the GMA 2015 estimates. Furthermore, other available inventories are typically based on different input data using different assumptions and approaches, are broken down to diverse combination of sectors. Therefore, for the most part direct comparisons are not possible and comparisons are discussed in a qualitative sense only.

For several European countries, the European Pollutant Release and Transfer Register (E-PRTR) provides a publically available resource that includes nationally reported values for Hg emission to air and releases to water and soil, as well as off-site transfers of waste. It reports pollutant emissions and releases from over 30,000 industrial facilities in European Union Member States, as well as Iceland, Liechtenstein, Norway, Serbia and Switzerland (UNEP, 2016). It should be noted that the EPTR applies a relatively high mandatory reporting requirement for mercury of 1 kg Hg/yr (at a given facility). This threshold means that not all industrial facilities with mercury emissions and releases report to the EPTR although some facilities with emissions/releases below this threshold report on a voluntary basis. . For the EU-28 countries, total Hg releases to water reported in the E-PRTR for 2015 are an order of magnitude lower than those estimated in GMMAR (3.5 vs. 34 t/yr). However, relative contribution of

sectors is similar. With the exception of NFMP sector, municipal sewage and thermal power stations dominate the releases in both inventories.

Canada, Mexico and the United States report data on emissions and releases of various pollutants including Hg to the North American Pollutant Release and Transfer Register (NA-PRTR). Data from 2006 to 2013 are available for states, provinces and territories at different levels of detail (http://www.cec.org/). Similar to, and for the same reasons as with the E-PRTR including differences in sector breakdown, on-site surface water discharges for North America (USA and Canada) as reported in the NA-PRTR are substantially lower compared to estimates for the North America region in the GMMAR (0.7-1.6 vs. 32.4 t/yr). Dominant sectors in the NA-PRTR register vary from year to year, and include among others paper and food manufacturing sectors not included in the GMMAR, while mining and electric power generation are recognised as important contributors in both inventories.

In addition to nationally reported inventories, there are other independent global inventories where releases of Hg to water are considered to some extent. For example, present day releases from commercial Hg use to water globally, as estimated by Horowitz et al. (2014) are comparable in magnitude with releases in GMMAR from comparable sectors, despite differences in the methodology used to derive the estimates. Similarly, sectors included, and their relative importance as indicated in GMMAR are to a large extent comparable to those considered important globally today by Streets et al. (2017), although it should be noted that in their work combined releases to land and water are estimated (see section 5.3.4 for details).

More detailed country-level inventories, including estimates for relases to water are becoming available as countries prepare these data as part of their commitments under the Minamata Convention. At the time of preparing the GMA estimates, few Minamata Initial Assessments (MIAs) were finalised and therefore most were not available for comparison.

5.3.4 Potential secondary sources of aquatic Hg releases

In addition to direct emissions/releases to air and water, respectively, for some of the sectors discussed here pathways to other environmental media can be equality if not more important. In this work primary global releases of Hg to land, waste and sector specific storage/treatment are estimated for Group 1 sectors using the UNEP Toolkit distribution factors. Using this approach sectors contributing

directly to land/soil are large scale Au mining, primary Hg production and chlor-alkali industry with approximately 2700, 60 and 16 t of annual Hg releases globally. Compared to releases to water, releases to land/soil from these sectors are 45, 12 and 6 times higher, respectively, and all this mercury initially released to land/soil acts as a potential secondary source of aquatic as well as atmospheric Hg. Large amounts of Hg being released as a general waste are also associated with production of Al (~76 t/yr), while even larger quantities of Hg are subjected to sector-specific waste treatment, with a vast majority of Hg being associated with production of Zn (~4200 t/yr), followed by VCM production (873 t/yr), Cu production (~490 t/yr), chlor-alkali industry (~190 t/yr), Al production (~12 t/yr) and oil refining (~8 t/yr). The fate of Hg associated with this latter pathway remains largely unknown, as facility specific information is usually lacking and it is therefore not possible to estimate what is the share of Hg that is ultimately reaching various environmental compartments. In case of VCM industry for example, the largest user of Hg in China, Lin et al. (2016) estimated that approximately 75% of all Hg used will end up as sector-specific waste of which 80-90% will be recycled with the rest equally distributed between air, water and landfills.

Large amounts of Hg secondary releases are also expected from various wastes associated with the use of Hg-added products. For example, out of ~1200 t/yr of Hg consumed on average globally for batteries, measuring devices, lamps, electrical and electronic devices, and other uses, only ~260 t/yr are estimated to be emitted/released directly to atmosphere and water, respectively (see section 5.3.2.5 and Annex 3 for details). Thus ~940 tons of Hg per year subsequently ends up in the waste stream and can be subjected to later remobilization, as it is estimated that only 6% of this amount is collected for safe storage globally and for which no further emissions/releases are expected to occur.

In addition to the abovementioned sectors, there are other sectors that can contribute significant amounts of Hg to various terrestrial environments, however are currently not covered in global inventories as no distribution factors exist for these categories that would enable estimation of the releases. One such example are releases associated with municipal sludge where it was recently established by Liu et al. (2018) that in contrast to some other sectors terrestrial environments can be the major sink of Hg. According to their material flow analysis for 2015, around 120 tons or 77% of all Hg from municipal sewage in China was releases to land (Liu et al., 2018). Similar, as discussed above (Section 5.3.2.3), large primary releases of Hg to terrestrial systems can result from disposal of Hg-

containing waste in a form of ash and slurry ponds due to the coal burning and washing, respectively, and the ultimate environmental fate of which is still very much unknown.

It should be noted however that in contrast to air emissions, it is extremely difficult in not impossible to fully separate the releases between land and water, either primary or secondary ones. This is, according to Streets et al. (2017), mostly because information on the way the waste is/was disposed is lacking for most of the installations. Therefore, Streets et al. (2017) reported cumulative releases to land and water as part of their all-time total historic releases and which are estimated to reach 7.000 −8.000 t/yr today. Due to differences in sectors covered and methodological approaches to derive the estimates, a direct comparisons of the results is not possible, however summing releases to water, land and waste for sectors discussed above results in a value comparable in magnitude to that of Streets et al. (2017). With the exception of Zn production which dominates the cumulative releases in the case of the Toolkit approach, also relative contribution of individual sectors is comparable with releases from large scale Au mining, ASGM, use and disposal of Hg containing products and NFMS prevailing.

5.3.5 Inventory in the context of global Hg cycle

Assessment of the contribution and significance of aquatic Hg releases quantified in this chapter in the global context is not straightforward for a number of reasons. In addition to all the uncertainties emphasised above, it should be noted that the inventory is still incomplete and it is not possible to assess the global relevance of the missing sources with any confidence. Moreover, for the largest global user of Hg nowadays – the ASGM sector – terrestrial releases cannot be distinguished between those to land and to water. Despite these limitations, it is apparent based on the magnitudes of aquatic Hg releases that these could be a substantial contributor to the terrestrial part of the global Hg budget.

When the sum of the non-ASGM water releases is compared with the magnitude of non-ASGM atmospheric emissions from Chapter 2, this results in a ratio between releases to water and air of approximately 1:2 (~ 600 vs. 1400 t/yr). This is comparable to the water/air ratio assessed for global releases in 2010 associated with intentional use of Hg in commercial products and processes (Horowitz et al., 2015), and so increases confidence in our estimates derived with a different methodology.

Primary anthropogenic sources quantified in this chapter may contribute Hg amounts to freshwaters that are similar to if not greater than that being delivered via atmospheric deposition. Only a small

fraction of the terrestrially-deposited Hg from air (globally estimated at 3,600 t/yr, see Chpt 2) will reach water bodies whereas the anthropogenic releases estimated in this chapter may directly enter freshwaters. Moreover, the evidence shows that primary releases to land and solid waste from anthropogenic sources can be very substantial compared to direct releases to water, and can, depending on the sector, contribute hundreds of tons of Hg per year to terrestrial ecosystems. These latter sources, following remobilisation and revolatilization, have a potential to act as secondary sources of Hg to both air and water (Amos et al., 2013).

Globally, releases of Hg to both freshwater and terrestrial systems are becoming more and more important, as the use of various emission abatement technologies caused a shifting trend from primary atmospheric emissions to revolatilization of legacy Hg from land and water over time (Streets et al., 2017). Nowadays, based on the recent work of Streets et al. (2017), cumulative global releases to land and water are estimated in the 7000 – 8000 t/yr range.

How much of the Hg released from individual anthropogenic sources directly reaches aquatic systems is usually unknown, as this depends on the waste disposal practices of individual facilities, information which is largely lacking. Similar, the time-lag between the releases to water/land and latter remobilisation within catchments, and the ultimate discharge to coastal waters, is mostly unknown. Regardless of these knowledge gaps, from a global perspective it is clear from the magnitude of the estimated inventory that primary anthropogenic Hg releases to waterways likely have a significant impact on Hg concentrations in many freshwater systems, upon which a large fraction of the world's population depends.

5.4 Conclusions

A new global inventory of aquatic Hg releases has been prepared as an extension of the global inventory of air emissions. This is the second time only global inventory of aquatic Hg releases is incorporated in the Global Mercury Assessment, and as such the current inventory is still a work in progress. New improved methodological approaches have been developed to fill some of the existing gaps in the inventories of anthropogenic Hg releases to the environment with the intention to better characterize differences between countries and sector-specifics in terms of technologies and practices applied. Moreover, the new inventory comprises some new source categories relevant for aquatic releases that

were not included in the 2010 inventory. This makes the 2015 inventory more complete. On the other hand, it is recognised that additional releases may arise from some sectors and activities not quantified in the current inventory, however lack of information is preventing any reliable global quantification of associated releases. While some of these non-included sectors identified are considered less important in terms of their relative global contribution to the aquatic systems (e.g. iron and steel manufacturing, dental industry), secondary releases resulting from remobilization of mercury initially released from industrial installations to terrestrial systems might be significant contributor. Magnitude and potential importance of such releases was evaluated for some selected sectors by quantifying primary releases to land and solid waste streams from relevant facilities using the distribution factors provided by the UNEP Toolkit.

Global releases of anthropogenic Hg to freshwater, excluding ASGM, based on revised estimates are XY t/y, compared to 180 t/yr in the 2010 estimate. The main sectors identified as sources of anthropogenic releases to water are non-ferrous metals production and releases associated with the use and disposal of Hg-added products, followed by the three newly added sectors: municipal sewage, coal washing and releases from coal-fired power plants. However, although not directly comparable - combined releases to land and water are estimated for this sector - ASGM is still considered as the major single current anthropogenic source of Hg for aquatic systems. In addition to direct releases to water, similar as in the case of ASGM activities, some industries release substantial amounts of Hg of the order of tens to hundreds of tonnes per year either directly to soil/land (e.g. large-scale and primary Hg mining) or to various waste streams (e.g. production of Zn, VCM production, Cu production and chlor-alkali industry).

Overall, there are a lot of knowledge gaps that were recognised when compiling the new inventory, and that should be filled in the future in order to decrease the still large uncertainties associated with these estimates, as follows:

- While levels of Hg associated with individual sectors included in the inventory are relatively well established, all other supporting information (e.g. production rates, waste-water generation, treatment practices etc.) is much more unreliable and inconsistently reported, and drives the uncertainties of the estimates. Better information about coal washing practices and fate of Hg during various water uses in coal fired power plants are needed, in particular.

- Some of the uncertainty is related to the lack of knowledge regarding the actual environmental fate of mercy once being releases form anthropogenic sources. In the current inventory only the air emission abatement technologies were considered. However, in installations where water abatement technologies are being used, these would decrease Hg releases ending in water and increase the share of Hg following sector-specific waste pathways. In the absence of such facility-level information, current releases for relevant sectors (XY) might be overestimated. On the other hand, there might be substantial secondary releases resulting from Hg initially being released to terrestrial pathways, however without detailed knowledge of processes controlling the time-lag between such releases and later remobilization into water, quantification of associated releases is not possible. One way to investigate these processes and their importance in the global Hg cycle is the use of biogeochemical cycling models.
- Additional sectors and anthropogenic activities, not taken into account in this inventory, as discussed in detail in Section 5.2.2.2, should be included in future inventories. Although recognised as less relevant in the global context in this work, some of these sources might be significant contributors of Hg to local aquatic systems.
- Estimates in the 2015 inventory are made based on country-level information. Future work would benefit from inclusion of more detailed facility-level information to improve the spatial distribution component of this work. Along these lines, more detailed knowledge on differences in technologies used, waste treatment practices and Hg consumption patterns in individual countries should be incorporated. Some of the information needed will be available as part of the Minamata Convention, as within the Convention each Party should identify relevant sources of releases and establish inventories of Hg releases from such sources.
- Harmonisation of methodological approaches for estimating the releases is needed, e.g. something along the lines of the UNEP Toolkit approach for air emissions but focused on aquatic Hg releases. Similar, reduction of uncertainties for all the sectors included in the inventory is needed by using more systematic and harmonised approaches in data collection. Not only information on Hg content must be improved, but especially information on related activity data needed to derive the estimates.
- Although out of the scope of this chapter, lack of knowledge regarding the fate of Hg once released from the source was recognised as a limiting factor for placing inventory results in the

context of the global Hg cycle. Future work should focus more on establishing relationships between catchments characteristics, sources within individual catchments and the Hg outflows. Nowadays, techniques like isotope tracer experiments and isotope ratio measurements of Hg are available to address this issues.

Annex X

Given the global nature of the inventory and general lack of data/information on aquatic Hg releases and associated information, assumptions had to be made to derive the estimated presented in this work. Often these assumptions are difficult to validate. For the transparency reasons details on the data/information and assumptions made within individual release category are given here.

X.1 Method used to estimate mercury releases to water, land and waste streams associated with Group 1 sectors

The following sectors for which the UNEP Toolkit provides "distribution factors" for water are included in Group 1: chlor-alkali industry, oil refining, large scale Au and non-ferrous metals production. Water releases for these sectors are estimated using water/air DF ratios as scaling factors together with the GMA atmospheric Hg emission inventory for which details regarding compiling data and derivation of emissions are given in Chapter 2 and Appendixes 1-6.

For the sectors where abatement is considered for calculation of atmospheric emissions, country/group specific abatement profiles are considered and the distribution factors revised accordingly, while for others distribution factors are directly adopted from the Toolkit. The former sectors comprise production of various non-ferrous metals (primary production of copper, lead, zinc and aluminium), large scale Au production and chlor-alkali industry. The methodology applied to calculate water releases comprise the following consecutive steps:

1. Using information on the country/group specific technology profiles (reduction efficiency and percentage and application rates), total air emissions are distributed between various types of abatement technologies.

2. Using information on air emissions by abatement technology combined with the information on reduction efficiency of individual technology profile, unabated/uncontrolled emissions to air are calculated.

3. Depending on the sector, input of Hg that is being directly (i.e. not via abatement) released to other pathways than air (non-air inputs) is calculated (see sector-specific comments below).

4. Total Hg input is calculated as a sum of unabated air emissions and the non-air inputs.

5. Actual distribution factor for air is calculated from air emissions and total Hg input.

6. Distribution factors for other pathways are revised depending whether they are assumed to originate from the abatement technologies or considered as direct releases (see sector-specific comments below).

7. Releases to water are calculated based on reported emissions to air and revised water/air ratios. In the same way by using appropriate DF ratios, outputs to other pathways considered in the Toolkit are estimated.

The water releases derived using the general methodological approach outlined above are based on sector-specific knowledge regarding the fate and pathways of Hg as described into more details in UNEP Toolkit (UNEP, 2017). In general, two types of releases to water are considered – direct ones and those resulting from the abatement technologies used. Direct releases are those where Hg goes to water directly without entering air pathway first, while abatement ones are associated with various wet cleaning technologies (e.g. scrubbers etc.). For the latter it is further assumed that Hg is initially re-allocated from the air pathway and then subjected to other pathways including water, with the same proportions as defined in the Toolkit. Whether dry-only abatement methods or wet-based abatement dominates in each particular country and sector have been decided based on technology profiles presented in Annex 6. For the purpose of these estimates, various sector-specific assumptions are made, as follows.

Primary production of copper, lead and zinc: Water releases for these sectors are assumed to originate from the use of wet gas cleaning technologies used. No direct releases to pathways other than air are considered. The exception is Hg bound in slag which, according to the data provided in Hui et al. 2016 varies from 3% to 14%, depending on metal. The share of slag is considered as a part of the sector-specific treatment which does not depend on air abatement and is kept constant in the calculations. It is further assumed that Hg once re-allocated from the air pathway is subjected to water, products (including sulphuric acid produced at acid plants considered as part of the abatement) and sector-specific treatment. In case where only dry abatement technologies are used, no water releases are considered.

Primary production of aluminium: Water releases for this sector are assumed to be a sum of direct releases and the abatement technologies used. Where wet cleaning abatement technologies prevail, Hg re-allocated from the air pathway is subjected to three pathways: water, general waste and sector-specific treatment. In cases where dry or no abatement is used, water pathway is excluded.

Production of gold from large-scale gold mining: Water releases for this sector are assumed to be a sum of direct releases and the abatement technologies used. Where wet cleaning dominates abatement profile Hg re-allocated from air is distributed between water and land. In cases where dry or no abatement is used, water pathway is excluded. Share of product-bound Hg is assumed to be constant.

Chlor-alkali industry: Water releases for this sector are assumed to be direct releases, while releases to land and sector-specific treatment are assumed to be a sum of direct releases and abatement technologies used. Hg re-allocated from the air pathway is distributed between these two pathways. Share of product-bound Hg is assumed to be constant.

Primary mercury production and oil refining: For these two sectors no wet abatement technologies are considered when calculation emissions to air. Therefore, distribution factors are directly adopted from the Toolkit. For the primary mercury production, in addition to air emissions, releases to water and land are considered. For the oil-refining sector, releases to water and sector-specific treatment are considered.

Gaps/needs to improve methodological approach:

- For the releases associated with abatement technologies used, this approach does not consider that part of Hg that is being abated by dry methods is not associated with water pathways, which for some cases may result in methodological overestimation of water releases. However, since 'dry-only' abatement technologies are in most countries significantly less spread than wet-based abatement, this issue can be neglected.

- For the production of Cu, Pb and Zn the distribution factors from the Toolkit reflect the distribution after abatement and no direct releases (except for slag) are assumed – so it is relatively easy to calculate unabated distribution factors. For the production of aluminium, large-scale Au mining and chlor-alkali industry the approach assumes that distribution factors from the Toolkit imply unabated emissions. Due

to the lack of more detailed information regarding abatement used in distribution factors given in the Toolkit – those are a combination of direct releases and releases via abatement so it is virtually impossible to derive actual unabated distribution factors. It is therefore assumed for simplicity that distribution factors in the Toolkit imply no abatement.

- The approach does not consider potential further abatement of water releases. Efficient water cleaning would also affect actual distribution factors resulting in lower water releases and more Hg going to sector-specific treatment; however lack of data does not make such corrections possible.

X.2 Method used to estimate mercury releases to water associated with municipal wastewater

The 2015 inventory for Hg releases associated with municipal wastewater is based on information regarding volumes of municipal wastewater produced, wastewater treatment practices and reported Hg ranges for concentrations measured in wastewater before (influent) and after the treatment (effluent). Municipal wastewater is defined here as water that has been used for municipal use and is afterwards released back to the environment. Treatment of this released water mostly depends on prosperity of the country and consequently its capacities and number of wastewater treatment plants. Bulk of the information for individual countries was obtained from the AQUASTAT database of the Food and Agriculture Organisation of the United Nations (FAO). AQUASTAT reports amounts of municipal wastewater generated within urban areas. Since not all countries are reporting their amounts of municipal wastewater on regular yearly basis, the last available data for each country was used. For countries with no data available, waste-water was calculated based on assumed water use per person per day. Water use averages for individual continent were selected and assigned to the countries with missing data: 230 for Asia (Kamal et al., 2008), 50 for Africa, 200 for Europe, 100 for Oceania and 100 l/person/day for Caribbean countries. Percentage of treated waste-water has been then assigned to each country. Most recent information on treatment practices in individual country was adopted from the global database compiled by Malik et al. (2015). For countries missing in that database, waste-water treatment data is based on regional averages as discussed by Malik et al. (2015) and in recent UN world water development report (UN, 2017), assuming similarities within regions and between the neighbouring countries. Based on these two sources, the following waste-water treatment rates were selected for individual regions: 80% for the EU28 and W Europe, 25% for East Europe and Central Asia, 20% for East Asia and Pacific, 5% for South Asia, 50% for N Africa, 15% for Sub-Saharan countries, 20% for Latin America and 50% for Middle East.

Magnitude of Hg releases from this sector will depend greatly on the amount of Hg products used, general waste handling practices and especially level of waste-water treatment - information lacking for most of the countries. In absence of such information, generic waste management profile of a country was used and different ranges of Hg concentrations applied for untreated wastewater and wastewater treated in treatment plants, to estimate releases for individual country. These estimates are based on an assumption that Hg concentrations in untreated wastewater are lower in more developed countries

compared to those in developing nations, as seen from values reported in scientific literature. Further assumption is that Hg removal is more efficient in developed countries due to greater levels of waste-water treatment (Table X.2).

Table X.2 Ranges of Hg concentrations in untreated and treated sewage used to derive the estimates

Profile	Hg in untreated wastewater [ng/L]	Hg removal efficiency [%]	Hg in treated wastewater [ng/L]
1	100-500	95	5-25
2	300-1500	80	60-300
3	300-1500	70	90-450
4	300-1500	60	120-600
5	300-1500	50	150-750

X.3 Method used to estimate mercury releases to water from coal-fired power plants

The 2015 inventory for Hg releases with wastewater from coal-fired power plants uses a very coarse approach for a first preliminary estimate of global magnitudes associated with this sector. In the absence of more detailed country-specific information, the approach largely relies on information available for China and work carried out by Liu et al. (2016), by upscaling globally relationships between CFPPs electric capacities, amounts of wastewater produced and associated reported ranges of Hg concentrations reported in their work.

The method applied is based on an assumption that on average global water use patterns in CFPPs are similar to those in China, country that is the single largest user of coal-derived electricity in the world. This is of course a rough generalisation, however inevitable in order to perform harmonised global calculation approach.

Based on wastewater volumes reported by Lie et al. (2016) and total electricity generation capacity of CFPPs in China, wastewater generation was estimated at 0.25-0.5 m^3 per MWh of energy produced. For the purpose of this wastewater generation estimate, realized energy output from CFPPs was calculated using the capacity factor of 0.55 (Biesheuvel et al., 2016). In order to estimate generation of wastewater in each country of the world with CFPP, wastewater generation rate from China was then used along with the information on country-wide CFPPs total capacity based on information provided in Global Coal Plant Tracer database (GCPT, 2017). Capacity factors used for calculation of the amount of energy produced in individual country were adopted from Biesheuvel et al. (2016). Final amounts of Hg releases per country were estimated using Hg concentrations in CFPPs generated wastewater in 5-25 mg/m^3 range (Liu et al., 2016 and references therein).

X.4 Method used to estimate mercury releases to water associated with coal washing

The 2015 inventory for Hg releases associated with coal washing is based on global coal production, coal Hg content, Hg removal efficiency and coal washing rates, following the approach of Liu et al. (2016).

Total coal production in 2015 for individual country was obtained from the Global Energy Statistical Yearbook 2016 (Enerdata, 2016). In the absence of detailed per-country information on amounts of different coal types, regional information on coal type produced (anthracite, metallurgical, bituminous, subbituminous and lignite) was obtained from International Energy Statistics available for the year 2014 (U.S. Energy Information Administration, 2017b). Regional ratios were then applied to individual country. For countries where information on Hg content in various Hg coals was available as summarised in Annex 6, country specific average Hg content was used, while for countries where this information is missing generic values were applied. Information on coal washing rates in individual countries is available for world's major coal producers only, China, United States, India and Australia, and varies in the 20-90% range. For the rest of the world we assume that higher percentages of coal produced are being washed in developed countries and assign the following washing rates using technology profiles (TP) of the country: TP1-80%, TP2-65%, TP3-50%, TP4-35% and TP5-20%. The Hg removal efficiency of coal washing is selected in 20-30% range (UNEP, 2017; Liu et al, 2016). It is further assumed that only part of Hg released during washing will reach local aquatic systems, the rest being deposited in slurry ponds. Using waste management profiles of individual country, following percentages for Hg reaching water courses were selected: WP1-20%, WP2-30%, WP3-40%, WP4-50% and WP5-60%.

X.5 Method used to estimate mercury releases to water from the use and wastes associated with Hg added products

In 2015 inventory mercury releases to water from Hg added products are produced using methodology comparable to that applied to estimate emissions to air (see Annex 3 for details). The approach uses regional patterns of consumption of Hg and Hg-containing products. Mercury releases at various points in the life-cycle of these products are estimated using assumptions regarding rates of breakage, waste handling, and factors for releases to water. The input data consist of estimated Hg consumption in one year (2015) covering following product groups: batteries, measuring devices, lamps, electrical and electronic devices, dental applications, and other uses. These amounts are then distributed to four different initial pathways (safe storage, breakage and releases of Hg during use, paths to the waste stream, products remained in use) using distribution factors. Waste pathways are further differentiated among waste recycling, waste incineration and waste landfill. This latter pathway is further distributed between two levels of waste management, controlled and uncontrolled waste landfill. All the initial and waste distribution factors used to determine the amount of Hg distributed to the abovementioned pathways are the same as those used in case of atmospheric emissions estimates (see Annex 3 for details). Within these pathways, releases to water are assumed for breakage/release during use, recycling and from waste landfills (Figure X.5.1).

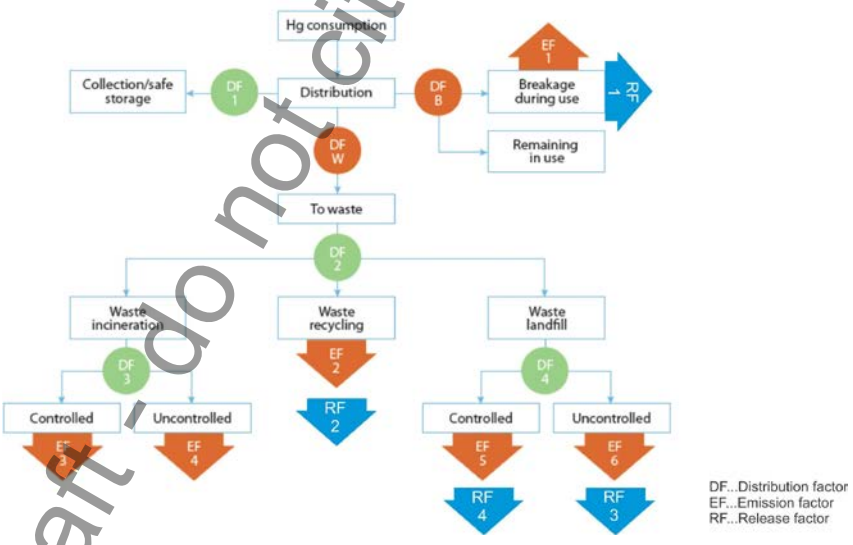

Figure X.5.1: Schematic representation of the model used to estimate mercury releases from waste streams associated with mercury added products and comparison with mercury emission streams.

Releases to water are then estimated by applying release factors (RF) according to Table X.4 to the distributed individual amounts of Hg. As in the case of atmospheric emissions for this sector, varying waste management practices were taken into account by using five different profiles of distribution of release factors. Each country has been assigned one of these five generic profiles based on assumptions and information available as discussed in detail in Chapter 2.X. For releases resulting from breakage during use, waste recycling and controlled landfills, release factors are the same for assigned generic profiles of waste management. A differentiation is introduced for releases from uncontrolled landfills by using different release factors for individual profiles.

Table X.4. Release factors (fraction released) applied to distributed amounts of mercury in Hg-added products

Profile	Break/release during use	Waste recycling	Landfill	
			controlled	uncontrolled
1	0.1	0.05	0.0001	0.05
2	0.1	0.05	0.0001	0.10
3	0.1	0.05	0.0001	0.15
4	0.1	0.05	0.0001	0.20
5	0.1	0.05	0.0001	0.25

Example calculation:

The following example shows the calculation scheme applied to estimate releases associated with the use and disposal of Hg added products for Mexico. Distribution of Hg between different distributions pathways, starting with the distribution of regional total amount of Hg consumed in intentional Hg use products is the same as that for atmospheric emissions and described in detail in Annex 3.

The flowchart Figure X.5.1 illustrates how, on the basis of this distribution, releases to water totalling about 2.5 tonnes are calculated. Of this, following breakage during use, 0.088 tons are released, while other releases are attributed to secondary waste pathways: 0.024 tonnes are estimated to be releases during waste recycling and 2.337 tonnes from managed and managed waste landfills.

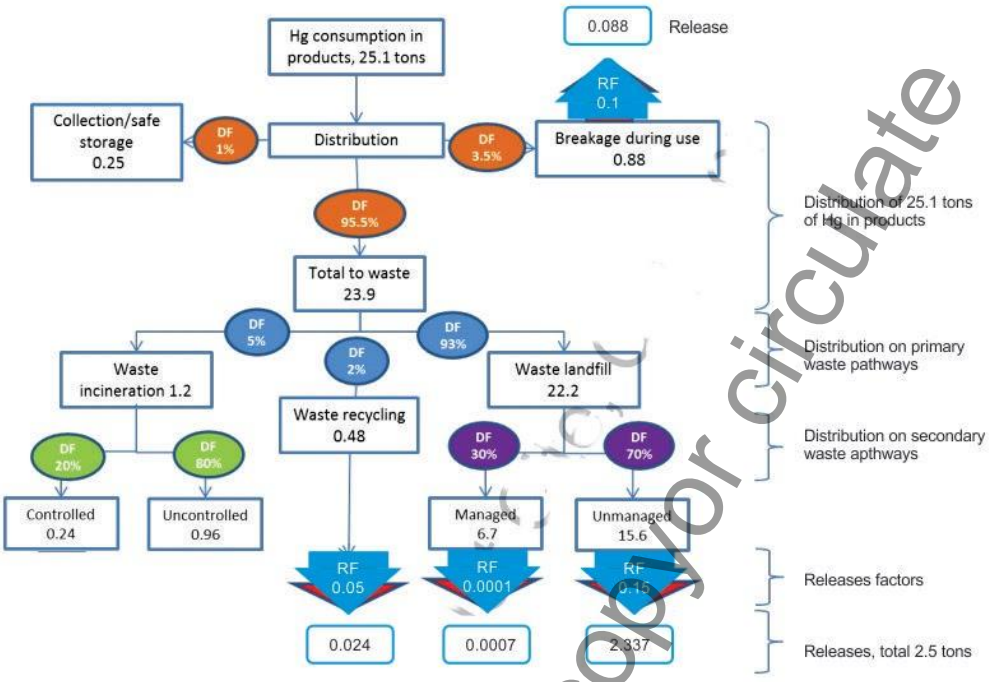

Figure X.5.3: Example calculation of mercury releases from waste streams associated with mercury added products

References:

AMAP, 2010. Updating Historical Global Inventories of Anthropogenic Mercury Emissions to Air. By: Wilson, S., J. Munthe, K. Sundseth, K. Kindbom, P. Maxson, J. Pacyna and F. Steenhuisen. AMAP Technical Report No. 3. Arctic Monitoring and Assessment Programme (AMAP), Oslo, Norway. 12 pp.

AMAP/UNEP, 2008. Technical Background Report to the Global Atmospheric Mercury Assessment. Arctic Monitoring and Assessment Programme / UNEP Chemicals Branch. 159 pp. Online at: www.chem.unep.ch/mercury/Atmospheric_Emissions/Technical_background_report.pdfAMAP/UNEP. Arctic Monitoring and Assessment Program: Oslo, Norway/UNEP Chemicals Branch: Geneva, Switzerland. Technical Background Report for the Global Mercury Assessment 2013, pp. vi–263.AQUASTAT, FAO, Produced Municipal Wastewater, 1985-2014.

AQUASTAT, 2017. Available at http://www.fao.org/nr/water/aquastat/main/index.stm

Biesheuvel et al. (2016), Modelling global water demand for coal based power generation, Methods and results report, Greenpeace.

BP, 2016, Statistical Review of World Energy. Available at https://www.bp.com/content/dam/bp/pdf/energy-economics/statistical-review-2016/bp-statistical-review-of-world-energy-2016-full-report.pdf

Budge et al., 2000. Review of worldwide status pf coal preparation technology, Available at: http://citeseerx.ist.psu.edu/viewdoc/download?doi=10.1.1.557.9262&rep=rep1&type=pdf

Carbon Locker, 2017. http://www.carbonlocker.org

Cheng, I., Lammi, H., 2016. The Great Water Grab. How the Coal Industry is Deepening the Global Water Crisis. Greenpeace.

Coal preparation, 2011. (http://webarchives.gov.uk/+/http:/www.berr.gov.uk/files/file19296.pdf)

Drainage Basins. William Rankin (personal communication) based on USGS Hydro1k database. Garretson, SD, USA.

EIA, 2017, International Energy Statistics, 2017 US Energy Information Administration. https://www.eia.gov/beta/international/data/browser/#/?pa=3g000000000000000000000000000000000000180000000000000g&c=4100000002000060000000000000g000200000000000000001&tl_id=1-A&vs=INTL.7-1-AFRC-TST.A&vo=0&v=H&start=1980&end=2014

EIP, 2016. Toxic Wastewater from Coal Plants, Available at: https://www.eenews.net/assets/2016/08/11/document_gw_05.pdf

Enerdata, 2016, Global Energy Statistical Yearbook 2016, https://yearbook.enerdata.net/coal-and-lignite-production.html

ENM, 2016. Energy News Monitor | Volume XII; Issue 30, https://indiaenergyanalysis.wordpress.com/2016/01/08/coal-washing-global-perspective/

E-PRTR, 2014, The European Pollutant Release and Transfer Register (E-PRTR), 2014. (http://prtr.ec.europa.eu)

Gallup, D. L. & Strong, J. B. (2006). Removal of Mercury and Arsenic from Produced Water. In 13th Annual International Petroleum Environmental Conference. http://www.hgsolution.com.my/research/paper2.asp

GCPT, 2017. Global Coal Plant Tracker, http://endcoal.org/global-coal-plant-tracker/

Gleick et al., 2014, The World's Water Volume 8.

Holmes C.D., Jacob D.J., Corbitt E.S., Mao J., Yang X., Talbot R., Slemr F. Global atmospheric model for mercury including oxidation by bromine atoms. Atmos. Chem. Phys. 2010;10:12037–12057. doi: 10.5194/acp-10-12037-2010.

IES, 2017. International Energy Statistics, 2015. (https://www.eia.gov/beta/international/data/browser/#/?pa=0000000000000000000000000000000000002&c=ruvvvvvfvtvnvv1urvvvvfvvvvvfvvvou20evvvvvvvvvvnvvuvo&ct=0&tl_id=5-A&vs=INTL.57-1-AFG-TBPD.A&vo=0&v=H&start=1980&end=2016)

IKIMP, 2012. Mercury arising from oil and gas production in the United Kingdom and UK continental shelf. By: Lang, D., M. Gardner and J.Holmes. Integrating Knowledge to Inform Mercury Policy (IKIMP). University of Oxford. 38 pp.

IOGP, 2016, Environmental performance indicators – 2015 data, International Association of Oil and Gas Producers. http://www.iogp.org/bookstore/product/environmental-performance-indicators-2015-data/

IPIECA, 2012. Industry input to the UN global mercury treaty negotiations focus on oil and gas. By: Doll, B.E., B.M. Knickerbocker and E. Nucci. The global oil and gas industry association for environmental and social issues (IPIECA).

Kamal, A.S.M., Goyer, K., Koottatep, T., Amin, A.T.M.N, 2008. Domestic wastewater management in South and Southeast Asia: the potential benefits of a decentralised approach. Urban Water Journal, 5, p. 345-354.

Kamal, A.S.M., Goyer, K., Koottatep, T., Amin, A.T.M.N., 2008. Domestic wastewater management in South and Southeast Asia: the potential benefits of a decentralized approach. Urban Water Journal 5, 345–354.

Lin et al., 2016 , Material Flow for the Intentional Use of Mercury in China.Environ Sci Technol. 2016 Mar 1;50(5):2337-44. doi: 10.1021/acs.est.5b04998

Liu, M.; Zhang, W.; Wang, X.; Chen, L.; Wang, H.; Luo, Y.; Zhang, H.; Shen, H.; Tong, Y.; Ou, L.; et al. Mercury Release to Aquatic Environments from Anthropogenic Sources in China from 2001 to 2012. Environ. Sci. Technol. 2016, 50, 8169–8177.

Lujala, Päivi; Jan Ketil Rød & Nadia Thieme, 2007. 'Fighting over Oil: Introducing A New Dataset', Conflict Management and Peace Science 24(3), 239-256.

Malik, O. M., Hsu, A., Johnson, de Sherbinin, A., A global indicator of wastewater treatment to inform the Sustainable Development Goals (SDGs), Environmental Science & Policy Volume 48, April 2015, Pages 172-185

Sato, T., Qadir, M., Yamamoto, S., Endo, T., Zahoor, A., 2013. Global, regional, and country level need for data on wastewater generation, treatment, and use. Agricultural Water Management, 130, p. 1-13.

Steenhuisen, F.; Wilson, S. Identifying and characterizing major emission point sources as a basis for geospatial distribution of mercury emissions inventories. Atmos. Environ. 2015, 112, 167–177

UN, 2017. The United Nations World Water Development Report 2017, http://www.unwater.org/publications/world-water-development-report-2017/

UNEP, 2017a, Toolkit for Identification and Quantification of Mercury Sources, Guideline for Inventory Level 1, UNEP Chemicals Branch: Geneva, Switzerland.

UNEP, 2017b. Toolkit for Identification and Quantification of Mercury Sources, Reference Report and Guideline for Inventory Level 2, UNEP Chemicals Branch: Geneva, Switzerland

UNEP. The state of the marine environment - trends and processes, 43 pp., United Nations Environment Programme and the Global Programme of Action for the Protection of the Marine Environment from Land-based Activities (GPA) of the United Nations Environment Programme (UNEP), The Hague, Netherlands. 2006.UNEP, 2017

Wilson, S., F. Steenhuisen, J.M. Pacyna and E.G. Pacyna, 2006. Mapping the spatial distribution of global anthropogenic mercury atmospheric emission inventories. Atmospheric Environment, 40: 4621-4632.

Zhao, C. and Luo, K,, Sulfur, arsenic, fluorine and mercury emissions resulting from coal-washing byproducts: A critical component of China's emission inventory, Atmospheric Environment 152 (2017) 270e278

7. Relationships between trends in atmospheric mercury and mercury in aquatic biota

Authors: Peter Outridge, Feiye Wang, Robert Mason, Lars-Eric Heimbürger, Xinbin Feng [order???]

Key messages

- *There are many transformative steps in the environmental cycle of mercury (Hg), between its emission into air from anthropogenic and natural sources to its eventual bioaccumulation in food chains leading to wildlife and human exposure. Multiple geochemical, climatic, biochemical, ecological and physiological processes and factors influence the environmental fate and bio-uptake of Hg. Therefore, there are good reasons to expect that the biological and atmospheric trends of Hg may not respond coincidentally or proportionately in future, after regulatory action to reduce anthropogenic emissions. This proposition is tested in this chapter.*
- *Methylation/demethylation, between inorganic Hg and methyl Hg (MeHg), is the key transformative step leading to humans in the environmental Hg cycle, as MeHg is the only Hg species to be biomagnified in food chains and is one of the most neurotoxic forms. Aquatic ecosystems are more favorable for methylation to occur than terrestrial ecosystems, because methylation is favored in anoxic and low oxygen environments. Marine ecosystems are of special concern from the perspective of human exposure to MeHg because of the widespread consumption of marine fish and mammals by many populations.*
- *The factors controlling methylation and demethylation in aquatic ecosystems (e.g., nutrient and carbon loading, acidity, chemical reduction-oxidation status) are complex and still poorly understood. This knowledge gap adds considerable uncertainty to our understanding of the relationship between atmospheric Hg deposition rates and MeHg concentrations in any given environment or aquatic animal population.*
- *In marine ecosystems, sediments are not the only important source of MeHg to estuarine, coastal and open ocean waters as was once believed. Recent extensive evidence points to in situ water column methylation occurring in coastal and pelagic waters in all ocean basins in the world. It is speculated that methylation occurs within the anoxic micro-environments inside 'marine snow' particles, namely the slowly-sinking, decaying organic remains of phytoplankton, zooplankton and their fecal pellets.*
- *Several regional groupings of case studies were synthesized for this assessment, involving data on atmospheric and aquatic biota Hg trends in the Arctic; Fennoscandia; reservoirs in Europe, North America and China; and North American lakes and coastal waters. Atmospheric Hg levels were either increasing, decreasing or stable, depending on the region in question, thus illustrating a range of possible future scenarios. Our analysis found numerous examples of biotic time-trend datasets that did not agree with the trends in regional atmospheric deposition or concentrations over recent decades; in a minority of cases, the atmosphere and biota trends did agree. In some cases, biota and air trends agreed for the first few decades of the study period but diverged in the most recent decade; in others, multiple species of fish and/or aquatic birds in the same area (and so subject to the same atmospheric Hg deposition trend) displayed significantly different directional patterns that either agreed or disagreed with atmospheric trends. A comparison of fish Hg trends in reservoirs was particularly compelling, with those in China generally exhibiting a quite different trend to North American and European reservoirs, and with biotic trends in both regions being unrelated to atmospheric trends. This finding clearly showed that local terrestrial and/or aquatic processes were more important than atmospheric deposition as drivers of biotic Hg concentrations in those systems.*
- *An over-arching general explanation for these results is that they reflect the dominant effects of other multi-causal factors, such as climate change, biogeochemical changes in aquatic ecosystems, and alterations in terrestrial or catchment soil processes, that masked any impact of changing atmospheric inputs. Further investigation is required to elucidate the specific explanations behind cases of non-concurrent atmospheric and biotic time-trends of Hg.*
- *In terms of implications for the future effects of regulatory action to restrict atmospheric Hg emissions, this assessment refined a general model of biotic responses to atmospheric Hg inputs to propose that a wide range of potential outcomes will be observed as atmospheric Hg declines. Small lakes with small, relatively uncontaminated catchment soils, and coastal marine waters with restricted water exchange with the open ocean, in general may show relatively rapid declines in biotic Hg levels. However, severely contaminated freshwaters, and most ocean basins of the world, will probably not show early and proportional declines in aquatic biota Hg concentrations. In fact, model predictions suggest that many marine food chains will remain significantly elevated in Hg for many decades to centuries after atmospheric Hg levels have returned to near-natural levels because of the long residence times of anthropogenic Hg in intermediate and deep waters, the revolatilization and redeposition of legacy anthropogenic Hg from global soils and surface waters, and the slow rate of penetration of historical and current anthropogenic emissions into deeper water masses.*

7.1 Introduction

The atmospheric and aquatic chemistry of mercury (Hg) is one of the most complex of all trace metals. The Hg that is emitted from anthropogenic (and natural) sources to air is almost exclusively in an inorganic form, as gaseous elemental mercury (Hg^0) and oxidized species (Hg^{II}) in gaseous and particulate forms (see Chapters 3 and 4). Because of the photo-oxidation of Hg^0 during its residence in the atmosphere, the bulk of the Hg deposited onto the Earth's surface is inorganic, divalent Hg^{II}, which is also the dominant species in terrestrial soils (Fitzgerald and Lamborg, 2014). Mercury entering the aquatic environment thus occurs mainly as different inorganic Hg^{II} species, directly deposited from the atmosphere following the oxidation of Hg^0, or released from anthropogenic and natural terrestrial sources in dissolved and particulate forms and transported via surface runoff and groundwater seepage (see Chapter 5).

In aquatic environments, the transformation of inorganic Hg^{II} through methylation to methylmercury (MeHg) is the key step in the Hg cycle leading to wildlife and human exposure. This chapter uses MeHg as a generic term when referring to methylated Hg species, which may include both monomethylmercury (MMHg) and dimethylmercury (DMHg) but often comprises only MMHg, depending on how MeHg is sampled and analyzed. MMHg is one of the most bioaccumulative and toxic Hg species, as well as being the only form that is biomagnified through food chains, whereas DMHg does not bioaccumulate or biomagnify (Fitzgerald and Lamborg, 2014). Thus, most references to 'methyl Hg' in the context of bio-uptake, and wildlife and human exposure, are in fact referring to MMHg (see Eagles-Smith et al., 2018). Mercury methylation occurs primarily in the aquatic environment, such that aquatic biota are generally more prone to Hg accumulation than terrestrial biota (see Chapter 8), and consumption of aquatic animals (marine fish, marine mammals and freshwater fish) is the most common Hg exposure pathway to humans (see Chapter 9). This chapter focuses on recent advances in understanding of the aquatic processes that determine MeHg exposure and accumulation by both aquatic biota and humans.

Many environmental and ecological factors (e.g., temperature, light intensity, pH, redox condition, organic carbon and nutrient concentrations, and food web structure and dynamics) have a strong influence on the rates of MeHg production (methylation) and degradation (demethylation), as well as the rate of uptake of inorganic Hg and MeHg by aquatic biota (Eagles-Smith et al., 2018; Hsu-Kim et al., 2018). The complexity of the Hg cycle through the atmospheric, terrestrial and aquatic environments, the limits of our understanding of Hg methylation/demethylation processes, and the number of factors affecting MeHg bioaccumulation and biomagnification, mean that there is considerable uncertainty about how closely and rapidly changes in the emissions and deposition of Hg into the environment brought about by regulatory action will be tracked by changes of Hg in aquatic food webs.

This chapter describes recent advances in our developing understanding of the aquatic chemistry of Hg, particularly focusing on the connectivity between atmospheric Hg and Hg concentrations in aquatic biota. Rather than provide a comprehensive synopsis of all the aspects that affect Hg dynamics in the aquatic environment, much of which can be found in the overviews by AMAP/UNEP (2013) and Fitzgerald and Lamborg (2014), this chapter focuses on the following major topics: recent advances in understanding of Hg methylation and demethylation in marine systems; and relationships between the trends in atmospheric Hg and in aquatic biota, and the reasons for the match or mis-match between those trends. These topics were chosen because they are of the greatest importance with respect to advances in understanding aquatic Hg processes since the 2013 Global Mercury Assessment (AMAP/UNEP, 2013) and because of their relevance to predicting the efficacy of international regulatory action in ultimately reducing Hg exposure in humans and wildlife.

7.2 New understanding of marine Hg methylation/demethylation

7.2.1 General remarks

The concentration of MeHg in an aquatic water column represents the culminating effect of various processes that influence the methylation of inorganic, divalent Hg^{II} to MeHg, its demethylation, as well as transport from the location of its formation to the water column. Generally, Hg is methylated by bacterial processes in sediments and the water column of large waterbodies, such as the ocean and large lakes, but not in the water column of most freshwater ecosystems. While MeHg can be produced by abiotic processes, its formation is thought to be primarily microbially-mediated (Paranjape and Hall, 2017). A major breakthrough was made recently with the discovery of two key genes, *hgcA* and *hgcB*, that control anaerobic Hg methylation first identified in sulfate-reducing bacteria (Parks et al., 2013). The *hgcA* and *hgcB* genes have since been found in many anaerobic microorganisms. An analysis of publicly available microbial metagenomes found the *hgcAB* genes in nearly all anaerobic environments, but much less abundantly in aerobic systems (Podar et al., 2015). In contrast, demethylation of MMHg and DMHg is thought to occur by both abiotic and biotic pathways, with DMHg being volatile and more unstable in the environment than MMHg. Overall, therefore, the concentration of MeHg in any given aquatic environment is the net result of many competing processes of formation, transport, and destruction.

Methylated Hg compounds constitute a small fraction of the total Hg present in some environments (e.g., <1% in air and typically <5% in marine sediments, but with somewhat higher relative concentrations in freshwater sediments and wetland soils; Paranjape and Hall, 2017). However, these compounds can be a much larger fraction of the total Hg in the water column and can exceed 30% of total Hg in the open ocean. In biota, the fraction as MeHg (specifically MMHg in this case) increases as a function of trophic level, from <20% of total Hg in phytoplankton to >90% in high trophic level biota. As MeHg poses the primary exposure risk to humans and other top predators it is of primary importance to understand the production and fate of this compound.

As discussed in later sections, due to the complexity of methylation and demethylation it is not possible to generalize these processes into either global or regional MeHg budgets, although some progress is being made in this regard. Furthermore, given the complexities that control

the *net* formation of MeHg in the environment, it is clear that while reducing total Hg emissions to the environment can be expected to ultimately reduce MeHg in biota in general and over time, more detailed predictions of the effects of regulatory action on Hg in biota in a specific ecosystem requires further investigation of the methylation/demethylation processes in the ecosystem in focus. The following text focuses on methylation/demethylation in marine systems, owing to the predominance of MeHg from marine food webs as the main exposure route in many human populations around the world (see Chapter 9). Other recent reviews (Lehnherr, 2014; Paranjape and Hall, 2017; Eagles-Smith et al., 2018; Hsu-Kim et al., 2018) should be consulted for syntheses of recent findings on methylation processes in freshwater ecosystems.

7.2.2 Coastal waters

Much of the earlier work concerning Hg methylation in coastal waters highlighted by AMAP/UNEP (2013) was focused on the factors controlling methylation in the sediments and the flux from sediments to the water column. The generally held view at that time was that in many settings, sediments were the major source of MeHg to coastal waters, although there were indications that inputs from terrestrial watersheds and/or from ocean exchange were important in some ecosystems.

In the last few years, several studies have challenged the predominance of sediments as the main MeHg source in coastal marine biota. First, Chen et al. (2014) found that the concentrations of MeHg in forage fish across multiple estuaries on the U.S. east coast did not track with the MeHg content of the sediments, but with the water column concentration, even though these fish were considered to forage at the sediment-water interface. Conversely, in the same study MeHg in benthic worms did track the sediment MeHg concentrations. Mercury stable isotope analyses also tended to confirm that the sediment may not have been the most important source of MeHg to the organisms in these ecosystems (Kwon et al., 2014). Li et al. (2016) used Hg isotope analyses to demonstrate that the source of MeHg in biota in Lake Melville, a large subarctic fjord, was from pelagic production. Similarly, sulfur isotope analyses of plankton from Long Island Sound did not support the idea that the accumulated MeHg had a substantial sediment component (Gosnell et al., 2017).

However, Buckman et al. (2017) showed that within the Delaware River estuary, these patterns were more complex and it was less easy to discern the importance of sediment inputs of MeHg compared to riverine inputs. Gosnell et al. (2016) found that for the Delaware River, sediment could be an important MeHg source at certain times of the year, suggesting that sediment sources should not be ignored. Jonsson et al. (2017) showed that changes in the concentration and type of dissolved organic carbon (DOC) as well as MeHg loading can influence MeHg bioaccumulation (see also Balcom et al., 2015; Schartup et al., 2015b; Gosnell et al., 2016). Comparison of water column and sediment MeHg concentrations indicated that in some ecosystems, such as the Hudson River, there is a reasonably strong relationship between dissolved water column MeHg and porewater MeHg, and between sediment and suspended particulate MeHg, but there are many ecosystems where there is little correlation.

One important factor that has received less attention is the degree to which the MeHg concentrations are influenced by demethylation of MeHg rather than by its formation. Many studies have assumed that demethylation is not a strong control on MeHg levels in coastal ecosystems but this assumption needs to be tested further. Overall, current literature suggests that there are no clear-cut trends across coastal ecosystems and that both internal and external sources of MeHg are likely to be important contributors of MeHg to the food chain.

Recent studies have reached contrasting conclusions on the effect of the nutrient and oxygen status of waterbodies on Hg methylation rates in sediments. In mesocosm studies using stable Hg isotopes, Liem-Nguyen et al. (2016) showed that the addition of nutrients could increase Hg methylation rates in sediments by increasing the activity of benthic microbial communities, but only for labelled Hg^{II} species with a high availability for methylation (such as labile dissolved forms and Hg-organic complexes). Mercury species with low availability in sediments (such as Hg sulfide) did not show an effect of nutrient loading (see also Jonsson et al., 2014). For oxygen status, the consensus is that increased eutrophication leading to oxygen depletion (hypoxia) in bottom waters results in increased MeHg production by providing ideal conditions for sulfate-reducing bacteria. A recent example of this process was provided by the modelling of Soerensen et al. (2016b), which suggested that increased MeHg in Baltic Sea plankton was associated with increasing eutrophication, although there is little evidence for this phenomenon in some estuaries (e.g., Gosnell et al., 2017). Contrary examples have also been reported recently, with no increase in sediment MeHg levels in some coastal regions with bottom water hypoxia (Liu et al., 2015; Chakraborty et al., 2016). In Long Island Sound, in the more eutrophic regions where bottom waters are seasonally hypoxic, plankton had lower MeHg than those from more oligotrophic regions (Gosnell et al., 2017). Again, these results suggest that the interaction between eutrophication and MeHg levels in biota is complex, and likely to vary between locations.

Organic carbon is an additional important factor influencing both Hg methylation and MeHg retention in sediments. For example, Mazrui et al. (2016) found that the binding of Hg to DOC enhanced methylation compared to Hg bound to particulate organic carbon (POC) and Hg present as cinnabar (the most common source mineral for refining elemental Hg). The origins and geochemical quality of the organic carbon (terrestrial or marine) are at least as important as its quantity in terms of its effect on Hg bioavailability (Jonsson et al., 2012, 2017; Schartup et al., 2015b). Additionally, it has been shown in pure cultures and laboratory sediment studies that nanoparticulate Hg has higher bioavailability for methylation than microparticulate forms (Zhang et al., 2014; Mazrui et al., 2016). These studies reinforce the conclusions of prior studies (Jonsson et al., 2012; Schartup et al., 2013; 2014) that the factors controlling Hg methylation in sediments are extremely complex given the interactions between Hg (and MeHg) and sediment biogeochemistry (primarily, the levels of organic carbon and reduced sulfur) which impact binding, bioavailability and sediment-water exchange. While speciation of the Hg is an important driver, desorption kinetics and microbial community activity are also important controls over the extent of Hg methylation in sediments.

The weight of evidence for the importance of water column methylation in coastal waters has increased in recent years. A number of studies have followed up on earlier work in the Thau Lagoon, France (Monperrus et al., 2007), examining the potential for methylation of Hg within the water column of coastal environments. Several research groups have now shown that there is potential for methylation in the water column of estuaries and coastal waters, especially in locations of mixing and flocculation of particulate material (Ortiz et al., 2015; Schartup et al., 2015a; Sharif et al., 2014). These studies point to the likely enhancement of methylation within aggregated particles where micro-anoxic conditions could exist, as demonstrated by the laboratory experiments of Ortiz et al. (2015). Overall, these studies do not suggest that Hg methylation is occurring through a different microbial biochemical pathway, but that it is occurring within the anoxic microzones within large particulates. Some of these studies have concluded that there is significant net Hg methylation within the water column (Ortiz et al., 2015; Schartup et al., 2015a) while in other cases, the rate of demethylation leads to a net decrease in MeHg (Sharif et al., 2014).

In summary, there is not one specific source for the MeHg accumulating in biota in coastal systems, and the sources are likely to vary spatially and temporally. In examining, and understanding, the dynamics of MeHg bioaccumulation in coastal environments it is necessary to examine both the potential external inputs (watershed and ocean inputs) and the internal production within the system (water column and sediment net Hg methylation). Furthermore, it is likely that their relative importance will change in the future due to climate and other human-caused alterations within these ecosystems.

7.2.3 Open ocean

Like coastal seas, there is increasing evidence for active Hg methylation in the oxygenated water column of open oceans. Early pioneering work by Mason and Fitzgerald (1990) suggested the potential for high rates of *in situ* production of MeHg in the open ocean, and later studies supported the idea of *in situ* MeHg formation (Monperrus et al., 2007; Cossa et al., 2009, 2011; Sunderland et al., 2009; Heimbürger et al., 2010). However, the prevailing paradigm continued to favor a coastal sediment MeHg source with offshore transport to the open oceans. There is now more recent published evidence for water column methylation from almost all major ocean basins: the Atlantic Ocean (Bowman et al., 2015; Bratkič et al., 2016), Pacific Ocean (Hammerschmidt and Bowman, 2012; Munson et al., 2015; Bowman et al., 2016; Kim et al., 2017), Arctic Ocean (Wang et al., 2012; Heimbürger et al., 2015), Southern Ocean (Gionfriddo et al., 2016), Mediterranean Sea (Cossa et al., 2012, 2018), Baltic Sea (Soerensen et al., 2016b) and the Black Sea (Rosati et al., 2018). No data have been published for the Indian Ocean thus far. Laboratory experiments confirm that net Hg methylation can occur in 'marine snow' (settling organic particles), with similar rates compared to marine sediments (Ortiz et al., 2015). Furthermore, several papers point out that open ocean methylation is required to balance the oceanic MeHg mass budget (Sunderland et al., 2009; Mason et al., 2012; Soerensen et al., 2016a).

A simplified marine Hg cycle describing *in situ* Hg methylation in the oceanic water column is shown in Figure 7.1. A common feature of the dissolved MeHg profiles in all ocean basins is a subsurface peak which coincides with a minimum in oxygen concentrations. At the surface, inorganic Hg adsorbs to organic matter, mostly phytoplankton, and is then exported to depth in

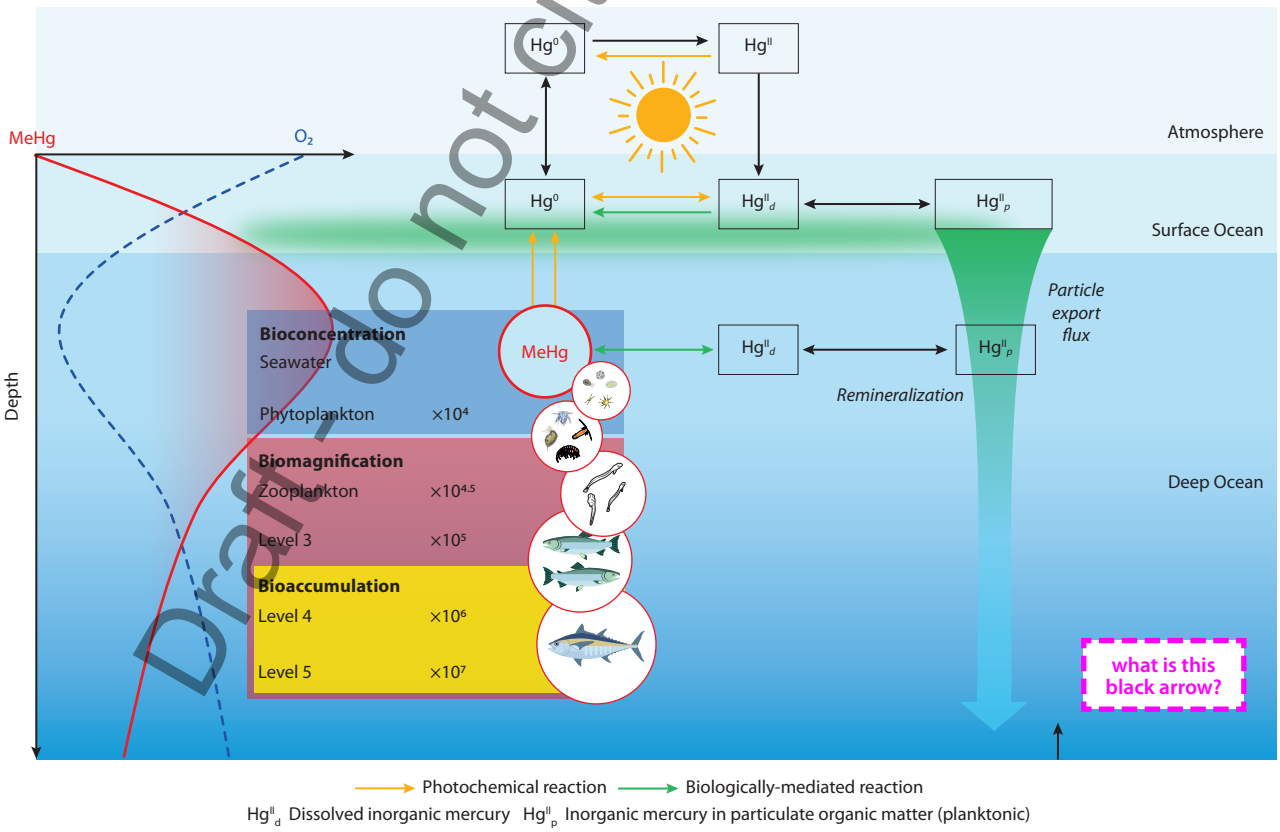

Figure 7.1 Simplified schematic of the marine Hg cycle, showing Hg methylation in the ocean water column. ~~Hg^{II}_d = dissolved inorganic Hg; Hg^{II}_p = inorganic Hg in particulate organic matter (planktonic). Yellow arrows indicate photochemical reactions, green arrows indicate biologically-mediated reactions.~~

marine snow, providing the key ingredients for Hg methylation – organic carbon and Hg. In the subsurface ocean, oxygen is consumed by bacteria that feed on the planktonic organic matter, a process known as organic matter remineralization. The correlation of dissolved MeHg with oxygen (or apparent oxygen utilization or organic carbon remineralization rates) suggests that organic matter remineralization fuels microbial MeHg production in the water column (Cossa et al., 2009, 2011, 2018; Sunderland et al., 2009; Heimbürger et al., 2010; Kim et al., 2017). The most likely explanation is that particle-attached bacteria generate anoxic micro-niches within marine snow (Sunderland et al., 2009; Ortiz et al., 2015), where anaerobic bacteria can methylate Hg. The dissolved MeHg produced at depth is then available for bioconcentration into phytoplankton, which exhibit the largest concentration factor (at least up to 10,000-fold) along marine food chains (Schartup et al., 2018). Bioconcentration, biomagnification and bioaccumulation processes in the upper trophic levels control the biotic MeHg concentrations at each trophic step. Different forms of isotopic evidence support this new paradigm. A pioneering study explored the carbon isotope composition of the MMHg compound in tuna and found $\delta^{13}C$ values similar to marine organic matter, suggesting its role as the carbon substrate for Hg methylation (Masbou et al., 2015). Additional evidence comes from Hg isotopic analysis of marine biota. Fish that foraged at different depths in the North Pacific Ocean showed Hg isotope gradients that could only be explained if 60–80% of their MeHg was produced in the water column below the surface mixed layer and not in sediments (Blum et al., 2013).

In general, the depth, shape and importance of the MeHg peak in ocean waters depend on the physical structuring and biological productivity of water columns. Several studies found Hg methylation hotspots at the density gradients of stratified systems (Wang et al., 2012; Heimbürger et al., 2015; Schartup et al., 2015a; Soerensen et al., 2016a; Rosati et al., 2018). High MeHg concentrations have also been observed in the oxygen minimum zones of upwelling regions (Conaway et al., 2009; Cossa et al., 2011; Bowman et al., 2016). Two field studies (Baya et al., 2015; St. Pierre et al., 2015) and a modelling study (Soerensen et al., 2016a) suggest the potential for enhanced DMHg evasion from the Arctic Ocean, where MeHg is produced at shallow depths (Heimbürger et al., 2015).

A marine microaerophilic bacterium has been identified as a potential Hg methylator within sea ice, where the anaerobic bacteria which are known to methylate Hg were absent (Gionfriddo et al., 2016). This bacterium could potentially be responsible for Hg methylation in the open ocean water column (Sunderland and Schartup, 2016). However, laboratory experiments have not found a clear relationship between the expression level of the key genes in this bacterium and net MeHg production (Gomi-Urriza et al., 2015), pointing again to complex interactions.

7.3 How closely do Hg levels in aquatic biota respond to changes in atmospheric Hg, and why?

In addition to methylation and demethylation processes, many other processes and factors affect the uptake of Hg by aquatic biota (Eagles-Smith et al., 2018; Hsu-Kim et al., 2018). These include the transport and speciation of Hg between emission sources and terrestrial and aquatic systems (see earlier chapters of this report), biological uptake of Hg (both inorganic Hg and MeHg), and biomagnification of MeHg in the food webs. The complexity of these processes, along with the large inventories of legacy anthropogenic and natural Hg stored in terrestrial and aquatic systems (see Chapter 2), dictate that the biotic Hg trends may or may not follow the same trends as atmospheric Hg. Furthermore, even if they do follow similar trends, there could be a significant time lag between them. This section compares recent trends in atmospheric Hg with those in aquatic biota, and discusses why they may or may not follow each other. This is done by examining major recent studies since GMA 2013 on biotic Hg trends as summarized in four case studies. These case studies are from North America, Europe, China, and the Arctic where Hg concentrations in certain aquatic biota have been monitored continuously or intermittently for several decades. No such long-term, time series data for biotic Hg are available for other regions of the world, especially for the Southern Hemisphere. A more thorough review of biotic Hg concentrations is provided in Chapter 8.

7.3.1 Trends in atmospheric Hg concentration and wet deposition

Before presenting the case studies, this section first reviews the general trends in Hg concentrations in air and in wet deposition, with which the aquatic biotic Hg trends will be compared.

North America and Europe are considered together here because their overall atmospheric Hg concentrations and deposition fluxes have trended similarly over the past few decades (Zhang et al., 2016). Measured Hg concentrations in the air (Hg^0, or total gaseous Hg) declined by 10–40% between 1990 and 2010 across most of North America and Europe (Slemr et al., 2011; Cole et al., 2014; Weiss-Penzias et al., 2016), a pattern that has been matched by trends in Hg concentrations and fluxes in wet deposition (Prestbo and Gay, 2009; Zhang and Jaeglé, 2013; Brigham et al., 2014; Weiss-Penzias et al., 2016). This general declining trend agrees very well with the declining Hg point-source emissions in North America and Europe over the same period (AMAP, 2010; AMAP/UNEP, 2013) and has been reasonably reproduced by a recent model study with revised global Hg emissions inventories (Zhang et al., 2016; Figure 7.2). This model study accounted for the declining emissions from commercial Hg-containing products since 1990, corrected for shifts in the speciation of airborne Hg emissions related to air pollution control technology, and reduced the putative importance of atmospheric Hg emissions from artisanal and small-scale gold mining (ASGM).

However, a closer analysis of the observational data in Figure 7.2 suggests that this systematic declining trend may have become less clear and uniform, and even reversed, over the most recent decade (i.e., since ~2008). This is demonstrated by a recent study in North America (Weiss-Penzias et al., 2016). Gaseous elemental Hg concentrations in the air were found to have stabilized since 2008 with a flat slope against time. While Hg concentrations in wet deposition continued to decline at some sites, a widespread increasing trend has been observed in Hg concentrations in wet deposition throughout North America and especially in the central and western USA (Weiss-Penzias et al., 2016).

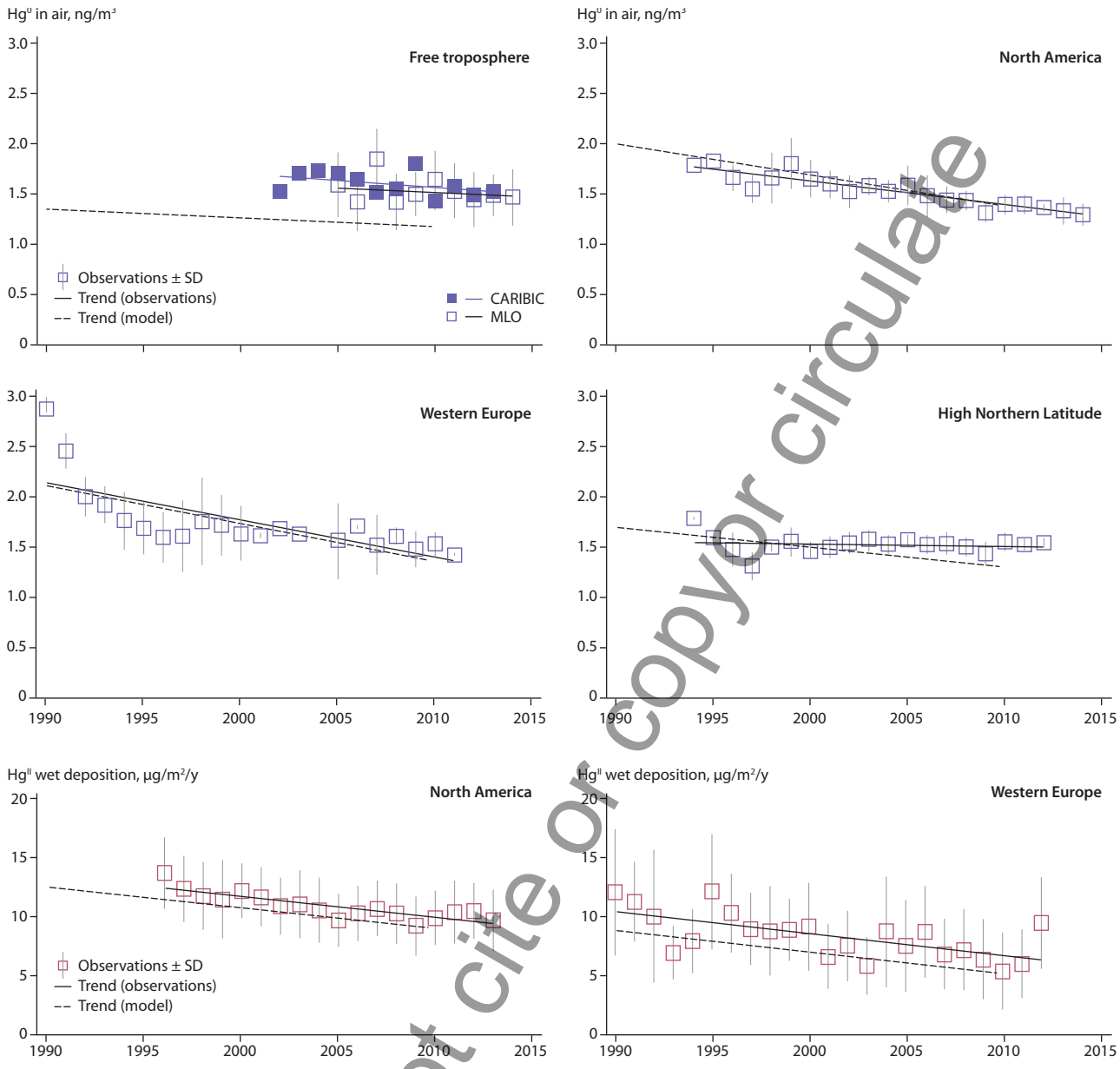

Figure 7.2 Observed and modelled trends for 1990 to 2013 in atmospheric gaseous elemental Hg concentrations (upper four plots) and divalent Hg^{II} wet deposition fluxes (lower two plots) in different regions of the Northern Hemisphere. Observations for individual years are shown as squares with linear regression as a solid line. The dashed line is the trend from the GEOS-CHEM simulation using the revised anthropogenic emissions inventory for 1990 and 2010. The data are averaged regionally across the free troposphere, North America, Western Europe, and high northern latitude regions. From Zhang et al. (2016).

Such a shift in the air Hg trends is not reproduced by the model of Zhang et al. (2016) (see Figure 7.2).

China is the largest national emitter of anthropogenic Hg to the atmosphere (Fu et al., 2015). In contrast to the global trend, anthropogenic Hg emissions in China increased rapidly from 1978 to as recently as 2007 at an average rate of ~5.5% per year, except for the period 1998–2000 when emissions decreased due to the Asian financial crisis, which led to a reduction in fuel consumption (Wu et al., 2016). Mercury emissions in China are reported to have plateaued around 2007 to 2010, and have shown a declining trend in the past few years (Wu et al., 2016). Available but limited data on atmospheric Hg concentrations over the past decade in China are in general agreement with this emissions trend. Direct measurements of Hg^0 at Guiyang (an urban site in southwest China) showed that annual mean Hg^0 concentrations increased at a rate of ~2.5% per year between 2002 and 2010 (Fu and Feng, 2015). Hg^0 concentrations also increased at Mt. Changbai (a remote site in northeastern China) at about the same rate from 2009 to 2013 but have since appeared to stabilize (Fu et al., 2015, 2016; Figure 7.3). Mercury passive sampling and plant biomonitoring on the Tibetan Plateau suggest that atmospheric Hg concentrations were stable during 2006 to 2009 and decreased during 2010 to 2015 (Tong et al., 2016).

In the *Arctic region* (above 60°N) atmospheric Hg^0 concentrations have also been declining, but at a markedly slower rate than elsewhere (see Figure 7.2). The observed and modelled trends also disagreed more than in other regions, with observed Hg^0 concentrations decreasing by 0.2±0.45% per year since 1994 compared to a modelled decrease of 1.3±0.11% per year. There are no decade-long observational data of Hg deposition flux available for the Arctic or subarctic regions; existing depositional data are limited to one to two years of measurements only (e.g., Sanei et al., 2010).

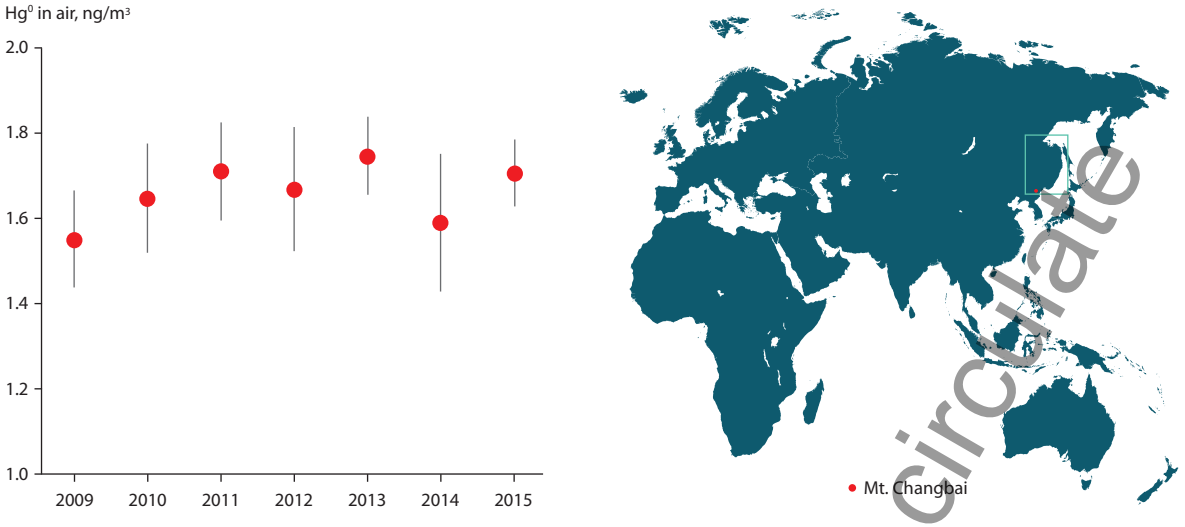

Figure 7.3. Annual mean gaseous elemental Hg concentrations measured at Mt. Changbai, a remote site in northeastern China (Fu et al., 2015).

7.3.2 Trends in Hg in aquatic biota and possible causes

7.3.2.1 Case Study 1: Fish and birds in lakes and coastal waters of North America

A large number of studies have reported inconsistent, diverging, or mixed temporal trends of Hg in aquatic biota throughout North America. The Great Lakes are an especially interesting study area because of the wide diversity of species monitored within the same general area, and the length of some of the biotic time trend datasets. Also, there is isotopic evidence from two predatory Great Lakes fish (lake trout *Salvelinus namaycush* and burbot *Lota lota*) which establishes that the atmosphere, rather than sediments or watershed soils, was the ultimate source of most of the Hg in fish tissues (Lepak et al., 2015). However, intervening ecological, geochemical or climatic processes may be acting to drive biological time trends along divergent paths. Blukacz-Richards et al. (2017) evaluated the temporal trends since the 1970s of Hg levels in eggs of a piscivorous bird (herring gull *Larus argentatus*), in two piscivorous fish (lake trout and walleye *Sander vitreus*), and in a planktivorous fish (rainbow smelt *Osmerus mordax*) in the Great Lakes. The results presented a mixed temporal pattern (Figure 7.4), with declining biotic Hg trends in all species in the first few decades (up to about the period 1995–2000), which matched the declining atmospheric Hg trend in North America (see Figure 7.2). After about 2005, however, trend reversals were detected in most but not all species at some sites. Zhou et al. (2017) also detected a breakpoint in fish Hg trends in the Great Lakes, with a significant decreasing trend before 2010 and no trend or an increasing trend since then.

Similar trend results were reported in fish populations across western Canada and the USA. When examining over 96,000 fish muscle samples from 206 species in over 4200 lakes, Eagles-Smith et al. (2016) found a significant, rapid decline in length-adjusted tissue Hg concentrations during the 1970s, with no subsequent significant trend up to 2012. In all these studies, the authors attributed the early decline in biotic Hg to regional and local declines in atmospheric Hg concentrations and deposition. They suggested that the subsequent trend reversal, or lack of a significant trend, were caused by factors such as increasing local emissions, food web changes, eutrophication and climate change.

Contrasting biotic Hg trends have also been reported for lakes in the same region. When examining temporal fish Hg trends in hundreds of small Ontario lakes in Canada, Gandhi et al. (2014) found a general decline in length-adjusted fish muscle Hg concentrations from the 1970s to 1990s for northern pike (*Esox lucius*), walleye and lake trout, followed by relatively small increases in some lakes starting about 1995–2000. Both the early declining trends and recent increasing trends were more pronounced in northern Ontario lakes than in southern Ontario lakes and more so in northern pike and walleye than in lake trout. In contrast, when examining changes in fish muscle Hg from 873 Ontario lakes, Tang et al. (2013) reported no significant decreases over the past several decades in any of the seven species (walleye, northern pike, lake trout, burbot, smallmouth bass *Micropterus dolomieu*, whitefish *Coregonus clupeaformis* and white sucker *Catostomus commersonii*). Instead, mean fish Hg concentrations were found to be slightly higher in the period 2005–2010 than in 1974–1981, and were significantly so in northern pike. Divergent trends are also reported in fish Hg in four small lakes within a national park in northern Minnesota (Brigham et al., 2014) and throughout the State of Massachusetts (Hutcheson et al., 2014) in the USA. Whereas the majority of these study lakes showed a decreasing trend in fish Hg between ~2000 and ~2010, a smaller set of lakes showed an increasing or no trend. The variety of trends in fish Hg among lakes from the same region clearly demonstrate the complexity of ecosystem responses to changes in atmospheric Hg concentration and deposition. Along the northeast coast of the USA, substantial reductions in muscle Hg (~30–40%) were reported between 1972–1974 and 2011 in a marine fish species, bluefish (*Pomatomus saltatrix*) (Figure 7.5) (Cross et al., 2015). However, the New York regional data suggest no further change in fish Hg levels up to 2007.

Most of these studies did not include stable carbon and nitrogen isotopic data, making it impossible to investigate whether changes in feeding behavior (prey trophic level and feeding location) influenced the Hg trends. The value of including trophic dynamic information in the interpretation of

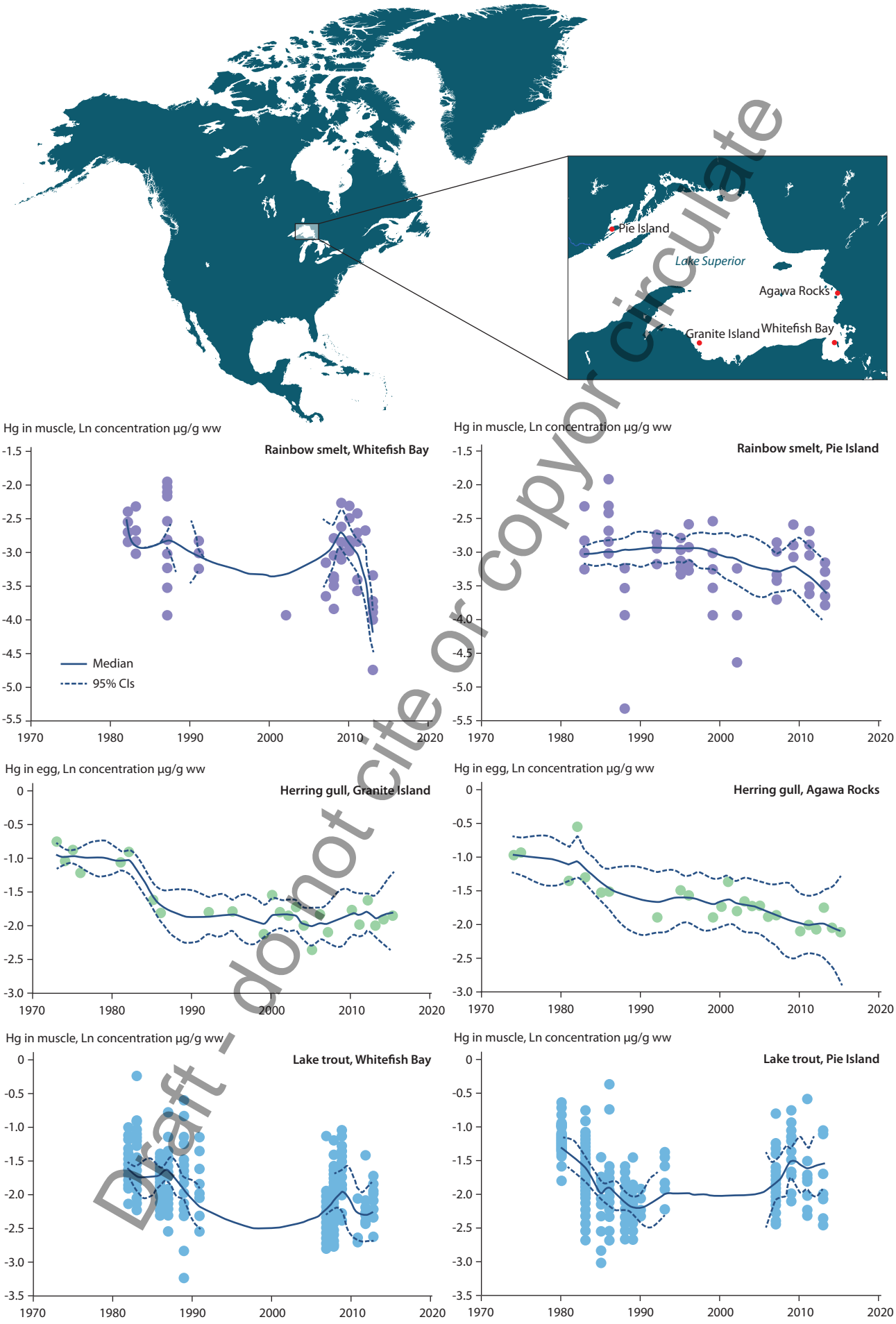

Figure 7.4. Mercury trends in fish and waterfowl of Lake Superior. The plots show Hg concentrations for rainbow smelt (planktivorous), lake trout (piscivorous) and herring gull (piscivorous). (Blukacz-Richards et al., 2017).

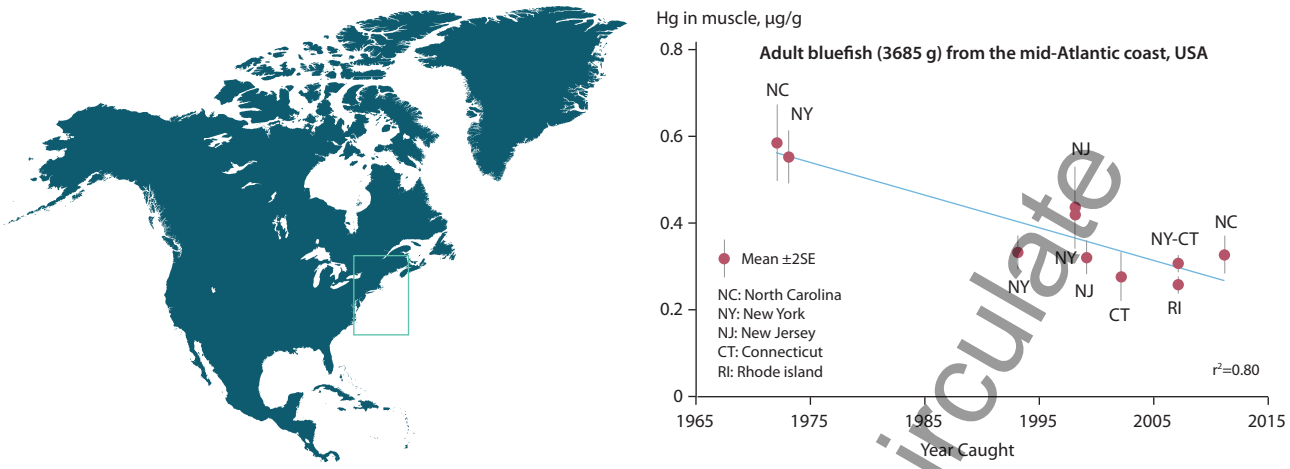

Figure 7.5 Mercury trends in the piscivorous bluefish (*Pomatomus saltatrix*) along the northeast coast of the USA from 1972 to 2011 (Cross et al. (2015).

Hg temporal trends was demonstrated by Burgess et al. (2013) in a study of Hg in herring gull eggs on the eastern Canadian seaboard. Between 1972 and 2008, two sites displayed a trend of significantly declining egg Hg, which is consistent with the declining atmospheric Hg deposition occurring at that time (see Figure 7.1). However, when trophic level changes over time were factored into the analysis using $\delta^{15}N$ isotope data, it was found that the Hg declines were due to feeding behavior shifts. $\delta^{15}N$ is a widely-used indictor of the trophic level of species' prey selection and was highly correlated with egg Hg in the birds. These results suggest that Hg in the coastal ecosystem in that region may have remained relatively constant over the past few decades despite the reduction in airborne Hg fluxes.

7.3.2.2 Case Study 2: Freshwater fish in Fennoscandia

Braaten et al. (2017) and Åkerblom et al. (2014) assessed the spatial and temporal trends of Hg in various species of freshwater fish (e.g., northern pike, Eurasian perch *Perca fluviatilis*, brown trout *Salmo trutta*, Arctic char *Salvelinus alpinus*, roach *Rutilus rutilus*) over the past 50 years (1965–2015) based on 54,560 observations from 2775 lakes across Fennoscandia (Sweden, Finland, Norway, and the Kola Peninsula in Russia). Some of the lakes were impacted by historical local industrial emissions of Hg directly to surface water, whereas others were impacted primarily by atmospheric Hg deposited onto catchment soils as well as water surfaces.

As expected, lakes that were affected by local pollution sources had higher mean observed fish Hg concentrations than lakes that were predominantly affected by atmospherically deposited Hg. When the fish Hg concentrations are normalized to a standard 1-kg pike, the Hg concentrations in '1-kg pike equivalent fish' showed a consistent and significant decreasing trend for the entire database (Figure 7.6). This declining trend matches well with the general declining atmospheric Hg trend over northern Europe (see Figure 7.2). Of particular interest is the finding that the declining fish Hg trend was much stronger for the entire database than for lakes only impacted by atmospheric Hg deposition. This could suggest that reduced Hg emissions, especially a reduction in local emission sources, lead to lower Hg in fish. However, Braaten et al. (2017) noted that the temporal trends varied with different standardization methods and cautioned that a better understanding of possible

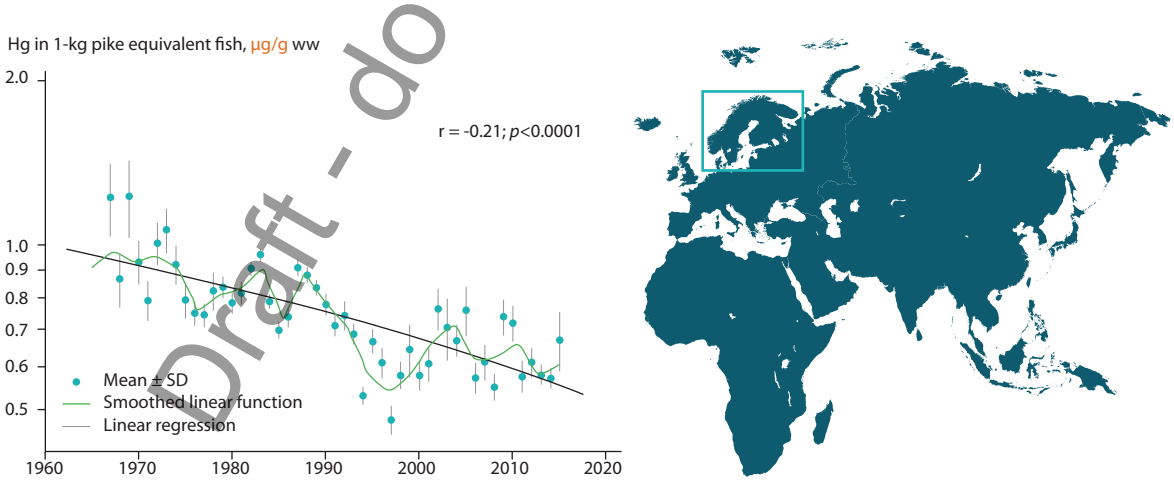

Figure 7.6. Mercury concentrations in five main freshwater fish species (Arctic char, brown trout, perch, pike and roach) over the past 50 years (1965–2015) in lakes across Fennoscandia. ~~Map in upper panel shows the locations of the 2775 lakes and the mean observed fish Hg concentration (without normalization) in each of the lakes.~~ The ~~lower~~ plot shows the temporal trend of fish Hg concentrations after being normalized to 'standard 1-kg pike Hg concentrations'. Data from Braaten et al. (2017).

CS: This graphic is missing the map showing spread of concentrations without normalization - i.e. colored dots across Europe. It is necessary for what is said in the text. The other locator map is not needed.
Author comment: if the bottom left panel is too complicated it can be left out
SW to obtain a file for this if possible. (26/4/2018)

confounding environmental processes (such as the impact of temperature and dissolved organic matter) is needed prior to concluding that the two declining trends are causally linked.

Also of note is that some of the lakes in Sweden were treated with lime in the 1970s and early 1980s to mitigate the impact of acidification. Fish Hg concentrations in these 'limed' lakes were found to be consistently higher than in lakes that were never-limed (Åkerblom et al., 2014), pointing to a significant effect on fish Hg from pH or other indirect ecosystem processes caused by lime treatment. The temporal trends in both limed and non-limed lakes are, however, similar (Åkerblom et al., 2014).

7.3.2.3 Case Study 3: Fish in reservoirs in North America and Europe versus China

Some of the longest time series of aquatic Hg data exist for man-made reservoirs due to concerns about the effects of impoundment on Hg methylation rates and thus on fish Hg levels. Although these reservoirs are not natural habitats for aquatic life they contain abundant fish and invertebrate communities and support important recreational fisheries in some areas and large aquaculture operations in others.

Studies in North America and Europe have shown that following impoundment, the large influx of flooded vegetation and organic matter in submerged soil stimulates microbial methylation of Hg, resulting in a sharp increase in fish Hg due to biomagnification of MeHg (Lucotte et al., 1999; St. Louis et al., 2004; Hall et al., 2005; Bodaly et al., 2007). Mercury methylation rates and fish Hg concentrations typically decrease as the reservoir ages and the organic matter further decomposes (Bodaly et al., 2007). This was demonstrated in a recent analysis of the temporal trends of Hg in a range of fish species from 883 reservoirs across western North America (Willacker et al., 2016). Temporal patterns (normalized for confounding variables such as species and body length) were clearly related to the time elapsed since reservoir impoundment, with maximum fish Hg concentrations being reached on average three years after the impoundment (Figure 7.7). Fish Hg concentrations thereafter declined relatively rapidly for four to 12 years, followed by a monotonic slow decline over many decades. Because the reservoirs were built at different dates over the past 150 years it may be concluded that the fish Hg trends are not directly related to changing atmospheric Hg deposition. Instead, water storage management is shown to be a key factor influencing this temporal pattern. Fish in reservoirs that experienced maximum drawdown during summer months (May–July) exhibited significantly higher concentrations (up to 11-fold) than fish in reservoirs in which drawdown occurred during other times of the year (Willacker et al., 2016).

As noted by Hsu-Kim et al. (2018), however, reservoirs in China present a different story. Unlike reservoirs in North America and Europe which are typically inhabited by native fish populations, reservoirs in much of China support aquaculture activities with fish harvested for human consumption. The fish in Chinese reservoirs thus tend to grow faster and are harvested younger. Therefore, the fish Hg concentrations from these reservoirs are typically low due to biodilution. However, monitoring of fish Hg concentrations in most of the Chinese reservoirs only started recently, making it impossible to deduce long-term temporal trends. One exception is the reservoirs in the Wujiang Basin in southwest China where extensive studies have been carried out in the past decade. Since these reservoirs vary greatly in age (time since their initial impoundment) an interesting evolution scheme in fish Hg concentrations starts to emerge when the data from all reservoirs are pooled (Feng et al., 2018).

The Wujiang River is the largest tributary of the upper Changjiang (Yangtze River). Since the 1960s, numerous large cascade reservoirs have been or are being constructed in the Wujiang Basin, including Wujiangdu (built in 1979), Dongfeng (1994), Puding (1994), Yingzidu (2003), Suofengying (2003), Hongjiadu (2004), and Pengshui (2008) on the main stream,

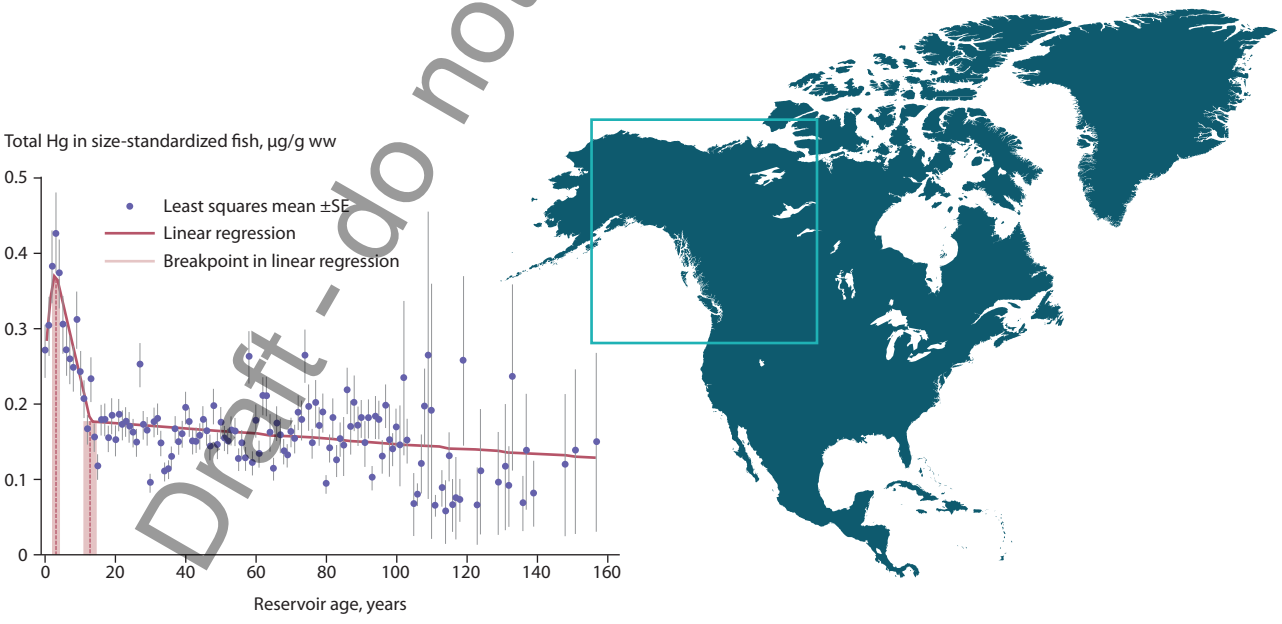

Figure 7.7 Fish tissue Hg trends from reservoirs across western North America. The data show least squares mean total Hg concentrations in size-standardized fish. Least squares means account for the effects of ecoregion, waterbody, species, and sampling year. Vertical red lines and shaded regions indicate estimated breakpoints (±standard error) from segmented linear regression (solid line) on fish Hg concentration when accounting for the effects of ecoregion, waterbody, species, and sampling year. From Willacker et al. (2016).

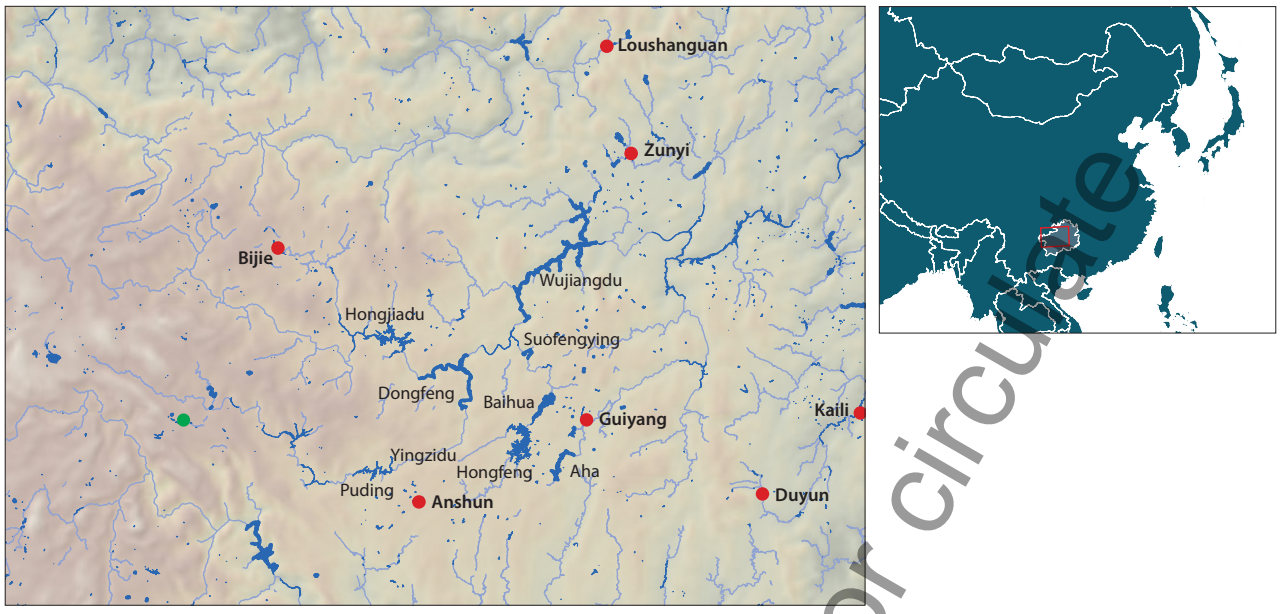

Figure 7.8 Reservoirs in the Wujiang River Basin, southwest China. From Feng et al. (2018).

and Aha (1960), Baihua (1966), and Hongfeng (1966) on its tributaries (Figure 7.8). Although impoundment was found to have significantly increased fish Hg concentrations in a newly constructed reservoir (Pengshui) (Li et al., 2013), fish Hg concentrations in this and another newly constructed reservoir (Hongjiadu) (Yao et al., 2011) were much lower than those in newly built reservoirs in North America and Europe (Yao et al., 2011; Li et al., 2013). For the much older Baihua reservoir, no statistically significant differences were observed in Hg concentrations in common carp (Cyprinidae) among the four sampling campaigns from 2003 to 2011, more than 40 years after the impoundment (Liu et al., 2012). In general, Hg concentrations in the various fish species studied, including carnivorous, omnivorous, planktivorous, and herbivorous fish, were remarkably low in all these reservoirs regardless of the age of the reservoir (Li et al., 2009, 2013; Yan et al., 2010; Yao et al., 2011; Liu et al., 2012), often an order of magnitude lower than the Codex guideline levels for MeHg in fish (i.e., predatory fish, 1.0 mg/kg; non-predatory fish, 0.5 mg/kg; wet weight) (FAO/WHO, 2011).

While biodilution and simple (short) food web structures clearly contribute to the generally low fish Hg concentrations (Feng et al., 2009a,b; Larssen, 2010; Meng et al., 2010, 2016; Yan et al., 2010; Yao et al., 2011; Liu et al., 2012), comparisons of fish Hg concentrations in reservoirs of different age in the same basin reveal three distinct stages of evolution due to changes in the source and concentration of organic matter in the submerged soil/sediment as the reservoir ages and cage aquaculture activities increase (Figure 7.9) (Feng et al., 2018). As much of the Wujiang Basin is located in a karst (eroded limestone) environment, the organic matter contents of the soils (typical range: 1.9–4.1%) are much lower than those in submersed soil (typically 30–50%) from the boreal forest or wetlands in North America and Europe (Lucotte et al., 1999; St. Louis et al., 2004; Hall et al., 2005; Yao et al., 2011). In addition, conditions were slightly alkaline in most of the reservoir water, which could restrain Hg methylation (Meng et al., 2010; Yao et al., 2011). Primary productivity in the newly constructed reservoirs in the Wujiang Basin is also low (oligotrophic–mesotrophic) due to the absence of cage aquaculture fishing (Meng et al., 2010, 2016; Yao et al., 2011) and thus the autochthonous contribution to organic matter is also very limited (Jiang, 2005; Yao et al., 2011). Therefore, in contrast to their counterparts in Europe and North America, the newly constructed reservoirs in the Wujiang Basin are not active sites of net Hg methylation due to the low organic carbon content in the submersed soils and/or low primary productivity (Meng et al., 2010; Yao et al., 2011). Consequently, the newly constructed reservoirs, such as Suofengying, Hongjiadu, and Yingzidu on the Wujiang River, are not a net source of MeHg and instead represent a net sink (Guo, 2008) (Figure 7.9 upper).

As these reservoirs became more productive (mesotrophic to eutrophic) with time, the organic matter content in the sediment increased due to continuous increases in autochthonous productivity due to the cage aquaculture activities. This tended to promote *in situ* Hg methylation, and as such reservoirs at this stage (e.g., Dongfeng and Puding) have transited from a net MeHg sink to a net MeHg source (Guo, 2008; Feng et al., 2009a,b; Zhang et al., 2009) (Figure 7.9 middle). Over the long-term evolution of the reservoir, primary productivity continues to increase and the reservoir will eventually become eutrophic. Phytoplankton-derived organic matter, and fish feed and feces become significant sources of organic matter input to the surface sediments, as shown in Wujingdu (Feng et al., 2009a; Zhang et al., 2009; Meng et al., 2010, 2016). The increased oxygen consumption during fresh organic matter degradation causes progressively more anoxic conditions at the sediment-water interface (Meng et al., 2010, 2016), which promotes the microbial Hg methylation processes (Figure 7.9 lower), as shown in Wujingdu (Guo, 2008) where both the surface sediment and the hypolimnetic water were sites of net MeHg production (Feng et al., 2009a; Meng et al., 2010, 2016). Thus, in contrast to fish in North American reservoirs, and despite the relatively high atmospheric Hg loading across much of China, fish Hg levels in Chinese impoundments reflect within-impoundment processes, especially organic matter loadings to sediments, water/soil quality, food web structure, and biodilution, rather than atmospheric inputs (Feng et al., 2018).

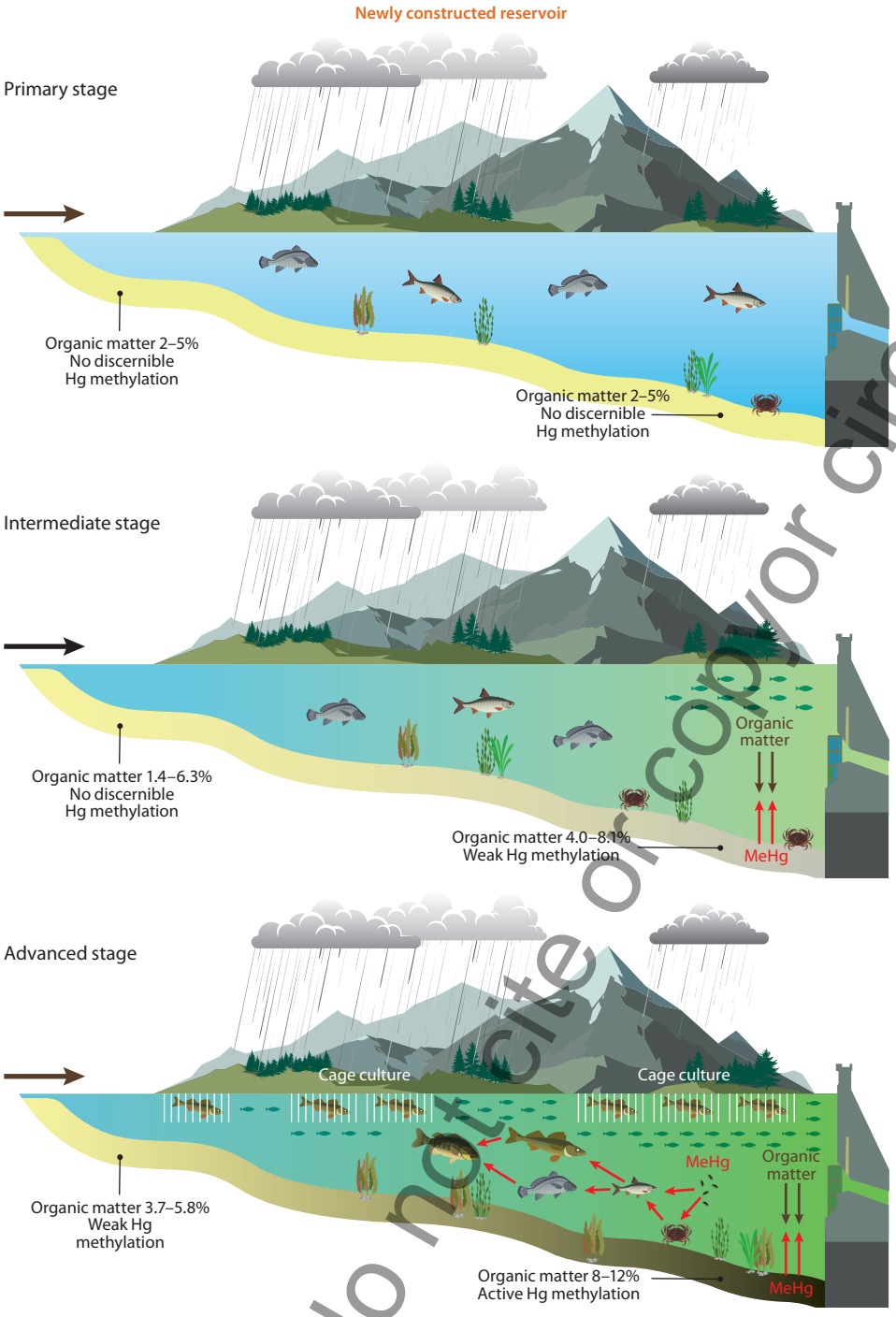

Figure 7.9 Conceptual models of Hg cycling in primary, intermediate, and advanced evolutionary stage reservoirs in the Wujiang River Basin, Southwest China. From Feng et al. (2018).

7.3.2.4 Case Study 4: The Arctic

Rigét et al. (2011) summarized all available temporal Hg datasets on Arctic biota up to about 2009 and found that some species in some locations had shown significant increases over recent decades, while others with closely adjacent or overlapping distributions exhibited non-significant changes. Most of the increasing biotic Hg trends occurred in marine species in the North American and West Greenlandic sector of the Arctic, whereas declining trends were mostly observed in East Greenlandic and European Arctic biota. This regional dichotomy is clearly seen in the hair of polar bears (*Ursus maritimus*) and has been suggested to be due to increased emissions from Asia entering the western Arctic coincident with decreasing emissions from North America and Europe in the eastern Arctic (Dietz et al., 2006).

A few additional studies have since been published. Rigét et al. (2012) analyzed temporal trends of Hg in livers of ringed seals (*Pusa hispida*) collected from the early 1980s to 2010 from Greenland. Increasing levels of Hg were found in ringed seals in two out of three Greenlandic seal populations (Central East and Northwest Greenland), rising at a rate of 10.3% per year and 2% per year, respectively. In addition to age and trophic position the study showed that the Atlantic Oscillation Index, a parameter related to climate variability was positively associated with Hg concentrations in seals although the specific mechanism involved was not clear.

By analyzing Hg in the teeth of polar bear from Svalbard in the Norwegian Arctic, Aubail et al. (2012) reported a decreasing trend in Hg concentration over the period 1964–2003 (Figure 7.10). Since no temporal changes were found in tooth $\delta^{15}N$ and $\delta^{13}C$ they concluded that the decrease in Hg was

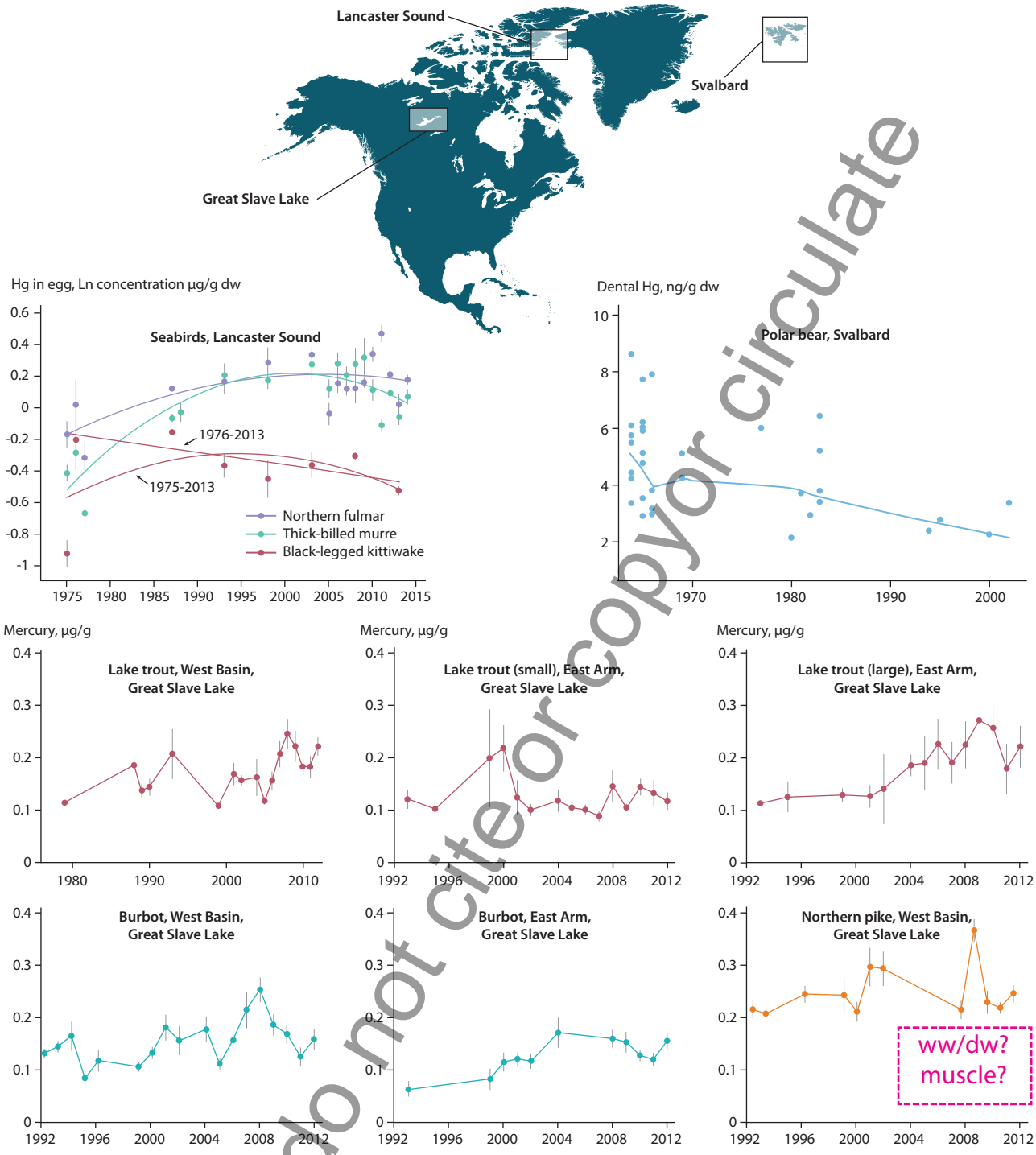

Figure 7.10 Mercury trends in Arctic aquatic biota. The data were derived from several sources: annual mean Hg concentrations adjusted for trophic position in eggs of thick-billed murres, northern fulmars, and black-legged kittiwakes from Lancaster Sound, Nunavut, 1975 to 2014 (Braune et al., 2016); for dental Hg concentrations in polar bears (aged three to 10 years) from Svalbard, smoothing lines (robust, locally weighted scatter plot smoothing system based on the LOWESS algorithm) represent the fitted non-linear trend of the values (Aubail et al., 2012); and Hg concentrations in burbot, lake trout [and northern pike] were collected from the West Basin and East Arm of Great Slave Lake, Northwest Territories, Canada (Evans et al., 2013).

not due to changes in trophic dynamics; instead, it was more likely to be due to a lower environmental Hg exposure in the region. McKinney et al. (2017) also reported a significant declining trend in hair Hg of the southern Beaufort Sea polar bear population, at an average rate of -13% per year between 2004 and 2011. This dataset differs from the general west-east pattern in Arctic biota Hg trends noted above. However, only males in the southern Beaufort Sea area exhibited significant decreases; females from the same area showed no significant trend. Mercury levels in the bears' main prey (ringed seal) also showed no change up to 2007 (Gaden et al., 2009), which argues against changes in Hg inputs or the biogeochemical Hg cycle as contributing to the decline. Analyses of body condition and diet led to the conclusion that the bears' Hg trend was due to changing foraging patterns over time and not to alteration in environmental Hg levels (McKinney et al., 2017).

Braune et al. (2014) reported the temporal trend of Hg in thick-billed murre (*Uria lomvia*) eggs from Coats Island, northern Hudson Bay, and Prince Leopold Island in Lancaster Sound, Nunvut. Although there was no significant change in

Hg concentrations in murre eggs from Coats Island from 1993 to 2013, $\delta^{15}N$ values for the eggs were found to be decreasing significantly, suggesting a decline in trophic position for the bird due to a dietary switch from Arctic cod (*Boreogadus saida*) to capelin (*Mallotus villosus*). After adjusting egg Hg concentrations for the decline in trophic position, time trends in Hg concentration at Coats Island changed from non-significant to significantly increasing. In contrast, at Prince Leopold Island, after adjustment for trophic position the egg Hg time trends changed from non-significant to significantly decreasing over the same period. These results suggest that in addition to trophic change in diet, there may have been other geographic factors at play that influenced Hg concentrations at the base of the marine food web, such as differences in Hg deposition or in Hg bioavailability related to climate change.

Subsequently, Braune et al. (2016) updated the Hg trends in High Arctic seabird eggs at Prince Leopold Island to 2014 for five species: thick-billed murre, northern fulmar (*Fulmarus glacialis*), black-legged kittiwake (*Rissa tridactyla*), black guillemot (*Cepphus grylle*), and glaucous gull (*Larus hyperboreus*). Eggs from the first three species had been collected from the Island as early as 1975, while the guillemots and gulls were sampled from 1993 to 2013. Egg Hg trends were adjusted for possible shifts in trophic position of the birds using $\delta^{15}N$ data. Adjusted Hg concentrations in eggs of murres, fulmars and kittiwakes increased from 1975 to the 1990s, followed by a plateauing or slight decline from the 1990s to 2014 (Figure 7.10). However, the kittiwake trend was strongly influenced by the 1975 samples; when these were excluded, kittiwake eggs actually displayed a significant decreasing trend from 1976 to 2013. Trends in the eggs of murres, fulmars, kittiwakes, and guillemots had negative slopes between 1993 and 2013. The pattern in glaucous gull eggs was unique: decreasing by 50% from 1993 to 2003 before increasing again.

Braune et al. (2016) concluded that the general increasing trends in egg Hg during the 1970s and 1980s were consistent with atmospheric Hg increases over the Arctic *during that period*. They noted that the migratory habits of the five bird species, which overwinter in different southern regions away from Lancaster Sound, complicated interpretation of the reasons for the temporal trends. Environmental Hg changes in their wintering areas could have been different to those in the Arctic. Interpretation is also complicated by significant differences in the findings from glacier archives of atmospheric Hg on the western and eastern edges of the North American Arctic. Greenland glacial snow/firn (Faïn et al., 2009) showed a monotonic decline in atmospheric Hg^0 concentrations during the 1970s and 1980s, following peak levels in the 1950s to 1960s. Glacial snow and ice core reconstructions of atmospheric Hg deposition from Mt. Logan (Yukon) showed increases in deposition through the 1990s, which could be an indication of increasing trans-Pacific contamination from Asia (Beal et al., 2015). Overall, these data, especially the declining Hg^0 trend on Greenland through the 1970s and 1980s, are inconsistent with Braune et al.'s (2016) conclusions. However, the flat or slightly declining egg Hg data from about 1990 onwards is consistent with the recent modelling of atmospheric Hg^0 in the Arctic (see Figure 7.2). Zheng (2015), on the other hand, reported that 20th-century total Hg accumulation in a Greenland ice core was relatively constant until increasing during the 1970s to 2000s, a pattern similar to those in most of the bird species but not in agreement with the Zhang et al. (2016) modelling. Thus, uncertainty about the actual trends in Arctic atmospheric Hg deposition is a limiting factor in assessing agreement between environmental and biological Hg trends in this region.

In Great Slave Lake in the western Canadian Arctic, temporal trends of Hg in lake trout, burbot, and northern pike were monitored irregularly between the late 1980s or early 1990s and 2012 (Evans et al., 2013; Figure 7.10). Muscle Hg data were adjusted for fish length, but not for trophic shifts over time. Mercury concentrations generally increased over time in lake trout and burbot but not in northern pike, with considerable interannual variation. These increasing or flat patterns are inconsistent with atmospheric Hg^0 concentrations and wet deposition fluxes that were declining at the time (see Figure 7.2) and with the Mt. Logan atmospheric deposition record of Beal et al. (2015). Statistical analysis of climate factors suggested that varying annual mean air temperatures, and particularly cold season temperatures, were related to the fish Hg patterns although a precise mechanism linking temperature to fish Hg could not be elucidated (Evans et al., 2013).

7.3.3 Causes of the match and mis-match between aquatic biota and atmospheric Hg trends

In contrast to the recent decadal datasets described in the previous section, the available century-scale biotic Hg trends since the pre-industrial era (from the Arctic; Dietz et al., 2009) generally matched remote glacial ice core archives showing increasing atmospheric Hg deposition and Hg^0 concentrations after about 1850 (Beal et al., 2015; Zheng, 2015; Kang et al., 2016; see Chapter 2). In both cases, starting in the mid- to late-19th century, and shortly after major anthropogenic uses and emissions of Hg became more common, Hg concentrations in the atmosphere and in aquatic biota increased steadily up to maxima typically attained at about the 1970s–1980s (Dietz et al., 2009; Rigét et al., 2011). The longer-term datasets thus clearly indicate the effects of anthropogenic contamination of aquatic systems on biotic Hg concentrations and trends over the century or more after about 1850.

As anthropogenic emissions to air began to stabilize after the 1970s, it became increasingly apparent that a mis-match between the aquatic biotic and atmospheric Hg trends was occurring in some areas, and in some co-occurring species in specific areas. In other areas and species, however, the atmospheric and biotic trends continued synchronously. The divergent patterns of match and mis-match between the atmosphere and biota have become more apparent over the past two decades or longer, as atmospheric and biological monitoring became more widespread and frequent.

Fundamentally, the mis-matches may be generally attributed to the large inventories of legacy Hg in soil and ocean reservoirs, and the exceptional sensitivity of Hg biogeochemical cycling to changes in climatic (e.g., temperature, light, hydrology), geochemical (e.g., pH, redox status, complexing ligands), biological (e.g., feeding behavior of an organism) and ecological (e.g., organic carbon flux, microbial processes, food web structure and dynamics) conditions (Table 7.1; see also Hsu-Kim et al., 2018). Some of the major processes that trigger changes in these conditions, and thus cause the decoupling between biotic and environmental Hg include changes in the soil and terrestrial environment, changes in the aquatic ecosystem, and climate change.

Table 7.1 Unique properties of Hg and implications for its biogeochemistry (Wang and Zhang, 2013)

Property	Implications
Redox between Hg^0 and Hg^{II}	Sensitive to changes in pe and pH; Sensitive to photochemical and microbial processes
High vapor pressure of Hg^0	Sensitive to changes in temperature; Long-range atmospheric transport; A global problem needing global solutions
Hg^{2+} ions being one of the softest Lewis acids	Strong affinity to ligands (e.g., reduced sulfides, halogens); Sensitive to changes in organic carbon
Methylation is primarily microbial, with MeHg being the most bioavailable and toxic	Sensitive to changes in organic carbon, nutrients, redox and microbial processes; Direct source control of MeHg difficult
MeHg biomagnifies in the food chain	Sensitive to changes in food web structure and dynamics

7.3.3.1 Changes in the soil and terrestrial environment

Globally the terrestrial environment represents the largest inventory of Hg (~1000 kt), with ~150 kt stored in surface organic soils (Figure 2.3, Chapter 2). Terrestrial biota are much less prone to Hg bioaccumulation as the conversion of inorganic Hg to MeHg is not favored in the terrestrial environment (Fitzgerald and Lamborg, 2014). Also, on a global scale, anthropogenic inputs have altered the Hg inventory in the soils to a lesser degree than in the oceans due to the naturally large mass of Hg that was present in terrestrial systems (see Figure 2.3). However, major changes in landscape and land-use in the watershed (such as urbanization, agricultural activities, flooding, damming, and deforestation) not only affect the net release of soil Hg to downstream aquatic systems (inland and coastal), more importantly they change the organic carbon flux and redox (pe) conditions that directly influence Hg methylation processes in the aquatic systems. The importance of such changes is perhaps best demonstrated by reservoir construction in the watershed. As shown in Case Study 3, fish Hg concentrations in reservoirs are primarily controlled by the influx and dynamics of terrestrially-derived organic carbon and Hg, and bear almost no relationship with trends in atmospheric Hg concentrations or deposition, even decades after reservoir impoundment.

7.3.3.2 Changes in the aquatic ecosystem

As MeHg biomagnifies in the food web (i.e., MeHg concentration increases from prey to predator), any changes in ecosystem structure, function and dynamics would result in major changes in Hg concentrations within the ecosystem. Processes such as acidification/liming (Case Study 2) and eutrophication (Case Study 3) affect not only MeHg production (see Section 7.2) by altering Hg speciation and bioavailability, but also Hg food-chain transfer and thus biotic Hg concentrations by altering species composition, biomass and growth rates (e.g., Clayden et al., 2013; Jardine et al., 2013). Aquaculture, overfishing, and invasion of non-native species can change not only the nutrient status of an aquatic ecosystem but also the structure, function, and dynamics of food webs, and thus could result in major changes in biotic Hg.

7.3.3.3 Climate change

On the global scale, climate change is the most prevalent contributor to the mis-match between biotic and environmental Hg. The impact of climate change on biotic Hg is perhaps most profoundly felt in the Arctic, where rapid climate warming has resulted in dramatic changes in many biogeochemical and ecological processes that drive Hg cycling (Wang et al., 2010; Stern et al., 2012). For instance, the rapid decline in the aerial coverage and thickness of Arctic sea ice and the replacement of multi-year sea ice by first-year ice have been shown to influence Hg distribution and transport across the ocean–ice–atmosphere interface, alter Hg methylation and demethylation rates, promote changes in primary productivity, and shift food web structures (bottom-up processes) (Chaulk et al., 2011; Beattie et al., 2014; Wang et al., 2017). The very large mass of mainly natural Hg found in northern permafrost deposits, which is projected to be released with further climate warming may profoundly affect biotic Hg levels around the Northern Hemisphere, especially as large amounts of organic carbon that may stimulate Hg methylation rates will be simultaneously released (Schuster et al., 2018).

Changes in animal social behavior associated with changing sea-ice regimes can also potentially affect dietary exposure to Hg (top-down processes) (Stern et al., 2012). As shown in Case Study 4, as sea ice declined in their feeding areas, thick-billed murre from Coats Island in northern Hudson Bay altered their feeding strategy to prey on a lower trophic level, open-water species (capelin) instead of Arctic cod which is an ice-associated species (Braune et al., 2014). This change would have tended to reduce the birds' Hg exposure. However, the population's egg Hg concentrations did not change significantly between 1993 and 2013; thus, to explain this stable trend the availability of MeHg in the environment and efficiency of Hg food web transfer must have increased. It has also been suggested that climate warming may cause a shift in energy flow from benthic to pelagic food webs as aquatic productivity increases in High Arctic lakes. Since zooplankton species such as *Daphnia* contain higher MeHg than benthic organisms, this shift could increase Hg transfer in the food web (Chételat and Amyot, 2009). The impact of climate change on biotic Hg has also been observed in lower latitude regions (e.g., Pinkney et al., 2014).

7.3.4 Implications for the effects on biotic Hg of regulatory action on atmospheric Hg emissions

Reports of biotic Hg trends not following the atmospheric Hg trends in recent decades should not be regarded as discouraging news when considering the efficacy of regulations to reduce atmospheric and other releases of Hg. The fact that the effectiveness of Hg emission control is expected to be followed by long delays before an ensuing reduction is seen in food-web Hg levels makes it all the more pressing to control and reduce Hg emissions as early as possible (Wang et al., 2010).

Wang et al. (2010) and Wang and Zhang (2013) proposed that the mis-match between biotic and environmental Hg trends is an indication that an aquatic ecosystem has entered a new paradigm in which the key controls on Hg bioaccumulation have switched from being emissions-driven to processes-driven. This switch occurs because the biotic Hg concentrations in an aquatic ecosystem are influenced not only by Hg influx (natural

or anthropogenic) to the system, but also by the internal processes in the ecosystem that control the recycling, speciation, bioavailability, methylation and biological uptake of Hg. As the accumulated mass of legacy Hg in a waterbody becomes large relative to the loading rate of newly emitted Hg, the internal biogeochemical processes that control its permanent removal (e.g., burial), re-emission, or uptake into the biota, increasingly become the determining steps in bioavailability and bioaccumulation.

The changing relationship over time between atmospheric Hg concentrations (or deposition) and biotic Hg is shown in Figure 7.11. Prior to anthropogenic influences (the exact timeline is subject to debate; see Chapter 2), when Hg emissions were at their natural level, the flux of Hg to the aquatic system was generally low, and so were its biotic concentrations (Phase I – 'Pre-anthropogenic background'). At around the mid-19th century, however, as rapid industrialization resulted in a sharp increase in anthropogenic Hg emissions, aquatic biota Hg concentrations responded rapidly due to increasing Hg deposition, exposure and uptake of Hg from a small but growing environmental Hg inventory (Phase II – 'Emissions-driven'). This phase is clearly seen in long-term retrospective studies of Hg levels in Arctic biota (Dietz et al., 2009). Once an aquatic ecosystem has accumulated sufficient Hg, additional increases in Hg influx become secondary to the amount that has been accumulated in the system after decades to centuries of loading (i.e., legacy Hg). Bioaccumulation then draws predominantly on this legacy Hg which is operated on by the internal biogeochemical processes (Phase III – 'Internal Processes-driven'). Throughout these three phases, biogeochemical processes (shown as sine-wave 'noise' in Figure 7.11) determine the transport of Hg from the abiotic part of the ecosystem to biota, but it is in Phase III that these processes emerge to create a variability that is large enough to obscure the external Hg emission trends and hence produces the mis-match between biotic and atmospheric Hg trends (Wang et al., 2010).

In the context of Hg emission controls mandated by the Minamata Convention, a new phase, Phase IV, can be envisioned (see Figure 7.11), based on observations of biotic Hg trends in the recent past (see Section 7.3.2) and predictions from modelling efforts of seawater Hg concentration trends in the future (see Chapter 2.4). As anthropogenic Hg emissions decrease, atmospheric Hg concentrations will decrease and eventually stabilize at a new steady state. However, recycling of the large quantities of legacy anthropogenic Hg presently contained in the world's oceans and soils, and revolatilization between oceans, soils and the atmosphere, means that atmospheric and dissolved Hg concentrations are likely to decrease much more slowly than changes in Hg emissions. While biotic Hg concentrations are also projected to decrease over the long term, the current phase of processes-driven bioaccumulation dictates that it will take much longer to establish a new steady-state in biotic Hg. The biotic Hg concentrations at the new steady-state are also likely to remain above the Holocene background levels for an extended period after atmospheric Hg levels have returned to natural levels, because of the continued presence of legacy Hg in aquatic and terrestrial systems. In the shorter term, in fact, aquatic biotic Hg concentrations in many instances, especially in some marine ecosystems, are likely to continue to increase despite recent emission controls (Sunderland and Selin, 2013). Biota in smaller waterbodies such as lakes and coastal marine systems with restricted water mass turnover are more likely to respond relatively rapidly to emissions controls.

Examples of this long and uneven recovery in biotic Hg can be found following the impoundment of a river, or following 'de-acidification' of a lake. As shown in Case Study 3, fish Hg in reservoirs decreases a few years after the impoundment but remains above the pre-impoundment level even after more than a century (see Figure 7.7). In the 1970s, liming was applied to many Swedish lakes that were acidified due to atmospheric acid deposition, to help restore the lake ecosystem. Following the liming, fish Hg in those lakes declined by 10–20% by the 1990s (Meili, 1995) and continued to decline to the present day (Åkerblom et al., 2014). Yet, more than 30 years after the liming, fish Hg concentrations in these lakes remained considerably higher (twice as high on average) than those in lakes that were not impacted by acidification (and not subject to liming) (Åkerblom et al., 2014).

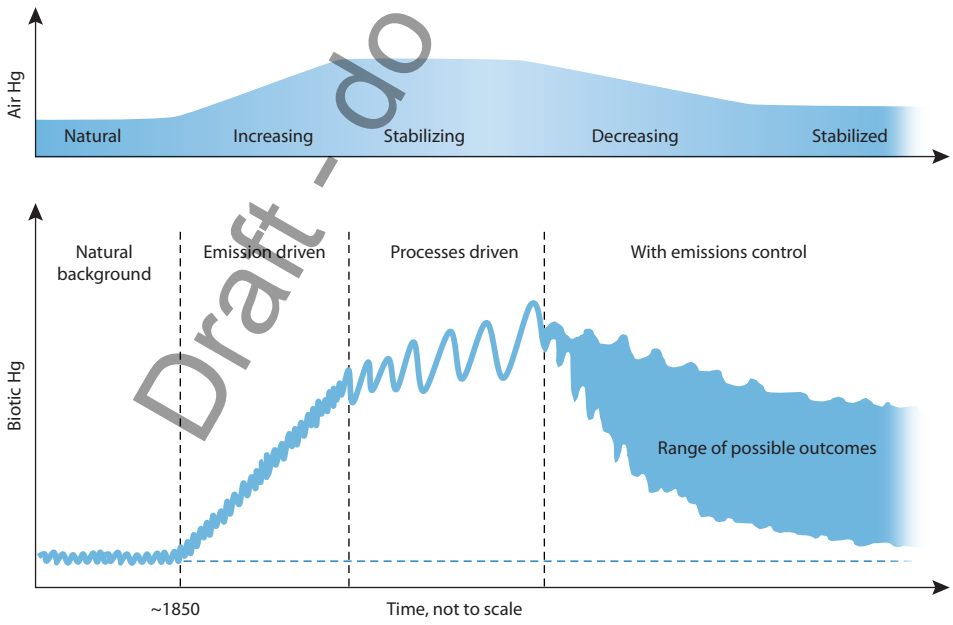

[GMA07-0100]Figure 7.11 A schematic representation of evolution in the Hg concentrations in the air (top panel) and aquatic biota (bottom panel), showing changes over time in the principal drivers of Hg bioaccumulation. Modified from Wang et al. (2010).

Note – includes not yet approved revision proposal

7 Mercury concentrations in biota

Authors: David Evers, Josh Ackerman, Staffan Åkerblom, Dominique Bally, Nil Basu, Joel Blum, Nathalie Bodin, David Buck, Paco Bustamante, Celia Chen, John Chetelat, Monica Costa, Rune Dietz, Paul Drevnick, Collin Eagles-Smith, José Lailson, Diego Henrique Costa Pereira, Frank Rigét, Carlos Rodriguez Brianza, Elsie Sunderland, Akinori Takeuchi, Eleuterio Umpiérrez, Hans Fredrik Veiteberg Braaten, Simon Wilson, Heleen de Wit, Younghee Kim

Key messages

- There is a preponderance of biotic Hg concentrations scientifically generated and available for fish and wildlife across most biomes and ecosystems of the world
- Food webs in many of the world's biomes and ecosystems have MeHg concentrations at levels of concern for ecological and human health around the world
- Spatial gradients of MeHg exposure vary greatly according to ecosystem sensitivity (i.e., there are many environmental variables that may accentuate or dampen MeHg generation and availability)
- Biotic MeHg exposure varies greatly and is linked to trophic level (which is related to food web structure), ecology, physiology, metabolism and demographics (e.g., lifespan)
- Biological MeHg hotspots (areas that have biota with above average MeHg body burdens that are at levels having potential significant human and ecological health impacts) are known throughout the world and can be linked to both contaminated sites and ecosystems/areas that are sensitive to Hg input
- Biological MeHg hotspots can be modelled and their identification could be crucial for effective and efficient biomonitoring
- Temporal trend data for Hg in biota are generally limited, but some key Hg monitoring datasets (e.g., AMAP and NCP Hg data), retrospective abilities (e.g., using museum specimens), and specific areas (e.g., Great Lakes Region in the U.S., Canada, and Fennoscandia) are insightful
- Mercury isotopes can be increasingly used as a tool for linking Hg source types with MeHg concentrations in fish, wildlife and humans
- Biota that best represent biomonitoring needs can generally be identified through current knowledge and reflect key overarching objectives, including (1) linking the source of MeHg exposure to humans, (2) tracking trends of MeHg in the environment, and (3) assessing the health of the environment

8.1 Introduction

The purpose of this chapter is to provide an overview of global methylmercury (MeHg) exposure to biota and so aid efforts to determine the source of MeHg for human exposure, identify biological MeHg hotspots, track temporal trends in environmental availability of MeHg, and assess ecological health. This has been achieved by reviewing existing biotic MeHg concentrations and biomonitoring programs, classifying

potential bioindicators that describe biotic MeHg exposure related to human and ecological health through the use of case studies, assessing overarching patterns of global spatial gradients and temporal trends of biotic MeHg exposure, identifying linkages among inorganic Hg sources and targeted bioindicators, and identifying critical knowledge gaps.

8.2 General remarks

Mercury (Hg) enters ecosystems via the air, water, and land. Atmospheric sources include emissions from coal-fired power plants and incinerators, aquatic sources include operational and non-operational chlor-alkali facilities and artisanal and small-scale gold mining, and terrestrial sources include natural geological formations, mine tailings, landfills, and other contaminated sites (UNEP, 2013; Pacyna et al., 2016; Kocman et al., 2017; Streets et al., 2017; Hsu-Kim et al., 2018; Obrist et al., 2018). Following emission, Hg can be retained in the environment for days to years and may be transported great distances (Driscoll et al., 2013). Mercury is a neurotoxin that can impair physiology, neurology, behavior, reproduction, and survival in fish, wildlife, and humans (Tan et al., 2009; Scheuhammer et al., 2011; Ackerman et al., 2016; Whitney and Cristol 2017; Evers, 2018). Mercury toxicity increases when inorganic Hg released into the environment is converted to MeHg by sulfur-reducing and iron-reducing bacteria, methanogens, and other microbes (Fleming et al., 2006; Gilmour et al., 2013; Yu et al., 2013). Conditions within some aquatic ecosystems are particularly conducive to MeHg production. Low oxygen conditions (hypoxia/anoxia) and the presence of sulfate, as is often found in wetlands and floodplains, provide optimal conditions for metabolism in bacteria (Hsu-Kim et al., 2013). Acidified conditions are also potentially important methylating environments (Wyn

et al., 2009), for example agricultural areas where sulfate is used as a soil amendment such as in the Everglades area of Florida (Gabriel et al., 2014). Dissolved organic carbon (DOC) is important. Mercury readily binds to DOC, which also serves as a metabolic substrate for some Hg-methylating microbes which means water with high DOC levels may generate and transport MeHg more readily (Schartup et al., 2015). However, DOC also affects Hg cycling through complexation processes and the amount of MeHg available for uptake in aquatic food chains can be reduced under high DOC concentrations (Gorski et al., 2008; Chaves-Ulloa et al., 2016; Chételat et al., 2018).

Such factors are important in assessing ecosystem sensitivity to inorganic Hg input and methylation potential (Eagles-Smith et al., 2018). Complex chemistry and transport pathways make it challenging to use Hg concentrations in air, water, and sediment to predict levels of potential concern in upper trophic level fish and wildlife (Gustin et al., 2016; Sunderland et al., 2016). In other words, areas with low Hg deposition may exhibit disproportionately high effects in biota if conditions are conducive to MeHg production. For example, MeHg concentrations in freshwater fish across western North America are poorly correlated with either total Hg or MeHg concentrations in aquatic sediments (Eagles-Smith et al., 2016a). Decoupling of inorganic Hg sources from MeHg production is evident at both the local level (Evers et al., 2007) and landscape level (Eagles-Smith et al., 2016b).

Methylmercury readily biomagnifies through ecosystems, even terrestrial ecosystems where spiders often serve as an important trophic link for MeHg to terrestrial wildlife (Cristol et al., 2008; Chaves-Ulloa, 2016). As a result, top predators such as fish, reptiles, birds, and mammals may have MeHg concentrations in their

tissues that are many orders of magnitude higher than in water (often more than 10^6 to 10^7 higher). Each trophic change in the food web generally accounts for about an order of magnitude increase in MeHg concentration, with the largest enrichment step occurring between water and phytoplankton in aquatic systems (Lee and Fisher, 2016; see Chapter 7 for more details).

Mercury exposure has been well documented in fish and wildlife. Contamination can arise directly from inorganic Hg point sources, such as those along rivers (Kinghorn et al., 2007; Jackson et al., 2011b; Nguetseng et al., 2015; Santschi et al., 2017; Geyer and Ralston 2018), around lakes (Anderson et al., 2008; Suchanek et al., 2008) and in estuaries (Eagles-Smith and Ackerman, 2009; Sullivan and Kopec 2018). Owing to atmospheric transport, inorganic Hg sources may be remote (>100 km) and are well described in most continents, including North America (Evers et al., 2005; Kamman et al., 2005; Evers et al., 2011a; Monson et al., 2011; Ackerman et al., 2016; Eagles-Smith et al., 2016b; Jackson et al., 2016; Scheuhammer et al., 2016), South America (Sebastiano et al., 2016; May Junior et al., 2017), Europe (Åkerblom et al., 2014; Nguetseng et al., 2015; Pacyna et al., 2017), Asia (Kim et al., 2012; Watanuki et al., 2016; Abeysinghe et al., 2017; Noh et al., 2017), Africa (Hanna et al., 2015; Rajaee et al., 2015; Daso et al., 2015), and ocean basins (Carravieri et al., 2014, 2017; Drevnick et al., 2015, 2017; Peterson et al., 2015; Lee et al., 2016; Bodin et al., 2017).

In fish, adverse impacts of MeHg exposure include reproductive, behavioral, and immunological impairment (Hammerschmidt et al., 2002; Depew et al., 2012a; Carvan et al., 2017) as well as reduced capacity for predator avoidance (Webber and Haines, 2003). In birds, studies document reduced reproductive success,

~~behavioral change and neurological problems (Depew et al., 2012a,b; Ackerman et al., 2016; Whitney and Cristol, 2017; Evers 2018). In mammals, elevated MeHg concentrations can result in biochemical changes in the brain, ataxia, and reduced reproductive output (Dietz et al., 2013; Evers, 2018). A complicating factor in determining Hg risk to wildlife is that many species vary in their sensitivity to MeHg toxicity (Heinz et al., 2009). For example, embryo survival and hatching success in songbirds (Passeriforms) seems more sensitive to MeHg toxicity than in other orders of birds, such as waterfowl (Anseriformes).~~

Identifying fish and wildlife species for MeHg biomonitoring is complex because their suitability differs according to geographic area, timescale of interest, conservation concern, and whether the overall goal is for ecological or human health. ~~This chapter reports spatial and temporal global patterns of MeHg exposure in fish and wildlife based on the peer-reviewed literature with an emphasis on bioindicators.~~

There is an extensive body of published data on total Hg concentrations in biota and many biomonitoring programs are in place worldwide, particularly in high-income countries (such as the USA, Canada, across several European countries, and Japan) that track global-scale spatio-temporal patterns of environmental inorganic Hg (with an emphasis on fish). Existing biomonitoring programs were identified in a recent United Nations Environment review (UNEP, 2016). Data within the peer-reviewed literature define the many case studies that include MeHg in taxa identified in Article 19 of the Minamata Convention on Mercury. Those published data are summarized here with an emphasis on fish, sea turtles, birds, and marine mammals. The type of Hg in tissues commonly sampled from biota is generally >95% MeHg.

8.3 Existing biotic Hg data

8.3.1 Literature search

The first step was to undertake a systematic literature search with an emphasis on long-term, standardized and large-scale monitoring efforts that included, among others, species identified in Article 19 of the Minamata Convention, species for human consumption, taxonomic groups at high risk of MeHg exposure, potential bioindicators, and species from areas of concern due to current Hg sources. Only peer-reviewed publications were used and the references are archived in the Global Biotic Mercury Synthesis (GBMS) database (Evers et al., 2017). Taxonomic groups with comprehensive coverage are shown in boldface in Appendix 8.1.

Studies included here are those for which there is reasonable confidence about their validity. For example, with a good description of the characteristics of the organism sampled (species, date, tissue analyzed), an appropriate method of sample collection, and detailed information on sampling location (i.e., market-based fish Hg concentrations are excluded). Terrestrial coverage of biotic Hg levels for North America is limited in in this chapter. However, extensive MeHg datasets synthesized during three regional workshops are available for the northeastern USA and eastern Canada for 2000–2004 (Evers and Clair, 2005), the Great Lakes Region of the USA and Canada for 2008–2010 (Evers et al., 2011a) and the western USA and Canada for 2012–2015 (Eagles-Smith et al., 2016b).

The data collected represent the arithmetic mean, standard deviation, minimum and maximum values, and total number of individuals for each species and tissue type that could be georeferenced within a peer-reviewed publication and were joined by taxa and tissue type to generate a global average and variation (see

Appendix 8.1). The raw data underlying the averaged statistics presented in Appendix 8.1 were not available. Each of the published studies' average Hg concentration was mapped by major taxonomic group (i.e., cartilaginous and bony fish, sea turtles, birds, and marine mammals) and tissue type and were placed in three risk categories based on human or ecological health thresholds (i.e., low, medium and high). Available data are summarized in Box 8.1.

The risk categories for human health are based on a combination of thresholds generated from standards used in the USA (Great Lakes Fish Advisory Workgroup, 2007), for Arctic communities (AMAP, 2015), and by the World Health Organization (i.e., <0.22 ppm low, 0.22–1.0 ppm moderate, >1.0 ppm high) that generally relate to MeHg exposure level concerns recognized for humans (Višnjevec Miklavčič et al., 2014; see also Chapter 9). For ecological health, risk categories by taxa for various tissue types are summarized by Evers (2018). This approach is conservative since it is the average Hg concentration for published data at the identified site that is ranked within one of the three risk categories.

Box 8.1 Overview of available datasets

Biotic Hg concentrations for targeted taxa were collected from nearly 1100 peer-reviewed scientific publications that represent about 515,000 individuals at over 2700 unique locations in 119 countries (Figure 8.1, Appendix 8.1). The data are housed in the GBMS database and represent an exhaustive literature review for field Hg concentrations in taxa targeted for this assessment including all elasmobranchs, marine teleosts (particularly tuna and billfish), freshwater teleosts (particularly in South America, Africa, and Asia), sea turtles, birds (especially Procellariformes, Gaviiformes, and Passeriformes), and marine mammals. The

literature review is less exhaustive, but still extensive in geographic and taxonomic coverage for freshwater teleosts in North America and birds in Orders other than the three listed above. A large number of Hg concentrations in biota, especially fish, have been generated by government agencies. Many of these data are not represented here because they are not published in the peer-reviewed literature or in English.

Elasmobranchs (sharks, skates, rays) are represented in 13 Orders by 10,038 individuals at 96 distinct locations. Marine teleosts were represented in 29 Orders by 40,491 individuals at 462 distinct locations, while freshwater teleosts included 31 Orders with 386,908 individuals at 9,314 distinct locations. For sea turtles, a total of 38 distinct locations were found with Hg concentrations in one of three tissue types of 1766 individuals. Marine birds were represented in 22 Orders by 67,987 individuals at 845 distinct locations. Marine mammals were placed in four groups and represented 8077 individuals at 328 locations.

Figure 8.1 Distribution of five major taxa and their total Hg concentrations in three risk categories based on mean data derived from a survey of the available peer-reviewed English literature. Risk categories by major taxa and tissue type are: **(1) cartilaginous fish (sharks and allies) and (2) bony fish** muscle (ppm, ww): <0.22=low, 0.22-1.0=moderate, >1.0=high; **(3) sea turtle** muscle and egg (ppm, ww): <0.22=low, 0.22-1.0=moderate, no samples were >1.0; **(4) bird** body feathers (adult; ppm, fw): <10.0=low, 10.0-20.0=moderate, >20.0=high; bird blood (adult; ppm, ww): <1.0=low, 1.0-3.0=moderate, .3.0=high; eggs (ppm, ww): <0.5=low, 0.5-1.0=moderate, >1.0=high; **(5) marine mammal** muscle (ppm, ww): <0.22=low, 0.22-1.0=moderate, >1.0=high. Letters indicate additional available fish Hg samples that were not mapped:

(a) 186,000 additional samples available in Canada; **(b)** 162,700 additional samples available in the United States; **(c)** >50,000 additional samples available throughout Scandinavia.

8.3.2 Preferred tissue types

This review focuses on tissues with well-established methods of measurement and interpretation and for which there is a large body of data. There are many matrices and tissue choice depends on monitoring objectives, interests, and outcomes. Often the most useful tissues can be nonlethally collected in the field. Samples that can be analyzed to assess total Hg or MeHg exposure are often from tissue (i.e., matrix) types for targeted biotic groups (Table 8.1). Composites samples are sometimes used to estimate Hg concentrations at decreased cost (Gandhi et al., 2016), and because most of the Hg in tissues that are commonly tested for biomonitoring purposes is in the MeHg form (generally >95%), analyses of total Hg (which is cheaper to analyze) is also more cost effective. The development of Direct Mercury Analyzers has simplified Hg determination and made analysis more accessible to those without advanced and costly laboratory facilities. Understanding MeHg concentrations in organisms is important because the organic form of Hg biomagnifies through the food web for Arctic (Ruus et al., 2015), temperate (Arcagni et al., 2018), and tropical (Seixas et al., 2014) ecosystems, and bioaccumulates over time in individual fish (Drevnick and Brooks, 2017), birds (Evers et al., 1998), and marine mammals (Krey et al., 2015). Understanding how the selection of tissue types dictate interpretative power in the biomagnification and bioaccumulation of MeHg and subsequent potential impacts is critical (Eagles-Smith et al., 2016b).

8.3.3 Other factors related to interpretation of biotic Hg data

Other metadata that are important to improve interpretive power include physiological, demographic, and ecological factors. For example, determining the health and fitness of bioindicators is important for standardized comparisons, as is the identification of size, age, and gender. However, for this data compilation biotic MeHg concentrations were not indexed or standardized according to size because individual or average lengths and/or weights were generally not available. In general, larger and older individuals have higher MeHg concentrations than smaller and younger individuals, and males that are larger in body size than females tend to have higher body burdens in fish (Eagles-Smith et al., 2016a) and birds (Evers et al., 2005; Ackerman et al., 2008, 2015, 2016; Robinson et al., 2012; Hartman et al., 2017), with a few exceptions related to foraging segregation between sexes such as in albatrosses (Carravieri et al., 2014). Changes in an animal's physiology or ecological life history events can also have a substantial effect on MeHg concentrations, regardless of an animal's actual environmental MeHg exposure. For example, rapid growth of juvenile birds can cause mass dilution of contaminants and substantially reduce MeHg concentrations as juvenile birds age (Ackerman et al., 2011). In contrast, annual life changes in adult body mass such as fasting- and breeding-associated declines in body mass during periods of haul-out on land for marine mammals, can substantially increase MeHg concentrations (Peterson et al., 2018).

Seasonality can have large implications for biotic Hg monitoring programs (Eagles-Smith and Ackerman, 2009). Seasonal changes in MeHg exposure may be related to changing methylation rates and bioavailability in estuaries (e.g., saltmarsh sparrows increase in blood Hg concentrations from early to late summer; Lane et al., 2011), molt strategies (Condon and Cristol, 2009), arrival to overwintering areas for migratory birds

(Eagles-Smith et al., 2009a), or lake-specific variation in Hg dynamics (e.g., Clark's and western grebes decrease in blood Hg from spring to autumn; Hartman et al., 2017).

8.4 Existing biomonitoring programs

Mercury biomonitoring programs were identified following a formal request to countries globally by the United Nations Environment Interim Secretariat. Responses were compiled (UNEP, 2016) and provide the most up-to-date record of existing local, regional, and global abiotic and biotic Hg monitoring programs. These include programs underway within many national networks, including initiatives in the EU (Norway, Sweden, Spain, UK, Poland), Canada, USA, Japan, Republic of Korea, Colombia and Brazil, and global or regional networks (UNEP, 2016). The Arctic is monitored through AMAP (AMAP, 2011) with valuable subsets from Canada's Northern Contaminants Program (Chételat et al., 2015; NCP 2017), the national monitoring program in Greenland and the Faroe Islands (Denmark), and the ARCTOX program based in Europe for tracking MeHg in seabirds. There are many programs in the temperate regions of the USA – such as the U.S. Environmental Protection Agency's seafood Hg monitoring program (Evers et al., 2008) and National Oceanic and Atmospheric Administration's mussel Hg watch program (Chase et al., 2001) – Europe (e.g., ROCCH, Reseau d'Observation de la Contamination Chimique), and Japan. In developing countries and countries in economic transition, there are fewer national or regional long-term initiatives. In particular, there are very few long-term Hg biomonitoring efforts in tropical biomes. In contrast, there are many oceanic Hg biomonitoring efforts within temperate and Arctic biomes (Evers et al., 2017).

AMAP is one of the best examples of how to operate a long-term MeHg biomonitoring field program for the benefit of both human and ecological health (AMAP, 2011, 2015). Whereas, the WHO Global Environment Monitoring System - Food Contamination Monitoring and Assessment Programme (commonly known as GEMS/Food) has one of the best global systems for collecting fish Hg data through its network of collaborating centers and recognized national institutions (WHO, 2018).

One of the longest running programs linking MeHg exposure in the environment to the foods that human communities depend on is that of AMAP (2011). This program uses standardized methodology across a large geographic area, involves multiple taxa (fish, birds, marine mammals), and incorporates other physical and chemical variables. AMAP has established an effective regional template for monitoring MeHg exposure in the environment that can be used concurrently for ecological and human health.

A review of the geographical coverage of Hg biomonitoring networks reveals a general lack of regional initiatives around the world, especially in Africa and Australia (UNEP, 2016). Most Asian countries are minimally involved with national initiatives to monitor Hg levels in biota, notable exceptions being Japan and the Republic of Korea where more extensive programs exist. Conversely, Hg biomonitoring is ongoing in many countries within Asia, Europe, Oceana and across the Western Hemisphere. Environmental Specimen Banks can be used as monitoring tools to provide long-term trends for contaminants in the environment, including Hg, as outlined within the EU.

One of the better examples for a national Hg biomonitoring effort is Canada's Northern Contaminants Program – an integrated initiative for Hg monitoring throughout Canada's vast Arctic territory (NCP, 2017).

Since its establishment in 1991, the program has focused on the measurement of contaminants (including Hg) in fish and wildlife that are traditional foods of northern Indigenous peoples (Figure 8.12). One of the strengths of the program is the interdisciplinary approach taken to assess and monitor risk of Hg to ecological and human health through the participation of Indigenous organizations, government departments (at federal and territorial level), environmental scientists, and human health professionals. Activities are managed under five subprograms: Human Health; Environmental Monitoring and Research; Community-Based Monitoring and Research; Communications, Capacity and Outreach; and Program Coordination and Indigenous Partnerships. A strategic long-term plan guides the development of subprograms and the links between them. For example, monitoring of Hg in biota is supported by Hg measurements in air as well as focused research on environmental processes that control Hg bioaccumulation. Data generated on Hg in wildlife can be used for human dietary exposure assessments, while community-based projects may focus on species that are local priorities but not covered by routine monitoring.

Figure 8.12 Map of long-term sampling sites for Arctic fish and wildlife monitored annually under Canada's Northern Contaminants Program in terrestrial, freshwater, and marine ecosystems. Biotic monitoring is one of several interdisciplinary subprograms (identified at the top of the map) to assess and monitor risks of contaminants (including Hg) to ecological and human health.

Monitoring of Hg in fish and wildlife under the Northern Contaminants Program includes terrestrial, freshwater and marine species in focal areas across northern Canada (Figure 8.12). Many of the samples are collected by Indigenous hunters in nearby communities as part of their subsistence activities. Annual

measurements track temporal trends of Hg bioaccumulation, and retrospective analyses of archived tissues from government specimen banks have provided opportunities to extend some time series (e.g., Braune, 2007). Intensive spatial sampling of several species including Arctic char (Evans et al., 2015) and ringed seal (Brown et al., 2016) have generated complementary information on geographic variation.

Another example of an international collaboration, ARCTOX, is a program whereby seabird blood and feather samples have been collected from more than 54 Arctic sites and a total of 14 seabird species (although not every species is sampled at each site). Samples are from Arctic countries, including the USA, Canada, Greenland, Scandinavia, and Russia.

Meanwhile, the hundreds of local studies conducted by the global scientific community that are reflected within the GBMS database provide a relatively comprehensive global data platform containing existing biotic Hg concentrations (Appendix 8.1; Evers et al., 2017). Based on the GBMS database, some of the regions with the highest fish consumption are poorly covered by biomonitoring efforts (e.g., Central America and the Caribbean Sea, western and central Africa, the southern Asian mainland, Indo-Pacific Asia). More efforts are needed to develop and implement projects to fill geographic and ecosystem gaps. Although national efforts are fundamental to regional biomonitoring networks, local scientific studies can make a significant contribution to better identifying where, for which species, and when to conduct biomonitoring. To provide sustainable and long-term biomonitoring capacity in key regions (e.g., Arctic, tropical areas associated with ASGM, and Small Island Developing States), the focus should be on expanding and stabilizing existing national initiatives that use sample sizes that can meet statistical power for confidence in

understanding spatial gradients (such as biological MeHg hotspots; Evers et al., 2011b) and temporal trends (Bignert et al., 2004). Moreover, it is crucial to foster international collaboration and coordination among national projects to create harmonized regional approaches, and to strive, where possible, to integrate biomonitoring activities into an interdisciplinary framework to assess ecological and human health risk that can be amalgamated to represent regional and eventually global spatio-temporal patterns.

8.5 Selection of bioindicators

A key initial step in bioindicator selection is to decide whether an organism is linked to a human health or ecological health endpoint – which can often be combined for both purposes if carefully considered. Biota that have been identified to best fit these two categories are well described and are categorized within their respective biomes and associated aquatic ecosystems (Table 8.2). The taxa of greatest interest for the Minamata Convention include fish, sea turtles, birds, and marine mammals. The extensive data on Hg in biota found in the published literature provides a selection of species for potential monitoring (Figure 8.1). Careful selection can ensure comparability at regional and global scales.

Organisms that are at risk of developing elevated MeHg body burdens, that represent specific ecological pathways or unique spatial or temporal scales, and that have well-established toxicity benchmarks can be grouped at relevant taxonomic resolutions to aid decisions concerning the selection of bioindicators (Evers et al., 2016; Appendix 8.1). The emphasis here is on the selection of biota that may pose concern for human exposure from dietary uptake of MeHg from marine or freshwater ecosystems; temporal timelines of interest (e.g., short-term timeframes [<6 years] should use young individuals with relatively low trophic level species

and long-term [>12 year] can use market fish); (3) spatial gradients of local to regional to global scales (e.g., wide-ranging predator species such as swordfish are key bioindicators for regional and global monitoring, while resident species fit better with local scales); or (4) conservation purposes (e.g., wildlife that are rare or are well-established as threatened by Hg exposure, such as albatrosses and loons).

8.5.1 Human health bioindicators

Many communities around the world depend in part, and sometimes completely, on wild animals for subsistence, including marine fish, freshwater fish, birds, and marine mammals. Patterns of dietary MeHg uptake in humans are described for all the world's major biomes from the Arctic and subarctic to temperate and tropical aquatic ecosystems, with mechanisms underlying source-exposure-human biomarker measures detailed in Chapter 9. The following case studies illustrate how biotic Hg exposure can be linked to human health concerns in each of these major biomes for key ecosystems in the world using select bioindicators.

8.5.1.1 Case study: Global oceans

Tuna species are one of the most important global sources of seafood. Commercial harvests tracked by the UN Food and Agriculture Organization (FAO) totaled 5 million tonnes in 2014, worth an estimated USD 42.21 billion (Galland et al., 2016) – although this total may not include all fisheries, and harvests could be higher than estimated (Pauly and Zeller, 2016). Muscle Hg concentrations and commercial harvests vary widely by species. The smallest tuna species (e.g., skipjack tuna) have average Hg concentrations under the U.S. EPA advisory level of 0.30 ppm (ww), while the largest (e.g., Pacific and Atlantic bluefin tunas) have the highest average Hg concentrations and often exceed advisory levels (Figure 8.2). These patterns vary by

size class within species and ocean basin origin. For example, yellowfin tuna tends to have lower average muscle Hg concentrations than seven of the nine tuna species with data (Figure 8.2), however individuals of that species from the south Atlantic Ocean weighing over 70 kg typically have higher Hg concentrations (Bosch et al., 2016). It is suggested to avoid consumption of yellowfin tuna larger than 70 kg. Yellowfin and bigeye tuna Hg concentrations grouped by major ocean basin indicate that the eastern and northern areas of the Pacific Ocean have significantly higher Hg concentrations than other ocean basins (Ferriss et al., 2011; Nicklisch et al., 2017). This is an area where increasing tuna Hg concentrations have been recorded over the past decade (Drevnick et al., 2015; Drevnick and Brooks 2017) and modelled for several decades into the future (Sunderland et al., 2009). As well as size and origin, other factors to consider include whether the tuna is canned or fresh (for the same species, canned tuna tend to have lower Hg concentrations; García et al., 2016) and farmed or wild. Although farmed tuna tend to have lower Hg concentrations (Balshaw et al., 2008), the amount of Hg bioaccumulation in muscle tissue in wild caught farmed tuna depends on time spent in rearing pens (Srebocan et al., 2007).

Figure 8.2 Arithmetic mean +/- SD of global total Hg concentrations (ppm, ww) in muscle tissue of nine tuna species, from the GBMS database (Evers et al., 2017), compared with the FAO harvests estimates (in tonnes) and tuna with harvests of 10-15,000 tonnes are depicted with ** while tuna with harvest of <5,000 tonnes are depicted with *.

8.5.1.2 Case study: Arctic

AMAP regularly fosters international collaboration and compiles measurements of Hg levels in Arctic biota, including shellfish, freshwater and marine fish, seabirds, marine and terrestrial mammals, and humans. Temporal trends from 83 long time-series for Hg in biota monitored at 60 sites around the Arctic establish one of the best standardized, long-term biomonitoring efforts for Hg in the world (AMAP, 2011). There is a need for concerted international effort to reduce Hg levels in the Arctic owing to long-range atmospheric transport of inorganic Hg from distant source regions, warmer and longer ice-free seasons potentially promoting MeHg production, the release of inorganic Hg stored from thawing permafrost, soils, sediments, and glaciers, and the reliance of indigenous communities on biota that are often upper trophic level species with long life spans and elevated MeHg body burdens (AMAP, 2011; Dietz et al., 2013; Scheuhammer et al., 2015). Studies show a ten-fold increase in Hg levels in birds and marine mammals over the past 150 years with an average annual rate of increase of 1–4% (AMAP, 2011). In contrast, recent temporal trends in Arctic fish and wildlife have been inconsistent, with Hg concentrations over the past 30 years increasing in some cases but declining elsewhere depending on species, location, and period monitored (Rigét et al., 2011). Continued long-term Hg biomonitoring is therefore critical for tracking changes in inorganic Hg emissions, deposition, and bioavailability of MeHg in food webs across the Arctic. This is necessary to protect indigenous communities (AMAP, 2011) and to determine the degree to which global climate change is altering Hg pathways within the Arctic (McKinney et al., 2015; Eagles-Smith et al., 2018).

8.5.1.3 Case study: Subarctic oceans

In some areas of North America, wildlife remains an important food source among natives and subsistence consumers. Baffin Island, located in eastern Arctic Canada, is an ecologically significant area, supporting many species of marine birds and mammals. Many Inuit communities rely upon Baffin Island's marine resources (Chan et al., 1995; Mallory, 2004). The presence of MeHg in biota (marine mammals, seabirds) throughout the Canadian Arctic is well established (Muir et al., 1999; Mallory 2004; Campbell et al., 2005; Mallory and Braune, 2012) with increasing trends observed in seabirds over recent decades (Canadian Mercury Science Assessment, 2016). Generally, MeHg concentrations in seabirds in the Canadian Arctic are below levels associated with health effects in wildlife. However, edible parts (breast muscle, eggs) approach or exceed the action level (0.22 µg/g) set by the Great Lakes Advisory Council (Figure 8.3).

Figure 8.3 Arithmetic mean +/- SD of total Hg (ppm,ww) in marine bird eggs from the Aleutian Islands, Alaska, United States (yellow) and the Canadian Arctic (blue).

Mercury concentrations in seabird eggs from the Canadian Arctic have increased significantly over recent decades using kittiwakes, fulmars and murres as bioindicators (Figure 8.3; Braune 2007, 2016; Campbell et al., 2005). In the Aleutian Islands of Alaska there has been an effort to quantify MeHg uptake by local North Pacific fisheries and wildlife due to potential cumulative inputs of Hg from historic military activity (Burger and Gochfeld, 2006; Anthony et al., 2007; Ricca et al., 2008), emissions from local volcanic activity (Ricca et al., 2008), and atmospheric and oceanic transport of Hg from Asia (Rocque and Winker, 2004; Anthony et al., 2007; Driscoll et al., 2013) and Russia (Fisher et al., 2012). Mercury accumulation in marine birds from

the Aleutian Islands has been well documented (Burger et al., 2007, 2008, 2009; Burger and Gochfeld, 2009; Savoy et al., 2017).

The Aleuts and subsistence hunters have a history of consuming seabirds (Burger et al., 2007), and especially eggs (Naves, 2009). According to Burger et al. (2007), 90% of households from an Aleutian village consumed birds to some degree each year. Previous studies have shown that some seabird species from the Aleutian Islands contain edible parts (e.g, breast meat, eggs) with Hg levels that approach or exceed human consumption advisory levels (0.22 µg/g, ww) (Burger et al., 2007, 2009). Abundance and ease of collection, mean the eggs of glaucous-winged gull (*Larus glaucescens*) are highly sought, and the number collected each year can exceed 6000 (Naves, 2009). Gulls routinely contain the highest Hg concentrations among seabirds.

8.5.1.4 Case study: Boreal and temperate lakes

Records of Hg in freshwater fish across Fennoscandia (Norway, Sweden, Finland, Kola Peninsula in Russian Federation) have been collected for over 50 years in almost 3000 lakes and rivers. These data have been collated into a single database by the International Cooperative Programme (or ICP Waters), under the UNECE Air Convention (Figure 8.4, Braaten et al., 2017). Fish Hg concentrations vary widely among lakes in Fennoscandia owing to differences in Hg pollution in the lakes, as well as other factors controlling the rates of methylation and subsequent biomagnification.

Figure 8.4 Lakes and streams that have been monitored for fish Hg concentrations over more than 50 years in northern Europe.

Measured Hg concentrations in the south (55°–60°N) are generally higher than in the north (60°–70°N), with over 40% of lakes containing fish muscle Hg concentrations exceeding the WHO/FAO limit of 0.5 ppm widely used as a trigger for human consumption safety (all data are total Hg concentrations in muscle tissue on a wet weight basis). The dataset includes important species for recreational fishing such as pike (*Esox lucius*; S: 0.63±0.01 ppm [n=24,849], N: 0.60±0.01 ppm [n=3360]), Arctic char (*Salvelinus alpinus*; S: 0.45±0.18ppm [n=284], N: 0.11±0.10 ppm [n=514]), perch (*Perca fluviatilis*; S: 0.26±0.02 ppm [n=20,276], N: 0.20±0.01 ppm [n=2326]), and brown trout (*Salmo trutta*; S: 0.14±0.03ppm [1816], N: 0.16±0.40 ppm [230]) (Figure 8.4).

Long-term patterns of fish Hg concentration in Fennoscandian lakes show a clear decline (Åkerblom et al., 2014; Braaten et al., 2017). However, there is no decline in those lakes for which Hg originates from atmospheric sources only. Closing of local industrial pollution sources over the past 50 years is likely to have led to a reduction in fish Hg concentrations.

To evaluate spatial and temporal variation of Hg in fish, the fish Hg data are first normalized with regard to size using well-established standard units (e.g., 55 cm and 1 kg for northern pike; Sorensen et al., 1990). Such standards have been applied to robust Hg datasets (i.e., >50,000 data points) in the USA, Canada, and northern Europe for northern pike, bass (*Micropterus* spp.) and walleye (*Sander vitreus*; Johnels et al., 1967; Kamman et al., 2005; Monson 2009; Monson et al., 2011; Gandhi et al., 2015; Eagles-Smith et al., 2016a).

8.5.1.5 Case study: Tropical rivers (Africa)

Mercury sources in Africa are concentrated in West Africa, the East African rift valley, and South Africa.

Around 70% of Hg emissions on the African continent are associated with artisanal and small-scale gold mining (ASGM; UNEP, 2013). A review of fish Hg levels (407 measures from 166 species) from 31 waterbodies in 12 African countries found that, in general, Hg levels were low but that in fish sampled near ASGM sites 25% of locations had mean fish Hg levels that exceeded the 0.3 ppm (ww) US EPA guideline value (Hanna et al., 2015). A similar pattern was found in Ghana (1305 measures in 65 species) in which four of 52 sampling sites associated with ASGM had fish Hg levels that exceeded the US EPA guideline value (Rajaee et al., 2015).

In Africa, subsistence and commercial fisheries are important to food and economic security, contributing up to 70% of animal protein consumption (FAO 2012; Hanna et al., 2015). Earlier studies documenting Hg concentrations in fish from uncontaminated lakes throughout Africa revealed relatively low concentrations (Black et al., 2011), but only 3.7% of inland water bodies have been studied for Hg contamination in fish (Hanna et al., 2015). Mercury concentrations in Nile perch and tilapia, the two most important commercial species, tend to be <0.5 ppm ww (FAO 2012; Hanna et al., 2016). However, local studies within individual countries show aquatic ecosystems that are impacted by Hg. Concentrations in fish from lakes and rivers in Ghana, Tanzania and South Africa have metal contaminants including Hg at levels of concern for human consumption (Hanna et al., 2015; Rajaee et al., 2015; Gbogbo et al., 2017; Walters et al., 2017). A study at a South African gold mine found an extremely high percentage (>90%) of MeHg in water suggesting very high methylation potential in mine watersheds (Lusilao-Makiese et al., 2016). Shellfish from ASGM sites on the Gambia River in Senegal had Hg concentrations above WHO safety guidelines, but fish samples did not

(Niane et al., 2015). Although local people consuming fish had elevated Hg levels in hair, the difficulty in measuring Hg in hair from people within ASGM communities is a concern (Chapter 9). Seventy percent of piscivorous fish in reservoirs in Burkina Faso have MeHg levels above the threshold for wildlife protection (Ouédraogo and Amyot, 2013). Although, some sites with elevated Hg levels in fish are associated with wetlands, power stations, and dams, associations with ASGM-related Hg contamination highlight the need for further biomonitoring near such sources.

Mercury in coastal and marine ecosystems has been less studied in Africa than in inland waters although studies of marine food webs in Senegal show Hg concentrations in invertebrates and fish to be below the health safety limits defined by the EU (Diop and Amara, 2016). In South Africa, the accumulation of metal contaminants in commercially consumed marine fish needs additional attention (Bosch et al., 2016a,b). In particular, sharks in coastal waters of South Africa have significantly higher Hg concentrations than conspecifics sampled in the North Atlantic and throughout the Pacific (McKinney et al., 2016). South Africa Hg concentrations in terrestrial and freshwater ecosystems also appear elevated as shown in southern ground-hornbills and wattled cranes with egg Hg concentrations above those benchmarkes where adverse reproductive effects have been observed in some avian species (Daso et al., 2015).

8.5.1.6 Case study: Coast and estuaries

The world's estuaries represent ecosystems that are sensitive to the input of Hg from contaminated sites and atmospheric deposition into watersheds draining into coastal river deltas (Correia and Guimarães, 2017; Fragoso et al., 2018). Estuaries within the Indo-Pacific area generally comprise mangrove wetlands and

associated seasonally-flooded forested areas, habitats which are well known for their ability to capture and methylate Hg (Li et al., 2016a; Haris et al., 2017; Sun et al., 2017).

ASGM activities and emissions from coal-fired power plants are two major contributors to the region's Hg burden. Atmospheric deposition of Hg from these and other sources are being monitored by the Asian-Pacific Mercury Monitoring Network, which helps provide a standard approach for determining temporal trends and spatial gradients (UNEP, 2016). Recent research using Hg isotope techniques shows Hg in the mangrove wetlands of southeast China to have originated from atmospheric deposition (Sun et al., 2017).

8.5.1.7 Case study: Tropical rivers (South America)

The major river basins of South America, including the Magdalena, Orinoco, Amazon, and La Plata, support a large freshwater fishery, providing livelihoods for small-scale artisanal fishers as well as major commercial enterprises (Barletta et al., 2010). In the remote interior areas of South America, indigenous communities are highly dependent on freshwater resources for subsistence, and for communities with high fish consumption the risk of Hg and MeHg exposure can be high (Uryu et al., 2001; Oliveira et al., 2010). Research over several decades in the Amazon Basin has repeatedly identified a link between a diet high in fish, especially piscivorous and omnivorous species, and elevated Hg concentrations in human biomarkers such as hair (Bidone et al., 1997; Lebel et al., 1997; Castilhos et al., 1998; Boischio and Henshel, 2000; Bastos et al., 2006; Costa et al., 2012; Faial et al., 2015).

The GBMS database for South America contains over 170 peer-reviewed publications on fish Hg concentrations from more than 240 sites across 100 different waterbodies (lakes, rivers, estuaries, bays);

more than 27,000 individual fish from more than 240 genera are represented (Evers et al., 2017). Mean Hg concentrations range from below detection limit to 4.4 ppm ww. The most commonly sampled taxa include species within the *Hoplias* (tigerfishes), *Serrasalmus* (piranhas), *Pseudoplatystoma* (sorubim catfishes), *Cichla* (neotropical cichlids) and *Odontesthes* (silversides) genera. Such data highlight areas of extensive freshwater sampling (e.g., Madeira and Tapajos Rivers of Brazil) as well as areas where extensive data gaps exist (e.g., the countries of Paraguay and Guyana) (Evers et al., 2017).

From these data, 'hotspots' of concern for ecological and human health start to emerge (Figure 8.1). Much of the research on Hg in environmental and human Hg exposure has been conducted in areas impacted by ASGM (Olivero-Verbel et al., 2015; Moreno-Brush et al., 2016; Salazar-Camacho, 2017). These and other Hg point sources (such as petroleum extraction; Webb et al., 2015) that are connected with river floodplain habitats, where daily and seasonal water level fluctuations can be extensive, appear to be sensitive to elevated methylation rates (Hsu-Kim et al., 2018).

8.5.1.8 Case study: Small Island Developing States

Large and relatively long-lived pelagic species such as billfishes are good bioindicators for understanding broad spatial gradients of MeHg contamination in the world's oceans using current commercial resources. Mercury body burdens in billfish, such as marlin (Drevnick and Brooks, 2017; Vega-Sánchez et al., 2017) and swordfish (Mendez et al., 2001; Branco et al., 2007), are some of the highest known for marine teleost fish (Table 8.1; Rodrigues and Amorim, 2016). In swordfish, Hg body burdens vary according to major ocean basin with a tendency for more elevated Hg concentrations in the Northern Hemisphere than the

Southern Hemisphere (Figure 8.5; 0.83±0.42 and 0.38±0.34 ppm, respectively). In addition to their high trophic level and relatively long lifespan (>10 years), swordfish have important commercial value and are an important source of income for many Small Island Developing States.

Figure 8.5 Arithmetic mean +/- SD of global total Hg concentrations (ppm, ww) in dorsal muscle tissue of swordfish from known ocean basins from the GBMS database (Evers et al., 2017; Bodin et al., in prep).

In the Indian Ocean, 27,000 tonnes of swordfish were harvested annually during 2006–2013 (including 270 tonnes caught by local semi-industrial fishing fleets in the Seychelles exclusive economic zone) and were mainly exported as whole fish to the EU (SFA, 2016). The Seychelles Fisheries Authority has recently reported total Hg concentrations of 0.70±0.40 ppm ww (n=226) in Seychelles swordfish edible muscle, with levels increasing with fish size (Hollanda et al., in prep). Similar concentrations were measured in swordfish across the Indian Ocean, except for swordfish caught in east India, Mozambique, and east Rodrigues, with total Hg concentrations >1.0 ppm (Figure 8.5; Kojadinovic et al., 2006; Bodin et al., in prep).

As for other Small Island Developing States such as Sri Lanka (Jinadasa et al., 2014), the Seychelles are required to determine the total Hg concentrations in muscle of swordfish and other large fish species when exporting to the EU – which requires fish imports to have <1.0 ppm ww in tissue for human consumption. Fish with concentrations over this EU advisory level are not permitted (i.e., large specimens with the highest commercial value) and either remain within the Seychelles or are exported to other countries for less value, which can have a significant adverse economic impact. The Seychelles semi-industrial fishing fleet are thus attempting to switch from swordfish to tuna, as Hg concentrations in tuna species within the EEZ are

generally <0.5 ppm ww (Bodin et al., 2017). However, this may not be a long-term solution owing to the declining status of tuna populations in the Indian Ocean (e.g., yellowfin tuna: overexploited; bigeye tuna: fully exploited; IOTC, 2016).

8.5.2 Ecological health bioindicators

Many species of fish and wildlife are impacted by the adverse effects of Hg on their physiology, behavior and reproductive success (Dietz et al., 2013; Scheuhammer et al., 2015; Ackerman et al., 2016; Whitney and Cristol, 2017; Evers, 2018). Some are considered high profile species and are included by IUCN on their Red List of Threatened Species, or listed as threatened or endangered by the USA.

Selection of the organism or suite of bioindicators depends on the objective. Taxa suitability may vary according to ecosystem interests (at habitat or biome levels of relevance), spatial resolution (local, regional or global), temporal scale (short- or long-term), human or ecological health interests, endpoints of importance (reproductive impairment), known adverse toxicity thresholds (by tissue and taxa using endpoints of interest), sample availability (simple or challenging), and sampling outcome (non-lethal or lethal). A provisional slate of some potential bioindicators for evaluating and monitoring environmental Hg loads for ecological health purposes can be grouped into four target biomes and their associated waterbodies and by major taxa of interest (Table 8.2; Evers et al., 2016).

8.5.2.1 Case study: Sharks

Many elasmobranchs (sharks, skates, rays) have tissue Hg concentrations well above the human health advisory levels set by the World Health Organization (1.0 ppm ww; Table 8.1, Figure 8.6). Species within

the mackerel and ground sharks generally have elevated Hg body burdens (de Pinho et al., 2010; de Carvalho et al., 2014; Teffer et al., 2014; Matulik et al., 2017) which is of concern because many of these species are already threatened with extinction from overfishing and their meat is also consumed globally. In marine ecosystems, pelagic foraging organisms tend to have higher Hg body burdens than those foraging in benthic habitats (Kim et al., 2012); sharks generally follow this pattern. The potential adverse impacts of MeHg on elasmobranchs are not well understood, although chronic dietary MeHg uptake above 0.2 ppm ww in freshwater fish can affect reproduction and other subclinical endpoints (Depew et al., 2012a). While most sharks have a dietary uptake of MeHg that is well over this benchmark level, it is unclear whether MeHg exposure is causing adverse effects or whether they are actually related to population declines. Of the 14 shark genera with published muscle Hg concentrations, average levels exceed 1.0 ppm ww in 71% of genera.

Figure 8.6 Arithmetic mean +/- SD of global total Hg concentrations (ppm, ww) in muscle tissue of sharks by genus from the Orders of Mackerel and Ground Sharks from the GBMS database (Evers et al., 2017).

8.5.2.2 Case study: Marine birds

Marine birds occupy a broad range of trophic levels, but most seabirds occur high in the food web and so biomagnify high levels of MeHg (Monteiro and Furness, 1995; Furness and Camphuysen, 1997; Mallory and Braune, 2012; Elliott and Eliott, 2013; Provencher et al., 2014). Due to their foraging strategies, behavioral ecologies, and life-history traits (breeding sequence, molting strategies, foraging ranges, migration patterns), seabirds generally have elevated body burdens of Hg which can ultimately reduce their reproductive capacity and affect their ability to sustain populations over time (Braune et al., 2006; Tartu et al., 2013; Goutte et al.,

2014a,b; Bond et al., 2015). Adverse Hg effects on the increasingly rare ivory gull are of particular concern (Braune et al., 2006; Bond et al., 2015). Many studies have focused on seabird Hg body burdens from tropical to polar regions and from coastal to oceanic zones, covering most of the world's oceans (Appendix 8.1). On a global scale, seabirds exhibit a wide range of Hg concentrations across tissue types (feathers, blood, eggs), driven by spatial differences as well as phylogeny. For example, penguins have the lowest Hg concentrations in eggs, blood, and feathers (except for in feathers for tropicbirds), whereas the Procellariiforms (petrels, shearwaters, albatrosses) generally have the highest Hg body burdens (Appendix 8.1, Figure 8.7). The Procellariiforms are the best studied group and display a wide range of tissue Hg concentrations which reflect some phylogenetic differences, with albatrosses exhibiting the highest Hg concentrations (Muirhead and Furness, 1988; Stewart et al., 1999; Anderson et al., 2010; Tavares et al., 2013; Bustamante et al., 2016).

Figure 8.7 Arithmetic mean +/- SD of global total Hg concentrations (ppm) in three tissues (fw in feathers, ww in blood and eggs) of seabird families within the Order Procellariiformes from the GBMS database (Evers et al., 2017).

The most important factor for predicting seabird Hg exposure is their foraging ecology. Because seabirds use a wide range of habitats, from the littoral zone to the open ocean (benthic and pelagic), different species or individuals with differing foraging behaviors can reflect Hg contamination from different parts of the ecosystems both horizontally (coastal and oceanic food webs) and vertically (benthic, epipelagic, and mesopelagic food webs). Therefore, the study of a group of seabirds with contrasting ecology from the same

region allows determination of MeHg availability for multiple marine zones and thus provides a more holistic view (Ochoa-Acuña et al., 2002; Bond and Diamond, 2009; Stenhouse et al., 2018). For example, crustacean-feeding seabirds have lower Hg exposure than cephalopod- and fish-feeders (Carravieri et al., 2014) and epipelagic seabirds have lower Hg exposure than those relying on mesopelagic prey (Ochoa-Acuña et al., 2002). Seabirds of the highest trophic levels with a regular dietary intake of MeHg (such as albatrosses or skuas) are therefore at risk of the effects of MeHg toxicity that are associated with potential long-term population declines (Goutte et al., 2014a,b).

Storm-petrels breeding in the Northern Hemisphere have feather Hg concentrations that are ten-fold higher (14.1±3.9 ppm) than populations breeding in the Southern Hemisphere (1.6±1.4 ppm) (Figure 8.7). Such a difference is not found for the Procellariidae (8.1±13.1 vs 7.4±13.7 µg/g, respectively). Differences between hemispheres should be explored further and should be based on seabirds with similar trophic ecology as well as close phylogeny.

Seabirds permit Hg monitoring across large geographical scales and variations within the same species over longitudinal (e.g., brown noddy) or latitudinal scales (e.g., skuas). The variation in Hg contamination in seabird tissues can reveal differences in the degree of contamination between major ocean basins, as well as latitudinal gradients of contamination within basins, and trends at a series of spatial and temporal scales.

8.5.2.3 Case study: Loons/Divers

Species within the Order Gaviiformes (loons or divers) are piscivores that breed on freshwater ponds and lakes in temperate and Arctic ecosystems of the Northern Hemisphere. The larger loon species (common

loon, *Gavia immer*, and yellow-billed loon, *Gavia adamsii*) are obligate piscivores and, as a result, have some of the highest average Hg body burdens of birds in the world (Appendix 8.1). In the winter, all loon species migrate to marine ecosystems (with parts of some populations overwintering on freshwater lakes). Loons have been used as bioindicators of MeHg availability in both their breeding and wintering areas for several decades (Evers et al., 1998, 2008, 2011a, 2014; Jackson et al., 2016). In Canada, the common loon and its prey are being studied to evaluate the success of national regulatory standards to reduce Hg emissions (Scheuhammer et al., 2016).

The effects of Hg on loon reproductive success are well established (Burgess and Meyer, 2008; Evers et al., 2011b; Depew et al., 2012b) and are used as benchmarks for evaluating ecological concern. Loons are being used as a standard bioindicator across continents and demonstrate a west to east increasing gradient of MeHg availability in lakes within temperate and boreal forest ecosystems, with Alaskan breeding populations having the lowest Hg concentrations and eastern North American populations the highest (Evers et al., 1998, Figure 8.8). The smaller loon/diver species, while less piscivorous and having lower Hg concentrations (Ackerman et al., 2016), remain potential bioindicators for MeHg availability.

Figure 8.8 Arithmetic mean +/- SD of global total Hg concentrations in common and yellow-billed loon indexed blood across parts of the northern hemisphere (from 10-180^{o} W) from the GBMS database (Evers et al., 2017).

8.5.2.4 Case study: Raptors

Birds of prey, or raptors, comprise a large and varied group of birds generally characterized as predators. Several raptors at the species or genus level have a near global distribution (i.e., peregrine falcons, ospreys, *Haliaeetus* eagles) and so are commonly used in spatial and temporal contaminant monitoring efforts (Bowerman et al., 2002; Weech et al., 2006; Grove et al., 2009; Henny et al., 2009a; DeSorbo et al., 2018). In breeding areas, developing nestlings of many raptor species are often more efficiently captured than resident adults. Adult raptors consistently exhibit higher Hg concentrations than nestlings, largely due to nestlings' ability to depurate Hg into growing feathers (Ackerman et al., 2011). Despite large home range sizes of many raptors, individuals sampled in association with nesting territories generally reflect MeHg exposure in the food web associated with the nesting territory (Bowerman et al., 1994; DeSorbo et al., 2018). Piscivorous raptors such as ospreys and *Haliaeetus* eagles tend to exhibit the highest adult blood Hg concentrations among raptors (Figure 8.9). Raptor species specializing in bird prey (e.g., many *Accipiter* and *Falco* spp.) generally have higher average Hg concentrations than those predominantly targeting small mammals (e.g., *Buteo* and *Circus* spp.), while obligate scavengers are generally exposed to low levels of Hg.

Figure 8.9 Global arithmetic mean +/- SD of total Hg concentrations in blood of adult and juvenile age classes of six selected Genera of raptors.

Piscivorous raptors, namely *Haliaeetus* eagles and ospreys are well-suited for Hg biomonitoring within and across multiple habitat types (marine, estuarine, freshwater river, lake) along the freshwater-marine gradient in ecosystems (Jackson et al., 2016; Rumbold et al., 2017; DeSorbo et al., 2018). *Haliaeetus* eagles are key sentinels in environmental programs used to monitor spatial and temporal Hg exposure patterns in North

America, particularly in the U.S. Great Lakes ecosystem (Bowerman et al., 2002). A study of bald eagles (*Haliaeetus leucocephalus*) in the Great Lakes of the USA found evidence that Hg adversely affects a proportion of this population (Rutkiewicz et al., 2011); in that study, 14–27% of individuals sampled were exposed to Hg at concentrations associated with subclinical neurological damage.

While piscivorous birds were predominantly emphasized in past Hg biomonitoring, recent studies show that MeHg is also prevalent in terrestrial-based food webs, and that invertivorous birds (Passeriformes) can have elevated MeHg concentrations (Jackson et al., 2011a, 2015; Evers, 2018) that result in levels of concern in bird-eating raptors such as Accipiters.

8.5.2.5 Case study: Landbirds

Many species of invertivorous birds (herein landbirds) are also at elevated risk of Hg exposure. In fact, some invertivore-feeding birds have higher tissue Hg concentrations than avian piscivores within the same ecosystem (Evers et al., 2005). They may also be more sensitive to MeHg, resulting in a higher likelihood of adverse impacts on reproductive success (Heinz et al., 2009; Jackson et al., 2011a). An increasing number of studies characterizing Hg exposure in songbirds (Passeriformes) are demonstrating that certain species are at higher risk than others, based largely on foraging behavior and breeding habitats. Generally, gleaning and flycatching songbirds that breed in wetland habitats (Figure 8.10; Edmonds et al., 2010; Jackson et al., 2011b, 2015; Lane et al., 2011; Hartman et al., 2013; Ackerman et al., 2016; Pacyna et al., 2017), including rice fields (Abeysinghe et al., 2017), are at highest risk of Hg exposure, especially species that forage on predaceous arthropods such as spiders (Cristol et al., 2008). The availability of MeHg to tropical resident

songbirds (and other landbird groups) remains relatively unknown, but indications are that some foraging guilds and habitat types are of concern (Lane et al., 2013; Townsend et al., 2013).

Figure 8.10 Arithmetic mean +/- SD of total Hg concentrations in Passeriform (songbird) blood in the United States from the GBMS database (Evers et al., 2017).

Songbird species that spend most of their annual life cycle within wetland-oriented ecosystems and that migrate long-distances (e.g., neotropical migrants or palearctic migrants) may also be at great risk of chronic Hg exposure adversely impacting reproductive success (Jackson et al., 2011a; Varian-Ramos et al., 2014). New findings on elevated Hg exposure and migration physiology/behavior indicate significant adverse impacts are possible, especially for long-distance migrants that may experience decreased flight endurance (Seewagen et al., 2016; Ma et al., 2018) that could also be related to increasing asymmetry in high Hg individuals (Herring et al., 2017).

8.5.2.6 Case study: Marine mammals

Toothed whales and some pinnipeds (or seals) are the marine mammal taxa of greatest concern for human and ecological health, with Hg concentrations regularly recorded in brain tissue that are associated with sub-clinical neurobiochemical changes (Dietz et al., 2013; Krey et al., 2015). Although the effect levels in marine mammals are little understood (Desforges et al., 2016), a study on bottle-nosed dolphins found lesions in the liver at 61 ppm ww and is being used by scientists as a benchmark for assessing ecological concern in marine mammals (Dietz et al., 2013). Because liver tissue has a broad percentage of MeHg content and is challenging to relate to muscle tissue (which is a more relevant tissue for human health purposes, Appendix

8.1) liver is less useful for rapidly assessing risk for human consumption. Muscle tissue is more useful to use for assessing the potential exposure of MeHg to humans.

Many subsistence communities, mostly in the Arctic, depend on the harvest of marine mammals such as narwhal, beluga, pilot whales, and ringed seals. Ringed seals are potentially important Holarctic bioindicators of MeHg availability to humans as they are common, widely distributed, and regularly harvested (Braune et al., 2015). Based on the GBMS database, over 20 species of toothed whales have average muscle tissue Hg concentrations >1.0 ppm ww. Therefore, toothed whales appear to be one of the more Hg contaminated groups of marine mammals. Toothed whales have global mean Hg concentrations (2.61 ppm, ww; Appendix 8.1) well above general recognized consumption advisory levels recognized by most national standards (and is most relevant for beluga and pilot whales) because of the dependence of certain Arctic human communities on them and several species have Hg concentrations >4.0 ppm ww (Figure 8.11). Various species of porpoises and dolphins (Aubail et al., 2013; Correa et al., 2013), as well as beaked whales (which specialize in foraging on deep-water cephalopods), also generally have elevated Hg body burdens (Figure 8.11; Bustamante et al., 2003; Garrigue et al., 2016). Other marine mammals foraging at lower depths in the mesopelagic zone also have elevated MeHg concentrations (Peterson et al., 2015) and are especially vulnerable when MeHg concentrations increase during haul-out periods when body mass declines as they fast and breed on land (Peterson et al., 2018).

Figure 8.11 Arithmetic mean +/- SD of global total Hg concentrations (ppm, ww) in muscle tissue of toothed whales by species (except beaked whales were combined under the family, Hyperoodontidae, and the two species of pilot whales were grouped).

8.6 Linkage between Hg source types and biota

Linkage between major Hg source types and Hg found in biota can be evaluated through the use of variations in stable Hg isotope ratios (e.g., Blum et al., 2014; Kwon et al., 2014; Li et al., 2016b). Mercury has seven stable isotopes and undergoes mass fractionation following many different patterns of isotope ratio variation during chemical reactions. The most widely used isotopic 'signals' of sources and chemical processes are: mass dependent fractionation (MDF); odd isotope mass independent fractionation (odd-MIF); and even isotope mass independent fractionation (even-MIF). The magnitude of the three 'signals' as well as the ratios between them can be used to distinguish Hg sources and chemical processes in the environment (Blum and Johnson, 2017).

By measuring the isotopic ratios of Hg in environmental samples, certain linkages can be established and others can be eliminated in investigations of Hg sources. The method is often not definitive by itself, but combined with other information based on Hg concentrations and chemical speciation, the evidence considered together can be conclusive. There are many examples in the literature where Hg isotopes have been used to separate the origin of Hg from global gaseous Hg background, global precipitation, coal burning facilities, chlor-alkali facilities, gold mining, and other industrial sources – particularly at local scales.

Several studies have shown that local atmospheric sources of Hg from industrial output can be identified in precipitation and in gaseous Hg because they contrast in isotopic composition with globally well-mixed atmospheric reservoirs (Sherman et al., 2012). Similarly, industrial inputs of Hg to rivers, lakes, and marine coastal areas can often be distinguished from natural background Hg and atmospherically deposited Hg based on isotopic composition (Donovan et al., 2014). Mercury isotopes have also been used as an indicator of Hg methylation and demethylation rates and hotspots within ecosystems, and more broadly as a tool in understanding Hg biogeochemistry (Donovan et al., 2016). In situations where at least two isotopically distinct sources of Hg are present, Hg isotopes have also been used to trace the source of Hg in biota and humans (Sherman et al., 2013).

Use of the Hg isotope technique to better track the effects of climate change on Hg dynamics in food webs is promising. For example, there is evidence that climate change may cause a shift in the depth of Hg methylation in the oceans and that could influence Hg levels in open ocean fisheries (Blum at al., 2014). Separating major Hg sources within existing contaminated sites would increase the potential for identifying how they influence human and ecological health as characterized through bioindicators for purposes related to the Minamata Convention (Evers et al., 2016).

~~8.7 Overarching global patterns~~

~~The compilation of existing biotic Hg data is an important approach to understand broad spatial gradients and temporal patterns. Models based on existing data and scientific findings are useful for extending observations in space and time. Recent global modelling efforts show 49% of global Hg^{II} deposition occurs~~

over the tropical oceans (Horowitz et al., 2017). The lifetimes of Hg in the ocean determined by considering coupling among the oceans, atmosphere, and land are decades in the upper ocean and up to millennia in the deep ocean (Amos et al., 2013). An alternate model suggests that the global ocean Hg turnover time against sediment burial to be about 1100 years (Semeniuk and Dastoor, 2017). Ocean cruise observations also show high dissolved gaseous Hg and MeHg concentrations in seawater in equatorial upwelling regions of the ocean (Mason and Fitzgerald, 1993; Soerensen et al., 2014; Bowman et al., 2016). Furthermore, studies now predict ocean regions with high organic carbon remineralization (e.g., equatorial Pacific Ocean) to have enhanced MeHg concentrations in both surface and subsurface waters (Kim et al., 2017). The equatorial Pacific region is an essential commercial harvesting location for many large pelagic species such as tunas that are responsible for a large fraction of human exposure to MeHg (Sunderland et al., 2018).

In freshwater ecosystems, large contaminated sites are expected to be an important driver of variability in freshwater biota concentrations. One recent effort to characterize global aquatic Hg releases to inland ecosystems is therefore especially important for understanding the spatial distribution of these locations (Kocman et al., 2017). A major driver of such spatial patterns is the location of ASGM activities (Annex within the Technical Report). Mercury releases from ASGM activities are greatest across much of Central and South America, most of Africa outside of the Sahara Desert, and broad areas across Asia, including the Indo-Pacific Region. Although the magnitude and patterns of occupational hazards associated with ASGM are beginning to be quantified (Steckling et al., 2017), understanding of the MeHg impacts on human and ecological health is poor (Macdonald et al., 2014). How releases of tonnes of ASGM-derived inorganic Hg

into the air, water, and land reach aquatic food webs and are transferred into higher trophic-level organisms varies greatly across these continents. Yet, the associated patterns over time and space are critical to understand for developing biomonitoring activities in a time-efficient and cost-effective manner. Enhanced atmospheric deposition of Hg from local sources is also apparent near regions with a large number of coal-fired power plants. In global modelling efforts, enhanced deposition is apparent in India and China owing to these concentrated sources (Giang et al., 2015). Regulations in the eastern USA and Europe have significantly decreased atmospheric Hg concentrations and local deposition from coal-fired utilities in those areas, thus protecting local biota and improving environmental quality (Zhang et al., 2016).

8.7.1 Spatial gradients

The availability of MeHg to high trophic level organisms is not uniform. Some ecosystems are more sensitive to inorganic Hg input than others (Driscoll et al., 2007; Eagles-Smith et al., 2016b) and it is in these areas that biological MeHg hotspots can form and are especially pronounced in higher trophic-level organisms (Evers et al., 2007). Such areas are generally associated with wetlands and other temporally wetted habitats, and can be particularly pronounced in ecosystems with water chemistry variables such as low pH, moderate to high dissolved organic carbon concentrations, and low to moderate primary productivity. In particular, fluctuating water levels can have a particularly important contribution in generating higher methylation rates and increases in MeHg bioavailability (Willacker et al., 2016); and, may happen at daily (tidal), monthly (artificial reservoirs and pools), or seasonal (river floodplains and dry tropical areas flooded during the wet season) timeframes, as well as under managed areas (rice agriculture).

Therefore, the determination of areas that may have elevated MeHg availability are generally not directly related to the deposition or release of inorganic Hg into the environment. For example, compared to the USA, relatively low precipitation-weighted mean concentrations and deposition of total Hg are in Kejimkujik National Park in Nova Scotia, Canada (an average of <5 ng/L and <7.5 ug/m^2 of Hg per year for the past four years of available data; NADP, 2017; Dastoor et al., 2004, 2015), yet the biotic MeHg exposure is some of the highest in North America where fish and birds within the National Park well exceed ecological health thresholds (i.e., 0.30 and 3.0 µg/g ww, respectively; Evers et al., 1998; Burgess and Hobson, 2006; Burgess and Meyer, 2008; Wyn et al., 2010). This is because most lakes in the area are sensitive to inorganic Hg input and have high methylation potential and MeHg bioavailability owing to a combination of low pH, high dissolved organic carbon, high percentage of shoreline wetlands, and low primary productivity. Ultimately, identification of biological MeHg hotspots can be made through the collection of existing biotic data (Evers et al., 2011b; Ackerman et al., 2016; Eagles-Smith et al., 2016b) and modelling ecosystem sensitivity at regional or global scales.

8.7.2 Temporal trends

New models simulating the deposition of Hg from anthropogenic emissions at global scales (using three anthropogenic emissions scenarios) indicate a best case scenario of a decrease of up to 50% in the Northern Hemisphere and up to 35% in the Southern Hemisphere by 2035 (Pacyna et al., 2016). Although tracking Hg emissions, deposition, and releases are important tools for understanding patterns of environmental Hg loads (Sundseth et al., 2017) the relationship between modelled (or measured) deposition and MeHg

concentrations in biota is poorly understood. Trends in inorganic Hg concentration are thought to differ among ocean basins because anthropogenic emissions have strongly declined in North America and Europe, leading to large declines in atmospheric concentrations, especially in the Atlantic Ocean (Zhang et al., 2016). Lee and Fisher (2016) postulated that this may also explain observed declines in Atlantic bluefin tuna MeHg concentrations between 2004 and 2012 in the North Atlantic Ocean – which are supported in measured Hg concentrations in blue marlin (*Makaira nigricans*; Barber and Cross, 2015).

The relationship of changing fish MeHg concentrations in different ocean basins is germane to a better understanding of the geographic origins of seafood by country or region. For example, for the USA, 45% of population-wide MeHg exposure originates from open oceans (particularly the Pacific Ocean), 37% from domestic coastal ecosystems, 9% from aquaculture, and 9% from freshwater fisheries (Sunderland et al., 2018).

By contrast, both atmospheric emissions and freshwater discharges of Hg have been growing on the Asian continent leading to increased Hg pollution in the North Pacific Ocean (Streets et al., 2009; Sunderland et al., 2009; Zhang et al., 2015). Temporal data on fisheries in the North Pacific are more limited but some researchers have suggested that there is evidence for increases in tuna MeHg concentrations over recent decades (Drevnick et al., 2015), which is further supported by additional analysis of bigeye tuna for the same area (Drevnick and Brooks, 2017).

In North America, long-term biomonitoring in Arctic freshwater (Chételat et al., 2015) and marine (Rigét et al., 2011; Braune et al., 2015) ecosystems provides an important regional platform for examining temporal

trends through Canada's Northern Contaminants Program and AMAP. In addition, in the Canadian province of Ontario projected temporal trends in over 200,000 game fish analyzed since 1970 indicate increasing MeHg concentrations in more than 250,000 lakes (which, when including the Great Lakes, represents about a third of the world's freshwater). Using one of the largest consistent Hg biomonitoring efforts in the world, a robust long-term trend in fish Hg concentrations can be determined. Using Hg concentrations in the muscle of walleye, northern pike, and lake trout, it is projected that 84–100% of the 250,000+ lakes will have "do not eat" advisories by 2050 for sensitive human populations (Gandhi et al., 2014, 2015). Although inorganic Hg emissions in North America are declining, other factors such as global emissions, climate change, invasive species, and local geochemistry may be impacting the response time and magnitude of biotic MeHg trends for this region (Gandhi et al., 2014). Climate drivers such as higher precipitation rates may be especially important in this area causing increased MeHg concentrations for both cool and warm water gamefish (Chen et al., 2018). Expected increases in input rates for terrestrial natural organic matter, due to climate change, are also linked to trophic shifts in aquatic food webs that lead to increased biomagnification of MeHg (Jonsson et al., 2017).

The influence of climate change on Hg cycling only increases the importance of generating baseline data for MeHg in bioindicators. An example can be found in Canada where total Hg levels in aquatic birds and fish communities have been monitored across the Canadian Great Lakes by Environment and Climate Change Canada at 22 stations for the past 42 years (1974–2015) (Blukacz-Richards et al., 2017). For the first three decades, Hg levels in gull eggs and fish declined at all stations. In the 2000s, trend reversals were apparent

~~for many stations and in most of the Great Lakes, although the specific taxa responsible varied. While strong trophic interactions among birds and fish are apparent, there also appears to be a high likelihood of trophic decoupling in some ecosystems. This indicates the importance not only of long-term Hg biomonitoring efforts, but also study designs that include other parameters such as food web structure (Pinkney et al., 2015), watershed disturbances including novel factors such as beaver activity (Brigham et al., 2014), and especially those related to climate change (magnitude and frequency of storm events, increasing wildfire activity, etc.; Sundseth et al., 2015).~~

8.7 Knowledge gaps

By identifying critical knowledge gaps and adopting quantitative and replicable approaches, a harmonized biomonitoring effort can be developed and made available to countries. A standardized approach that quantifies where, when, how, and what to monitor for tracking environmental inorganic Hg loads, their changes over time, and potential impacts on human and ecological health is now needed. Although there are a few large biological Hg datasets, they do not provide the ability to determine changes in biotic Hg exposure at regional or global scales over decadal periods. Robust statistical approaches are critical for confidently tracking biotic Hg concentrations in the many different biomes around the world, and controlling for the effects of other factors, such as global climate change, altered foraging habitat, changes in primary productivity and changing growth rates that can drive changes in biotic MeHg concentrations with no actual change in inorganic Hg availability (Eagles-Smith et al., 2018).

One factor in particular, global climate change, will alter future Hg concentration levels across the landscape (Sundseth et al., 2017), especially in Arctic marine (McKinney et al., 2015; Sundseth et al., 2015), subarctic and temperate lakes (Chen et al., 2018), temperate estuarine (Willacker et al., 2017), and terrestrial ecosystems (Eagles-Smith et al., 2018). Specific effects of global climate change include enhanced air-seawater exchange, melting of polar ice caps and glaciers, increased thawing of permafrost, and changes in estuarine sulfur biogeochemistry, but how these landscape processes relate to changes in biotic Hg exposure is relatively unknown.

Iterative efforts to link realistic and applied biomonitoring efforts at local levels with science groups aimed at assisting the Conference of Parties of the Minamata Convention will ultimately help keep pace with the many emerging scientific findings that may fill existing information gaps that are key for global policymaking.

8.8 Conclusions

In summary, the careful selection and use of bioindicators that closely match objectives of the interested parties can be a cost-effective and time-efficient way to track human and ecological health from the anthropogenic loading of Hg onto the water and landscape at a global level (Evers et al., 2016). The methods for biomonitoring and the interpretation of the tissues sampled are generally well-described for many target taxa. The extensive knowledge of Hg exposure in a wide range of fish and wildlife that are available in the peer-reviewed literature, and now available in the GBMS database (Evers et al., 2017), provides a platform for selecting the appropriate taxa within a certain biome or waterbody. Biomonitoring should build from

existing programs, which are generally found within developed countries at local, national, and sometimes regional levels. Global pilot projects based on existing networks with local organizations and governmental agencies have been tested for fish (Buck et al., in press) and humans (Trasande et al., 2016) and biomonitoring approaches in temperate marine ecosystems are well described (Evers et al., 2008). Generating a more global approach that can amalgamate existing biomonitoring programs and identify the ecosystem, taxa, or geographic gaps is feasible. There are many landscape, ecological, and demographic factors that influence MeHg generation and bioavailability – many of which are known and can be used for scaling models, whereas other factors that affect spatial gradients of biotic MeHg exposure still need further investigation (e.g., climate change). Once country needs and interests of the Minamata Convention are determined by the Conference of Parties, it is feasible to generate cost-efficient and reliable biomonitoring approaches at geographic scales of interest.

References

Abeysinghe, K.S., G. Qiu, E. Goodale, C.W. Anderson, K. Bishop, D.C. Evers, M.W. Goodale, H. Hintelmann, S. Liu, C. Mammides and R.C. Quan, 2017. Mercury flow through an Asian rice-based food web. Environmental Pollution, 229:219-228.

Abma, R.A., G. Paterson, A. McLeod and G.D. Haffner, 2015. Cross-basin comparison of mercury bioaccumulation in Lake Huron lake trout emphasizes ecological characteristics. Environmental Toxicology and Chemistry, 34:355-359.

Ackerman, J.T., C.A. Eagles-Smith, J.Y. Takekawa, S.A. Demers, T.L. Adelsbach, J.D. Bluso, A.K. Miles, N. Warnock, T.H. Suchanek and S.E. Schwarzbach, 2007. Mercury concentrations and space use of pre-breeding American avocets and black-necked stilts in San Francisco Bay. Science of the Total Environment, 384:452-466.

Ackerman, J.T., C.A. Eagles-Smith, J.Y. Takekawa, J.D. Bluso and T.L. Adelsbach, 2008. Mercury concentrations in blood and feathers of pre-breeding Forster's terns in relation to space use of San Francisco Bay habitats. Environmental Toxicology and Chemistry, 27:897-908.

Ackerman, J.T., C.A. Eagles-Smith and M.P. Herzog, 2011. Bird mercury concentrations change rapidly as chicks age: toxicological risk is highest at hatching and fledging. Environmental Science and Technology, 45:5418-5425.

Ackerman, J.T., M.P. Herzog and S.E. Schwarzbach, 2013. Methylmercury is the predominant form of mercury in bird eggs: a synthesis. Environmental Science and Technology, 47:2052-2060.

Ackerman, J.T., C.A. Hartman, C.A. Eagles-Smith, M.P. Herzog, J. Davis, G. Ichikawa and A. Bonnema, 2015. Estimating mercury exposure of piscivorous birds and sport fish using prey fish monitoring. Environmental Science and Technology, 49:13596-13604.

Ackerman, J.T., C.A. Eagles-Smith, M.P. Herzog, C.A. Hartman, S.H. Peterson, D.C. Evers, A.K. Jackson, J.E. Elliott, S.S. Vander Pol and C.E. Bryan, 2016. Avian mercury exposure and toxicological risk across western North America: A synthesis. Science of the Total Environment, 568:749-769.

Affum, A.O., S.O. Dede, B.J.B. Nyarko, S.O. Acquaah, E.E. Kwaansa-Ansah, G. Darko, A. Dickson, E.A. Affum and J.R. Fianko, 2016. Influence of small-scale gold mining and toxic element concentrations in Bonsa river, Ghana: a potential risk to water quality and public health. Environmental Earth Sciences, 75:178.

Åkerblom, S. and J. de Jong, 2017. Mercury in fur of Daubenton's bat (*Myotis daubentonii*) in southern Sweden and comparison to ecotoxicological thresholds. Bulletin of Environmental Contamination and Toxicology, 99:561-566.

Åkerblom, S., A. Bignert, M. Meili, L. Sonesten and M. Sundbom, 2014. Half a century of changing mercury levels in Swedish freshwater fish. Ambio, 43:91-103.

AMAP, 2011. AMAP Assessment 2011: Mercury in the Arctic. Arctic Monitoring and Assessment Programme (AMAP), Oslo.

AMAP, 2015. AMAP Assessment 2015: Human Health in the Arctic. Arctic Monitoring and Assessment Programme (AMAP), Oslo.

Amos, H.M., D.J. Jacob, D.G. Streets and E.M. Sunderland, 2013. Legacy impacts of all-time anthropogenic emissions on the global mercury cycle. Global Biogeochemical Cycles, 27:410-421.

Anderson, D.W., T.H. Suchanek, C.A. Eagles-Smith and T.M. Cahill, 2008. Mercury residues and productivity in osprey and grebes from a mine-dominated ecosystem. Ecological Applications, 18:A227-A238.

Anderson, O.R.J., R.A. Phillips, R.F. Shore, R.A.R. McGill, R.A. McDonald and S. Bearhop, 2010. Element patterns in albatrosses and petrels: influence of trophic position, foraging range, and prey type. Environmental Pollution, 158:98-107.

Anthony, R.G., A.K. Miles, M.A. Ricca and J.A. Estes, 2007. Environmental contaminants in bald eagle eggs from the Aleutian archipelago. Environmental Toxicology and Chemistry, 26:1843-1855.

Arcagni, M., R. Juncos, A. Rizzo, M. Pavlin, V. Fajon, M.A. Arribére, M. Horvat and S.R. Guevara, 2018. Species- and habitat-specific bioaccumulation of total mercury and methylmercury in the food web of a deep oligotrophic lake. Science of the Total Environment, 612:1311-1319.

Aubail, A., P. Méndez-Fernandez, P. Bustamante, C. Churlaud, M. Ferreira, J.V. Vingada and F. Caurant, 2013. Use of skin and blubber tissues of small cetaceans to assess the trace element content of internal organs. Marine Pollution Bulletin, 76:158-169.

Balshaw, S., J.W. Edwards, K.E. Ross and B.J. Daughtry, 2008. Mercury distribution in the muscular tissue of farmed southern bluefin tuna (*Thunnus maccoyii*) is inversely related to the lipid content of tissues. Food Chemistry, 111:616-621.

Barber, R.T. and F.A. Cross, 2015. Mercury bioaccumulation response to recent Hg pollution abatement in an oceanic predatory fish, blue marlin, versus the response in a Coastal predatory species, bluefish, in the western North Atlantic Ocean. In: AGU December 2015 Fall Meeting.

Barletta, M., A.J. Jaureguizar, C. Baigun, N.F. Fontoura, A.A. Agostinho, V.M.F. Almeida-Val, A.L. Val, R.A. Torres, L.F. Jimenes-Segura, T. Giarrizzo, N.N. Fabre, V.S. Batista, C. Lasso, D.C. Taphorn, M.F. Costa, P.T. Chaves, J.P. Vieira and M.F.M. Correa, 2010. Fish and aquatic conservation in South America: a continental overview with emphasis on neotropical systems. Journal of Fish Biology, 76:2118-2176.

Bastos, W.R., J.P.O. Gomes, R.C. Oliveira, R. Almeida, E.L. Nascimento, J.V.E. Bernardi, L.D. de Lacerda, E.G. da Silveira and W.C. Pfeiffer, 2006. Mercury in the environment and riverside population in the Madeira River basin, Amazon, Brazil. Science of the Total Environment, 368:344-351.

Bastos, W.R., J.G. Dórea, J.V. Bernardi, L.C. Lauthartte, M.H. Mussy, L.D. Lacerda and O. Malm, 2015. Mercury in fish of the Madeira River (temporal and spatial assessment), Brazilian Amazon. Environmental Research, 140:191-197.

Bidone, E.D., Z.C. Casilhos, T.M. Cid de Souza and L.D. Lacerda, 1997. Fish contamination and human exposure to mercury in the Tapajoas River Basin, Para State, Amazon, Brazil: a screening approach. Bulletin of Environmental Contamination and Toxicology, 59:194-201.

Bignert, A., F. Riget, B. Braune, P. Outridge and S. Wilson, 2004. Recent temporal trend monitoring of mercury in Arctic biota – how powerful are the existing data sets? Journal of Environmental Monitoring, 6:351-355.

Black, F.J., T. Bokhutlo, A. Somoxa, M. Maethamako, O. Modisaemang, T. Kemosedile, C. Cobb-Adams, K. Mosepele and M. Chimbari, 2011. The tropical African mercury anomaly: lower than expected mercury concentrations in fish and human hair. Science of the Total Environment, 409:1967-1975.

Bloom, N.S., 1992. On the chemical form of mercury in edible fish and marine invertebrate tissue. Canadian Journal of Fisheries and Aquatic Sciences, 49:1010-1017.

Blukacz-Richards, E.A., A. Visha, M.L. Graham, D.L. McGoldrick, S.R. de Solla, D.J. Moore and G.B. Arhonditsis, 2017. Mercury levels in herring gulls and fish: 42 years of spatio-temporal trends in the Great Lakes. Chemosphere, 172:476-487.

Blum, J.D. and M.W. Johnson, 2017. Recent developments in mercury stable isotope analysis. Reviews in Mineralogy and Geochemistry, 82:733-757.

Blum, J.D., L.S. Sherman and M.W. Johnson, 2014. Mercury isotopes in earth and environmental sciences. Annual Review of Earth and Planetary Sciences, 42:249-269.

Bodin, N., D. Lesperance, R. Albert, S. Hollanda, P. Michaud, M. Degroote, C. Churlaud and P. Bustamante, 2017. Trace elements in oceanic pelagic communities in the western Indian Ocean. Chemosphere, 174:354-362.

Bodin, N., R. Albert, N. Pillay, C. Churlaud, P. Bustamante and S. Hollanda, (in prep). Spatio-temporal distribution of mercury in swordfish from the Indian Ocean. In prep.

Boischio, A.A.P. and D. Henshel, 2000. Fish consumption, fish lore, and mercury pollution – risk communication for the Madeira River people. Environmental Research, 84A:108-126.

Bond, A.L. and A.W. Diamond, 2009. Mercury concentrations in seabird tissues from Machias Seal Island, New Brunswick, Canada. Science of the Total Environment, 407:4340-4347.

Bond, A.L., K.A. Hobson and B.A. Branfireun, 2015. Rapidly increasing methyl mercury in endangered ivory gull (*Pagophila eburnea*) feathers over a 130 year record. Proceedings of the Royal Society of London B, 282:20150032.

Bosch, A.C., B. O'Neill, G.O. Sigge, S.E. Kerwath and L.C. Hoffman, 2016a. Mercury accumulation in yellowfin tuna (*Thunnus albacares*) with regards to muscle type, muscle position and fish size. Food Chemistry, 190:351-356.

Bosch, A.C., B. O'Neill, G.O. Sigge, S.E. Kerwath and L.C. Hoffman, 2016b. Heavy metals in marine fish meat and consumer health: A review. Journal of the Science of Food and Agriculture, 96:32-48.

Bowerman, W.W., E.D. Evans, J.P. Giesy and S. Postupalsky, 1994. Using feathers to assess risk of mercury and selenium to bald eagle reproduction in the Great Lakes region. Archives of Environmental Contamination and Toxicology, 27:294-298.

Bowman, K.L., C.R. Hammerschmidt, C.H. Lamborg, G.J. Swarr and A.M. Agather, 2016. Distribution of mercury species across a zonal section of the eastern tropical South Pacific Ocean (US GEOTRACES GP16). Marine Chemistry, 186:156-166.

Braaten, H.F.V., S. Åkerblom, H.A. de Wit, G. Skotte, M. Rask, J. Vuorenmaa, K.K. Kahilainen, T. Malinen, S. Rognerud, E. Lydersen and P.A. Amundsen, 2017. Spatial and Temporal Trends of Mercury in Freshwater fish in Fennoscandia (1965-2015). NIVA-Report 7179/2017, ICP Waters Report 132/2017.

Branco, V., C. Vale, J. Canário and M.N. dos Santos, 2007. Mercury and selenium in blue shark (*Prionace glauca*, L. 1758) and swordfish (*Xiphias gladius*, L. 1758) from two areas of the Atlantic Ocean. Environmental Pollution, 150:373-380.

Braune, B.M., 1987. Comparison of total mercury levels in relation to diet and molt for nine species of marine birds. Archives of Environmental Contamination and Toxicology, 16:217-224.

Braune, B.M., 2007. Temporal trends of organochlorines and mercury in seabird eggs from the Canadian Arctic, 1975–2003. Environmental Pollution, 148:599-613.

Braune, B.M., M.L. Mallory and H.G. Gilchrist, 2006. Elevated mercury levels in a declining population of ivory gulls in the Canadian Arctic. Marine Pollution Bulletin, 52:978-982.

Braune, B., J. Chételat, M. Amyot, T. Brown, M. Clayden, M. Evans, A. Fisk, A. Gaden, C. Girard, A. Hare and J. Kirk, 2015. Mercury in the marine environment of the Canadian Arctic: Review of recent findings. Science of the Total Environment, 509:67-90.

Braune, B.M., A.J. Gaston and M.L. Mallory, 2016. Temporal trends of mercury in eggs of five sympatrically breeding seabird species in the Canadian Arctic. Environmental Pollution, 214:124-131.

Brigham, M.E., M.B. Sandheinrich, D.A. Gay, R.P. Maki, D.P. Krabbenhoft and J.G. Wiener, 2014. Lacustrine responses to decreasing wet mercury deposition rates: Results from a case study in northern Minnesota. Environmental Science and Technology, 48:6115-6123.

Brookens, T.J., T.M. O'Hara, R.J. Taylor, G.R. Bratton and J.T. Harvey, 2008. Total mercury body burden in Pacific harbor seal, *Phoca vitulina richardii*, pups from central California. Marine Pollution Bulletin, 56:27-41.

Brown, T.M., A.T. Fisk, X. Wang, S.H. Ferguson, B.G. Young, K.J. Reimer and D.C. Muir, 2016. Mercury and cadmium in ringed seals in the Canadian Arctic: Influence of location and diet. Science of the Total Environment, 545:503-511.

Buck, D.G., D.C. Evers, E. Adams, J. DiGangi, B. Beeler, J. Samanek, J. Petrlik, M.A. Turnquist, O. Speranskaya, K. Reagan, In press. A global-scale assessment of fish mercury concentrations and the identification of biological hotspots. Science of the Total Environment, In press.

Burger, J., 1993. Metals in avian feathers: bioindicators of environmental pollution. Reviews in Environmental Toxicology, 5:203-311.

Burger, J. and M. Gochfeld, 2000. Metal levels in feathers of 12 species of seabirds from Midway Atoll in the northern Pacific Ocean. Science of the Total Environment, 257:37-52.

Burger, J., and M. Gochfeld, 2006. Locational differences in heavy metals and metalloids in Pacific blue mussels *Mytilus [edulis] trossulus* from Adak Island in the Aleutian Chain, Alaska. Science of the Total Environment, 368:937-950.

Burger, J. and M. Gochfeld, 2009. Comparison of arsenic, cadmium, chromium, lead, manganese, mercury and selenium in feathers in bald eagle (*Haliaeetus leucocephalus*), and comparison with common eider (*Somateria mollissima*), glaucous-winged gull (*Larus glaucescens*), pigeon guillemot (*Cepphus columba*), and tufted puffin (*Fratercula cirrhata*) from the Aleutian Chain of Alaska. Environmental Monitoring and Assessment, 152:357-367.

Burger, J., M. Gochfeld, C. Jeitner, S. Burke, T. Stamm, R. Snigaroff, D. Snigaroff, R. Patrick and J. Weston, 2007. Mercury levels and potential risk from subsistence foods from the Aleutians. Science of the Total Environment, 384:93-105.

Burger, J., M. Gochfeld, C. Jeitner, D. Snigaroff, R. Snigaroff, T. Stamm and C. Volz, 2008. Assessment of metals in down feathers of female common eiders and their eggs from the Aleutians: arsenic, cadmium, chromium, lead, manganese, mercury, and selenium. Environmental Monitoring and Assessment, 143:247-256.

Burger, J., M. Gochfeld, C. Jeitner, S. Burke, C. Volz, R. Snigaroff, D. Snigaroff, T. Shukla and S. Shukla, 2009. Mercury and other metals in eggs and feathers of glaucous-winged gulls (*Larus glaucescens*) in the Aleutians. Environmental Monitoring and Assessment, 152:179-194.

Burgess, N.M. and K.A. Hobson, 2006. Bioaccumulation of mercury in yellow perch (*Perca flavescens*) and common loons (*Gavia immer*) in relation to lake chemistry in Atlantic Canada. Hydrobiologia, 567:275-282.

Burgess, N.M. and M.W. Meyer, 2008. Methylmercury exposure associated with reduced productivity in common loons. Ecotoxicology, 17:83-91.

Burgess, N.M., A.L. Bond, C.E. Hebert, E. Neugebauer and L. Champoux, 2013. Mercury trends in herring gull (*Larus argentatus*) eggs from Atlantic Canada, 1972–2008: temporal change or dietary shift? Environmental Pollution, 172:216-222.

Bustamante, P., C. Garrigue, L. Breau, F. Caurant, W. Dabin, J. Greaves and R. Dodémont, 2003. Trace elements in two odontocetes species (*Kogia breviceps* and *Globicephala macrorhynchus*) stranded in New Caledonia (South Pacific). Environmental Pollution, 124:263-271.

Bustamante, P., A. Carravieri, A. Goutte, C. Barbraud, K. Delord, O. Chastel, H. Weimerskirch and Y. Cherel, 2016. High feather mercury concentrations in the wandering albatross are related to sex, breeding status and trophic ecology with no demographic consequences. Environmental Research, 144:1-10.

Cai, Y., J.R. Rooker, G.A. Gill and J.P. Turner, 2007. Bioaccumulation of mercury in pelagic fishes from the northern Gulf of Mexico. Canadian Journal of Fisheries and Aquatic Sciences, 64:458-469.

Campbell, L.M., R.J. Norstrom, K.A. Hobson, D.C. Muir, S. Backus and A.T. Fisk, 2005. Mercury and other trace elements in a pelagic Arctic marine food web (Northwater Polynya, Baffin Bay). Science of the Total Environment, 351:247-263.

Carravieri, A., Y. Cherel, P. Blévin, M. Brault-Favrou, O. Chastel and P. Bustamante, 2014. Mercury exposure in a large subantarctic avian community. Environmental Pollution, 190C:51-57.

Carravieri, A., Y. Cherel, A. Jaeger, C. Churlaud and P. Bustamante, 2016. Penguins as bioindicators of mercury contamination in the southern Indian Ocean: geographical and temporal trends. Environmental Pollution, 213:195-205.

Carravieri, A., Y. Cherel, M. Brault-Favrou, C. Churlaud, L. Peluhet, P. Labadie, H. Budzinski, O. Chastel and P. Bustamante, 2017. From Antarctica to the subtropics: Contrasted geographical concentrations of selenium, mercury, and persistent organic pollutants in skua chicks (*Catharacta* spp.). Environmental Pollution, 228:464-473.

Carvan, M.J., T.A. Kalluvila, R.H. Klingler, J.K. Larson, M. Pickens, F.X. Mora-Zamorano, V.P. Connaughton, I. Sadler-Riggleman, D. Beck and M.K. Skinner, 2017. Mercury-induced epigenetic transgenerational inheritance of abnormal neurobehavior is correlated with sperm epimutations in zebrafish. PloS ONE, 12:e0176155.

Castilhos, Z.C., E.D. Bidone and L.D. Lacerda, 1998. Increase of the background human exposure to mercury through fish consumption due to gold mining at the Tapajos River region, Para State, Amazon. Bulletin of Environmental Contamination and Toxicology, 61:202-209.

Cerveny, D., S. Roje, J. Turek and T. Randak, 2016. Fish fin-clips as a non-lethal approach for biomonitoring of mercury contamination in aquatic environments and human health risk assessment. Chemosphere, 163:290-295.

Chan, H.M., C. Kim, K. Khoday, O. Receveur and H.V. Kuhnlein, 1995. Assessment of dietary exposure to trace-metals in Baffin Inuit food. Environmental Health Perspectives, 103:740-746.

Chase, M.E., S.H. Jones, P. Hennigar, J. Sowles, G.C.H. Harding, K. Freeman, P.G. Wells, C. Krahforst, K. Coombs, R. Crawford and J. Pederson, 2001. Gulfwatch: Monitoring spatial and temporal patterns of trace metal and organic contaminants in the Gulf of Maine (1991–1997) with the blue mussel, *Mytilus edulis* L. Marine Pollution Bulletin, 42:490-504.

Chaves-Ulloa, K., B.W. Taylor, H.J. Broadley, K.L. Cottingham, N.A. Baer, K.C. Weathers, H.A. Ewing and C.Y. Chen, 2016. Dissolved organic carbon modulates mercury concentrations in insect subsidies from streams to terrestrial consumers. Ecological Applications, 26:1771-1784.

Chen, C.Y., M.E. Borsuk, D.M. Bugge, T. Hollweg, P.H. Balcom, D.M. Ward, J. Williams and R.P. Mason, 2014. Benthic and pelagic pathways of methylmercury bioaccumulation in estuarine food webs of the northeast United States. PloS ONE, 9:89305.

Chen, M.M., L. Lopez, S.P. Bhavsar and S. Sharma, 2018. What's hot about mercury? Examining the influence of climate on mercury levels in Ontario top predator fishes. Environmental Research, 162:63-73.

Chételat, J., B. Braune, J. Stow and S. Tomlinson, 2015. Special issue on mercury in Canada's North: Summary and recommendations for future research. Science of the Total Environment, 509:260-262.

Chételat, J., M.C. Richardson, G.A. MacMillan, M. Amyot and A.J. Poulain, 2018. Ratio of methylmercury to dissolved organic carbon in water explains methylmercury bioaccumulation across a latitudinal gradient from North-Temperate to Arctic Lakes. Environmental Science and Technology, 52:79-88.

Cizdziel, J.V., T.A. Hinners and E.M. Heithmar, 2002. Determination of total mercury in fish tissues using combustion atomic absorption spectrometry with gold amalgamation. Water, Air and Soil Pollution, 135:355-370.

Condon, A.M. and D.A. Cristol, 2009. Feather growth influences blood mercury level of young songbirds. Environmental Toxicology and Chemistry, 28:395-401.

Correia, R.R.S. and J.R.D. Guimarães, 2017. Mercury methylation and sulfate reduction rates in mangrove sediments, Rio de Janeiro, Brazil: The role of different microorganism consortia. Chemosphere, 167:438-443.

Correa, L., J.M. Castellini, R.S. Wells and T. O'Hara, 2013. Distribution of mercury and selenium in blood compartments of bottlenose dolphins (*Tursiops truncatus*) from Sarasota Bay, Florida. Environmental Toxicology and Chemistry, 32:2441-2448.

Costa, M., W. Landing, H. Kehrig, M. Barletta, C. Holmes, P. Barrocas, D.C. Evers, D. Buck, A. Vasconcellos, S. Hacon, J. Moreia, and O. Malm, 2012. Mercury in tropical and sub-tropical coastal environments. Environmental Research, 119:88-100.

Cristol, D.A., R.L. Brasso, A.M. Condon, R.E. Fovargue, S.L. Friedman, K.K. Hallinger, A.P. Monroe and A.E. White, 2008. The movement of aquatic mercury through terrestrial food webs. Science, 320:335-335.

Dam, M. and D. Bloch, 2000. Screening of mercury and persistent organochlorine pollutants in long-finned pilot whale (*Globicephala melas*) in the Faroe Islands. Marine Pollution Bulletin, 40:1090-1099.

Daso, A.P., J.O. Okonkwo, R. Jansen, J.D. Brandao and A. Kotzé, 2015. Mercury concentrations in eggshells of the southern ground-hornbill (*Bucorvus leadbeateri*) and wattled crane (*Bugeranus carunculatus*) in South Africa. Ecotoxicology and Environmental Safety, 114:61-66.

Dastoor, A.P. and Y. Larocque, 2004. Global circulation of atmospheric mercury: A modelling study. Atmospheric Environment, 38:147-161.

Dastoor, A., A. Ryzhkov, D. Durnford, I. Lehnherr, A. Steffen and H. Morrison, 2015. Atmospheric mercury in the Canadian Arctic. Part II: Insight from modeling. Science of The Total Environment, 509:16-27.

Day, R.D., S.J. Christopher, P.R. Becker and D.W. Whitaker, 2005. Monitoring mercury in the loggerhead sea turtle, *Caretta caretta*. Environmental Science and Technology, 39:437-446.

de Carvalho, G.G.A., I.A.M. Degaspari, V. Branco, J. Canário, A.F. de Amorim, V.H. Kennedy and J.R. Ferreira, 2014. Assessment of total and organic mercury levels in blue sharks (*Prionace glauca*) from the south and southeastern Brazilian coast. Biological Trace Element Research, 159:128-134.

de Pinho, A.P., J.R.D. Guimarães, A.S. Martins, P.A.S. Costa, G. Olavo and J. Valentin, 2010. Total mercury in muscle tissue of five shark species from Brazilian offshore waters: effects of feeding habit, sex, and length. Environmental Research, 89:250-258.

Depew, D.C., N. Basu, N.M. Burgess, L.M. Campbell, E.W. Devlin, P.E. Drevnick, C.R. Hammerschmidt, C.A. Murphy, M.B. Sandheinrich and J.G. Wiener, 2012a. Toxicity of dietary methylmercury to fish: derivation of ecologically meaningful threshold concentrations. Environmental Toxicology and Chemistry, 31:1536-1547.

Depew, D.C., N. Basu, N.M. Burgess, L.M. Campbell, D.C. Evers, K.A. Grasman and A.M. Scheuhammer, 2012b. Derivation of screening benchmarks for dietary methylmercury exposure for the common loon (*Gavia immer*): rationale for use in ecological risk assessment. Environmental Toxicology and Chemistry, 31:2399-2407.

Desforges, J.P.W., C. Sonne, M. Levin, U. Siebert, S. De Guise and R. Dietz, 2016. Immunotoxic effects of environmental pollutants in marine mammals. Environment International, 86:126-139.

DesGranges, J.L., J. Rodrigue, B. Tardif and M. Laperle, 1998. Mercury accumulation and biomagnification in ospreys (*Pandion haliaetus*) in the James Bay and Hudson Bay regions of Quebec. Archives of Environmental Contamination and Toxicology, 35:330-341.

DeSorbo, C.R., N.M. Burgess, C.S. Todd, D.C. Evers, R.A. Bodaly, B.H. Massey, S.E. Mierzykowski, C.P. Persico, R.B. Gray, W.E. Hanson, D.E. Meattey and K.J. Regan, 2018. Mercury concentrations in bald eagles across an impacted watershed in Maine, USA. Science of the Total Environment, 627:1515-1527.

Dietz, R., C. Sonne, N. Basu, B. Braune, T. O'Hara, R.J. Letcher, T. Scheuhammer, M. Andersen, C. Andreasen, D. Andriashek and G. Asmund, 2013. What are the toxicological effects of mercury in Arctic biota? Science of the Total Environment, 443:775-790.

Diop, M. and R. Amara, 2016. Mercury concentrations in the coastal marine food web along the Senegalese coast. Environmental Science and Pollution Research, 23:11975-11984.

Dolgova, S., D. Crump, E. Porter, K. Williams and C.E. Hebert, in press. Stage of development affects dry weight mercury concentrations in bird eggs: Laboratory evidence and adjustment method. Environmental Toxicology and Chemistry, In press.

Donovan, P.M., J.D. Blum, J.D. Demers, B. Gu, S.C. Brooks and J. Peryam, 2014. Identification of multiple mercury sources to stream sediments near Oak Ridge, TN, USA. Environmental Science and Technology, 48:3666-3674.

Donovan, P.M., J.D. Blum, M.B. Singer, M. Marvin-DiPasquale and M.T. Tsui, 2016. Isotopic composition of inorganic mercury and methylmercury downstream of a historical gold mining region. Environmental Science and Technology, 50:1691-1702.

Drevnick, P.E. and B.A. Brooks, 2017. Mercury in tunas and blue marlin in the North Pacific Ocean. Environmental Toxicology and Chemistry, 36:1365-1374.

Drevnick, P.E., C.H. Lamborg and M.J. Horgan, 2015. Increase in mercury in Pacific yellowfin tuna. Environmental Toxicology and Chemistry, 34:931-934.

Driscoll, C.T., Y.J. Han, C.Y. Chen, D.C. Evers, K.F. Lambert, T.M. Holsen, N.C. Kamman and R. Munson, 2007. Mercury contamination in remote forest and aquatic ecosystems in the northeastern U.S.: Sources, transformations and management options. Bioscience, 57:17-28.

Driscoll, C.T., R.P. Mason, H.M. Chan, D.J. Jacob and N. Pirrone, 2013. Mercury as a global pollutant: sources, pathways, and effects. Environmental Science and Technology, 47:4967-4983.

Eagles-Smith, C.A. and J.T. Ackerman, 2009. Rapid changes in small fish mercury concentrations in estuarine wetlands: Implications for wildlife risk and monitoring programs. Environmental Science and Technology, 43:8658-8664.

Eagles-Smith, C.A. and J.T. Ackerman, 2014. Mercury bioaccumulation in estuarine wetland fishes: evaluating habitats and risk to coastal wildlife. Environmental Pollution, 193:147-155.

Eagles-Smith, C.A., J.T. Ackerman, S.E.W. De La Cruz and J.Y. Takekawa, 2009a. Mercury bioaccumulation and risk to three waterbird foraging guilds is influenced by foraging ecology and breeding stage. Environmental Pollution, 157:1993-2002.

Eagles-Smith, C.A., J.T. Ackerman, J. Yee and T.L. Adelsbach, 2009b. Mercury demethylation in waterbird livers: dose-response thresholds and differences among species. Environmental Toxicology and Chemistry, 28:568-577.

Eagles-Smith, C.A., J.T. Ackerman, J.J. Willacker, M.T. Tate, M.A. Lutz, J.A. Fleck, A.R. Stewart, J.G. Wiener, D.C. Evers, J.M. Lepak and J.A. Davis, 2016a. Spatial and temporal patterns of mercury concentrations in freshwater fish across the Western United States and Canada. Science of the Total Environment, 568:1171-1184.

Eagles-Smith, C.A., J.G. Wiener, C.S. Eckley, J.J. Willacker, D.C. Evers, M. Marvin-DiPasquale, D. Obrist, J.A. Fleck, G.R. Aiken, J.M. Lepak and A.K. Jackson, 2016b. Mercury in western North America: A

synthesis of environmental contamination, fluxes, bioaccumulation, and risk to fish and wildlife. Science of the Total Environment, 568:1213-1226.

Eagles-Smith, C.A., E.K. Silbergeld, N. Basu, P. Bustamante, F. Diaz-Barriga, W.A. Hopkins, K.A. Kidd and J.F. Nyland, 2018. Modulators of mercury risk to wildlife and humans in the context of rapid global change. Ambio, 47:170-197.

Edmonds, S.T., D.C. Evers, N.J. O'Driscoll, C. Mettke-Hoffman, L. Powell, D. Cristol, A.J. McGann, J.W. Armiger, O. Lane, D.F. Tessler and P. Newell, 2010. Geographic and seasonal variation in mercury exposure of the declining rusty blackbird. Condor, 112:789-799.

Elliott, J.E. and K.H. Elliott, 2013. Tracking marine pollution. Science, 340:556-558.

Evans, R.D., E.M. Addison, J.Y. Villeneuve, K.S. MacDonald and D.G. Joachim, 2000. Distribution of inorganic and methylmercury among tissues in mink (*Mustela vison*) and otter (*Lutra canadensis*). Environmental Research, 84:133-139.

Evans, M.S., D.C. Muir, J. Keating and X. Wang, 2015. Anadromous char as an alternate food choice to marine animals: A synthesis of Hg concentrations, population features and other influencing factors. Science of the Total Environment, 509:175-194.

Evers, D.C., 2018. The Effects of Methylmercury on Wildlife: A Comprehensive Review and Approach for Interpretation. Encyclopedia of the Anthropocene. Elsevier.

Evers, D.C. and T.A. Clair, 2005. Mercury in northeastern North America: A synthesis of existing databases. Ecotoxicology, 14:7-14.

Evers, D.C., J.D. Kaplan, M.W. Meyer, P.S. Reaman, A. Major, N. Burgess and W.E. Braselton, 1998. Bioavailability of environmental mercury measured in common loon feathers and blood across North American. Environmental Toxicology and Chemistry, 17:173-183.

Evers, D.C., N. Burgess, L. Champoux, B. Hoskins, A. Major, M.W. Goodale, R. Taylor, R. Poppenga and T. Daigle, 2005. Patterns and interpretation of mercury exposure in freshwater avian communities in northeastern North America. Ecotoxicology 14:193-222.

Evers, D.C., Y.J. Han, C.T. Driscoll, N.C. Kamman, M.W. Goodale, K.F. Lambert, T.M. Holsen, C.Y. Chen, T.A. Clair and T. Butler, 2007. Identification and evaluation of biological hotspots of mercury in the northeastern U.S. and eastern Canada. Bioscience, 57:29-43.

Evers, D.C., R.P. Mason, N.C. Kamman, C.Y. Chen, A.L. Bogomolni, D.H. Taylor, C.R. Hammerschmidt, S.H. Jones, N.M. Burgess, K. Munney and K.C. Parsons, 2008. An integrated mercury monitoring program for temperate estuarine and marine ecosystems on the North American Atlantic Coast. EcoHealth, 5:426-441.

Evers, D.C., R.T. Graham, P. Perkins, R. Michener and T. Divoll, 2009. Mercury concentrations in the goliath grouper of Belize: an anthropogenic stressor of concern. Endangered Species Research, 7:249-256.

Evers D.C., J.G. Wiener, N. Basu, R.A. Bodaly, H.A. Morrison and K.A. Williams, 2011a. Mercury in the Great Lakes region – Bioaccumulation, spatial and temporal patterns, ecological risks, and policy. Ecotoxicology, 20:1487-1499.

Evers, D.C., K.A. Williams, M.W. Meyer, A.M. Scheuhammer, N. Schoch, A.T. Gilbert, L. Siegel, R.J. Taylor, R. Poppenga and C.R. Perkins, 2011b. Spatial gradients of methylmercury for breeding common loons in the Laurentian Great Lakes region. Ecotoxicology, 20:1609-1625.

Evers, D.C., J.A. Schmutz, N. Basu, C.R. DeSorbo, J.S. Fair, C.G. Osborne, J. Paruk, M. Perkin, K. Regan, B.D. Uher-Koch and K.G. Wright, 2014. Mercury exposure and risk in yellow-billed loons breeding in Alaska and Canada. Waterbirds, 37:147-159.

Evers, D.C., S.E. Keane, N. Basu and D. Buck, 2016. Evaluating the effectiveness of the Minamata Convention on Mercury: Principles and recommendations for next steps. Science of the Total Environment, 569:888-903.

Evers, D.C., D.G. Buck, S.M. Johnson and M. Burton, 2017. Mercury in the Global Environment: Understanding spatial patterns for biomonitoring needs of the Minamata Convention on Mercury. Biodiversity Research Institute Science Communications Series 2017-12. Portland, Maine, USA.

Faial, K., R. Deus, S. Deus, R. Neves, I. Jesus, E. Santos, C.N. Alves and D. Brasil, 2015. Mercury levels assessment in hair of riverside inhabitants of the Tapajos River, Para State, Amazon, Brazil: fish consumption as a possible route of exposure. Journal of Trace Elements in Medicine and Biology, 30:66-76.

Ferriss, B.E. and T.E. Essington, 2011. Regional patterns in mercury and selenium concentrations of yellowfin tuna (*Thunnus albacares*) and bigeye tuna (*Thunnus obesus*) in the Pacific Ocean. Canadian Journal of Fisheries and Aquatic Sciences, 68:2046-2056.

Finkelstein, M., B.S. Keitt, D.A. Croll, B. Tershy, W.M. Jarman, S. Rodriguez-Pastor, D.J. Anderson, P.R. Sievert and D.R. Smith, 2006. Albatross species demonstrate regional differences in North Pacific marine contamination. Ecological Applications, 16:678-686.

Fisher, J.A., D.J. Jacob, A.L. Soerensen, H.M. Amos, A. Steffen and E.M. Sunderland, 2012. Riverine source of Arctic Ocean mercury inferred from atmospheric observations. Natural Geoscience, 5:499-504.

Fleming, E.J., E.E. Mack, P.G. Green and D.C. Nelson, 2006. Mercury methylation from unexpected sources: molybdate-inhibited freshwater sediments and an iron-reducing bacterium. Applied and Environmental Microbiology, 72:457-64.

Fonseca, F.R.D., O. Malm and H.F. Waldemarin, 2005. Mercury levels in tissues of giant otters (*Pteronura brasiliensis*) from the Rio Negro, Pantanal, Brazil. Environmental Research, 98:368-371.

Fragoso, C.P., E. Bernini, B.F. Araújo, M.G. de Almeida and C.E. de Rezende, 2018. Mercury in litterfall and sediment using elemental and isotopic composition of carbon and nitrogen in the mangrove of southeastern Brazil. Estuarine, Coastal and Shelf Science, 202:30-39.

Frederick, P.C., M.G. Spalding and R. Dusek, 2002. Wading birds as bioindicators of mercury contamination in Florida, USA: Annual and geographic variation. Environmental Toxicology and Chemistry, 21:163-167.

Furness, R.W. and K.C.J. Camphuysen, 1997. Seabirds as monitors of the marine environment. ICES Journal of Marine Science, 54:726-737.

Gabriel, M.C., N. Howard and T.Z. Osborne, 2014. Fish mercury and surface water sulfate relationships in the Everglades Protection Area. Environmental Management, 53:583-593.

Gandhi, N., R.W. Tang, S.P. Bhavsar and G.B. Arhonditsis, 2014. Fish mercury levels appear to be increasing lately: a report from 40 years of monitoring in the province of Ontario, Canada. Environmental Science and Technology, 48:5404-5414.

Gandhi, N., S.P. Bhavsar, R.W. Tang and G.B. Arhonditsis, 2015. Projecting fish mercury levels in the province of Ontario, Canada and the implications for fish and human health. Environmental Science and Technology, 49:14494-14502.

Gandhi, N., S.P. Bhavsar, S.B. Gewurtz, K.G. Drouillard, G.B. Arhonditsis and S. Petro, 2016. Is it appropriate to composite fish samples for mercury trend monitoring and consumption advisories? Environment International, 88:80-85.

Gantner, N., M. Power, D. Iqaluk, M. Meili, H. Borg, M. Sundbom, K.R. Solomon, G. Lawson and D.C. Muir, 2010. Mercury concentrations in landlocked Arctic char (*Salvelinus alpinus*) from the Canadian Arctic. Part I: insights from trophic relationships in 18 lakes. Environmental Toxicology and Chemistry, 29:621-632.

García, M.Á., R. Núñez, J. Alonso and M.J. Melgar, 2016. Total mercury in fresh and processed tuna marketed in Galicia (NW Spain) in relation to dietary exposure. Environmental Science and Pollution Research, 23:24960-24969.

Garrigue, C., M. Oremus, R. Dodémont, P. Bustamante, O. Kwiatek, G. Libeau, C. Lockyer, J.C. Vivier and M.L. Dalebout, 2016. A mass stranding of seven Longman's beaked whales (*Indopacetus pacificus*) in New Caledonia, South Pacific. Marine Mammal Science, 32:884-910.

Gbogbo, F., S.D. Otoo, R.Q. Huago and O. Asomaning, 2017. High levels of mercury in wetland resources from three river basins in Ghana: a concern for public health. Environmental Science and Pollution Research, 24:5619-5627.

Geyer, W.R. and D.K. Ralston, 2018. A mobile pool of contaminated sediment in the Penobscot Estuary, Maine, USA. Science of the Total Environment, 612:694-707.

Giang, A., L.C. Stokes, D.G. Streets, E.S. Corbitt and N.E. Selin, 2015. Impacts of the Minamata Convention on mercury emissions and global deposition from coal-fired power generation in Asia. Environmental Science and Technology, 49:5326-5335.

Gibb, H. and K.G. O'Leary, 2014. Mercury exposure and health impacts among individuals in the artisanal and small-scale gold mining community: a comprehensive review. Environmental Health Perspectives, 122:667-672.

Gilmour, C.C., M. Podar, A.L. Bullock, A.M. Graham, S.D. Brown, A.C. Somenhally, A. Johs, R.A. Hurt Jr., K.L. Bailey and D.A. Elias, 2013. Mercury methylation by novel microorganisms from new environments. Environmental Science and Technology, 47:11810-11820.

Goodale, M.W., D.C. Evers, S.E. Mierzykowski, A.L. Bond, N.M. Burgess, C.I. Otorowski, L.J. Welch, C.S. Hall, J.C. Ellis, R.B. Allen, A.W. Diamond, S.W. Kress and R.J. Taylor, 2008. Marine foraging birds as bioindicators of mercury in the Gulf of Maine. EcoHealth, 5:409-425.

Gorski, P.R., D.E. Armstrong, J.P. Hurley and D.P. Krabbenhoft, 2008. Influence of natural dissolved organic carbon on the bioavailability of mercury to a freshwater alga. Environmental Pollution, 154:116-123.

Goutte, A., C. Barbraud, A. Meillère, A. Carravieri, P. Bustamante, P. Labadie, H. Budzinski, K. Delord, Y. Cherel, H. Weimeskirch and O. Chastel, 2014a. Demographic consequences of heavy metals and persistent organic pollutants in a vulnerable long-lived bird, the wandering albatross. Proceedings of the Royal Society B, 281:20133313.

Goutte, A., P. Bustamante, C. Barbraud, K. Delord, H. Weimeskirch and O. Chastel, 2014b. Demographic responses to mercury exposure in two closely-related Antarctic top predators. Ecology, 95:1075-1086.

Great Lakes Fish Advisory Workgroup, 2007. A protocol for mercury-based fish consumption advise. Available from the International Joint Commission. 30pp.

Grove, R.A., C.J. Henny and J.L. Kaiser, 2009. Osprey: worldwide sentinel species for assessing and monitoring environmental contamination in rivers, lakes, reservoirs, and estuaries. Journal of Toxicology and Environmental Health B, 12:25-44.

Gustin, M., D.C. Evers, M. Bank, C.R. Hammerschmidt, A. Pierce, N. Basu, J. Blum, P. Bustamante, C. Chen, C.T. Driscoll, M. Horvat, D. Jaffe, J. Pacyna, N. Pirrone and N. Selin, 2016. Importance of integration and implementation of emerging and future mercury research into the Minamata Convention. Environmental Science and Technology, 50:2767-2770.

Hammerschmidt, C.R., M.B. Sandheinrich, J.G. Wiener and R.G. Rada, 2002. Effects of dietary methylmercury on reproduction of fathead minnows. Environmental Science and Technology, 36:877-883.

Hanna, D.E., C.T. Solomon, A.E. Poste, D.G. Buck and L.J. Chapman, 2015. A review of mercury concentrations in freshwater fishes of Africa: Patterns and predictors. Environmental Toxicology and Chemistry, 34:215-223.

Hanna, D.E., D.G. Buck and L.J. Chapman, 2016. Effects of habitat on mercury concentrations in fish: a case study of Nile perch (*Lates niloticus*) in Lake Nabugabo, Uganda. Ecotoxicology, 25:178-191.

Haris, H., A.Z. Aris and M. bin Mokhtar, 2017. Mercury and methylmercury distribution in the intertidal surface sediment of a heavily anthropogenically impacted saltwater-mangrove-sediment interplay zone. Chemosphere, 166:323-333.

Hartman, C.A., J.T. Ackerman, G. Herring, J. Isanhart and M.P. Herzog, 2013. Marsh wrens as bioindicators of mercury in wetlands of Great Salt Lake: Do blood and feathers reflect site-specific exposure risk to bird reproduction? Environmental Science and Technology, 47:6597-6605.

Hartman, C.A., J.T. Ackerman, M.P. Herzog and C.A. Eagles-Smith, 2017. Season, molt, and body size influence mercury concentrations in grebes. Environmental Pollution, 229:29-39.

Heinz, G.H., D.J. Hoffman, J.D. Klimstra, K.R. Stebbins, S.L. Kondrad and C.A. Erwin, 2009. Species differences in the sensitivity of avian embryos to methylmercury. Archives of Environmental Contamination and Toxicology, 56:129-138.

Henny, C.J., M.A. Yates and W.S. Seegar, 2009a. Dramatic declines of DDE and other organochlorines in spring migrant peregrine falcons from Padre Island, Texas, 1978-2004. Journal of Raptor Research, 43:37-42.

Henny, C.J., J.L. Kaiser and R.A. Grove, 2009b. PCDDs, PCDFs, PCBs, OC pesticides and mercury in fish and osprey eggs from Willamette River, Oregon (1993, 2001 and 2006) with calculated biomagnification factors. Ecotoxicology, 18:151-173.

Herring, G., C.A. Eagles-Smith and J.T. Ackerman, 2017. Mercury exposure may influence fluctuating asymmetry in waterbirds. Environmental Toxicology and Chemistry, 36:1599-605.

Hollanda, S.J., P. Bustamante, C. Churlaud and N. Bodin, in prep. Trace metal concentrations in swordfish caught in the Republic of Seychelles exclusive economic zone. Science of the Total Environment. In prep.

Horowitz, H.M., D.J. Jacob, Y. Zhang, T.S. Dibble, F. Slemr, H.M. Amos, J.A. Schmidt, E.S. Corbitt, E.A. Marais and E.M. Sunderland, 2017. A new mechanism for atmospheric mercury redox chemistry: Implications for the global mercury budget. Atmospheric Chemistry and Physics, 17:6353-6371.

Hsu-Kim, H., K.H. Kucharzyk, T. Zhang and M.A. Deshusses, 2013. Mechanisms regulating mercury bioavailability for methylating microorganisms in the aquatic environment: a critical review. Environmental Science and Technology, 47:2441-2456.

Hsu-Kim, H., C.S. Eckley, D. Achá, X. Feng, C.C. Gilmour, S. Jonsson and C.P. Mitchell, 2018. Challenges and opportunities for managing aquatic mercury pollution in altered landscapes. Ambio, 47:141-169.

Hughes, K.D., P.J. Ewins and K.E. Clark, 1997. A comparison of mercury levels in feathers and eggs of osprey (*Pandion haliaetus*) in the North American Great Lakes. Archives of Environmental Contamination and Toxicology, 33:441-452.

IOTC, 2016. Report of the 19th Session of the IOTC Scientific Committee. Indian Ocean Tuna Commission (IOTC), Seychelles, 1-5 December 2016.

Jackson, A.K., D.C. Evers, M.A. Etterson, A.M. Condon, S.B. Folsom, J. Detweiler, J. Schmerfeld and D.A. Cristol, 2011a. Mercury exposure affects the reproductive success of free-living terrestrial songbird, the Carolina wren (*Thryothorus ludovicianus*). Auk, 128:759-769.

Jackson, A.K., D.C. Evers, S.B. Folsom, A.M. Condon, J. Diener, L.F. Goodrick, A.J. McGann, J. Schmerfeld, D.A. Cristol, 2011b. Mercury exposure in terrestrial birds far downstream of an historical point source. Environmental Pollution, 159:3302-3308.

Jackson, A.K., D.C. Evers, E. Adams, C.A. Eagles-Smith, C. Osborne, O. Lane, S. Edmonds, T. Tear, D. Cristol, A. Sauer and N. O'Driscoll, 2015. Mercury exposure in songbirds of eastern North America across habitats and guilds. Ecotoxicology, 24:453-467.

Jackson, A.K., D.C. Evers, C.A. Eagles-Smith, J.T. Ackerman, J.J. Willacker, J.E. Elliot, J.M. Lepak, S.S. Vander Pol and C.E. Bryan, 2016. Mercury risk to avian piscivores across the western United States and Canada. Science of the Total Environment, 568:685-696.

Jinadasa, B.K.K.K., E.M.R.K.B. Edirisinghe and I. Wickramasinghe, 2014. Total mercury, cadmium and lead levels in main export fish of Sri Lanka. Food Additives and Contaminants B, 7:309-314.

Johnels, A.G., T. Westermark, W. Berg, P.I. Persson and B. Sjöstrand, 1967. Pike (*Esox lucius* L.) and some other aquatic organisms in Sweden as indicators of mercury contamination in the environment. Oikos, 1967:323-333.

Jonsson, S., A. Andersson, M.B. Nilsson, U. Skyllberg, E. Lundberg, J.K. Schaefer, S. Åkerblom and E. Björn, 2017. Terrestrial discharges mediate trophic shifts and enhance methylmercury accumulation in estuarine biota. Science Advances, 3(1):e1601239.

Kalisinska, E., J. Gorecki, N. Lanocha, A. Okonska, J.B. Melgarejo, H. Budis, I. Rzad and J. Golas, 2014. Total and methylmercury in soft tissues of white-tailed eagle (*Haliaeetus albicilla*) and osprey (*Pandion haliaetus*) collected in Poland. Ambio, 43:858-870.

Kamman, N.C., N.M. Burgess, C.T. Driscoll, H.A. Simonin, W. Goodale, J. Linehan, R. Estabrook, M. Hutcheson, A. Major, A.M. Scheuhammer and D.A. Scruton, 2005. Mercury in freshwater fish of northeast

North America – a geographic perspective based on fish tissue monitoring databases. Ecotoxicology, 14:163-180.

Kenney, L.A., C.A. Eagles-Smith, J.T. Ackerman and F.A. von Hippel, 2014. Temporal variation in fish mercury concentrations within lakes from the western Aleutian archipelago, Alaska. PloS ONE, 9(7):102244.

Kim, E., H. Kim, K.H. Shin, M.S. Kim, S.R. Kundu, B.G. Lee and S. Han, 2012. Biomagnification of mercury through the benthic food webs of a temperate estuary: Masan Bay, Korea. Environmental Toxicology and Chemistry, 31:1254-1263.

Kim, H., A.L. Soerensen, J. Hur, L.E. Heimburger, D. Hahm, T.S. Rhee, S. Noh and S. Han, 2017. Methylmercury mass budgets and distribution characteristics in the western Pacific Ocean. Environmental Science and Technology, 51:1186-1194.

Kinghorn, A., P. Solomon and H.M. Chan, 2007. Temporal and spatial trends of mercury in fish collected in the English–Wabigoon river system in Ontario, Canada. Science of the Total Environment, 372:615-623.

Kiszka, J.J., A. Aubail, N.E. Hussey, M.R. Heithaus, F. Caurant and P. Bustamante, 2015. Plasticity of trophic interactions among sharks from the oceanic south-western Indian Ocean revealed by stable isotope and mercury analyses. Deep Sea Research I, 96:49-58.

Klenavic, K., L. Champoux, P.Y. Daoust, R.D. Evans and H.E. Evans, 2008. Mercury concentrations in wild mink (*Mustela vison*) and river otters (*Lontra canadensis*) collected from eastern and Atlantic Canada: relationship to age and parasitism. Environmental Pollution, 156:359-366.

Kocman, D., S.J. Wilson, H.M. Amos, K.H. Telmer, F. Steenhuisen, E.M. Sunderland, R.P. Mason, P. Outridge and M. Horvat, 2017. Toward an assessment of the global inventory of present-day mercury releases to freshwater environments. International Journal of Environmental Research and Public Health, 14:138. doi:10.3390/ijerph14020138.

Kojadinovic, J., M. Potier, M. Le Corre, R.P. Cosson and P. Bustamante, 2006. Mercury content in commercial pelagic fish and its risk assessment in the Western Indian Ocean. Science of the Total Environment, 366:688-700.

Kojadinovic, J., P. Bustamante, C. Churlaud, R.P. Cosson and M. Le Corre, 2007. Mercury in seabird feathers: Insight on dietary habits and evidence for exposure levels in the western Indian Ocean. Science of the Total Environment, 384:194-204.

Korstian, J.M., M.M. Chumchal, V.J. Bennett and A.M. Hale, 2018. Mercury contamination in bats from the central United States. Environmental Toxicology and Chemistry, 37:160-165.

Krey, A., S.K. Ostertag and H.M. Chan, 2015. Assessment of neurotoxic effects of mercury in beluga whales (*Delphinapterus leucas*), ringed seals (*Pusa hispida*), and polar bears (*Ursus maritimus*) from the Canadian Arctic. Science of the Total Environment, 509:237-247.

Kwon, S.Y., J.D. Blum, C.Y. Chen, D.E. Meattey, D.E. and R.P. Mason, 2014. Mercury isotope study of sources and exposure pathways of methylmercury in estuarine food webs in the Northeastern US. Environmental Science and Technology, 48:10089-10097.

Lane, O.P., K.M. O'Brien, D.C. Evers, T.P. Hodgman, A. Major, N. Pau, M.J. Ducey, R. Taylor and D. Perry, 2011. Mercury in breeding saltmarsh sparrows (*Ammodramus caudacutus*). Ecotoxicology, 20:1984-1991.

Lane, O.P., W.J. Arendt, M.A. Tórrez and J.C.G. Castellón, 2013. Pilot assessment of mercury exposure in selected biota from the lowlands of Nicaragua. Mesoamericana, 17:19-28.

Lebel, J., M. Roulet, D. Mergler, M. Lucotte and F. Larribe, 1997. Fish diet and mercury exposure in a riparian Amazonian population. Water, Air and Soil Pollution, 97:31-44.

Lee, C.S. and N.S. Fisher, 2016. Methylmercury uptake by diverse marine phytoplankton. Limnology and Oceanography, 61:1626-1639.

Lee, C.S., M.E. Lutcavage, E. Chandler, D.J. Madigan, R.M. Cerrato and N.S. Fisher, 2016. Declining mercury concentrations in bluefin tuna reflect reduced emissions to the North Atlantic Ocean. Environmental Science and Technology, 50:12825-12830.

Li, R., H. Xu, M. Chai and G.Y. Qiu, 2016a. Distribution and accumulation of mercury and copper in mangrove sediments in Shenzhen, the world's most rapid urbanized city. Environmental Monitoring and Assessment, 188:87. doi.org/10.1007/s10661-016-5103-z

Li, M., A.T. Schartup, A.P. Valberg, J.D. Ewald, D.P. Krabbenhoft, R. Yin, P.H. Balcom and E.M. Sunderland, 2016b. Environmental origins of methylmercury accumulated in subarctic estuarine fish indicated by mercury stable isotopes. Environmental Science and Technology, 50:11559-11568.

Little, M.E., N.M. Burgess, H.G. Broders and L.M. Campbell, 2015. Distribution of mercury in archived fur from little brown bats across Atlantic Canada. Environmental Pollution, 207:52-58.

Lucia, M., N. Verboven, H. Strøm, C. Miljeteig, M.V. Gavrilo, B.M. Braune, D. Boertmann and G.W. Gabrielsen, 2015. Circumpolar contamination in eggs of the high-Arctic ivory gull *Pagophila eburnea*. Environmental Toxicology and Chemistry, 34:1552-1561.

Lucia, M., H. Strøm, P. Bustamante and G.W. Gabrielsen, 2016. Trace element concentrations in relation to the trophic behaviour of endangered ivory gulls (*Pagophila eburnea*) during their stay at a breeding site in Svalbard. Archives of Environmental Contamination and Toxicology, 71:518-529.

Lusilao-Makiese, J.G., E. Tessier, D. Amouroux, H. Tutu, L. Chimuka, I. Weiersbye and E.M. Cukrowska, 2016. Mercury speciation and dispersion from an active gold mine at the West Wits area, South Africa. Environmental Monitoring and Assessment, 188:47. doi.org/10.1007/s10661-015-5059-4

Ma, Y., C.R. Perez, B.A. Branfireun and C.G. Guglielmo, 2018. Dietary exposure to methylmercury affects flight endurance in a migratory songbird. Environmental Pollution, 234:894-901.

Macdonald, K.F., M.A. Lund, M.L. Blanchette and C.D. Mccullough, 2014. Regulation of artisanal small scale gold mining (ASGM) in Ghana and Indonesia as currently implemented fails to adequately protect aquatic ecosystems. Proceedings of International Mine Water Association Symposium. pp. 401-405. Xuzhou, China. IMWA. http://ro.ecu.edu.au/ecuworkspost2013/863

Maffucci, F., F. Caurant, P. Bustamante and F. Bentivegna, 2005. Trace element (Cd, Cu, Hg, Se, Zn) accumulation and tissue distribution in loggerhead turtles (*Caretta caretta*) from the western Mediterranean Sea (southern Italy). Chemosphere, 58:535-542.

Mallory, M.L. and B.M. Braune, 2012. Tracking contaminants in seabirds of Arctic Canada: Temporal and spatial insights. Marine Pollution Bulletin, 64:1475-1484.

Mallory, M.L., M. Wayland, B.M. Braune and K.G. Drouillard, 2004. Trace elements in marine birds, arctic hare and ringed seals breeding near Qikiqtarjuaq, Nunavut, Canada. Marine Pollution Bulletin, 49:136-141.

Marcovecchio, J.E., M.S. Gerpe, R.O. Bastida, D.H. Rodríguez and S.G. Morón, 1994. Environmental contamination and marine mammals in coastal waters from Argentina: an overview. Science of the Total Environment, 154:141-151.

Mason, R.P. and W.F. Fitzgerald, 1993. The distribution and biogeochemical cycling of mercury in the equatorial Pacific Ocean. Deep Sea Research I, 40:1897-1924.

Matulik, A.G., D.W. Kerstetter, N. Hammerschlag, T. Divoll, C.R. Hammerschmidt and D.C. Evers, 2017. Bioaccumulation and biomagnification of mercury and methylmercury in four sympatric coastal sharks in a protected subtropical lagoon. Marine Pollution Bulletin, 116:357-364.

May Junior, J.A., H. Quigley, R. Hoogesteijn, F.R. Tortao, A. Devlin, R.M. Carvalho Junior, R.G. Mortato, L.R. Sartorello, L.E. Rampim, M. Haberfeld and R.C. Paula, 2017. Mercury content in the fur of jaguars (*Panthera onca*) from two areas under different levels of gold mining impact in the Brazilian Pantanal. Anais da Academia Brasileira de Ciências, doi.org/10.1590/0001-3765201720170190.

Maz-Courrau, A., C. López-Vera, F. Galvan-Magaña, O. Escobar-Sánchez, R. Rosíles-Martínez and A. Sanjuán-Muñoz, 2012. Bioaccumulation and biomagnification of total mercury in four exploited shark species in the Baja California Peninsula, Mexico. Bulletin of Environmental Contamination and Toxicology, 88:129-134.

McKinney, M.A., S. Pedro, R. Dietz, C. Sonne, A.T. Fisk, D. Roy, B.M. Jenssen and R.J. Letcher, 2015. A review of ecological impacts of global climate change on persistent organic pollutant and mercury pathways and exposures in arctic marine ecosystems. Current Zoology, 61:617-628.

McKinney, M.A., K. Dean, N.E. Hussey, G. Cliff, S.P. Wintner, S.F.J. Dudley, M.P. Zungu and A.T. Fisk, 2016. Global versus local causes and health implications of high mercury concentrations in sharks from the east coast of South Africa. Science of the Total Environment, 541:176-183.

Mendez, E., H. Giudice, A. Pereira, G. Inocente and D. Medina, 2001. Total mercury content – fish weight relationship in swordfish (*Xiphias gladius*) caught in the southwest Atlantic Ocean. Journal of Food Composition and Analysis, 14:453-460.

Miljeteig, C., H. Strom, M.V. Gavrilo, A. Volkov, B.M. Jenssen and G.W. Gabrielsen, 2009. High levels of contaminants in ivory gull *Pagophila eburnea* eggs from the Russian and Norwegian Arctic. Environmental Science and Technology, 43:5521-5528.

Mol, J.H., J.S. Ramlal, C. Lietar and M. Verloo, 2001. Mercury contamination in freshwater, estuarine, and marine fishes in relation to small-scale gold mining in Suriname, South America. Environmental Research, 86:183-197.

Monson, B.A. 2009. Trend reversal of mercury concentrations in piscivorous fish from Minnesota Lakes: 1982−2006. Environmental Science and Technology, 43:1750-1755.

Monson, B.A., D.F. Staples, S.P. Bhavsar, T.M. Holsen, C.S. Schrank, S.K. Moses, D.J. McGoldrick, S.M. Backus and K.A. Williams, 2011. Spatiotemporal trends of mercury in walleye and largemouth bass from the Laurentian Great Lakes region. Ecotoxicology, 20:1555-1567.

Monteiro, L.R. and R.W. Furness, 1995. Seabirds as monitors of mercury in the marine environment. Water, Air and Soil Pollution, 80:851-870.

Moreno-Brush, M., J. Rydberg, N. Gamboa, I. Storch and H. Biester, 2016. Is mercury from small-scale gold mining prevalent in the southeastern Peruvian Amazon? Environmental Pollution, 218:150-159.

Mott, R., A. Herrod and R.H. Clarke, 2017. Post-breeding dispersal of frigatebirds increases their exposure to mercury. Marine Pollution Bulletin, 119:204-210.

Muir, D., B. Braune, B. DeMarch, R. Norstrom, R. Wagemann, L. Lockhart, B. Hargrave, D. Bright, R. Addison, J. Payne and K. Reimer, 1999. Spatial and temporal trends and effects of contaminants in the Canadian Arctic marine ecosystem: A review. Science of the Total Environment, 230:83-144.

Muirhead, S.J. and R.W. Furness, 1988. Heavy metal concentrations in the tissues of seabirds from Gough Island, South Atlantic Ocean. Marine Pollution Bulletin, 19:278-283.

NADP, 2017. National Atmospheric Deposition Program (NADP) Program Office, Illinois State Water Survey, University of Illinois, Champaign, IL 61820.
http://nadp.sws.uiuc.edu/maplib/pdf/mdn/hg_Conc_2015.pdf.

Naves, L.C., 2009. Alaska Migratory Bird Subsistence Harvest Estimates, 2004–2007. Alaska Migratory Bird Co-Management Council. Anchorage.

NCP, 2017. Northern Contaminants Program (NCP). Indigenous and Northern Affairs, Government of Canada. www.science.gc.ca/eic/site/063.nsf/eng/h_7A463DBA.html.

Newtoff, K.N. and S.D. Emslie, 2017. Mercury exposure and diet in brown pelicans (*Pelecanus occidentalis*) in North Carolina, USA. Waterbirds, 40:50-57.

Nguetseng, R., A. Fliedner, B. Knopf, B. Lebreton, M. Quack and H. Rüdel, 2015. Retrospective monitoring of mercury in fish from selected European freshwater and estuary sites. Chemosphere, 134:427-434.

Niane, B., S. Guédron, R. Moritz, C. Cosio, P.M. Ngom, N. Deverajan, H.R. Pfeifer and J. Poté, 2015. Human exposure to mercury in artisanal small-scale gold mining areas of Kedougou region, Senegal, as a function of occupational activity and fish consumption. Environmental Science and Pollution Research, 22: 7101-7111.

Nicklisch, S.C., L.T. Bonito, S. Sandin and A. Hamdoun, 2017. Mercury levels of yellowfin tuna (*Thunnus albacares)* are associated with capture location. Environmental Pollution, 229:87-93.

Noh, S., C.K. Kim, Y. Kim, J.H. Lee and S. Han, 2017. Assessing correlations between monomethylmercury accumulation in fish and trophic states of artificial temperate reservoirs. Science of the Total Environment, 580:912-919.

Obrist, D., J.L. Kirk, L. Zhang, E.M. Sunderland, M. Jiskra and N.E. Selin, 2018. A review of global environmental mercury processes in response to human and natural perturbations: Changes of emissions, climate, and land use. Ambio, 47:116-140.

Ochoa-Acuña, H., M.S. Sepulveda and T.S. Gross, 2002. Mercury in feathers from Chilean birds: Influence of location, feeding strategy and taxonomic affiliation. Marine Pollution Bulletin, 44:340-349.

Odsjö, T., A. Roos and A.G. Johnels, 2004. The tail feathers of osprey nestlings (*Pandion haliaetus* L.) as indicators of change in mercury load in the environment of southern Sweden (1969-1998): Case study with a note on the simultaneous intake of selenium. Ambio, 33:133-137.

Oliveira, R.C., J.G. Dorea, J.V.E. Bernardi, W.R. Bastos, R. Almeida and A.G. Manzatto, 2010. Fish consumption by traditional subsistence villagers of the Rio Madeira (Amazon): impact on hair mercury. Annals of Human Biology, 37:629-642.

Olivero-Verbel, J., K. Caballero-Gallardo and A. Turizo-Tapia, 2015. Mercury in the gold mining district of San Martin de Loba, South of Bolivar (Colombia). Environmental Science and Pollution Research, 22:5895-5907.

Ouédraogo, O. and M. Amyot, 2013. Mercury, arsenic and selenium concentrations in water and fish from sub-Saharan semi-arid freshwater reservoirs (Burkina Faso). Science of the Total Environment, 444:243-254.

Pacyna, J.M., O. Travnikov, F. De Simone, I.M. Hedgecock, K. Sundseth, E.G. Pacyna, F. Steenhuisen, N. Pirrone, J. Munthe and K. Kindbom, 2016. Current and future levels of mercury atmospheric pollution on a global scale. Atmospheric Chemistry and Physics, 16:12495-12511.

Pacyna, A.D., C.Z. Martínez, D. Miguélez, F. Jiguet, Ż. Polkowska and K. Wojczulanis-Jakubas, 2017. Mercury contamination, a potential threat to the globally endangered aquatic warbler *Acrocephalus paludicola*. Environmental Science and Pollution Research, 24:26478-26484.

Pauly, D. and D. Zeller, 2016. Catch reconstructions reveal that global marine fisheries catches are higher than reported and declining. Nature Communications, 7:10244.

Pelletier, A.R., L. Castello, A.V. Zhulidov, T.Y. Gurtovaya, R.D. Robarts, R.M. Holmes, D.A. Zhulidov and R.G. Spencer, 2017. Temporal and longitudinal mercury trends in burbot (*Lota lota*) in the Russian Arctic. Environmental Science and Technology, 51:13436-13442.

Perkins, M., L. Ferguson, R.G. Lanctot, I.J. Stenhouse, S. Kendall, S. Brown, H.R. Gates, J.O. Hall, K. Regan and D.C. Evers, 2016. Mercury exposure and risk in breeding and staging Alaskan shorebirds. Condor, 118:571-582.

Peterson, S.A., J. Van Sickle, R.M. Hughes, J.A. Schacher and S.F. Echols, 2004. A biopsy procedure for determining filet and predicting whole-fish mercury concentration. Archives of Environmental Contamination and Toxicology, 48:99-107.

Peterson, S.H., J.T. Ackerman and D.P. Costa, 2015. Marine foraging ecology influences mercury bioaccumulation in deep-diving northern elephant seals. Proceedings of the Royal Society B, 282:20150710.

Peterson, S.H., J.T. Ackerman and D.P. Costa, 2016a. Mercury correlations among blood, muscle, and hair of northern elephant seals during the breeding and molting fasts. Environmental Toxicology and Chemistry, 35:2103-2110.

Peterson, S.H., E.A. McHuron, S.N. Kennedy, J.T. Ackerman, L.D. Rea, J.M. Castellini, T.M. O'Hara and D.P. Costa, 2016b. Evaluating hair as a predictor of blood mercury: the influence of ontogenetic phase and life history in pinnipeds. Archives of Environmental Contamination and Toxicology, 70:28-45.

Peterson, S.H., J.T. Ackerman, C.A. Eagles-Smith, C.A. Hartman and M.P. Herzog, 2017. A critical evaluation of the utility of eggshells for estimating mercury concentrations in avian eggs. Environmental Toxicology and Chemistry, 36:2417-2427.

Peterson, S.H., J.T. Ackerman, D.E. Crocker and D.P. Costa, 2018. Foraging and fasting can influence contaminant concentrations in animals: an example with mercury contamination in a free-ranging marine mammal. Proceedings of the Royal Society B, 285:20172782.

Pinkney, A.E., C.T. Driscoll, D.C. Evers, M.J. Hooper, J. Horan, J.W. Jones, R.S. Lazarus, H.G. Marshall, A. Milliken, B.A. Rattner and J. Schmerfeld, 2015. Interactive effects of climate change with nutrients,

mercury, and freshwater acidification on key taxa in the North Atlantic Landscape Conservation Cooperative region. Integrated Environmental Assessment and Management, 11:355-369.

Provencher, J.F., M.L. Mallory, B.M. Braune, M.R. Forbes and H.G. Gilchrist, 2014. Mercury and marine birds in Arctic Canada: effects, current trends, and why we should be paying closer attention. Environmental Reviews, 22:244-255.

Reif, J.S., A.M. Schaefer and G.D. Bossart, 2015. Atlantic bottlenose dolphins (*Tursiops truncatus*) as a sentinel for exposure to mercury in humans: closing the loop. Veterinary Sciences, 2:407-422.

Ricca, M.A., M.A. Keith and R.G. Anthony, 2008. Sources of organochlorine contaminants and mercury in seabirds from the Aleutian archipelago of Alaska: Inferences from spatial and trophic variation. Science of the Total Environment, 406:308-323.

Rigét, F., R. Dietz, E.W. Born, C. Sonne and K.A. Hobson, 2007. Temporal trends of mercury in marine biota of west and northwest Greenland. Marine Pollution Bulletin, 54:72-80.

Rigét, F., B. Braune, A. Bignert, S. Wilson, J. Aars, E. Born, M. Dam, R. Dietz, M. Evans, T. Evans and M. Gamberg, 2011. Temporal trends of Hg in Arctic biota, an update. Science of the Total Environment, 409:3520-3526.

Rimmer, C.C., K.P. McFarland, D.C. Evers, E.K. Miller, Y. Aubry, D. Busby and R.J. Taylor, 2005. Mercury concentrations in Bicknell's thrush and other insectivorous passerines in montane forests of northeastern North America. Ecotoxicology, 14:223-240.

Robinson, S.A., M.J. Lajeunesse and M.R. Forbes, 2012. Sex differences in mercury contamination of birds: testing multiple hypotheses with meta-analysis. Environmental Science and Technology, 46:7094-7101.

Rocque, D.A., and K. Winker, 2004. Biomonitoring of contaminants in birds from two trophic levels in the North Pacific. Environmental Toxicology and Chemistry, 23:759-766.

Rodrigues, T. and A.F. Amorim, 2016. Review and analysis of mercury levels in blue marlin (*Makaira nigricans*, Lacepède 1802) and swordfish (*Xiphias gladius*, Linnaeus 1758). bioRxiv, p.043893. doi.org/10.1101/043893.

Routti, H., R.J. Letcher, E.W. Born, M. Branigan, R. Dietz, T.J. Evans, A.T. Fisk, E. Peacock and C. Sonne, 2011. Spatial and temporal trends of selected trace elements in liver tissue from polar bears (*Ursus maritimus*) from Alaska, Canada and Greenland. Journal of Environmental Monitoring, 13:2260-2267.

Rumbold, D.G., K.E. Miller, T.A. Dellinger and N. Haas, 2017. Mercury concentrations in feathers of adult and nestling osprey (*Pandion haliaetus*) from coastal and freshwater environments of Florida. Archives of Environmental Contamination and Toxicology, 72:31-38.

Rutkiewicz, J., D.-H. Nam, T. Cooley, K. Neumann, I.B. Padilla, W. Route, S. Strom and N. Basu, 2011. Mercury exposure and neurochemical impacts in bald eagles across several Great Lakes states. Ecotoxicology, 20:1669-1676.

Ruus, A., I.B. Øverjordet, H.F.V. Braaten, A. Evenset, G. Christensen, E.S. Heimstad, G.W. Gabrielsen and K. Borgå, 2015. Methylmercury biomagnification in an Arctic pelagic food web. Environmental Toxicology and Chemistry, 34:2636-2643.

Salazar-Camacho, C., M. Salas-Moreno, S. Marrugo-Madrid, J. Marrugo-Negrete and S. Díez, 2017. Dietary human exposure to mercury in two artisanal small-scale gold mining communities of northwestern Colombia. Environment International, 107:47-54.

Santschi, P.H., K.M. Yeager, K.A. Schwehr and K.J. Schindler, 2017. Estimates of recovery of the Penobscot River and estuarine system from mercury contamination in the 1960s. Science of the Total Environment, 596:351-359.

Savoy, L., P. Flint, D. Zwiefelhofer, H. Brant, C. Perkins, R. Taylor, O. Lane, J. Hall, D. Evans and J. Schamber, 2017. Geographic and temporal patterns of variation in total mercury concentrations in blood of harlequin ducks and blue mussels from Alaska. Marine Pollution Bulletin, 117:178-183.

Schartup, A.T., U. Ndu, P.H. Balcom, R.P. Mason and E.M. Sunderland, 2015. Contrasting effects of marine and terrestrially derived dissolved organic matter on mercury speciation and bioavailability in seawater. Environmental Science and Technology, 49:5965-5972.

Scheuhammer, A.M., A.H. Wong and D. Bond, 1998. Mercury and selenium accumulation in common loons (*Gavia immer*) and common mergansers (*Mergus merganser*) from eastern Canada. Environmental Toxicology and Chemistry, 17:197-201.

Scheuhammer, A.M., N. Basu, D.C. Evers, G.H. Heinz, M.B. Sandheinrich and M.S. Bank, 2011. Ecotoxicology of mercury in fish and wildlife: Recent advances. In: M. Bank (ed.). Mercury in the Environment: Pattern and Process. pp. 223-238. University of California Press.

Scheuhammer, A., B. Braune, H.M. Chan, H. Frouin, A. Krey, R. Letcher, L. Loseto, M. Noël, S. Ostertag, P. Ross and M. Wayland, 2015. Recent progress on our understanding of the biological effects of mercury in fish and wildlife in the Canadian Arctic. Science of the Total Environment, 509:91-103.

Scheuhammer, A.M., S.I. Lord, M. Wayland, N.M. Burgess, L. Champoux and J.E. Elliott, 2016. Major correlates of mercury in small fish and common loons (*Gavia immer*) across four large study areas in Canada. Environmental Pollution, 210:361-370.

Schneider, L., S. Eggins, W. Maher, R.C. Vogt, F. Krikowa, L. Kinsley, S.M. Eggins and R. Da Silveira, 2015. An evaluation of the use of reptile dermal scutes as a non-invasive method to monitor mercury concentrations in the environment. Chemosphere, 119:163-170.

Sebastiano, M., P. Bustamante, D. Costantini, I. Eulaers, G. Malarvannan, P. Mendez-Fernandez, C. Churlaud, P. Blévin, A. Hauselmann, G. Dell'Omo and A. Covaci, 2016. High levels of mercury and low levels of persistent organic pollutants in a tropical seabird in French Guiana, the magnificent frigatebird, *Fregata magnificens*. Environmental Pollution, 214:384-393.

Sebastiano, M., P. Bustamante, I. Eulaers, G. Malarvannan, P. Mendez-Fernandez, C. Churlaud, P. Blévin, A. Hauselmann, A. Covaci, M. Eens, D. Costantini and O. Chastel, 2017. Trophic ecology drives contaminant concentrations within a tropical seabird community. Environmental Pollution, 227:183-193.

Seewagen, C.L., D.A. Cristol and A.R. Gerson, 2016. Mobilization of mercury from lean tissues during simulated migratory fasting in a model songbird. Scientific Reports, 6: 10.1038/srep25762 .

Seixas, T.G., I. Moreira, S. Siciliano, O. Malm and H.A. Kehrig, 2014. Differences in methylmercury and inorganic mercury biomagnification in a tropical marine food web. Bulletin of Environmental Contamination and Toxicology, 92:274-278.

Semeniuk, K. and A. Dastoor, 2017. Development of a global ocean mercury model with a methylation cycle: Outstanding issues. Global Biogeochemical Cycles, 31:400-433.

SFA, 2016. Fisheries Statistical Report, 2015. Seychelles Fishing Authority (SFA), Victoria, Seychelles.

Sherman, L.S., J.D. Blum, T.A. Douglas and A. Steffen, 2012. Frost flowers growing in the Arctic ocean-atmosphere–sea ice–snow interface: 2. Mercury exchange between the atmosphere, snow, and frost flowers. Journal of Geophysical Research, 117, D00R10, doi:10.1029/2011JD016186.

Sherman, L.S., J.D. Blum, A. Franzblau and N. Basu, 2013. New insight into biomarkers of human mercury exposure using naturally occurring mercury stable isotopes. Environmental Science and Technology, 47:3403-3409.

Sorensen, J.A., G.E. Glass, K.W. Schmidt, J.K. Huber and G.R. Rapp Jr, 1990. Airborne mercury deposition and watershed characteristics in relation to mercury concentrations in water, sediments, plankton, and fish of eighty northern Minnesota lakes. Environmental Science and Technology, 24:1716-1727.

Soerensen, A.L., R.P. Mason, P.H. Balcom, D.J. Jacob, Y. Zhang, J. Kuss and E.M. Sunderland, 2014. Elemental mercury concentrations and fluxes in the tropical atmosphere and ocean. Environmental Science and Technology, 48:11312-11319.

Spalding, M.G., P.C. Frederick, H.C. McGill, S.N. Bouton and L.R. McDowell, 2000. Methylmercury accumulation in tissues and its effects on growth and appetite in captive great egrets. Journal of Wildlife Diseases, 36:411-422.

Srebocan, E., J. Pompe-Gotal, A. Prevendar-Crnic and E. Ofner, 2007. Mercury concentrations of captive Atlantic bluefin tuna (*Thunnus thynnus*) farmed in the Adriatic Sea. Veterinarni Medicina, 52:175-177.

Steckling, N., M. Tobollik, D. Plass, C. Hornberg, B. Ericson, R. Fuller and S. Bose-O'Reilly, 2017. Global burden of disease of mercury used in artisanal small-scale gold mining. Annals of Global Health, 83:234-247.

Stenhouse, I.J., E.M. Adams, J.L. Goyette, K.J. Regan, M.W. Goodale and D.C. Evers, 2018. Changes in mercury exposure of marine birds breeding in the Gulf of Maine, 2008-2013. Marine Pollution Bulletin, 128:156-161.

Stewart, F.M., R.A. Phillips, J.A. Bartle, J. Craig and D. Shooter, 1999. Influence of phylogeny, diet, moult schedule and sex on heavy metal concentrations in New Zealand Procellariiformes. Marine Ecology Progress Series, 1999:295-305.

Storelli, M.M. and G.O. Marcotrigiano, 2001. Total mercury levels in muscle tissue of swordfish (*Xiphias gladius*) and bluefin tuna (*Thunnus thynnus*) from the Mediterranean Sea (Italy). Journal of Food Protection, 64:1058-1061.

Streets, D.G., Q. Zhang and Y. Wu, 2009. Projections of global mercury emissions in 2050. Environmental Science and Technology, 43:2983-2988.

Streets, D.G., H.M. Horowitz, D.J. Jacob, Z. Lu, L. Levin, A.F.H. Ter Schure and E.M. Sunderland, 2017. Total mercury released to the environment by human activities. Environmental Science and Technology, 51:5969-5977.

Suchanek, T.H., C.A. Eagles-Smith, D.G. Slotton, E.J. Harner, A.E. Colwell, N.L. Anderson, L.H. Mullen, J.R. Flanders, D.P. Adam and K.J. McElroy, 2008. Spatiotemporal trends in fish mercury from a mine-dominated ecosystem: Clear Lake, California. Ecological Applications, 18(8) Supplement. A177-A195.

Sullivan, K.M. and A.D. Kopec, 2018. Mercury in wintering American black ducks (*Anas rubripes*) downstream from a point-source on the lower Penobscot River, Maine, USA. Science of the Total Environment, 612:1187-1199.

Sun, L., B. Lu, D. Yuan, W. Hao and Y. Zheng, 2017. Variations in the isotopic composition of stable mercury isotopes in typical mangrove plants of the Jiulong estuary, SE China. Environmental Science and Pollution Research, 24:1459-1468.

Sunderland, E.M., D.P. Krabbenhoft, J.W. Moreau, S.A. Strode and W.M. Landing, 2009. Mercury sources, distribution, and bioavailability in the North Pacific Ocean: Insights from data and models. Global Biogeochemical Cycles, 23:GB2010, doi:10.1029/2008GB003425.

Sunderland, E.M., C.T. Driscoll Jr, J.K. Hammitt, P. Grandjean, J.S. Evans, J.D. Blum, C.Y. Chen, D.C. Evers, D.A. Jaffe, R.P. Mason, S. Goho and W. Jacobs, 2016. Benefits of regulating hazardous air pollutants from coal and oil-fired utilities in the United States. Environmental Science and Technology, 50:2117-2120.

Sunderland, E.M., M. Li and K. Bullard, 2018. Decadal changes in the edible supply of seafood and methylmercury exposure in the United States. Environmental Health Perspectives, 126:017006-1-017006-6.

Sundseth, K., J.M. Pacyna, A. Banel, E.G. Pacyna and A. Rautio, 2015. Climate change impacts on environmental and human exposure to mercury in the Arctic. International journal of Environmental Research and Public Health, 12:3579-3599.

Sundseth, K., J.M. Pacyna, E.G. Pacyna, N. Pirrone and R.J. Thorne, 2017. Global sources and pathways of mercury in the context of human health. International journal of Environmental Research and Public Health, 14:105. 10.3390/ijerph14010105.

Tan, S.W., J.C. Meiller and K.R. Mahaffey, 2009. The endocrine effects of mercury in humans and wildlife. Critical Reviews in Toxicology, 39:228-269.

Tartu, S., A. Goutte, P. Bustamante, F. Angelier, B. Moe, C. Clément-Chastel, C. Bech, G.W. Gabrielsen, J.O. Bustness and O. Chastel, 2013. To breed or not to breed: endocrine response to mercury contamination by an arctic seabird. Biology Letters, 9:20130317. 10.1098/rsbl.2013.0317.

Tavares, S., J.C. Xavier, R.A. Phillips, M.E. Pereira and M.A. Pardal, 2013. Influence of age, sex and breeding status on mercury accumulation patterns in the wandering albatross *Diomedea exulans*. Environmental Pollution. 181:315-320.

Teffer, A.K., M.D. Staudinger, D.L. Taylor and F. Juanes, 2014. Trophic influences on mercury accumulation in top pelagic predators from offshore New England waters of the northwest Atlantic Ocean. Marine Environmental Research, 101:124-134.

Titcomb, E.M., J.S. Reif, P.A. Fair, H.C.W. Stavros, M. Mazzoil, G.D. Bossart and A.M. Schaefer, 2017. Blood mercury concentrations in common bottlenose dolphins from the Indian River Lagoon, Florida: Patterns of social distribution. Marine Mammal Science, 33:771-784.

Townsend, J.M., C.C. Rimmer, C.T. Driscoll, K.P. McFarland and E. Inigo-Elias, 2013. Mercury concentrations in tropical resident and migrant songbirds on Hispaniola. Ecotoxicology, 22:86-93.

Trasande, L., J. DiGangi, D.C. Evers, P. Jindrich, D.G. Buck, J. Samanek, B. Beeler, M.A. Turnquist and K. Regan, 2016. Economic implications of mercury exposure in the context of the global mercury treaty: hair mercury levels and estimated lost economic productivity in selected developing countries. Journal of Environmental Management, 183:229-235.

UNEP, 2013. Sources, Emissions, Releases and Environmental Transport. UNEP Chemicals Branch, Geneva, Switzerland.

UNEP, 2016. UNEP Global Review of Mercury Monitoring Networks. United Nations Environment, Geneva, Switzerland.

University of Michigan Animal Diversity Web, 2018. University of Michigan Museum of Zoology Animal Diversity Web. University of Michigan, Ann Arbor, Michigan. http://animaldiversity.org/.

Uryu, Y., O. Malm, I. Thornton, I. Payne and D. Cleary. 2001. Mercury contamination of fish and its implications for other wildlife of the Tapajós Basin, Brazilian Amazon. Conservation Biology, 15:438-446.

Varian-Ramos, C.W., J.P. Swaddle and D.A. Cristol, 2014. Mercury reduces avian reproductive success and imposes selection: an experimental study with adult- or lifetime-exposure in zebra finch. PLoS ONE 9:e95674. doi.org/10.1371/journal.pone.0095674.

Vega-Sánchez, B., S. Ortega-García, J. Ruelas-Inzunza, M. Frías-Espericueta, O. Escobar-Sánchez and J. Guzmán-Rendón, 2017. Mercury in the blue marlin (*Makaira nigricans*) from the southern Gulf of California: Tissue distribution and inter-annual variation (2005–2012). Bulletin of Environmental Contamination and Toxicology, 98:156-161.

Višnjevec Miklavčič, A.M., D. Kocman and M. Horvat, 2014. Human mercury exposure and effects in Europe. Environmental Toxicology and Chemistry, 33:1259-1270.

Wagemann, R. and H. Kozlowska, 2005. Mercury distribution in the skin of beluga (*Delphinapterus leucas*) and narwhal (*Monodon monoceros*) from the Canadian Arctic and mercury burdens and excretion by moulting. Science of the Total Environment, 351:333-343.

Wagemann, R., E. Trebacz, G. Boila and W.L. Lockhart, 1998. Methylmercury and total mercury in tissues of arctic marine mammals. Science of the Total Environment, 218:19-31.

Walters, C., M. Couto, N. McClurg, B. Silwana and V. Somerset, 2017. Baseline monitoring of mercury levels in environmental matrices in the Limpopo Province. Water, Air, and Soil Pollution, 228:57. doi.org/10.1007/s11270-016-3230-3

Wang, H., W. Xu, Z. Chen, Z. Cheng, L. Ge, Y. Man, J.P. Giesy, J.Du, C.K.C. Wong and M. Wong, 2013. In vitro estimation of exposure of Hong Kong residents to mercury and methylmercury via consumption of market fishes. Journal of Hazardous Materials, 248:387-393.

Watanuki, Y., A. Yamashita, M. Ishizuka, Y. Ikenaka, S.M. Nakayama, C. Ishii, T. Yamamoto, M. Ito, T. Kuwae and P.N. Trathan, 2016. Feather mercury concentration in streaked shearwaters wintering in separate areas of southeast Asia. Marine Ecology Progress Series, 546:263-269.

Webb, J., O.T. Coomes, N. Mainville and D. Mergler, 2015. Mercury contamination in an indicator fish species from Andean Amazonian rivers affected by petroleum extraction. Bulletin of Environmental Contamination and Toxicology, 95:279-285.

Webber, H.M. and T.A. Haines, 2003. Mercury effects on predator avoidance behavior of a forage fish, golden shiner (*Notemigonus crysoleucas*). Environmental Toxicology and Chemistry, 22:1556-1561.

Weech, S.A., A.M. Scheuhammer and J.E. Elliott, 2006. Mercury exposure and reproduction in fish-eating birds breeding in the Pinchi Lake region, British Columbia, Canada. Environmental Toxicology and Chemistry, 25:1433-1440.

Weis, J.S. and A.A. Khan, 1990. Effects of mercury on the feeding behavior of the mummichog, *Fundulus heteroclitus* from a polluted habitat. Marine Environmental Research, 30:243-249.

Weseloh, D.C., D.J. Moore, C.E. Hebert, S.R. de Solla, B.M. Braune and D.J. McGoldrick, 2011. Current concentrations and spatial and temporal trends in mercury in Great Lakes Herring Gull eggs, 1974–2009. Ecotoxicology, 20:1644-1658.

Whitney, M.C. and D.A. Cristol, 2017. Impacts of sublethal mercury exposure on birds: A detailed review. Reviews of Environmental Contamination and Toxicology, 244:113-163.

Wiemeyer, S.N., C.M. Bunck and A.J. Krynitsky, 1988. Organochlorine pesticides, polychlorinated biphenyls, and mercury in osprey eggs – 1970–79 – and their relationships to shell thinning and productivity. Archives of Environmental Contamination and Toxicology, 17:767-787.

Wiener, J.G., M.B. Sandheinrich, S.P. Bhavsar, J.R. Bohr, D.C. Evers, B.A. Monson and C.S. Schrank, 2012. Toxicological significance of mercury in yellow perch in the Laurentian Great Lakes region. Environmental Pollution, 161:350-357.

Willacker, J.J., C.A. Eagles-Smith and J.T. Ackerman, 2017. Mercury bioaccumulation in estuarine fishes: Novel insights from sulfur stable isotopes. Environmental Science and Technology, 51:2131-2139.

Wyn, B., K.A. Kidd, N.M. Burgess and R.A. Curry, 2009. Mercury biomagnification in the food webs of acidic lakes in Kejimkujik National Park and National Historic Site, Nova Scotia. Canadian Journal of Fisheries and Aquatic Sciences, 66:1532-1545.

Wyn, B., K.A. Kidd, N.M. Burgess, R.A. Curry and K.R. Munkittrick, 2010. Increasing mercury in yellow perch at a hotspot in Atlantic Canada, Kejimkujik National Park. Environmental Science and Technology, 44:9176-9181.

Yates, D.E., D.T. Mayack, K. Munney, D.C. Evers, A. Major, T. Kaur and R.J. Taylor, 2005. Mercury levels in mink (*Mustela vison*) and river otter (*Lontra canadensis*) from northeastern North America. Ecotoxicology, 14:263-274.

Yates, D.E., E.M. Adams, S.E. Angelo, D.C. Evers, J. Schmerfeld, M.S. Moore, T.H. Kunz, T. Divoll, S.T. Edmonds, C. Perkins and R. Taylor, 2014. Mercury in bats from the northeastern United States. Ecotoxicology, 23:45-55.

Yu, R.Q., J.R. Reinfelder, M.E. Hines and T. Barkay, 2013. Mercury methylation by the methanogen *Methanospirillum hungatei*. Applied and Environmental Microbiology, 79:6325-6330.

Zhang, Y., D.J. Jacob, S. Dutkiewicz, H.M. Amos, M.S. Long and E.M. Sunderland, 2015. Biogeochemical drivers of the fate of riverine mercury discharged to the global and Arctic oceans. Global Biogeochemical Cycles, 29:854-864.

Zhang, Y., D.J. Jacob, H.M. Horowitz, L. Chen, H.M. Amos, D.P. Krabbenhoft, F. Slemr, V.L. St Louis and E.M. Sunderland, 2016. Observed decrease in atmospheric mercury explained by global decline in anthropogenic emissions. Proceedings of the National Academy of Sciences, 113:526-531.

Table 8.1 Major biota groupings and tissues recommended for MeHg monitoring. All tissues can be non-lethally sampled (including biopsies of liver and kidney).

Group	Matrix	MeHg proportion	Sample prep type* (preferred is underlined)	Analysis type	Source reference for MeHg %	Comments
Fish	Muscle fillet	>95% (but varies)	ww or <u>dw</u>	THg	Bloom, 1992	Dark muscle is significantly higher than white muscle (Bosch et al., 2016a). New evidence indicates that %MeHg may be lower for some fish species and some cooking approaches (Wang

						et al., 2013) and 10% of fish should be analyzed for MeHg content.
	Muscle biopsy	>95% (but varies)	dw	THg	Peterson et al., 2004	dw is best owing to moisture loss concerns. Muscle biopsy to muscle fillet has a $r^2 = 0.96$. Biopsy plug depth may impact Hg measured – 5 mm plugs are best below dorsal fin (Cizdziel et al., 2002) and are without skin and adipose tissue.
	Fin clips	unknown	dw	THg	Cerveny et al., 2016	There is a significant correlation between fin clips and muscle fillet ($p<0.01$)
	Blood	>95%	ww or dw	THg	-	Assumed to be >95% MeHg based on other vertebrates
Sea turtles	Scutes	>95%?	fw (or dw if scutes need washing)	THg	Schneider et al., 2015	Recommended and assumed nearly all MeHg as scutes are composed of keratin
	Blood	>95%?	ww or dw	THg	-	Assumed to be >95% MeHg based on other vertebrates
	Muscle	>95%?	ww or dw	THg	-	Assumed to be >95% MeHg based on other vertebrates
Birds	Blood	>95%	ww or dw	THg	Rimmer et al., 2005; Edmonds et al., 2010	Bird blood is approximately 75% water
	Feather	~100%	fw (or dw if feathers are washed due to external contamination)	THg	Burger, 1993	If feathers are not washed, fw = dw because mean feather moisture is <1%, n = 490; R. Taylor, pers. comm.
	Eggs	>96%	ww or dw or fww	THg	Ackerman et al., 2013 (96% for 22 species)	ww and dw can be problematic if eggs are not collected immediately after laying (Dolgova et al., in press).
	Eggshells and membranes	>95%	dw	THg	Peterson et al., 2017	Membranes are assumed to be primarily MeHg, but shells are entirely inorganic Hg.
	Liver and kidney	5–7% in loons and mergansers; 56–90% in egrets; 88% (20–100%) terns and shorebirds	dw	MeHg	Scheuhammer et al., 1998; Spalding et al., 2000; Eagles-Smith et al., 2009b	These tissues are not recommended for monitoring; %MeHg can vary widely
Mammals	Skin	>90%	dw	THg	Wagemann et al., 1998	Muktuk (in marine mammals) includes layers of skin and blubber
	Fur or hair	>90%	fw (or dw if fur needs to be washed)	THg	Evans et al., 2000	Fur/hair may not relate to blood and muscle depending on growth patterns (Peterson et al., 2016a)
	Muscle	>90%	ww or dw	THg	Wagemann et al., 1998	
	Liver and kidney	3–12% in whales/seals 57–91% in mink/otter	dw	MeHg	Wagemann et al., 1998; Evans et al., 2000	These tissues are not recommended for monitoring; %MeHg can vary widely

*Reported as wet weight (ww), dry weight (dw), fresh weight (fw), or fresh wet weight (fww) analyses. Fw denotes samples that are not cleaned or dried prior to total Hg analysis.

Table 8.2 Potential bioindicator choices for ecological and human health grouped by major terrestrial biomes and their associated aquatic ecosystems (as described and adapted from Evers et al., 2016).

Target Terrestrial Biomes	**Associated Aquatic Ecosystems**	**Ecological Health Bioindicators**						**Human and Ecological Health Bioindicators**	
		Freshwater and Marine Fish	***Sea Turtles***	***Freshwater/ Terrestrial Birds***	***Marine Birds***	***Mammals***	***Freshwater Fish***	***Marine Fish***	***Marine Mammals***
Arctic Tundra	***Arctic Ocean and associated estuaries, lakes, rivers***	Sticklebacks[1] (freshwater); Arctic Cod[2] Sculpin[3] Sticklebacks[1] (marine)		Loons[4,5] Shorebirds[100]	Fulmars[6] Murres[6] Gulls[61,62, 63, 64, 65,66]	Polar Bears[7,99] Seals[8]	Arctic Char[9,60] Arctic Burbot[67] Grayling[10]	Halibut[11] Cod[11]	Beluga[2, 12,99] Narwhal[2, 12] Ringed Seal[57,99] Hooded Seal[8]
Boreal Forest and Taiga	***North Pacific and Atlantic Oceans and associated estuaries, lakes, rivers***	Perch[13] (freshwater); Mummichogs and Silversides[14, 82, 82] Gobies and Sticklebacks[101,102] (marine)		Loons[15] Osprey[17,98] Songbirds[18] (blackbirds, flycatchers, warblers)	Ducks[107] Eagles[105] Osprey[19] Herring Gulls[58,68] Petrels[20,]	Mink[21,22] Otter[21,22] Seals[23]	Catfish[11] Lake Trout[69,70] Pike[10,70] Sauger[10] Walleye[10,70]	Flounder[11] Snapper[11] Tuna[11]	Pilot Whale[24]
Temperate Broadleaf and Mixed Forest	***North Pacific and Atlantic Oceans, Mediterranean and Caribbean Seas, and associated estuaries, lakes rivers***	Perch[13] Cyprinnids[78, 83] (freshwater); Mummichogs and Silversides[14, 82, 82] Rockfish[11] Sticklebacks[25] (marine)	Sea Turtles[29, 52]	Eagles[16,72,92] Egrets[27] Grebes[5,26,71, 95] Gulls[59] Herons[27] Loons[4] Osprey[17,91,93,94,95] Shorebirds[104] Terns[26,101,103] Songbirds[18, 81] (blackbirds, fly-catchers, sparrows, swallows, warblers, wrens)	Cormorants[28] Eagles[72] Osprey[5,19] Pelicans[73] Shearwaters[76] Skuas[49] Terns[26,28]	Bats[85,86,87,88] Otter[21,22] Seals[23,97] Toothed whales[53,54, 90,98]	Bass[10,30,31] Bream[11] Lake Trout[70] Mullet[11] Pike[70] Walleye[31,70]	Barracuda[11] Mackerel[11] Mullet[11] Scabbard-fish[11] Sharks[11,32] Swordfish[11,45] Tuna[11,32]	

Tropical Rainforest	***South Pacific and South Atlantic and Indian Oceans and associated estuaries, lakes, rivers***	Catfish[23] Piranha[34] Snook[11] (freshwater); Bay Snook[11,34] (marine)	Sea Turtles[29]	Cranes[80] Egrets[27] Herons[27] Kingfishers[3,5] Songbirds[36] (Wrens, Thrushes, Flycatchers)	Albatrosses[37,38,50,51] Frigatebirds[4,7,4,75] Noddy[39,47] Penguins[48] Shearwaters[39,76] Skuas[49] Terns[39,47] Tropicbirds[39]	Jaguar[89] Otter[40] Seals[41] Toothed whales[55,56]	Catfish[11] Nile Perch[79] Snakehead[11] Tigerfish[84]	Barracuda[11] Grouper[42] Sharks[43,4,4,46] Snapper[11] Swordfish[46] Tuna[46,77.106]	

[1]Kenney et al. 2014, [2]AMAP 2011, [3]Rigét et al. 2007, [4]Evers et al. 2014, [5]Jackson et al. 2016, [6]Braune 2007, [7] Routti et al. 2011, [8]Dietz et al. 2013, [9]Gantner et al. 2010, [10]Eagles-Smith et al. 2016a, [11]Evers et al. 2016, [12]Wagemann, and Kozlowska 2005, [13]Wiener et al. 2012, [14]Weis and Kahn 1990, [15]Evers et al. 2011b, [16]Bowerman et al. 1994, [17]Odsjö et al. 2004, [18]Jackson et al. 2015, [19]Wiemeyer et al. 1988, [20]Goodale et al. 2008, [21]Yates et al. 2005, [22]Klenavic et al. 2008, [23]Brookens et al. 2008, [24]Dam and Bloch 2000, [25]Eagles-Smith and Ackerman 2009, [26]Ackerman et al. 2016, [27]Frederick et al. 2002, [28]Braune 1987, [29]Day et al. 2005, [30]Kamman et al. 2005, [31]Monson et al. 2011, [32]Cai et al. 2007, [33]Bastos et al. 2015, [34]Mol et al. 2001, [35]Lane et al. 2011, [36]Townsend et al. 2013, [37]Finkelstein et al. 2006, [38]Burger and Gochfeld 2000, [39]Kojadinovic et al. 2007, [40]Fonseca et al. 2005, [41]Marcovecchio et al. 1994, [42]Evers et al. 2009, [43]Kiszka et al. 2015, [44]Maz-Courrau et al. 2012, [45]Storelli and Marcotrigiano 2001, [46]Bodin et al. 2017, [47]Sebastiano et al. 2017, [48]Carravieri et al. 2016, [49]Carravieri et al. 2017, [50]Bustamante et al. 2016, [51]Anderson et al. 2010, [52]Maffucci et al. 2005, 53 Correa et al. 2013, 54 Aubail et al. 2013, 55 Bustamante et al. 2003, 56 Garrigue et al. 2016, [57]Brown et al. 2016, [58]Burgess et al. 2013, [59]Weseloh et al. 2011, [60]Evans et al. 2014, [61]Braune et al. 2006, [62]Lucia et al. 2015, [63]Lucia et al. 2016, [64]Braune et al. 2016, [65]Miljeteig et al. 2009, [66]Bond et al. 2015, [67]Pelletier et al. 2017, [68]Blukacz-Richards et al. 2017, [69]Abma et al. 2015, [70]Gandhi et al. 2014, [71]Hartman et al. 2017, [72]DeSorbo et al. 2018, [73]Newtoff and Emslie 2017, [74]Sebastiano et al. 2016, [75]Mott et al. 2017, [76]Watanuki et al. 2016, [77]Bosch et al. 2016b, [78]Cerveny et al. 2016, [79]Hanna et al. 2016, [80]Daso et al. 2015, [81]Pacyna et al. 2017, [82]Chen et al. 2014, [83]Buckman et al. 2015, [84]Webb et al. 2015, [85]Yates et al. 2014, [86]Little et al. 2015,[87]Åkerblom and de Jong 2017, [88]Korstian et al. 2018, [89]May Junior et al. 2017, [90]Titcomb et al. 2017, [91]Rumbold et al. 2017, [92]Kalisinska et al. 2014,[93]Hughes et al. 1997,[94]Henny et al. 2009b,[95]Anderson et al. 2008,[96]DesGranges et al. 1998, [97]Peterson et al. 2016b, [98]Reif et al. 2015, [99]Krey et al. 2015, [100]Perkins et al. 2016, [101]Eagles-Smith and Ackerman 2009a, [102]Eagles-Smith and Ackerman 2014, [103]Ackerman et al. 2008, [104]Ackerman et al. 2007, [105]Burger and Gochfeld 2009, [106] Chouvelon et al. 2017, [107]Savoy et al. 2017

Appendix 8.1 Global arithmetic mean ± SD of total Hg (µg/g or ppm) concentrations for selected fish, sea turtle, birds and marine mammals at the taxonomic level of Order (or other groupings for marine mammals). Biota are arranged by major group, then mean Hg concentrations from high to low. Relevant tissue types of target biota vary by major taxonomic classification (i.e., Order) (based on University of Michigan Animal Diversity Web, 2018).

Common Name	Order	# of locations	# of individuals	Mean	SD	Min	Max
SHARKS, SKATES, AND RAYS	***CHONDRICHTHYES***	***Muscle (ww)***					
Chimaeras	Chimaeriformes	6	225	2.81	1.04	0.07	5.16
Cow sharks	Hexanchiformes	6	38	2.51	0.90	0.48	3.43
Electric rays	Torpediniformes	7	47	1.56	1.10	0.02	3.59
Dogfishes	Squaliformes	28	786	1.45	2.11	0.03	10.51
Mackerel sharks	Lamniformes	35	526	1.24	1.02	0.00	10.00
Ground sharks	Carcharhiniformes	205	7806	1.07	0.83	0.00	21.07
Carpet sharks	Orectolobiformes	5	120	0.96	0.29	0.05	3.40
Angel sharks	Squatiniformes	3	98	0.40	0.07	0.03	0.48
Stingrays	Myliobatiformes	33	229	0.33	0.30	0.01	3.50
Guitarfishes	Rhinobatiformes	11	59	0.22	0.28	0.01	2.05
Skates and Rays	Rajiformes	9	88	0.14	0.08	0.01	0.63
MARINE FISH	***TELEOSTEI***	***Muscle (ww)***					
Roughy	Beryciformes	18	71	0.53	0.36	0.03	1.91

Tarpons	Elopiformes	15	277	0.46	0.78	0.02	5.78
Perch-like fishes	Perciformes	1430	26231	0.37	0.48	0	24.61
Eels	Anguilliformes	20	349	0.31	0.17	0.01	2.20
Toadfish	Batrachoidiformes	6	117	0.30	0.14	0.03	0.37
Bonefishes	Albuliformes	6	47	0.27	0.19	0.03	1.10
Flatfishes, Flounders, Soles	Pleuronectiformes	112	2713	0.26	0.26	0.00	1.10
Catfishes	Siluriformes	71	1159	0.17	0.14	0.01	1.80
Pipefishes, Sticklebacks	Gasterosteiformes	3	232	0.16	0.13	0.08	0.31
Minnows, Suckers	Cypriniformes	12	312	0.15	0.04	0.00	0.19
Scorpion fishes, Sculpins	Scorpaeniformes	71	1273	0.13	0.11	0.00	1.23
Silversides	Atheriniformes	13	662	0.12	0.07	0.02	0.51
Anglerfishes	Lophiiformes	8	115	0.12	0.10	0.01	0.68
Cods, Hakes, Haddocks	Gadiformes	85	1769	0.12	0.14	0.00	2.35
Mullets	Mugiliformes	91	1048	0.08	0.15	0.00	2.38
Needlefishes	Beloniformes	7	54	0.07	0.03	0.016	0.35
Puffers, Triggerfishes, Leatherjackets	Tetraodontiformes	11	72	0.07	0.06	0.01	0.17
Salmons	Salmoniformes	40	646	0.06	0.03	0.01	0.55
Herrings, Sardinesm Anchovies	Clupeiformes	142	2894	0.06	0.18	0.00	6.48
Aulopiforms, Lizardfishes	Aulopiformes	19	93	0.05	0.08	0.00	0.58
Smelts	Osmeriformes	16	143	0.05	0.09	0.00	0.79
Dragonfishes, Lightfishes	Stomiiformes	5	31	0.05	0.04	0.01	0.19
Lanternfishes	Myctophiformes	11	97	0.04	0.04	0.01	0.32
FRESHWATER FISH	***TELEOSTEI, CHONDROSTEI, HOLOSTEI, DIPNOI***	***Muscle (ww)***					
Bowfins	Amiiformes	544	607	0.97	0.75	0.02	7.00
Needlefishes	Beloniformes	5	116	0.59	0.92	0.02	5.40
Gars	Semionotiformes	164	295	0.45	0.36	0.04	2.41
Bonytongues	Osteoglossiformes	215	1821	0.42	0.84	0.00	20.74
Perch-like fishes	Perciformes	38981	186940	0.37	0.60	0.00	181.00
Mudminnows, Pikes	Esociformes	7953	31755	0.32	0.23	0.00	9.99
Milkfish	Gonorynchiformes	1	68	0.28		0.11	0.83
Piranhas, Leporins	Characiformes	722	11239	0.26	0.35	0.00	13.44
Catfishes	Siluriformes	6171	21630	0.21	1.24	0.00	175.00
Cods, Hakes, Haddocks	Gadiformes	350	1708	0.20	0.13	0.01	6.40
Eels	Anguilliformes	68	253	0.18	0.12	0.01	0.45
Herrings, Sardinesm Anchovies	Clupeiformes	334	2255	0.16	0.23	0.01	6.64
Knifefishes	Gymnotiformes	16	43	0.16	0.30	0.01	1.92
Sturgeons, Spoonfishes, Paddlefishes	Acipenseriformes	210	614	0.16	0.13	0.00	3.60
Salmons	Salmoniformes	11783	46593	0.14	0.18	0.00	12.30
Minnows, Suckers	Cypriniformes	9420	58094	0.13	0.45	0.00	22.46
Mullets	Mugiliformes	18	67	0.13	0.27	0.00	3.19
Killifishes	Cyprinodontiformes	89	5985	0.13	0.20	0.01	28.50
Scorpion fishes, Sculpins	Scorpaeniformes	1098	4529	0.10	0.14	0.00	2.19
Pipefishes, Sticklebacks	Gasterosteiformes	60	1544	0.08	0.05	0.01	0.46
Silversides	Atheriniformes	1417	6109	0.06	0.05	0.00	0.88

Smelts	Osmeriformes	27	924	0.06	0.07	0.00	2.08
Flatfishes, Flounders, Soles	Pleuronectiformes	1285	3800	0.05	0.21	0.00	5.00
Lungfishes	Lepidosireniformes	15	107	0.01	0.01	0.00	0.04
REPTILES	***REPTILIA***	***Scutes (fw)***					
Sea turtles	Testunides	14	222	0.34	0.57	0.05	2.33
		Blood (ww)					
Sea turtles	Testunides	25	897	0.02	0.02	0.00	0.40
		Muscle (ww)					
Sea turtles	Testunides	41	246	0.06	0.03	0.00	0.66
		Egg Contents (ww)					
Sea turtles	Testunides	15	401	0.07	0.23	0.00	0.13
BIRDS	***AVES***	***Adult Body Feathers (fw)***					
Hawks, Eagles, Vultures	Accipitriformes	37	537	18.13	12.46	0.10	193.00
Loons	Gaviiformes	5	637	12.61	1.05	1.72	63.40
Albatrosses, Petrels, Shearwaters	Procellariiformes	183	4206	12.13	10.04	0.08	94.72
Pelecans, Ibises, Herons	Pelecaniformes	6	72	7.24	3.23	0.78	19.07
Rails and Cranes	Gruiformes	4	167	6.88	4.38	0.03	9.04
Grebes	Podicipediformes	3	16	6.16	1.87	4.00	8.00
Kingfishers	Coraciiformes	4	93	6.13	2.28	0.60	46.10
Cormorants	Suliformes	22	252	5.40	2.88	0.25	27.40
Gulls, Terns, Other Shorebirds	Charadriiformes	174	2865	4.20	3.73	0.03	57.00
Tropicbirds	Phaethontiformes	5	79	4.09	3.06	0.80	6.41
Perching Birds	Passeriformes	16	539	2.87	2.04	0.18	10.76
Waterfowl	Anseriformes	26	446	1.92	2.25	0.19	18.00
Penguins	Sphenisciformes	123	1296	1.26	1.28	0.02	9.43
Owls, Goatsuckers	Strigiformes	5	96	1.19	0.36	0.03	12.80
		Adult Blood (ww)					
Pelecans, Ibises, Herons	Pelecaniformes	14	437	5.80	3.72	0.22	20.28
Albatrosses, Petrels, Shearwaters	Procellariiformes	109	1530	4.52	13.11	0.06	209.37
Loons	Gaviiformes	101	4927	2.01	2.14	0.00	20.32
Grebes	Podicipediformes	10	473	1.67	1.54	0.36	5.37
Cormorants	Suliformes	49	893	1.30	1.75	0.19	17.14
Rails and Cranes	Gruiformes	17	311	1.22	1.18	0.00	3.31
Kingfishers	Coraciiformes	10	275	0.94	0.81	0.04	3.35
Hawks, Eagles, Vultures	Accipitriformes	80	1320	0.90	0.83	0.00	7.40
Woodpeckers	Piciformes	2	18	0.75	0.83	0.09	1.27
Gulls, Terns, Other Shorebirds	Charadriiformes	277	3031	0.65	0.65	0.01	4.26
Falcons	Falconiformes	10	788	0.64	0.69	0.04	2.59
Waterfowl	Anseriformes	248	4230	0.55	1.15	0.00	6.62
Owls, Goatsuckers	Strigiformes	15	147	0.54	0.63	0.02	2.26
Perching Birds	Passeriformes	309	7668	0.50	0.69	0.01	6.72
Penguins	Sphenisciformes	29	330	0.31	0.22	0.04	0.75
Tropicbirds	Phaethontiformes	1	32	0.27		0.27	0.27
Doves, Pigeons	Columbiformes	3	49	0.00	0.00	0.00	0.00
		Eggs (ww)					

Loons	Gaviiformes	25	1941	0.87	0.41	0.00	9.03
Kingfishers	Coraciiformes	1	16	0.56		0.03	3.03
Gulls, Terns, Other Shorebirds	Charadriiformes	433	16413	0.48	0.39	0.00	3.74
Albatrosses, Petrels, Shearwaters	Procellariiformes	26	534	0.44	0.27	0.12	1.74
Falcons	Falconiformes	33	972	0.43	0.20	0.01	1.01
Cormorants	Suliformes	20	586	0.27	0.08	0.00	1.07
Rails and Cranes	Gruiformes	13	761	0.20	0.18	0.03	2.70
Hawks, Eagles, Vultures	Accipitriformes	81	1031	0.17	0.18	0.00	2.48
Pelecans, Ibises, Herons	Pelecaniformes	60	1491	0.17	0.17	0.00	1.90
Waterfowl	Anseriformes	64	1838	0.15	0.21	0.00	3.93
Perching Birds	Passeriformes	68	3856	0.10	0.04	0.00	1.50
Grebes	Podicipediformes	13	639	0.09	0.03	0.04	0.18
Penguins	Sphenisciformes	8	109	0.08	0.05	0.02	0.12
Owls, Goatsuckers	Strigiformes	3	14	0.02	0.01	0.00	0.11
Doves, Pigeons	Columbiformes	2	32	0.01	0.00	0.00	0.06
MARINE MAMMALS	***MAMMALIA***	***Muscle (ww)***					
Toothed Whales	Cetacea: Odontoceti	526	5068	2.64	4.66	0.00	93.52
Seals and Walruses	Carnivora: Odobenidae, Otariidae, Phocidae	166	2338	0.39	0.38	0.00	3.22
Baleen Whale	Cetacea: Mysticeti	34	594	0.08	0.07	0.02	0.74
Polar Bears	Carnivora: Ursus maritimus	5	77	0.08	0.05	0.06	0.24

Please leave Track Changes switched on for all work on this file. Also, please do not accept any revisions – just work over them or flag anything with which you disagree

9. Mercury levels and trends in human populations worldwide

Credits ???

Key messages

- **All people are exposed to mercury (Hg) to some extent.** For many communities worldwide, dietary consumption of fish, shellfish, marine mammals, and other food items that are contaminated with methylmercury (MeHg), is the most important source of exposure. Exposures to elemental and inorganic mercury mainly occur in occupational settings as well as via contact with products containing mercury.

- **There is great variability in Hg exposure worldwide. A** review of over 240,000 biomarker measurements suggests that individuals in background populations (i.e. without significant Hg exposures) have blood Hg levels generally <5 µg/L and urine Hg levels generally <3 µg/L.

- **Concern remains about Hg exposure in vulnerable groups who are sensitive owing to extrinsic (e.g., high exposures) and intrinsic (e.g., lifestage) factors.** Elevated Hg exposures in key groups of concern for which there are relatively robust datasets include fetuses, Arctic populations (e.g., Inuit) who regularly consume fish and marine mammals, tropical riverine communities (e.g., Amazonian), coastal and/or small-island communities who are high seafood consumers, and individuals who either work or live among artisanal and small-scale gold mining sites, or who otherwise have high occupational exposures.

- **Assessing Hg exposure is relatively straightforward by the use of biomarkers.** Mercury can be measured in blood, hair and urine. Measurements in hair and urine samples are particularly suitable because they provide information on the two main forms of Hg, and their collection is relatively non-invasive, requires no specialized training or handling and storage regiment, and is relatively cheap. In addition, the results can be interpreted against guideline values, over different spatial and temporal scales, and following interventions to gauge their effectiveness.

9.1 Background

9.1.1 Sources of human exposure to mercury

Mercury is a naturally occurring element that can enter the environment via natural or anthropogenic-mediated processes. There are three major chemical forms of mercury (Hg) relevant to human exposure: elemental Hg (Hg^0), inorganic Hg compounds (Hg^{2+}), and organic Hg compounds, the most important form of which is methylmercury (MeHg). The source, environmental fate, exposure, and toxicity of these different Hg forms vary.

Mercury has unique physical and chemical properties that have rendered it attractive for use in a range of industrial and medical applications. Human exposure to Hg^0 and Hg^{2+} may occur in occupational settings, for example artisanal and small-scale gold mining (ASGM) and dentistry, as well as through contact with products containing Hg, such as dental amalgams, skin-lightening creams and other cosmetics, traditional

medicines, broken thermometers and fluorescent lamps. In addition, thimerosal, which contains MeHg, is used as a preservative in some vaccines (WHO, 2017).

Mercury released into the environment may be converted to MeHg which bioaccumulates and biomagnifies through the food chain, particularly in aquatic systems (see Chapter 7). Seafood is the main source of protein for about one billion people worldwide (FAO, 2014) and some organisms that are widely consumed are likely to be contaminated with MeHg. These include predatory fish such as tuna, swordfish, grouper, and mackerel. For many communities, therefore, dietary consumption of contaminated fish, shellfish, marine mammals, and other food items is arguably the most important source of exposure. Foods such as rice grown in sites heavily contaminated with Hg may also represent a source of exposure for some communities (Rothenberg et al., 2014). Figure 9.1 illustrates some key sources of Hg exposure around the world.

Figure 9.1 Selected studies depicting strong and representative evidence of Hg source-exposure relationships.

9.1.2 Health effects of mercury

Mercury is a pollutant of global concern principally due to its adverse effects on human health. The current state of knowledge concerning human health impacts has been extensively reviewed by international agencies (IPCS, 1990, 2003; JECFA 2007a,b, 2011; EFSA CONTAM panel, 2012) as well as by national agencies and other authors (US EPA, 1997, 2001; ATSDR, 1999; Clarkson and Magos, 2006; Karagas et al. 2012; Ha et al., 2017; Eagles-Smith et al., 2018).

All individuals worldwide are exposed to some amount of Hg, and the possibility of exposure-related adverse health effects is dependent upon a range of factors (e.g., chemical form, concentration, duration of exposure, lifestage). The embryo and fetus are the most vulnerable lifestages with respect to the adverse effects of MeHg (JECFA, 2007).

All forms of Hg are toxic but the principal target organs differ according to the form. Exposure to Hg^0 may affect the nervous system. Exposure to Hg^{2+} compounds may affect the kidneys. Exposure to MeHg is associated with adverse neurodevelopmental outcomes. The latter has received the most attention largely due to notorious MeHg poisoning events in Japan and Iraq following high exposures (IPCS, 1990). Studies on the toxicity of MeHg carried out over recent decades have provided a growing body of evidence that chronic, relatively low-level MeHg exposure can be associated with a range of adverse health outcomes targeting, for example, the cardiovascular and immune systems (Karagas et al., 2012).

9.1.3 Mercury exposure assessment using biomarkers

Detailed reviews of methodology for assessing Hg exposure have been undertaken by WHO/UNEP (2008) and the US EPA (1997). Human exposure to Hg can be estimated by measuring Hg in human tissue and other samples (WHO/UNEP, 2008). This report focuses on biomarkers of Hg exposure for which there are well-validated methods of measurement and interpretation and for which there is a reasonably large body of knowledge. The most commonly used biomarkers are the concentrations of Hg in hair, urine, blood, and cord blood, and their selection can depend on factors such as the potential source of exposure, chemical form, and exposure lifestage. The logistical requirements and costs differ for each sample type. In all cases it is

important that steps are taken to avoid sample contamination during collection, storage, transportation, and analysis, and to be mindful of ethical considerations (WHO Regional Office for Europe, 2015).

Most of the Hg in hair occurs as MeHg and once incorporated the Hg remains in the hair. This biomarker can therefore provide an integrated measurement of Hg exposure given that hair grows at roughly 1 cm per month and thus exposure can be tracked over time by careful sampling. Hair has the advantage that it is easy to collect and transport, although it should be noted that in some communities there may be cultural objections to taking hair samples. On the other hand, in highly contaminated areas such as ASGM sites there is a danger of external contamination of the hair, which can confound interpretation of the results. Studies using stable isotope analysis have, for example, found external contamination of hair in ASGM communities by Hg^0, thus calling for special attention to be paid to the interpretation of hair Hg levels to monitor exposure at ASGM sites (Sherman et al., 2015) and the need to analyze hair for MeHg in such scenarios.

Urine analysis primarily provides information about exposure to Hg^{2+} and Hg^0, although MeHg may also contribute to the burden of urinary Hg, particularly among avid seafood consumers (Sherman et al., 2013). The concentration of the analyte may depend on the dilution of the urine, which can vary. It is therefore common for the Hg measurement to be expressed in terms of its concentration per unit of creatinine. Another approach is to relate the Hg concentration to the specific gravity of the urine sample, which is gaining favor given that creatinine measures may be confounded by factors such as diet and age. Urine is a relatively easy and non-invasive sample to collect.

Mercury is measured in whole blood and this provides information about recent exposure (~1–2 months) to both MeHg and Hg^{2+}. In most communities the measurement of blood total Hg is an accepted biomarker for MeHg exposure as it correlates relatively well to seafood consumption (Sheehan et al., 2014). Speciation can provide an indication of potential Hg sources but requires careful sample preparation and sophisticated instrumentation. The measurement of Hg in cord blood provides information about developmental exposure. Blood collection, storage, and transport pose certain logistical and financial barriers, however.

Each biomarker can provide pertinent exposure information on the type of Hg (organic vs. inorganic) and timeline of exposure (acute vs. chronic). When multiple biomarker measures are taken from a given individual, and also combined with surveys, a deeper exposure assessment can be performed. In general, careful measurement of Hg in hair and urine offers the most convenient and cost-effective scheme to monitor Hg in a given population, particularly those populations situated in resource-limited settings. For a more detailed discussion of Hg biomarkers, including potential challenges in their use, see WHO/UNEP (2008).

To maximize the use of Hg biomarker data, it is sometimes necessary to convert across biomarker types and there are two conventions to be noted for exposure cases that largely involve MeHg (N.B. applicability to Hg^0 and Hg^{2+} is not known). First, the Joint Food and Agriculture Organization (FAO) and World Health Organization (WHO) Expert Committee on Food Additives (JECFA) established a MeHg hair-to-blood ratio of 250 (JECFA, 2004) that is now commonly used by the research community. Second, cord blood levels are on average 70% higher than maternal blood levels, as discussed by Stern and Smith (2003). While these two biomarker ratios are both used in the current assessment, it is acknowledged that there is ongoing debate in

the literature concerning the validity of these approaches particularly in terms of heterogeneity across individuals with respect to influential factors such as sex, age, and ethnicity (Bartell et al., 2000; Stern and Smith, 2003). There is also growing awareness that inter-individual differences in the toxicokinetics of Hg and resulting biomarker measures may be influenced by polymorphisms in certain genes (Basu et al., 2014), although at this time such information cannot be put into practice. Nonetheless, biomarker conversions facilitate comparability across studies, and have been effective at helping derive large, regional biomonitoring assessments and maps – for example, in Europe by Višnjevec Miklavčič et al. (2014) and in the Arctic by AMAP (2015) – that are effective communication tools. In addition, to make judgements from biomarker measures it is necessary to have reference values. Proposals by stakeholder organizations are summarized in Appendices 9.1 and 9.2. The colour scale used by Višnjevec Miklavčič et al. (2014) in their European assessment of Hg exposure was adapted for the purposes of this assessment (Appendix 9.3).

9.2 Objective

The aim of this chapter is to provide an overview of worldwide human exposures to Hg as reflected by concentrations in biomarker samples. The specific objectives of this study are to outline:

- whether exposures have changed over time in specific populations
- geographical variations in exposure
- exposures in vulnerable groups who are sensitive owing to extrinsic (e.g., high exposures) and intrinsic (e.g., susceptible lifestage) factors
- exposure biomarker data with respect to guideline values

- links between Hg sources and biomarker levels
- key knowledge gaps.

9.3 Method

9.3.1 Identification of studies

An international advisory group of scientific experts on Hg exposure was convened to guide the work. The group (i.e., report authors) decided to focus this initial global assessment on three study population types: A, B and C.

A-National human biomonitoring programs. These programs are usually sponsored and/or operated by official government agencies and provide high quality data.

B-Longitudinal birth cohort studies. These studies are usually well designed and most pertinent for establishing exposure-outcome relationships. They tend to provide high quality exposure data for vulnerable groups (i.e., those with high exposures and/or susceptibility to toxic effects; such as fetuses, newborns, and children), and these data can be used to explore geographic differences and temporal trends, as well as to characterize Hg source-exposure-biomarker relationships.

C-Cross-sectional studies on vulnerable populations. While many vulnerable populations exist, this study focused on groups according to Hg sources (a-populations exposed to Hg^{2+} inorganic mercury from point sources, i.e., artisanal and small-scale gold miners and community members; people living and working in

former Hg-contaminated sites; and n-methylmercury exposure from high consumption of fish and other aquatic animals), and lifestages (c-fetuses).

9.3.2 Search strategy

A systematic search of the peer-reviewed scientific literature was performed using three databases: Medline, Biosis, and the Web of Science Core Collection. The search strategy included the following Boolean search phrases: “mercury OR methylmercury OR (methyl AND mercury) OR MeHg”; and “blood OR hair OR urine”. Other information sources include grey literature, key researchers identified by report authors, and stakeholders via UN Environment outreach activities. When a study was reported upon in multiple articles, the article with the most complete dataset was chosen to serve as a representative piece.

Scientific papers were reviewed through a two-stage process: the title and abstract fields were searched to ascertain relevancy; and the full text was reviewed on papers that were deemed relevant. In brief, national biomonitoring studies (Study Population Type A) were identified through a list compiled by UN Environment (UN Environment, 2016), WHO-Europe (WHO Regional Office for Europe 2005), and subsequent outreach efforts, authors’ knowledge, and an electronic search. All national biomonitoring programs that measured Hg in hair, blood, urine, or cord blood were included (i.e., no exclusion criteria were applied). Longitudinal birth cohort studies (Study Population Type B) were also identified through the 2016 UN Environment survey, authors’ knowledge, and an electronic search. Similar to the national biomonitoring studies, exclusion criteria were not applied with the exception that the studies included needed to have at least two discrete sampling periods, one of which needed to be a biomarker measured during pregnancy or

birth. Vulnerable population group studies (Study Population Type C) were identified through a review of the bibliographic search results. For brevity, this study focused on the most illustrative works but it should be noted that this information was extracted from a companion effort led by the World Health Organization (WHO) that is more comprehensive (Basu et al., in prep).

9.3.3 Data analyses

For all studies, data were extracted on population characteristics (age, lifestage, sex, city/country/region location), Hg exposure measurements (sample size, Hg biomarker and speciation information, quality control measures), and measures of central tendencies (geometric mean, median) and high-end (90th or 95th percentile or maximum) biomarkers. To compare across biomarker types, datasets were converted to blood Hg equivalents using the conventions mentioned earlier. To further interpret the results, the values were compared against ranges that were derived based on a scan of existing reference range and guidance resources (Appendix 9.1) and a color scale (Appendix 9.3) was used to visually represent the findings.

9.4 Results

9.4.1 National biomonitoring studies

Data were obtained from nine countries (Belgium, Canada, Czech Republic, France, Germany, Republic of Korea, Slovenia, Sweden, USA) that were identified by those countries as being nationally-representative (Table 9.1). The total sample population of these surveys was 121,437 people from which 192,675 biomarker measurements of Hg exposure were extracted (Table 9.2). The survey data were compared with a particular focus on: country, lifestage, sex, sampling year(s), and biomarker type.

Table 9.1 Summary of national human biomonitoring programs that measure mercury.

Country	Survey	Lead organization	Start date	Frequency	Size/cycle	Age; Sex	Biomarkers	Key reference
Belgium	FLEHS	Vlaanderen Departement Omgeving	2002	2; every 2 years	~5000	1–65; female adults, children both sexes	hair	Croes et al., 2014
Canada	CHMS	Statistics Canada	2007	4; every 2 years	~5000	3–79; both	blood, urine	Haines et al., 2017
Czech Republic	CZ-HBM	National Institute of Public Health	1994	16; ~every year	~400	8–64; both	blood, urine, hair	NIPH, 2017
France	Elfe	Santé publique France	2011	1	~1800	18–47; pregnant women	hair	Dereumeaux et al., 2016
Germany	GerES	German Environment Agency	1985	5; variable	~2000–5000	3–79; both	blood, urine	German Federal Environment Agency, 2017
Germany	ESB	German Environment Agency	1981	37; each year	500	20–29; both	blood, urine	
Republic of Korea	KoNEHS	Korean Ministry of Environment	2009	3; every 3 years	~6000	3–19+; both	blood, urine	Seo et al., 2015; Burm et al., 2016
Slovenia	SLO-HBM	Jozef Stefan Institute	2008	2; every 2 years	~300–~900	18–49; both	blood, urine, breast milk, hair	Snoj Tratnik et al., subm.
Sweden	Riksmaten	Swedish National Food Agency	1990	2; variable	~300	18–80; both	blood	Bjermo et al., 2013
USA	NHANES	Centers for Disease Control and Prevention	1999	6; every 2 years	~8000	1–70+; both	blood, urine	US CDC, 2015

Table 9.2 Count of individuals and mercury biomarker measures from the national biomonitoring programs.

	Demographics					Number of Hg measurements				
Country	Total sample size	Children	Adults	Males	Females	Total	Blood total Hg	Blood MeHg	Urine	Hair

Belgium	465	210	255		255	465				465
Canada	22,805	9,491	13,314	11,227	11,578	41,235	22,425	2,075	16,734	
Czech Republic	7,542	3,623	3,919			13,845	4,700		6,459	2,686
France	1,799		1,799		1,799	1,799				1,799
Germany	25,772	2,602	23,170			41,045	17,056		23,989	
Republic of Korea	14,688	2,346	12,342			14,688	14,688			
Slovenia	1,095		1,095	553	542	3,523	1,085		1,020	947
Sweden	297			128	145	297	297			
USA	46,974	19,086	27,888	23,292	23,682	75,778	46,974	13,016	15,788	
Total	121,437					192,675				

Across the national biomonitoring programs the majority of participants had blood Hg levels that fell below 5 μg/L (Figure 9.2). Blood Hg levels were consistently highest in Republic of Korea versus the other countries. Blood Hg levels in adults were approximately 2.1-fold higher than in children, and this varied across lifestage. For example, median blood Hg levels in Canadians from the CHMS increased with age as follows: 0.24 μg/L (6–11 years), 0.28 μg/L (12–19 years), 0.76 μg/L (20–39 years), 1.1 μg/L (40–59 years), and 0.96 μg/L (60–79 years). Similar trends were observed in the U.S. and Korean datasets.

Figure 9.2 Comparison of median blood total Hg (μg/L) measurements across children (<19 years) and adults from national biomonitoring datasets between the years 2003 and 2014. Note, for Belgium and France that blood Hg values were estimated based on hair Hg levels in women (adults) and children (both sexes).

Table 9.3 Cross-sectional comparison of blood total Hg concentrations (μg/L) in adults and children via national biomonitoring data. Males and females are grouped together. Note, for Belgium and France that blood Hg values were estimated based on hair Hg levels in women (adults) and children (both sexes).

Republic of Korea	Germany	USA	Canada	Belgium	France	Czech Republic	Slovenia	Sweden

	Survey Name	KoNEHS-2 (Adults), KorEHS-C (Children)	GerES-III (Adults), GerES-IV (Children)	NHANES	CHMS Cycle 2	FLEHS2	Elfe (Adults), ENNS (Children)	CZ-HBM	SLO-HBM	Riksmaten
Adults	Year	2014	1998	2011-2012	2009-2011	2007-2011	2011	2015	2008-2012	2010-2011
	Age	19+	18-69	20+	20-39	18-42	18-47	18-64	18-49	18-80
	Sample Size	6457	3973	5030	1313	255	1799	302	1,085	297
	Blood Hg[a]	3.05	0.70	0.79	0.65	1.36	1.68	0.65	1.20	1.13
	Blood Hg[b]	9.05	2.40	5.02	5.20	3.44	5.56	2.50	4.78	3.45
Children	Year	2012-2014	2003-2006	2011-2012	2009-2011	2007-2011	2006-2007	2008	2008	
	Age	3-18	3-14	6-11	6-11	14-16	3-17	8-10	6-11	
	Sample Size	2346	1240	1048	961	210	1364	198	174	
	Blood Hg[a]	1.80	0.30	0.32	0.21	0.76	1.52	0.40	0.79	
	Blood Hg[b]	3.68	1.00	1.40	2.00	1.88	4.8	1.40	2.19	

[a] 50th percentile concentration; [b] 95th percentile concentration.

Urine Hg levels were consistent across the countries from which data were obtained, with the majority of values falling below 3 μg/L (Table 9.4). Like blood, urine Hg levels were higher in adults than in children.

Table 9.4 Cross-sectional comparison of urinary total Hg measurement (μg/L) in adults and children via national biomonitoring data. Males and females are grouped together. When available, creatinine-adjusted values are indicated in parenthesis.

		Germany	USA	Canada	Czech Republic	Slovenia
Adults	Year	1998	2013–2014	2012–2013	2015	2008–2012
	Age	18–69	20+	20–39	18–64	18–49
	Sample size	4052	1813 (1812)	1048	234	1020
	Urine Hg[a]	0.40	0.24 (0.30)	0.20 (0.22)	0.91 (0.91)	0.45

						(0.47)
	Urine Hg[b]	3.00	1.76 (1.76)	1.10 (1.20)	6.34 (4.67)	3.47 (2.48)
Children	Year	2003–2006	2013–2014	2012–2013	2008	2008
	Age	3–14	6–11	6–11	8–10	6–11
	Sample size	1734	401	1010	318	164
	Urine Hg[a]	<MDL, i.e. 0.1	<MDL, i.e. 0.13 (<MDL, i.e. 0.13)	<MDL, i.e. 0.2 (<MDL, i.e. 0.2)	(0.20)	0.76 (0.73)
	Urine Hg[b]	0.5	0.89 (1.11)	0.93 (1.9)	(1.10)	4.64 (4.15)

MDL: Method detection limit; [a] 50th percentile concentration; [b] 95th percentile concentration.

Temporal changes in Hg exposure were evaluated by reviewing national datasets in which there were two or more comparable sampling periods (Figure 9.3). For blood Hg, datasets from four countries (USA, Canada, Czech Republic, Republic of Korea) were reviewed and in general they showed declining exposures. For example, combining the data for the USA, Canada, and the Czech Republic into a linear regression model showed annual decreases in blood Hg of approximately 0.026 μg/L or 2.25% (i.e., over 10 years this would be a decrease of 0.26 μg/L or ~22.5%) with median blood Hg levels stabilizing around 0.75 μg/L (Figure 9.3A). For urinary Hg, similar over-time decreases can be observed particularly when examining the US NHANES dataset as the Hg levels in the latest dataset is approximately 50% lower than it was 10 years earlier (Figure 9.3B). Urinary Hg values in the US are currently similar to those Canada and hover around 0.2 μg/L.

Figure 9.3. Temporal trends of adult A) blood and B) urinary total Hg (μg/L; median values) measurements across the national biomonitoring studies in which data were available from two or more comparable sampling periods.

9.4.2 Longitudinal birth cohorts

Twenty-four birth cohort studies were found (many of which had multiple sub-cohorts or sites) from 17 countries in which there was at least one Hg exposure measurement during pregnancy or birth, as well as a follow-up period in which an outcome measurement was taken (Figure 9.4; Appendix 9.4). The total sample population of these birth cohort studies was 23,374 mother-child pairs, from which 47,699 biomarker measurements were taken. Of these birth cohort studies, 17 (53%) measured Hg in cord blood, 9 (28%) measured Hg in maternal blood during pregnancy, and 19 (59%) measured Hg in maternal hair. In general, the birth cohort studies focused on MeHg exposures.

Figure 9.4. Locations of the selected Hg birth cohort studies. Data represent 24 cohort studies and 47,699 Hg biomarker measures. The cohort ID is indicated in the first box as a letter (see Appendix 9.4 for details). The first three boxes refer to group average Hg measures taken during pregnancy, at birth, and up until age 18 years, respectively. Blank cells represent lifestages without a Hg measurement. If the final box has a star, then a Hg-associated adverse outcome was reported in that cohort. Color codes are based on the work by Višnjevec Miklavčič et al. (2014) with minor modifications as detailed in Appendix 9.3.

The overview presented in Figure 9.4 leads to several observations: (1) groups consuming large amounts of seafood (Seychelles, Spain), freshwater fish (Brazil) and/or marine mammals (e.g., Faroe Islands, Inuit communities of the Arctic) have the highest Hg exposures, which often exceed 10 μg/L in cord blood; (2) cord blood Hg levels range between 5 and 10 μg/L across several Mediterranean populations, are approximately 5 μg/L in Asia, and generally less than 5 μg/L across communities in North America and

Europe (excluding Indigenous Peoples and the Mediterranean area); and (3) exposures in the Faroe Islands show an almost five-fold decline between ~1987 and ~2008 (blood Hg from 22.3 to 4.6 μg/L), and in the Seychelles an approximately two-fold decline between ~1989 and ~2008 (hair Hg from 5.9 to 2.9 μg/g). In these birth cohort studies, a range of health outcomes were measured in the newborn, infant, toddler, or child, including for example, birth weight, motor function, and intelligence (see reviews by Karagas et al., 2012 and Ha et al., 2017). In flagging cohorts in which a MeHg-associated adverse health outcome was observed (by asterisks in Figure 9.4), such as neurobehavior and motor function, it is apparent that these cohorts span a range of exposures and are not restricted to highly exposed groups or particular regions (Figure 6).

9.4.3 Vulnerable populations

This section presents a selection of illustrative findings from the bibliometric search and group discussions, the purpose is to showcase the current state of knowledge concerning Hg exposure in particularly vulnerable groups. In general, conclusions from high-quality review papers were prioritized. Some of these examples were captured in Figure 9.1. It should be noted that the information presented here is from a more comprehensive companion effort led by the World Health Organization (Basu et al., in prep).

9.4.3.1 Pregnant women and fetuses

MeHg-contaminated seafood (and other MeHg-contaminated food items) pose risk-benefit dilemmas to all populations since there are both health benefits (e.g., from the selenium and polyunsaturated fatty acids they contain) and risks (from the MeHg they contain) associated with their consumption (FAO/WHO, 2010).

Sheehan et al. (2014) conducted a systematic review of Hg exposure biomarkers in these populations worldwide (164 studies from 43 countries) and drew some significant conclusions: (1) exposures are highest among riverine gold mining communities (median hair Hg 5.4 μg/g; n=10,152 participants) and Arctic Indigenous Peoples (median hair Hg 2.1 μg/g; n=5935 participants); and (2) coastal Pacific regions of Asia have higher median hair Hg levels (1.3 μg/g; n=14,704 participants) than coastal population in the Mediterranean (0.7 μg/g; n=6536) and Atlantic (0.4 μg/g; n=9675), as well as inland populations (0.4 μg/g; n=10,745).

9.4.3.2 Indigenous Peoples

Indigenous Peoples worldwide may be exposed to Hg given that many communities are reliant upon traditional foods such as fish and marine mammals for sustenance. Cisneros-Montemayor et al. (2016) compiled data from over 1900 coastal Indigenous groups (27 million people from 87 countries) and showed that per capita seafood consumption in these communities is 15-times higher than in non-Indigenous groups. Because traditional foods also form a strong basis for the culture, spirituality, recreation, and economy of many of these communities, contamination of food by Hg presents an issue of environmental justice (Landrigan et al., 2018). The Inuit in the Arctic are exposed to some of the highest MeHg levels globally largely due to their reliance on fish and marine mammals as culturally important food staples. The latest AMAP Human Health Assessment (AMAP, 2015) reviewed several human biomonitoring programs across the circumpolar region. As an example, in Canada as part of the International Polar Year study, the geometric mean of blood Hg across four study regions ranged from 2.8 to 12 μg/L, with individual values

ranging from 0.1 to 240 μg/L. In another example, the Greenlandic Inuit Health and Transition Study of 3105 participants from all geographic areas and community sizes (nine towns, 13 villages) reported blood Hg levels ranging from 0.1 to 400 μg/L. Indigenous Peoples living within the Amazon Basin have also been documented to be highly exposed to Hg through both fish consumption and proximity to gold mining (Berzas Nevado et al., 2010).

9.4.3.3 Artisanal and small-scale gold mining communities

ASGM is rapidly growing worldwide with over 15 million miners estimated to be directly involved in the sector and potentially 100 million people living in ASGM communities (UNEP, 2012; WHO, 2016). There are several public health concerns in ASGM communities (Basu et al., 2015; WHO, 2016) and a growing number of human biomonitoring studies (reviewed by Gibb and O'Leary, 2014). One meta-analysis of data from 1245 miners from across Indonesia, Philippines, Tanzania, Zimbabwe, and Mongolia reported median urine Hg values of 3.6 μg/L (95^{th} percentile 119 μg/L) with upward values in excess of 1000 μg/L, and median blood Hg levels in 1121 miners of 5.1 μg/L (95^{th} percentile 38.2 μg/L) (Baeuml et al., 2011).

9.5 Summary of findings

This assessment documents great variability in Hg exposures worldwide. All people are exposed to some amount of Hg. Individuals in select background populations worldwide with insignificant exposures to Hg sources have blood Hg levels that are generally <5 μg/L and urine Hg levels that are <3 μg/L, and corresponding levels in hair and cord blood may be determined using the ratios outlined in Appendix 9.1. There are a number of notable groups with relatively high Hg exposures. Elevated exposures to Hg in key

groups of concern for which there exist a relatively robust dataset include Arctic populations who consume fish and marine mammals as a significant component of their diet (e.g. many Indigenous communities), tropical riverine communities (such as those in the Amazon Basin), coastal and/or small-island communities who are high seafood consumers, and individuals who either work or reside at ASGM sites.

Despite a relatively large dataset – this study used 192,675 and 47,699 biomarker measurements from national biomonitoring programs and birth cohort studies, respectively – there remain various outstanding issues.

First, there are several countries and geographic regions for which data are completely lacking. Given that the Minamata Convention is motivated by human health concerns (i.e., Article 1), there is a need for Parties to have data that is nationally representative so that temporal changes in human exposure (and ultimately risk) may be tracked. There is general agreement concerning the methods to assess Hg exposure. Measures of Hg in hair and urine samples are particularly suitable as they provide information on the two main forms of Hg, and their collection is relatively non-invasive, requires no specialized training or handling and storage regimen, and is relatively cheap (Evers et al., 2016). Such methods are being scaled across countries to help harmonize Hg biomonitoring. For example, the DEMOnstration of a study to COordinate and Perform Human biomonitoring on a European Scale (DEMOCOPHES) project showed that hair Hg could be measured in 1799 mother-child pairs from 17 European countries to yield comparable values (Castaño et al., 2015).

Exposures to Hg in vulnerable groups who are sensitive owing to extrinsic (e.g., high exposures) and intrinsic (e.g., susceptible lifestage) factors remain of utmost concern. There are several highly exposed groups – such as individuals living in Hg-contaminated sites (Trasande et al., 2016), consumers of rice from contaminated sites (Rothenberg et al., 2014), and users of skin-lightening creams (WHO/UNEP, 2008) – for which there is growing awareness but relatively few data from which to draw firm conclusions. In addition to vulnerability based on elevated exposures, there is also concern about Hg susceptibility during certain lifestages (e.g., fetus), the range of physiological systems targeted (Karagas et al., 2012), the complex interactions between Hg and other chemical and non-chemical stressors, particularly in the context of global change drivers (Eagles-Smith et al., 2018), and the increasing acceptance that genetic differences in sub-populations can influence exposure biomarkers and exposure-outcome relationships (Basu et al., 2014).

Concerns over Hg pollution and human health risks are firmly established, nevertheless there are success stories to be noted. This review found studies that showed steps to limit Hg exposures – intentional or otherwise – may be effective. First, the roughly two-fold reduction in urinary Hg levels measured over the past decade across the U.S. population is likely to be due to a combination of the development of encapsulated amalgams, increasing use of composite resins, and overall awareness of the occupational and environmental risks associated with Hg use (Figure 9.3B). Similar trends have been observed elsewhere such as in German children (Link et al., 2007) and among U.S. dental professionals (Anglen et al., 2015; Goodrich et al., 2016).

Second, although Hg exposures across Arctic circumpolar regions remain elevated, levels have declined over the past two decades, probably owing to local dietary advisories and changing consumption patterns. According to AMAP (2015) these decreases may be a sign that risk management efforts are having a beneficial effect, but there remain concerns about changing consumption patterns and how these may affect Indigenous culture, identity and spirituality, recreational opportunities, and human nutrition. In other jurisdictions, there have been cases of decreased Hg exposures as a result of dietary consumption advisories (e.g., Knobeloch et al., 2011; Kirk et al., 2017). Decreases have also been observed in both the Faroe Islands and the Seychelles (Figures 4 and 5). However, in other Small Island Developing States the awareness of Hg exposure and its potential health impacts may be lower and thus the decrease observed in the Seychelles is not necessarily representative of other islands.

Third, within the ASGM sector there is increasing interest in assessing the efficacy of interventions aimed at reducing exposures. Calys-Tagoe et al. (2017a) found urinary Hg levels to be significantly lower in workers from licensed ASGM sites than unlicensed sites in Ghana. While sociodemographic profiles, use of personal protective equipment, and education can differ between licensed and unlicensed miners, relating these to Hg exposures is not straightforward (Calys-Tagoe et al., 2017b).

References

ACGIH, 2007. TLVs and BEIs: Based on the Documentation of the Threshold Limit Values for Chemical Substances and Physical Agents and Biological Exposure Indices. American Conference of Governmental Industrial Hygienists (ACGHI). Signature Publications.

AMAP, 2015. AMAP Assessment 2015: Human Health in the Arctic. Arctic Monitoring and Assessment Programme (AMAP), Oslo.

Anglen, J., S.E. Gruninger, H.N. Chou, J. Weuve, M.E. Turyk, S. Freels and L.T. Stayner, 2015. Occupational mercury exposure in association with prevalence of multiple sclerosis and tremor among US dentists. Journal of the American Dental Association, 146:659-668.

ATSDR, 1999. Toxicological Profile for Mercury. Agency for Toxic Substances and Disease Registry (ATSDR).

Baeuml, J., S. Bose-O'Reilly, R. Matteucci Gothe, B. Lettmeier, G. Roider, G. Drasch and U. Siebet, 2011. Human biomonitoring data from mercury exposed miners in six artisanal small-scale gold mining areas in Asia and Africa. Minerals, 1:122-143.

Bartell, S.M., R.A. Ponce, R.N. Sanga and E.M. Faustman, 2000. Human variability in mercury toxicokinetics and steady state biomarker ratios. Environmental Research, 84:127-132.

Basu, N., J.M. Goodrich and J. Head, 2014. Ecogenetics of mercury: from genetic polymorphisms and epigenetics to risk assessment and decision-making. Environmental Toxicology and Chemistry, 33:1248-1258.

Basu, N., E. Clarke, A. Green, B. Calys-Tagoe, L. Chan, M. Dzodzomenyo, J. Fobil, R.N. Long, R.L. Neitzel, S. Obiri, E. Odei, L. Ovadje, R. Quansah, M. Rajaee and M.L. Wilson, 2015. Integrated assessment of artisanal and small-scale gold mining in Ghana–part 1: human health review. International Journal of Environmental Research and Public Health, 12:5143-5176.

Basu, N., J. Tempowski, D. Evers, M. Horvat, P. Weihe and I. Zastenskaya, in prep. A systematic review of mercury levels and trends in human populations worldwide. For submission to a pertinent open access journal by end-March 2018.

Berzas Nevado, J.J., R.C. Rodríguez Martín-Doimeadios, F.J. Guzmán Bernardo, M. Jiménez Moreno, A.M. Herculano, J.L. do Nascimento and M.E. Crespo-López, 2010. Mercury in the Tapajós River basin, Brazilian Amazon: a review. Environment International, 36:593-608.

Bjermo, H., S. Sand, C. Nälsén, T. Lundh, H. Enghardt Barbieri, M. Pearson, A.K. Lindroos, B.A. Jönsson, L. Barregård and P.O. Darnerud, 2013. Lead, mercury, and cadmium in blood and their relation to diet among Swedish adults. Food and Chemical Toxicology, 57:161-169.

Burm, E., I. Song, M. Ha, Y.M. Kim, K.J. Lee, H.C. Kim, S. Lim, S.Y. Kim, C.G. Lee, S.Y. Kim, H.K. Cheong, J. Sakong, H.T. Kang, M. Son, G.J. Oh, Y. Kim, J.Y. Yang, S.J. Hong, J.H. Seo, J. Kim, S. Oh, J. Yu, S.S. Chang, H.J. Kwon, Y.H. Choi, W. Choi, S. Kim and S.D. Yu, 2016. Representative levels of blood lead, mercury, and urinary cadmium in youth: Korean Environmental Health Survey in Children and Adolescents (KorEHS-C), 2012-2014. International Journal of Hygiene and Environmental Health, 219:412-418.

Calys-Tagoe, B., N. Basu, E. Clarke and T. Robins, 2017a. Mercury exposure biomarkers differ between licensed and un-licensed ASGM miners in Tarkwa, Ghana. Presented at the 13th International Conference on Mercury as a Global Pollutant, July 16-21 2017, Rhode Island, USA.

Calys-Tagoe, B.N.L., E. Clarke, T. Robins and N. Basu, 2017b. A comparison of licensed and un-licensed artisanal and small-scale gold miners (ASGM) in terms of socio-demographics, work profiles, and injury rates. BMC Public Health, 17:862. doi:10.1186/s12889-017-4876-5.

Castaño, A., F. Cutanda, M. Esteban, P. Pärt, C. Navarro, S. Gómez, M. Rosado and 53 others, 2015. Fish consumption patterns and hair mercury levels in children and their mothers in 17 EU countries. Environmental Research, 141:58-68.

Cisneros-Montemayor, A.M., D. Pauly, L.V. Weatherdon and Y. Ota, 2016. A global estimate of seafood consumption by coastal indigenous Peoples. PLoS One, 11(12):e0166681.

Clarkson, T.W. and L. Magos, 2006. The toxicology of mercury and its chemical compounds. Critical Reviews in Toxicology, 36:609-662.

Croes, K., S. De Coster, S. De Galan, B. Morrens, I. Loots, E. Van de Mieroop, V. Nelen, I. Sioen, L. Bruckers, T. Nawrot, A. Colles, E. Den Hond, G. Schoeters, N. van Larebeke, W. Baeyens and Y. Gao, 2014. Health effects in the Flemish population in relation to low levels of mercury exposure: from organ to transcriptome level. International Journal of Hygiene and Environmental Health, 217:239-247.

Dereumeaux, C., A. Saoudi, M. Pecheux, B. Berat, P. de Crouy-Chanel, C. Zaros, S. Brunel, C. Delamaire, A. Tertre, A. Lefranc, S. Vandentorren and L. Guldner, 2016. Biomarkers of exposure to environmental contaminants in French pregnant women from the Elfe cohort in 2011. Environment International, 97:56-67.

Eagles-Smith, C., E. Silbergeld, N. Basu, P. Bustamante, F. Diaz-Barriga, W. Hopkins, K. Kidd and J. Nyland, 2018. A synthesis of how global change drivers modulate mercury exposure, bioaccumulation, and adverse outcomes in wildlife and humans. Ambio, 47:170-197.

EFSA CONTAM Panel, 2012. Scientific Opinion on the risk for public health related to the presence of mercury and methylmercury in food. EFSA Journal. 10(12):2985. doi:10.2903/j.efsa.2012.2985. European Food Safety Authority (EFSA) Panel on Contaminants in the Food Chain (CONTAM).

Evers, D.C., S.E. Keane, N. Basu and D. Buck, 2016. Evaluating the effectiveness of the Minamata Convention on Mercury: Principles and recommendations for next steps. Science of the Total Environment, 569-570:888-903.

FAO, 2014. The State of World Fisheries and Aquaculture: Opportunities and Challenges. Food and Agriculture Organization (FAO), Rome.

FAO/WHO, 2010. Report of the Joint FAO/WHO Expert Consultation on the Risks and Benefits of Fish Consumption. Food and Agriculture Organization (FAO), Fisheries and Aquaculture Report No. 978.

Florida Health Department, 2009. Guidelines for mercury. Document No. document HG05-2009. www.floridahealth.gov/environmental-health/mercury-spills/mercury-poisoning/_documents/guidelines-for-mercury.pdf

German Federal Environment Agency, 2017. German Environmental Survey. www.umweltbundesamt.de/en/topics/health/assessing-environmentally-related-health-risks/german-environmental-survey-geres [Accessed 30 November 2017]

Gibb, H. and K.G. O'Leary, 2014. Mercury exposure and health impacts among individuals in the artisanal and small-scale gold mining community: a comprehensive review. Environmental Health Perspectives, 122:667-672.

Goodrich, J.M., H.N. Chou, S.E. Gruninger, A. Franzblau and N. Basu, 2016. Exposures of dental professionals to elemental mercury and methylmercury. Journal of Exposure Science and Environmental Epidemiology, 26:78-85.

Ha, E., N. Basu, S. Bose-O'Reilly, J.G. Dórea, E. McSorley, M. Sakamoto and H.M. Chan, 2017. Current progress on understanding the impact of mercury on human health. Environmental Research, 152:419-433.

Haines, D.A., G. Saravanabhavan, K. Werry and C. Khoury, 2017. An overview of human biomonitoring of environmental chemicals in the Canadian Health Measures Survey: 2007-2019. International Journal of Hygiene and Environmental Health, 220:13-28.

Health Canada, 2015. Third Report on Human Biomonitoring of Environmental Chemicals in Canada. Health Canada, Ottawa.

IPCS, 1990. Methylmercury. Environmental Health Criteria 101. World Health Organization, International Programme on Chemical Safety (IPCS). www.inchem.org/documents/ehc/ehc/ehc101.htm [Accessed 30 November 2017].

IPCS, 2003. Elemental Mercury and Inorganic Mercury Compounds: Human Health Aspects. World Health Organization, International Programme on Chemical Safety (IPCS). Concise international chemical assessment document No. 50.

JECFA, 2004. Evaluation of Certain Food Additives and Contaminants. Sixty-first report of the Joint FAO/WHO Expert Committee on Food Additives (JECFA). World Health Organization (WHO) Technical Report Series 922.

JECFA, 2007a. Methylmercury (addendum). In: Safety Evaluation of Certain Food Additives and Contaminants. Prepared by the sixty-seventh meeting of the Joint FAO/WHO Expert Committee on Food Additives (JECFA). Food Additives Series 58. pp. 269-315.

JECFA, 2007b. Methylmercury. In: Evaluation of Certain Food Additives and Contaminants. Sixty-seventh Report of the Joint FAO/WHO Expert Committee on Food Additives. Geneva: World Health Organization/Food and Agriculture Organization (JECFA). WHO Technical Report Series 940. pp. 53-59.

JECFA, 2011. Safety Evaluation of Certain Contaminants in Food. Prepared by the seventy-second meeting of the Joint FAO/WHO Expert Committee on Food Additives (JECFA). WHO Food Additives Series 63.

Karagas, M.R., A.L. Choi, E. Oken, M. Horvat, R. Schoeny, E. Kamai, W. Cowell, P. Grandjean and S. Korrick, 2012. Evidence on the human health effects of low-level methylmercury exposure. Environmental Health Perspectives, 120:799-806.

Kirk, L.E., J.S. Jørgensen, F. Nielsen and P. Grandjean, 2017. Public health benefits of hair-mercury analysis and dietary advice in lowering methylmercury exposure in pregnant women. Scandinavian Journal of Public Health, 45:444-451.

Knobeloch, L., C. Tomasallo and H. Anderson, 2011. Biomonitoring as an intervention against methylmercury exposure. Public Health Reports, 126:568-574.

Landrigan, P.J., R. Fuller, N.J.R. Acosta, O. Adeyi, R. Arnold, N.N. Basu, A.B. Baldé, R. Bertollini, S. Bose-O'Reilly, J.I. Boufford, P.N. Breysse, T. Chiles, C. Mahidol, A.M. Coll-Seck, M.L. Cropper, J. Fobil, V. Fuster, M. Greenstone, A. Haines, D. Hanrahan, D. Hunter, M. Khare, A. Krupnick, B. Lanphear, B. Lohani, K. Martin, K.V. Mathiasen, M.A. McTeer, C.J.L. Murray, J.D. Ndahimananjara, F. Perera, J. Potočnik, A.S. Preker, J. Ramesh, J. Rockström, C. Salinas, L.D. Samson, K. Sandilya, P.D. Sly, K.R. Smith, A. Steiner, R.B. Stewart, W.A. Suk, O.C.P. van Schayck, G.N. Yadama, K. Yumkella and M. Zhong, 2018. The Lancet Commission on pollution and health. Lancet, 391:462-512.

Legrand, M., M. Feeley, C. Tikhonov, D. Schoen and A. Li-Muller, 2010. Methylmercury blood guidance values for Canada. Canadian Journal of Public Health, 101:28-31.

Link, B., T. Gabrio, I. Piechotowski, I. Zöllner and M. Schwenk, 2007. Baden-Wuerttemberg Environmental Health Survey (BW-EHS) from 1996 to 2003: toxic metals in blood and urine of children. International Journal of Hygiene and Environmental Health, 210:357-371.

Mahaffey, K.R., E.M. Sunderland, H.M. Chan, A.L. Choi, P. Grandjean, K. Mariën, E. Oken, M. Sakamoto, R. Schoeny, P. Weihe, C.H. Yan and A. Yasutake, 2011. Balancing the benefits of n-3 polyunsaturated fatty acids and the risks of methylmercury exposure from fish consumption. Nutrition Reviews, 69:493-508.

Mergler, D., H.A. Anderson, L.H. Chan, K.R. Mahaffey, M. Murray, M. Sakamoto and A.H. Stern, 2007. Methylmercury exposure and health effects in humans: a worldwide concern. Ambio, 36:3-11.

NIPH, 2016. Systém monitorování zdravotního stavu obyvatelstva České republiky ve vztahu k životnímu prostředí Souhrnná zpráva za rok 2015 [Environmental Health Monitoring System in the Czech Republic. Summary Report, 2015]. National Institute of Public Health (NIPH), Prague. www.szu.cz/uploads/documents/chzp/souhrnna_zprava/Souhrnna_15_CD.pdf.

NIPH, 2017. Environmental Health Monitoring Reports. Czech Republic National Institute of Public Health (NIPH). www.szu.cz/topics/environmental-health/environmental-health-monitoring [Accessed 30 Nov 2017]

Puklová, V., A. Krsková, M. Černá, M. Cejchanová, I. Rehůrková, J. Ruprich, K. Kratzer, R. Kubínová and M. Zimová, 2010. The mercury burden of the Czech population: An integrated approach. International Journal of Hygiene and Environmental Health, 213:243-251.

Rothenberg, S.E., L. Windham-Myers and J.E. Creswell, 2014. Rice methylmercury exposure and mitigation: a comprehensive review. Environmental Research, 133:407-423.

Schulz, C., J. Angerer, U. Ewers and M. Kolossa-Gehring, 2007. The German Human Biomonitoring Commission. International Journal of Hygiene and Environmental Health, 210:373-382.

Seo, J.W., B.G. Kim, Y.M. Kim, R.B. Kim, J.Y. Chung, K.M. Lee and Y.S. Hong, 2015. Trend of blood lead, mercury, and cadmium levels in Korean population: data analysis of the Korea National Health and Nutrition Examination Survey. Environmental Monitoring and Assessment, 187:146. doi:10.1007/s10661-015-4348-2.

Shamlaye, C.F., D.O. Marsh, G.J. Myers, C. Cox, P.W. Davidson, O. Choisy, E. Cernichiari, A. Choi, M.A. Tanner and T.W. Clarkson, 1995. The Seychelles child development study on neurodevelopmental outcomes

in children following in utero exposure to methylmercury from a maternal fish diet: background and demographics. Neurotoxicology, 16:597-612.

Sheehan, M.C., T.A. Burke, A. Navas-Acien, P.N. Breysse, J. McGready and M.A. Fox, 2014. Global methylmercury exposure from seafood consumption and risk of developmental neurotoxicity: a systematic review. Bulletin of the World Health Organization, 92:254-269F.

Sherman, L., J.D. Blum, A. Franzblau and N. Basu, 2013. New insight into biomarkers of human mercury exposure using naturally occurring mercury stable isotopes. Environmental Science and Technology, 47:3403-3409.

Sherman, L.S., J.D. Blum, N. Basu, M. Rajaee, D.C. Evers, D.G. Buck, J. Petrlik and J. DiGangi, 2015. Assessment of mercury exposure amongst small-scale gold miners using mercury stable isotopes. Environmental Research, 137:226-234.

Snoj Tratnik, J., D. Mazej, M. Jagodic, D. Kocman, A. Stajnko, A. Trdin, Z. Šlejkovec, I. Falnoga, J. Osredkar, M. Prezelj, M. Skitek, M. Krsnik, A. Sešek-Briški, A.B. Kobal, L. Kononenko, M. Horvat, Subm. Results of the first National Human Biomonitoring in Slovenia: trace elements in lactating women and their partners and sources of exposure. Submitted to International Journal of Hygiene and Environmental Health.

Stern, A.H. and A.E. Smith, 2003. An assessment of the cord blood:maternal blood methylmercury ratio: implications for risk assessment. Environmental Health Perspectives, 111:1465-1670.

Trasande, L., J. DiGangi, D.C. Evers, J. Petrlik, D.G. Buck, J. Šamánek, B. Beeler, M.A. Turnquist and K. Regan, 2016. Economic implications of mercury exposure in the context of the global mercury treaty: hair mercury levels and estimated lost economic productivity in selected developing countries. Journal of Environmental Management, 183:229-235.

UN Environment, 2016. Global Review of Mercury Monitoring Networks. United Nations Environment Programme.

UNEP, 2012. Reducing Mercury Use in Artisanal and Small-Scale Gold Mining: A Practical Guide. United Nations Environment Programme (UNEP). Available at http://wedocs.unep.org/handle/20.500.11822/11524.

US CDC, 2015 Fourth National Report on Human Exposure to Environmental Chemicals, Updated Tables, February 2015. Centers for Disease Control and Prevention (CDC).

US EPA, 1997. Mercury Study Report to Congress. United States Environmental Protection Agency (US EPA). www.epa.gov/mercury/mercury-study-report-congress

US EPA, 2001. Risk assessment for methylmercury. In: Water Quality Criterion for the Protection of Human Health: Methylmercury. Chapter 4. United States Environmental Protection Agency (US EPA), Office of Science and Technology.

US NAS / US NRC, 2000. Toxicological Effects of Methylmercury. US National Academy of Sciences (US NAS) / US National Research Council (US NRC). National Academy Press.

Višnjevec Miklavčič, A.M., D. Kocman and M. Horvat, 2014. Human mercury exposure and effects in Europe. Environmental Toxicology and Chemistry, 33:1259-1270.

WHO, 2016. Environmental and Occupational Health Hazards Associated with Artisanal and Small-scale Gold Mining. World Health Organization (WHO).

WHO, 2017. Mercury and Health. Fact sheet. World Health Organization (WHO). www.who.int/mediacentre/factsheets/fs361/en/ [Accessed 10 November 2017]

WHO Regional Office for Europe, 2015. Human Biomonitoring: Facts and Figures. World Health Organization (WHO).

WHO/UNEP, 2008. Guidance for Identifying Populations at Risk from Mercury Exposure. World Health Organization (WHO) / United Nations Environment Programme (UNEP).

Yasutake, A., M. Matsumoto, M. Yamaguchi and N. Hachiya, 2004. Current hair mercury levels in Japanese for estimation of methylmercury exposure. Journal of Health Science, 50:120-125.

Appendix 9.1 Reference Values for Mercury Biomarkers. *Italicized values* denoted with an asterisk (*) are estimated based on biomarker conversions indicated in the text.

	Blood	Hair	Cord Blood	Urine
US National Academy of Sciences (NAS) and US National Research Council's Benchmark Dose Lower Limit (BMDL) concerning women of child-bearing age) (US NAS / US NRC, 2000)	*3.5 µg/L* *	1 µg/g	5.8 µg/L	
Qualitative conclusions by expert panel on "High" Levels (Karagas et al., 2012)	>12 µg/L	>4 µg/g	>20 µg/L	
Health Canada (Legrand et al., 2010)	8 µg/L (pregnant women); 20 µg/L (non-pregnant adults); 100 µg/L for "general" men/women	*2 µg/g *; 5 µg/g *; 25 µg/g **	*13.6 µg/L *; 29 µg/L *; not relevant for the 3rd group*	
German HBM-1 (concentration of a substance in human biological material at which and below which, according to the current knowledge and assessment by the HBM-Commission, there is no risk of adverse health effects) (Schulz et al., 2010)	5 µg/L	*1.25 µg/g **	*8.5 µg/L **	7 µg/L
German HBM-2 (concentration of a substance in human biological material at which and above which adverse health effects are possible and, consequently, an acute need for the reduction of exposure and the provision of biomedical advice is given) (Schulz et al., 2010)	15 µg/L	*3.75 µg/g **	*25.5 µg/L **	25 µg/L
The ACGIH (2007) https://www.osha.gov/dts/osta/otm/otm_ii/pdfs/otmii_chpt2_appb.pdf				Not exceed 35 µg/g creatinine among occupationally exposed
Florida Health Department (2009)	<10 µg/L (background); >50µg/L (clinical effects)	*<2.5 µg/g *; >12.5 µg/g **		<40µg/L (no clinical effects); 40-60 (medium); 60+ (high)

Appendix 9.2 Reference Values for Mercury Intake. References from WHO/UNEP (2008) unless otherwise indicated.

	Inorganic Hg (µg/kg bw/wk)	MeHg (µg/kg bw/wk)
European Food Safety Authority (CONTAM panel), 2012	4	1.3
Joint FAO/WHO Expert Committee on Food Additives (JECFA), 2011	4*	
Joint FAO/WHO Expert Committee on Food Additives (JECFA), 2007b		1.6*
US EPA Reference Dose (adopted 2001)		0.7
Canada (adopted 1997)		1.4
Japan (adopted 2005)		2.0
Netherlands (adopted 2000)		0.7

*Provisional tolerable weekly intake values

Appendix 9.3. Colour scale related to mercury biomarker values. Adapted from Višnjevec Miklavčič et al. (2014) with minor modifications.

	Assigned color	Hair (ug/g)	Blood (ug/L)	Cord Blood (ug/L)	Urine (ug/L)
Background Levels (non seafood consumers)	Blue	<0.5	<2	<3.4	<1
Background Levels (seafood consumers)	Cyan	0.5-2	2-8	3.4-13.6	1-3
Elevated Levels	Yellow	2-5	8-20	13.6-34	3-10
Moderately High Levels	Orange	5-10	20-40	34-68	10-50
High Levels	Red	>10	>40	>68	>50

Appendix 9.4. Summary of birth cohort studies that were reviewed. Color codes are based on the work by Višnjevec Miklavčič et al. (2014) with minor modifications as detailed in Appendix 3.

				Lifestage exposures (blood Hg equivalents)								
Cohort-ID	Cohort-Name	n	Yr	Pregnancy	Birth	Infant (0-1)	Toddler (1-3)	Child (3-11)	Adolescence (12-17)	Adult (18+)	Outcome ?	Key reference
H	POUCH (Michigan)	1024	1998	0.92							*	Xue et al., 2007
N	Poland	313	2002	0.83	1.09						*	Jedrychowski et al., 2006
E	MIREC	1673	2008	2.24	0.80						*	Arbuckle et al., 2016
D	VIVA	135	2002	1.80							*	Oken et al., 2005
T	Massachusetts	421	1993	1.80							*	Sagiv et al., 2012
F	ALSPAC	4131	1991	1.86								Golding et al., 2013
U	Shanghai	1652	2008		1.88						*	Yu et al., 2011
O	Oswego	212		2.00							*	Stewart et al., 2003
K	EDEN	665	2003	2.08								Drouillet-Pinard et al., 2010
I	World Trade Center	280	2001	1.60	4.44						*	Lederman et al., 2008
S	Italy	128	2001	3.20				2.16			*	Deroma et al., 2013
B	ELEMENT	348	1994	2.80	4.10			1.37				Basu et al., 2014
J	MOCEH (Korea)	797	2006	3.10	5.20						*	Kim et al., 2011
V	PELAGIE	349	2002		4.24							Chevrier et al., 2013
A5	Faroe Islands	500	2008		4.60							AMAP 2015
Q1	PHIME-Italy	573		4.00	5.60							Llop et al., 2017
M	Zhoushan	406	2004	4.98	5.58							Gao et al., 2007

Q2	PHIME-Greece	281		5.60	7.50							Llop et al., 2017
R	Hong Kong	1057	2000	4.92	8.80				2.62		*	Fok et al., 2007
L	Tohoku	498	2001	7.80							*	Suzuki et al., 2010
P	INMA	1883	2004		8.20							Ramon et al., 2011
C3	Seychelles		2008	11.68								Strain et al., 2015
A3	Faroe Islands	475	1999		12.40				2.60		*	AMAP 2015
G	Nunavik Child Development	130	1994	12.60	15.90				5.90		*	Muckle et al., 2001
A2	Faroe Islands	182	1995		21.00				3.20		*	AMAP 2015
A1	Faroe Islands	1022	1987		22.30				8.40	4.10	2.53 *	AMAP 2015
C1	Seychelles	779	1989	23.60		26.40	19.20		25.20	32.40	27.30	Strain et al., 2015
W4	Madeira R (Tin Mine)	294	2006		30.26						*	Marques et al., 2013
C2	Seychelles		2001	22.50	39.30							Davidson et al., 2008
W2	Madeira R (Urban)	676	2006		36.45							Marques et al., 2013
W3	Madeira R (Rural)	67	2006		53.18							Marques et al., 2013
W1	Madeira R (Riverine)	396	2006		82.42							Marques et al., 2013